Aspects of Cosmological, Celestial and String Amplitudes

by

Shounak De

A dissertation submitted in partial fulfillment of the requirements for the Degree of Doctor of Philosophy in the Department of Physics at Brown University

Providence, Rhode Island
May 2025

This dissertation by Shounak De is accepted in its present form by the Department of Physics as satisfying the dissertation requirement for the degree of Doctor of Philosophy.

Date ________________ ________________________________
Anastasia Volovich, Advisor

Recommended to the Graduate Council

Date ________________ ________________________________
Anastasia Volovich, Reader

Date ________________ ________________________________
Stephon Alexander, Reader

Date ________________ ________________________________
JiJi Fan, Reader

Approved by the Graduate Council

Date ________________ ________________________________
Thomas A. Lewis
Dean of the Graduate School

Abstract of “Aspects of Cosmological, Celestial and String Amplitudes” by Shounak De, Ph.D., Brown University, May 2025.

In this thesis, we present novel perspectives on the explicit evaluation and analytic structure of correlation functions and scattering amplitudes in flat and expanding spacetimes. Specifically, we analyze wavefunction coefficients in a toy model theory of conformally coupled scalars within power-law FRW cosmologies, examine unitarity constraints on dual resonant string amplitudes, and further our understanding of the flat-space $\mathcal{S}$-matrix using the framework of celestial amplitudes.

First, we explore intriguing connections between positive geometries, on-shell methods, and bootstrap principles studied within the modern scattering amplitudes program to the Bunch-Davies wavefunction in toy models of FRW cosmologies. Leveraging recent advances in twisted cohomology and generalized unitarity from the Feynman integral literature, we develop an algorithm to construct a physical basis that simplifies the computation of differential equations for all tree and loop-level wavefunction contributions. Furthermore, we unravel the existence of hidden zeros in the cosmological wavefunction and demonstrate a universal factorization behavior associated with the kinematics of near-zero configurations for all tree and loop graphs.

Second, we investigate the constraints of partial wave unitarity on dual resonant amplitudes from the viewpoint of the modern $\mathcal{S}$-matrix bootstrap. Focusing on the Coon amplitude – a one-parameter deformation of the Veneziano amplitude with logarithmic Regge trajectories – we establish manifest positivity on certain Regge trajectories while identifying regions of unitarity violation in parameter space using tools from q-calculus and numerical methods.

Finally, we make substantial advances in the study of celestial amplitudes by investigating the dual celestial conformal field theory (CCFT) and the role of light-ray operators, which are increasingly recognized as fundamental components of the CCFT spectrum. We present new computations of tree-level correlation functions for these operators, demonstrating their appearance in the operator product expansion of gluon primaries. Additionally, we examine the treatment of distributional low-point correlators by introducing a background that breaks bulk translation invariance, yielding correlators that more closely resemble those found in traditional two-dimensional CFTs.

SHOUNAK DE | Curriculum Vitae

Brown University, Box 1843, 182 Hope Street, Providence, RI 02912, USA

shounak_de@brown.edu
orcid.org/0000-0002-2013-3201 google scholar/Shounak De arXiv/Shounak De

EDUCATION

Brown University **Providence, RI, USA**
Doctor of Philosophy (PhD) *2021-Present*
Advisor: Prof. Anastasia Volovich

University of Cambridge **Cambridge, UK**
Master of Advanced Study (MASt) *2019-20*
Part III Mathematical Tripos

Indian Institute of Technology Guwahati **Guwahati, Assam, India**
Master of Science (M.Sc.) *2016-18*
Thesis title "*Geometric Representation of a Fluid*"

St. Xavier's College, University of Calcutta **Kolkata, West Bengal, India**
Bachelor of Science (B.Sc. Hons) *2013-16*
Dissertation title "*Gravity and Thermodynamics At Work in Stellar Clusters*"

PROFESSIONAL APPOINTMENTS

Kavli Institute for Theoretical Physics **Santa Barbara, CA, USA**
KITP Graduate Fellow *January-June 2025*
Mentor: Prof. David Gross

AWARDS & HONORS

Kavli Institute for Theoretical Physics Graduate Fellowship	*2024*
Award of Excellence as a Graduate Teaching Assistant	*2022*
University of Cambridge Lundgren and Pillman Research Fund Awards	*2020*
Oxford and Cambridge Society of India (OCSI) Scholarship	*2019*
Honorary Life Membership to the Oxford and Cambridge Society of India	*2019*
Honorable Mention in the Gravity Research Foundation Awards for Essays on Gravitation	*2019*

PUBLICATIONS (authors listed in alphabetical order except for *)

- **Hidden zeros of the cosmological wavefunction** [2503.23579 [hep-th]]
  under review in JHEP
  S. De, S. Paranjape, A. Pokraka, M. Spradlin, A. Volovich
- **A physical basis for cosmological correlators from cuts** [2411.09695 [hep-th]]
  JHEP **03**, (2025) 040
  S. De, A. Pokraka
- **From Feynman diagrams to the amplituhedron: a gentle review** [2410.11757 [hep-th]]
  contribution to special volume "Positive Geometry" for Le Matematiche
  S. De, D. Pavlov, M. Spradlin, A. Volovich

- **Surfaceology for colored Yukawa theory** [2406.04411 [hep-th]]
  JHEP **09**, (2024) 160
  S. De, A. Pokraka, M. Skowronek, M. Spradlin, A. Volovich

- **Scalar-graviton amplitudes and celestial holography** [2310.00520 [hep-th]]
  JHEP **02**, (2024) 097
  A. Ball, S. De, A. Yelleshpur Srikant, A. Volovich

- **Dual resonant amplitudes from Drinfeld twists** [2309.07214 [hep-th]]
  under review in Phys. Rev. D
  R. Bhardwaj, S. De

- **Cosmology meets cohomology** [2308.03753 [hep-th]]
  JHEP **03**, (2024) 156
  S. De, A. Pokraka

- **On unitarity of the Coon amplitude** [2212.00764 [hep-th]]
  JHEP **08**, (2023) 082
  R. Bhardwaj, S. De, M. Spradlin, A. Volovich

- **Correlators of four light-ray operators in CCFT** [2206.08875 [hep-th]]
  JHEP **10**, (2022) 170
  S. De, Y. Hu, A. Yelleshpur Srikant, A. Volovich

- **Beyond-Newtonian dynamics of a planar circular restricted three-body problem with Kerr-like primaries*** [2011.12533 [gr-qc]]
  MNRAS **501**, 713 (2021)
  S. De, S. Roychowdhury, R. Banerjee

- **Gravity dual of Navier-Stokes equation in a rotating frame through parallel transport**
  Phys. Rev. D **102**, 064003 (2020) [2002.06801 [hep-th]]
  S. Dey, S. De, B. R. Majhi

- **Quantum gravity as an emergent phenomenon** [1903.11066 [gr-qc]]
  Int. J. Mod. Phys. D **28**, 1944003 (2019)
  Honorable Mention in the Gravity Research Foundation 2019 Awards for Essays on Gravitation
  S. De, T. P. Singh, A. Varma

- **Effective metric in fluid-gravity duality through parallel transport: a proposal**
  Phys. Rev. D **99**, 124024 (2019) [1901.05735 [hep-th]]
  S. De, S. Dey, B. R. Majhi

- **Fluid description of gravity on a timelike cut-off surface: beyond Navier-Stokes equation**
  JHEP **01**, (2019) 044 [1810.07017 [hep-th]]
  S. De, B. R. Majhi

INVITED TALKS & PRESENTATIONS

"A Physical Basis for Cosmological Correlators from Cuts" *November 2024*
Combinatorics of Fundamental Physics Workshop, Institute for Advanced Study, USA

"A Physical Basis for Cosmological Correlators from Cuts" *November 2024*
Loop-the-Loop Workshop, Mainz Institute for Theoretical Physics, Mainz, Germany

"A Canonical Basis for Cosmological Correlators" *June 2024*
Amplitudes Gong Show, Institute for Advanced Study, Princeton, USA

"Surfaceology for Colored Yukawa Theory" *June 2024*
Amplitudes Poster Presentation, Institute for Advanced Study, Princeton, USA

"q-CFTs from Quantum Groups" *November 2023*
HEP Theory Journal Club, McGill University, Montréal, Canada

"The Coon Amplitude and its Unitarity" *August 2023*
Poster Presentation, Amplitudes 2023 Conference, CERN, Geneva, Switzerland

"On Unitarity of the Coon Amplitude" *July 2023*
PiTP Student Talks, Institute for Advanced Study, Princeton, USA

"Veneziano Variations" *June 2023*
TASI Student Talks, University of Colorado, Boulder, USA

"Dualities: Introduction and Beyond" *March 2019*
Physics Colloquium, St. Xavier's College, Kolkata, India

SCHOOLS & WORKSHOPS

Combinatorics of Fundamental Physics Workshop *November 2024*
Institute for Advanced Study, Princeton, USA

Amplitudes 2024 Conference & Summer School *June 2024*
Institute for Advanced Study, Princeton, USA

Amplituhedra, Cluster Algebras, and Positive Geometry *May 2024*
Center of Mathematical Sciences and Applications, Harvard University, USA

Simons Collaboration on Celestial Holography Annual Meeting *April 2024*
Flatiron Institute, New York, USA

Mathematical Aspects of $\mathcal{N} = 4$ Super-Yang-Mills Theory *February 2024*
Simons Center for Geometry and Physics, Stony Brook, USA

Amplitudes 2023 Conference & Summer School *August 2023*
CERN, Geneva, Switzerland

Prospects in Theoretical Physics (PiTP) - Understanding Confinement *July 2023*
Institute for Advanced Study, Princeton, USA

TASI 2023 - Aspects of Symmetry *June 2023*
University of Colorado, Boulder, USA

Preface

This thesis is based on the following works:

Hidden Zeros of the Cosmological Wavefunction
S. De, S. Paranjape, A. Pokraka, M. Spradlin, A. Volovich
arXiv:2503.23579 [hep-th]

A Physical Basis for Cosmological Correlators from Cuts
S. De, A. Pokraka
JHEP **03**, (2025) 040 [arXiv:2311.09695 [hep-th]]

Cosmology Meets Cohomology
S. De, A. Pokraka
JHEP **03**, (2024) 156 [arXiv:2308.03753 [hep-th]]

On Unitarity of the Coon Amplitude
R. Bhardwaj, S. De, M. Spradlin, A. Volovich
JHEP **08**, (2023) 082 [arXiv:2212.00764 [hep-th]]

Scalar-graviton Amplitudes and Celestial Holography
A. Ball, S. De, A. Y. Srikant, A. Volovich
JHEP **02**, (2024) 097 [arXiv:2310.00520 [hep-th]]

Correlators of Four Light-ray Operators in CCFT
S. De, Y. Hu, A. Yelleshpur Srikant, A. Volovich
JHEP **10**, (2022) 170 [arXiv:2206.08875 [hep-th]]

Acknowledgments

I owe a special debt of gratitude to my advisor, Professor Anastasia Volovich, for her constant and invaluable support, guidance, and mentorship throughout my PhD journey. She has been the ideal advisor – always available to discuss research problems and generous with her time, encouragement, and insight. She instilled in me the importance of articulating complex research ideas with clarity and simplicity, a lesson that has profoundly shaped the way I approach both thinking about and presenting my research. Over the past four years, Professor Volovich has played a pivotal role in my growth as a PhD student, guiding me through the challenges of research and academia, and helping me evolve into a thoughtful, independent researcher. I will always cherish her confidence in me at several crucial moments during my PhD, which gave me the belief to push forward. Her contributions to my academic career will remain close to my heart.

I am equally grateful to Professor Marcus Spradlin, who has also been very instrumental in my progress during these years. His mentorship, unwavering support, and readiness to engage in physics discussions have been invaluable. I have greatly enjoyed our many collaborations, and Professor Spradlin has, in many ways, acted as a second advisor to me. His influence on my development as a researcher has been immense, and I am deeply thankful for the patience, knowledge, and enthusiasm he has shared.

Along the way, I have been fortunate to receive guidance and encouragement from several mentors who took me under their wing at different stages of my early academic life. I would like to express my sincerest thanks to Dr. Suparna Roychowdhury, Prof. Bibhas Ranjan Majhi, Prof. Tejinder Pal Singh, Prof. Blake Sherwin, Prof. Shiraz Minwalla, Prof. David Simmons-Duffin, and Prof. David Gross. A special thank you goes to my high school physics teacher, Basab Sir, whose infectious enthusiasm for physics and creative problem-solving with I. E. Irodov's textbook first inspired me to pursue physics seriously.

I am also grateful to the faculty of the High Energy Theory Group at Brown, in particular Professor Stephon Alexander and Professor JiJi Fan, for serving on my prelim and PhD defense committees and for their kind words of encouragement, which have meant a great deal to me. I would also like to thank our wonderful department administrators – Jess, Jessie, Linda, and Douglas – for their ever-quick and friendly help with everything from reimbursements to logistics; their efficiency and warmth have made the day-to-day much easier.

I have learned a tremendous amount from the postdoctoral researchers at Brown during my time here. In particular, Adam Ball, Shruti Paranjape, Andrzej Pokraka, and Akshay Yelleshpur Srikant have shaped my PhD experience in meaningful ways. I think I spent more time in their offices than in my own, and I'll always treasure the ideas we puzzled over together and the collaborations we shared. I've also had the pleasure of learning from my peers on the 5th floor – Luke, Lecheng, Yangrui, He-Chen, Marcos, and Rishabh – whose insights and camaraderie have brightened many long days. A special shoutout to my office mates at KITP for making my final semester of graduate school both productive and joyful.

I could not have made it through graduate school and life in Providence without the support of Rishabh and Madhuja. Beyond being a research collaborator, Rishabh has been a best friend and roommate throughout my time at Brown. Sharing this journey with him – through highs, lows, and everyday conversations – has been one of the most rewarding parts of my PhD. Madhuja has been nothing short of a lifeline. I quite literally owe her my life for her care and support during times of illness. She is one of the finest people I have had the privilege of knowing, and quite simply, without her presence, completing this PhD journey would have been immeasurably more difficult.

To my dear friends from growing up – Ankan, Joydipto, Bihan, Snepa, Sounok, Saumyajit, Pichik, Sukhjovan, Daniel, Nour, and Yanky – thank you for teaching me about life, friendship, and occasionally physics. Your encouragement and humour have kept me grounded through it all.

Lastly, and most importantly, I thank my family for their endless love and the sacrifices they have made for me every single day. This thesis is dedicated to the memory of my beloved grandmother, Baguima, and to my incredible parents, Shyamal and Swapna De. It is impossible to adequately express what they have done for me – this journey would not have been possible without them. I am also deeply grateful to my sister Tanima, my brother-in-law Soumik, and my amazing nephews Kiaan and Viaan, whose love and faith in me inspire me to strive for greater heights every day.

Contents

List of Figures

Dedicated to the memory of my beloved grandmother, Baguima. And to my parents, Maa and Baba, for their endless love and sacrifices.

Chapter 1

Introduction

Quantum Field Theory (QFT) provides the foundational framework for describing the fundamental forces of Nature. The Standard Model of particle physics unifies the weak, electromagnetic, and strong interactions into a single theoretical structure. A cornerstone of this framework is the study of scattering processes, which have played a crucial role in testing and refining our understanding of physical laws – from Rutherford's identification of the atomic nucleus to the discovery of the Higgs boson at the Large Hadron Collider. In quantum mechanics, the outcomes of scattering experiments are inherently probabilistic, with their likelihoods determined by the squared absolute values of quantum transition amplitudes, commonly known as *scattering amplitudes*.

Sparked by the remarkable simplicity that emerges from extensive calculations, scattering amplitudes have become central to a modern reformulation of perturbative QFT, driving a wave of breakthroughs in theoretical high-energy physics. Traditional approaches based on fields, Lagrangians and an action principle rely on Feynman diagrams, which are defined only up to field redefinitions and gauge transformations, introducing redundancies that obscure the underlying physics. While such redundancies are necessary in the QFT formulation to account for unphysical degrees of freedom, they also lead to unnecessary computational complexity, masking the deeper structures and inherent simplicity of scattering processes. In contrast, on-shell scattering amplitudes bypass these limitations by remaining independent of field-based redundancies, offering a more direct and efficient framework for computing physical observables while revealing striking hidden mathematical structures.

This unexpected simplicity is perhaps laid bare in the case of $2 \to n$ gluon scattering in Yang-Mills theory at tree-level. While textbooks often discuss the case of $n = 2$ involving four Feynman diagrams, the number grows factorially as the multiplicity n increases

n	2	3	4	5	6	7	8	9
# of diagrams	4	25	220	2,485	34,300	559,405	10,525,900	224,449,225

Strikingly, the computational complexity does not grow with the multiplicity n and there are families of amplitudes for which all-multiplicity expressions are available. The most famous one is the infinite sequence of Maximally Helicity Violating (MHV) gluon amplitudes given by the celebrated Parke-Taylor formula [3] in spinor-helicity variables

$$A_n^{\text{MHV}}(1^+, \ldots, i^-, \ldots, j^+, \ldots, n) = ig^{n-2}\frac{\langle ij\rangle^4}{\langle 12\rangle\langle 23\rangle\ldots\langle n1\rangle} \ , \tag{1.1}$$

whose striking simplicity is not captured by Feynman diagrams. Moreover, this simplicity of the above Parke-Taylor formula becomes manifest via the BCFW recursion relation [4] for Yang-Mills tree level amplitudes, which relates generic n-point amplitudes to its lower point counterparts

$$A_n = \sum_I \hat{A}_L(-\hat{P}_I, z_I)\frac{1}{P_I^2}\hat{A}_R(\hat{P}_I, z_I) \ , \tag{1.2}$$

where the sum is over all possible factorization channels I. In fact, it has been proven that *any* tree-level scattering amplitude satisfy either a BCFW recursion relation or a generalization [5] of the same.[1] For supersymmetric extensions of Yang-Mills theory like $\mathcal{N} = 4$ super-Yang-Mills (sYM) theory, such recursion relations are also valid for constructing loop integrands at *any* loop order [6].

While understanding the analytic structure of amplitudes and the symmetries that leave them invariant has proven invaluable, the past decade has uncovered even deeper mathematical structures, revealing that scattering amplitudes can be expressed purely in terms of geometric and combinatorial building blocks. It turns out that amplitudes in certain theories naturally "live" in more abstract spaces in which they can be interpreted as volumes of geometric objects known as "polytopes".[2] This perspective has led to the formulation of the amplituhedron [7] for planar $\mathcal{N} = 4$ sYM amplitudes[3], ABHY associahedron for the bi-adjoint ϕ^3 scalar theory [9], the Stokes polytopes for planar ϕ^4 theory [10], the accordiohedra for planar ϕ^k theories [11, 12]. These *positive geometries* are defined independently of physical concepts, yet they inherently encode fundamental properties of flat-space scattering. This perspective suggests that key principles such as *unitarity*, *causality*, and *locality* emerge naturally from these mathematical frameworks rather than being imposed as fundamental constraints (see [13, 14] and references therein). Such developments have deepened our understanding of the fundamental properties of QFTs by uncovering hidden mathematical structures in scattering amplitudes and leveraging these structures to streamline practical calculations for collider physics at the LHC.

This transformative progress in the scattering amplitudes program raises intriguing questions about the applicability of these techniques to computing observables and understanding its analytic structure in other domains. This thesis, therefore, is driven by the following key questions:

- *Can such modern on-shell techniques that often aid loop-level computations relevant to collider physics be imported to the computation of observables in cosmological spacetimes?*

  In chapters 2-4, we will attempt to answer this question by exploring intriguing connections between positive geometries, on-shell methods, and bootstrap principles studied within the

[1] This is true even for tree-level amplitudes in effective field theories (EFTs).
[2] These are higher-dimensional generalizations of polygons.
[3] Please refer to [8] for an introductory review on the amplituhedron.

modern scattering amplitudes program to the Bunch-Davies wavefunction in toy models of FRW cosmologies.

- *The analytic $\mathcal{S}$-matrix program of the 1960s sought to non-perturbatively bootstrap scattering amplitudes using fundamental principles of locality, causality, and crossing symmetry, ultimately leading to dual-resonant models such as string theory. In the modern revival of this decades-old effort, what constraints does unitarity impose on candidate UV-complete amplitudes?*

  In chapter 5, we will investigate the constraints of partial wave unitarity on dual resonant amplitudes from the viewpoint of the modern $\mathcal{S}$-matrix bootstrap, focusing on a particular dual resonant model, the Coon amplitude.

- *Can the asymptotic symmetries on the celestial sphere provide new insights into the analytic structure of the flat-space $\mathcal{S}$-matrix? Conversely, can our understanding of traditional conformal field theories help refine the celestial dictionary and clarify the properties of the dual celestial conformal field theory?*

  In Chapters 6 and 7, we attempt to answer such questions by investigating key aspects of the dual celestial conformal field theory (CCFT), including its operator structure, correlation functions, and symmetries.

In the remainder of the introduction, we further explore the three key questions outlined above, providing a more detailed discussion of the relevant concepts that play a crucial role in shaping the developments presented in the subsequent chapters of this thesis.

Cosmological amplitudes: the wavefunction approach

Our understanding of the analytic structure of observables away from asymptotically flat-spacetimes remains relatively underdeveloped. In particular, gaining deeper insights into quantum mechanical observables in expanding spacetimes is crucial, as it provides a window into physics at energy scales far beyond those accessible in earth-based accelerators. The Hubble parameter during the early Universe could reach values as high as 10^{14} GeV – exceeding LHC energies by 10 to 11 orders of magnitude – offering a unique arena to probe fundamental high-energy physics. An important clue in this quest lies in the large-scale correlations observed in the structure of the Universe, which are not randomly distributed but instead serve as a fossil imprint of the very early Universe. By measuring these correlations, we hope to uncover insights into how cosmological perturbations formed and evolved, offering a valuable probe of the universe's high-energy past. The correlations in late-time cosmological observables – like the distribution of the large-scale structure (LSS) or the anisotropies of the cosmic microwave background (CMB) – can be traced back in time to primordial correlations on the "reheating surface" (marking the initial surface of the hot Big Bang universe or the final surface at the end of inflation), imprinted in these correlations is the physics of the inflationary era (see figure 1.1). The main observable predictions of inflation are spatial correlation functions and

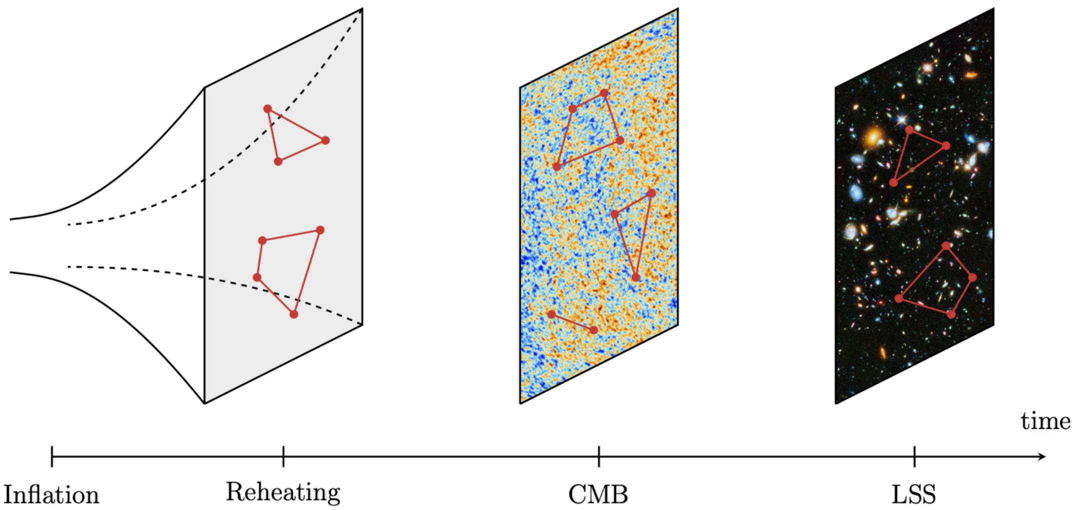

Figure 1.1: Correlations in the large-scale structure (LSS) or in the cosmic microwave background (CMB) can be traced back to correlations of quantum fields at the end of inflation, which are dubbed as inflationary correlators.

a major portion of this thesis will be devoted to understand such correlations via the *wavefunction approach*.

Cosmological correlations can also be computed by means of the so-called "wavefunction of the Universe." The wavefunction is a slightly more primitive object than cosmological correlators themselves – the relation between them is roughly the same as that between the $\mathcal{S}$-matrix and scattering cross-sections. Formally, this is computed as a path integral by integrating over all bulk field configurations $\phi(\vec{x},\eta)$ with non-vanishing Dirichlet boundary condition in the future $\phi(\vec{x},\eta = 0) = \Phi(\vec{x})$. It is standard to work in momentum space where the wavefunction can be expanded as

$$\Psi[\Phi] = \int_{\phi(-\infty(1-i\epsilon))}^{\phi(0)=\Phi} \mathcal{D}\phi\, e^{iS[\phi]} \equiv \exp\left[i\sum_n \frac{1}{n!}\int \prod_i \mathrm{d}^d\vec{k}_i\, \Phi(\vec{k}_i)\, \tilde{\psi}_n(\{\vec{k}_i\})\right], \tag{1.3}$$

and the standard $i\epsilon$ prescription selects the adiabatic/Bunch-Davies/Hartle-Hawking vacuum at the early-time boundary $\eta \to -\infty$. The kernels $\tilde{\psi}_n$ are called *wavefunction coefficients* and $\{\vec{k}_i\}$ denotes the set of all *spatial* momentum. Due to *spatial* translation invariance on the future boundary, the wavefunction coefficients contain an overall momentum-conserving δ-function. It is useful to extract this δ-function and compute the "stripped" wavefunction coefficients ψ_n:

$$\tilde{\psi}_n(\{\vec{k}_i\}) = \delta^{(d)}\left(\sum_{i=1}^{n} \vec{k}^{(i)}\right) \psi_n(\{\vec{k}_i\}) . \tag{1.4}$$

Our main objective is the computation of these stripped wavefunction coefficients.

Traditionally, the wavefunction coefficients ψ_n are obtained perturbatively, using Feynman diagrammatics, which we review here. We approximate the path integral (1.3) by its saddle point $\Psi[\Phi] \approx \exp\left(iS[\Phi_{\rm cl}]\right)$ where $\Phi_{\rm cl}$ is the boundary profile corresponding to the classical solution to the equations of motion $\phi_{\rm cl}$. To derive the Feynman rules, we write the classical solution as

$$\phi_{\rm cl}(\vec{k},\eta) = \mathcal{K}(E,\eta)\Phi(\vec{k}) + \int {\rm d}\eta' \mathcal{G}(E;\eta,\eta') \frac{\delta S_{\rm int}}{\delta\phi(\vec{k},\eta')} \ . \tag{1.5}$$

Substituting the above solution into the action, one can verify that the path integral evaluates to the expression in (1.3) by taking functional derivatives of the path integral with respect to the boundary value $\Phi(\vec{k})$ (which acts like a source term). To ensure that the solution (1.5) satisfies the correct Dirichlet boundary conditions, one needs to appropriately solve for the two distinct Green's functions, the bulk-to-boundary propagator $\mathcal{K}(E_v,\eta_v)$ associated with a vertex v and the bulk-to-bulk propagator $\mathcal{G}(E_e,\eta_v,\eta_v')$ associated with an edge e connecting a vertex at time η_v to another one at time η_v'. In a flat-space theory of a single scalar field with polynomial self-interactions

$$S[\phi] = \int {\rm d}^d x \, {\rm d}\eta \left[-\frac{1}{2}(\partial\phi)^2 - \sum_{k\geq 3} \frac{\lambda_k}{k!}\phi^k \right] \ . \tag{1.6}$$

the propagators are given by the expressions

$$\mathcal{K}(E_v,\eta_v) = e^{iE_v\eta_v} \ , \tag{1.7}$$

$$\mathcal{G}(E_e,\eta_v,\eta_v') = \frac{1}{2E_e}\left(e^{-iE_e(\eta_v-\eta_v')}\theta\left(\eta_v-\eta_v'\right) + e^{-iE_e(\eta_v'-\eta_v)}\theta\left(\eta_v'-\eta_v\right) - e^{iE_e(\eta_v+\eta_v')} \right) \ , \tag{1.8}$$

where $E_v = \sum_j |\vec{k}_j|$ denotes the sum of the energies of j external lines connected to the vertex v, and $E_e = |\vec{k}_e|$ is the energy of an internal line. The bulk-to-boundary propagator, $\mathcal{K}(E,\eta)$, solves the linearized, homogeneous EOM, oscillates with positive frequency in the far past, and approaches unity at the late time boundary as $\eta \to 0$. The bulk-to-bulk propagator, $\mathcal{G}(E,\eta,\eta')$, solves the inhomogeneous wave equation $\sqrt{-g}(\Box - m^2)\mathcal{G}(E,\eta,\eta') = i\delta(\eta-\eta')$, subject to the boundary condition that it vanishes identically when either of its time arguments approach zero. The combined boundary conditions on the Green's functions guarantee that the path integral in (1.3) as well as the classical solution (1.5) satisfy the correct Dirichlet boundary conditions. With these preliminaries, we can now state the Feynman rules for the computation of the flat-space wavefunction coefficients $\psi_{n,\rm flat}$:

- Draw all graphs with a fixed number of lines, n, ending on the boundary.
- Assign a vertex factor, iV, to each bulk interaction.
- Assign a bulk-to-bulk propagator (1.8), $\mathcal{G}$, to each internal line and a bulk-to-boundary propagator (1.7), $\mathcal{K}$, to each external line.
- Integrate over all the time insertions of all bulk vertices.

The vertex factors are obtained from the action following the same procedure as in S-matrix Feynman rules, with the key distinction that only spatial variables are treated in Fourier space. Consequently, each vertex retains an explicit time dependence, requiring integration over time. A significant challenge in computing wavefunction coefficients arises from these time integrals, highlighting the need for alternative computational techniques explored in this thesis.[4]

In particular, when the couplings in the flat-space action have a particular time dependence

$$\lambda_k(\eta) \equiv \lambda_k[a(\eta)]^{(2-k)(d-1)/2+2} \ , \tag{1.9}$$

we can do a Weyl rescaling to obtain the action of conformally coupled scalars in an FRW cosmology with scale factor $a(\eta)$

$$\mathcal{S} = \int \mathrm{d}^d x \, \mathrm{d}\eta \sqrt{-g} \left[-\frac{1}{2} g^{\mu\nu} \partial_\mu \phi \partial_\nu \phi - \frac{1}{2} \xi R \phi^2 - \sum_{k \geq 3} \frac{\lambda_k}{k!} \phi^k \right] \ . \tag{1.10}$$

As a consequence, starting from the flat-space wavefunction coefficients $\psi_{n,\text{flat}}$ for a theory (1.6) one can obtain its counterparts in a generic FRW cosmology (parametrized by ε) via a simple integral transform

$$\psi_{n,\text{FRW}}(X_v, Y_e) = \int_0^\infty \prod_{v \in \mathcal{V}} \mathrm{d}x_v \, x_v^\varepsilon \, \psi_{n,\text{flat}}(x_v + X_v, Y_e) \ . \tag{1.11}$$

Such *twisted* integrals arise in the computation of one-loop scattering amplitudes in dimensional regularization (in that context, $2\varepsilon = 4 - D$ is the deviation from the canonical spacetime dimension). This connection allows us to import tools from the treatment of loop amplitudes to the study of tree-level FRW correlators. In particular, an important insight is that loop amplitudes can be written in terms of a set of master integrals which span a finite-dimensional vector space. The finiteness of this vector space guarantees that the master integrals themselves satisfy interesting differential equations (DEQ) with respect to the kinematic data, which then provides a powerful way to compute the original Feynman integrals (see for nice reviews). In chapters 2 and 3, we will see how the DEQ method can be translated to the cosmological context.

As was highlighted earlier in the context of flat-space scattering amplitudes, there also exists purely combinatorial-geometrical formulation of the perturbative wavefunction coefficients. As we will soon seen in the course of the first three chapters, positive geometries such as the *cosmological polytope* and the *graph associahedron* encode the wavefunction as its volume form. Such geometric formulations allow us to sharpen questions about the relation between cosmology and flat-space physics, providing a concrete framework that makes precise the sense in which Lorentz invariance as well as flat-space unitarity and causality emerge. Moreover, in chapter 4, we will exploit such polytopal realizations to unravel the existence of hidden zeros of the cosmological wavefunction and demonstrate a novel factorization-type behavior termed splitting associated to near-zero kinematical configurations.

While recent years have seen techniques from scattering amplitudes applied to the evaluation of cosmological correlation functions, much remains to be explored. A key future direction is to derive a compact "Parke-Taylor-like" formula for spinning four-point functions in de Sitter space

[4]We note that while one must integrate over the loop momenta as part of the Feynman rules, our focus in the remainder of this thesis will be on *loop integrands*.

using newly developed twistor space kinematic variables, thereby paving the way for cosmological "BCFW-like" recursion relations. These advances could dramatically streamline computations and provide a unifying framework for organizing cosmological observables, much like the revolution in flat-space amplitudes nearly three decades ago.

String amplitudes and the $\mathcal{S}$-matrix bootstrap program

A cornerstone of the modern $\mathcal{S}$-matrix program is the quest to uncover fundamental constraints on scattering amplitudes from first principles such as *locality*, *causality*, and *unitarity*. In this context, the Veneziano amplitude – the first known example of a meromorphic four-point amplitude with polynomial residues and exact crossing symmetry – has played a pivotal role in shaping our understanding of string scattering. Introduced in 1968 [15], the Veneziano amplitude takes the form

$$\mathcal{A}^V(s,t) = -(s+t)^{\alpha_0-1}\frac{\Gamma(-\alpha_0-s)\Gamma(-\alpha_0-t)}{\Gamma(-2\alpha_0-s-t)}, \tag{1.12}$$

where the parameter α_0 depends on the specific string theory under consideration. Its worldsheet interpretation as a dual resonance model was subsequently established[16, 17, 18].

Given its simple pole structure, the Veneziano amplitude admits an alternative infinite product representation

$$\mathcal{A}^V(s,t) = \frac{1}{st}\prod_{n=1}^{\infty}\frac{1-\frac{s+t}{n}}{\left(1-\frac{s}{n}\right)\left(1-\frac{t}{n}\right)}\ , \tag{1.13}$$

which makes manifest its underlying algebraic structure when $\alpha_0 = 0$. This discovery motivated a broader search for alternative amplitudes that retain key analytic properties while potentially relaxing others.

Shortly thereafter, Coon proposed a one-parameter deformation of the Veneziano amplitude by introducing logarithmic Regge trajectories [19], leading to what is now known as the Coon amplitude

$$\mathcal{A}^C(s,t) = (q-1)\exp\left(\frac{\log\sigma\log\tau}{\log q}\right)\prod_{n=0}^{\infty}\frac{\left(1-\frac{q^n}{\sigma\tau}\right)(1-q^{n+1})}{\left(1-\frac{q^n}{\sigma}\right)\left(1-\frac{q^n}{\tau}\right)}, \tag{1.14}$$

where the deformed kinematic variables are given by

$$\sigma = 1-(1-q)(\alpha_0+s), \qquad \tau = 1-(1-q)(\alpha_0+t). \tag{1.15}$$

This amplitude smoothly interpolates between the Veneziano amplitude as $q \to 1$ and a sum of contact interactions in the limit $q \to 0$

$$\mathcal{A}^C(s,t) \xrightarrow{q\to 0} \frac{1}{s+\alpha_0} + \frac{1}{t+\alpha_0} + 1. \tag{1.16}$$

A crucial requirement for dual resonant amplitudes to have physical relevance is that it must be *unitary*. An initial study of the unitarity of the Coon amplitude [20] suggested the absence of ghosts, but a more refined numerical analysis [2] revealed a boundary in (q, D) space separating unitary and non-unitary regions, with an analytically determined critical value $q = q_\infty(-\alpha_0)$. However, a full analytic understanding of its unitarity structure remains an open question. An analytic understanding of this unitarity constraint remains an outstanding problem. In chapter 5, we study the unitarity of the Coon amplitude through the positivity of its partial wave expansion coefficients, leveraging techniques recently applied to the Veneziano amplitude [1]. Similar analyses of partial wave unitarity have been crucial in understanding the viability of other dual resonant amplitudes, including those with modified Regge trajectories and higher-spin generalizations [21, 22]. By extending these techniques to the Coon amplitude, we take steps toward clarifying its physical interpretation and assessing whether it can be embedded into a broader framework of consistent dual resonant models.

The analytic structure of celestial amplitudes

Celestial holography proposes a duality between gravitational scattering in $(d+2)$-dimensional asymptotically flat spacetimes and a conformal field theory (CFT) defined on the celestial sphere $\mathcal{CS}^d$. This duality is rooted in the observation that the Lorentz group in Minkowski spacetime, $\mathrm{SO}(1,d+1)$, is isomorphic to the conformal group $\mathrm{SL}(d,\mathbb{C})$ on the celestial sphere, modulo a $\mathbb{Z}_2$ quotient

$$\mathrm{SO}(1,d+1) \cong \mathrm{SL}(d,\mathbb{C})/\mathbb{Z}_2 \ , \tag{1.17}$$

which provides the geometric foundation for mapping $\mathcal{S}$-matrix elements in Minkowski spacetime to conformal correlators on the celestial sphere.

The directions of massless scattering particles in the bulk are parametrized by coordinates on the celestial sphere, with their momenta embedded as null vectors $q^\mu(z,\bar{z})$ in the compactified light cone

$$q^\mu(z,\bar{z}) = (1+z\bar{z}, z+\bar{z}, i(\bar{z}-z), 1-z\bar{z}) \ , \tag{1.18}$$

where z and $\bar{z}$ are stereographic coordinates. The energy ω of the scattering particles scales this null vector, yielding $p^\mu = \omega q^\mu(z,\bar{z})$. This embedding establishes a direct link between the momentum-space description in the bulk and the conformal coordinates of the celestial sphere.

Transitioning to the celestial basis involves a *Mellin transform* of the on-shell momentum eigenstates. The *celestial amplitudes*, $\mathcal{A}^{h_1,\ldots,h_n}(\{z_i,\bar{z}_i;\Delta_i\})$, are constructed by applying the Mellin transform to the momentum-space $\mathcal{S}$-matrix elements $A_n^{h_1,\ldots,h_n}(\{\omega_i,z_i,\bar{z}_i\})$ [23, 24, 25]

$$\begin{aligned}\mathcal{A}_n^{h_1,\ldots,h_n}(\{z_i,\bar{z}_i;\Delta_i\}) &\equiv \langle \mathcal{O}_{\Delta_1,h_1}(z_1,\bar{z}_1)\ldots\mathcal{O}_{\Delta_n,h_n}(z_n,\bar{z}_n)\rangle \\ &= \int_{\mathbb{R}^n_{\geq 0}} \prod_{i=1}^n \mathrm{d}\omega_i\, \omega_i^{\Delta_i-1} A_n^{h_1,\ldots,h_n}(\{\omega_i,z_i,\bar{z}_i\}) \ ,\end{aligned} \tag{1.19}$$

where Δ_i is the conformal dimension, and h_i denotes the i^{th} particle's helicity. This transformation recasts the scattering amplitudes into conformal correlators on the celestial sphere, with the primary operators $\mathcal{O}_{\Delta,h}(z,\bar{z})$ defined through this process.

A key challenge in celestial holography is understanding how bulk translational symmetry emerges. Celestial CFT (CCFT) correlators must obey not only conformal invariance but also translation invariance, which acts as an "external symmetry" and forces low-point correlators to be distributional

[26]. At higher points, correlators are non-distributional but remain constrained, preventing arbitrary placement of operators on the celestial sphere [27]. These properties make CCFT correlators distinct from those in conventional 2D CFTs and complicate the search for a top-down CCFT construction.

One approach to circumventing this difficulty is to introduce nontrivial backgrounds in the bulk [28, 29, 30, 31, 32, 33, 34, 35, 36, 37, 38, 39]. Such backgrounds must preserve Lorentz invariance—thus maintaining the 2D conformal symmetry of CCFT—while remaining asymptotically flat. The celestial counterparts of scattering amplitudes on these backgrounds often exhibit desirable features: they are unconstrained by translation invariance (as the background acts as a source/sink of momentum), they resemble traditional CFT correlators, and they have better convergence properties [28, 33, 40]. These characteristics suggest that the background-free CCFT and its deformations might be closely related, motivating further study of these correlators to establish an independent CCFT definition [31, 41].

To that end, we explore gravity amplitudes in 4D Minkowski and Klein spacetimes [42] in chapter 6, generalizing results from [40] where gluon amplitudes were studied on a massive scalar background. Unlike gluons, a non-dynamical scalar background breaks diffeomorphism invariance in gravity, necessitating scalar exchange in amplitudes involving gravitons. Nevertheless, the corresponding celestial correlators retain key features of CCFT correlators while avoiding translation invariance constraints. This motivates further study of how backgrounds influence CCFT structure and operator algebras, paving the way for a more complete celestial holographic duality.

Another important question in the field of celestial holography has been to understand the constituents of the CCFT spectrum. Light-ray operators play a central role in CCFT, particularly in identifying a suitable operator basis [43, 44]. Their correlation functions are light-ray transforms of ordinary CCFT correlators, and they provide a natural framework for understanding symmetries and operator product expansions (OPEs) in CCFT. It was shown in [45] that certain three-point correlators involving light-ray operators take the form of standard CFT three-point functions, in contrast to the distributional nature of standard CCFT correlators [24]. Moreover, the light transform is closely related to Witten's half Fourier transform, with conformal primary twistor eigenstates expressible as linear combinations of light-transformed boost eigenstates. The light transform also elucidates CCFT symmetries; in gravity, the single-helicity sector exhibits an enhanced $w_{1+\infty}$ symmetry, identified in [46] as the light transform of the soft current mode.

Four-point correlators involving one and two gluon light-ray operators have been computed [47, 48], revealing their non-distributional nature and their role in the OPE of CCFT primaries. These contributions are not visible from the collinear limits of four-point celestial amplitudes. Extending these results, we will investigate the four-gluon light-ray operator correlators in chapter 7, demonstrating that they can be expressed in terms of Fox H-functions and generalized I-functions.

Chapter 2

Cosmology Meets Cohomology

This chapter is based on the work [49].

Over the past decade, an increasing number of concepts from the theory of hypergoemetric functions and more broadly algebraic geometry have entered modern methods for studying scattering amplitudes. In particular, the framework of twisted cohomology (originally formulated to study the linear relations among hypergoemetric functions) has been used to construct CHY amplitudes [50, 51], provide a geometric framework for understanding KLT relations in string amplitudes [52, 53, 54, 55], the double copy [56] and more.

In the Feynman integral community, twisted intersection theory [57, 58, 59, 60, 61, 62, 63, 64] provides an algebraic alternative to integral reduction[1] via integration-by-parts (IBP) identities [65, 66, 67]. While these techniques are still being optimized for applications to physics, they have the potential to circumvent solving large linear systems of IBPs thereby streamlining one of the most expensive steps in the pipeline for multi-loop phenomenological calculations.

Recently, the procedure for calculating intersection numbers of Feynman integrals has been streamlined by using *relative* twisted cohomology [68, 69]. By working with relative twisted cohomology, one can set the regulator in previous works to zero at the start of the calculation. As a consequence, many intermediate quantities vanish or simplify, streamlining the overall algorithm.

The last decade has also seen the discovery of rich geometrical structures in the study of flat-space scattering amplitudes which provide answers to elegant questions posed purely in the kinematic space. While such insights have transformed our understanding of the flat-space S-matrix, the situation for cosmological correlators is still underdeveloped. The lack of such methods for cosmology and the complexity of even tree-level results[2] means that the repository of theoretical data is significantly smaller. The problem is further complicated by the fact that inflationary correlators live on the late-time boundary of de Sitter, which is space-like. The understanding of the holographic

[1] Integral reduction is the process of decomposing an arbitrary integral into a linear combination of basis (also called master) integrals that only need to be computed once.

[2] One already encounters branch cuts at the level of trees in cosmological correlators whereas their flat-space counterparts are rational functions in the kinematic invariants.

dual to theories with space-like boundaries is still in its infancy, while the boundary description for anti-de Sitter space is well established due to the time-like nature of its boundary. Having said that, the cosmological polytope and bootstrap programs have taken important steps towards a boundary description of inflationary correlators.

While de Sitter models the accelerated expansion of the early Universe, the Friedmann-Robertson-Walker (FRW)[3] metric describes a homogeneous, isotropic, expanding (or contracting) Universe. The FRW spacetime is often considered to be the standard model of cosmology post inflation. Field theoretic correlation functions in FRW cosmologies represent quantum fluctuations, which in the early Universe are thought to have sourced the observed distribution of matter. Comparing these predictions to current and future cosmological datasets will help constrain new physics beyond the Standard Model.

Unlike the de Sitter geometry (which has provided a rich playground for studying inflationary correlators in the literature so far), FRW Universes are not maximally symmetric spacetimes and have a reduced isometry group. This reduces the applicability of the cosmological bootstrap program to derive differential equations for correlators beyond de Sitter space. However, it turns out that correlators in FRW cosmologies (the main focus of this work[4]) furnish some of the simplest examples of relative twisted cohomology.[5] Thus, they provide fertile testing ground for developing our understanding of relative twisted cohomologies, which in turn will deepen our understanding of the underlying physics.

While the standard tool for computing cosmological correlation functions is perturbation theory, the past decade has seen novel computational methods with interesting and fruitful connections to scattering amplitudes (e.g., symbology [70]) and mathematics (the combinatorial description in terms of the cosmological polytope [71, 72, 73, 74]). Many of these methods manifest the simplicity of the final answer that is hidden at intermediate steps in perturbation theory. In particular, the singularity structure of these correlators is particularly evident in the polytopal picture and encodes principles of unitary (by cutting rules) as well as causality (Steinmann relations).

Our main goal is two fold. First, we aim to provide efficient methods for computing the differential equations of FRW wavefunction coefficients. Deriving differential equations for cosmological correlators was first considered in [75, 76]. We also hope that by formally constructing the cohomology associated to the integrals appearing in the FRW wavefunction coefficients and elucidating their mathematical structure will lead to a deeper physical understanding of these objects. Secondly, our techniques are quite general and are applicable to many integrals seen in both physics and mathematics. Thus, we expect this work to be useful beyond the current setting of cosmological correlators.

While primarily aimed at physicists, we think that much of this work will interest mathematicians.

[3]While the most commonly used term is the FRW metric, it is also sometimes called the FLRW metric after Friedmann, Lemaitre, Robertson and Walker.

[4]We will consider FRW cosmologies with a future spacelike boundary where our boundary observables live.

[5]Mathematically, FRW correlators are integrals associated to hyperplane arrangements where the coordinate hyperplanes are twisted and all other divisors are left untwisted.

While many of our claims have been well tested, this chapter lacks formal proofs and it would be interesting to understand these claims more formally. As far as the authors know, [77] is the only paper discussing relative twisted cohomology in the mathematics literature.

The chapter is organized as follows. In section 2.1, we set up the toy model of conformally coupled scalars in a general FRW background studied in this work and explain how to uplift flat-space wavefunction coefficients to their FRW counterparts. In section 2.2, we study the integral representation of the two-site/four-point FRW integral in detail. To evaluate this integral, we derive the differential equation satisfied by a basis of integrals for the corresponding integral family. We obtain these differential equations using three different perspectives: twisted cohomology and standard IBPs in section 2.2.1, the dual (relative) twisted cohomology and dual IBPs in section 2.2.2, and intersection numbers in section 2.2.3. The dual perspective (section 2.2.2) yields computational advantages as well as novel geometric understanding and is central to this work. In section 2.2.4, we explicitly integrate these differential equations to obtain the first correction to the de Sitter two-site/four-point function. In section 2.3, we provide two more worked examples: the one-loop two-site/two-point and the tree-level three-site/five-point FRW integrals. In this section, we illustrate how to use the techniques developed in section 2.2 on more complicated examples. We conclude in section 2.4 with a discussion of our results and directions for future work.

2.1 Cosmological correlators and the Wavefunction of the Universe

We consider the model of a conformally-coupled scalar field in a general FRW cosmology with non-conformal polynomial interactions, studied extensively in [71, 72, 70, 78]. The action for such a theory in a $(d+1)$-dimensional spacetime is

$$\mathcal{S} = \int \mathrm{d}^d x \, \mathrm{d}\eta \sqrt{-g} \left[-\frac{1}{2} g^{\mu\nu} \partial_\mu \phi \partial_\nu \phi - \frac{1}{2} \xi R \phi^2 - \sum_{k \geq 3} \frac{\lambda_k}{k!} \phi^k \right] , \tag{2.1}$$

with the FRW metric and the constant ξ defined as

$$\mathrm{d}s^2 \equiv g_{\mu\nu} \mathrm{d}x^\mu \mathrm{d}x^\nu = a^2(\eta) \left[-\mathrm{d}\eta^2 + \mathrm{d}x_i \mathrm{d}x^i \right] , \quad \xi = \frac{d-1}{4d} . \tag{2.2}$$

The FRW metric above has been written in comoving coordinates with conformal time $\eta \in (-\infty, 0]$ and the index $i = 1, \ldots, d$ runs over the spatial dimensions. $a(\eta)$ denotes the scale factor and the choice of its representation in various stages of the Universe's evolution will be crucial for the class of integrals dealt with in our chapter. Importantly, the choice of ξ sets the scalar to be conformally-coupled thereby making the action $\mathcal{S}$ conformally equivalent to the following flat-space action

$$S[\phi] = \int \mathrm{d}^d x \, \mathrm{d}\eta \left[-\frac{1}{2} (\partial \phi)^2 - \sum_{k \geq 3} \frac{\lambda_k(\eta)}{k!} \phi^k \right] . \tag{2.3}$$

More precisely, the conformal transformation

$$g_{\mu\nu} \to a^2(\eta) g_{\mu\nu} \ , \quad \phi \to a^{-\Delta}(\eta)\phi \ , \quad \Delta = \frac{d-1}{2} \ , \tag{2.4}$$

allows one to rewrite the original action $\mathcal{S}$ (2.1) as the action of a massless scalar field in $(d+1)$-dimensional flat-space (2.3) with time-dependent couplings given by

$$\lambda_k(\eta) \equiv \lambda_k [a(\eta)]^{(2-k)\Delta+2} \ . \tag{2.5}$$

It is worth stressing that the conformal equivalence between the original action $\mathcal{S}$ (2.1) and the flat-space action $S[\phi]$ (2.3) allows us to do meaningful computations in a general FRW cosmology (described by the scale factor $a(\eta)$) simply by doing flat-space perturbation theory (albeit with time-dependent couplings given by (2.5)), as we shall see below.

Of central importance, is the wavefunction of the universe $\Psi[\Phi]$. Formally, this is computed as a path integral by integrating over all bulk field configurations $\phi(\vec{x}, \eta)$ with non-vanishing Dirichlet boundary condition in the future $\phi(\vec{x}, \eta = 0) = \Phi(\vec{x})$. It is standard to work in momentum space where the wavefunction can be expanded as

$$\Psi[\Phi] = \int_{\phi(-\infty(1-i\epsilon))}^{\phi(0)=\Phi} \mathcal{D}\phi \, e^{iS[\phi]} \equiv \exp\left[i \sum_n \frac{1}{n!} \int \prod_i \mathrm{d}^d \vec{k}_i \, \Phi(\vec{k}_i) \, \tilde{\psi}_n(\{\vec{k}_i\}) \right] \ , \tag{2.6}$$

and the standard $i\epsilon$ prescription selects the adiabatic/Bunch-Davies/Hartle-Hawking vacuum at the early-time boundary $\eta \to -\infty$. The kernels $\tilde{\psi}_n$ are called *wavefunction coefficients* and $\{\vec{k}_i\}$ denotes the set of all *spatial* momentum. Due to *spatial* translation invariance on the future boundary, the wavefunction coefficients contain an overall momentum-conserving δ-function. It is useful to extract this δ-function and compute the "stripped" wavefunction coefficients ψ_n:

$$\tilde{\psi}_n(\{\vec{k}_i\}) = \delta^{(d)}\left(\sum_{i=1}^n \vec{k}^{(i)} \right) \psi_n(\{\vec{k}_i\}) \ . \tag{2.7}$$

Our main objective is the computation of these stripped wavefunction coefficients.

Traditionally, the wavefunction coefficients ψ_n are obtained perturbatively, using Feynman diagrammatics, which we review here. We approximate the path integral (2.6) by its saddle point $\Psi[\Phi] \approx \exp\left(iS[\Phi_{\rm cl}]\right)$ where $\Phi_{\rm cl}$ is the boundary profile corresponding to the classical solution to the equations of motion $\phi_{\rm cl}$. To derive the Feynman rules, we write the classical solution as

$$\phi_{\rm cl}(\vec{k}, \eta) = \mathcal{K}(E, \eta)\Phi(\vec{k}) + \int \mathrm{d}\eta' \mathcal{G}(E; \eta, \eta') \frac{\delta S_{\rm int}}{\delta \phi(\vec{k}, \eta')} \ . \tag{2.8}$$

Substituting the above solution into the action, one can verify that the path integral evaluates to the expression in (2.6) by taking functional derivatives of the path integral with respect to the boundary value $\Phi(\vec{k})$ (which acts like a source term). To ensure that the solution (2.8) satisfies the correct Dirichlet boundary conditions, one needs to appropriately solve for the two distinct Green's functions, the bulk-to-boundary propagator $\mathcal{K}(E_v, \eta_v)$ associated with a vertex v and the bulk-to-bulk propagator $\mathcal{G}(E_e, \eta_v, \eta_v')$ associated with an edge e connecting a vertex at time η_v to another one at time η_v'. Explicitly, they are given by the expressions

$$\mathcal{K}(E_v,\eta_v) = e^{iE_v\eta_v} \ , \tag{2.9}$$

$$\mathcal{G}(E_e,\eta_v,\eta_v') = \frac{1}{2E_e}\left(e^{-iE_e(\eta_v-\eta_v')}\theta\left(\eta_v-\eta_v'\right) + e^{-iE_e(\eta_v'-\eta_v)}\theta\left(\eta_v'-\eta_v\right) - e^{iE_e(\eta_v+\eta_v')}\right) \ , \tag{2.10}$$

where $E_v = \sum_j |\vec{k}_j|$ denotes the sum of the energies of j external lines connected to the vertex v, and $E_e = |\vec{k}_e|$ is the energy of an internal line. The bulk-to-boundary propagator, $\mathcal{K}(E,\eta)$, solves the linearized, homogeneous EOM, oscillates with positive frequency in the far past, and approaches unity at the late time boundary as $\eta \to 0$. The bulk-to-bulk propagator, $\mathcal{G}(E,\eta,\eta')$, solves the inhomogeneous wave equation $\sqrt{-g}(\Box - m^2)\mathcal{G}(E,\eta,\eta') = i\delta(\eta-\eta')$, subject to the boundary condition that it vanishes identically when either of its time arguments approach zero. The combined boundary conditions on the Green's functions guarantee that the path integral in (2.6) as well as the classical solution (2.8) satisfy the correct Dirichlet boundary conditions. The problem of computing the wavefunction coefficients ψ_n is now thus reduced to an exercise in perturbative diagrammatic expansion using Feynman rules for the fluctuations of the theory at hand. We note that to compute these wavefunction contributions, it suffices to implement flat-space perturbation theory which thereby surpasses the need to introduce complicated Green's functions for a general FRW spacetime. As we shall see in the subsequent sections, for various FRW cosmologies this is facilitated by an operation involving integration over the external energies that accounts for the time-dependent couplings (2.5) of the theory.

2.1.1 FRW cosmologies

In this work, we study the analytic structure of integrals associated to the wavefunction coefficients in a general FRW Universe, going beyond the inflationary expansion modelled by a de Sitter Universe. Before presenting the integrals tackled in this chapter, we give a brief description of the FRW backgrounds describing the Universe's evolution at its various stages:

de Sitter Universe de Sitter (dS) space models the accelerated expansion of the inflationary Universe to a good approximation and thus provides a starting point for a boundary description of inflationary correlators. The isometry group of dS space has been utilized to exploit the conformal symmetry of cosmological correlators in the recent cosmological bootstrap program [79, 80, 81]. We recall that the de Sitter line element in flat slicing is given by

$$\mathrm{d}s^2 = \frac{-\mathrm{d}\eta^2 + \mathrm{d}x_i\mathrm{d}x^i}{\eta^2} \ , \tag{2.11}$$

with $\eta \in (-\infty, 0]$ and the Hubble scale set to unity. Comparing with the FRW metric (2.2), one sees that the scale factor behaves as $a(\eta) = 1/\eta$ for a de Sitter Universe. Much of the theoretical data concerning cosmological correlators come from our understanding of polynomial interactions in dS space. A particularly well-studied model is the $\lambda_3\phi^3$ theory in dS_4, which provides a rich framework for understanding the analytic structure of inflationary correlators [82].

Radiation/Matter dominated Universe For most of its history the Universe was dominated by a single component, as suggested by the different scalings of the energy density ρ with the scale factor $a(\eta)$. A phase of radiation domination (RD) where $\rho \propto a^{-4}$ was followed by an era of matter domination (MD) where $\rho \propto a^{-3}$. The dependencies of the scale factor on the conformal time in these phases are obtained by integrating the first Friedmann equation for a flat, single-component Universe [83]. This leads to the following FRW solutions for the scale factor

$$a(\eta) \propto \begin{cases} \eta & \text{(RD)} \\ \eta^2 & \text{(MD)} \end{cases}, \tag{2.12}$$

where the proportionality factors depend on dimensionless density parameters and will be set to unity for our discussions.

Given the above dependencies of the scale factor $a(\eta)$, the different FRW solutions (2.2) corresponding to a de Sitter (2.11), flat, radiation or a matter-dominated Universe (2.12) can be encapsulated by the following metric parameterized by ε

$$\mathrm{d}s^2 = \eta^{-2\varepsilon}\left[\frac{-\mathrm{d}\eta^2 + \mathrm{d}x_i\mathrm{d}x^i}{\eta^2}\right] \begin{cases} \varepsilon = 0 & \text{(dS)} \\ \varepsilon = -1 & \text{(flat)} \\ \varepsilon = -2 & \text{(RD)} \\ \varepsilon = -3 & \text{(MD)} \end{cases}, \tag{2.13}$$

such that the scale factor is

$$a(\eta) = \frac{1}{\eta^{1+\varepsilon}}. \tag{2.14}$$

While the differential equations (DEQ) that we derive in this chapter hold for any value of ε, the solution to them is always presented as a Laurent series expansion in ε, as we shall soon see. When solving the DEQ, our analysis will thereby be restricted to cosmologies closely resembling a dS Universe. The consequence of $\varepsilon \sim 0$ is two fold: i) in the analysis of inflationary correlators so far, the literature assumes a perfect dS expansion ($\varepsilon = 0$). However, inflationary cosmology dictates that for inflation to end one has to consider small departures from dS, often leading to inflation being referrred as a quasi-dS period. ii) Even if one models inflation as a perfect dS expansion, computing wavefunction coefficients as a series in ε could potentially shed crucial insights into physics beyond inflation, i.e., after the reheating surface.

Mathematically, the parameter ε corresponds to the exponent of the "*twist*" associated to the wavefunction coefficients of an FRW Universe. This identification, allows us to import the technology of *relative twisted cohomology* and *intersection theory* to cosmological correlators. Such ideas were first introduced in physics in the context of Feynman integrals. There, the parameter ε is the dimensional regularization parameter. In both cases, this exponent is generally non-integer giving rise to branch cut singularities on the integration manifold that partially dictates the singularity structure of the final object.

For the sake of simplicity, we shall focus on a theory of conformally coupled scalars described by a cubic $\lambda_3\phi^3$ interaction in a (1+3)-dimensional FRW Universe described by the action

$$\mathcal{S} = \int \mathrm{d}^3x\, \mathrm{d}\eta \sqrt{-g}\left[-\frac{1}{2}g^{\mu\nu}\partial_\mu\phi\partial_\nu\phi - \frac{1}{12}R\phi^2 - \frac{\lambda_3}{3!}\phi^3\right] \ . \tag{2.15}$$

However, it is straightforward to generalize our analysis to theories with polynomial interactions $\lambda_k\phi^k$ in an FRW Universe (2.13) obeying the condition

$$[a(\eta)]^{(2-k)\frac{(d-1)}{2}+2} = \frac{1}{\eta^{1+\varepsilon}} \ , \tag{2.16}$$

such that the time-dependent couplings (2.5) are given by $\lambda_k(\eta) = \frac{\lambda_k}{\eta^{1+\varepsilon}}$. These time-dependent couplings are most conveniently treated in (temporal) Fourier space

$$\frac{1}{\eta^{1+\varepsilon}} = \frac{(-i)^{1+\varepsilon}}{\Gamma(1+\varepsilon)}\int_0^{\infty(1-i\epsilon)} \mathrm{d}x\, x^\varepsilon e^{ix\eta} \ . \tag{2.17}$$

Before proceeding to furnish the integral representations for FRW correlators, a few comments are in order regarding the above Fourier-space expression. First, it is worth noting the difference between the FRW parameter ε and the standard $i\epsilon$ regulator ensuring the convergence of the integral. Secondly, it is crucial to note that the integral converges only for $\varepsilon > -1$ due to the presence of the gamma functions. This is seemingly in contradiction with our boundary choices of ε denoting the various FRW solutions in (2.13). However, as we will see in section 2.2, the differential equations satisfied by the FRW cosmological correlators can be solved for any value of the parameter ε. In what follows, we suppress the overall constants arising from the gamma functions and the factors of i appearing in (2.17) to avoid clutter. Given a choice of ε for the FRW Universe one lives in, such overall factors and coupling constants can be reinstated as they are needed.

2.1.2 Cosmological correlators in FRW backgrounds

Equipped with the above conceptual preliminaries, we now turn our attention to the construction of the wavefunction coefficients in flat-space and their uplifts to a general FRW cosmology.

We first define the flat-space n-site wavefunction coefficient at L-loops $\psi^{(L)}_{n,\text{flat}}$ which essentially makes up the *energy integrand* of the FRW wavefunction coefficient

$$\psi^{(L)}_{n,\text{flat}}(X_v, Y_e) = \int_{-\infty}^{0}\prod_{v\in\mathcal{V}} \mathrm{d}\eta_v\, e^{iX_v\eta_v}\prod_{e\in\mathcal{E}}\mathcal{G}(Y_e,\eta_v,\eta_v') \ , \tag{2.18}$$

where $\mathcal{V},\mathcal{E}$ denotes the set of vertices and edges of a given n-site, L-loop Feynman graph. We also introduce the notation X_v associated with the sum of energies flowing to the boundary from a vertex v and Y_e denote the energies of the edges (internal lines) e.

The computation of the nested time integrals given by the formal expression (2.18) has been carried out in the literature using several approaches: i) explicitly computing the 3^e *bulk* time integrals arising from the three-term structure of the propagator (2.10), ii) a combinatorial representation to implement *boundary* old-fashioned perturbation theory which one would obtain via the Lippmann-Schwinger kernel [71], iii) *triangulations* of the cosmological polytope (and its dual) [71, 73, 72, 84]. Using any of the approaches, one can compute the two- and three-site flat-space wavefunction coefficients at tree-level to be

$$\psi^{(0)}_{2,\text{flat}} = \frac{1}{(X_1+X_2)(X_1+Y)(X_2+Y)} \ , \tag{2.19}$$

$$\psi^{(0)}_{3,\text{flat}} = \frac{X_1+Y_1+2X_2+Y_2+X_3}{(X_1+X_2+X_3)(X_1+Y_1)(X_3+Y_2)(X_2+Y_1+Y_2)(X_1+X_2+Y_2)(X_2+X_3+Y_1)} \ , \tag{2.20}$$

while the two-site contribution at one loop is given by

$$\psi^{(1)}_{2,\text{flat}} = \frac{2(X_1+X_2+Y_1+Y_2)}{(X_1+X_2)(X_1+X_2+2Y_1)(X_1+Y_1+Y_2)(X_2+Y_1+Y_2)(X_1+X_2+2Y_2)} \ . \tag{2.21}$$

To compute wavefunction coefficients relevant to FRW cosmologies, we perform an uplift by integrating the *integrand* (2.18) over the energies related to the time-dependent coupling constants (2.17). To account for this extra time-dependence, we denote the *shifted* vertex energies as $E_v = x_v + X_v$ while also tacking on the twist factor x_v^ε at each vertex. As a result, the full FRW wavefunction contributions take the form

$$\psi^{(L)}_{n,\text{FRW}}(X_v, Y_e) = \int_0^\infty \prod_{v\in\mathcal{V}} \mathrm{d}x_v\, x_v^\varepsilon\, \psi^{(L)}_{n,\text{flat}}(x_v + X_v, Y_e) = \int_{\mathcal{R}} \prod_{v\in\mathcal{V}} \mathrm{d}x_v\, x_v^\varepsilon\, \psi^{(L)}_{n,\text{flat}}(E_v, Y_e) \ , \tag{2.22}$$

where $\mathcal{R}$ defines the rectangular region $E_v > X_v$ for each vertex v. In the mathematics literature, the integrals (2.22) belong to the class of functions which are often called generalized Euler integrals or GKZ[6] hypergeometric functions [85]. As we will see in section 2.2.4, the FRW wavefunction coefficients belong to the subset of this function space whose series expansion in ε involves only multiple polylogarithms. It is worth noting that (2.22) is actually the spatial loop momentum integrand for loop level corrections. While we will only study the integrals given by (2.22) in this work, the mathematical framework developed here can straightforwardly accommodate the integration over the spatial loop momentum and is left for future work.

As an example of this prescription, consider the uplift of $\psi^{(0)}_{2,\text{flat}} \to \psi^{(0)}_{2,\text{FRW}}$. Using the two-site flat-space wavefunction coefficient (2.19) and the uplift relation (2.22), one obtains the explicit realization of the corresponding FRW wavefunction coefficient given by the integral expression

$$\psi^{(0)}_{2,\text{FRW}}(X_1, X_2; Y) = \int_0^\infty \mathrm{d}x_1 \wedge \mathrm{d}x_2\ \frac{(x_1x_2)^\varepsilon}{(x_1+x_2+X_1+X_2)(x_1+X_1+Y)(x_2+X_2+Y)} \ . \tag{2.23}$$

The $\varepsilon \to 0$ limit of such integrals reduces to the well-studied cases arising in inflationary correlators in dS_4 [79, 82]. It is worth mentioning that while this prescription for the uplift of $\psi_{n,\text{flat}} \to \psi_{n,\text{FRW}}$ is technically true only for $\varepsilon \neq -1$, the flat-space wavefunction coefficient appears as the coefficient of the leading log divergence in the $\varepsilon \to -1$ limit. Explicitly setting $\varepsilon \to -1+\mu$ in (2.23) yields

$$\begin{aligned}
\psi^{(0)}_{2,\text{FRW}}(X_1, X_2, ; Y)\big|_{\varepsilon\to-1+\mu} &= \int_0^\infty x_1^{-1+\mu}\ \mathrm{d}x_1 \int_0^\infty \mathrm{d}x_2\ x_2^{-1+\mu}\ \psi^{(0)}_{2,\text{flat}}(x_1+X_1, x_2+X_2; Y) \\
&= \int_0^\infty \mathrm{d}x_1\ x_1^{-1+\mu}\ \frac{\psi^{(0)}_{2,\text{flat}}(x_1+X_1, X_2; Y)}{\mu} + \mathcal{O}(\mu^0) \\
&= \frac{\psi^{(0)}_{2,\text{flat}}(X_1, X_2; Y)}{\mu^2} + \mathcal{O}(\mu^{-1}) \ .
\end{aligned} \tag{2.24}$$

[6]Gelfand, Kapranov and Zelevinsky.

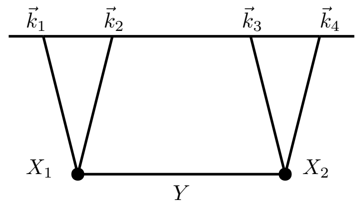

Figure 2.1: The Feynman diagram for the tree-level two-site/four-point wavefunction coefficient in $\lambda_3\phi^3$ theory.

Thus, for the flat-space case, the integral (2.23) returns the original wavefunction coefficient multiplied by a divergent factor $1/\mu^2$. This factor corresponds to the infinite volume of the energy integrals that we should not have integrated over.

The main objective of this chapter is to illustrate how one can study the analytic structure of FRW wavefunction coefficients using techniques from *relative twisted cohomology*, *intersection theory* and canonical differential equations that has already been developed in context to flat-space scattering amplitudes. In particular, in the subsequent sections, we will derive the differential equations for the tree-level two-site/four-point and three-site/five-point and the one-loop two-site/two-point FRW wavefunction coefficients in a theory comprised of conformally coupled scalars obeying a $\lambda_3\phi^3$ interaction (2.15). In the process, we argue that *relative twisted cohomology* provides a particularly efficient and powerful formalism for studying FRW wavefunction coefficients.

2.2 The tree-level two-site FRW correlator

For the $\lambda_3\phi^3$ theory of conformally coupled scalars (2.15), the two-site flat-space wavefunction coefficient at tree-level is also the four-point function from the boundary perspective as depicted in figure 2.1. With the uplift prescription laid out in section 2.1.2, the corresponding FRW wavefunction coefficient has the integral representation

$$\psi^{(0)}_{2,\mathrm{FRW}}(X_1, X_2; Y) = \int_0^\infty \mathrm{d}x_1 \wedge \mathrm{d}x_2 \, \frac{(x_1 x_2)^\varepsilon}{(x_1+x_2+X_1+X_2)(x_1+X_1+Y)(x_2+X_2+Y)} \, . \tag{2.25}$$

While it is possible to integrate the above two-site/four-point integral, direct integration becomes intractable at higher points. Similar integrals often appear in the study of dimensionally regulated Feynman integrals where there is a rich literature describing their evaluation and understanding their analytic structure (see [86, 65, 87, 66, 67, 88, 89, 90, 91, 92, 93, 94, 95, 96, 85] for a very incomplete list). In particular, we will use the method of canonical differential equations [97, 98] and some ideas from intersection theory [57, 58, 59, 60, 61, 62, 63, 68, 69] to evaluate the two-site FRW correlator (2.25).

In order to implement these methods, we have to consider the family of integrals defined by the singularities of the integrand in (2.25). This family is made up of integrals whose integrands are rational differential forms on the manifold X (to be defined later) multiplied by a universal multi-valued function, u, called the twist

$$\psi^{(0)}_{2,\mathrm{FRW}}(X_1, X_2; Y; \boldsymbol{\mu}, \boldsymbol{\nu}) = \int u \, \frac{N(\mathbf{x})}{\prod_{j=1}^{2} T_j^{\mu_j} \prod_{k=1}^{3} S_k^{\nu_k}(\mathbf{x})} \mathrm{d}^2\mathbf{x} \quad (\nu_i, \mu_i \in \{0, 1, 2, \dots\}), \tag{2.26}$$

$$u = \prod_{i=1}^{2} T_i^{\varepsilon} \qquad (\varepsilon \notin \mathbb{C} \setminus \mathbb{Z} \text{ for FRW cosmologies}) \ . \tag{2.27}$$

In particular, the integral (2.25) corresponds to $\mu = \{0, 0\}$ and $\nu = \{1, 1, 1\}$ above. While we can have any arbitrary polynomial numerator $N(\mathbf{x})$, the analytic structure of the integral is (mostly) determined by the singular surfaces $T_a = 0$ and $S_a = 0$. Moreover, the behavior of the integrand at the singular surfaces $T_a = 0$ and $S_a = 0$ is very different and needs distinct mathematical treatment. The hyperplanes[7]

$$T_1 = x_1 \quad \text{and} \quad T_2 = x_2 \ , \tag{2.28}$$

correspond to branch surfaces or *twisted singularities* of the integrand. These singularities are said to regulated by ε and are mild in the sense that the integral in the neighbourhood of any $T_a = 0$ has a well defined analytic continuation. On the other hand, the (hyper-)planes

$$S_1 = x_1 + X_1 + Y \ , \tag{2.29}$$

$$S_2 = x_2 + X_2 + Y \ , \tag{2.30}$$

$$S_3 = x_1 + x_2 + X_1 + X_2 \ . \tag{2.31}$$

correspond to poles or *relative singularities*. These singularities are dangerous and cannot be avoided by analytic continuation.

Having understood the possible locations of singularities, we can define the integration manifold $X = \mathbb{C}^2 \setminus (T \cup S)$ where $T = \cup_{i=1}^{2}\{T_i = 0\}$ are the twisted singular surfaces and $S = \cup_{i=1}^{3}\{S_i = 0\}$ are the relative singular surfaces. The analytic structure of this family of integrals is almost entirely determined by how the surfaces T_a and S_a intersect amongst themselves.

One perhaps surprising fact is that such families of integrals are spanned by a finite basis of integrals $\{I_a\}$ [99, 100]. This means that the partial derivatives of these integrals with respect to the kinematic (non-integration) variables can be expressed as a linear combination of the original basis of integrals

$$\partial_z I_a = B^{(z)}_{ab} I_b \ , \tag{2.32}$$

where $z \in \{X_1, X_2, Y\}$ for the example at hand. Such systems of differential equations have a closed solution in terms of a path-ordered exponential. Then, since we can can choose a basis such that the differential equation is proportional to ε: $\underline{\boldsymbol{B}} = \varepsilon \underline{\boldsymbol{A}}$, the path-ordered exponential

$$\mathbf{I} = \mathbf{I}_0 + \varepsilon \int \underline{\boldsymbol{A}} \cdot \mathbf{I}_0 + \varepsilon^2 \int \underline{\boldsymbol{A}} \cdot \int \underline{\boldsymbol{A}} \cdot \mathbf{I}_0 + \cdots \tag{2.33}$$

[7]By a hyperplane, we mean a codimension-1 surface cut out by a linear equation. We will use this terminology even for lines in 2-dimensions and planes in 3-dimensions.

can be truncated at any desired order in ε.[8] For each order in ε, sophisticated technology exists in the amplitudes literature for handling the resulting iterated integrals [101]. Lastly, $\mathbf{I}_0$ corresponds to the boundary conditions of our basis integrals.

Thus, we can integrate by differentiation! Since obtaining $\underline{\boldsymbol{A}}$ and the boundary conditions $\mathbf{I}_0$ are orders of magnitude easier than direct integration, we pursue this strategy in the following sections.

Before moving on, we note that the iterated integrals appearing in (2.33) will not produce anything more complicated than multiple polylogarithms because the matrix $\underline{\boldsymbol{A}}$ contains at most simple poles (see [90, 92, 102, 93] for some of the mathematical techniques used to simplify such integrals). If one was powerful enough to sum the series (2.33), one would recover the corresponding generalized hypergeometric function. Further, note that ε carries weight -1 so that the expansion of these hypergeometric functions have uniform transcendental weight.

To aid us in the computation of differential equations, we introduce a few ideas from intersection theory. In section 2.2.1, we introduce the twisted cohomology of FRW integrals, compute the differential equation and obtain the basis size from geometric quantities. Along the way we will comment on some computation bottlenecks of the usual twisted cohomology picture. To simplify the computation of the differential equation as well as improve our geometric understanding of such integrals, we introduce the vector space dual to FRW integrals in section 2.2.2. In particular, the analogous algorithm for computing the DEQ presented in section 2.2.1 simplifies and in some cases becomes trivial in the dual space. We also describe how to compute differential equations of logarithmic forms using the intersection number (an inner product on the FRW cohomology) bypassing integration-by-parts in section 2.2.3. In particular, we describe how to compute the differential equations without leaving the space of logarithmic forms. Lastly, in section 2.2.4, we will integrate the differential equation found in both sections 2.2.1 and 2.2.2 to obtain an explicit formula for the two-site/four-point FRW correlator.

2.2.1 Differential equations from twisted cohomology

To compute the differential equations, it is useful to change perspective and consider the *integrands* as the fundamental objects of interest instead of the corresponding integrals.[9] The allowed FRW integrands are any holomorphic rational differential top-forms φ on X,[10] multiplied by the multi-valued twist

$$\text{FRW integrands: } u\ \varphi. \tag{2.34}$$

Mathematically, we denote the space of (holomorphic) differential p-forms by $\Omega^p(X)$. Since the twist is universal to all FRW integrands, we can factor it out and only work with the single-valued forms φ by introducing a covariant derivative: $\mathrm{d}(u\ \varphi) = u\nabla\varphi$ where $\nabla = \mathrm{d} + \omega\wedge$ and $\omega = \mathrm{d}\log u$ is a flat

[8] FRW integrals turn out to be sufficiently simple that it is always possible to chose such a basis.

[9] Since we will always be dealing with a basis of integrals there is no loss of information by considering integrands instead of integrals.

[10] Holomorphic differential forms only contain the holomorphic variables of the complex manifold X. A top form has form degree equal to the complex dimension of the manifold $\dim_{\mathbb{C}} X$. In this example, $\dim_{\mathbb{C}} X = 2$.

connection ($\mathrm{d}\omega = 0$). The connection ω is analogous to the gauge field A_μ of QED and keeps track of the phase of u.

Notice that integrands are not uniquely defined. One can always shift an integrand by a total derivative without changing the resulting integral

$$\int u\ \varphi = \int \Big(u\ \varphi + \mathrm{d}(u\ \psi)\Big) = \int u\Big(\varphi + \nabla\psi\Big) \tag{2.35}$$

for any $\psi \in \Omega^{\dim_{\mathbb{C}} X-1}(X)$.[11] Thus, the unique objects are holomorphic top-forms modulo covariant derivatives. This is is made precise by the *twisted cohomology group*

$$[\varphi] \in H^p(X,\nabla) = \frac{\{\varphi \in \Omega^n(X)|\nabla\varphi = 0\}}{\{\nabla\psi|\psi \in \Omega^{p-1}(X)\}}. \tag{2.36}$$

The numerator corresponds to "covariantly closed" differential forms where the condition $\nabla\varphi = 0$ ensures that the integral of $u\varphi$ does not depend on the choice of path – only on the end points. The denominator corresponds to the set of all possible "covariantly exact" forms (covariant derivatives) that we can add to φ without changing the resulting integral. We will use the freedom to add any $\nabla\psi$ to φ to derive the FRW differential equations. In the Feynman integral literature, this procedure often goes by the name *integration-by-parts*.

Since twisted cohomology is well studied, we can borrow a key fact from the mathematical literature: only the top-dimensional twisted cohomology group is non-trivial.[12] As a consequence, the dimension of the top-dimensional cohomology (or equivalently the size of the FRW basis) is equal to the Euler characteristic $\chi(X)$. Moreover, it is known that for hyperplane arrangements the Euler characteristic is equal to the number of bounded chambers [103, 104].[13] For our particular example, there are four bounded chambers (figure 2.2). This should be familiar from the positive geometry and cosmological polytope picture [71, 72, 73, 105, 84, 106]. In fact, the canonical forms associated to the bounded chambers provide a natural ε-form basis for this family of integrals[14]

$$\vartheta_1 = \mathrm{d}\log\frac{S_1}{S_2} \wedge \mathrm{d}\log\frac{S_2}{S_3}, \tag{2.37}$$

$$\vartheta_2 = \mathrm{d}\log\frac{T_1}{S_2} \wedge \mathrm{d}\log\frac{S_2}{S_3}, \tag{2.38}$$

$$\vartheta_3 = \mathrm{d}\log\frac{T_2}{S_1} \wedge \mathrm{d}\log\frac{S_1}{S_3}, \tag{2.39}$$

$$\vartheta_4 = \left(\frac{x_1+X_1+X_2}{T_2S_1S_3} + \frac{x_2+X_1+X_2}{T_1S_2S_3} - \frac{1}{T_1T_2}\right)\mathrm{d}x_1 \wedge \mathrm{d}x_2. \tag{2.40}$$

[11] In the example at hand, $\dim_{\mathbb{C}} X - 1 = 2 - 1 = 1$.

[12] The usual proof of these theorems assume some conditions that we break by letting the S_i have integer exponents. Fortunately, in most cases, this statement remains true even when the S_i have integer exponents. A proof of this fact will appear in a forthcoming publication by one of the authors.

[13] When all singularities are twisted, a more practical way to compute this Euler characteristic is by counting the critical points of the connection [99, 51]. While this formula does not hold for FRW cohomology, it does hold for the dual cohomology. Thus, it is the recommend way for computing the dual basis size when working in higher dimensions.

[14] The canonical form of a chamber bounded by the lines A, B, C is given by the d log-form $\mathrm{d}\log\frac{A}{B} \wedge \mathrm{d}\log\frac{B}{C}$ or any permutation of A, B and C. The canonical form for a chamber bounded by more than three lines is obtained by triangulating the bounded chamber and adding up the canonical forms associated to the triangulation. This construction generalizes straightforwardly to higher dimensional spaces.

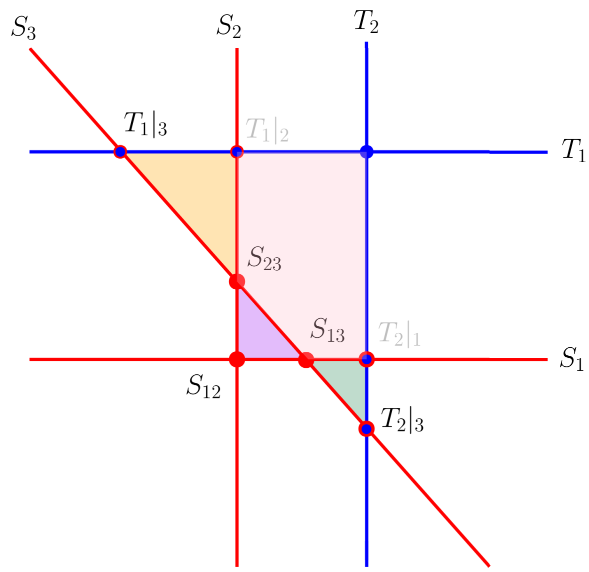

Figure 2.2: Hyperplane arrangement for the two-site/four-point integrand. The twisted planes are pictured in blue while the untwisted planes are red. For the FRW-cohomology, it is common to use the canonical forms of the bounded chambers, which are colored in orange, purple, green and pink (section 2.2.1). For the dual-cohomology, the basis is determined by uplifting the basis on each 1- and 2-boundary since the bulk cohomology is empty. On each 2-boundary, the cohomology is spanned by the constant function. Each 1-boundary only has a non-trivial cohomology if it crosses both twisted lines (section 2.2.2).

The last form has been written out explicitly, since its construction requires one to triangulate the pink bounded chamber in figure 2.2 and add up the canonical forms on each piece of the triangulation. Notice that $u\ \vartheta_1$ is simply the integrand of (2.25) (up to a sign).

Let us now compute the differential equation for ϑ_1. Taking the kinematic covariant derivative of ϑ_1 yields

$$\begin{aligned}\dot{\vartheta}_1 \equiv \nabla_{\text{kin}}\vartheta_1 = &\frac{2\left(2x_1+x_2+2X_1+X_2+Y\right)}{S_1^2S_2S_3^2}\,\mathrm{d}x_1\wedge\mathrm{d}x_2\wedge\mathrm{d}X_1\\ &+\frac{2\left(x_1+2x_2+X_1+2X_2+Y\right)}{S_1S_2^2S_3^2}\,\mathrm{d}x_1\wedge\mathrm{d}x_2\wedge\mathrm{d}X_2\\ &+\frac{2\left(x_2X_1+x_1X_2+x_1x_2+X_1X_2-Y^2\right)}{S_1^2S_2^2S_3}\,\mathrm{d}x_1\wedge\mathrm{d}x_2\wedge\mathrm{d}Y,\end{aligned}\tag{2.41}$$

where $\nabla_{\text{kin}}=\mathrm{d}_{\text{kin}}+\mathrm{d}_{\text{kin}}\log u=\mathrm{d}_{\text{kin}}$ and $\mathrm{d}_{\text{kin}}=\partial_{X_1}\mathrm{d}X_1+\partial_{X_2}\mathrm{d}X_2+\partial_Y\mathrm{d}Y$ for the current example. Note that $\dot{\vartheta}_1$ is not directly expressible in terms of our basis (2.37). However, we have the freedom to add the covariant derivative of any 1-form to (2.41) without changing the value of the integral. One can check that

$$\begin{aligned}\dot{\vartheta}_1+\nabla\text{IBP} = &\,\varepsilon\ \mathrm{d}\log\left((X_1+Y)\,(X_2+Y)\right)\wedge\vartheta_1\\ &+\varepsilon\ \mathrm{d}\log\left(\frac{Y-X_1}{X_1+Y}\right)\wedge\vartheta_2+\varepsilon\ \mathrm{d}\log\left(\frac{X_2+Y}{Y-X_2}\right)\wedge\vartheta_3,\end{aligned}\tag{2.42}$$

where

$$\mathrm{IBP} = \frac{2(x_1+X_1)\mathrm{d}x_2\wedge\mathrm{d}Y - 2(x_2+X_2)\mathrm{d}x_1\wedge\mathrm{d}Y + 2Y(\mathrm{d}x_1\wedge\mathrm{d}X_2 - \mathrm{d}x_2\wedge\mathrm{d}X_1)}{S_1S_2S_3}. \tag{2.43}$$

The IBP form above is not so difficult to guess or construct for the current example. However, constructing such IBP forms at the level of the three-site/five-point graph or higher is much more difficult. This integration-by-parts step can be simplified and in some cases trivialized by working in the dual cohomology of section 2.2.2. While the change to the dual cohomology requires a new layer of abstraction, the computational and conceptual simplifications are well worth it!

Equation (2.42) corresponds to the first row of our differential equation. Computing the other rows of $\underline{\boldsymbol{A}}$ in an analogous fashion yields

$$\underline{\boldsymbol{A}}_{\vartheta} = \varepsilon\,\mathrm{d}\begin{pmatrix} \log\left((X_1+Y)(X_2+Y)\right) & \log\left(\frac{Y-X_1}{X_1+Y}\right) & \log\left(\frac{X_2+Y}{Y-X_2}\right) & 0 \\ 0 & \log\left((X_1-Y)(X_1+X_2)\right) & \log\left(\frac{X_2+Y}{X_1+X_2}\right) & \log\left(\frac{X_2+Y}{X_1+X_2}\right) \\ 0 & \log\left(\frac{X_1+Y}{X_1+X_2}\right) & \log\left((X_2-Y)(X_1+X_2)\right) & \log\left(\frac{X_1+X_2}{X_1+Y}\right) \\ 0 & \log\left(\frac{Y-X_1}{X_1+Y}\right) & \log\left(\frac{X_2+Y}{Y-X_2}\right) & \log\left((X_1+Y)(X_2+Y)\right) \end{pmatrix}, \tag{2.44}$$

where we have included a subscript ϑ on $\underline{\boldsymbol{A}}$ to signify the choice of basis. Indeed, such differential equations come with an inherent gauge redundancy that is the choice of basis. Under a change of basis $\vartheta_i = U_{ij}\varphi_j$, the matrix $\underline{\boldsymbol{A}}$ transforms like a gauge field

$$\nabla_{\mathrm{kin}}\boldsymbol{\varphi} = \underline{\boldsymbol{A}}_{\varphi}\cdot\boldsymbol{\varphi}, \tag{2.45}$$

where

$$\underline{\boldsymbol{A}}_{\varphi} = \underline{\boldsymbol{U}}^{-1}\cdot\underline{\boldsymbol{A}}_{\vartheta}\cdot\underline{\boldsymbol{U}} - \underline{\boldsymbol{U}}\cdot\mathrm{d}_{\mathrm{kin}}\underline{\boldsymbol{U}}. \tag{2.46}$$

The equation above gives the rule for how to compare the differential equations for different choices of bases. Notice that (2.44) is actually quite dense. This hints that there may be a better choice of basis that simplifies the form of $\underline{\boldsymbol{A}}$. In fact, the dual cohomology will point us to such a basis in section 2.2.2.

Before moving onto describe the dual cohomology, we note that the matrix $\underline{\boldsymbol{A}}$ is integrable: $\mathrm{d}_{\mathrm{kin}}A_{ij} + A_{ik}\wedge A_{kj} = 0$. This condition places strong consistency conditions on $\underline{\boldsymbol{A}}$ and provides an important check of our calculations. If $\underline{\boldsymbol{A}}$ were not integrable, the path ordered exponential would depend on the path of integration in kinematic space.

2.2.2 Differential equations from the dual (relative twisted) cohomology

Since the twisted cohomology is a vector space, there exists a dual vector space and an associated inner product called the *intersection number*. The dual cohomology is the *relative twisted* cohomology $\chi H^p(X,\nabla) = H^p(\chi X, \chi X\cap S, \chi\nabla)$ where $\chi X = \mathbb{C}^2\backslash T$, $\chi\nabla = \mathrm{d}+\check{\omega}\wedge$ is the dual covariant derivative, $\check{\omega} = \mathrm{d}\log\check{u}$ is the dual connection and $\check{u} = 1/u$ is the dual twist [77, 68, 69]. In this section, we will unpack the ideas underlying relative twisted cohomology and describe how this simplifies computing differential equations.

We also opt to avoid delving into the details of how the intersection number is computed. Instead, we give a simple formula for the intersection of logarithmic forms in appendix 2.5 that covers all cases considered in this work. However, to provide some motivation for why the dual cohomology takes its particular form, it is useful to give the definition of the intersection number in the main text.

The intersection number of a FRW-form $\varphi \in H^n(X,\nabla)$ with a dual form $\check{\varphi} \in H^n(\chi X, \chi X \cap S, \chi\nabla)$ is given by

$$\langle\check{\varphi}|\varphi\rangle \propto \frac{1}{(2\pi i)^{\dim_{\mathbb{C}} X}} \int_X \mathrm{Reg}[\check{\varphi}] \wedge \varphi \tag{2.47}$$

where the overall sign is conventional and $\mathrm{Reg}[\check{\varphi}]$ is a regulated version of the dual form.[15] While this looks like it could be a difficult integral to perform, the intersection number localizes on the maximal codimension intersections of the singular surfaces T_i and S_i (the point S_{12} in figure 2.1 for example). Thus, the intersection number is actually algebraically evaluated as a series of residues. Moreover, it is simple to compute for logarithmic forms, which encompass all FRW-forms.

Like any vector space, we can construct a resolution of the identity from a basis for the FRW and dual cohomologies $\{\varphi_a\}$ and $\{\check{\varphi}_a\}$

$$\mathbb{1} = \sum_{a,b} |\varphi_a\rangle\ C^{-1}_{ab}\ \langle\check{\varphi}_b|. \tag{2.48}$$

Here, $C_{ab} = \langle\check{\varphi}_a|\varphi_b\rangle$ is the intersection matrix associated to our choice of bases. Using this resolution of identity, any FRW-form φ (and hence integral $\int u\ \varphi$) can be projected onto the basis $\{\varphi_a\}$

$$|\varphi\rangle = \sum_a c_a\varphi_a, \qquad c_a = C^{-1}_{ab}\langle\check{\varphi}_b|\varphi\rangle. \tag{2.49}$$

Roughly speaking, this projection is a form of generalized unitary [87, 109, 88, 110, 111, 112, 113, 114, 115]. It can also be used instead of the integration-by-parts identities of the previous section to derive the differential equations (section 2.2.4).

The reason that the dual cohomology takes a different form from the FRW cohomology is due to the nature of the regularization map in (2.47). Since the twisted singularities T_a can be regularized thanks to the fact that $\varepsilon \notin \mathbb{Z}$ is generic, dual forms can have singularities at the zero loci of the T_i. On the other hand, singularities at the zero loci of the relative singularities S_i *cannot* be regularized. Thus, dual forms must be regular on $\chi X \cap S$. This is why we only excise T in the definition of the dual manifold $\chi X = \mathbb{C}^2 \setminus T$.

The last piece of mathematical terminology that we need to explain before moving to the calculation of the differential equation is what the adjective "relative" means. It is simply a fancy name for keeping track of boundary terms that arise form Stokes' theorem. For the FRW cohomology, we did not allow boundaries and the total covariant derivative always integrated to zero. For the dual

[15] We skip the details of the regularization procedure in this work since the simple formula in appendix 2.5 covers all cases encountered in this work. For details on the regularization procedure we direct the interested reader to [107, 51, 59, 60, 108, 62, 63, 69, 68] and the references therein.

cohomology, the relative singular surfaces become boundaries and the integral of a total covariant derivative only vanishes up to boundary terms. These boundary terms are integrals arising from lower-degree forms that live on the boundary surfaces.

Mechanically, this boundary information is kept track by the so-called coboundary symbol δ_J. A generic dual form $\check{\varphi} \in H^n(\chi X, \chi X \cap S, \chi\nabla)$ should be thought of as a vector with components labeled by each boundary J

$$\check{\varphi} = \sum_J \delta_J \left(\check{\phi}_J\right). \tag{2.50}$$

Here, δ_J can be thought of as picking out the component of $\check{\varphi}$ that corresponds to the boundary $S_J = \chi X \cap_{j \in J} S_j$ and $\check{\phi}_J$ is an element of the twisted cohomology of the boundary indexed by J: $H^{n-|J|}(\chi X \cap S_J, \chi\nabla)$.[16] Naturally, the corresponding dual integrals

$$\chi I_J = \int_\gamma \check{u}\ \check{\varphi} = \sum_J \int_\gamma \check{u}\ \delta_J\Big(\check{\phi}_J\Big) = \sum_J \int_{\gamma|_J} \check{u}|_J\ \check{\phi}_J, \tag{2.51}$$

are simply integrals defined on the boundaries.

In addition to indexing the components of $\check{\varphi}$, the δ_J act like differential forms. They anti-commute with themselves

$$\delta_{ij} = \delta_i \wedge \delta_j = -\delta_j \wedge \delta_i = -\delta_{ji} \tag{2.52}$$

and the exterior derivative is given by

$$\mathrm{d}\delta_J(\check{\phi}) = (-1)^{|J|}\delta_J\left(\mathrm{d}\check{\phi}\right) + (-1)^{|J|}\sum_{k \notin J} \delta_{Jk}\left(\check{\phi}|_k\right) \tag{2.53}$$

up to boundary terms. The δ_J also convert the covariant derivative on bulk space to the covariant derivative on the boundary

$$\chi\nabla\delta_J(\check{\phi}) = (-1)^{|J|}\delta_J\left(\chi\nabla|_J\ \check{\phi}\right) + (-1)^{|J|}\sum_{k \notin J} \delta_{Jk}\left(\check{\phi}|_k\right) \tag{2.54}$$

where $\chi\nabla|_J = \mathrm{d} + \check{\omega}|_J\wedge$. Equations (2.53) and (2.54) will do virtually all the heavy lifting in this formalism. To the zeroth order approximation, the δ_i can be thought of as being dual to the $\mathrm{d}\log$-form $\mathrm{d}\log S_i$ since the δ_i correspond to residues about $S_i = 0$ in the intersection number (see equation (2.110)). The main job of the δ_J is to take care of the combinatorics of Stokes' theorem on a manifold with boundary.

[16] For the mathematically inclined, the formal definition of relative twisted cohomology is the direct sum of the twisted cohomology on each boundary

$$\Omega^n(\chi X, S; \chi\nabla) = \Omega^n(\chi X; \chi\nabla) \bigoplus_{a=1}^{m} \Omega^{n-1}(\chi X \cap S_a; \chi\nabla|_a) \bigoplus_{\substack{a,b=1\\a\neq b}}^{m} \Omega^{n-2}(\chi X \cap S_a \cap S_b; \chi\nabla|_{ab})$$
$$\bigoplus \cdots \bigoplus_{\substack{a_1,\ldots,a_n=1\\a_i\neq a_j}}^{m} \Omega^0(\chi X \cap S_{a_1} \cap \cdots \cap S_{a_n}; \chi\nabla|_{a_1\cdots a_n})$$

where m is the number of relative surfaces S_i.

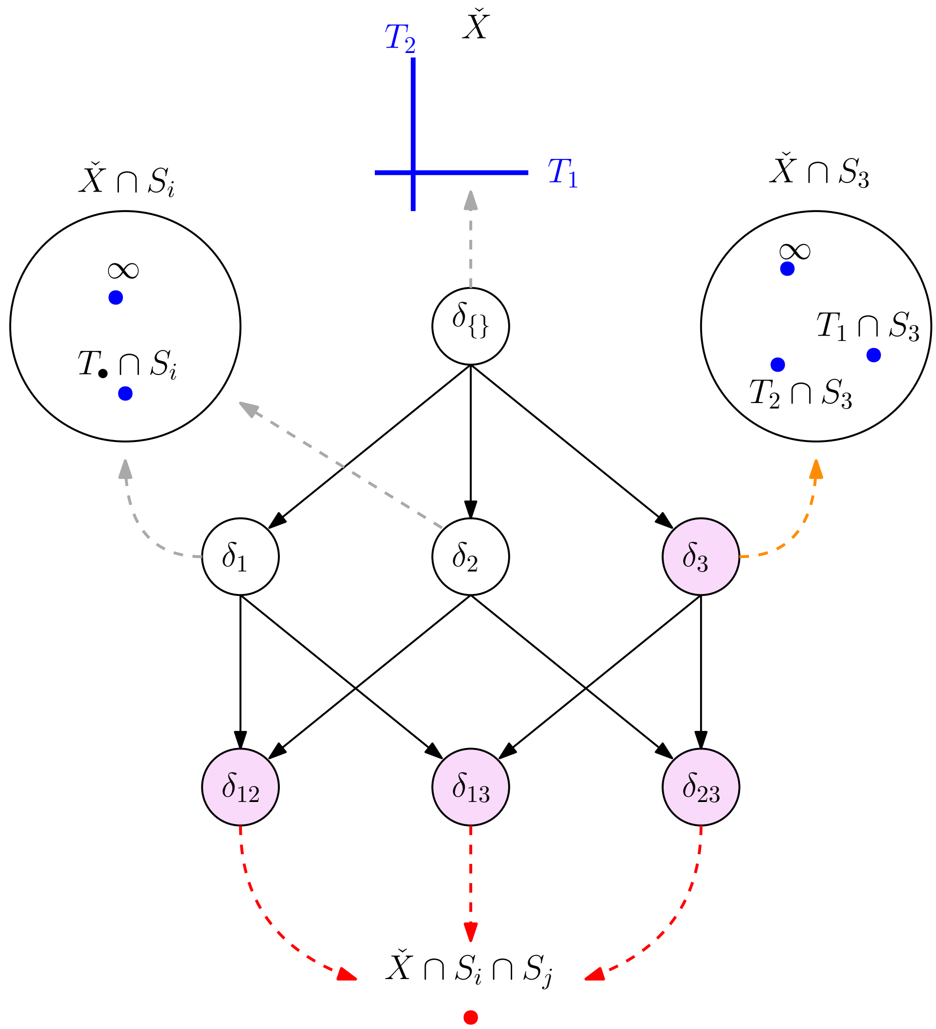

Figure 2.3: The topological spaces appearing in the direct sum decomposition of the relative cohomology. Since the twist is sufficiently generic, only the corresponding middle dimensional cohomology is non-trivial. The first diagram is a real slice of the bulk space where the coordinate planes (in blue) have been removed. Since the planes defined by the T_i do not form a bounded chamber, $\dim H^2(\check{X}, \check{\nabla}) = 0$. Each 1-boundary $\check{X} \cap S_i$ is topologically a Riemann sphere with either 2- or 3-punctures. Only $X \cap S_3$ has enough punctures to have a non-trivial topology. Thus, $\dim H^1(\check{X} \cap S_3, \check{\nabla}) = 1$ while $\dim H^1(\check{X} \cap S_{i=1,2}, \check{\nabla}) = 0$. The last diagram represents the 2-boundaries $\check{X} \cap S_i \cap S_j$. While there is no twisting, the 0^{th} cohomology of a point is known to be 1-dimensional: $\dim H^0(\check{X} \cap S_1 \cap S_j) = 1$.

Returning to the two-site/four-point example, we need to choose a basis for the dual-cohomology. To do this, we simply write down a basis for the cohomology on each boundary. First, we look at the bulk twisted cohomology $H^2(\chi X, \chi\nabla)$. The topological space χX is pictured at the top of figure 2.3. Clearly there are no bounded chambers cut out by the twisted singularities so $\dim H^2(\chi X, \chi\nabla) = 0$. Next, we look at the cohomologies on all possible 1-boundaries. We find two distinct cases of 1-boundaries (pictured on the left and right in figure 2.3). Both boundaries S_1 and S_2 are twice punctured Riemann spheres. From a well known result [104], the dimension of the twisted cohomology of a punctured Riemann sphere is $\#(\text{punctures}) - 2$ (this is the analogue of counting bounded chambers in 1-dimension). Thus, both $H^1(S_1, \chi\nabla|_1)$ and $H^1(S_2, \chi\nabla|_2)$ are trivial. On the other hand, the twisted cohomology on S_3 is 1-dimensional since S_3 has 3 punctures. We can choose

$$\check{\phi}_1 = \varepsilon \, \mathrm{d}\log \frac{T_1|_3}{T_2|_3} \tag{2.55}$$

for the basis of $H^1(S_3, \chi\nabla|_3)$ and then uplift this into the full dual cohomology by simply tacking on a δ_3

$$\check{\varphi}_1 = \delta_3\left(\check{\phi}_1\right) = \varepsilon \, \delta_3\left(\mathrm{d}\log \frac{T_1|_3}{T_2|_3}\right). \tag{2.56}$$

The 1-boundary form has been normalized by ε to ensure that the differential equation is in ε-form.[17]

Lastly, there are three 2-boundaries: S_{12}, S_{23} and S_{13}. Each of these are simply a point (bottom of figure 2.3). While the corresponding cohomology $H^0(S_{ij})$ is not twisted, it is non-trivial and spanned by the constant function: 1. Thus, we choose

$$\check{\varphi}_2 = \delta_{12}(1), \qquad \check{\varphi}_3 = \delta_{23}(1), \qquad \check{\varphi}_4 = \delta_{13}(1), \tag{2.57}$$

as the remaining elements for our basis of the dual cohomology. Notice that the basis size is the same as in section 2.2.1. In the dual cohomology, the basis size is computed by adding the dimensions of the twisted cohomology on each possible boundary![18] For higher dimensional manifolds, one can no longer visualize and count bounded chambers and we have to switch to alternative methods for computing the Euler characteristic of each boundary. A practical way to do this is provided by footnote 13.

The components of the kinematic connection associated to the 2-boundary forms are trivial to obtain. Taking the (dual) kinematic covariant derivative and using equation (2.54), we find

$$\check{\nabla}_{\mathrm{kin}}\check{\varphi}_2 = \delta_{12}\left(\check{\omega}_{\mathrm{kin}}|_{12}\right) = \check{\omega}_{\mathrm{kin}}|_{12} \wedge \check{\varphi}_2 \equiv \check{A}_{22} \wedge \check{\varphi}_2, \tag{2.58}$$

$$\check{\nabla}_{\mathrm{kin}}\check{\varphi}_3 = \delta_{23}\left(\check{\omega}_{\mathrm{kin}}|_{23}\right) = \check{\omega}_{\mathrm{kin}}|_{23} \wedge \check{\varphi}_3 \equiv \check{A}_{33} \wedge \check{\varphi}_3, \tag{2.59}$$

$$\check{\nabla}_{\mathrm{kin}}\check{\varphi}_4 = \delta_{13}\left(\check{\omega}_{\mathrm{kin}}|_{13}\right) = \check{\omega}_{\mathrm{kin}}|_{13} \wedge \check{\varphi}_4 \equiv \check{A}_{44} \wedge \check{\varphi}_4, \tag{2.60}$$

[17] Intuitively, the more a form is localized to a boundary the less transcendental the resulting integral is. Thus, we normalize the more transcendental 1-boundary form by ε so that it has the same transcendentality as the 2-boundary forms.

[18] Sometimes this can over count the basis size when the hyperplane arrangement is non-generic and some boundaries need to be identified. We will see an example of this in section 2.3.2.

where $\check{\nabla}_{\text{kin}} = \mathrm{d}_{\text{kin}} + \check{\omega}_{\text{kin}}$, $\check{\omega}_{\text{kin}} = \mathrm{d}_{\text{kin}} \log \check{u}$ and $\check{\omega}_{\text{kin}}|_J = \mathrm{d}_{\text{kin}} \log \check{u}|_J$. Consequently, we see that the dual differential equation has the following upper triangular form

$$\check{\nabla}_{\text{kin}} \check{\varphi}_a = \check{A}_{ab} \wedge \check{\varphi}_b \quad \text{where} \quad \underline{\check{\boldsymbol{A}}} = \begin{pmatrix} \check{A}_{11} & \check{A}_{12} & \check{A}_{13} & \check{A}_{14} \\ 0 & \check{\omega}_{\text{kin}}|_{12} & 0 & 0 \\ 0 & 0 & \check{\omega}_{\text{kin}}|_{23} & 0 \\ 0 & 0 & 0 & \check{\omega}_{\text{kin}}|_{13} \end{pmatrix}. \tag{2.61}$$

To compute the remaining components associated to the 1-boundary form, we perform IBP on the 1-boundary. That is, we look for some kinematic 1-forms A_{1i} such that

$$\check{\nabla}_{\text{kin}} \check{\varphi}_1 + \check{\nabla}\text{IBP} = \sum_{i=1}^{4} \check{A}_{1i} \wedge \check{\varphi}_i, \tag{2.62}$$

for some integration-by-parts form IBP. Since $\check{\varphi}_1$ is a form on the boundary S_3, IBP should also be a form on this boundary: IBP $= \delta_3 \left(\check{\xi}\right)$ where $\check{\xi}$ is a 1-form in the kinematic variables but a 0-form in the integration variables. Inserting this definition of IBP into (2.62), we obtain

$$\begin{aligned} &\delta_3 \left(\check{A}_{11} \wedge \check{\phi}_1 - \check{\nabla}_{\text{kin}}|_3 \; \check{\phi}_1 - \check{\nabla}_{\text{int}}|_3 \; \check{\xi}\right) \\ &\qquad + \delta_{12} \left(\check{A}_{12}\right) + \delta_{23} \left(\check{A}_{13} + \check{\xi}|_2\right) + \delta_{13} \left(\check{A}_{14} + \check{\xi}|_1\right) = 0 \; . \end{aligned} \tag{2.63}$$

Again, we see that the 2-boundary components are fixed rather trivially

$$\check{A}_{12} = 0 \; , \quad \check{A}_{13} = -\check{\xi}|_2 \; , \quad \check{A}_{14} = -\check{\xi}|_1 \; . \tag{2.64}$$

All that remains is to specify $\chi\xi$. It is easily verified that equation (2.63) is satisfied by setting $\check{A}_{11} = -2\varepsilon \; \mathrm{d} \log(X_1 + X_2)$ and

$$\check{\xi} = -\varepsilon \frac{\mathrm{d}(X_1 + X_2)}{T_2|_3}. \tag{2.65}$$

Putting everything together, we find the dual differential equation

$$\underline{\check{\boldsymbol{A}}} = -\varepsilon \; \mathrm{d} \begin{pmatrix} 2\log(X_1 + X_2) & 0 & \log\left(\frac{X_2+Y}{X_1-Y}\right) & \log\left(\frac{X_2-Y}{X_1+Y}\right) \\ 0 & \log(X_1+Y)(X_2+Y) & 0 & 0 \\ 0 & 0 & \log\left((X_1-Y)(X_2+Y)\right) & 0 \\ 0 & 0 & 0 & \log\left((X_2-Y)(X_1+Y)\right) \end{pmatrix} \tag{2.66}$$

for our basis of the dual-cohomology (2.55) and (2.57).

The differential equation for the basis of canonical forms (2.44) is obtained from the dual differential equation (2.66) by a gauge transform

$$\begin{aligned} \underline{\boldsymbol{A}}_\vartheta &= -\left(\underline{\boldsymbol{C}}_\vartheta^{-1} \cdot \underline{\check{\boldsymbol{A}}} \cdot \underline{\boldsymbol{C}}_\vartheta\right)^\top \\ &= \varepsilon \; \mathrm{d} \begin{pmatrix} \log\left((X_1+Y)(X_2+Y)\right) & \log\left(\frac{Y-X_1}{X_1+Y}\right) & \log\left(\frac{X_2+Y}{Y-X_2}\right) & 0 \\ 0 & \log\left((X_1-Y)(X_1+X_2)\right) & \log\left(\frac{X_2+Y}{X_1+X_2}\right) & \log\left(\frac{X_2+Y}{X_1+X_2}\right) \\ 0 & \log\left(\frac{X_1+Y}{X_1+X_2}\right) & \log\left((X_2-Y)(X_1+X_2)\right) & \log\left(\frac{X_1+X_2}{X_1+Y}\right) \\ 0 & \log\left(\frac{Y-X_1}{X_1+Y}\right) & \log\left(\frac{X_2+Y}{Y-X_2}\right) & \log\left((X_1+Y)(X_2+Y)\right) \end{pmatrix} \end{aligned} \tag{2.67}$$

where

$$(C_\vartheta)_{ab} = \langle \check{\varphi}_a | \vartheta_b \rangle = \begin{pmatrix} 0 & -1 & 1 & 0 \\ 1 & 0 & 0 & 0 \\ 1 & 1 & 0 & 1 \\ -1 & 0 & 1 & -1 \end{pmatrix} \tag{2.68}$$

is the intersection matrix. The intersection matrix is analogous to the computation of generalized unitary coefficients in the context of Feynman integrals. In particular, the simple formula for the intersection number of d log-forms (appendix 2.5) make such calculations straightforward!

Furthermore, the intersection matrix is a realization of the isomorphism between the FRW- and dual-cohomologies since it has full rank. However, in some sense, the canonical forms (2.37) are not the most direct way of establishing the duality between the FRW- and dual-cohomologies since the intersection matrix is dense.

Instead, one can directly construct a basis for the FRW-cohomology that is orthonormal to the basis of dual-cohomology (2.55) and (2.57). By choosing d log forms that do not share singularities on the maximal intersections of the hyperplanes $\{T_i, S_i\}$, one guarantees that the corresponding intersection matrix is diagonal. For example, the following basis

$$\begin{aligned} \varphi_1 &= -\frac{1}{2} \mathrm{d}\log(S_3) \wedge \mathrm{d}\log\left(\frac{T_1}{T_2}\right) , & \varphi_2 &= \mathrm{d}\log S_1 \wedge \mathrm{d}\log S_2 , \\ \varphi_3 &= \mathrm{d}\log S_2 \wedge \mathrm{d}\log S_3 , & \varphi_4 &= \mathrm{d}\log S_1 \wedge \mathrm{d}\log S_3 , \end{aligned} \tag{2.69}$$

is orthonormal to the $\check{\varphi}_a$

$$(C_\varphi)_{ab} = \langle \check{\varphi}_a | \varphi_b \rangle = \delta_{ab} . \tag{2.70}$$

Generally, it is much easier to build a basis in the dual-cohomology that has a simple DEQ. Thus, the basis φ_a is extremely useful since the resulting differential equation is the minus transpose of $\check{\underline{\boldsymbol{A}}}$

$$\underline{\boldsymbol{A}}_\varphi = -\left(\check{\underline{\boldsymbol{A}}}\right)^\top , \tag{2.71}$$

which is much more sparse than $\underline{\boldsymbol{A}}_\vartheta$. Then, since the integral of physical interest is simply related to the φ-basis $\vartheta_1 = \varphi_2 + \varphi_3 - \varphi_4$[19], one can integrate the simpler DEQ $\underline{\boldsymbol{A}}_\varphi$ instead of $\underline{\boldsymbol{A}}_\vartheta$. Moreover, the φ-basis never needs to be explicitly constructed – only its existence is important! One can obtain any FRW integral of interest by integrating $\left(-\check{\underline{\boldsymbol{A}}}\right)^\top$ (without choosing a basis for the FRW cohomology) and using the intersection matrix to project out the correct linear combination.

2.2.3 Trivializing the DEQ computation using intersection theory

As advertised in the introduction, one can compute the differential equations for a family of relative twisted differential forms using the intersection number instead of IBPs. Explicitly,

$$A_{ij} = C^{-1}_{jk} \langle \check{\varphi}_k | \nabla_{\mathrm{kin}} \varphi_i \rangle , \qquad \check{A}_{ij} = \langle \check{\nabla}_{\mathrm{kin}} \check{\varphi}_i | \varphi_k \rangle C^{-1}_{kj} , \tag{2.72}$$

[19] These signs simply correspond to the first column of $\underline{\boldsymbol{C}}_\vartheta$. By inserting identity $\mathbb{1} = |\varphi_a\rangle \left(C^{-1}_\varphi\right)_{ab} \langle \check{\varphi}_b|$, one finds $|\vartheta_1\rangle = |\varphi_a\rangle \left(C^{-1}_\varphi\right)_{ab} \langle \check{\varphi}_b | \vartheta_1 \rangle = \langle \check{\varphi}_a | \vartheta_1 \rangle |\varphi_a\rangle = (C_\vartheta)_{a1} |\varphi_a\rangle$ as claimed.

where $C_{ij} = \langle \check{\varphi}_i | \varphi_j \rangle$ is the intersection matrix for a given choice of basis. In general, this usually requires more sophisticated methods for computing the intersection numbers than those presented in appendix 2.5 since the forms $\nabla_{\text{kin}}\varphi_j$ and $\check{\nabla}_{\text{kin}}\check{\varphi}_i$ no longer have at most simple poles. However, since our forms are logarithmic, we can use a simple trick that avoids the introduction of double poles and allows us to compute the differential equations using only the formula presented in appendix 2.5![20]

The idea is to simply promote the exterior derivative d that acts on the integration variables to the exterior derivative that acts on both the integration and external variables: $\mathrm{d} \to \mathrm{D} = \mathrm{d} + \mathrm{d}_{\text{kin}}$. This promotes our basis to forms valued on the total space. For example,

$$
\begin{aligned}
\vartheta_1 \to \mathrm{D}\log\frac{S_1}{S_2} \wedge \mathrm{D}\log\frac{S_2}{S_3}
&= \frac{-2Y\ \mathrm{d}x_1 \wedge \mathrm{d}x_2}{(x_1+x_2+X_1+X_2)(x_1+X_1+Y)(x_2+X_2+Y)} \\
&\quad + \frac{2(x_2+X_2)\ \mathrm{d}x_1 \wedge \mathrm{d}Y}{(x_1+x_2+X_1+X_2)(x_1+X_1+Y)(x_2+X_2+Y)} \\
&\quad + \frac{2Y\ \mathrm{d}x_2 \wedge \mathrm{d}X_1}{(x_1+x_2+X_1+X_2)(x_1+X_1+Y)(x_2+X_2+Y)} \\
&\quad - \frac{2Y\ \mathrm{d}x_1 \wedge \mathrm{d}X_2}{(x_1+x_2+X_1+X_2)(x_1+X_1+Y)(x_2+X_2+Y)} \\
&\quad - \frac{2(x_1+X_1)\ \mathrm{d}x_2 \wedge \mathrm{d}Y}{(x_1+x_2+X_1+X_2)(x_1+X_1+Y)(x_2+X_2+Y)} \\
&\quad + \text{kinematic 2-forms}\,.
\end{aligned}
\tag{2.73}
$$

Note that the FRW connection does not change since it is independent of kinematics $\omega \to \mathrm{D}\log(u) = \mathrm{d}\log(u)$.[21]

Now, since the difference between $(\mathrm{D}+\mathrm{D}\log(u)\wedge)$ and ∇_{kin} is a total derivative ∇, we can replace ∇_{kin} in (2.72) by $(\mathrm{D}+\mathrm{D}\log(u)\wedge)$ without changing the intersection number.[22] Explicitly, for ϑ_1, this amounts to the replacement

$$
\begin{aligned}
\dot{\vartheta}_1 = \nabla_{\text{kin}}\vartheta_1 \to (\mathrm{D}+\mathrm{D}\log(u)\wedge)\ \vartheta_1
&= \frac{-2\varepsilon\ (x_2X_1 + x_1X_2 + 2x_1x_2)\ \mathrm{d}x_1 \wedge \mathrm{d}x_2 \wedge \mathrm{d}Y}{x_1x_2(x_1+x_2+X_1+X_2)(x_1+X_1+Y)(x_2+X_2+Y)} \\
&\quad + \frac{2\varepsilon\ Y\ \mathrm{d}x_1 \wedge \mathrm{d}x_2 \wedge \mathrm{d}X_1}{x_1(x_1+x_2+X_1+X_2)(x_1+X_1+Y)(x_2+X_2+Y)} \\
&\quad + \frac{2\varepsilon\ Y\ \mathrm{d}x_1 \wedge \mathrm{d}x_2 \wedge \mathrm{d}X_2}{x_2(x_1+x_2+X_1+X_2)(x_1+X_1+Y)(x_2+X_2+Y)} \\
&\quad + \text{kinematic 2-forms}\,.
\end{aligned}
\tag{2.74}
$$

Notice that the right hand side above only has simple poles! Using the formulae given in appendix

[20]The methods outlined here also help streamline the integration-by-parts algorithm presented in sections 2.2.1 and 2.2.2.

[21]On the other hand, the dual connection does change since the restriction to boundaries introduces kinematic dependence.

[22]The intersection number of any total covariant derivative ∇ or $\chi\nabla$ always vanishes.

2.5, one finds the first row of the differential equation $\underline{\boldsymbol{A}}_\vartheta$

$$(A_\vartheta)_{1j} = (C_\vartheta^{-1})_{jk}\langle\check{\varphi}_k|(\mathrm{D} + \mathrm{D}\log(u)\wedge)\ \vartheta_1\rangle\,. \tag{2.75}$$

The above formula is attractive since it only involves algebraic (residue) operations. We know where the intersection number localizes and don't have to go through the process of constructing IBP-forms.

Before moving on to actually integrating our differential equation, we note that the ideas outlined here are applicable to the algorithm for computing the symbol in [116]. By promoting the external derivative to a derivative on the total space, the two-step algorithm for computing the intersection number could potentially be reduced to one-step!

2.2.4 Integrating the differential equations

Having constructed the DEQ system for the two-site/four-point FRW correlator in subsections 2.2.1 (ϑ-basis) and 2.2.2 (φ-basis), we now turn our attention to solving them. We implement conventional techniques that have become widespread in the computation of Feynman integrals over the last decade [98, 117]. Differential equations of the form constructed in sections 2.2.1 and 2.2.2 are known as Pfaffian systems whose solutions are given by the path-ordered exponential as expressed in equation (2.33). For small ε, as is the case for FRW cosmologies, such solutions can be expanded and truncated to any desired order in ε. In this subsection, we will reproduce the well known de Sitter result corresponding to the $\mathcal{O}(\varepsilon^0)$ term of the FRW wavefunction coefficient. Then, for the first time, we derive an expression for the $\mathcal{O}(\varepsilon)$ term of the two-site/four-point FRW wavefunction coefficient.

We begin by reviewing how to integrate systems of coupled linear DEQs in the context of the two-site/four-point example. The physical integral ϑ_1 can be obtained by directly integrating the $\underline{\boldsymbol{A}}_\vartheta$ system associated to the canonical basis, for which ϑ_1 is a basis element, or by integrating the $\underline{\boldsymbol{A}}_\varphi$ system and using the fact that $\vartheta_1 = \varphi_2 + \varphi_3 - \varphi_4$.

In either case, the DEQ is

$$\nabla_{\mathrm{kin}}\alpha_i = A_{\alpha;ij}\wedge\alpha_j\ , \tag{2.76}$$

where $\alpha = \vartheta, \varphi$ denotes our choice of basis. In terms of actual integrals instead of differential forms, this DEQ becomes

$$\mathrm{d}_{\mathrm{kin}}\,\vec{g}_\alpha(z,\varepsilon) = \underline{\boldsymbol{A}}_\alpha\cdot\vec{g}_\alpha(z,\varepsilon)\ , \tag{2.77}$$

where $\vec{g}_\alpha = \int u\,\alpha$ is the vector of integrals associated to our choice of basis. Here, $z \in \{X_1, X_2, Y\}$ refers to the external scales for the tree-level two-site/four-point example at hand and $\mathrm{d}_{\mathrm{kin}} = \sum_{\{z\}}\partial_z\mathrm{d}z = \partial_{X_1}\mathrm{d}X_1 + \partial_{X_2}\mathrm{d}X_2 + \partial_Y\mathrm{d}Y$ as before. The 4×4 DEQ matrix $\underline{\boldsymbol{A}}_\alpha$ can be expanded as

$$\underline{\boldsymbol{A}}_\alpha = \varepsilon\sum_{\{z\}}\underline{\boldsymbol{\Omega}}_z\mathrm{d}z = \varepsilon\left(\underline{\boldsymbol{\Omega}}_{X_1}\mathrm{d}X_1 + \underline{\boldsymbol{\Omega}}_{X_2}\mathrm{d}X_2 + \underline{\boldsymbol{\Omega}}_Y\mathrm{d}Y\right)\ , \tag{2.78}$$

where the entries of the $\underline{\mathbf{\Omega}}_z$ matrices are rational one-forms. The solution $\vec{g}_\alpha(z,\varepsilon)$ is a Laurent series in ε

$$\vec{g}_\alpha(z,\varepsilon) = \sum_{n=-2}^{\infty} \varepsilon^n \, \vec{f}_\alpha^{(n)}(z) \ , \tag{2.79}$$

where the minimal value of n is determined by boundary conditions (in this case, it happens to be -2).

For the two-site/four-point example, the boundary conditions are generated by taking the $Y \to 0$ limit where the integrals can actually be performed and then expanded in ε. We denote this boundary condition by $\vec{g}_\alpha^*$

$$\vec{g}_\alpha^*(X_1,X_2,\varepsilon) := \vec{g}_\alpha^*(X_1,X_2,0,\varepsilon) = \sum_{n=-2}^{\infty} \varepsilon^n \, \vec{f}_\alpha^{*(n)}(X_1,X_2) \ . \tag{2.80}$$

For the ϑ-basis, the boundary condition integrals are straightforward to compute. On the other hand, the integral associated to φ_1 is divergent. However, due to the simplicity of the $\underline{\boldsymbol{A}}_\varphi$ DEQ, it is easy to see that the function $a(\varepsilon)(X_1+X_2)^{2\varepsilon}$ is a solution for the first component of $\vec{g}_\varphi$. Expanding $a(\varepsilon)$ as a series in ε, each coefficient can be fixed by demanding that the vector of boundary conditions $\vec{g}_\varphi^*$ satisfies the DEQ. In particular, using $a(\varepsilon) = -\frac{1}{2\varepsilon^2} - \frac{\pi^2}{4} + \mathcal{O}(\varepsilon)$ is enough to fix the physical integral to $\mathcal{O}(\varepsilon)$.

Having generated the boundary conditions, we are now in a position to integrate the DEQ system at hand. Given our Laurent series ansatz (2.79), the DEQ system takes the form

$$\partial_z \, \vec{g}_\alpha(z,\varepsilon) = \underline{\mathbf{\Omega}}_z \cdot \vec{g}_\alpha(z,\varepsilon) \implies \begin{cases} \partial_z \vec{f}^{(-2)} = 0 \\ \partial_z \vec{f}^{(a)} = \underline{\mathbf{\Omega}}_z \cdot \vec{f}^{(a-1)} \quad \forall \ a > 2 \ . \end{cases} \tag{2.81}$$

Following conventional DEQ techniques, we can now solve order by order in the twist parameter ε. Thus, we are led to the following solution at order $\varepsilon = 0$ for the two-site/four-point correlator, i.e., the solution corresponding to the physical chamber denoted by ϑ_1

$$\psi_{2,\mathrm{dS}}^{(0)} = \mathrm{Li}_2\left(\frac{X_1-Y}{X_1+Y}\right) + \mathrm{Li}_2\left(\frac{X_2-Y}{X_2+Y}\right) - \mathrm{Li}_2\left(\frac{X_1-Y}{X_1+Y}\frac{X_2-Y}{X_2+Y}\right) - \frac{\pi^2}{6} \ . \tag{2.82}$$

Up to a sign,[23] the above solution corresponds to the well-know two-site contribution to the wave-function coefficient in a dS Universe ($\varepsilon = 0$) [82, 79, 70].

In order to go beyond dS, we solve the differential equations arising at the next order in ε (only for the physical component ϑ_1) leading us to the following two-site/four-point contribution to the

[23]The sign difference arises from the arbitrariness in the choice of orientation when constructing a canonical form.

wavefunction coefficient in a FRW Universe in the region $X_1 > X_2 > Y$

$$
\begin{aligned}
\psi^{(0)}_{2,\mathrm{FRW}} =& -\mathrm{Li}_3\left(\frac{Y+X_1}{Y-X_2}\right) + \mathrm{Li}_3\left(-\frac{X_1-Y}{Y+X_2}\right) + 2\mathrm{Li}_3\left(\frac{X_1-Y}{X_1+X_2}\right) - 2\mathrm{Li}_3\left(\frac{Y+X_1}{X_1+X_2}\right) \\
&+ 2\log\left(X_1+X_2\right)\mathrm{Li}_2\left(-\frac{Y+X_2}{X_1-Y}\right) - 2\log\left(X_1+X_2\right)\mathrm{Li}_2\left(\frac{Y-X_2}{Y+X_1}\right) \\
&+ \frac{1}{6}\log^3\left(X_2-Y\right) - \frac{1}{6}\log^3\left(X_2+Y\right) - \frac{1}{2}\log\left(X_1+Y\right)\log^2\left(X_2-Y\right) \\
&- \frac{1}{2}\log^2\left(X_1+Y\right)\log\left(X_2-Y\right) - \log^2\left(X_1+X_2\right)\log\left(X_2-Y\right) \\
&+ \frac{1}{2}\log\left(X_1+Y\right)\log^2\left(X_2+Y\right) + \log^2\left(X_1+X_2\right)\log\left(X_2+Y\right) \\
&+ \frac{1}{2}\log^2\left(X_1+Y\right)\log\left(X_2+Y\right) + \log\left(X_1+X_2\right)\log^2\left(X_1-Y\right) \\
&- \log\left(X_1+X_2\right)\log^2\left(X_1+Y\right) + 2\log\left(X_1+X_2\right)\log\left(X_1+Y\right)\log\left(X_2-Y\right) \\
&+ \frac{1}{6}\pi^2\left(\log\left(X_2-Y\right) - \log\left(X_2+Y\right)\right) \\
&- 2\log\left(X_1+X_2\right)\log\left(X_1-Y\right)\log\left(X_2+Y\right) \ .
\end{aligned}
\tag{2.83}
$$

It is worth noting a few important features of the above expression. First, the integral representation of $\psi^{(0)}_{2,\mathrm{FRW}}$ is *not* manifestly symmetric in X_1 and X_2. We have sacrificed this symmetry for the simple presentation above. A formula valid in the whole physical region that is manifestly symmetric has been included in the ancillary files. Second, the above expression has uniform transcendental weight three. This is expected since the FRW wavefunction is the integral of the dS wavefunction thereby increasing the transcendental weight from two to three. In the next section, we will derive the differential equation for the tree-level three-site/five-point and one-loop two-site/two-point FRW wavefunction coefficients. While we leave the integration of these differential equation for future work, the resulting $\mathcal{O}(\varepsilon)$ terms will have transcendental weight four and three since the corresponding dS wavefunction coefficients are know to be weight three and two respectively. Interestingly, loop-diagrams corresponding to cosmological correlators are not more transcendental than their tree-level counter parts because the integration over the spatial loop momentum is not performed.

2.3 Further examples

In this section, we provide two further examples illustrating how to construct cosmological correlators associated to FRW integrals and the differential equations they satisfy. In particular, we show that there are no obstructions to extending the techniques applied in this work to loop integrands.[24] To illustrate this point, we construct the cohomologies for the one-loop two-site/two-point FRW

[24]To go beyond and explicitly perform the integral over the spatial loop momenta, one needs to account for the integration measure, which introduces new polynomials into the numerator of the integrals [118] that can be naturally accommodated in the framework of relative twisted cohomology. While polynomial numerators don't pose any technical problems, numerators with square roots may need additional regularization: $\sqrt{\bullet} \to (\bullet)^{\frac{1}{2}+\delta}$ where δ is a regulator much like the dimensional regulator. We leave the technical details of the L-loop FRW problem to upcoming work.

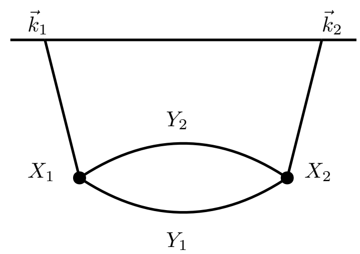

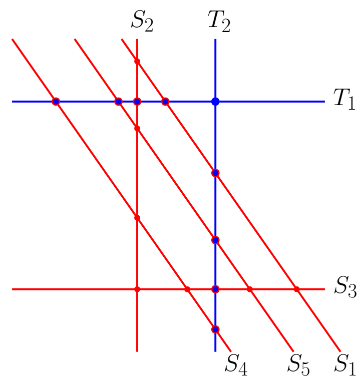

Figure 2.4: The Feynman diagram for the one-loop two-site/two-point wavefunction coefficient in $\lambda_3\phi^3$ theory and the associated hyperplane arrangement.

integrand as well as their differential equations in section 2.3.1. Then, in section 2.3.2, we construct the cohomologies and associated differential equations for the tree-level three-site/five-point FRW wavefunction coefficient. Here, we see a new feature due to the degeneration of boundaries that will be present in most higher-site/point examples and explain how to account for this degeneracy.

2.3.1 The one-loop two-site FRW correlator

In $\lambda_3\phi^3$ theory, the flat-space one-loop two-site/two-point wavefunction coefficient receives contributions from a single graph (see the left of figure 2.4) given by equation (2.21), which we quote here for convenience

$$\psi^{(1)}_{2,\text{flat}} = \frac{2\,(X_1+X_2+Y_1+Y_2)}{(X_1+X_2)\,(X_1+X_2+2Y_1)\,(X_1+Y_1+Y_2)\,(X_2+Y_1+Y_2)\,(X_1+X_2+2Y_2)}\ . \tag{2.84}$$

The FRW uplift prescription (2.22) yields the associated hyperplane arrangement for the FRW correlator (see the right of figure 2.4). As usual, the hyperplane arrangement is determined by the twisted coordinate hyperplanes

$$T_i = x_i \quad \text{for} \quad i = 1, 2\ , \tag{2.85}$$

and the singular/boundary hyperplanes are defined by the linear divisors of $\psi^{(1)}_{2,\text{flat}}|_{X_i\to x_i+X_i}$

$$\begin{aligned} &S_1 = x_1+x_2+X_1+X_2, && S_2 = x_1+X_1+Y_1+Y_2,\\ &S_3 = x_2+X_2+Y_1+Y_2, && S_4 = x_1+x_2+X_1+X_2+2Y_1,\\ &S_5 = x_1+x_2+X_1+X_2+2Y_2. && \end{aligned} \tag{2.86}$$

Note that this hyperplane arrangement is incredibly similar to the tree-level case and not any more difficult.

Counting the bounded chambers in figure 2.4 (right), we see that the FRW cohomology and its dual are 10-dimensional. A convenient choice for the dual 1-boundary forms is

$$\check{\varphi}_1 = \varepsilon\ \delta_1\left(\mathrm{d}\log\frac{T_1|_1}{T_2|_1}\right), \qquad \check{\varphi}_2 = \varepsilon\ \delta_4\left(\mathrm{d}\log\frac{T_1|_2}{T_2|_2}\right), \qquad \check{\varphi}_3 = \varepsilon\ \delta_5\left(\mathrm{d}\log\frac{T_1|_3}{T_2|_3}\right). \tag{2.87}$$

A similarly convenient choice for the 2-boundary forms is

$$\begin{aligned}
&\check{\varphi}_4 = \delta_{12}(1), \quad \check{\varphi}_5 = \delta_{13}(1), \quad \check{\varphi}_6 = \delta_{23}(1), \quad \check{\varphi}_7 = \delta_{24}(1), \\
&\check{\varphi}_8 = \delta_{25}(1), \quad \check{\varphi}_9 = \delta_{34}(1), \quad \check{\varphi}_{10} = \delta_{35}(1).
\end{aligned} \tag{2.88}$$

A set of FRW forms dual to the 1-boundary forms (2.87) is

$$\begin{aligned}
&\varphi_1 = -\tfrac{1}{2}\, \mathrm{d}\log S_1 \wedge \mathrm{d}\log \tfrac{T_1}{T_2}, \quad \varphi_2 = -\tfrac{1}{2}\, \mathrm{d}\log S_4 \wedge \mathrm{d}\log \tfrac{T_1}{T_2}, \\
&\varphi_3 = -\tfrac{1}{2}\, \mathrm{d}\log S_5 \wedge \mathrm{d}\log \tfrac{T_1}{T_2},
\end{aligned} \tag{2.89}$$

while a set of FRW forms dual to (2.88) is

$$\begin{aligned}
&\varphi_4 = \mathrm{d}\log S_1 \wedge \mathrm{d}\log S_2, \quad \varphi_5 = \mathrm{d}\log S_1 \wedge \mathrm{d}\log S_3, \quad \varphi_6 = \mathrm{d}\log S_2 \wedge \mathrm{d}\log S_3, \\
&\varphi_7 = \mathrm{d}\log S_2 \wedge \mathrm{d}\log S_4, \quad \varphi_8 = \mathrm{d}\log S_2 \wedge \mathrm{d}\log S_5, \quad \varphi_9 = \mathrm{d}\log S_3 \wedge \mathrm{d}\log S_4, \\
&\varphi_{10} = \mathrm{d}\log S_3 \wedge \mathrm{d}\log S_5.
\end{aligned} \tag{2.90}$$

With these choices for our basis, it is easy to see that only the diagonal intersection numbers are non-trivial. Moreover, the normalization of $-\frac{1}{2}$ in (2.87) ensures that our choice of basis are orthonormal: each $T_i|_\bullet$ contributes a $\frac{1}{-\varepsilon}$ to the intersection number while the point at infinity does not contribute since of the forms (2.87) are regular at infinity.

Computing the differential equation using the methods of section 2.2.2 or 2.2.3 yields

$$\underline{\boldsymbol{A}} = \varepsilon \begin{pmatrix}
2a_1 & 0 & 0 & 0 & 0 & 0 & 0 & 0 & 0 & 0 \\
0 & 2a_2 & 0 & 0 & 0 & 0 & 0 & 0 & 0 & 0 \\
0 & 0 & 2a_3 & 0 & 0 & 0 & 0 & 0 & 0 & 0 \\
a_5-a_4 & 0 & 0 & a_4+a_5 & 0 & 0 & 0 & 0 & 0 & 0 \\
a_7-a_6 & 0 & 0 & 0 & a_6+a_7 & 0 & 0 & 0 & 0 & 0 \\
0 & 0 & 0 & 0 & 0 & a_5+a_6 & 0 & 0 & 0 & 0 \\
0 & a_8-a_5 & 0 & 0 & 0 & 0 & a_5+a_8 & 0 & 0 & 0 \\
0 & 0 & a_{10}-a_5 & 0 & 0 & 0 & 0 & a_5+a_{10} & 0 & 0 \\
0 & a_6-a_9 & 0 & 0 & 0 & 0 & 0 & 0 & a_6+a_9 & 0 \\
0 & 0 & a_6-a_{11} & 0 & 0 & 0 & 0 & 0 & 0 & a_6+a_{11}
\end{pmatrix}. \tag{2.91}$$

Here, one should read the a_i's above as $\mathrm{d}\log(a_i)$ where the a_i are the letters

$$\begin{aligned}
a_{i=1,\ldots,11} = \Big\{ &X_1 + X_2,\ X_1 + X_2 + 2Y_1,\ X_1 + X_2 + 2Y_2,\ X_2 - Y_1 - Y_2, \\
&X_1 + Y_1 + Y_2,\ X_2 + Y_1 + Y_2,\ X_1 - Y_1 - Y_2,\ X_2 + Y_1 - Y_2, \\
&X_1 + Y_1 - Y_2,\ X_2 - Y_1 + Y_2,\ X_1 - Y_1 + Y_2 \Big\}.
\end{aligned} \tag{2.92}$$

The known de Sitter limit of this alphabet [70] is a subset of the above FRW alphabet with the new letters being $X_1 + Y_1 + Y_2$ and $X_2 + Y_1 + Y_2$.

After integrating the above differential equation, the physical integral can be computed by taking the appropriate linear combination. In our chosen basis,

$$\psi^{(1)}_{2,\mathrm{FRW}} = \frac{1}{4Y_1Y_2} \int u \left(-\varphi_4 + \varphi_5 + \varphi_6 - \varphi_7 - \varphi_8 + \varphi_9 + \varphi_{10}\right). \tag{2.93}$$

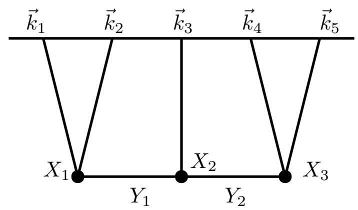

Figure 2.5: The Feynman diagram for the three-site/five-point FRW wavefunction coefficient in $\lambda_3\phi^3$-theory.

While one can get the FRW IBPs algorithm of section 2.2.1 to finish in a reasonable amount of time on a laptop for this example, the dual IBPs of section 2.2.2 or the intersection algorithm of section 2.2.3 becomes noticeably faster here. The simplicity of dual IBPs is essential for the next example. There, we could not get a *simple* implementation of the algorithm in section 2.2.1 to finish in a reasonable time unless supplemented with knowledge of the dual differential equation.

Our basis choice is motivated by the geometry of the dual cohomology and produces a sparse differential equation. While this is desirable, there may be better choices. Since only the un-twisted hyperplanes appear in the physical FRW form, it would be interesting if one could find a basis that factorizes the differential equation (2.91) into physical and un-physical sectors that can be solved separately.[25] We leave such questions to future work.

2.3.2 The tree-level three-site FRW correlator

We now turn our attention to the tree-level three-site/five-point FRW wavefunction coefficient where we will find new features not seen at the level of the two-site/four-point example but are expected to be present for most higher-site diagrams. Substituting equation (2.20) into (2.22), one obtains

$$\psi^{(0)}_{3,\text{FRW}} = \int_0^\infty \left(\bigwedge_{i=1}^{3} \mathrm{d}x_i\right)\left(\prod_{a=1}^{3} T_a^\varepsilon\right) \psi^{(0)}_{3,\text{flat}}\Big|_{X_i\to x_i+X_i} , \tag{2.94}$$

where we duplicate the flat space three-site wavefunction coefficient (2.20) below for ease of reading

$$\psi^{(0)}_{3,\text{flat}} = \frac{X_1+Y_1+2X_2+Y_2+X_3}{(X_1+X_2+X_3)(X_1+Y_1)(X_3+Y_2)(X_2+Y_1+Y_2)(X_1+X_2+Y_2)(X_2+X_3+Y_1)} . \tag{2.95}$$

The corresponding hyperplane arrangement is determined by the twisted coordinate hyperplanes

$$T_i = x_i \quad \text{for} \quad i = 1,2,3, \tag{2.96}$$

and the linear denominators of $\psi^{(0)}_{3,\text{flat}}|_{X_i\to x_i+X_i}$

$$\begin{aligned} S_1 &= x_1+x_2+x_3+X_1+X_2+X_3+Y_3 , & S_2 &= x_1+X_1+Y_1 , \\ S_3 &= x_3+X_3+Y_2 , & S_4 &= x_2+X_2+Y_1+Y_2 , \\ S_5 &= x_1+x_2+X_1+X_2+Y_2 , & S_6 &= x_2+x_3+X_2+X_3+Y_1 . \end{aligned} \tag{2.97}$$

[25] Indeed, it looks like this had been achieved to some extent in [75]. While the FRW cohomology of the 3-site/5-point is 26-dimensional, in [75] they seem to only need 16 elements to get the DEQ for the physical integral.

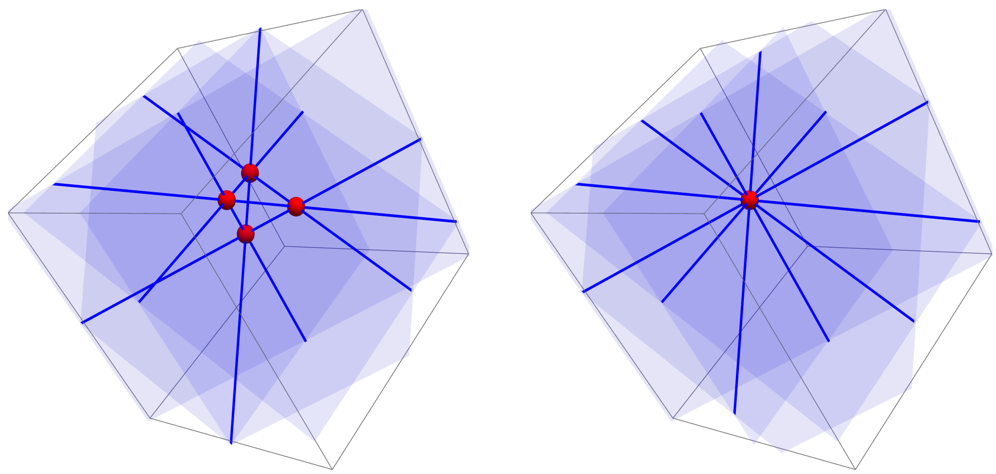

Figure 2.6: Plots of the planes $S_{i=1,4,5,6}$. The dark blue lines denote the intersection of these planes and the red dots mark where these lines intersect. The left plot corresponds to the unphysical but generic hyperplane arrangement with $Y_3 \neq 0$. The right plot is the degeneration of the left plot in the $Y_3 \to 0$ limit. The bounded chamber with the red dots as vertices in the right plot vanishes in the $Y_3 \to 0$ limit. This degeneration corresponds to the drop in dimension of the cohomology group.

Note that we have added an extra factor of Y_3 into S_1 that is not present in the physical arrangement. This has been done for purely pedagogical reasons since the physical arrangement ($Y_3 = 0$) is non-generic – there are 4-planes crossing at a single point (see figure 2.6). Adding a non-zero Y_3 will help us understand how to think about non-generic arrangements. However, in the end, one can directly set $Y_3 = 0$ at the beginning of the calculation as we will explain later.

For the generic arrangement ($Y_3 \neq 0$), the basis size or dimension of the cohomology group is 26. The basis size is obtained by adding up the dimension of each twisted cohomology group on each of the non-maximal codimension boundaries.[26] Additionally, (for generic arrangements) each maximal codimension boundary generates a cohomology class/basis element. The boundary stratification for the three-site/five-point arrangement is presented in figure 2.7. Each node denotes the twisted cohomology on the given boundary. The blue nodes represent boundaries with trivial cohomology (zero dimensional) while the purple nodes represent boundaries with non-trivial cohomology. Example arrangements of the twisted hyperplanes on some boundaries are illustrated in figure 2.7. Since the twisted hyperplanes do not form bounded chambers in the bulk space $\delta_{\{\}}$ only the cohomologies on the boundaries are non-trivial. The 1-boundary δ_6 is also pictured in figure 2.7 and is clearly trivial since there are no bounded chambers. On the other hand, the cohomology on δ_1 is 1-dimensional since the twisted hyperplanes form a single bounded chamber. For the cohomologies on 2-boundaries, the dimension is determined by the number of twisted singularities minus two. Thus, the dimension on boundary δ_{12} is 1-dimensional while the cohomology on the boundary δ_{46} is trivial. For the generic arrangement, the untwisted 3-boundaries are all distinct and 1-dimensional.

[26]Recall that the dimension of the top-dimensional twisted cohomology group is given by the Euler characteristic of the underlying manifold or equivalently by counting the critical points of the dual connection $\check{\omega}$ (see footnote 13) or by counting the number of bounded chambers formed by the twisted hyperplanes.

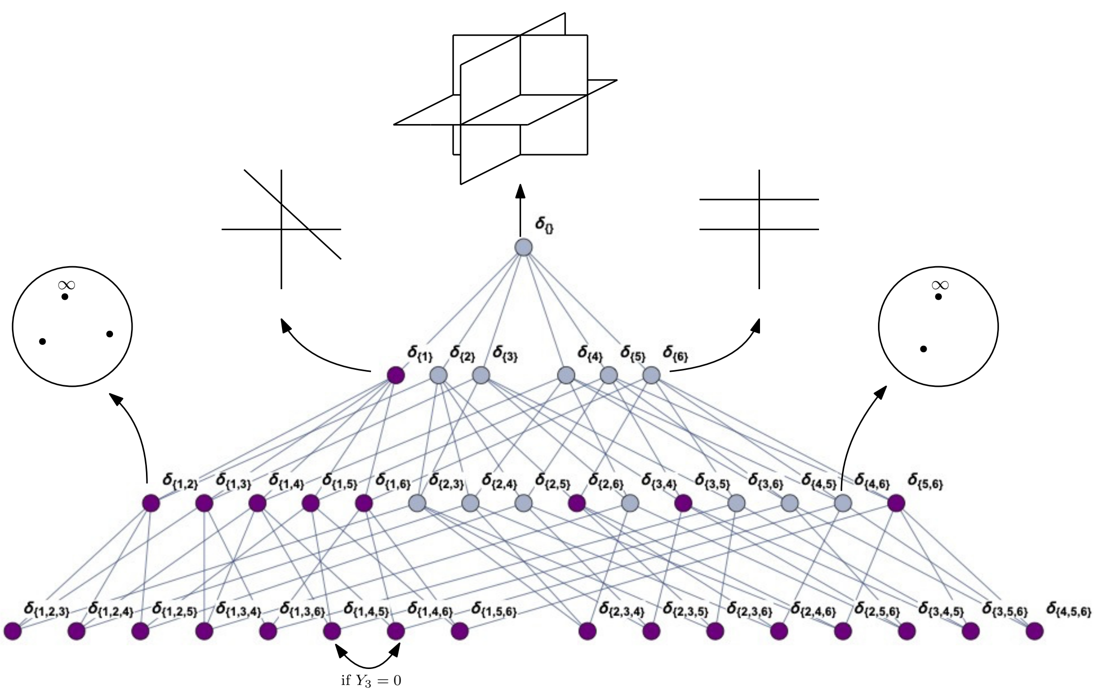

Figure 2.7: Boundary stratification of the relative twisted cohomology associated to the three-site/five-point hyperplane arrangement. The purple vertices are boundaries with non-trivial cohomology while all the blue vertices are boundaries with trivial cohomology. Notice that there are some missing 3-boundaries, $\delta_{126}, \delta_{135}, \delta_{245}, \delta_{346}$, since $S_1 \cap S_2 \cap S_6 = S_1 \cap S_3 \cap S_5 = S_2 \cap S_4 \cap S_5 = S_3 \cap S_4 \cap S_6 = \emptyset$.

For the physical ($Y_3 = 0$) arrangement, the basis size decreases to 25 because the four hyperplanes S_1, S_4, S_5 and S_6 all intersect at a point (see figure 2.6). Sending $Y_3 \to 0$ shrinks the bounded chamber pictured in the left of figure 2.6 to a point decreasing the basis size. Since we expect that there will be many more instances of such degeneracies for higher site FRW integrals, we provide a careful treatment of how the generic arrangement degenerates to the physical arrangement below.[27] Again, we emphasize that one does not need to introduce additional parameters to make the arrangement generic as long as one knows how to consistently treat the non-generic/degenerate case directly.

Below, we give a natural basis associated to the generic arrangement where the element that drops out when passing to the physical arrangement has been colored in gray.[28] The only non-trivial 1-boundary cohomology occurs on the boundary δ_1 and is generated by the single form

$$\check{\varphi}_1 = \varepsilon^2\ \delta_1 \left(\mathrm{d}\log\left(\frac{T_1|_1}{T_3|_1}\right) \wedge \mathrm{d}\log\left(\frac{T_3|_1}{T_2|_1}\right)\right). \tag{2.98}$$

This is nothing but the canonical form associated to the bounded chamber on the boundary δ_1. We have also normalized by ε^2 since we expect the intersection of 2-boundary forms to be proportional to $1/\varepsilon^2$. The 2-boundary cohomologies are generated by the following 9 forms

$$\begin{aligned}
&\check{\varphi}_2 = \varepsilon\ \delta_{12}\left(\mathrm{d}\log\tfrac{T_2|_{12}}{T_3|_{12}}\right), \quad \check{\varphi}_3 = \varepsilon\ \delta_{13}\left(\mathrm{d}\log\tfrac{T_1|_{13}}{T_2|_{13}}\right), \quad \check{\varphi}_4 = \varepsilon\ \delta_{14}\left(\mathrm{d}\log\tfrac{T_1|_{14}}{T_3|_{14}}\right), \\
&\check{\varphi}_5 = \varepsilon\ \delta_{15}\left(\mathrm{d}\log\tfrac{T_1|_{15}}{T_2|_{15}}\right), \quad \check{\varphi}_6 = \varepsilon\ \delta_{16}\left(\mathrm{d}\log\tfrac{T_2|_{16}}{T_3|_{16}}\right), \quad \check{\varphi}_7 = \varepsilon\ \delta_{26}\left(\mathrm{d}\log\tfrac{T_2|_{26}}{T_3|_{26}}\right), \\
&\check{\varphi}_8 = \varepsilon\ \delta_{35}\left(\mathrm{d}\log\tfrac{T_1|_{35}}{T_2|_{35}}\right), \quad \check{\varphi}_9 = \varepsilon\ \delta_{56}\left(\mathrm{d}\log\tfrac{T_1|_{56}}{T_2|_{56}}\right), \quad \check{\varphi}_{10} = \varepsilon\ \delta_{56}\Big(\mathrm{d}\log T_3|_{56}\Big).
\end{aligned} \tag{2.99}$$

Note that the cohomology on all 2-boundaries is 1-dimensional except for the δ_{56} boundary, which is 2-dimensional. The 2-boundary forms are normalized by a single power of ε since we expect the 2-boundary intersection to be proportional to $1/\varepsilon$. Finally, the 3-boundary cohomologies are generated by the following 16 forms

$$\begin{aligned}
&\check{\varphi}_{11} = \delta_{123}\,(1)\,, \quad \check{\varphi}_{12} = \delta_{124}\,(1)\,, \quad \check{\varphi}_{13} = \delta_{125}\,(1)\,, \quad \check{\varphi}_{14} = \delta_{134}\,(1)\,, \\
&\check{\varphi}_{15} = \delta_{136}\,(1)\,, \quad \check{\varphi}_{16} = \delta_{145}\,(1)\,, \quad \check{\varphi}_{17} = \delta_{146}\,(1)\,, \quad \check{\varphi}_{18} = \delta_{156}\,(1)\,, \\
&\check{\varphi}_{19} = \delta_{234}\,(1)\,, \quad \check{\varphi}_{20} = \delta_{235}\,(1)\,, \quad \check{\varphi}_{21} = \delta_{236}\,(1)\,, \quad \check{\varphi}_{22} = \delta_{246}\,(1)\,, \\
&\check{\varphi}_{23} = \delta_{256}\,(1)\,, \quad \check{\varphi}_{24} = \delta_{345}\,(1)\,, \quad \check{\varphi}_{25} = \delta_{356}\,(1)\,, \quad \check{\varphi}_{26} = \delta_{456}\,(1)\,.
\end{aligned} \tag{2.100}$$

Notice that there are some missing 3-boundaries $(\delta_{126}, \delta_{135}, \delta_{245}, \delta_{346})$ since some triples of the relative surfaces do not intersect at a point: $S_1 \cap S_2 \cap S_6 = S_1 \cap S_3 \cap S_5 = S_2 \cap S_4 \cap S_5 = S_3 \cap S_4 \cap S_6 = \emptyset$.

[27]For the four-site graph, there are two topologically distinct Feynman diagrams: a line and a three-pointed star. For example, the hyperplane arrangement corresponding to the *generic* three-point star graph consists of 11 boundary hyperplanes in generic position and the 3 twisted coordinate hyperplanes as usual. We find that this generic arrangement of the star graph has a total of 377 elements. The degenerate/physical arrangement has 12 lines where 4 of the boundary hyperplanes intersect, 18 points where 5 of the boundary hyperplanes intersect and 1 point where 8 of the boundary hyperplanes intersect. This is expected to reduce the number of independent elements by a considerable amount.

[28]While we have chosen to eliminate the forms associated with the intersection $S_1 \cap S_4 \cap S_5$, we could have chosen to eliminate the form associated to the intersections $S_1 \cap S_5 \cap S_6$, $S_1 \cap S_4 \cap S_6$ or $S_4 \cap S_5 \cap S_6$ instead.

Next we provide a basis of d log-forms orthonormal to the above dual basis. A d log-form dual to the 1-boundary form (2.98) is

$$\varphi_1 = \frac{1}{3}\,\mathrm{d}\log S_1 \wedge \mathrm{d}\log\left(\frac{T_1}{T_3}\right) \wedge \mathrm{d}\log\left(\frac{T_3}{T_2}\right). \tag{2.101}$$

The normalization of $1/3$ ensures that the intersection of (2.101) with (2.98) is unity. It is a simple exercise to see that this is indeed the correct normalization. First, it is easy to see that φ_1 only has a non-trivial overlap with $\check{\varphi}_1$. Their intersection $\langle\check{\varphi}_1|\varphi_1\rangle$ is proportional to the self-intersection of the canonical form corresponding to the chamber bounded on $X \cap S_1$. Thus, there are three-intersection points contributing to the intersection number. Since each T_i has the same twist, we expect each intersection point to contribute with the same factor. Hence, the normalization of $1/3$.

A set of d log-forms orthonormal to the 2-boundary forms (2.99) is

$$\begin{aligned}
&\varphi_2 = -\tfrac{1}{2}\,\mathrm{d}\log S_1 \wedge \mathrm{d}\log S_2 \wedge \mathrm{d}\log \tfrac{T_2}{T_3}, && \varphi_3 = -\tfrac{1}{2}\,\mathrm{d}\log S_1 \wedge \mathrm{d}\log S_3 \wedge \mathrm{d}\log \tfrac{T_1}{T_2},\\
&\varphi_4 = -\tfrac{1}{2}\,\mathrm{d}\log S_1 \wedge \mathrm{d}\log S_4 \wedge \mathrm{d}\log \tfrac{T_1}{T_3}, && \varphi_5 = -\tfrac{1}{2}\,\mathrm{d}\log S_1 \wedge \mathrm{d}\log S_5 \wedge \mathrm{d}\log \tfrac{T_1}{T_2},\\
&\varphi_6 = -\tfrac{1}{2}\,\mathrm{d}\log S_1 \wedge \mathrm{d}\log S_6 \wedge \mathrm{d}\log \tfrac{T_2}{T_3}, && \varphi_7 = -\tfrac{1}{2}\,\mathrm{d}\log S_2 \wedge \mathrm{d}\log S_6 \wedge \mathrm{d}\log \tfrac{T_2}{T_3},\\
&\varphi_8 = -\tfrac{1}{2}\,\mathrm{d}\log S_3 \wedge \mathrm{d}\log S_5 \wedge \mathrm{d}\log \tfrac{T_1}{T_2}, && \varphi_9 = -\tfrac{1}{2}\,\mathrm{d}\log S_5 \wedge \mathrm{d}\log S_6 \wedge \mathrm{d}\log \tfrac{T_1}{T_2},\\
&\varphi_{10} = -\tfrac{3}{2}\,\mathrm{d}\log S_5 \wedge \mathrm{d}\log S_6 \wedge \mathrm{d}\log T_3.
\end{aligned} \tag{2.102}$$

Following a similar argument as that below (2.98), the normalization's of these forms are simple to fix. The relative sign difference between the normalization of (2.102) and (2.101) comes from the fact that the dual twist has exponent $-\varepsilon$ and for each boundary we lose a power of $-\varepsilon$ in the intersection number. Furthermore, the reason why the normalization of φ_{10} differs from the rest is because it is the only form where the point at infinity (on $X \cap S_5 \cap S_6$) contributes to its self-intersection.

Lastly, a set of d log forms orthonormal to the 3-boundary forms (2.100) is

$$\begin{aligned}
&\varphi_{11} = \mathrm{d}\log S_1 \wedge \mathrm{d}\log S_2 \wedge \mathrm{d}\log S_3, && \varphi_{12} = \mathrm{d}\log S_1 \wedge \mathrm{d}\log S_2 \wedge \mathrm{d}\log S_4,\\
&\varphi_{13} = \mathrm{d}\log S_1 \wedge \mathrm{d}\log S_2 \wedge \mathrm{d}\log S_5, && \varphi_{14} = \mathrm{d}\log S_1 \wedge \mathrm{d}\log S_3 \wedge \mathrm{d}\log S_4,\\
&\varphi_{15} = \mathrm{d}\log S_1 \wedge \mathrm{d}\log S_3 \wedge \mathrm{d}\log S_6, && \varphi_{16} = \mathrm{d}\log S_1 \wedge \mathrm{d}\log S_4 \wedge \mathrm{d}\log S_5,\\
&\varphi_{17} = \mathrm{d}\log S_1 \wedge \mathrm{d}\log S_4 \wedge \mathrm{d}\log S_6, && \varphi_{18} = \mathrm{d}\log S_1 \wedge \mathrm{d}\log S_5 \wedge \mathrm{d}\log S_6 - \varphi_{10},\\
&\varphi_{19} = \mathrm{d}\log S_2 \wedge \mathrm{d}\log S_3 \wedge \mathrm{d}\log S_4, && \varphi_{20} = \mathrm{d}\log S_2 \wedge \mathrm{d}\log S_3 \wedge \mathrm{d}\log S_5,\\
&\varphi_{21} = \mathrm{d}\log S_2 \wedge \mathrm{d}\log S_3 \wedge \mathrm{d}\log S_6, && \varphi_{22} = \mathrm{d}\log S_2 \wedge \mathrm{d}\log S_4 \wedge \mathrm{d}\log S_6,\\
&\varphi_{23} = \mathrm{d}\log S_2 \wedge \mathrm{d}\log S_5 \wedge \mathrm{d}\log S_6 - \varphi_{10}, && \varphi_{24} = \mathrm{d}\log S_3 \wedge \mathrm{d}\log S_4 \wedge \mathrm{d}\log S_5,\\
&\varphi_{25} = \mathrm{d}\log S_3 \wedge \mathrm{d}\log S_5 \wedge \mathrm{d}\log S_6 - \varphi_{10}, && \varphi_{26} = \mathrm{d}\log S_4 \wedge \mathrm{d}\log S_5 \wedge \mathrm{d}\log S_6 - \varphi_{10}.
\end{aligned} \tag{2.103}$$

To have a orthogonal basis, we have to subtract φ_{10} from forms with non-trivial $S_5 \cap S_6$ residues since the intersections $\langle\check{\varphi}_{10}|\mathrm{d}\log S_\bullet \wedge \mathrm{d}\log S_5 \wedge \mathrm{d}\log S_6\rangle \sim \langle \mathrm{d}\log T_3|_{56}|\mathrm{d}\log S_\bullet\rangle \neq 0$ are non-vanishing. This is because both forms share a singularity at infinity on $X \cap S_5 \cap S_6$ and why it is best to choose d log-forms built out of ratios of the twisted hyperplanes when constructing a dual basis. Computing the dual differential equation using the method outlined in section 2.2.2 or 2.2.3 yields

$$\check{\nabla}\check{\varphi} = \varepsilon\, \check{\underline{\boldsymbol{A}}} \cdot \check{\varphi}, \tag{2.104}$$

$$\check{\underline{\boldsymbol{A}}} = \sum \check{\underline{\boldsymbol{A}}}\ \mathrm{dlog} a_i, \tag{2.105}$$

$X_1+X_2+X_3+Y_3$,	X_1+Y_1,	$X_2+X_3-Y_1+Y_3$,	X_3+Y_2,
$X_1+X_2-Y_2+Y_3$,	$X_2+Y_1+Y_2$,	$X_1+X_3-Y_1-Y_2+Y_3$,	$X_1+X_2+Y_2$,
$X_3-Y_2+Y_3$,	$X_2+X_3+Y_1$,	$X_1-Y_1+Y_3$,	$X_2-Y_1-Y_2+Y_3$,
$X_3-2Y_1-Y_2+Y_3$,	$X_2-Y_1+Y_2$,	$X_1-Y_1-2Y_2+Y_3$,	$X_2+Y_1-Y_2$,
X_1-Y_1,	X_3-Y_2,	$X_2+Y_1+Y_2-Y_3$,	$X_3+2Y_1-Y_2$,
	$X_1-Y_1+2Y_2$,	$X_1-X_3-Y_1+Y_2$	

Table 2.1: The alphabet for the differential equation a_i. For the generic arrangement, there are a total of 22 different letters. None of these letters are singular in the $Y_3 \to 0$ limit. The colored pairs of letters correspond to letters that are to be identified in the $Y_3 \to 0$ limit. Thus, the physical DEQ has only 19 letters. The symbol alphabet of the de Sitter three-site/five-point integral forms a subset of the physical 19 letters as expected [71, 70].

where the a_i are the letters in table 2.1 and the $\check{\underline{\boldsymbol{A}}}_i$ are 26×26 $\mathbb{Q}$-valued matrices. The exact form of these coefficient matrices can be found in the ancillary file (see figure 2.8 for the general structure or equation 2.118 for the explicit result). Of course, since $\langle\check{\varphi}_a|\varphi_b\rangle = \delta_{ab}$, we also have $\nabla\varphi_a = \varepsilon\, A_{ab}\wedge\varphi_b$ where $\underline{\boldsymbol{A}} = -(\check{\underline{\boldsymbol{A}}})^\top$.

Starting from the generic arrangement we will illustrate how to degenerate $\check{\underline{\boldsymbol{A}}}$ to the physical arrangement. This will suggest a way to treat the physical case directly without deforming the physical arrangement. Both methods have been checked to yield the same resulting differential equation.

In the limit $Y_3 \to 0$, the boundaries (or equivalently residues) $\delta_{145}, \delta_{146}, \delta_{156}$ and δ_{456} are not independent since the following intersection matrix does not have full rank

$$\langle\check{\varphi}_a|\varphi_b\rangle = \begin{pmatrix} 1 & 1 & 0 & 0 \\ 1 & 1 & 0 & 0 \\ -1 & 0 & 1 & 0 \\ 1 & 0 & 0 & 1 \end{pmatrix} \quad \text{where} \quad a,b \in \{16,17,18,26\}. \tag{2.106}$$

Choosing to eliminate φ_{16} and $\check{\varphi}_{16}$, yields

$$\check{\varphi}_{16} = \check{\varphi}_{17} \implies \delta_{145} = \delta_{146}, \tag{2.107}$$

$$\varphi_{16} = \varphi_{17} - \varphi_{18} + \varphi_{26}, \tag{2.108}$$

The second equation is an equivalence among $\mathrm{d}\log$-forms that can be checked directly. On the other hand, the first equation tells us that the residue operators Res_{145} and Res_{156} are equivalent and that we should identify δ_{145} and δ_{156}. Since all the $S_i \cap S_j \cap S_k$ are the same for $i,j,k \in \{1,4,5,6\}$ one might wonder why we do not identify all the δ_{ijk} with $i,j,k \in \{1,4,5,6\}$. Loosely speaking, the different δ_{ijk} with $i,j,k \in \{1,4,5,6\}$ represent the "directions" that one can approach the degenerate boundary. Such degenerate configurations often need careful treatment by blow-ups to resolve. Thankfully, the hyperplane arrangements associated to cosmological correlators are sufficiently simple that we can get by *without* introducing additional mathematical formalism – one simply finds the independent residues.

The physical DEQ is obtained from $\check{\underline{\boldsymbol{A}}}$ by eliminating the 16$^{\text{th}}$ row and adding the 16$^{\text{th}}$ column to the 17$^{\text{th}}$ column as instructed by equation (2.107). For the explicit form of $\underline{\boldsymbol{A}}_{\text{phys}}$, see the ancillary

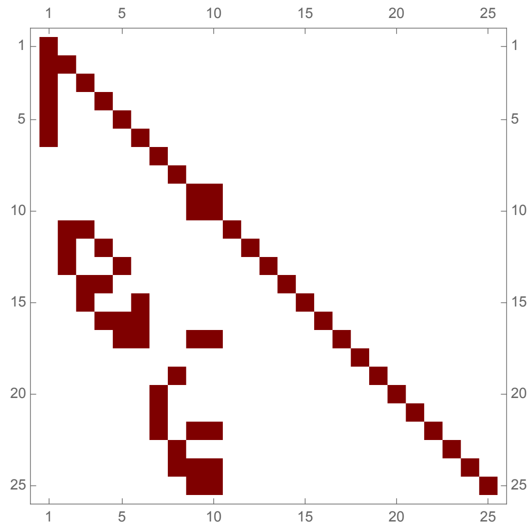

Figure 2.8: Matrix plot of the connection $\underline{\boldsymbol{A}}_{\text{phys}} = -\check{\underline{\boldsymbol{A}}}^{\top}_{\text{phys}}$. Each colored square on this 25×25 grid represents a non-zero element of $\check{\underline{\boldsymbol{A}}}_{\text{phys}}$. Note that this DEQ is very sparse!

files or equation (2.118). Figure 2.8 also provides a rough sketch of the structure of $\underline{\boldsymbol{A}}_{\text{phys}}$ without using up a whole page. Once again, a natural basis of the dual cohomology has lead to a remarkably sparse differential equation! As a consistency check, we note that the symbol alphabet for the dS wavefunction coefficient is a subset of our FRW symbol alphabet (2.117), as expected [71, 70].

Equivalently, one could compute the physical DEQ without introducing Y_3 by making the identification $\delta_{145} = \delta_{156}$ at the start of the calculation. To avoid missing potential boundary elements of the dual cohomology, we recommend that one assumes that all boundaries are independent and then check for relations among them. Complications from non-generic arrangements are unavoidable and present in both the dual and FRW cohomologies.

Once the $\underline{\boldsymbol{A}}_{\text{phys}}$ system has been integrated, the three-site/five-point FRW integral (2.94) can be recovered from the decomposition of its integrand

$$\psi^{(0)}_{3,\text{FRW}} = \frac{1}{4Y_1Y_2} \int u \, (\varphi_{11}-\varphi_{13}+\varphi_{15}-\varphi_{18}+\varphi_{19}-\varphi_{20}-\varphi_{21}+\varphi_{22}-\varphi_{24}+\varphi_{26})\,. \tag{2.109}$$

Since the dS wavefunction coefficient $\psi^{(0)}_{3,\text{dS}}$ has transcendental weight three, the leading FRW ($\mathcal{O}(\varepsilon)$) term must have transcendental weight four.

2.4 Discussions and future directions

The main goal of this work is to elucidate how (relative) twisted cohomology and intersection theory can be used to study the analytic structure of FRW integrals. In particular, we construct the differential equations obeyed by families of FRW integrals. The techniques presented here provide a geometric framework for understanding Euler/generalized hypergeometric integrals arising from hyperplane arrangements.

Families of FRW integrals form a particularly simple subset of such integrals where not all singularities are twisted. The un-twisted singularities correspond to boundaries in the associated dual cohomology leading to a simple geometric picture where dual forms are supported only on the boundaries. By working in the dual space, we gain both conceptual and computational advantages. In particular, integration-by-parts is much simpler in the dual cohomology since all forms are restricted to boundaries.

After defining the proper dual cohomology, we can use the intersection number – an inner product on the vector space of FRW integrals – to decompose any FRW integral into a chosen basis. In particular, the intersection number can be used to derive differential equations for a family of FRW integrals bypassing traditional integration-by-parts algorithms. Intersection numbers have several advantages over integration-by-parts algorithms. Most importantly, the intersection number is an algebraic procedure given by a sequence of residues localizing onto the maximal codimension intersection points of the FRW hyperplane arrangement. The use of the intersection number for studying FRW integrals is efficient and practical since the intersection number of $\mathrm{d}\log$-forms is easy to compute.

For various examples (tree-level two-site/four-point and three-site/five-point integrals as well as the one-loop two-site/two-point integral), we have constructed explicit representatives for a basis of the associated (relative) twisted cohomology. Then, using dual integration-by-parts identities or intersection numbers, we derived the corresponding differential equations. For the tree-level two-site/four-point example, we have explicitly integrated the differential equation to $\mathcal{O}(\varepsilon)$ and obtained the first correction (2.83) to the known de Sitter result (2.82).

As already mentioned a few times throughout the text, finding/choosing a "good" basis is often artisanal. Motivated by the geometry of the dual cohomology, our choices for a good basis yielded simple intersection matrices and sparse differential equations. Yet, from [75] it seems that one may be able to choose a basis where the differential equation decomposes into physical and un-physical sectors that can be integrated separately. It would be interesting to further study the physical and mathematical principles behind this basis choice and subsequent factorization of the differential equations.[29]

It would also be interesting to understand the cohomology in the de Sitter limit $\varepsilon \to 0$ where the twist disappears. Such an understanding would also be useful in the context of $\mathcal{N} = 4$ SYM amplitudes where one could hope to understand soft and collinear singularities cohomologically. Similarly, it would be interesting to understand the un-twisted cohomology of the $m = 1$ amplituhedron, which has been identified as the complex of bounded faces of a cyclic hyperplane arrangement in [119].

Another interesting question is whether the tools of intersection theory can be utilised to help understand how the constraints of bulk unitarity are encoded in cosmological correlators in a general FRW Universe (with a boundary). It has been recently pointed out in [120, 121, 122, 123] that unitarity imposes specific constraints that inflationary correlators have to satisfy, closely resembling

[29] A preliminary analysis reveals that the dual forms in the physical sector correspond to unitarity cuts of the physical integrand. The full analysis of this fact and the possibility of a canonical basis of physical integrals can be found in Chapter 3.

the optical theorem in flat space. These systematic cutting rules that cosmological correlators obey rely on very general properties of the Green's functions used to compute the wavefunction [123]. As a result, there lies no conceptual obstruction to generalizing these cutting rules to FRW wavefunction coefficients. However, with the Green's functions being rather complicated in a given FRW spacetime, such generalizations could be computationally cumbersome. Since intersection theory has also enhanced our understanding of d-dimensional generalized unitarity in multi-loop Feynman integrals [69, 68], it would be interesting to see if such techniques simplify some aspects of the cosmological cutting rules in a general FRW Universe, both at the level of trees and loops.

In this chapter, we considered correlation functions of a simplistic, toy-model FRW theory comprising solely of conformally coupled scalars with a cubic interaction. In such a scenario, our new result for the leading ε correction to the four-point function in dS (equation 2.83) could pave the way for understanding distinctive signatures during inflation and beyond. Like the analysis conducted in [82] where the four-point function in dS was utilised to understand distinctive signatures of primordial non-Gaussianities and also as a probe to predict new particles during inflation, the four-point function for $\varepsilon \neq 0$ (equation 2.83) is perhaps a first step towards understanding physics in an inflationary regime described by a quasi-dS period or physics beyond the reheating surface. Moreover, correlators of conformally-coupled scalars act as seeds from which correlators of massless/massive fields with higher-spin exchanges can be deduced by acting with differential operators [124]. Thus, our analysis serves as an initial step towards analysing physically relevant theories in FRW cosmologies and facilitating concrete cosmological predictions.

2.5 Appendix: Simple formulae for the intersection number of logarithmic forms

Fortunately, FRW-forms and their duals are always logarithmic so that the needed intersection numbers are easy to compute and purely combinatorial. To avoid getting bogged down by unnecessary mathematical formalism, we provide simple formulas to compute logarithmic intersection numbers without proof. The interested reader is encouraged to consult [107, 51, 59, 60, 108, 62, 63, 69, 68] and the references therein for more details.

To compute the intersection number, one first takes care of any δ_I's via

$$\left\langle \delta_I(\check{\phi}_I) \middle| \varphi \right\rangle = \left\langle \check{\phi}_I \middle| \mathrm{Res}_I \left[\frac{u}{u|_I} \varphi \right] \right\rangle \underset{\text{if } \varphi \text{ d log}}{=} \left\langle \check{\phi}_I \middle| \mathrm{Res}_I \left[\varphi \right] \right\rangle \equiv \langle \check{\phi}_I | \phi_I \rangle \,, \tag{2.110}$$

where ϕ_I is a short had for $\mathrm{Res}_I[\varphi]$. Since FRW-forms have only simple poles on S, the ratio $u/u|_I$ is not needed and can be set to unity in the second equality above. It is also important to note that the residue is anti-symmetric with respect to the ordering of I. In our conventions, we define Res_I by $\mathrm{Res}_I[\bullet] = \mathrm{Res}_{i_{|I|}} \cdots \mathrm{Res}_{i_2} \mathrm{Res}_{i_1}[\bullet]$.

After using up all the δ_J's, the remaining intersection number is an intersection number on the submanifold $X_I = X \cap S_I$. We provide a simple formula for its computation that localizes to the maximal codimension intersection points of the twisted surfaces. The algorithm presented here was first developed in [107] and we aim to provide a user friendly summary of this work.

The first step is to identify maximal intersection points of the twisted hyperplanes with themselves and the hyperplane at infinity (H_∞): $\mathbb{CP}^{n-|I|} \setminus (T \cap S_I) \cup H_\infty$. Let us call this set Int_I. For each intersection point, choose *normal* coordinates $\boldsymbol{z}^*$ such that the origin $\mathbf{0}$ corresponds to the intersection point. Then, the intersection number of logarithmic forms is given by

$$\left\langle \check{\phi}_I \middle| \mathrm{Res}_I\left[\varphi\right] \right\rangle = \sum_{\boldsymbol{z}^* \in \mathrm{Int}_I} \frac{\mathrm{Res}_{\boldsymbol{z}^*=\mathbf{0}}\left[\check{\phi}_I\right]}{\prod_{i=1}^{n-|I|}(\check{\alpha}_i)} \mathrm{Res}_{\boldsymbol{z}^*=\mathbf{0}}\Big[\mathrm{Res}_I\left[\varphi\right]\Big] \ , \tag{2.111}$$

where, near $\boldsymbol{z}^* = \mathbf{0}$, $\check{\omega}_I|_{\boldsymbol{z}^*} = \sum_{i=1}^{n-|I|} \check{\alpha}_i \ \mathrm{d}\log z_i^* + \mathcal{O}(\boldsymbol{z}^*)$. For those familiar with intersection theory, the first term in the product above is a stand-in for the leading term of the maximal primitive for $\check{\phi}_I$.

This formula makes it obvious that the intersection number vanishes if $\check{\phi}_I$ and $\mathrm{Res}_I\left[\varphi\right]$ do not share a singularity at any $\boldsymbol{z}^* \in \mathrm{Int}_I$. For FRW integrals, the $\check{\alpha}_i$ are simply multiples of ε (intersection points at infinity can introduce non-trivial multiples of ε).

2.5.1 Tree-level two-site example

As a simple example, we compute the intersection number $\langle\check{\varphi}_1|\vartheta_2\rangle$. Using the δ_3 in $\check{\varphi}_1$, we find

$$\langle\check{\varphi}_1|\vartheta_2\rangle = \left\langle \varepsilon \ \mathrm{d}\log\frac{T_1|_3}{T_2|_3} \middle| \mathrm{Res}_3\left[\mathrm{d}\log\frac{T_1}{S_2} \wedge \mathrm{d}\log\frac{S_2}{S_3}\right] \right\rangle = \varepsilon \left\langle \mathrm{d}\log\frac{T_1|_3}{T_2|_3} \middle| \mathrm{d}\log\frac{T_1|_3}{S_2|_3} \right\rangle . \tag{2.112}$$

Supposing that we eliminated x_2 when taking the δ_3 residue, there are three twisted intersection points in x_1: $\mathrm{Int} = \{0, -(X_1+X_2), \infty\}$. The left and right forms in the intersection number share singularities only at $x_1 = 0$. Thus, the intersection number evaluates to

$$\langle\check{\varphi}_1|\vartheta_2\rangle = \varepsilon \ \frac{\mathrm{Res}_{x_1=0}\left[\mathrm{d}\log\frac{T_1|_3}{T_2|_3}\right]}{-\varepsilon} \mathrm{Res}_{x_1=0}\left[\mathrm{d}\log\frac{T_1|_3}{S_2|_3}\right] = -1 \ , \tag{2.113}$$

since $\check{\omega} \sim -\varepsilon \ \mathrm{d}\log z^* + \mathcal{O}(z^*)$ near $z^* = x_1 = 0$.

2.5.2 Tree-level three-site example

In this section, we work through a more involved example: the intersection number $\langle\check{\varphi}_1|\varphi_1\rangle$ in the context of the tree-level three-site example. Taking care of the δ_1 in $\check{\varphi}_1$, yields

$$\langle\check{\varphi}_1|\varphi_1\rangle = \frac{\varepsilon^2}{3}\left\langle \mathrm{d}\log\left(\frac{T_1|_1}{T_3|_1}\right) \wedge \mathrm{d}\log\left(\frac{T_3|_1}{T_2|_1}\right) \middle| \mathrm{d}\log\left(\frac{T_1|_1}{T_3|_1}\right) \wedge \mathrm{d}\log\left(\frac{T_3|_1}{T_2|_1}\right) \right\rangle. \tag{2.114}$$

On $X \cap S_1$ there are three finite intersection points: $T_i|_1 \cap T_j|_1$ for $i,j \in \{1,2,3\}$ and $i \neq j$. Additionally, there are possible intersection points with the hyperplane at infinity H_∞. Thus, the set of intersection points are

$$\mathrm{Int} = \{T_1|_1 \cap T_2|_1, \ T_1|_1 \cap T_3|_1, \ T_2|_1 \cap T_3|_1, \ T_2|_1 \cap H_\infty, \ T_1|_1 \cap H_\infty, \ T_3|_1 \cap H_\infty\} \ . \tag{2.115}$$

Note that the intersection point $T_3|_1 \cap H_\infty$ appears in multiple charts of the $\mathbb{CP}^2$ and should only be counted once.

For the example at hand, only the finite intersection points will contribute since the forms are regular on the hyperplane at infinity. Then, for each of these intersection points, we use the corresponding hyperplanes as the normal coordinates $\boldsymbol{z}^* = \{T_i|_1, T_j|_1\}$. In these coordinates, the dual connection becomes $\check{\omega}|_1 = -\varepsilon\ \mathrm{d}\log z_1^* - \varepsilon\ \mathrm{d}\log z_2^* + \mathcal{O}(1)$ near each of the finite intersection points. Using (2.111), the intersection (2.114) becomes

$$\langle \check{\varphi}_1 | \varphi_1 \rangle = \frac{\varepsilon^3}{3} \left(\frac{3}{(-\varepsilon)^2} \right) = 1\ . \tag{2.116}$$

The factor of 3 simply comes from the fact that each of the three finite intersection points contribute the same factor of $1/(-\varepsilon)^2$ to the intersection number.

2.6 Appendix: Explicit presentation of the three-site/five-point differential equation

In this appendix, we record the physical differential equation $\underline{\boldsymbol{A}}_{\text{phys}} = -(\chi \underline{\boldsymbol{A}}_{\text{phys}})^\top$. Explicitly, the physical alphabet is

$$\begin{aligned} a_{i=1,\dots,19} = \big\{ & X_1{+}X_2{+}X_3,\ X_1{-}Y_1,\ X_2{+}X_3{-}Y_1,\ X_1{+}Y_1,\ X_2{+}X_3{+}Y_1,\ X_1{-}Y_1{-}2Y_2, \\ & X_1{+}X_2{-}Y_2,\ X_3{-}Y_2,\ X_3{-}2Y_1{-}Y_2,\ X_2{-}Y_1{-}Y_2,\ X_1{+}X_3{-}Y_1{-}Y_2, \\ & X_2{+}Y_1{-}Y_2,\ X_3{+}2Y_1{-}Y_2,\ X_1{+}X_2{+}Y_2,\ X_3{+}Y_2,\ X_2{-}Y_1{+}Y_2, \\ & X_1{-}X_3{-}Y_1{+}Y_2,\ X_2{+}Y_1{+}Y_2,\ X_1{-}Y_1{+}2Y_2 \big\}\ . \end{aligned} \tag{2.117}$$

Though a slight abuse of notation, we denote $\mathrm{d}\log(a_i)$ as a_i below in order to fit $\underline{\boldsymbol{A}}_{\text{phys}}$ on the page

$$\underline{\boldsymbol{A}}_{\text{phys}} = \left(\begin{array}{ccccccccccccccccccccccccc}
3a_1 & 0 & 0 & 0 & 0 & 0 & 0 & 0 & 0 & 0 & 0 & 0 & 0 & 0 & 0 & 0 & 0 & 0 & 0 & 0 & 0 & 0 & 0 & 0 & 0 \\
a_3-a_4 & 2a_3+a_4 & 0 & 0 & 0 & 0 & 0 & 0 & 0 & 0 & 0 & 0 & 0 & 0 & 0 & 0 & 0 & 0 & 0 & 0 & 0 & 0 & 0 & 0 & 0 \\
a_7-a_{15} & 0 & 2a_7+a_{15} & 0 & 0 & 0 & 0 & 0 & 0 & 0 & 0 & 0 & 0 & 0 & 0 & 0 & 0 & 0 & 0 & 0 & 0 & 0 & 0 & 0 & 0 \\
a_{18}-a_{11} & 0 & 0 & 2a_{11}+a_{18} & 0 & 0 & 0 & 0 & 0 & 0 & 0 & 0 & 0 & 0 & 0 & 0 & 0 & 0 & 0 & 0 & 0 & 0 & 0 & 0 & 0 \\
a_{14}-a_8 & 0 & 0 & 0 & a_8+2a_{14} & 0 & 0 & 0 & 0 & 0 & 0 & 0 & 0 & 0 & 0 & 0 & 0 & 0 & 0 & 0 & 0 & 0 & 0 & 0 & 0 \\
a_5-a_2 & 0 & 0 & 0 & 0 & a_2+2a_5 & 0 & 0 & 0 & 0 & 0 & 0 & 0 & 0 & 0 & 0 & 0 & 0 & 0 & 0 & 0 & 0 & 0 & 0 & 0 \\
0 & 0 & 0 & 0 & 0 & 0 & a_4+2a_5 & 0 & 0 & 0 & 0 & 0 & 0 & 0 & 0 & 0 & 0 & 0 & 0 & 0 & 0 & 0 & 0 & 0 & 0 \\
0 & 0 & 0 & 0 & 0 & 0 & 0 & 2a_{14}+a_{15} & 0 & 0 & 0 & 0 & 0 & 0 & 0 & 0 & 0 & 0 & 0 & 0 & 0 & 0 & 0 & 0 & 0 \\
0 & 0 & 0 & 0 & 0 & 0 & 0 & 0 & \frac{a_5}{2}+2a_{14}+\frac{a_{17}}{2} & \frac{a_5}{2}-\frac{a_{17}}{2} & 0 & 0 & 0 & 0 & 0 & 0 & 0 & 0 & 0 & 0 & 0 & 0 & 0 & 0 & 0 \\
0 & 0 & 0 & 0 & 0 & 0 & 0 & 0 & \frac{3a_5}{2}-\frac{3a_{17}}{2} & \frac{3a_5}{2}+\frac{3a_{17}}{2} & 0 & 0 & 0 & 0 & 0 & 0 & 0 & 0 & 0 & 0 & 0 & 0 & 0 & 0 & 0 \\
0 & a_{10}-a_{15} & a_{10}-a_4 & 0 & 0 & 0 & 0 & 0 & 0 & 0 & a_4+a_{10}+a_{15} & 0 & 0 & 0 & 0 & 0 & 0 & 0 & 0 & 0 & 0 & 0 & 0 & 0 & 0 \\
0 & a_{18}-a_9 & 0 & a_9-a_4 & 0 & 0 & 0 & 0 & 0 & 0 & 0 & a_4+a_9+a_{18} & 0 & 0 & 0 & 0 & 0 & 0 & 0 & 0 & 0 & 0 & 0 & 0 & 0 \\
0 & a_{16}-a_8 & 0 & 0 & a_{16}-a_4 & 0 & 0 & 0 & 0 & 0 & 0 & 0 & a_4+a_8+a_{16} & 0 & 0 & 0 & 0 & 0 & 0 & 0 & 0 & 0 & 0 & 0 & 0 \\
0 & 0 & a_6-a_{18} & a_{15}-a_6 & 0 & 0 & 0 & 0 & 0 & 0 & 0 & 0 & 0 & a_6+a_{15}+a_{18} & 0 & 0 & 0 & 0 & 0 & 0 & 0 & 0 & 0 & 0 & 0 \\
0 & 0 & a_2-a_{12} & 0 & 0 & a_{15}-a_{12} & 0 & 0 & 0 & 0 & 0 & 0 & 0 & 0 & a_2+a_{12}+a_{15} & 0 & 0 & 0 & 0 & 0 & 0 & 0 & 0 & 0 & 0 \\
0 & 0 & 0 & 2a_2-2a_8 & a_{18}-a_2 & a_8-a_{18} & 0 & 0 & 0 & 0 & 0 & 0 & 0 & 0 & 0 & a_2+a_8+a_{18} & 0 & 0 & 0 & 0 & 0 & 0 & 0 & 0 & 0 \\
0 & 0 & 0 & 0 & a_2-a_{18} & a_8-a_{18} & 0 & 0 & a_2+\frac{a_{17}}{2}-a_{18}-\frac{a_5}{2} & -\frac{a_5}{2}+a_8-\frac{a_{17}}{2} & 0 & 0 & 0 & 0 & 0 & 0 & a_2+a_8+a_{18} & 0 & 0 & 0 & 0 & 0 & 0 & 0 & 0 \\
0 & 0 & 0 & 0 & 0 & 0 & 0 & 0 & 0 & 0 & 0 & 0 & 0 & 0 & 0 & 0 & 0 & a_4+a_{15}+a_{18} & 0 & 0 & 0 & 0 & 0 & 0 & 0 \\
0 & 0 & 0 & 0 & 0 & 0 & 0 & a_4-a_{16} & 0 & 0 & 0 & 0 & 0 & 0 & 0 & 0 & 0 & 0 & a_4+a_{15}+a_{16} & 0 & 0 & 0 & 0 & 0 & 0 \\
0 & 0 & 0 & 0 & 0 & 0 & a_{15}-a_{12} & 0 & 0 & 0 & 0 & 0 & 0 & 0 & 0 & 0 & 0 & 0 & 0 & a_4+a_{12}+a_{15} & 0 & 0 & 0 & 0 & 0 \\
0 & 0 & 0 & 0 & 0 & 0 & a_8-a_{18} & 0 & 0 & 0 & 0 & 0 & 0 & 0 & 0 & 0 & 0 & 0 & 0 & 0 & a_4+a_8+a_{18} & 0 & 0 & 0 & 0 \\
0 & 0 & 0 & 0 & 0 & 0 & a_{13}-a_{16} & 0 & a_4-a_{16}+\frac{a_{17}}{2}-\frac{a_5}{2} & -\frac{a_5}{2}+a_{13}-\frac{a_{17}}{2} & 0 & 0 & 0 & 0 & 0 & 0 & 0 & 0 & 0 & 0 & 0 & a_4+a_{13}+a_{16} & 0 & 0 & 0 \\
0 & 0 & 0 & 0 & 0 & 0 & 0 & a_{18}-a_2 & 0 & 0 & 0 & 0 & 0 & 0 & 0 & 0 & 0 & 0 & 0 & 0 & 0 & 0 & a_2+a_{15}+a_{18} & 0 & 0 \\
0 & 0 & 0 & 0 & 0 & 0 & 0 & a_{19}-a_{12} & -\frac{a_5}{2}-a_{12}+\frac{a_{17}}{2}+a_{19} & -\frac{a_5}{2}+a_{15}-\frac{a_{17}}{2} & 0 & 0 & 0 & 0 & 0 & 0 & 0 & 0 & 0 & 0 & 0 & 0 & 0 & a_{12}+a_{15}+a_{19} & 0 \\
0 & 0 & 0 & 0 & 0 & 0 & 0 & 0 & a_2+\frac{a_{17}}{2}-a_{18}-\frac{a_5}{2} & -\frac{a_5}{2}+a_8-\frac{a_{17}}{2} & 0 & 0 & 0 & 0 & 0 & 0 & 0 & 0 & 0 & 0 & 0 & 0 & 0 & 0 & a_2+a_8+a_{18}
\end{array}\right) \tag{2.118}$$

Chapter 3

A Physical Basis for Cosmological Correlators from Cuts

This chapter is based on the work [125].

Cosmological correlators, or primitively, the wavefunction of the universe, are important quantum mechanical observables in cosmology. Recently, there has been tremendous progress in our perturbative understanding of the analytic structure of these observables in certain toy models of quantum cosmology, specifically for a theory of conformally coupled scalars with general polynomial interactions evolving in power-law Friedmann–Robertson–Walker (FRW) cosmologies.

Underlying many of these advances are the cosmological bootstrap [79, 80, 124, 126, 81, 127] and polytope [71, 128, 73] programs. The cosmological polytope provides a geometric and combinatorial way to compute wavefunction coefficients independent of the notions of locality, causality and unitarity baked into the formalism of Feynman diagrams. Techniques from the Feynman integral community[1] (related to algebraic geometry) have been used to compute canonical differential equations for both massless and massive wavefunction coefficients [49, 131, 132]. In particular, the kinematic flow algorithm has identified a powerful yet mysterious structure in these canonical differential equations [75, 76, 133, 134]. After accounting for the loop-momentum integration, elliptic sectors in these differential equations were identified in [135]; this is not surprising since the loop integrals defining wavefunction coefficients include all Feynman integrals, which are known to contain elliptic sectors. Ideas from tropical geometry and sector decomposition have been used to identify the origin of infrared divergences in the integration space and develop subtraction schemes [118]. Hypergeometric solutions, relations to GKZ-systems and D-modules have also been explored [136, 137, 138, 139, 140]. Cosmological cutting rules and implications from unitarity have been formalized [141, 142, 143, 144, 123, 121, 122, 120, 72, 145] and will play an important role in this paper.

In this toy model of conformal scalars in power-law FRW cosmologies, the wavefunction coefficient

[1] Additional connections include symbology [70] and Landau analysis [129, 130].

corresponding to a given Feynman graph $\mathcal{G}$ is represented as a certain *twisted* integral

$$\psi_n^{(\ell)} = \int_0^\infty u\, \Psi_n^{(\ell)} \quad \Psi_n^{(\ell)} := \hat{\Omega}_n^{(\ell)}(\mathbf{x}+\mathbf{X},\mathbf{Y})\, \mathrm{d}^n\mathbf{x}\ , \tag{3.1}$$

where n and ℓ are the number of vertices and loops in $\mathcal{G}$; for loop graphs, $\psi_n^{(\ell)}$ is the *loop integrand.* $\hat{\Omega}_n^{(\ell)}(\mathbf{X},\mathbf{Y})$ is the canonical function of the cosmological polytope $\mathcal{P}_{\mathcal{G}}$ associated to the graph $\mathcal{G}$ and is essentially the wavefunction coefficient for flat spacetimes. It depends on the kinematic parameters $X_i = \sum_{m=n_{i-1}+1}^{n_i} |\mathbf{k}_m|$, the sum of external energies flowing from the vertex i to the boundary, and $Y_i = |\sum_{m=n_{i-1}+1}^{n_i} \mathbf{k}_m|$, the energy exchanged through the i^{th} edge of a given graph $\mathcal{G}$:

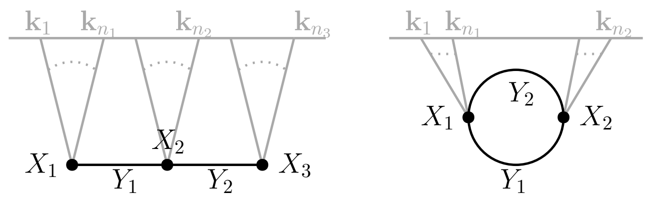

The *twist* u is a multi-valued function associated to a given graph. It is a product of polynomials raised to specific powers that depend on the underlying power-law cosmology (see below (3.9)).

The mathematical structure of these integrals is largely governed by the theory of twisted (co)homology [104, 146, 85, 49, 69, 57, 68, 108, 60]. Moreover, the twisted cohomology is a finite $|\chi|$-dimensional vector space, where χ is the Euler characteristic of the underlying hyperplane arrangement (equivalently, the number of bounded chambers). Due to the finite dimensionality of this vector space, the twisted integrals must satisfy coupled first-order linear differential equations (DEQs)

$$\mathrm{d}_{\text{kin}} \int u\, \varphi_i = B_{ij} \int u\, \varphi_j\ . \tag{3.2}$$

Here, the $\varphi_{j=1,\ldots,|\chi|}$ form a basis of differential forms for the twisted cohomology and $\mathrm{d}_{\text{kin}} = \sum_{i=1}^n \mathrm{d}X_i\ \partial_{X_i} + \sum_{i=1}^{n+\ell-1} \mathrm{d}Y_i\ \partial_{Y_i}$ is the exterior derivative with respect to the kinematic parameters.

When the connection matrix $\underline{\boldsymbol{B}}$ is proportional to the cosmological parameter ε, $\underline{\boldsymbol{B}} = \varepsilon\underline{\boldsymbol{A}}$, the associated basis is said to be *canonical* [97]. Such differential equations (DEQs) efficiently separate the kinematic dependence from the dependence on the cosmological parameter and are easy to integrate order-by-order in ε. They play a central role in the evaluation of dimensionally regulated Feynman integrals in flat-space and now cosmology.

Recently, efficient methods for computing the connection matrix $\underline{\boldsymbol{A}}$ have been developed [49, 76, 75, 118, 131]. In particular, the kinematic flow algorithm [76, 75, 134, 133] provides a diagrammatic way to choose a basis and evaluate the connection matrix $\underline{\boldsymbol{A}}$. Surprisingly, these universal graphical rules pick out a distinguished subset of integrals that include the physical wavefunction coefficient (3.1) and whose DEQs close. This physical subspace of integrals is vastly smaller than the total size of the twisted cohomology, which is easy to see at tree-level where the kinematic flow basis has size 4^{n-1}:

				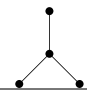
χ	4	25	213	312
4^{n-1}	4	16	64	64

So far the kinematic flow algorithm is an empirical observation; there is no satisfactory characterization of the physical subspace. Using intuition from generalized unitarity and algebro-geometric tools, we provide physical and mathematical origin for the physical subset of the twisted cohomology.

Our paper is organized as follows. In section 3.1, we review how to construct the relevant flat-space and FRW wavefunction coefficients for any Feynman graph. We also introduce the minimal set of ideas from (relative) twisted cohomology and intersection theory—mathematics underpinning the structure of cosmological wavefunction coefficients—needed to identify the physical subspace. In section 3.2, we demonstrate how the structure of the relative twisted cohomology—organized by cuts—clearly separates the space of all differential forms into three categories: physical, unphysical and degenerate. As a pedagogical example, we illustrate how to construct a basis for the physical subspace of the 3-site chain graph by further separating the space of degenerate differential forms into physical and unphysical forms in section 3.3. Section 3.4 systematically classifies the degeneracy of cosmological hyperplane arrangements by providing a simple graphical rule that generates all linear relations among hyperplane polynomials. Furthermore, we show how linear relations among hyperplane polynomials result in linear relations among residue operators and differential forms. In fact, the set of linear relations in conjunction with a cohomological condition is enough to classify all physical differential forms. Utilizing this, we develop graphical rules for constructing a basis of differential forms for the physical subspace by enumerating all physical cuts in section 3.5 for all tree and loop graphs.

3.1 Correlators from twisted integrals

As mentioned, our playground will be a theory of conformally-coupled scalars in a power-law FRW cosmology with (non-conformal) polynomial interactions. The action for such a theory in a $(d+1)$-dimensional spacetime is

$$\mathcal{S} = \int \mathrm{d}^d x \, \mathrm{d}\eta \sqrt{-g} \left[-\frac{1}{2} g^{\mu\nu} \partial_\mu \phi \partial_\nu \phi - \frac{d-1}{8d} R \phi^2 - \sum_{p \geq 3} \frac{\lambda_p}{p!} \phi^p \right] , \tag{3.3}$$

where the FRW metric $\mathrm{d}s^2 = a^2(\eta) \left[-\mathrm{d}\eta^2 + \mathrm{d}x_i \mathrm{d}x^i \right]$ is written in comoving coordinates with conformal time $\eta \in (-\infty, 0]$ and the index $i = 1, \dots, d$ runs over the spatial dimensions. The scale factor is a power-law controlled by the cosmological parameter ε: $a(\eta) = (\eta/\eta_0)^{-(1+\varepsilon)}$. Setting ε to specific integer values recovers well studied cosmologies [49, 75]. In particular, $0 < \varepsilon \ll 1$ is expected to capture the essential features of a near de Sitter inflationary cosmology.

Central to our analysis is the wavefunction of the universe $\Psi[\Phi]$. Formally, this is computed as a path integral by integrating over all bulk field conurations $\phi(\vec{x}, \eta)$ with non-vanishing Dirichlet boundary condition in the future $\phi(\vec{x}, \eta = 0) = \Phi(\vec{x})$. It is standard to work in momentum space where the wavefunction has the expansion

$$\begin{aligned}\Psi[\Phi] &= \int_{\phi(-\infty(1-i\epsilon))}^{\phi(0)=\Phi} \mathcal{D}\phi\, e^{iS[\phi]} \\ &\equiv \exp\left[i \sum_n \frac{1}{n!} \int \left(\prod_{i=1}^{n} \frac{\mathrm{d}^d \vec{k}_i}{(2\pi)^d} \Phi(\vec{k}_i) \right) \int \left(\prod_{j=1}^{\ell} \mathrm{d}^d \vec{L}_j \right) \psi^{(n,\ell)}(\{\vec{k}_i\})\, \delta^{(d)} \left(\sum_{i=1}^{n} \vec{k}_i \right) \right], \end{aligned} \tag{3.4}$$

and the standard $i\epsilon$ prescription selects the adiabatic/Bunch-Davies/Hartle-Hawking vacuum at the early-time boundary $\eta \to -\infty$. The kernels $\psi^{(n,\ell)}$ are the n-point *wavefunction coefficients* with n denoting the number of field insertions on the late-time boundary and $\{\vec{k}_i\}$ the corresponding set of all *spatial* momentum. In our analysis, we will be more interested in the number of vertices (or equivalently sites) in a graph $\mathcal{G}$ rather than the number of external fields on the future boundary. To differentiate this fact, the wavefunction coefficient for the n-site, ℓ-loop graph will be denoted by $\psi_n^{(\ell)}$. There has been significant progress in the perturbative computations of these wavefunction coefficients in the Bunch-Davies state, both for conformally-coupled scalars as well as massless and light states [71, 73]. Also, we note that $\vec{L}_j$ denote the loop momenta and consequently the wavefunction coefficient $\psi_n^{(\ell)}$ corresponds to the *loop integrand* of a given graph. For a discussion on the associated loop integrals and recent progress, please refer to [118, 147, 135].

The FRW wavefunction coefficients $\psi_n^{(\ell)}$ can be constructed out of their (*shifted*) flat-space counterparts $\hat{\Omega}_n^{(\ell)}$ (as expressed in (3.1)), which admit a purely geometric description in terms of the associated cosmological polytope. We review the cosmological polytope and the corresponding hyperplane arrangement in section 3.1.1. Then in section 3.1.2, we elaborate on how to uplift the flat-space canonical form to FRW spacetimes and the associated twisted cohomology. Section 3.1.3 reviews the the intersection number and dual relative twisted cohomology; our main tools for analyzing the analytic structure of FRW integrals.

3.1.1 The universal integrand

From a traditional QFT perspective, the FRW wavefunction coefficient $\psi_n^{(\ell)}$ is represented by a Feynman diagram $\mathcal{G}$ with n vertices and ℓ loops. However, the corresponding flat space coefficient $\hat{\Omega}_n^{(\ell)}$ from which it emerges can be defined without ever referencing "Feynman rules" and has a purely combinatorial-geometric origin as the *canonical form* of the cosmological polytope $\mathcal{P}_{\mathcal{G}}$ [71].

The cosmological polytope $\mathcal{P}_{\mathcal{G}}$ is a *positive geometry* encoding the singularity structure of wavefunction coefficients for conformally coupled scalars in flat spacetimes. A canonical form is the unique differential form (up to sign) that can be associated to a bounded region $\check{\Delta}$ with logarithmic singularities on its corresponding boundaries $\partial\check{\Delta}$. Moreover, the residue of a canonical form with respect to a boundary divisor is the canonical form of that boundary. The existence of a canonical form whose residues are all canonical forms is a recursive way to define a positive geometry [148].

For a given graph $\mathcal{G}$ (without external legs), there are a total of $2n+\ell-1$ kinematic parameters: $\{X_i\}_{i=1}^{n}$ and $\{Y_i\}_{i=1}^{n+\ell-1}$. The hyperplane polynomials, S_i, are generated by the 1-tubings of $\mathcal{G}$. A

1-tubing τ_i consists of two sets: the vertices $\mathcal{V}_i$ encircled by the tubing and the edges $\mathcal{E}_i$ that this tubing crosses. To each 1-tubing τ_i of the Feynman graph, the associated hyperplane polynomial is

$$S_i(\mathbf{X},\mathbf{Y}) = \sum_{v\in\mathcal{V}_i} X_v + \sum_{e\in\mathcal{E}_i} Y_e\,. \tag{3.5}$$

For example, the hyperplane polynomials for the 3-site tree level graph are

$S_1 =$ 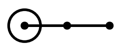 $= X_1{+}Y_1$, $S_2 =$ 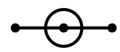 $= X_2{+}Y_1{+}Y_2$,

$S_3 =$ 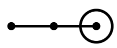 $= X_3{+}Y_2$, $S_4 =$ 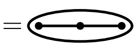 $= X_1{+}X_2{+}X_3$,   (3.6)

$S_5 =$ 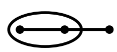 $= X_1{+}X_2{+}Y_2$, $S_6 =$ 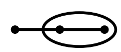 $= X_2{+}X_3{+}Y_1$.

This 3-site tree level chain graph will be an important pedagogical example to illustrate our main ideas in section 3.3.

Usually, the simplest way to compute the canonical form is by summing rational functions associated with the set of compatible complete tubings (non-crossing $(2n{+}\ell{-}1)$-tubings) of a given graph $\mathcal{G}$ [71]. Explicitly, if T is the set of compatible complete tubings, the canonical form $\Omega_n^{(\ell)}$ and function $\hat{\Omega}_n^{(\ell)}$ are

$$\Omega_n^{(\ell)} = \hat{\Omega}_n^{(\ell)}(\mathbf{X},\mathbf{Y})\frac{\mathrm{d}^n\mathbf{X}\wedge\mathrm{d}^{n+\ell-1}\mathbf{Y}}{\mathrm{GL}(1)}, \qquad \hat{\Omega}_n^{(\ell)}(\mathbf{X},\mathbf{Y}) = \mathcal{N}_n^{(\ell)}\sum_{\tau\in\mathsf{T}}\prod_{t\in\tau}\frac{1}{S_t}\,, \tag{3.7}$$

and $\mathcal{N}_n^{(\ell)} = \prod_{i=1}^{n+\ell-1} 2Y_i$ is a normalization factor ensuring that the canonical form has unit residues. Returning to the 3-site example, the canonical function is

$\hat{\Omega}^{(0)}_{\text{3-chain}}(\mathbf{X},\mathbf{Y}) = 4Y_1Y_2 \Big[$ 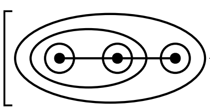 $+$ 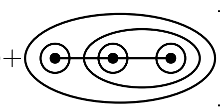 $\Big] = \dfrac{4Y_1Y_2}{S_1\cdots S_4}\left(\dfrac{1}{S_5}+\dfrac{1}{S_6}\right)$ (3.8)

where, in this context, each 5-tubing corresponds to the inverse of the product of the depicted S_i's.

3.1.2 From flat-space to FRW spacetimes

Importantly, the flat-space wavefunction coefficients/canonical forms define a universal integrand for their counterparts in *any* power-law FRW spacetime. For any $\varepsilon \notin \mathbb{Q}$, this is obtained by integrating the shifted flat-space wavefunction against a specific kernel u called the *twist*,

$$\psi_n^{(\ell)} = \int_0^\infty u\ \Psi_n^{(\ell)}\,, \quad \text{where} \quad \Psi_n^{(\ell)} = \hat{\Omega}_n^{(\ell)}(\mathbf{x}+\mathbf{X},\mathbf{Y})\ \mathrm{d}^n\mathbf{x}\,, \tag{3.9}$$

Here, $u = \prod_{i=1}^n x_i^{\alpha_i}$ is a multi-valued function ($\alpha_i \notin \mathbb{Z}$) called the *twist* whose vanishing loci defines the twisted hyperplanes $\mathcal{T}_i = \{x_i = 0\}$ (coordinate hyperplanes). The exponents α_i are related to the underlying power-law cosmology (ε), number of spatial dimensions (d) and valency of the i^{th} vertex (p_i):

$$\alpha_i = d + \varepsilon(d+1) + \frac{1}{2}p_i(1+\varepsilon)(1-d) \notin \mathbb{Z}\,. \tag{3.10}$$

The condition $\varepsilon \notin \mathbb{Q}$ guarantees that $\alpha_i \notin \mathbb{Z}$, which is essential for the techniques of twisted cohomology employed in this paper. However, it is important to note that one can often specialize to the case $\alpha_i \in \mathbb{Z}$ by an analytic continuation of the case $\alpha_i \notin \mathbb{Z}$. In the remainder of this paper, we assume $d = 3$ and $p_i = 3$ such that $\alpha_i = \varepsilon$ for all vertices and $u = \prod_{i=1}^{n} x_i^{\varepsilon}$.[2]

As seen above in (3.9), the FRW form $\Psi_n^{(\ell)}$ is simply generated from the canonical function $\hat{\Omega}_n^{(\ell)}(\mathbf{X}, \mathbf{Y})$ of the cosmological polytope by a shift in its $\mathbf{X}$-variables. We denote the shifted linear factors appearing in the FRW form $\Psi_n^{(\ell)}$ by

$$B_i(\mathbf{x}; \mathbf{X}, \mathbf{Y}) = S_i(\mathbf{x} + \mathbf{X}, \mathbf{Y}) \,. \tag{3.11}$$

Then,

$$\Psi_n^{(\ell)} = \mathrm{d}^n\mathbf{x} \left(\prod_{i=1}^{n+\ell-1} 2Y_i \right) \left(\sum_{\tau \in \mathsf{T}} \prod_{t \in \tau} \frac{1}{B_t} \right) \,, \tag{3.12}$$

where T is the set of compatible complete tubings of a given graph $\mathcal{G}$.

Since our objective is understanding the mathematical structure of wavefunction coefficients for arbitrary ε, our primary focus is the hyperplane arrangement generated by both the B_i and T_i not the cosmological polytope $\mathcal{P}_{\mathcal{G}}$ (generated solely by the S_i's).[3] Explicitly, we wish to classify the differential forms on the topological space $M \setminus \mathcal{B}$ where

$$M{:=}\mathbb{C}^n \setminus \mathcal{T} \,, \quad \mathcal{T}{:=}\bigcup_{i=1}^{n} \mathcal{T}_i \,, \quad \mathcal{T}_i{:=}\{x_i = 0\} \,, \quad \mathcal{B}{:=}\bigcup_{j} \mathcal{B}_j \,, \quad \text{and} \qquad \mathcal{B}_j{:=}\{B_j = 0\} \,. \tag{3.13}$$

This requires understanding the associated twisted cohomology $H^n(M \setminus \mathcal{B}; \nabla)$; the cohomology with respect to the covariant derivative $\nabla := \mathrm{d} + \omega \wedge$ with flat connection $\omega = \mathrm{d}\log u$

$$H^n(M \setminus \mathcal{B}; \nabla) := \frac{\text{covariantly closed } n\text{-forms on } M \setminus \mathcal{B}}{\text{covariantly exact } n\text{-forms on } M \setminus \mathcal{B}} \,. \tag{3.14}$$

It classifies all non-trivial (do not integrate to zero) differential n-forms on $M \setminus \mathcal{B}$ that can have poles on the untwisted singular loci $\mathcal{B}$ and twisted loci $\mathcal{T}$ (coordinate axes). Explicitly, the twisted cohomology of FRW integrals is populated by forms

$$\varphi \sim \frac{P(\mathbf{x})\, \mathrm{d}^n\mathbf{x}}{\prod_i T_i^{\mu_i} \prod_j B_j^{\nu_j}} \in H^n(M \setminus \mathcal{B}; \nabla) \tag{3.15}$$

where $\mu_i, \nu_i \in \mathbb{Z}$ and $P(\mathbf{x})$ is any polynomial in $\mathbf{x}$. While the above is automatically covariantly closed ($\nabla\varphi = 0$) since it is a holomorphic top-form, it may or may not be covariantly exact. Depending on P, it is possible for φ to be exact $\varphi = \nabla[(n-1)\text{-form}] \simeq 0$ and lie outside of $H^n(M \setminus \mathcal{B}; \nabla)$.

Importantly, the integrand of these twisted integrals (i.e., $u\, \Psi_n^{(\ell)}$ or any other $u\, \varphi$) exhibit very different behavior near the twisted and untwisted singular loci. Due to the twist u, there exists

[2] Technically, our cosmological model (3.3) needs at least quartic interactions (only terms with $p \geq 4$ in (3.3)) to ensure that the kinematic space of the ($\ell \geq 1$)-loop 2-site graphs are non-trivial. However, when we treat these integrals in section 3.5, the specific form of the twist is not important.

[3] We refer to this structure as the "FRW cosmological polytope" to remind ourselves that it is defined in $\mathbf{x}$-space like the FRW form $\Psi_n^{(\ell)}$. In an abuse of notation, we will also refer to the FRW cosmological polytope by $\mathcal{P}_{\mathcal{G}}$.

a choice of ε such that integral in a local neighborhood of where an x_i vanishes converges; the integral for all other "non-convergent" values of ε are well defined through analytic continuation. On the other hand, nothing saves the integral from blowing up whenever a B_i vanishes. Therefore, singularities at $B_i = 0$ and $x_i = 0$ must be managed differently. This has already been partially accounted for in the covariant derivative ∇ since the connection ω has singularities on the twisted hyperplanes. From the perspective of contours, B_i-residues of the integrand are allowed but x_i-residues are not since the coordinate axes are branch surfaces ($u \sim x_i^{\alpha_i}$ with $\alpha_i \notin \mathbb{Z}$).[4] This distinction places crucial restrictions on the kind of allowed contours and cuts. This will be most obvious in the dual cohomology defined in section 3.1.3 where each dual form can be thought of as a coarse approximation to a cut contour. This is made precise in appendix 3.7 and will play an important role in the development of a diagrammatic coaction method [149, 150].

3.1.3 The intersection number and relative twisted cohomology

The *intersection number* $\langle\check{\varphi}|\varphi\rangle$ defines an *inner product* on the space of twisted differential forms (and therefore, cosmological integrals) by pairing an element of FRW cohomology $\varphi \in H^n(M\setminus\mathcal{B};\nabla)$ (recall (3.14)) with an element of the associated dual cohomology $\check{\varphi} \in \chi H^n$ (defined in (3.17)). The dual cohomology has more structure than its FRW counterpart since it is essentially the direct sum of the the twisted cohomology of each cut. Therefore, it is automatically organized in an ideal way for understanding cuts. It is also easily linked to the space of contours on the topological space $M \setminus \mathcal{B}$ (see appendix 3.7).

The intersection number is the link between the FRW cohomology and dual cohomology

$$\langle\check{\varphi}|\varphi\rangle : H^n(M,\mathcal{B};\chi\nabla) \times H^n(M\setminus\mathcal{B};\nabla) \mapsto \mathbb{C}\,. \tag{3.16}$$

For FRW correlators, the intersection number is easy to compute; it is simply a weighted residue where the dual forms dictate the exact linear combination ((3.19) and (3.21)). Moreover, the intersection number facilitates a simple formula for computing the differential equation in a way that emphasizes the role of cuts (demonstrated in section 3.2). From this formula, we deduce that an FRW form φ couples to $\partial_{X_i}\Psi_n^{(\ell)}$ or $\partial_{Y_i}\Psi_n^{(\ell)}$ if and only if φ shares a cut with the FRW form $\Psi_n^{(\ell)}$ (also in section 3.2).

The dual cohomology to (3.14) is the *relative*[5] twisted cohomology

$$\chi H^n := H^n(M,\mathcal{B};\chi\nabla) \subseteq \bigoplus_{p=0}^{n}\bigoplus_{|J|=p} \delta_J\left(H^{n-p}(M_J;\chi\nabla|_J)\right)\,, \qquad \chi\nabla = \mathrm{d} - \omega\wedge\,, \tag{3.17}$$

where J is a multi-index denoting a cut, $M_J = M \cap \mathcal{B}_J$ is the topological space associated to this cut and $\mathcal{B}_J = \cap_{j\in J}\{B_j = 0\}$. Importantly, dual forms are represented by twisted differential forms

[4] For forging connections to cosmological spacetimes one will generally encounter cases where $\alpha_i = \varepsilon \in \mathbb{Z}$. We note that the DEQs (and their solutions) for twisted cosmological integrals can be analytically continued in ε and one can extract the physical wavefunction by taking appropriate limits.

[5] Name for the cohomology of a topological space with boundaries ($\mathcal{B}$ in our case).

localized to the cuts M_J. The localization to the cut M_J is denoted by the coboundary symbol δ_J[6] and its argument contains a differential form on M_J:

$$\check{\varphi} = \sum_J \delta_J(\phi_J)\,, \qquad\qquad \phi_J \in H^{n-|J|}(M_J; \chi\nabla|_J)\,. \tag{3.18}$$

The δ_J indexes the component of the direct sum corresponding to the J-boundary cohomology and keeps track of boundary terms.[7] They are also anti-symmetric in their indices $\delta_{ij} = -\delta_{ji}$ and induce a residue/cut inside the intersection number

$$\langle \delta_J(\check{\phi})|\varphi\rangle = \left\langle \check{\phi} \middle| \mathrm{Res}_J[\varphi] \right\rangle_J =: \langle \check{\phi}|\phi_J\rangle_J\,, \tag{3.19}$$

where

$$\mathrm{Res}_J[\bullet] := \mathrm{Res}_{j_1\cdots j_{|J|}}[\bullet] := \mathrm{Res}_{\mathcal{B}_{j_{|J|}}\cap\cdots\cap\mathcal{B}_{j_2}\cap\mathcal{B}_{j_1}} \circ \mathrm{Res}_{\mathcal{B}_{j_2}\cap\mathcal{B}_{j_1}} \circ \mathrm{Res}_{\mathcal{B}_{j_1}}\;, \tag{3.20}$$

denotes the iterated residue.

After taking care of the coboundary operators, the remaining intersection number $\langle\check{\phi}|\phi_J\rangle_J$ localizes to the maximal codimension intersection points of the twisted surfaces on the cut.[8] Since $\langle\check{\phi}|\phi_J\rangle_J$ only plays a minor role in the remainder of this article, its definition has been relegated to footnote 8. While equation (3.19) (and (3.21)) are sufficient for our purposes, it is important to note that they are *only valid for logarithmic differential forms*; there are known corrections to these formulas if the forms have higher order poles [107, 60].

3.2 DEQs from residues and finding the physical subspace

We choose a spanning set for both dual and FRW forms that makes the cut structure manifest. The first step is to determine which cuts have a non-trivial twisted cohomology. This is done by computing the Euler characteristic of each cut surface $\chi_J = \chi(M_J)$ and putting $|\chi_J|$-many canonical forms into the coboundary operator

$$\{\check{\varphi}_a\}_{a=1}^{\sum_J |\chi_J|} = \bigcup_J \left\{\delta_J(\Omega_{J,k})\right\}_{k=1}^{|\chi_J|}\,, \tag{3.22}$$

Importantly, the canonical forms are non-singular at infinity and are always a linear combination of $\mathrm{dlog}T_i|_J \wedge \cdots \wedge \mathrm{dlog}T_k|_J$. Dual forms are closely related to cut contours; they are the *dual canonical*

[6] See [49, 69, 68] for a more in-depth explanation of the coboundary and its properties. See [151] for a more formal exposition in the context of (untwisted) homology.

[7] While not explicitly used in this work, boundary terms are generated by the derivative in the dual relative twisted cohomology: $\mathrm{d}\delta_J(\phi_J) = (-1)^{|J|}\left[\delta_J(\mathrm{d}\phi_J) + \sum_{i\notin J}\delta_{Ji}(\phi_J|_i)\right]$.

[8] Explicitly,

$$\langle\check{\phi}|\phi_J\rangle_J = \sum_{\boldsymbol{z}^*\in\mathrm{Int}_J} \frac{\mathrm{Res}_{\boldsymbol{z}^*=\boldsymbol{0}}[\check{\phi}]\mathrm{Res}_{\boldsymbol{z}^*=\boldsymbol{0}}[\phi_J]}{\prod_{i=1}^{n-|J|}\mathrm{Res}_{z_i^*=0}[\omega]}\,, \tag{3.21}$$

and only plays a minor role in the remainder of this paper. Here, $\mathrm{Int}_J = \bigcup_{K:|K|=n-|J|}(\mathcal{B}_J\cap\mathcal{T}_K)$ and $\mathcal{T}_K := \bigcap_{k\in K}\mathcal{T}_k$. See appendix A of [49] for a more detailed discussion.

form of a cut contour and the intersection number is the leading order term of the cut integral (see appendix 3.7).

For the FRW cohomology, we choose the set

$$\{\varphi_a\}_{a=1}^{\sum_J |\chi_J|} = \bigcup_J \left\{ \mathrm{dlog}_J \wedge \tilde{\Omega}_{J,k} \right\}_{k=1}^{|\chi_J|} \quad \text{where} \quad \mathrm{dlog}_J := \bigwedge_{j \in J} \mathrm{dlog} B_j \,, \tag{3.23}$$

and $\tilde{\Omega}_{J,k}$ is obtained from $\Omega_{J,k}$ by removing the restriction to the cut J acting on the T_i's (an explicit example of this procedure is given in section 3.3 and diagrammatic rules are provided in section 3.5). By organizing the bases according to the cuts automatically produces a block diagonal intersection matrix

$$C_{ab} := \langle \check{\varphi}_a | \varphi_b \rangle = \langle \delta_I(\Omega_{I,k}) | \mathrm{dlog}_J \wedge \tilde{\Omega}_{J,l} \rangle = \delta_{IJ} \langle \Omega_{J,k} | \Omega_{J,l} \rangle_J \ . \tag{3.24}$$

where $\Omega_{J,k} = \tilde{\Omega}_{J,k}|_J$. Note that it is easy to translate between these two sets via the replacement $\delta_J(\Omega) \leftrightarrow \mathrm{dlog}_J \wedge \tilde{\Omega}$.[9]

The intersection number facilitates a simple formula for the DEQs in terms of residues that highlights the importance of cuts. Schematically, the connection matrix takes the form[10]

$$A_{ab} \sim \left\langle \delta_{J_b}(\check{\phi}_b) \middle| \nabla_{\mathrm{kin}} \varphi_a \right\rangle = \left\langle \check{\phi}_b \middle| \mathrm{Res}_J [\nabla_{\mathrm{kin}} \varphi_a] \right\rangle_{J_b} \to 0 \text{ whenever } \mathrm{Res}_{J_b}[\nabla_{\mathrm{kin}} \varphi] = 0 \,. \tag{3.25}$$

This equation implies that φ_b couples to φ_a in the DEQ if and only if both φ_a and φ_b share a residue since[11]

$$\mathrm{Res}_{J_b}[\nabla_{\mathrm{kin}} \varphi_a] = 0 \iff \mathrm{Res}_{J_b}[\varphi_a] = 0 \,. \tag{3.26}$$

This implies that the physical subspace is spanned by all FRW forms in (3.23) that have overlapping residues with the physical wavefunction. More explicitly,

$$\boxed{H^n_{\mathrm{phys}} \subset \mathrm{Span} \left\{ \mathrm{dlog}_J \wedge \tilde{\Omega}_J \right\}_J \quad \text{such that} \quad \mathrm{Res}_J[\Psi^{(\ell)}_n] \neq 0 \,.} \tag{3.27}$$

This is the first main result of this paper. Moreover, (3.25) and (3.26) imply that dlog_J-forms only couple to themselves and $\mathrm{dlog}_{J\setminus j}$-forms where $j \in J$.

If the FRW hyperplane arrangement was non-degenerate, (3.27) would be the whole story. However, as we will see shortly (section 3.3), even simple cosmological examples are *non-generic* or *degenerate* and we have to work a bit harder to reduce (3.27) from a spanning set to a basis. We will discuss how to systematically work with this degeneracy in the remainder of this article.

---

[9] Technically, the sets (3.22) and (3.23) are not quite dual since the intersection matrix (3.24) is only block diagonal and not full rank. However, this technicality will dealt with shortly in a simple way.

[10] The precise formula is $A_{ab} = C^{-1}_{bc} \langle \check{\varphi}_c | \nabla_{\mathrm{kin}} \varphi_a \rangle$. It will be used to compute the DEQs in section 3.3 as well as appendices 3.9.2 and 3.9.4.

[11] In order to use equations (3.19) and (3.21), one needs a representation for $\nabla_{\mathrm{kin}} \varphi$ that has at most simple poles. We provide a simple recipe for such a representative for $\nabla_{\mathrm{kin}} \varphi$ *without* invoking integration-by-parts in appendix 3.8. We also derive (3.26) as a consequence.

3.3 A pedagogical example: the 3-site chain

We illustrate how the physical subspace arises by organizing the basis of forms according to whether they have compatible sequential residues with the physical FRW form in the context of the simplest example: the 3-site chain. Moreover, we highlight how the associated hyperplane arrangement dictates this organization; a ubiquitous feature for all tree-level and loop-level cosmological arrangements. We comment on further worked examples (the 4-site chain, 4-site star and 1-loop 3-gon of appendix 3.9) near the end of this section.

The hyperplane polynomials: For the convenience of the reader, we collect the 3-site FRW hyperplane polynomials B_i (shifted versions of (3.6))

$B_1 =$ 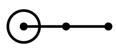 $= x_1+X_1+Y_1$, $\quad B_2 =$ 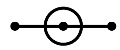 $= x_2+X_2+Y_1+Y_2$,

$B_3 =$ 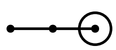 $= x_3+X_3+Y_2$, $\quad B_4 =$ 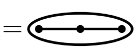 $= x_1+x_2+x_3+X_1+X_2+X_3$, (3.28)

$B_5 =$ 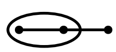 $= x_1+x_2+X_1+X_2+Y_2$, $\quad B_6 =$ 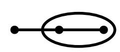 $= x_2+x_3+X_2+X_3+Y_1$.

The FRW form: Following the discussion in section 3.1.2, the FRW form (shifted version of (3.8)) is

$$\Psi_3^{(0)} = \frac{4Y_1Y_2}{B_1\cdots B_4}\left(\frac{1}{B_5}+\frac{1}{B_6}\right)\mathrm{d}^3\mathbf{x}\,. \tag{3.29}$$

Recalling (3.13), this is a differential form on the space $M \setminus \mathcal{B}$ where

$$M := \mathbb{C}^3 \setminus \{x_1x_2x_3 = 0\}\,, \qquad \mathcal{B} := \bigcup_{i=1}^{6} \mathcal{B}_i\,, \qquad \mathcal{B}_i := \{B_i = 0\}\,. \tag{3.30}$$

In the following, we will also be interested in the space M after taking a sequential residue Res_J. We denote these topological spaces by $M_J := M \cap \mathcal{B}_J$ where $\mathcal{B}_J = \cap_{j\in J}\mathcal{B}_j$.

A linear relation among hyperplane polynomials: The associated hyperplane arrangement is highly non-generic or degenerate due to a linear relation between the FRW hyperplane polynomials of (3.28).[12] A graphical representation for the 3-site hyperplane polynomial relation is

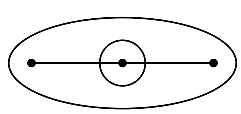 $\Big|_+ =$ 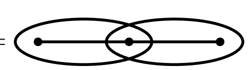 $\Big|_+ \iff B_2 + B_4 = B_5 + B_6\,,$ (3.31)

where $|_+$ instructs us to add the B_i associated to the 2-tubings. This relation implies that the four hyperplanes $\{\mathcal{B}_4, \mathcal{B}_5, \mathcal{B}_6, \mathcal{B}_2\}$ intersect in codimension-3 instead of codimension-4. Therefore, the geometry of the following 3-cuts is not unique: $M_{4,5,2} = M_{4,6,2} = M_{4,5,6} = M_{5,6,2}$. This will have important consequences for the space of residue operators and differential forms.

[12] By non-generic or degenerate, we mean that there exists a collection of $|J|$ hyperplanes $\{\mathcal{B}_{j\in J}\}$ that intersect in codimension-m where $m < |J|$.

Cuts and residues: Following the discussion in section 3.1.3 (in particular (3.17) and (3.22)), it is clear that the dual cohomology is built by constructing the cohomology of each cut. Excluding the 0-cut, which is M itself (recall (3.13)), the 3-site chain has a total of 37 cuts:

- There are 6 possible 1-cuts (the space M after taking the residues on each of the six B_i's in (3.28))

$$\{M_1, M_2, M_3, M_5, M_6, M_4\}\ . \tag{3.32}$$

  These are 2-dimensional topological spaces (codimension-1). As we will see, the gray M_J will turn out to have trivial cohomology.

- There are $\binom{6}{2} = 15$ possible 2-cuts, each of which are 1-dimensional (codimension-2)

$$\begin{aligned}\{&M_{1,2}, M_{1,3}, M_{5,1}, M_{2,3}, M_{5,2}, M_{6,2}, M_{6,3},\\ &M_{4,1}, M_{6,1}, M_{4,2}, M_{4,3}, M_{5,3}, M_{4,5}, M_{4,6}, M_{5,6}\}\ .\end{aligned} \tag{3.33}$$

- Lastly, there are sixteen 3-cuts

$$\begin{aligned}\Big\{&M_{1,2,3}, M_{4,1,2}, M_{6,1,2}, M_{4,1,3}, M_{5,1,3}, M_{6,1,3}, M_{4,5,1}, M_{5,6,1},\\ &M_{4,2,3}, M_{5,2,3}, M_{4,6,3}, M_{5,6,3}, M_{4,5,2}, M_{4,6,2}, M_{5,6,2}, M_{4,5,6}\Big\}\ .\end{aligned} \tag{3.34}$$

  These are 0-dimensional topological spaces consisting of only a point. Note that a fully generic arrangement would have produced $\binom{6}{3} = 20$ codimension-3 boundaries. In our case, four are missing because some cuts do not exist: $M_{4,5,3} = M_{4,6,1} = M_{5,1,2} = M_{6,2,3} = \varnothing$. That is, the associated hyperplanes to these cuts do not intersect.

Cut ordering

The cut multi-index J in δ_J, Res_J and M_J is *always* ordered such that the associated 1-tubings with the most vertices comes first. For tubings of the same size, we proceed in lexicographical order. Symbolically, if $|\tau_i| = |\mathcal{V}_i|$ is the number of vertices inside the tubing τ_i, we require $|\tau_{j_i}| \geq |\tau_{j_{i+1}}|$ for $J = \{j_1, j_2, \cdots\}$.

While ad hoc now, the physical reason will become clear in section 3.5. Mathematically, an order is necessary to resolve the mentioned degeneracies (more in section 3.4).[13]

Building a basis from the geometry of cuts: To generate elements of the dual cohomology, we search for cuts with bounded chambers. The 0-cut, M, has no bounded chambers and therefore does not generate a potential basis element. This is a general feature of all FRW arrangements; the 0-cut will never generate an interesting form.

[13]We thank Clément Dupont and Lecheng Ren for important discussions regarding this point.

Of all the 1-cuts, only the total energy cut M_4 has a bounded chamber. For example,

$M_5 =$ 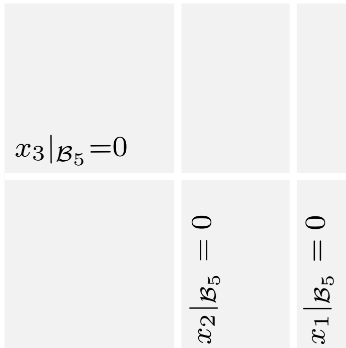

, $M_4 =$ 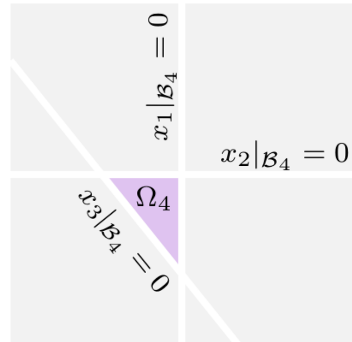

, (3.35)

where the white lines are removed from $\mathbb{C}^2$. Evidently, there is no bounded chamber in M_5. To see this, solve $B_5 = 0$ by eliminating x_2. Then, $\mathbf{x}|_{\mathcal{B}_5} = (x_1, -(x_1 + X_1 + X_2 + Y_2), x_3)$. Clearly, the first two components define parallel lines as depicted above. However, there is a single bounded chamber in M_4. This can be seen by solving the condition $B_4 = 0$ and eliminating x_3. Then, $\mathbf{x}|_{\mathcal{B}_4} = (x_1, x_2, -(x_1{+}x_3{+}X_1{+}X_2{+}X_3))$ generates the plot above. The canonical form associated to this bounded chamber is

$$\check{\varphi}_1 = \delta_4(\Omega_4) \quad \text{where} \quad \Omega_4 = \frac{\varepsilon^2}{3}\mathrm{dlog}\frac{x_1}{x_2}\Big|_{\mathcal{B}_4} \wedge \mathrm{dlog}\frac{x_2}{x_3}\Big|_{\mathcal{B}_4}\,, \tag{3.36}$$

The powers of ε in the normalization ensure ε-form DEQs. The overall rational number is convenient.

The remaining dual forms are generated in the same way and can be found in [49]. The 2-boundary dual forms are generated by the line segments between the removed twisted points on the 2-cuts

$$\begin{aligned}
&\check{\varphi}_2 = \frac{\varepsilon}{2}\delta_{4,1}\left(\mathrm{dlog}\frac{x_2}{x_3}\Big|_{\mathcal{B}_{41}}\right), \quad \check{\varphi}_3 = \frac{\varepsilon}{2}\delta_{6,1}\left(\mathrm{dlog}\frac{x_2}{x_3}\Big|_{\mathcal{B}_{61}}\right), \quad \check{\varphi}_4 = \frac{\varepsilon}{2}\delta_{4,3}\left(\mathrm{dlog}\frac{x_1}{x_3}\Big|_{\mathcal{B}_{43}}\right), \\
&\check{\varphi}_5 = \frac{\varepsilon}{2}\delta_{5,3}\left(\mathrm{dlog}\frac{x_1}{x_2}\Big|_{\mathcal{B}_{53}}\right), \quad \check{\varphi}_6 = \frac{\varepsilon}{2}\delta_{4,5}\left(\mathrm{dlog}\frac{x_1}{x_2}\Big|_{\mathcal{B}_{45}}\right), \quad \check{\varphi}_7 = \frac{\varepsilon}{2}\delta_{4,6}\left(\mathrm{dlog}\frac{x_1}{x_2}\Big|_{\mathcal{B}_{46}}\right), \\
&\check{\varphi}_8 = \frac{\varepsilon}{2}\delta_{4,2}\left(\mathrm{dlog}\frac{x_2}{x_3}\Big|_{\mathcal{B}_{42}}\right), \quad \check{\varphi}_9 = \frac{\varepsilon}{2}\delta_{5,6}\left(\mathrm{dlog}\frac{x_1}{x_2}\Big|_{\mathcal{B}_{56}}\right), \quad \check{\varphi}_{10} = \frac{\varepsilon}{2}\delta_{5,6}\left(\mathrm{dlog}\frac{x_2}{x_3}\Big|_{\mathcal{B}_{56}}\right).
\end{aligned} \tag{3.37}$$

Note that the cut M_{56} has two canonical forms since the restriction of all coordinate axes to the cut form two line segments

$M_{56} =$ 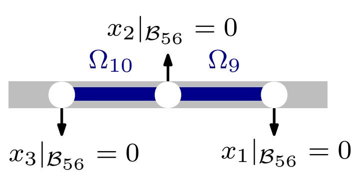

. (3.38)

The 3-boundary forms are

$$\begin{aligned}
&\check{\varphi}_{11} = \delta_{1,2,3}(1) &&\check{\varphi}_{12} = \delta_{6,1,2}(1)\,, &&\check{\varphi}_{13} = \delta_{4,1,3}(1)\,, &&\check{\varphi}_{14} = \delta_{5,1,3}(1)\,, \\
&\check{\varphi}_{15} = \delta_{6,1,3}(1)\,, &&\check{\varphi}_{16} = \delta_{4,5,1}(1)\,, &&\check{\varphi}_{17} = \delta_{5,2,3}(1)\,, &&\check{\varphi}_{18} = \delta_{4,6,3}(1)\,, \\
&\check{\varphi}_{19} = \delta_{4,5,2}(1)\,, &&\check{\varphi}_{20} = \delta_{4,6,2}(1)\,, &&\check{\varphi}_{21} = \delta_{5,6,2}(1)\,, &&\check{\varphi}_{22} = \delta_{4,5,6}(1)\,, \\
&\check{\varphi}_{23} = \delta_{4,1,2}(1)\,, &&\check{\varphi}_{24} = \delta_{5,6,1}(1)\,, &&\check{\varphi}_{25} = \delta_{4,2,3}(1)\,, &&\check{\varphi}_{26} = \delta_{5,6,3}(1)\,.
\end{aligned} \tag{3.39}$$

Note that the argument of each δ_J is simply the the 0-form 1; the canonical form for a point.

The physical, unphysical and degenerate/mixed cuts: The non-trivial dual forms corresponding to the 1-, 2- and 3-cuts given by (3.36), (3.37) and (3.39) will now be color-coded according to whether they are physical, unphysical or degenerate/mixed.

The physical dual forms induce residues that do not annihilate $\Psi_n^{(\ell)}$ in the intersection number

$$\mathrm{Res}_J[\Psi_3^{(0)}] \neq 0\,, \tag{3.40}$$

where

$$\begin{aligned} J \in \Big\{ &\{1\},\{4,1\},\{6,1\},\{4,3\},\{5,3\},\{4,5\},\{4,6\},\{1,2,3\},\\ &\{6,1,2\},\{4,1,3\},\{5,1,3\},\{6,1,3\},\{4,5,1\},\{5,2,3\},\{4,6,3\}\Big\}\,. \end{aligned} \tag{3.41}$$

These generate the physical FRW forms in (3.46), (3.47) and (3.48) via the replacement $\delta_J(\Omega) \to \mathrm{dlog}_J \wedge \tilde{\Omega}$.

The unphysical dual forms induce residues that annihilate $\Psi_n^{(\ell)}$ in the intersection number

$$\mathrm{Res}_J[\Psi_3^{(0)}] = 0\,, \tag{3.42}$$

where

$$J \in \Big\{\{4,2\},\{5,6\},\{4,1,2\},\{5,6,1\},\{4,2,3\},\{5,6,3\}\Big\}\,. \tag{3.43}$$

These generate unphysical FRW forms. Importantly, note that the unphysical dual forms correspond to sequential residues that set either side of the linear relation (3.31) to zero. The unphysical residues correspond to Steinmann relations in the cosmological context [152, 74].

The degenerate/mixed class of dual forms correspond to residues that may or may not annihilate $\Psi_n^{(\ell)}$

$$\begin{aligned} &\mathrm{Res}_{4,5,2}[\Psi_3^{(0)}] = -\mathrm{Res}_{4,6,2}[\Psi_3^{(0)}] = \mathrm{Res}_{4,5,6}[\Psi_3^{(0)}] = 1\\ &\mathrm{Res}_{5,6,2}[\Psi_3^{(0)}] = 0\,. \end{aligned} \tag{3.44}$$

As discussed earlier all four of these cuts correspond to the same loci $M_{452} = M_{462} = M_{562} = M_{456}$ and are therefore called degenerate. Additionally, the associated residues operators induced by the δ_J satisfy linear relations. For example,

$$\mathrm{Res}_{4,5,2} = \mathrm{Res}_{4,5,6}\,, \quad \text{and} \quad \mathrm{Res}_{4,6,2} = \mathrm{Res}_{4,6,5}\,. \tag{3.45}$$

From the point of view of direct computation, it takes additional work to understand which FRW forms generated by dual forms on the degenerate cut should be associated to the physical sector. A cut is degenerate whenever all but one hyperplane in a linear relation appears in a sequential residue. In this example, it happens whenever a cut involves three of the hyperplane polynomials that appear in the linear relation (3.31).

This classification of cuts with a non-trivial cohomology into physical, unphysical and degenerate/mixed directly follows from the linear relation(s) of the hyperplane arrangement. Simple rules, that circumvent direct computation, for classifying the non-trivial cuts are provided in section 3.4 and 3.5. Further rules for generating the exact physical differential forms are also provided.

The FRW forms: A spanning set of FRW forms is obtained from the dual forms by the rule $\delta_J(\Omega_J) \to \mathrm{dlog}_J \wedge \tilde{\Omega}_J$ and guarantees that the intersection matrix is block diagonal on the cuts. We also drop any normalization associated to the dual forms in this procedure.

There is one physical FRW form associated to the only non-trivial 1-cut from (3.36)

$$\varphi_1 = \mathrm{dlog}_4 \wedge \mathrm{dlog}\frac{x_1}{x_2} \wedge \mathrm{dlog}\frac{x_2}{x_3}\,. \tag{3.46}$$

The nine dual forms (3.37) generate the physical φ_{2-7} and unphysical φ_{8-10} FRW forms

$$\begin{aligned}
\varphi_2 &= \mathrm{dlog}_{4,1} \wedge \mathrm{dlog}\frac{x_2}{x_3}\,, & \varphi_3 &= \mathrm{dlog}_{6,1} \wedge \mathrm{dlog}\frac{x_2}{x_3}\,, & \varphi_4 &= \mathrm{dlog}_{4,3} \wedge \mathrm{dlog}\frac{x_1}{x_3}\,,\\
\varphi_5 &= \mathrm{dlog}_{5,3} \wedge \mathrm{dlog}\frac{x_1}{x_2}\,, & \varphi_6 &= \mathrm{dlog}_{4,5} \wedge \mathrm{dlog}\frac{x_1}{x_2}\,, & \varphi_7 &= \mathrm{dlog}_{4,6} \wedge \mathrm{dlog}\frac{x_1}{x_2}\,,\\
\varphi_8 &= \mathrm{dlog}_{4,2} \wedge \mathrm{dlog}\frac{x_2}{x_3}\,, & \varphi_9 &= \mathrm{dlog}_{5,6} \wedge \mathrm{dlog}\frac{x_1}{x_2}\,, & \varphi_{10} &= \mathrm{dlog}_{5,6} \wedge \mathrm{dlog}\frac{x_2}{x_3}\,.
\end{aligned} \tag{3.47}$$

The ten dual forms (3.39) generate the physical φ_{11-18}, unphysical φ_{23-26} and degenerate φ_{19-22} FRW forms

$$\begin{aligned}
\varphi_{11} &= \mathrm{dlog}_{1,2,3}\,, & \varphi_{12} &= \mathrm{dlog}_{6,1,2}\,, & \varphi_{13} &= \mathrm{dlog}_{4,1,3}\,, & \varphi_{14} &= \mathrm{dlog}_{5,1,3}\,,\\
\varphi_{15} &= \mathrm{dlog}_{6,1,3}\,, & \varphi_{16} &= \mathrm{dlog}_{4,5,1}\,, & \varphi_{17} &= \mathrm{dlog}_{5,2,3}\,, & \varphi_{18} &= \mathrm{dlog}_{4,6,3}\,,\\
\varphi_{19} &= \mathrm{dlog}_{4,5,2}\,, & \varphi_{20} &= \mathrm{dlog}_{4,6,2}\,, & \varphi_{21} &= \mathrm{dlog}_{5,6,2}\,, & \varphi_{22} &= \mathrm{dlog}_{4,5,6}\,,\\
\varphi_{23} &= \mathrm{dlog}_{4,1,2}\,, & \varphi_{24} &= \mathrm{dlog}_{5,6,1}\,, & \varphi_{25} &= \mathrm{dlog}_{4,2,3}\,, & \varphi_{26} &= \mathrm{dlog}_{5,6,3}\,.
\end{aligned} \tag{3.48}$$

The only remaining task is to understand how to deal with the degenerate forms.

Disentangling the degenerate cuts via direct computation: Since we will soon describe how to find the physical subspace without performing any direct computation, we focus on conceptual details; some explicit computations can be found in appendix 3.9.

As mentioned above, the intersection matrix is block diagonal with one block coming from the unphysical two-dimensional cohomology on the 56-cut and the other from the degenerate 452-, 462-, 562- and 456-cuts

$\underline{\boldsymbol{C}} =$ 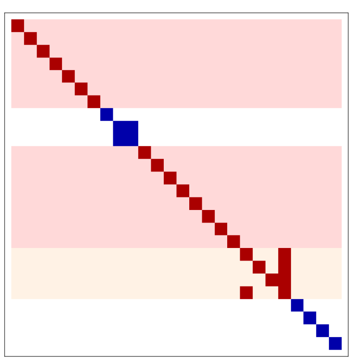 where

$$\underline{\boldsymbol{C}}_{\text{degen}} = \begin{pmatrix} 1 & 0 & 0 & 1\\ 0 & 1 & 0 & -1\\ 0 & 0 & 1 & 1\\ 1 & 0 & 0 & 1 \end{pmatrix}. \tag{3.49}$$

Each row of this matrix corresponds to a dual form and therefore to a cut and are color coded according to their classification. In particular, the degenerate rows in orange correspond to residues that localize to the same loci. Yet, some annihilate $\Psi_3^{(0)}$ and some do not (c.f., (3.45)). Therefore, it is not clear if they should be classified as physical or unphysical.

Also, the rank of the 4×4 degenerate block $\underline{\boldsymbol{C}}_{\text{degen}}$ is only three. This is a consequence of a linear relation among dlog-forms and a generic feature of degenerate hyperplane arrangements (see section 3.4.2). Therefore, we have to remove one element in this 4×4 block from our spanning sets to get a basis. We remove the elements associated to the 456-cut (elements $\check{\varphi}_{22}$ and φ_{22}) to form the bases $\check{\varphi}'$ and $\boldsymbol{\varphi}'$. The corresponding intersection matrix $\underline{\boldsymbol{C}}'$ is full rank.

At this stage, the number of linearly independent elements in cohomology that share cuts with $\Psi_3^{(0)}$ are the number of red elements along the diagonal of $\underline{\boldsymbol{C}}'$: 18. To reduce this more, we need to decompose the degenerate space into a component along $\Psi_3^{(0)}$ and its orthogonal complement. This is accomplished by constructing a gauge transformations $\underline{\boldsymbol{\chi U}}$ and $\underline{\boldsymbol{U}} = (\underline{\boldsymbol{\chi U}} \cdot \underline{\boldsymbol{C}}')^{-1\top}$ detailed in appendix 3.9.1. Applying these gauge transformations we obtain the bases $\check{\varphi}'' = \underline{\boldsymbol{\chi U}} \cdot \check{\varphi}'$ and $\varphi'' = \underline{\boldsymbol{U}} \cdot \varphi'$. Since these bases have unit intersection matrix $\underline{\boldsymbol{C}}'' = \mathbb{1}$, they are truly dual making it easy to map between the FRW and dual cohomologies (c.f., footnote 9).

The new basis $\check{\varphi}''$ contains only 16 dual forms that correspond to residues that do not annihilate $\Psi_3^{(0)}$; the corresponding FRW forms share sequential residues with $\Psi_3^{(0)}$ and make up the physical subspace. Computing the φ''-DEQs, $A''_{ab} = (C''_{bc})^{-1}\langle\check{\varphi}''_c|\nabla_{\text{kin}}\varphi''_a\rangle = \langle\check{\varphi}''_b|\nabla_{\text{kin}}\varphi''_a\rangle$, we find that the 16-dimensional physical subspace closes and is integrable

∇_{kin} = 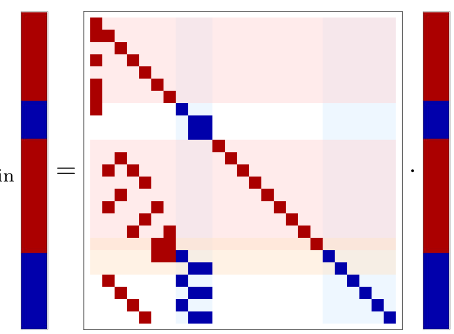 . (3.50)

Clearly the derivative of any physical FRW form only talks to other physical FRW forms. Explicitly, the physical subspace contains all forms in red and one linear combination of the orange forms of the degenerate cut

$$\{\varphi_{\text{phys},i}\}_{i=1}^{16} = \{\varphi_1, \ldots \varphi_7, \varphi_{11}, \ldots \varphi_{18}, (\varphi_{19} - \varphi_{20})/2\}\,. \tag{3.51}$$

From the perspective of direct calculation, the linear combination $(\varphi_{19} - \varphi_{20})/2$ in (3.51) comes from the gauge transformation matrix $\underline{\boldsymbol{U}}$. `Mathematica` files with the physical basis, gauge transformations and DEQs can be found in appendix 3.9.1 and at the `github` repository.

Of course, we need to decompose $\Psi_3^{(0)}$ into the physical basis in order to use the DEQs for the physical quantity of interest. One can either use partial fractions (see appendix 3.10 for a diagrammatic approach) or the intersection number:

$$\Psi_3^{(0)} = (0,0,0,0,0,0,0,1,-1,-1,1,1,-1,-1,1,2) \cdot \boldsymbol{\varphi}_{\text{phys}}\,. \tag{3.52}$$

Further examples and loops: At no step in any part of our algorithm has the specification to tree-level cosmological correlators been needed; everything generalizes straightforwardly to loop-level. We demonstrate the splitting of the full cohomology into physical and unphysical subspaces via direct calculation for the 4-site chain (appendix 3.9.2), 4-site star (appendix 3.9.3) and 1-loop 3-gon (appendix 3.9.4). Using the intersection matrix, we demonstrate that the full cohomologies with dimensions 213, 312 and 99 reduce to a physical basis with 64, 64 and 50 elements in agreement with both the kinematic flow algorithm [76, 75, 133, 134] and those obtained from a time integral perspective [131]. The DEQs for the 4-site chain and 1-loop 3-gon can be found in the `Mathematica` files at the `github` repository.

Disentangling the degenerate cuts avoiding direct computation: Before moving on, we preview how to find the physical subspace and avoid direct calculation. A systematic algorithm is developed in sections 3.4 and 3.5.

To every δ_J or equivalently Res_J, we can associate a cut tubing. For example, the total energy residue can be represented diagrammatically by the dashed tubing

$\delta_4 \leftrightarrow \text{Res}_4 :=$ 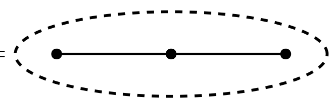 , (3.53)

Next, note that *only* cut tubings with *no crossings* appear in the physical basis (3.51). This is because of the two following facts:

i) The set of compatible complete tubings of a graph $\mathcal{G}$ only involves non-crossed tubings (see (3.8), (3.149) and (3.160) for examples).

ii) Due to our ordering, the only residues with crossed cut tubings that do not annihilate $\Psi_n^{(\ell)}$ are degenerate. Moreover, the degenerate crossed cut tubings that do not annihilate $\Psi_n^{(\ell)}$ are equivalent to a non-crossed cut tubings. For example, in the context of the 3-site example, $\text{Res}_{4,5,6} = \text{Res}_{4,5,2}$

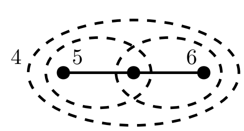

$=$
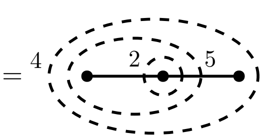

. (3.54)

The generalization of such residue relations is presented in section 3.4.1.

No crossed cut tubings

The physical subspace only contains forms associated to non-crossed tubings:

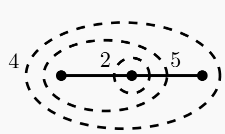

✓ ,
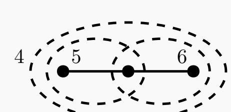

✗ .

Each degenerate block also only contributes one form to the physical subspace since we decompose the degenerate block into a component along $\Psi_3^{(0)}$ and its orthogonal complement. The dlog_J-part of the physical form associated to a degenerate cut is a linear combination of dlog_J-forms associated to the non-crossing cut tubings of the degenerate cut. Specifically, there is a relative sign between all pairs of dlog_J's that only differ by tubings that cross. Indeed, $\varphi_{\text{phys},16} \propto \varphi_{19} - \varphi_{20} = \mathrm{dlog}_{4,5,2} - \mathrm{dlog}_{4,6,2}$ satisfies this rule; the dlog's share all but one factor and these unshared B_i have tubings that cross.

3.4 Linear relations and degenerate arrangements

The classification of cuts/residues with non-trivial cohomologies into physical, unphysical and degenerate/mixed cuts is controlled entirely by the system of linear relations associated to the hyperplane arrangement of the graph $\mathcal{G}$. Importantly, these hyperplane arrangements (section 3.1.2) are non-generic in the sense that there exists codimension m loci where more than m hyperplanes intersect. This non-genericity in cosmological hyperplane arrangements is entirely encoded in the linear relations among the corresponding hyperplane polynomials B_i. As a consequence of this degeneracy, some sequential residues do not necessarily anti-commute and satisfy linear relations (recall (3.44) and (3.45)).

The linear relations among the B_i (equivalently the S_i) are generated by 2-tubings that intersect.[14] For the 3-site chain, there is just one relation

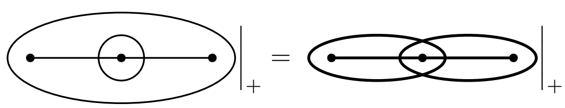

$$\iff B_2 + B_4 = B_5 + B_6\,, \tag{3.55}$$

where $|_+$ instructs us to add the B_i associated to the 2-tubings. Via equation (3.5), this graphical rule is easy to verify since the crossed 2-tubings encircle the same vertices and cross the same edges the same number of times. Moreover, this graphical rule holds beyond tree-level graphs and generates all possible linear relations. Indeed, it is easy to check the following identity for the 1-loop 3-gon graph below

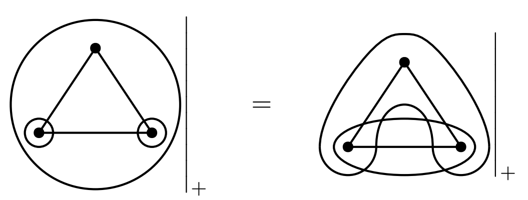

(3.56)

We also note that not all linear relations between hyperplane polynomials will generate interesting consequences for the physical basis; some only effect the unphysical subspace.

To keep track of the linear relations and deduce their consequences, we introduce the notion of

[14] This is not always a minimal presentation; the set of all pairs of crossed tubings often produces an over complete set of relations.

a minimally dependent indexing set I. A minimally dependent indexing set

$$I = \{I_{\text{LHS}}|I_{\text{RHS}}\}\,, \tag{3.57}$$

is a collection of two sets indexing the hyperplane polynomials B_i that appear on the LHS and RHS of linear relations. For example, in this notation, equation (3.55) is equivalent to $I = \{2,4|5,6\}$ or with some abuse of notation $I = \{B_2, B_4|B_5, B_6\}$. Furthermore, note that I_{RHS} is always a set of two 1-tubings that cross.

The set I is minimally dependent in the sense that removing any single element, say B_j, results in a linearly independent set of B_i[15]

$$\sum_{i\in I} \underbrace{\alpha_i}_{\neq 0} B_i{=}0 \quad \text{but} \quad \sum_{i\in I\setminus i_j} \alpha_i B_i{=}0 \Longleftrightarrow \alpha_i{=}0\,. \tag{3.58}$$

Every minimally dependent set I generates a relation between sequential residues (section 3.4.1) as well as a relation among dlog-forms (section 3.4.2). After identifying a degenerate boundary, we also provide a simple prescription for constructing the physical form without computing the intersection matrix in section 3.5.3.

3.4.1 Consequences for residue operations

As a consequence of the linear relations among hyperplane polynomials, iterated residues do not necessarily anti-commute under ordering exchanges and satisfy relations. To see why iterated residues do not necessarily anti-commute, consider the following example of a toy (non-cosmological) arrangement below where the lines $\mathcal{B}_1$, $\mathcal{B}_2$ and $\mathcal{B}_3$ all intersect at the same point (in red)

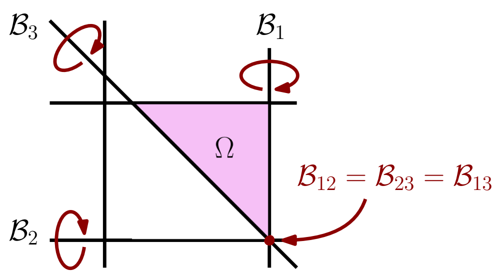

While the canonical form Ω is singular at the point $\mathcal{B}_{12} = \mathcal{B}_{23} = \mathcal{B}_{31}$, its residue at this point depends on the order. The 13-residues of Ω behave normally

$$\text{Res}_{13}[\Omega] = -\text{Res}_{31}[\Omega]\,. \tag{3.59}$$

On the other hand, one ordering of the 23- and 12-residues vanish

$$\text{Res}_{21}[\Omega] = \text{Res}_{23}[\Omega] = 0\,. \tag{3.60}$$

[15] In some of the relations that follow, we suppress the B's and denote a hyperplane polynomial B_i simply by its label i.

The other ordering is equal to an ordering of the 13-residues

$$\mathrm{Res}_{32}[\Omega] = \mathrm{Res}_{31}[\Omega] \neq 0\,, \tag{3.61}$$

$$\mathrm{Res}_{12}[\Omega] = \mathrm{Res}_{13}[\Omega] \neq 0\,. \tag{3.62}$$

For this reason, we need to fix an ordering when taking residues. As mentioned in section 3.3, we always order residues such that the B_i associated to the tubing that encircles the most vertices always comes first. Diagrammatically, this means that we work outward-in for residue tubings

$\mathrm{Res}_{452} :=$ 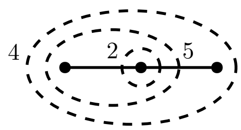

$\neq \mathrm{Res}_{425} \neq \mathrm{Res}_{542} \neq \cdots\,.$ (3.63)

For tubings of the same size, we assign lexicographical order

$\mathrm{Res}_{413} :=$ 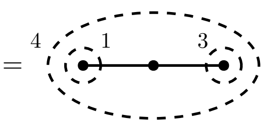

. (3.64)

For now, this ordering is a mathematical necessity. However, in section 3.5, we will show that our ordering choice aligns with physical intuition.

Every minimally dependent set, I, of hyperplane polynomials (3.58) seeds a residue relation

$$\mathrm{Res}_{i_j} \circ \mathrm{Res}_{\sigma(I\setminus\{i_j,i_k\})} = \mathrm{Res}_{i_k} \circ \mathrm{Res}_{\sigma(I\setminus\{i_j,i_k\})}\,, \tag{3.65}$$

where $i_j, i_k \in I$ and $\sigma \in S_{|I|-2}$ is a permutation acting on $I \setminus \{i_j, i_k\}$. To see why this is the case, note that when restricted to the cut $I \setminus \{i_j, i_k\}$, the linear relation between the hyperplane polynomials now becomes $\alpha_{i_j} B_{i_j}|_{I\setminus\{i_j,i_k\}} + \alpha_{i_k} B_{i_k}|_{I\setminus\{i_j,i_k\}} = 0$. Since $B_{i_j}|_{I\setminus\{i_j,i_k\}}$ and $B_{i_k}|_{I\setminus\{i_j,i_k\}}$ are proportional, the final residues in the above equation are equivalent. Note that this relation is insensitive to the actual values of the coefficients α_i appearing in the linear relations (3.58).

3.4.2 Consequences for differential forms

Similarly, linear relations among the hyperplane polynomials generate linear relations among differential forms. Like before, we identify a minimally dependent set of hyperplane polynomials I. After fixing an order for I, the following identity holds

$$\sum_{j=1}^{|I|} (-1)^{j-1} \left(\bigwedge_{k \in I\setminus i_j} \mathrm{dlog} B_k \right) = 0\,, \tag{3.66}$$

where i_j is the j^{th} element of I. For example, it is easy to verify the relation

$$\mathrm{dlog}_{456} - \mathrm{dlog}_{452} + \mathrm{dlog}_{462} - \mathrm{dlog}_{562} = 0\,, \tag{3.67}$$

in terms of the 3-site example (section 3.3), which can be deduced from the nullspace of the intersection matrix (3.49). Such relations are known in the mathematical literature as Orlik-Solomon relations [153, 154]. In fact, the Orlik-Solomon algebra generates all linear relations of degenerate hyperplane arrangements circumventing the need to use blow-ups. Furthermore, a nice presentation for the Gröbner basis of monomials in dlog's is known.

Equation (3.66), also gives a relations between the $(|I|-2)$-residues of $(|I|-1)$-forms. Let I be a minimally dependent set and $j,k \in \{1,\dots,|I|\}$. Then,

$$\mathrm{Res}_{I\setminus\{i_j i_k\}}\mathrm{dlog}_{I\setminus i_j} = (-1)^{j-k}\mathrm{Res}_{I\setminus\{i_j i_k\}}\mathrm{dlog}_{I\setminus i_k}. \tag{3.68}$$

The sign in (3.68) comes from the fact that we are comparing the residues of different dlog-forms.

3.5 Cut tubings – a basis for all trees and loops

In this section, we demonstrate how to construct a basis of physical forms for *any* n-site, ℓ-loop FRW wavefunction coefficient $\psi_n^{(\ell)}$ via simple universal graphical rules that systematize the construction of *residue* or equivalently *cut tubings*.

As mentioned in section 3.3, an ℓ-loop cut tubing, $\mathcal{C}^{(\ell)}_{n_i,B_i}$, is denoted by a dashed tube (in comparison to the solid tubings τ_i of (3.6)) and defines an instruction to compute a residue on the hyperplane polynomial $B_i = 0$. The label n_i in $\mathcal{C}^{(\ell)}_{n_i,B_i}$ denotes the number of vertices enclosed by the tubing. For example, a residue on the total energy pole $B_{T=4} = 0$ in the tree-level 3-site graph is represented by the following cut tubing:

$$\mathcal{C}^{(0)}_{3,B_4} :=$$

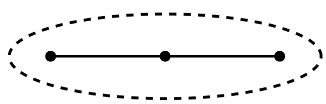

$$:= \mathrm{Res}_{\mathcal{B}_4}\Psi_3^{(0)}\ . \tag{3.69}$$

While primarily a bookkeeping tool to enumerate the basis elements of any given graph $\mathcal{G}$, these cut tubings carry both physical and mathematical information:

1. From a mathematical perspective, they correspond to all physical boundaries M_J that have a one-dimensional twisted cohomology and count each degenerate cut exactly once.

2. From a physics perspective, they correspond to all ways to factorize the shifted flat-space wavefunction coefficient $\Psi_n^{(\ell)}$ solely into product(s) of lower-point flat-space scattering amplitudes.

We elaborate on these connections as we present the universal rules for generating the physical cut tubings, which remarkably hold true for *all* tree and loop level wavefunction coefficients.

In section 3.5.1, we present a set of simple universal graphical rules (with detailed examples) associated to cut tubings that arise from the associated system of linear relations as well as from cohomological arguments. In section 3.5.2, we will see how these simple rules systematize the construction of the space of all tubings corresponding to each physical cut M_J (i.e., the space of physical 1-tubings, 2-tubings, and so on), thereby enumerating the physical subspace of forms that couple to $\Psi_n^{(\ell)}$ in the DEQs. We end by explicitly implementing these universal rules to generate the physical basis for the tree-level 3-site graph in section 3.5.4 and the 2-loop 2-site sunset graph in section 3.5.5. In section 3.5.6, we present some remarkable patterns that our analysis reveals.

3.5.1 Universal selection rules for physical cut tubings

The linear relations of section 3.4 constrain the space of physical cuts. In particular, they constrain how cut tubings can be nested. In subsection 3.5.1, we present the *good cut* and *degenerate cut* conditions that govern the mechanism for evolving any cut tubing (i.e., going from a J-cut to $(J+1)$-cut) in a sequentially nested fashion. Following this, we present an additional set of rules in subsection 3.5.1 motivated by cohomological arguments, which accounts for cuts beyond this scope of sequential nesting.

The good cut and degenerate cut conditions

For a given graph $\mathcal{G}$, the residue of the wavefunction coefficient $\Psi_n^{(\ell)}$ on its total energy pole $B_T = 0$ is called the *(true) scattering facet* of $\mathcal{P}_\mathcal{G}$ [71]. At tree level, we have

$$\mathcal{C}^{(0)}_{n,B_T} := \mathrm{Res}_{\mathcal{B}_T}\Psi_n^{(0)} := \tag{3.70}$$

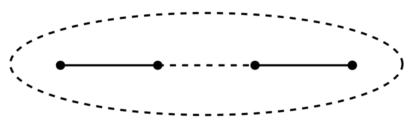

Subsequent cut tubings contained inside the true facet $\mathcal{C}^{(0)}_{n_i,B_i} \subset \mathcal{C}^{(0)}_{n,B_T}$ behave as scattering facets associated to a lower n_i-point wavefunction coefficient $\Psi^{(0)}_{n_i<n}$. This extends to any loop and number of sites and means that a $\mathcal{C}^{(\ell')}_{n_i,B_i} (\subset \mathcal{C}^{(\ell)}_{n,B_T})$ evolves like an $(n_i < n)$-site $(\ell' < \ell)$-level cut tubing regardless of what other cut tubings surround $\mathcal{C}^{(\ell')}_{n_i,B_i}$. This observation implies that $\mathcal{C}^{(\ell')}_{n_i,B_i}$ only directly constrains whether a (dashed) tubing placed wholly inside of B_i lead to a physical cut. In particular, this means that the evolution of a cut tubing—what further cut tubings can be drawn inside it—does not depend on the details of the larger graph outside of it. In this way, information from lower-point and lower-loop cuts is recycled! This structure is reflected in the good-cut and degenerate-cut conditions discussed below.

The good cut condition

Suppose we want to evolve the cut tubing $\mathcal{C}^{(\ell)}_{n_i,B_i}$ by nesting the cut tubing $\mathcal{C}^{(\ell')}_{n_j,B_j}$: $\mathcal{C}^{(\ell')}_{n_j,B_j} \subset \mathcal{C}^{(\ell)}_{n_i,B_i}$. We first identify all minimal dependent sets (3.57) where τ_i (corresponding to B_i) is the largest tubing[16]

$$I^{(i)}_\alpha = \{I^{(i)}_{\alpha,\mathrm{LHS}} | I^{(i)}_{\alpha,\mathrm{RHS}}\}\,. \tag{3.71}$$

The residue tubings that can be paired with $\mathcal{C}^{(\ell)}_{n_i,B_i}$ to form physical cuts *do not* set all elements of $I^{(i)}_{\alpha,\mathrm{LHS}}$ to zero (also no element of $I^{(i)}_{\alpha,\mathrm{RHS}}$ should be set to zero). This is the *good cut condition* associated to the cut tubing $\mathcal{C}^{(\ell)}_{n_i,B_i}$. It constrains the space of physical cuts with $|I^{(i)}_{\alpha,\mathrm{LHS}}| - 1$ further cuts inside $\mathcal{C}^{(\ell)}_{n_i,B_i}$.

Sequential residues that set all elements in $I^{(i)}_{\alpha,\mathrm{LHS}}$ (and none in $I^{(i)}_{\alpha,\mathrm{RHS}}$) to zero annihilate the

[16] Note that τ_i is always an element of $I^{(i)}_{\alpha,\mathrm{LHS}}$.

physical form $\Psi_n^{(\ell)}$. Therefore, the good cut condition tells us how to avoid these unphysical boundaries and generate physical cuts.[17]

For example, the tree-level 3-site chain graph has a single minimal dependent set $I_1^{(T)} = \{B_2, B_{T=4} | B_5, B_6\}$ (depicted in (3.55)) that constrains the space of physical 2-cuts. The double residue $\text{Res}_{42}[\Psi_3^{(0)}]$ annihilates $\Psi_3^{(0)}$ (as shown in (3.42)) implying that $\mathcal{C}_{1,B_2}^{(0)} \subset \mathcal{C}_{3,B_4}^{(0)}$ is an unphysical 2-cut

$$\mathcal{C}_{1,B_2}^{(0)} \subset \mathcal{C}_{3,B_{T=4}}^{(0)} = \quad \text{[diagram]} \quad = 0\ . \tag{3.72}$$

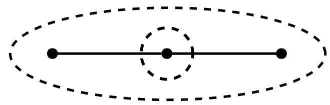

Thus, the good cut condition for the true facet $C_{3,B_{T=4}}^{(0)}$ implies that pairing any of the cut tubings $\mathcal{C}_{1,B_1}^{(0)}, \mathcal{C}_{1,B_3}^{(0)}, \mathcal{C}_{2,B_5}^{(0)}, \mathcal{C}_{2,B_6}^{(0)}$ with it corresponds to physical 2-cuts (see (3.115)). In general, $|I_{\alpha,\text{LHS}}| = 2$ for all tree-level graphs. Therefore, the good cut condition only restricts the next cut $\mathcal{C}_{n_j,B_j}^{(0)} \subset \mathcal{C}_{n_i,B_i}^{(0)}$ such that $B_j \notin I_{\alpha,\text{LHS}}^{(i)}$.

For loop-level graphs, $|I_{\alpha,\text{LHS}}| \geq 2$ and the next cut $\mathcal{C}_{n_j,B_j}^{(\ell')} \subset \mathcal{C}_{n_i,B_i}^{(\ell)}$ is unconstrained whenever $|I_{\alpha,\text{LHS}}| > 2$. For example, let's understand how the minimal dependent set $I_1^{(T)} = \{B_1, B_2, B_{T=5} | B_6, B_{14}\}$ of the the 1-loop 4-gon box graph affects the evolution of its true facet. While the space of 2-tubings involving $\mathcal{C}_{4,B_{T=5}}^{(1)}$ is unconstrained, the 3-element set $I_{1,\text{LHS}}^{(T)}$ constrains the space of physical 3-cuts according to the good cut condition of the true facet. Explicitly, the the following 3-cut is unphysical

$$(\mathcal{C}_{1,B_2}^{(0)} \times \mathcal{C}_{1,B_1}^{(0)}) \subset \mathcal{C}_{4,B_{T=5}}^{(1)} = \quad \text{[diagram]} \quad = 0\ . \tag{3.73}$$

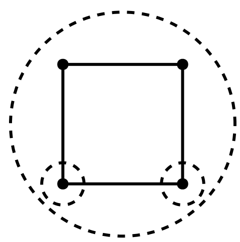

The degenerate cut condition

Suppose that we want to evolve an $m = |I_{\alpha,\text{LHS}}^{(i)}|$ cut

$$\mathcal{C}_{n_{j_{m-1}},B_{j_{m-1}}}^{(\ell_{j_{m-1}})} \subset \cdots \subset \mathcal{C}_{n_{j_1},B_{j_1}}^{(\ell_{j_1})} \subset \mathcal{C}_{n_i,B_i}^{(\ell)}\ , \tag{3.74}$$

(that could be embedded inside another cut) into an $(m+1)$-tubing. The next tubing is placed in accordance with the good cut condition of the most recent cut $\mathcal{C}_{n_{j_{m-1}},B_{j_{m-1}}}^{(\ell_{j_{m-1}})}$

$$\mathcal{C}_{n_{j_m},B_{j_m}}^{(\ell_{j_m})} \subset \mathcal{C}_{n_{j_{m-1}},B_{j_{m-1}}}^{(\ell_{j_{m-1}})} \subset \cdots \subset \mathcal{C}_{n_{j_1},B_{j_1}}^{(\ell_{j_1})} \subset \mathcal{C}_{n_i,B_i}^{(\ell)}\ . \tag{3.75}$$

Then, the resulting $(m+1)$-cut tubing is degenerate, in the sense of section 3.4, if all elements in $I_{\alpha,\text{LHS}}^{(i)}$ appear in the sequence (3.75) (the good cut condition ensures one cut corresponding

[17] Recall that all elements of $I_{\alpha,\text{RHS}}^{(i)}$ contain crossed tubings and correspond to sequential residues/cuts that are either unphysical or degenerate. For degenerate cuts, these crossed tubings can always be uncrossed using the linear relation of section 3.4.1. Hence such crossed residue tubings do not appear in our analysis. See the discussion around the no crossed cuts box for more.

to an element of $I^{(i)}_{\alpha,\mathrm{LHS}}$ is present in the sequence (3.75)). This is the *degenerate cut* condition of $\mathcal{C}^{(\ell)}_{n_i,B_i}$ or more precisely $I^{(i)}_\alpha$.

Physical degenerate cuts need to be identified and counted *exactly* once since they form a single degenerate sub-block in the DEQ matrix $\underline{\boldsymbol{A}}$ and only contribute a single differential form to the physical basis.

To illustrate this condition in action, we provide a short discussion with selected examples below:

- Consider a 4-term minimal dependent set $I^{(j)}_\alpha = \{B_i, B_j | B_k, B_l\}$. While the 2-tubing $\mathcal{C}^{(\ell_i)}_{n_i,B_i} \subset \mathcal{C}^{(\ell_j)}_{n_j,B_j}$ is an unphysical 2-cut, $\mathcal{C}^{(\ell_k)}_{n_k,B_k} \subset \mathcal{C}^{(\ell_j)}_{n_j,B_j}$ is a physical 2-cut consistent with the good cut condition of B_j. This 2-tubing can now be followed by a residue tubing $\mathcal{C}^{(\ell_i)}_{n_i,B_i}$ (with τ_i entirely inside τ_j) since this is consistent with the good cut evolution of $\mathcal{C}^{(\ell_j)}_{n_j,B_j}$. However, this 3-tubing satisfies the degenerate cut condition of $\mathcal{C}^{(\ell_i)}_{n_i,B_i}$ associated to $I^{(j)}_\alpha$ and must be classified as degenerate. This example is essentially a diagrammatic restatement of the residue relation (3.65) discussed in section 3.4.

  The first example of such a degenerate cut occurs in the tree-level 3-site graph when the physical 2-tubings $\mathcal{C}^{(0)}_{2,B_5} \subset \mathcal{C}^{(0)}_{3,B_{T=4}}$ or $\mathcal{C}^{(0)}_{2,B_6} \subset \mathcal{C}^{(0)}_{3,B_{T=4}}$ are evolved into a 3-tubing and is a consequence of the minimal dependent set $I^{(T)}_1 = \{B_2, B_{T=4} | B_5, B_6\}$. As discussed above, the cuts $\mathcal{C}^{(0)}_{2,B_5}$ and $\mathcal{C}^{(0)}_{2,B_6}$ effectively evolve as 2-site graphs, producing the 3-cuts

  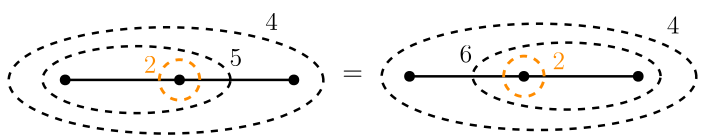

  (3.76)

  However, the new cut tubing in orange saturates $I^{(T)}_1$ and satisfies the degenerate cut condition of the true scattering facet $\mathcal{C}^{(0)}_{3,B_{T=4}}$. Therefore, these 3-cuts must be identified.

- A similar identification of a degenerate cut can be made for 1-loop graphs where one encounters 5-term minimal dependent sets. For example, for the case of the 1-loop 4-site box graph, we encounter a degenerate cut as a consequence of the minimal dependent set $I^{(T)}_1 = \{B_1, B_3, B_{T=5} | B_{10}, B_{12}\}$. Below, the 4th cut tubing $\mathcal{C}^{(0)}_{1,B_3}$ saturates $I^{(T)}_1$ and is identified:

  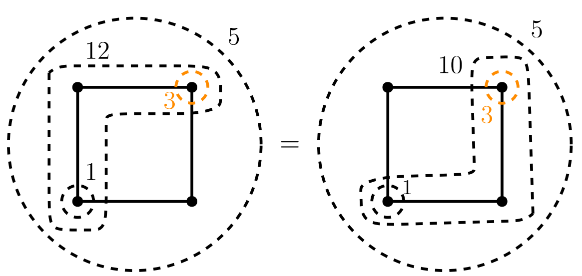

  (3.77)

- The further evolution of physical degenerate cuts occurs in the usual fashion; adding a new tubing inside the most recent tubing in accordance with its good cut condition and the degenerate cut conditions (of previous tubings).

- One often encounters scenarios where on the locus of a degenerate cut arising from some system, say $I^{(i)}$, is equivalent to the locus of another degenerate cut arising from a separate system $I^{(j)}$. In such a case, one simply identifies all $(m+1)$-cuts where the latest red tubing is common to all of them. For example, the first instance where one has to account for this is in the case of the tree-level 4-site chain graph due to the minimal dependent sets $I_1^{(9)} = \{B_2, B_9|B_6, B_7\}$ and $I_1^{(T)} = \{B_{T=5}, B_7|B_9, B_{10}\}$:

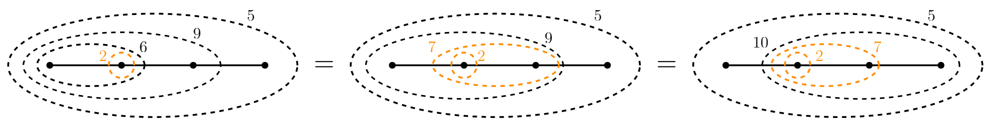

(3.78)

Importantly, we note that such degenerate cuts are different from the following degenerate cut, which arises from a distinct system $I_2^{(T)} = \{B_2, B_{T=5}|B_6, B_{10}\}$:

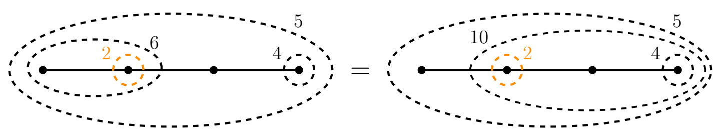

(3.79)

The uni-dimensional cohomology condition(s)

The above good and degenerate cut conditions associated to any cut tubing are simple manifestations of the linear relations of the associated hyperplane arrangement and constrain sequentially nested cut tubings. In addition to these, we need one more set of conditions—the *uni-dimensional cohomology* condition(s)—that goes beyond nested evolution, to generate all physical cuts. This graphical rule tells us how to avoid cuts with trivial cohomology (do not contribute forms to the basis).

The uni-dimensional cohomology condition(s)

The uni-dimensional cohomology condition(s) dictates that:

1. An m cut tubing of an n-site ℓ-loop graph $\mathcal{G}$ must enclose all the sites/vertices of $\mathcal{G}$ to yield a physical m-cut.

2. Inside each physical cut tube *containing more than a single vertex*, further good cut tubes must leave *at least* one unenclosed vertex.

Below, we provide the reasoning behind these conditions as well as a short discussion of selected examples.

- To have a non-trivial cohomology, the cut must contain a bounded chamber with boundaries made from the coordinate axes restricted to this cut. For a 1-cut of $\mathcal{G}$, this implies that all physical 1-cut tubings are associated to hyperplane polynomials B_i that contain the factor $\sum_{i=1}^{n}(x_i + X_i)$ in them. This ensures that one twisted hyperplane on the cut intersects the remaining other twisted hyperplanes creating a bounded chamber (see the right ure in (3.35) corresponding to the 3-site tree graph for an example).

For tree-level wavefunction coefficients $\Psi_n^{(0)}$, this condition implies that the only allowed 1-tubing with a one-dimensional cohomology is the true scattering facet $\mathcal{C}^{(0)}_{n,B_T}$:

$$\mathcal{C}^{(0)}_{n,B_T} := \quad . \tag{3.80}$$

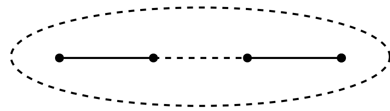

It is imperative to note that 1-tubings of tree graphs that do not correspond to the true facet tubing $\mathcal{C}^{(0)}_{n,B_T}$ violate this condition despite corresponding to non-vanishing residues of $\Psi_n^{(0)}$. This is because such 1-cuts $\mathcal{C}^{(0)}_{n_i,B_i\neq B_T}$ do not have a bounded chamber and therefore have trivial cohomology (the arrangement of twisted hyperplanes on the cut contains a pair of parallel hyperplanes; see left ure in (3.35) corresponding to the 3-site tree graph for an example). Such cuts correspond to unphysical cut tubings.

For example, the 1-cut $\mathcal{C}^{(0)}_{n,B_5}$ in the 3-site graph that encloses only two vertices out of the possible three

$$\mathcal{C}^{(0)}_{n,B_5} := \mathrm{Res}_{\mathcal{B}_5}\Psi_3^{(0)} := \quad \neq 0 \; , \qquad \text{(invalid tubing)} \tag{3.81}$$

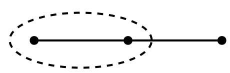

yields a non-zero residue; however, such 1-cuts have *trivial cohomology* and are therefore *inconsistent* with the condition above. From a cuts perspective, such residues split the graph into a flat-space amplitude times a (shifted) lower-point wavefunction coefficient, as discussed in [123].

For loop integrands, in addition to the true facet $\mathcal{C}^{(\ell)}_{n,B_T}$, there are further 1-cut tubings corresponding to hyperplanes $B_{T'}$ that enclose all the sites of the graph and have a one-dimensional cohomology. For example, the n-gon has a total of n+1 physical 1-cuts. In the case of the 3-gon (triangle) graph, these four tubings are

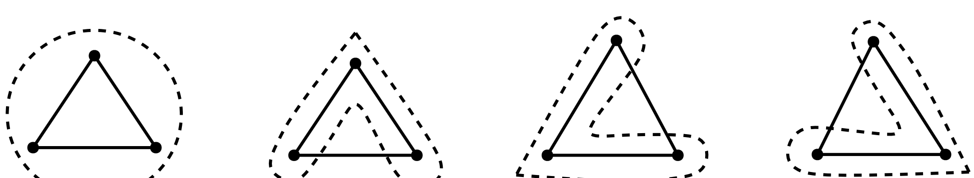

$$\mathcal{C}^{(1)}_{3,B_{T=4}} \qquad \mathcal{C}^{(0)}_{3,B_8} \qquad \mathcal{C}^{(0)}_{3,B_9} \qquad \mathcal{C}^{(0)}_{3,B_{10}} \quad . \tag{3.82}$$

Note that in addition to the true scattering facet tubing $\mathcal{C}^{(1)}_{3,B_{T=4}}$ of the 3-gon, the three other 1-tubings corresponding to the hyperplane polynomials $B_{T'=8,9,10} = \sum_{i=1}^{3}(x_i + X_i) + 2Y_{1,2,3}$, enclose all the three vertices of the triangle graph and are therefore consistent with the uni-dimensional cohomology condition.

For higher cuts, to be consistent with the first uni-dimensional cohomology condition, one has to partition the set of n-vertices of an ℓ-loop graph into non-empty, non-overlapping subsets to give a physical product of residue tubings $\mathcal{C}^{(\ell_1)}_{n_1,B_1} \times \mathcal{C}^{(\ell_2)}_{n_2,B_2} \times \cdots \times \mathcal{C}^{(\ell_m)}_{n_m,B_m}$ such that $n_1 + n_2 + \cdots + n_m = n$, which means no vertices are left unenclosed, thus ensuring a one-dimensional cohomology. An example of such a 2-tubing of the 4-site star graph is

$$\mathcal{C}^{(0)}_{3,B_{10}} \times \mathcal{C}^{(0)}_{1,B_2} = \tag{3.83}$$

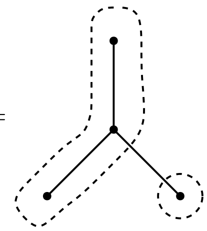

An example of a 4-cut of the double box consistent with this condition is

$$\mathcal{C}^{(0)}_{2,B_{12}} \times \mathcal{C}^{(0)}_{2,B_{10}} \times \mathcal{C}^{(0)}_{1,B_2} \times \mathcal{C}^{(0)}_{1,B_1} = \tag{3.84}$$

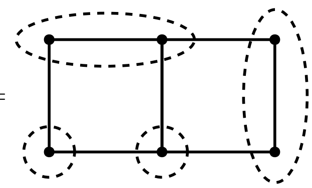

- Given any cut tubing, the subsequent cut tubings (consistent with its good cut condition) contained inside it must leave *at least* one vertex unenclosed to guarantee a one-dimensional cohomology and a non-trivial residue for the corresponding cut. When all vertices inside a cut tubing are enclosed again, the linear system cannot be solved and the corresponding cut/residue does not exist.

  For example, one can check this condition explicitly in the case for the 3-site tree graph. The following 3-cuts do not exist

  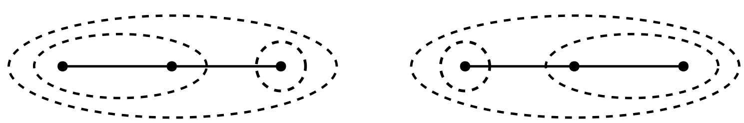

  (invalid tubings)

  while, on the other hand,

  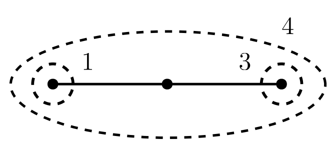

  (3.85)

  is a physical 3-cut. It abides by both the good cut condition and the uni-dimensional cohomology condition.

  In general, the n_i-vertices inside any cut tubing $\mathcal{C}^{(\ell)}_{n_i,B_i}$ can be partitioned into non-empty, non-overlapping subsets to give a physical product of residue tubings $\mathcal{C}^{(\ell_1)}_{n_1,B_1} \times \mathcal{C}^{(\ell_2)}_{n_2,B_2} \times \cdots \times \mathcal{C}^{(\ell_m)}_{n_m,B_m}$ such that $n_1 + n_2 + \cdots + n_m < n_i$. This leaves at least one vertex unenclosed and satisfies the second uni-dimensional cohomology condition.

The set of three conditions presented above — the good cut condition, the degenerate cut condition and the uni-dimensional cohomology condition — universally determine the set of all possible physical cuts contributing to the space of physical forms in the DEQs of *any* given $\Psi^{(\ell)}_n$, as we demonstrate in the following.

3.5.2 Enumerating physical cut tubings

Equipped with a universal set of rules for identifying physical cut tubings, we elucidate how to systematically construct all physical cuts for *any* n-site, ℓ-loop graph. Moreover, we will demonstrate how these conditions (that identify the space of physical boundaries) are in correspondence with all possible ways to factorize $\Psi_n^{(\ell)}$ *solely* into product(s) of flat-space scattering amplitudes.

<u>1-cut tubings</u>

As discussed above, for tree-level wavefunction coefficients $\Psi_n^{(\ell)}$, the only allowed 1-tubing consistent with the uni-dimensional cohomology condition is the true scattering facet $\mathcal{C}^{(0)}_{n,B_T}$, which yields the corresponding flat-space amplitude A_n:[18]

$\mathcal{C}^{(0)}_{n,B_T} =$ 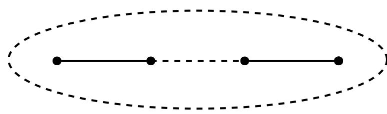 $\leftrightarrow$ 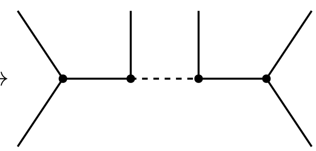 . (3.86)

At loop level there exist additional 1-tubings that have one-dimensional cohomology as illustrated in (3.82) for the 1-loop 3-gon. Note that the three 1-cuts $\mathcal{C}^{(0)}_{3,B_{i=8,9,10}}$ carry a superscript label (0) in comparison to the true facet 1-cut $\mathcal{C}^{(1)}_{3,B_T=5}$. The difference between these tubings is that the total energy pole $B_{T=5}$ is involved in 5-term minimal dependent sets $I^{(T)}_{\alpha}$ (or more specifically, with a 3-term $I^{(T)}_{\alpha,\mathrm{LHS}}$) whereas the hyperplane polynomials $B_{i=8,9,10}$ appear in 4-term sets (with a 2-term $I^{(i)}_{\beta,\mathrm{LHS}}$) meaning that such 1-cuts effectively evolve as tree-level 3-site 1-cut tubings. This is a generic feature for all n-gon graphs and is an explicit example of how lower-site lower-loop data gets gets recycled for the n-site ℓ-loop graph under study!

<u>2-cut tubings</u>

Consistent with the rules presented in section 3.5.1, there are two possible ways to construct physical 2-tubings that generates the entire space of physical 2-cuts contributing to the DEQ basis:

- *Evolution of the 1-cut(s)*: For tree level graphs, the true scattering facet $\mathcal{C}^{(0)}_{n,B_T}$ is evolved into physical 2-tubings by inserting a cut tubing inside $\mathcal{C}^{(0)}_{n,B_T}$ that is consistent with its good cut condition, as described in section 3.5.1. These 2-cuts factorize the tree-level 1-cut $\mathcal{C}^{(0)}_{n,B_T}$ or, equivalently the flat-space amplitude A_n, into a product of lower-point amplitudes.

  For example in the 3-site tree graph, two possible physical 2-cuts evolved according to the

[18] In order to demonstrate factorization properties, we will now restrict to a ϕ^3 vertex for simplicity. However, our analysis holds true for arbitrary polynomial interactions.

good cut condition of the true facet factorizes $A_5^{(0)}$ as follows:

$$\mathcal{C}^{(0)}_{1,B_3} \subset \mathcal{C}^{(0)}_{3,B_{T=4}} :=$$ 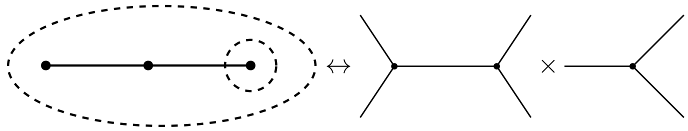 , (3.87)

$$\mathcal{C}^{(0)}_{2,B_5} \subset \mathcal{C}^{(0)}_{3,B_{T=4}} :=$$ 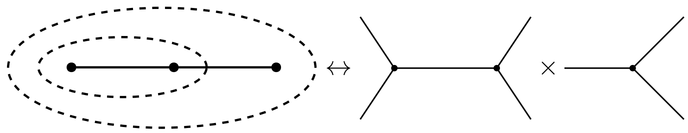 . (3.88)

It is important to note that while the above 2-cuts result in a the same product of flat-space amplitudes $A_4 \times A_3$, they are distinct cut tubings and hence generate distinct physical forms. This is a manifestation of the fact that the flat-space Mandelstam invariants are obtained from a product of two hyperplane polynomials B_i, B_j (on the residue of the total energy pole) appearing in the wavefunction coefficient. An explicit residue computation for the tubings above in (3.88) gives a result proportional to $g \times \frac{-g^2}{s_{12}}$, where g is the three-point coupling and $s_{12} = -(Y_1 - X_1)(Y_1 + X_1)$ is the flat-space Mandelstam invariant.

For 1-loop n-gons, the 1-tubings $\mathcal{C}^{(0)}_{n,B_i}$ that are not the true facet evolve according to their good cut condition, which is analogous to an n-site tree-level 1-tubing. The true facet $\mathcal{C}^{(1)}_{n,B_T}$ is evolved without any restriction; any cut tubing can be placed inside it. This discussion readily generalizes to generic ℓ-loop graphs.

- *Product of lower-point facets*: As discussed in section 3.5.1, a physical 2-cut consistent with the uni-dimensional cohomology condition involves partitioning the set of n-vertices of an ℓ-loop graph into two non-empty, non-overlapping subsets to give a product of two residue tubings $\mathcal{C}^{(\ell_1)}_{n_1,B_i} \times \mathcal{C}^{(\ell_2)}_{n_2,B_j}$ such that $n_1 + n_2 = n$. An example of such a 2-tubing for the tree-level 4-site star graph was given in (3.83) and corresponds to the factorization:

$$\mathcal{C}^{(0)}_{3,B_{10}} \times \mathcal{C}^{(0)}_{1,B_2} =$$ 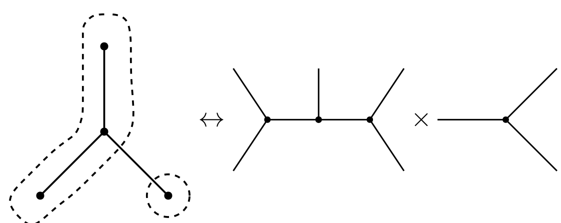 . (3.89)

Some examples of such 2-cuts in the 3-gon (triangle) and 4-gon (box) graphs are:

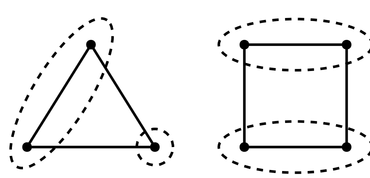 . (3.90)

It is important to note that each cut tubing in these 2-cuts will evolve as independent 1-cut tubings, in accordance with its own set of good and degenerate cut conditions. What guarantees this is the existence of linear relations where B_i, B_j now act as the "true" facets of lower-point functions with n_1 and n_2 vertices.

For example, in the 4-site star example presented above, the hyperplane B_{10} is the "true facet" in the minimal dependent set $I_1^{(10)} = \{B_4, B_{10}|B_6, B_8\}$ represented graphically by

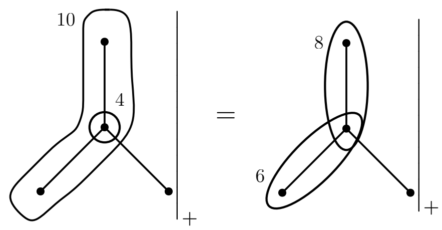

$$. \tag{3.91}$$

As a consequence, the 1-cut tubing $\mathcal{C}^{(0)}_{3,B_{10}}$ evolves as a 3-site 1-tubing.

The same story extends to product 2-tubings of the n-gon. For example, in the 4-gon 2-cut presented above, the two 1-cuts will each evolve as the 1-cut of the 2-site tree-level graph!

One can similarly work out higher loop examples. For example, in the double-box 6-site 2-loop graph, we have the following possible physical 2-cut:

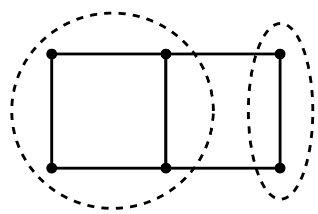

$$. \tag{3.92}$$

While the first 1-cut evolves as that of a 4-gon box, the second 1-cut evolves as the 1-cut of the 2-site tree-level graph. This allows us to effectively reuse lower-site, lower-loop data for complicated loop graphs under study!

3-cut tubings

There are now three possible ways to construct physical 3-tubings that generates the entire space of physical 3-cut forms, while accounting for the appearance of degenerate cuts:

- *Evolution of the 1-cut(s)*: At tree level, the evolution of the physical 2-tubings involving the true facet $\mathcal{C}^{(0)}_{n,B_T}$ occurs via the two possible options.

  i) Evolving the latest cut tubing consistent with its good cut condition. In such a scenario, one has to also account for the degenerate cut condition of section 3.5.1. An example of a non-degenerate and degenerate 3-cut for the tree-level 4-site star graph are:

$$\mathcal{C}^{(0)}_{1,B_1} \subset \mathcal{C}^{(0)}_{3,B_9} \subset \mathcal{C}^{(0)}_{4,B_{T=5}} =$$ 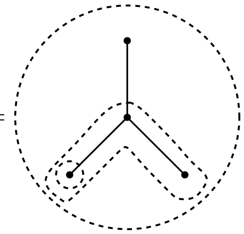 ,

$$\mathcal{C}^{(0)}_{2,B_6} \subset \mathcal{C}^{(0)}_{3,B_9} \subset \mathcal{C}^{(0)}_{4,B_{T=5}} =$$ 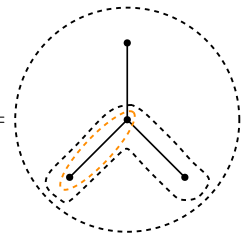 . (3.93)

ii) Introducing an additional good cut tubing inside the true facet consistent with the second uni-dimensional cohomology condition, i.e., $(\mathcal{C}^{(0)}_{n_1,B_i} \times \mathcal{C}^{(0)}_{n_2,B_j}) \subset \mathcal{C}^{(0)}_{n,B_T}$ such that $n_1 + n_2 < n$. From a factorization perspective, this ensures that we avoid cutting an internal edge of the flat amplitude twice simultaneously.

An example of such a 3-tubing for the 3-site graph is (3.85), This is also the maximal number of tubings one can draw for such a graph and decomposes the flat-space amplitude into its three 3-pt building blocks $A_3^{(0)}$:

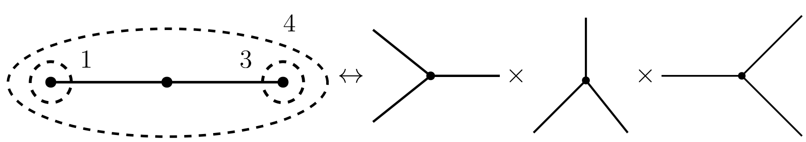

. (3.94)

- *Evolution of the lower-point facets*: As discussed, the evolution of the 2-cut $\mathcal{C}^{(\ell_1)}_{n_1,B_i} \times \mathcal{C}^{(\ell_2)}_{n_2,B_j}$ proceed without extra subtleties except that any evolution of the individual 1-cuts has to be consistent with its good cut conditions. An example of such a 3-tubing for the 4-gon is shown as follows:

$$(\mathcal{C}^{(0)}_{1,B_3} \subset \mathcal{C}^{(0)}_{3,B_{12}}) \times \mathcal{C}^{(0)}_{1,B_2} :=$$ 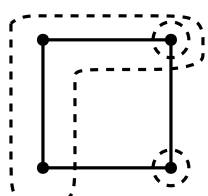 . (3.95)

- *Product of lower-point facets*: As before, one can construct physical 3-cuts consistent with the uni-dimensional cohomology condition, which involves a simple partition of the n-vertices into three non-empty, non-overlapping subsets to give a product of three 1-cuts $\mathcal{C}^{(\ell)}_{n_1,B_i} \times \mathcal{C}^{(\ell)}_{n_2,B_j} \times \mathcal{C}^{(\ell)}_{n_3,B_k}$ such that $n_1 + n_2 + n_3 = n$. An example of such a 3-tubing for the 4-site star tree graph is:

$$\mathcal{C}^{(0)}_{2,B_8} \times \mathcal{C}^{(0)}_{1,B_1} \times \mathcal{C}^{(0)}_{1,B_2} \; := \quad \tag{3.96}$$

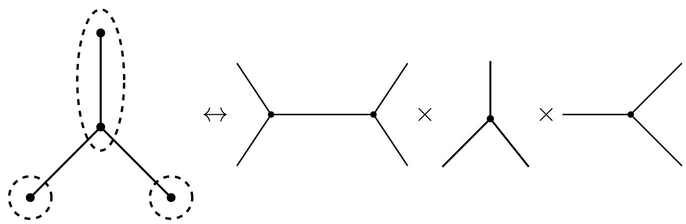

<u>n-cut tubings</u>

The procedure to generate the n-cut tubings for any n-site, ℓ-loop graph proceeds in a similar fashion — evolution and construction of each cut tubing such that it is consistent with its *good cut*, *degenerate cut* and the *uni-dimensional cohomology* conditions at each step. For a generic graph, the maximal number of residue operations one can perform is n, which from a cuts perspective corresponds to decomposing the flat-space amplitude A_n into its n 3-point building blocks. The process ends when one has generated all physical boundaries contributing to 1-, 2-, ..., n-cuts, which in turn enumerate all the physical forms contributing to the physical subspace of the DEQs!

3.5.3 From cut tubings to physical FRW forms

This space of physical cut tubings can be translated to the corresponding physical FRW forms that constitute physical DEQ basis. Not only do these cut tubings enumerate the space of physical cuts and therefore, the dlog_J part of a basis form (c.f., (3.23)), they also determine $\tilde{\Omega}_J$ (and consequently Ω_J), giving the full FRW form φ_a. We provide the rule to generate non-degenerate physical forms before providing the rule for degenerate forms.

Non-degenerate physical FRW forms: Enumerating the physical cut tubings via the rules presented in sections 3.5.1 and 3.5.2 is equivalent to listing all good δ_J's. For non-degenerate cuts, each δ_J is dual via the intersection number to dlog_J. The remaining part of the FRW form is linked to the the canonical form of the cut M_J (recall each physical cut has a 1-dimensional cohomology and unique canonical form).

To determine $\tilde{\Omega}_J$ (or equivalently $\Omega_J = \tilde{\Omega}|_J$) from the cut tubings, one links each pair of vertices $\{i, j\}$ without crossing a cut tubing.[19] Each linked pair of vertices corresponds to the dlog-form: $\mathrm{dlog}\frac{x_i}{x_j}$. Wedging together all pairs produces $\tilde{\Omega}_J$. We illustrate this procedure using selected examples

[19] The variable x_i is fully determined if it is the only unenclosed vertex inside another cut tubing. Therefore, it cannot participate in the dlog-form contributing to $\tilde{\Omega}_J$.

from the physical basis of the 4-site chain (see appendix 3.9.2)

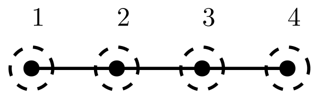

$$= \varphi_{38}^{\text{4-chain}} = \mathrm{dlog}_{1,2,3,4}\,, \tag{3.97}$$

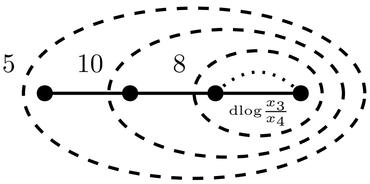

$$= \varphi_{34}^{\text{4-chain}} = \mathrm{dlog}_{5,10,8} \wedge \mathrm{dlog}\frac{x_3}{x_4}\,, \tag{3.98}$$

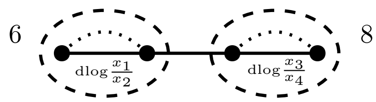

$$= \varphi_{10}^{\text{4-chain}} = \mathrm{dlog}_{6,8} \wedge \mathrm{dlog}\frac{x_1}{x_2} \wedge \mathrm{dlog}\frac{x_3}{x_4}\,, \tag{3.99}$$

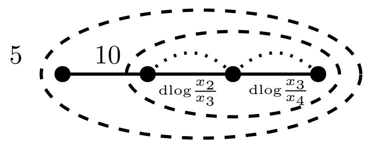

$$= \varphi_{7}^{\text{4-chain}} = \mathrm{dlog}_{5,10} \wedge \mathrm{dlog}\frac{x_2}{x_3} \wedge \mathrm{dlog}\frac{x_3}{x_4}\,, \tag{3.100}$$

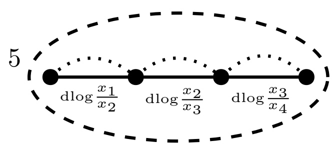

$$= \varphi_{1}^{\text{4-chain}} = \mathrm{dlog}_{5} \wedge \mathrm{dlog}\frac{x_1}{x_2} \wedge \mathrm{dlog}\frac{x_2}{x_3} \wedge \mathrm{dlog}\frac{x_3}{x_4}\,, \tag{3.101}$$

and the 1-loop 3-gon (see appendix 3.9.4)

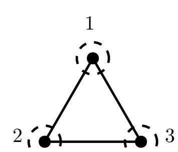

$$= \varphi_{24}^{\text{3-gon}} = \mathrm{dlog}_{1,2,3}\,, \tag{3.102}$$

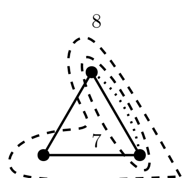

$$= \varphi_{24}^{\text{3-gon}} = \mathrm{dlog}_{8,7} \wedge \mathrm{dlog}\frac{x_1}{x_3}\,, \tag{3.103}$$

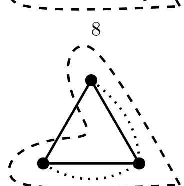

$$= \varphi_{2}^{\text{3-gon}} = \mathrm{dlog}_{8} \wedge \mathrm{dlog}\frac{x_1}{x_2} \wedge \mathrm{dlog}\frac{x_2}{x_3}\,, \tag{3.104}$$

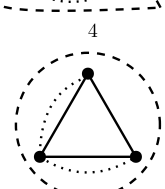

$$= \varphi_{1}^{\text{3-gon}} = \mathrm{dlog}_{4} \wedge \mathrm{dlog}\frac{x_1}{x_2} \wedge \mathrm{dlog}\frac{x_2}{x_3}\,. \tag{3.105}$$

Note that the indices in the dlog_J have been ordered according to our cut ordering rules: larger tubes come before smaller tubes.

Degenerate physical FRW forms: As discussed previously, there are no crossed cut tubings in the physical subspace. The physical forms associated to degenerate cuts always come with a specific linear combination of dlog_J's where each J is associated to a non-crossing tubing of the degenerate cut. For example, in the 3-site chain we have

$$\varphi_{\text{phys},16} = \frac{\varphi_{19} - \varphi_{20}}{2} = \mathrm{dlog} B_4 \wedge \mathrm{dlog} \frac{B_5}{B_6} \wedge \mathrm{dlog} B_2 \,. \tag{3.106}$$

We conjecture that the physical linear combination of dlog's associated to any degenerate cut is obtained by first identifying all non-crossed cut tubings associated to this degenerate cut. Then, the corresponding dlog's are added with coefficients ± 1 such that the B_i corresponding to crossed tubings appear in ratios like in (3.106) whenever possible.

To further illustrate this point, consider the degenerate 4-cut involving B_5, B_9, B_{10}, B_7 and B_3. There are three non-crossing cut tubings associated to this cut

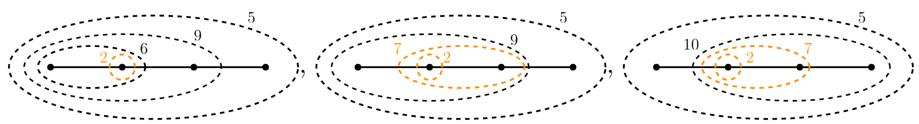

(3.107)

From the discussion above, we want the crossing tubings to appear as ratios in the physical form

$$\varphi_{63} = \mathrm{dlog}_{5,9,6,2} - \mathrm{dlog}_{5,9,7,2} + \mathrm{dlog}_{5,10,7,2} \,, \tag{3.108}$$

as given in (3.155) (produced via the direct calculation method outlined in section 3.3). Indeed this is easy to check

$$\begin{aligned} \varphi_{63} &= \mathrm{dlog} B_5 \wedge \mathrm{dlog} \frac{B_6}{B_7} \wedge \mathrm{dlog} B_7 \wedge \mathrm{dlog} B_3 + \mathrm{dlog}_{5,10,7,3} \\ &= \mathrm{dlog}_{5,9,6,2} + \mathrm{dlog} B_5 \wedge \mathrm{dlog} \frac{B_{10}}{B_9} \wedge \mathrm{dlog} B_7 \wedge \mathrm{dlog} B_2 \end{aligned} \tag{3.109}$$

where the tubings $\{\tau_6, \tau_7\}$ and $\{\tau_9, \tau_{10}\}$ cross. However, the pair $\{\tau_{10}, \tau_6\}$ also cross but cannot be put into a ratio because they differ by more than one factor of B_i.

In general, the physical dlog form for a degenerate k-cut is

$$\sum_{a=1}^{r} \underbrace{\left(\frac{\bigwedge_{i \in J_a^{(k)}} \mathrm{d}B_i}{\bigwedge_{j \in J_1^{(k)}} \mathrm{d}B_j} \right)}_{\pm 1} \mathrm{dlog}_{J_a^{(k)}} \,, \tag{3.110}$$

where $J_a^{(k)}$ is a set indexing the B_i generated by the non-crossing k-tubings associated to the degenerate k-cut: $\{\tau_a^{(k)}\}$ with $a = 1, \ldots, r \geq 2$. The only freedom is the overall sign which is fixed by a choice of $\tau_1^{(k)}$ or equivalently $J_1^{(k)}$.

To see why this formula must be correct, recall that all FRW forms are generated by the set of compatible complete tubings of $\mathcal{G}$, which by definition, do not contain crossed tubings. Additionally, note that each term in this set comes with coefficient $+1$. Up to a sign, the non-crossing residues of $\Psi_n^{(\ell)}$ corresponding to a degenerate cut must be the same. Because of this, the relative sign of the residues and corresponding combination of dlog's that appear in $\Psi_n^{(\ell)}$ comes solely from the relative sign of the differentials $\bigwedge_{j\in J_a^{(k)}} \mathrm{d}B_j$'s.

From the formula (3.110), it is easy to see that the B_i that cross must come with signs such that they form ratios in the dlog-form. Choose two terms corresponding to sets J_a and J_b that share $k-1$ elements

$$J_a^{(k)} = \{(J_a^{(k)} \cap J_b^{(k)}), p\} \quad \text{and} \quad J_b^{(k)} = \{(J_a^{(k)} \cap J_b^{(k)}), q\}\,. \tag{3.111}$$

The tubings τ_p and τ_q necessarily cross which means that they appear on the same side of a linear relation with a "+"-sign. Thus, $B_q = -B_p + \cdots$ and therefore there is a relative sign between the differentials $\wedge_{i\in J_a^{(k)}} \mathrm{d}B_i$ and $\wedge_{j\in J_1^{(k)}} \mathrm{d}B_j$. When combined, we find a dlog-form with the ratio B_p/B_q.

An alternative construction of the physical form associated to a degenerate boundary using a diagrammatic method for partial fractions can be found in appendix 3.10.

Since all degenerate cuts correspond to the same topological space, the associated $\tilde{\Omega}_{J^{(k)}}$ are the same and generated in the same way as for non-degenerate cuts. For example,

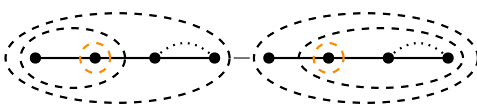

$$= \varphi_{35}^{\text{4-chain}} = \big(\mathrm{dlog}_{5,6,2} - \mathrm{dlog}_{5,10,2}\big) \wedge \mathrm{dlog}\frac{x_3}{x_4}\,, \tag{3.112}$$

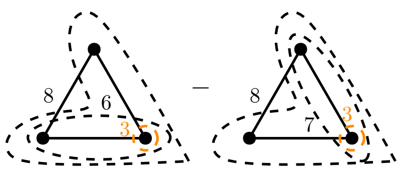

$$= \varphi_{48}^{\text{3-gon}} = \mathrm{dlog}_{8,6,3} - \mathrm{dlog}_{8,7,3}\,, \tag{3.113}$$

where $\varphi_{35}^{\text{4-chain}}$ and $\varphi_{48}^{\text{3-gon}}$ can be found in appendix 3.9.2 and 3.9.4.

3.5.4 Example: the physical basis for the 3-site tree graph from cut tubings

We now demonstrate the rules governing the evolution and construction of cut tubings to enumerate the physical boundaries contributing to the DEQ system with explicit examples. We begin with the 3-site tree graph and show that our prescription involving drawing consistent residue tubings land us on the 16 physical forms listed in (3.51). For the hyperplane polynomials B_i and the associated linear relation system I for the 3-site tree graph, please refer to (3.28) and (3.31) respectively.

<u>1-cut tubing</u>

As discussed in section 3.5.2, the only allowed 1-tubing consistent with the uni-dimensional cohomology condition is the true scattering facet of the 3-site tree graph $\mathcal{C}^{(0)}_{3,B_{T=4}}$. This corresponds to the residue that yields the 5-pt flat-space tree amplitude A_5:

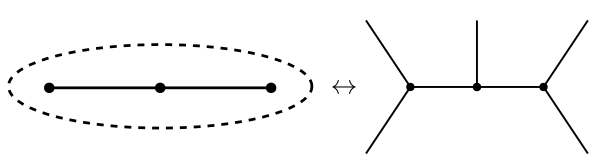

$$, \tag{3.114}$$

as well as the physical form φ_1 given in (3.46).

2-cut tubings

Now, there are two possible ways to construct physical 2-tubings, as discussed in section 3.5.2:

i) Evolve the scattering facet tubing (3.114) consistent with its good cut condition. Following the discussion leading up to (3.72), we obtain four such good 2-tubings that evolve from the scattering facet which generate the physical forms $\varphi_2, \varphi_4, \varphi_6, \varphi_4$ listed in (3.47):

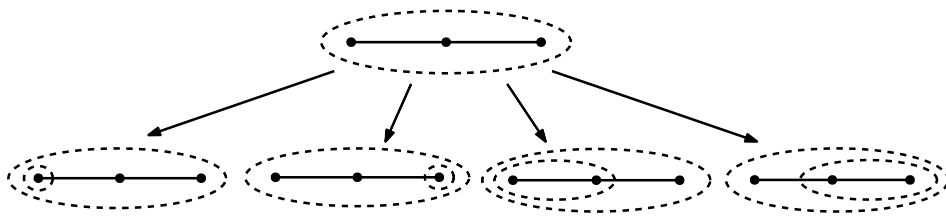

(3.115)

Each of these 2-cuts above factorize the 5-pt flat amplitude A_5 into the product $A_4 \times A_3$, as was shown in (3.88) for two such 2-cuts.

ii) Construct physical 2-tubings by decomposing the graph into a product of two lower-point residue tubings. For the 3-site graph, we have two such possibilities:

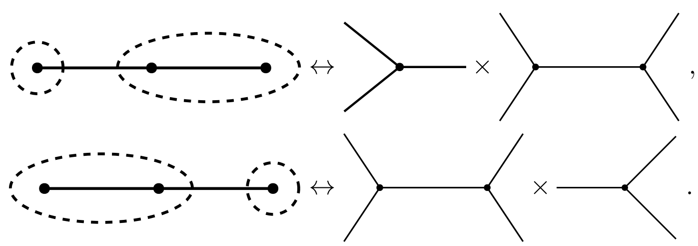

(3.116)

These 2-cuts correspond to the physical forms φ_3 and φ_5 in (3.47).

3-cut tubings

The construction of 3-cut tubings proceeds in three different ways, as outlined in section 3.5.2:

i) Continue evolving the 2-tubings that originated from the scattering facet (3.115), except that now we have to be consistent with the appropriate degenerate cut condition. Additionally, we can construct a 3-cut consistent with the uni-dimensional cohomology condition, as shown in (3.94). Thus, we get three non-degenerate physical 3-tubings that correspond to the forms $\varphi_{13}, \varphi_{16}, \varphi_{18}$ in (3.48). The degenerate 3-cuts (3.76) are identified and counted precisely *once*; they correspond to the physical form $(\varphi_{19} - \varphi_{20})/2$. The full evolution of the scattering facet tubing into 3-cuts is depicted below:

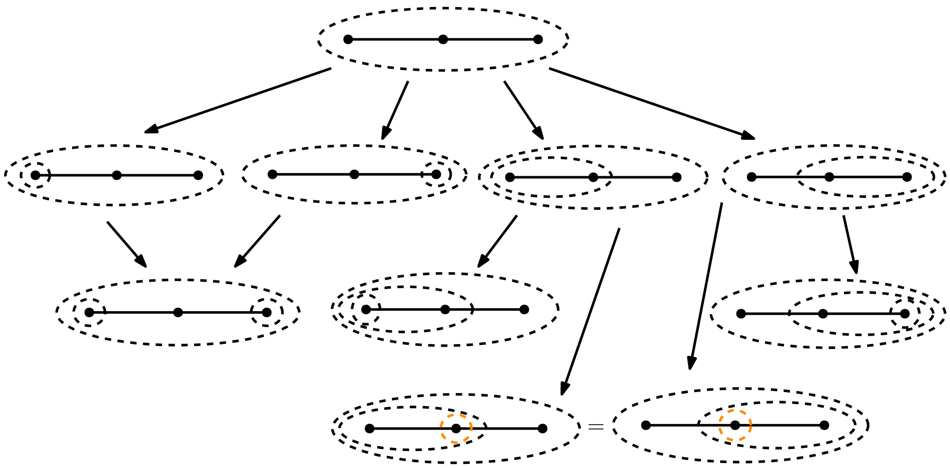

(3.117)

All the 3-cuts above correspond to the product $A_3 \times A_3 \times A_3$, as shown explicitly for the 3-cut in (3.94).

ii) The second set of physical 3-tubings are obtained by evolving the 2-tubings constructed in (3.116). We note the tubings $\mathcal{C}^{(0)}_{2,B_5}$ and $\mathcal{C}^{(0)}_{2,B_6}$ in (3.116) are effectively scattering facets of a 2-site tree graph, which can be evolved without restriction (as there are no associated minimal dependent sets I associated with $\Psi^{(0)}_2$):

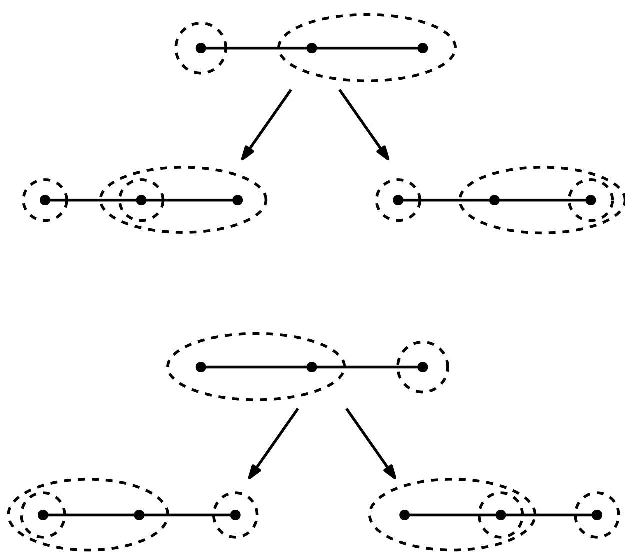

(3.118)

These 3-cuts correspond to the physical forms $\varphi_{12}, \varphi_{15}, \varphi_{14}, \varphi_{17}$ in (3.48) and also decompose the flat amplitude A_5 into its three building blocks A_3.

iii) The remaining physical 3-cut:

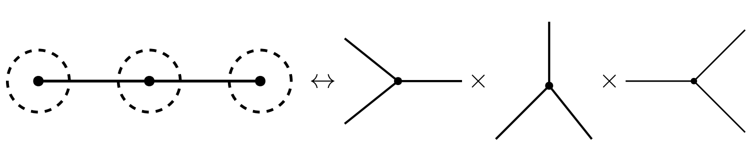

(3.119)

generates the remaining physical 3-form φ_{11} in (3.48).

For the 3-site tree graph, the maximal number of residues one can take is three and hence the flow ends with drawing all consistent 1-, 2- and 3-tubings, which are in *one-to-one* correspondence with all possible ways to factorize the 5-pt flat amplitude down to its 3-point building blocks, as demonstrated above. Therefore, these simple rules for evolving cut tubings generate the 16 physical forms in the DEQs of the 3-site tree-level wavefunction coefficient!

3.5.5 Example: the physical basis for 2-site 2-loop sunset graph from cut tubings

Having demonstrated the universal rules for residue tubings for the simplest 3-site tree-level graph, we show these rules in action for the 2-site 2-loop sunset graph.

Hyperplane polynomials: The FRW hyperplane polynomials B_i associated with the sunset graph are

$B_1=$ 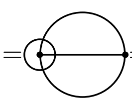 $=x_1+X_1+Y_1+Y_2+Y_3,$ $B_2=$ 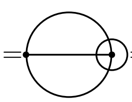 $=x_2+X_2+Y_1+Y_2+Y_3,$

$B_{T=3}=$ 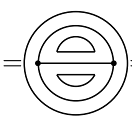 $=x_1+x_2+X_1+X_2,$ $B_4=$ 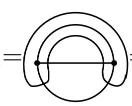 $=x_1+x_2+X_1+X_2+2Y_2+2Y_3,$

$B_5=$ 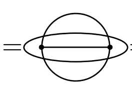 $=x_1+x_2+X_1+X_2+2Y_1+2Y_3,$ $B_6=$ 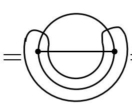 $=x_1+x_2+X_1+X_2+2Y_1+2Y_2,$

$B_7=$ 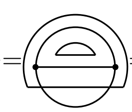 $=x_1+x_2+X_1+X_2+2Y_3,$ $B_8=$ 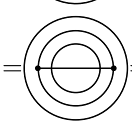 $=x_1+x_2+X_1+X_2+2Y_2,$

$B_9=$ 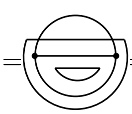 $=x_1+x_2+X_1+X_2+2Y_1.$ (3.120)

Linear relations: There exists several linear relations involving the total energy hyperplane $B_{T=3}$. These include three 4-term relations giving us the minimal dependent sets

$$I_1^{(T)}=\{B_{T=3},B_4|B_7,B_8\}\quad,\quad I_2^{(T)}=\{B_{T=3},B_5|B_7,B_9\}\quad,\quad I_3^{(T)}=\{B_{T=3},B_6|B_8,B_9\}\;. \tag{3.121}$$

There also exists linear relations involving the other hyperplane polynomials, which all give 5-term minimal dependent sets. For example, a set involving B_9 gives us

$$I^{(9)}=\{B_1,B_2,B_9|B_5,B_6\}\;. \tag{3.122}$$

However, such 5-term sets constrain the space of physical 3-cuts as per the good cut condition; hence, they will not affect our analysis for the sunset graph, where the maximal number of residues one can perform is two.

We can now construct the physical 1- and 2-cuts that contribute to the physical basis of the sunset graph.

<u>1-cut tubings</u>

There are seven 1-tubings that are consistent with the uni-dimensional cohomology condition:

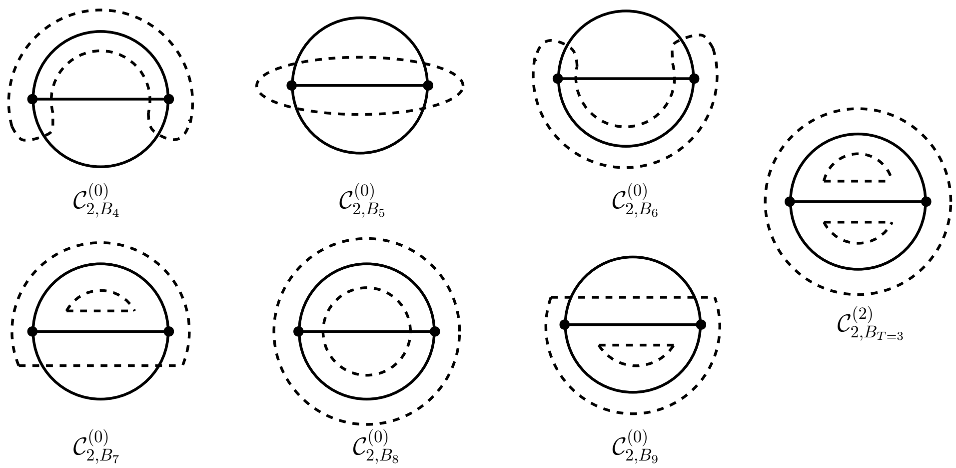

(3.123)

We note that in addition to the true scattering facet $\mathcal{C}^{(2)}_{2,B_{T=3}}$, there are six further physical 1-tubings.

<u>2-cut tubings</u>

Now, the true scattering facet $\mathcal{C}^{(2)}_{2,B_{T=3}}$ is evolved to 2-tubings consistent with its good cut condition resulting from the sets $I^{(T)}_{\alpha}$ listed in (3.121). However, coupled with the uni-dimensional cohomology condition, we only get the following two physical 2-cuts arising from the true facet:

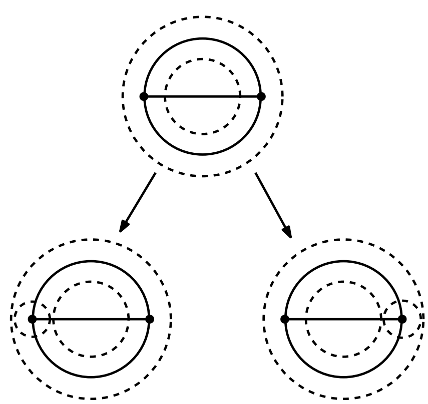

(3.124)

Each of the remaining six 1-tubings are evolved to give two physical 2-cuts, consistent with the uni-dimensional cohomology condition:

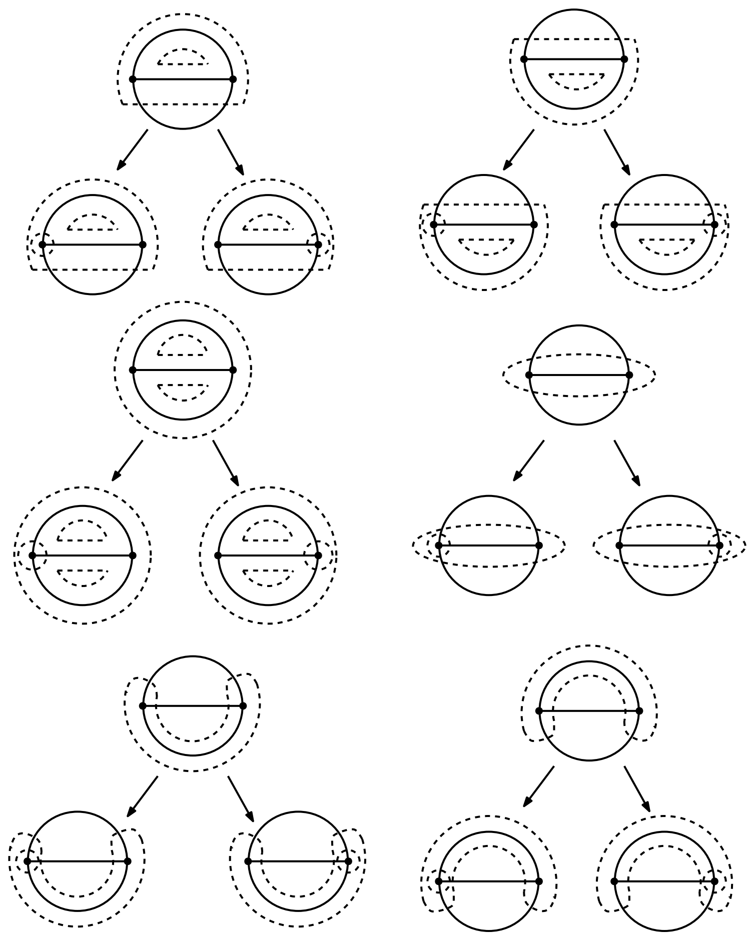

(3.125)

The remaining 2-tubing is simply given by the product of two 1-tubings enclosing each of the vertices:

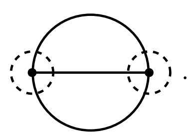

(3.126)

Counting all the seven 1-cut tubings in (3.5.5) along with the fifteen 2-cut tubings in (3.124), (3.125) and (3.126), yields the 22 physical forms for the sunset graph.

More generally, it is interesting to note that for a 2-site ℓ-loop graph, the uni-dimensional cohomology condition implies all its 1-cuts behave as those corresponding to a 2-site tree level graph. This, along with accounting for the single 2-cut of the form (3.126), allows us to predict the number of the physical forms contributing to the DEQs of the 2-site ℓ-loop wavefunction coefficient $\psi_2^{(\ell)}$:

$$\underbrace{(2^{\ell+1}-1)}_{\#\text{ 1-cuts}}+\underbrace{(2^{\ell+2}-1)}_{\#\text{ 2-cuts}}=2(3\cdot 2^{\ell}-1)\,. \tag{3.127}$$

This matches the counting of the physical forms for the bubble ($\ell = 1$) and the sunset ($\ell = 2$) graphs using the rules of kinematic flow [134, 133]. Moreover, at ℓ-loop order, (3.127) matches the counting presented in [131] obtained by adding the number of functions at each level in their corresponding DEQ system.

3.5.6 Cut stratification for trees and loops

We end this section on residue tubings with comments on certain surprising patterns associated to the space of physical boundaries/cuts for tree and loop graphs. At tree-level, the number of physical cut tubings/forms is 4^{n-1} and splits according to the codimension of the b-cuts

$$4^{n-1} = \sum_{b=1}^{n} \binom{n-1}{b-1} 3^{b-1} \, , \tag{3.128}$$

which can be organized into a Pascal triangle:

	1-cuts	2-cuts	3-cuts	4-cuts	5-cuts	6-cuts	$\cdots$
	3^0	3^1	3^2	3^3	3^4	3^5	$\cdots$
$n=2$	1	1					
$n=3$	1	2	1				
$n=4$	1	3	3	1			
$n=5$	1	4	6	4	1		
$n=6$	1	5	10	10	5	1	
$\vdots$	$\vdots$	$\vdots$	$\vdots$	$\vdots$	$\vdots$	$\vdots$	$\vdots$

Importantly, we note that this stratification is topology *independent*!

The number of physical forms for n-gons at 1-loop generated by this flow of residue tubings matches the number $(= 4^n - 2(2^n - 1))$ predicted in [131]. While this data does not form a Pascal triangle structure as in the case of tree graphs, its cut stratification is given by

	1-cuts	2-cuts	3-cuts	4-cuts	$\cdots$
$n=2$ (bubble)	3	7			
$n=3$ (triangle)	4	21	25		
$n=4$ (box)	5	42	100	79	
$\vdots$	$\vdots$	$\vdots$	$\vdots$	$\vdots$	

3.6 Discussion and Outlook

The FRW wavefunction coefficient is expressed as a twisted integral whose integrand is associated to a particular hyperplane arrangement (geometry). Recently, the kinematic flow algorithm [76, 75, 134, 133] demonstrated that the twisted cohomology of FRW cosmological integrands vastly over counts the number of integrands needed to define DEQs for FRW wavefunction coefficients. The minimal space of integrands that couple to the wavefunction coefficient is called the physical subspace and its characterization is imperative for understanding how to build DEQs for loop integrated wavefunction coefficients.

In this article, we demonstrate that the physical subspace is intimately tied to the physical (non-trivial) cuts/residues of the FRW form $\Psi_n^{(\ell)}$ (integrand of the FRW wavefunction coefficient). Using the intersection number (an inner product on the space of integrands) and exploiting extra structure in the dual relative twisted cohomology (automatically organized by cuts), we show that the physical subspace is spanned by the forms that share cuts/residues with $\Psi_n^{(\ell)}$ via equations (3.25) and (3.27).

We compute the DEQs for the full twisted cohomology of the 3-site chain (section 3.3), 4-site chain (appendix 3.9.2) and 1-loop 3-gon (appendix 3.9.4) graphs using the intersection number. Then, we demonstrate how to construct the physical subspace and check that this subspace has an integrable DEQs that closes. `Mathematica` files for these examples can be found at the github repository .

We provide geometric and graphical rules for generating the differential forms that make up the physical subspace. Importantly, one has to disentangle differential forms associated to so-called degenerate cuts. Degenerate cuts are codimension-m surfaces that correspond to the intersection of more than m (untwisted) hyperplanes ($\mathcal{B}_i = \{B_i = 0\}$). As a consequence, transposing the order of two resides in a sequential residue does not necessarily (anti-) commute. Moreover, there are relations among sequential resides and differential forms. We show that each degenerate cut contributes *only* one differential form to the physical subspace and provide a simple rule to construct this form.

Degenerate cuts are a consequence of linear relations satisfied by the polynomials that generate the cosmological hyperplane arrangement. In section 3.4, we show how all linear relations of a cosmological hyperplane arrangement are a result of simple graphical rules. Since each hyperplane is generated by a graphical 1-tubing of the Feynman graph, linear relations are the result of uncrossing a crossed 2-tubing.

Amazingly, these linear relations classify all physical, unphysical and degenerate cuts as well as differential forms. In section 3.5, we develop graphical rules for enumerating all physical cuts and identifying degenerate cuts. We also provide rules that map the diagrammatics to explicit forms. The good cut, degenerate cut and uni-dimensional cohomology conditions enumerate the physical subspace for any graph at any loop order (at the level of loop integrands). At tree-level, the physical subspace has a nice interpretation: the physical subspace is all forms associated to cuts that factorize the FRW form into exclusively flat space amplitudes. A completely satisfactory explanation of this fact is missing and left for future work.

Our results for the size of the physical subspace is in perfect agreement with other methods (kinematic flow [76, 75, 134, 133]). Moreover, we find that there is a simple Pascal's triangle structure to how many of the 4^{n-1} physical forms are associated with each b-cut (see (3.128)). For the ℓ-loop 2-site graph, we verified that the size of the physical subspace is $2(3 \cdot 2^{\ell} - 1)$ and break down how it is organized on each cut in equation (3.127).

The flow of cut tubings—how to evolve a physical m-cut to a physical $(m+1)$-cut—also predict which physical dual forms couple to each other in the DEQs. This is a consequence of the structure of dual cohomology; specifically, how the derivative produces boundary terms (see footnote 7). Then, since the dual and FRW DEQs are related by a sign and transposition, one simply reverses the arrows to get the flow of FRW forms. This effectively predicts all the zeros of the DEQs and provides a possible explanation for the mechanism responsible for the structure observed in the kinematic flow algorithm. Graphical rules for determining the entries of the connection matrix akin to the kinematic flow is currently under investigation.

3.7 Appendix: From cut contours to the dual canonical form

In this appendix, we provide more intuition for the nature of dual forms by relating them to more familiar objects: cut contours. The ideas presented here are also important for the development of a diagrammatic coaction and are part of some work in progress [149].

For a positive geometry, the canonical form maps a dual contour $\check{\Delta}$ (bounded chamber with boundaries on either $\mathcal{B}_i$ or $\mathcal{T}_i$) to an FRW form $\Omega[\check{\Delta}]$ with logarithmic singularities on $\partial\check{\Delta}$. There also exists a dual version of this map, which maps a cut contour $\Delta_J \wedge \circlearrowleft_J$ (where Δ_J is a bounded chamber on the cut M_J with boundaries $\mathcal{T}_i \cap \mathcal{B}_J$) to an FRW form via the blue arrow(s)

$$\begin{tikzcd} \text{dual forms} \arrow[r, dashed, "\langle\bullet|\bullet\rangle=\mathbb{1}"] & \text{FRW forms} \\ \text{dual contours} \arrow[ur, "\Omega"'] & \text{FRW contours} \arrow[u] \arrow[ul, dashed, "\check{\Omega}"] \end{tikzcd} \quad . \tag{3.129}$$

In this way, our basis of FRW forms inherits the essential properties of cut contours: we map contours on the space of interest to forms on the space of interest. This should be contrasted with the usual positive geometry workflow where the canonical form maps contours belonging to an axillary space to forms on the space of interest.

The first (diagonal) blue dashed arrow in (3.129) represents the dual canonical form associated to a cut contour

$$\gamma = \Delta_J \wedge \circlearrowleft_J \quad \mapsto \quad \check{\Omega}[\Delta_J \wedge \circlearrowleft_J] := \delta_J(\Omega[\Delta_J]) \, . \tag{3.130}$$

This is exactly how we build up our basis of dual forms in (3.22). The second (horizontal) blue dashed arrow in (3.129), represents choosing a basis of FRW forms that diagonalizes the intersection matrix. The following replacement rule

$$\delta_J(\Omega[\Delta_J]) \quad \mapsto \quad \mathrm{dlog}[J] \wedge \tilde{\Omega}[\Delta_J] \, . \tag{3.131}$$

generates a basis of FRW forms that almost diagonalizes the intersection matrix as demonstrated by (3.24). Recall that $\tilde{\Omega}[\Delta_J]$ is obtained from $\Omega[\Delta_J]$ by removing the restriction to the cut J acting on the T_i's (an explicit example of this procedure is given in section 3.3). A simple recipe for diagonalizing the degenerate cuts in physical subspace is provided in section 3.4.

Intuitively, the action of a dual canonical form $\check{\varphi} = \delta_J(\Omega[\Delta_J])$ on an FRW form φ via the intersection number should be thought of as an approximation to the the integral $\int_\gamma u\,\varphi$ where

$\gamma = \Delta_J \wedge \circlearrowleft_J$ is the cut contour that generates the dual canonical form $\check{\varphi}$. That is,

$$\int_{\Delta_J \wedge \circlearrowleft_J} (u \times \bullet) \approx \langle \delta_J(\Omega_J[\Delta_J]) | \bullet \rangle \,. \tag{3.132}$$

Formally, this is because the dual canonical form is a realization of Poincaré duality: $H_n(M \backslash \mathcal{B}; \mathcal{L}_u) \simeq \check{H}^n(M \setminus \mathcal{B}; \nabla) = H^n(M, \mathcal{B}; \check{\nabla})$.[20,21,22] Since we diagonalize the intersection matrix of the physical subspace, this implies, that our physical FRW forms have a diagonal pairing with physical cut contours to leading order

$$\int_{\gamma_{\mathrm{phys},a}} u\, \varphi_{\mathrm{phys},b} \approx \delta_{ab} \,. \tag{3.133}$$

Like physical dual forms, physical contours do not contain residues that annihilate the physical FRW form. The problems with degenerate residues of cosmological arrangements is dealt with in the same way as dual forms (section 3.4).

Equation (3.133) can also be thought of as a generalization of prescriptive unitarity for integrals with multi-valued integrands. Usually, prescriptive unitarity instructs one to find a basis of forms that is diagonal with respect to cut contours [114]. However, due to the twist u, the best one can do is diagonalize the leading order part of this matrix. Moreover, achieving this using the intersection number is much easier that actually carrying out the integrations and expanding in ε.

3.8 Appendix: No new poles

In this appendix, we derive a simple representation for $\nabla_{\mathrm{kin}}\varphi$ that has at most simple poles. Such a representation is needed to use the simplified formulas (3.19) and (3.21) for computing the intersection number. Then, we show that $\mathrm{Res}_{J_b}[\nabla_{\mathrm{kin}}\varphi_a] = 0 \iff \mathrm{Res}_{J_b}[\varphi_a] = 0$ from which we can deduce equation (3.27).

To this end, it is easiest to work on on the full space of kinematic and integration variables: $\mathcal{M} \setminus \mathcal{B}$. Here, we set $\mathcal{M} = \mathbb{C}^{3n+\ell-1} \setminus \mathcal{T}$ where there are $3n-1$ total variables: n integration variables x_i, n kinematic variables X_i and an additional $n+\ell-1$ kinematic variables Y_i. We also interpret the vanishing loci $\{T_i = 0\}$ and $\{B_i = 0\}$ on $\mathbb{C}^{3n+\ell-1}$ instead of just the integration space M.

Then all dlog-forms on the integration space M can be canonically uplifted to the full space $\mathcal{M}$ simply by swapping all instances of dlog for $\mathrm{D}\log = \mathrm{dlog} + \mathrm{d}_{\mathrm{kin}}\log$. We also upgrade the covariant derivative $\nabla \to \nabla_{\mathrm{D}} = \nabla + \nabla_{\mathrm{kin}} = \mathrm{D} + \mathrm{D}\log u \wedge$. Denoting the uplift of φ by Φ, the part of $\nabla_{\mathrm{D}}\Phi$

[20] In general, Poincaré duality is an isomorphism between the p^{th} homology and the $(2n-p)^{\mathrm{th}}$ cohomology where n is the complex dimension of the topological space ($M \setminus \mathcal{B}$ or $(M, \mathcal{B})$ in our case). For $p = n$, this is an isomorphism between the n^{th} homology and cohomology as stated in the main text.

[21] The symbol $\mathcal{L}_u$ is the local system to associated to the twist. Intuitively, this is extra information in the contour specifying which branch of the multi-valued function u should be used when integrating. It is only here for completeness and can be ignored for the purposes of this work.

[22] The existence of the dual canonical form should not be surprising since $H_n(M \setminus \mathcal{B}; \mathcal{L}_u)$ has an analogous decomposition to (3.17) (see [151, 155] for such a decomposition in the untwisted case).

that is a 1-form on kinematic space is cohomologous to $\nabla_{\text{kin}}\varphi$ in the usual sense. Thus, we have a closed form dlog representation of $\nabla_{\text{kin}}\phi$

$$\nabla_{\text{kin}}\varphi \simeq \varepsilon\, \mathrm{D}\log(T_1 \cdots T_n) \wedge \Phi|_{(\text{kin } p>1)\text{-forms}\to 0} \tag{3.134}$$

since Φ only has simple poles and $\Delta\Phi = 0$. The projection (kin $p > 1$)-forms $\to 0$ is equivalent to adding up all possible ways one can assign one $\mathrm{D} \to \mathrm{d}_{\text{kin}}$ with all others $\mathrm{D} \to \mathrm{d}$. Having a simple representation for $\nabla_{\text{kin}}\varphi$ with only simple poles allows for the use of formulas (3.19) and (3.21).

Then, the claim that $\mathrm{Res}_K[\varphi] = 0 \implies \mathrm{Res}_K[\nabla_{\text{kin}}\varphi] = 0$ follows straightforwardly from (3.134). Explicitly, start with the following representation for the physical differential form

$$\Psi_n^{(\ell)} = \sum_{J:|J|=n} \psi_J\, \mathrm{dlog}_J \tag{3.135}$$

for some coefficients $\psi_J \in \mathbb{Q}$. Since $\Psi_n^{(\ell)}$ does not have any poles on the twisted hyperplanes, only dlog_J forms need to be included in the above decomposition. Next, we make the replacement $\mathrm{dlog} \to \mathrm{D}\log$ to uplift $\Psi_n^{(\ell)}$ and compute its total covariant derivative

$$\Psi_n^{(\ell)} \to \sum_{J:|J|=n} \psi_J\, \mathrm{D}\log_J \tag{3.136}$$

$$\nabla_{\mathrm{D}}(3.136) = \varepsilon \sum_{J:|J|=n} \psi_J\, \mathrm{D}\log(T_1 \cdots T_n) \wedge \mathrm{D}\log_J \tag{3.137}$$

Since the residue Res_K is simply the coefficient of $\mathrm{D}\log_K$, we have

$$\mathrm{Res}_K[(3.136)] = \sum_{J\supset K} (-1)^{J\setminus K} \psi_J \bigwedge_{j\in J\setminus K} \mathrm{D}\log B_j|_K \tag{3.138}$$

and

$$\mathrm{Res}_K[(3.137)]{=}\varepsilon\ (-1)^{|K|}\mathrm{D}\log(T_1{\cdots}T_n|_K){\wedge}(3.138) \tag{3.139}$$

Therefore,

$$\mathrm{Res}_K[\Psi_n^{(\ell)}] = (3.138)|_{(\text{kin } p>1)\text{-forms}\to 0} = 0\,, \tag{3.140}$$
$$\Downarrow$$
$$\mathrm{Res}_K[\nabla_{\text{kin}}\Psi_n^{(\ell)}] = (3.139)|_{(\text{kin } p>1)\text{-forms}\to 0} = 0\,, \tag{3.141}$$

as claimed. The same manipulations work for all other basis elements, not just Ψ_n^{ℓ}.

3.9 Appendix: Further examples (including loops) via direct computation

In this appendix, we elaborate on how to construct the gauge transformation that splits the twisted cohomology into a physical and unphysical subspace (appendix 3.9.1). Then we apply the methods of section 3.3 to the 4-site chain (appendix 3.9.2), the 4-site star (appendix 3.9.3) and the 1-loop 3-gon (appendix 3.9.4) graphs. Using the intersection matrix, we demonstrate that the corresponding full cohomologies with dimensions 213, 312 and 99 reduce to a physical basis with 64, 64 and 50 elements, respectively, in agreement with both the kinematic flow algorithm [76, 75, 134, 133] and those obtained from a time integral perspective [131]. The DEQs for the 4-site chain and the 1-loop 3-gon can be found in the `Mathematica` files at the `github` repository.

3.9.1 Explicit decomposition of the 3-site chain degenerate block

To decompose the degenerate block in the 3-site chain example, we compute the vector

$$\vec{w}_{4562} := \left(\mathrm{Res}_{452}[\Psi_3^{(0)}], \mathrm{Res}_{462}[\Psi_3^{(0)}], \mathrm{Res}_{562}[\Psi_3^{(0)}]\right) = (1, -1, 0)\,, \tag{3.142}$$

and its nullspace, $\underline{\boldsymbol{W}}_{4562} := \mathrm{Null}(\vec{w}_{4562})$. Next, we build the matrix

$$\underline{\boldsymbol{\chi U}} = \begin{pmatrix} \mathbb{1}_{18\times18} & & \\ & (\vec{w}_{4562})_{1\times3} & \\ & (\underline{\boldsymbol{W}}_{4562})_{2\times3} & \\ & & \mathbb{1}_{4\times4} \end{pmatrix} = \begin{pmatrix} \mathbb{1}_{18\times18} & & & & \\ & 1 & -1 & 0 & \\ & 0 & 0 & 1 & \\ & 1 & 1 & 0 & \\ & & & & \mathbb{1}_{4\times4} \end{pmatrix}. \tag{3.143}$$

A basis of FRW forms with the analogous property is given by the basis $\boldsymbol{\varphi}'' = \underline{\boldsymbol{U}} \cdot \boldsymbol{\varphi}'$ where

$$\underline{\boldsymbol{U}} = (\underline{\boldsymbol{\chi U}} \cdot \underline{\boldsymbol{C}}')^{-1^\top} = \begin{pmatrix} \mathbb{1}_{8\times8} & & & & & & \\ & \underline{\boldsymbol{\mathcal{U}}}_{2\times2} & & & & & \\ & & \mathbb{1}_{8\times8} & & & & \\ & & & \frac{1}{2} & -\frac{1}{2} & 0 & \\ & & & 0 & 0 & 1 & \\ & & & \frac{1}{2} & \frac{1}{2} & 0 & \\ & & & & & & \mathbb{1}_{4\times4} \end{pmatrix}, \tag{3.144}$$

and $\underline{\boldsymbol{\mathcal{U}}}_{2\times2}$ is a matrix corresponding to the unphysical 56-cut with a 2-dimensional cohomology; its exact form is not needed.

The forms of (3.51) make up the physical subspace. Their corresponding differential equation is

$$\underline{\boldsymbol{A}}_{\mathrm{phys}} = \underline{\boldsymbol{A}}_{\mathrm{phys}}^{\mathrm{diag}} + \underline{\boldsymbol{A}}_{\mathrm{phys}}^{\mathrm{off\text{-}diag}}\,, \tag{3.145}$$

where

$$\begin{aligned}\underline{\boldsymbol{A}}_{\mathrm{phys}}^{\mathrm{diag}} = -\varepsilon\,\mathrm{diag}\Big(&[\![s_4^3]\!], [\![s_1^+(s_6^-)^2]\!], [\![s_1^+(s_6^+)^2]\!], [\![s_3^+(s_5^-)^2]\!], [\![s_3^+(s_5^+)^2]\!], [\![-s_3^-(s_5^+)^2]\!],\\ &[\![-s_1^-(s_6^+)^2]\!], [\![s_1^+s_2^{++}s_3^+]\!], [\![s_1^+s_2^{++}s_3^-]\!], [\![-s_1^+s_2^{--}s_3^+]\!], [\![-s_1^+s_2^{-+}s_3^+]\!],\\ &[\![s_1^+s_2^{+-}s_3^+]\!], [\![-s_1^+s_2^{-+}s_3^-]\!], [\![-s_1^-s_2^{++}s_3^+]\!], [\![-s_1^-s_2^{+-}s_3^+]\!], [\![-s_1^-s_2^{++}s_3^-]\!]\Big)\,,\end{aligned} \tag{3.146}$$

and

$$
\underline{\boldsymbol{A}}^{\text{off-diag}}_{\text{phys}} = \varepsilon \begin{pmatrix}
0 & 0 & 0 & 0 & 0 & 0 & 0 & 0\cdots \\
\frac{2}{3}\left\llbracket -\frac{S_1^+}{S_6^-}\right\rrbracket & 0 & 0 & 0 & 0 & 0 & 0 & 0\cdots \\
0 & 0 & 0 & 0 & 0 & 0 & 0 & 0\cdots \\
\frac{2}{3}\left\llbracket -\frac{S_3^+}{S_5^-}\right\rrbracket & 0 & 0 & 0 & 0 & 0 & 0 & 0\cdots \\
0 & 0 & 0 & 0 & 0 & 0 & 0 & 0\cdots \\
\frac{2}{3}\left\llbracket -\frac{S_3^-}{S_5^+}\right\rrbracket & 0 & 0 & 0 & 0 & 0 & 0 & 0\cdots \\
\frac{2}{3}\left\llbracket -\frac{S_1^-}{S_6^+}\right\rrbracket & 0 & 0 & 0 & 0 & 0 & 0 & 0\cdots \\
0 & 0 & 0 & 0 & 0 & 0 & 0 & 0\cdots \\
0 & 0 & \frac{1}{2}\left\llbracket \frac{S_2^{++}}{S_3^-}\right\rrbracket & 0 & 0 & 0 & 0 & 0\cdots \\
0 & \frac{1}{2}\left\llbracket \frac{S_2^{--}}{S_3^+}\right\rrbracket & 0 & \frac{1}{2}\left\llbracket -\frac{S_2^{--}}{S_1^+}\right\rrbracket & 0 & 0 & 0 & 0\cdots \\
0 & 0 & 0 & 0 & \frac{1}{2}\left\llbracket -\frac{S_2^{-+}}{S_1^+}\right\rrbracket & 0 & 0 & 0\cdots \\
0 & 0 & \frac{1}{2}\left\llbracket \frac{S_2^{+-}}{S_3^+}\right\rrbracket & 0 & 0 & 0 & 0 & 0\cdots \\
0 & \frac{1}{2}\left\llbracket -\frac{S_3^-}{S_2^{-+}}\right\rrbracket & 0 & 0 & 0 & \frac{1}{2}\left\llbracket -\frac{S_1^+}{S_2^{-+}}\right\rrbracket & 0 & 0\cdots \\
0 & 0 & 0 & 0 & \frac{1}{2}\left\llbracket -\frac{S_2^{++}}{S_1^-}\right\rrbracket & 0 & 0 & 0\cdots \\
0 & 0 & 0 & \frac{1}{2}\left\llbracket -\frac{S_2^{+-}}{S_1^-}\right\rrbracket & 0 & 0 & \frac{1}{2}\left\llbracket \frac{S_2^{+-}}{S_3^+}\right\rrbracket & 0\cdots \\
0 & 0 & 0 & 0 & 0 & \frac{1}{2}\left\llbracket -\frac{S_1^-}{S_2^{++}}\right\rrbracket & \frac{1}{2}\left\llbracket \frac{2S_3^-}{S_2^{++}}\right\rrbracket & 0\cdots
\end{pmatrix} . \tag{3.147}
$$

To fit the connection matrix on the page, we have introduced the shorthand notation $\llbracket \bullet \rrbracket := \mathrm{dlog}(\bullet)$ and defined

$$
\begin{aligned}
S_1^{\pm} &= X_1 \pm Y_1 \,, \qquad & S_2^{\pm\pm} &= X_2 \pm Y_1 \pm Y_2 \,, \quad & S_3^{\pm} &= X_3 \pm Y_2 \,, \\
S_4 &= X_1 + X_2 + X_3 \,, \qquad & S_5^{\pm} &= X_1 + X_2 \pm Y_2 \,, \quad & S_6^{\pm} &= X_2 + X_3 \pm Y_1 \,.
\end{aligned} \tag{3.148}
$$

Of course, whenever all superscripts are a "+" sign, these reduce to the familiar linear forms of equation (3.6).

3.9.2 Physical basis for the tree-level 4-site chain

Below we present a basis for H^4_{phys}. To present the basis efficiently, we introduce the short hand $\mathrm{dlog}[i, j, \cdots] = \mathrm{dlog}(i) \wedge \mathrm{dlog}(j) \wedge \cdots$ with $i = B_i$ and $\mathbf{i} = x_i$.

We use the following labeling for the tubings/hyperplanes:

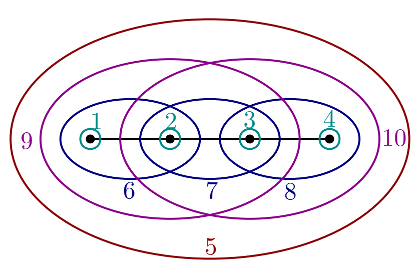

.

The flat-space wavefunction coefficient of the 4-site chain graph is (recall (3.7))

$$\frac{\hat{\Omega}^{(0)}_{\text{4-chain}}}{8Y_1Y_2Y_3} =$$

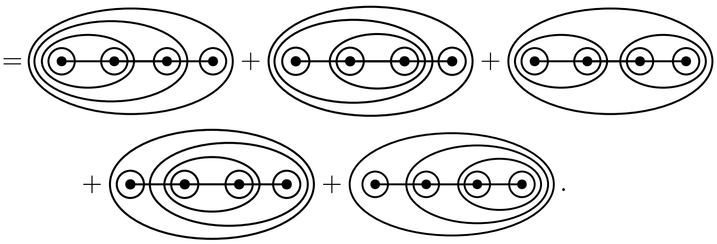

(3.149)

For the 4-site chain graph, (3.22) and (3.23) produce an over complete set of 234 forms. However, the Euler characteristic or equivalently the rank of the intersection matrix is 213. We choose a linearly independent set of 213 forms from the over complete set by removing the linearly dependent form from the three degenerate 3-boundaries and six degenerate 4-boundaries; the largest degenerate block being 12×12. Constructing the analogous gauge transformation (3.143), we arrive at a differential equation with the physical and unphysical sectors separated.

The physical basis contains a single 1-cut form,

$$\varphi_1 = \mathrm{dlog}[5, \tfrac{\mathbf{1}}{\mathbf{2}}, \tfrac{\mathbf{2}}{\mathbf{3}}, \tfrac{\mathbf{3}}{\mathbf{4}}]\,, \tag{3.150}$$

and nine 2-cut forms

$$\begin{aligned} &\varphi_2 = \mathrm{dlog}[5, 1, \tfrac{\mathbf{2}}{\mathbf{3}}, \tfrac{\mathbf{3}}{\mathbf{4}}], \quad &&\varphi_3 = \mathrm{dlog}[10, 1, \tfrac{\mathbf{2}}{\mathbf{3}}, \tfrac{\mathbf{3}}{\mathbf{4}}], \quad &&\varphi_4 = \mathrm{dlog}[5, 4, \tfrac{\mathbf{1}}{\mathbf{2}}, \tfrac{\mathbf{2}}{\mathbf{3}}], \\ &\varphi_5 = \mathrm{dlog}[9, 4, \tfrac{\mathbf{1}}{\mathbf{2}}, \tfrac{\mathbf{2}}{\mathbf{3}}], \quad &&\varphi_6 = \mathrm{dlog}[5, 9, \tfrac{\mathbf{1}}{\mathbf{2}}, \tfrac{\mathbf{2}}{\mathbf{3}}], \quad &&\varphi_7 = \mathrm{dlog}[5, 10, \tfrac{\mathbf{2}}{\mathbf{3}}, \tfrac{\mathbf{3}}{\mathbf{4}}], \\ &\varphi_8 = \mathrm{dlog}[5, 6, \tfrac{\mathbf{1}}{\mathbf{2}}, \tfrac{\mathbf{3}}{\mathbf{4}}], \quad &&\varphi_9 = \mathrm{dlog}[5, 8, \tfrac{\mathbf{1}}{\mathbf{2}}, \tfrac{\mathbf{3}}{\mathbf{4}}], \quad &&\varphi_{10} = \mathrm{dlog}[6, 8, \tfrac{\mathbf{1}}{\mathbf{2}}, \tfrac{\mathbf{3}}{\mathbf{4}}]. \end{aligned} \tag{3.151}$$

Note that once restricted to the 56-, 58- and 68-cuts, the form $\mathrm{dlog}\left(\frac{x_1}{x_2}, \frac{x_3}{x_4}\right)$ becomes the corresponding non-simplicial canonical form on that cut.

The 3-cut forms corresponding to non-degenerate boundaries are

$$\begin{aligned} &\varphi_{11} = \mathrm{dlog}[8, 1, 2, \tfrac{\mathbf{3}}{\mathbf{4}}], \quad &&\varphi_{12} = \mathrm{dlog}[10, 1, 2, \tfrac{\mathbf{3}}{\mathbf{4}}], \quad &&\varphi_{13} = \mathrm{dlog}[5, 1, 4, \tfrac{\mathbf{2}}{\mathbf{3}}], \\ &\varphi_{14} = \mathrm{dlog}[7, 1, 4, \tfrac{\mathbf{2}}{\mathbf{3}}], \quad &&\varphi_{15} = \mathrm{dlog}[9, 1, 4, \tfrac{\mathbf{2}}{\mathbf{3}}], \quad &&\varphi_{16} = \mathrm{dlog}[10, 1, 4, \tfrac{\mathbf{2}}{\mathbf{3}}], \\ &\varphi_{17} = \mathrm{dlog}[5, 6, 1, \tfrac{\mathbf{3}}{\mathbf{4}}], \quad &&\varphi_{18} = \mathrm{dlog}[1, 5, 8, \tfrac{\mathbf{3}}{\mathbf{4}}], \quad &&\varphi_{19} = \mathrm{dlog}[5, 9, 1, \tfrac{\mathbf{2}}{\mathbf{3}}], \\ &\varphi_{20} = \mathrm{dlog}[6, 8, 1, \tfrac{\mathbf{3}}{\mathbf{4}}], \quad &&\varphi_{21} = \mathrm{dlog}[10, 7, 1, \tfrac{\mathbf{2}}{\mathbf{3}}], \quad &&\varphi_{22} = \mathrm{dlog}[10, 8, 1, \tfrac{\mathbf{3}}{\mathbf{4}}], \\ &\varphi_{23} = \mathrm{dlog}[8, 6, 2, \tfrac{\mathbf{3}}{\mathbf{4}}], \quad &&\varphi_{24} = \mathrm{dlog}[6, 3, 4, \tfrac{\mathbf{1}}{\mathbf{2}}], \quad &&\varphi_{25} = \mathrm{dlog}[9, 3, 4, \tfrac{\mathbf{1}}{\mathbf{2}}], \\ &\varphi_{26} = \mathrm{dlog}[6, 8, 3, \tfrac{\mathbf{1}}{\mathbf{2}}], \quad &&\varphi_{27} = \mathrm{dlog}[5, 6, 4, \tfrac{\mathbf{1}}{\mathbf{2}}], \quad &&\varphi_{28} = \mathrm{dlog}[5, 8, 4, \tfrac{\mathbf{1}}{\mathbf{2}}, \\ &\varphi_{29} = \mathrm{dlog}[5, 10, 4, \tfrac{\mathbf{2}}{\mathbf{3}}, \quad &&\varphi_{30} = \mathrm{dlog}[6, 8, 4, \tfrac{\mathbf{1}}{\mathbf{2}}], \quad &&\varphi_{31} = \mathrm{dlog}[9, 6, 4, \tfrac{\mathbf{1}}{\mathbf{2}}], \\ &\varphi_{32} = \mathrm{dlog}[9, 7, 4, \tfrac{\mathbf{2}}{\mathbf{3}}], \quad &&\varphi_{33} = \mathrm{dlog}[5, 9, 6, \tfrac{\mathbf{1}}{\mathbf{2}}], \quad &&\varphi_{34} = \mathrm{dlog}[5, 10, 8, \tfrac{\mathbf{3}}{\mathbf{4}}], \end{aligned} \tag{3.152}$$

while the 3-boundary forms corresponding to degenerate boundaries are

$$\varphi_{35} = \mathrm{dlog}[5, \tfrac{6}{10}, 2, \tfrac{\mathbf{3}}{\mathbf{4}}], \quad \varphi_{36} = \mathrm{dlog}[5, \tfrac{8}{9}, 3, \tfrac{\mathbf{1}}{\mathbf{2}}], \quad \varphi_{37} = \mathrm{dlog}[5, \tfrac{9}{10}, 7, \tfrac{\mathbf{2}}{\mathbf{3}}]\,. \tag{3.153}$$

The non-degenerate 4-boundary forms:

$$
\begin{aligned}
&\varphi_{38} = \mathrm{dlog}[1,2,3,4], \quad &&\varphi_{39} = \mathrm{dlog}[8,1,2,3], \quad &&\varphi_{40} = \mathrm{dlog}[7,1,2,4],\\
&\varphi_{41} = \mathrm{dlog}[8,1,2,4], \quad &&\varphi_{42} = \mathrm{dlog}[10,1,2,4], \quad &&\varphi_{43} = \mathrm{dlog}[10,7,1,2],\\
&\varphi_{44} = \mathrm{dlog}[6,1,3,4], \quad &&\varphi_{45} = \mathrm{dlog}[7,1,3,4], \quad &&\varphi_{46} = \mathrm{dlog}[9,1,3,4],\\
&\varphi_{47} = \mathrm{dlog}[6,8,1,3], \quad &&\varphi_{48} = \mathrm{dlog}[5,6,1,4], \quad &&\varphi_{49} = \mathrm{dlog}[5,8,1,4],\\
&\varphi_{50} = \mathrm{dlog}[6,8,1,4], \quad &&\varphi_{51} = \mathrm{dlog}[9,6,1,4], \quad &&\varphi_{52} = \mathrm{dlog}[10,8,1,4],\\
&\varphi_{53} = \mathrm{dlog}[5,9,6,1], \quad &&\varphi_{54} = \mathrm{dlog}[6,2,3,4], \quad &&\varphi_{55} = \mathrm{dlog}[6,8,2,3],\\
&\varphi_{56} = \mathrm{dlog}[6,8,2,4], \quad &&\varphi_{57} = \mathrm{dlog}[9,7,3,4], \quad &&\varphi_{58} = \mathrm{dlog}[5,10,8,4]\,.
\end{aligned}
\tag{3.154}
$$

The degenerate 4-boundary forms:

$$
\begin{aligned}
&\varphi_{59} = \mathrm{dlog}[5,\tfrac{8}{9},1,3], \qquad &&\varphi_{60} = \mathrm{dlog}[10,\tfrac{7}{8},1,3],\\
&\varphi_{61} = \mathrm{dlog}[5,\tfrac{6}{10},2,4], \qquad &&\varphi_{62} = \mathrm{dlog}[9,\tfrac{6}{7},2,4],\\
&\varphi_{63} = \mathrm{dlog}[5,9,6,2]-\mathrm{dlog}[5,9,7,2]+\mathrm{dlog}[5,10,7,2], &&\\
&\varphi_{64} = \mathrm{dlog}[5,9,7,3]-\mathrm{dlog}[5,10,7,3]+\mathrm{dlog}[5,10,8,3]\,. &&
\end{aligned}
\tag{3.155}
$$

The resulting differential equation for the whole 213-dimensional cohomology has the following structure:

$$\underline{\boldsymbol{A}}_{\text{4-chain}} =$$

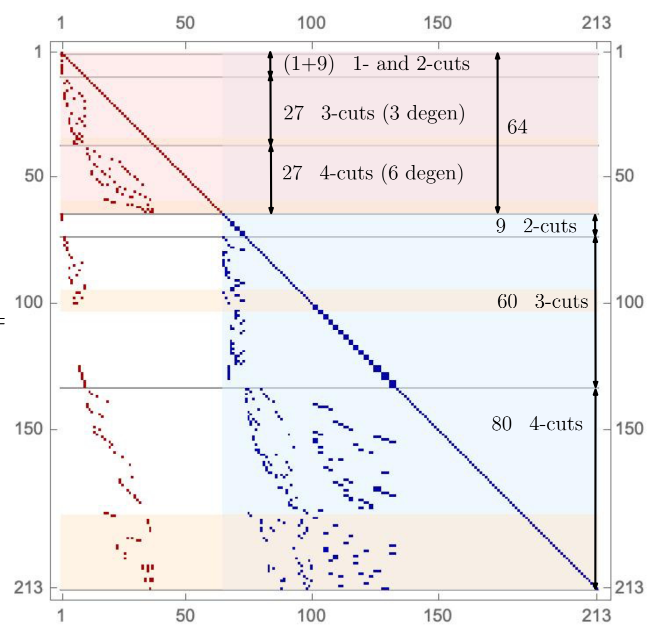

. (3.156)

This procedure outlined in section 3.3 picks out a physical space with 64 elements exactly as the kinematic flow algorithm [76, 75, 134, 133] and those obtained from a time integral perspective [131]. Moreover, we have verified that the physical 64×64 submatrix of (3.156) is integrable and can be found in the `github` repository.

3.9.3 Physical basis for the tree-level 4-site star

For the 4-site star graph, we computed the intersection matrix of the over complete basis of 377 forms. The corresponding intersection matrix

$$\underline{\boldsymbol{C}}_{\text{4-star}} = \begin{pmatrix} \underline{\boldsymbol{C}}_{\text{1- and 2-cuts}} & & \\ & \underline{\boldsymbol{C}}_{\text{3-cuts}} & \\ & & \underline{\boldsymbol{C}}_{\text{4-cuts}} \end{pmatrix}, \tag{3.157}$$

has rank 312 which is the dimension of the FRW cohomology. The intersection matrix corresponding to 1- and 2-cut forms is full rank and contains 10 elements that couple to the physical FRW form. There are three degenerate 3-cuts: manifesting as three 4×4 blocks in the intersection matrix:

$$\underline{\boldsymbol{C}}_{\text{1- and 2-cuts}} =$$

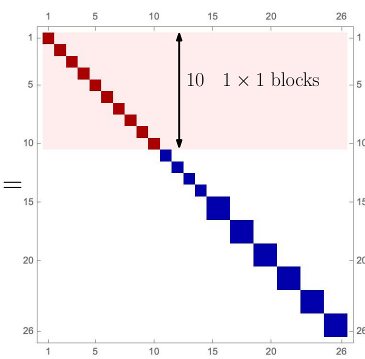

$$, \quad \underline{\boldsymbol{C}}_{\text{3-cuts}} =$$

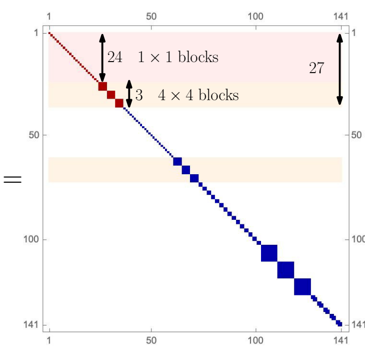

$$. \tag{3.158}$$

There are seven degenerate 4-cuts: six 4×4 blocks and one 60×60 block that couple to $\Psi^{(0)}_{\text{4-star}}$

$$\underline{\boldsymbol{C}}_{\text{4-cuts}} =$$

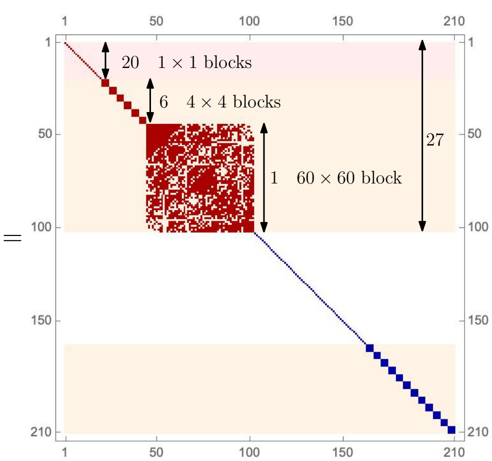

$$. \tag{3.159}$$

Knowing that each degenerate block only contributes one element to the physical basis, we obtain 64 elements for the physical basis.

It is highly non-trivial that the degenerate blocks of different topologies conspire in just the right way to produce the 2^{n-1} counting for tree-level FRW correlators. It is a special feature of the hyperplane arrangement generated by the cosmological polytope.

3.9.4 Physical basis for the 1-loop 3-gon

The hyperplane arrangement corresponding to the 1-loop 3-site diagram is generated by the 10 tubings below:

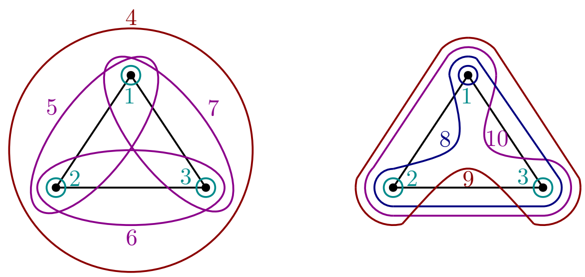

.

The flat space wavefunction coefficient for the 1-loop 3-gon is (recall (3.7))

$$\frac{\hat{\Omega}^{(1)}_{\text{3-gon}}}{8Y_1Y_2Y_3} =$$ 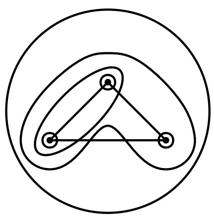 $+\, 2\times \text{rotations} +$ 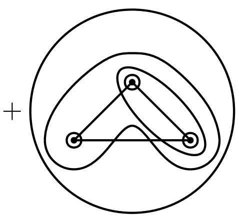 $+\, 2\times \text{rotations}\,. \qquad (3.160)$

The over complete set of forms (3.22) and (3.23) for the 1-loop 3-gon has 102 elements while the Euler characteristic/rank of the intersection matrix is 99. There are three degenerate 4×4 block (3-cuts).

Unlike at tree-level, there are $1{+}n$ non-trivial 1-boundaries for any n-gon at 1-loop. In this example, $n = 3$ and there are 4 non-trivial 1-boundary forms:

$$\varphi_1 = \mathrm{dlog}[4, \tfrac{\mathbf{1}}{\mathbf{2}}, \tfrac{\mathbf{2}}{\mathbf{3}}], \quad \varphi_2 = \mathrm{dlog}[8, \tfrac{\mathbf{1}}{\mathbf{2}}, \tfrac{\mathbf{2}}{\mathbf{3}}], \quad \varphi_3 = \mathrm{dlog}[9, \tfrac{\mathbf{1}}{\mathbf{2}}, \tfrac{\mathbf{2}}{\mathbf{3}}], \quad \varphi_4 = \mathrm{dlog}[10, \tfrac{\mathbf{1}}{\mathbf{2}}, \tfrac{\mathbf{2}}{\mathbf{3}}], \tag{3.161}$$

There are 21 2-boundary forms:

$$\begin{aligned}
&\varphi_5 = \mathrm{dlog}[4,1,\tfrac{\mathbf{2}}{\mathbf{3}}], && \varphi_6 = \mathrm{dlog}[6,1,\tfrac{\mathbf{2}}{\mathbf{3}}], && \varphi_7 = \mathrm{dlog}[8,1,\tfrac{\mathbf{2}}{\mathbf{3}}], && \varphi_8 = \mathrm{dlog}[10,1,\tfrac{\mathbf{2}}{\mathbf{3}}],\\
&\varphi_9 = \mathrm{dlog}[4,2,\tfrac{\mathbf{1}}{\mathbf{3}}], && \varphi_{10} = \mathrm{dlog}[7,2,\tfrac{\mathbf{1}}{\mathbf{3}}], && \varphi_{11} = \mathrm{dlog}[8,2,\tfrac{\mathbf{1}}{\mathbf{3}}], && \varphi_{12} = \mathrm{dlog}[9,2,\tfrac{\mathbf{1}}{\mathbf{3}}],\\
&\varphi_{13} = \mathrm{dlog}[4,3,\tfrac{\mathbf{1}}{\mathbf{2}}], && \varphi_{14} = \mathrm{dlog}[5,3,\tfrac{\mathbf{1}}{\mathbf{2}}], && \varphi_{15} = \mathrm{dlog}[9,3,\tfrac{\mathbf{1}}{\mathbf{2}}], && \varphi_{16} = \mathrm{dlog}[10,3,\tfrac{\mathbf{1}}{\mathbf{2}}],\\
&\varphi_{17} = \mathrm{dlog}[4,5,\tfrac{\mathbf{1}}{\mathbf{2}}], && \varphi_{18} = \mathrm{dlog}[4,6,\tfrac{\mathbf{2}}{\mathbf{3}}], && \varphi_{19} = \mathrm{dlog}[4,7,\tfrac{\mathbf{1}}{\mathbf{3}}], && \varphi_{20} = \mathrm{dlog}[9,5,\tfrac{\mathbf{1}}{\mathbf{2}}],\\
&\varphi_{21} = \mathrm{dlog}[10,5,\tfrac{\mathbf{1}}{\mathbf{2}}], && \varphi_{22} = \mathrm{dlog}[8,6,\tfrac{\mathbf{2}}{\mathbf{3}}], && \varphi_{23} = \mathrm{dlog}[10,6,\tfrac{\mathbf{2}}{\mathbf{3}}], && \varphi_{24} = \mathrm{dlog}[8,7,\tfrac{\mathbf{1}}{\mathbf{3}}],\\
&\varphi_{25} = \mathrm{dlog}[9,7,\tfrac{\mathbf{1}}{\mathbf{3}}].
\end{aligned} \tag{3.162}$$

There are 25 3-boundary forms:

$$\begin{aligned}
&\varphi_{26} = \mathrm{dlog}[1,2,3], && \varphi_{27} = \mathrm{dlog}[6,1,2], && \varphi_{28} = \mathrm{dlog}[7,1,2], && \varphi_{29} = \mathrm{dlog}[8,1,2],\\
&\varphi_{30} = \mathrm{dlog}[5,1,3], && \varphi_{31} = \mathrm{dlog}[6,1,3], && \varphi_{32} = \mathrm{dlog}[10,1,3], && \varphi_{33} = \mathrm{dlog}[5,1,4],\\
&\varphi_{34} = \mathrm{dlog}[7,1,4], && \varphi_{35} = \mathrm{dlog}[10,1,5], && \varphi_{36} = \mathrm{dlog}[8,7,1], && \varphi_{37} = \mathrm{dlog}[5,2,3],\\
&\varphi_{38} = \mathrm{dlog}[7,2,3], && \varphi_{39} = \mathrm{dlog}[9,2,3], && \varphi_{40} = \mathrm{dlog}[4,5,2], && \varphi_{41} = \mathrm{dlog}[4,6,2],\\
&\varphi_{42} = \mathrm{dlog}[9,5,2], && \varphi_{43} = \mathrm{dlog}[8,6,2], && \varphi_{44} = \mathrm{dlog}[4,6,3], && \varphi_{45} = \mathrm{dlog}[4,7,3],\\
&\varphi_{46} = \mathrm{dlog}[10,6,3], && \varphi_{47} = \mathrm{dlog}[9,7,3]\,.
\end{aligned} \tag{3.163}$$

Note that there are three degenerate blocks in this example

$$\varphi_{48} = \mathrm{dlog}[8,\tfrac{7}{6},3], \qquad \varphi_{49} = \mathrm{dlog}[9,\tfrac{5}{7},1], \qquad \varphi_{50} = \mathrm{dlog}[10,\tfrac{6}{5},2]\,. \tag{3.164}$$

Computing the differential equation for the 99 linearly independent elements and partitioning into a physical and unphysical space we find

$$\underline{\boldsymbol{A}}^{\text{1-loop}}_{\text{3-gon}} = \tag{3.165}$$

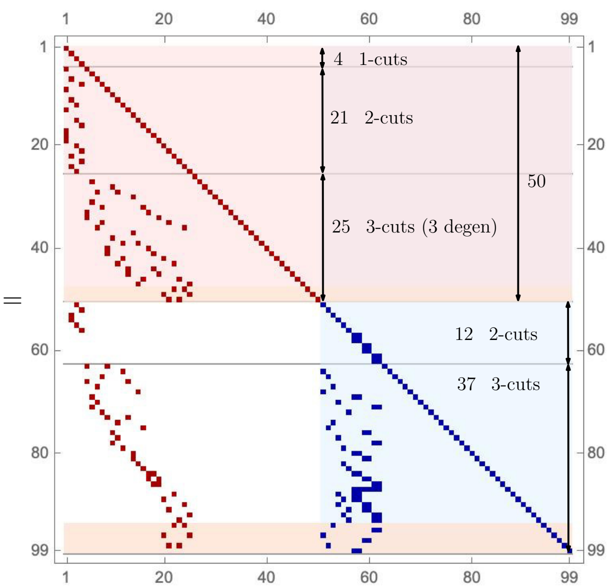

In particular, we find that the size of the physical basis is 50 elements, which agrees with [131]. Moreover, we have also checked that the 50×50 physical submatrix of (3.165) is integrable. `Mathematica` files for this example can be found at .

3.10 Appendix: Diagrammatic partial fractions

Usually, the simplest way to compute the canonical form is by summing forms associated to the set of compatible complete tubings associated to a graph $\mathcal{G}$.[23] Explicitly, if T is the set of all complete

[23] A complete non-crossing tubing is a tubing with $2n + \ell - 1$ tubings that do not intersect.

non-crossing tubings, the canonical form and function are

$$\Omega_n^{(\ell)} = \hat{\Omega}_n^{(\ell)} \frac{\mathrm{d}^n\mathbf{X}\wedge\mathrm{d}^{n+\ell-1}\mathbf{Y}}{\mathrm{GL}(1)}\,, \qquad \hat{\Omega}_n^{(\ell)} = \left(\prod_{i=1}^{n+\ell-1} 2Y_i\right)\left(\sum_{\tau\in\mathsf{T}}\prod_{t\in\tau}\frac{1}{S_t}\right). \tag{3.166}$$

For FRW correlators, we are interested in the form (3.9) which is an n-form in $\mathbf{x}$-space. Each complete non-crossing tubing contains $2n+\ell-1$ tubings or equivalently each term of (3.7) contains $2n+\ell-1$ denominators.

To isolate the specific linear combination of dlog-forms of a degenerate boundary in the physical wavefunction, it is useful to think of the canonical function as a rational function of only the $\mathbf{X}$ (or $\mathbf{x}$ after the shift). From this perspective, each term in (3.7) has more linear factors in the denominator than variables. Therefore, we partial fraction each term until there are only n denominators. Thankfully, this can be done in a simple graphical way that leads to an analytic formula without any calculation!

Start by identifying a "large" tubing S^{out} and a set of its subtubings that encircle all vertices in S^{out} once $S_1^{\text{in}},\ldots,S_m^{\text{in}}$

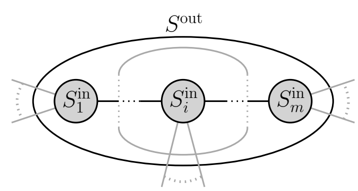

$$:= \prod_{i:S_i \text{ inside } S^{\text{out}}} \frac{1}{S_i}\,. \tag{3.167}$$

Here, each S_i^{in} *must be* a "large" tubing that contains further nested subtubings or a bare vertex. The gray external lines denote the possibility that S^{out} is only a small piece of larger tubing. The gray internal tubing is a place holder for the possibility of tubings that encircle the S_i^{in} as a whole. Then,

$$(3.167) = \frac{1}{2Y^{\text{out}}}\left[\sum_{i=1}^{m}\right.$$

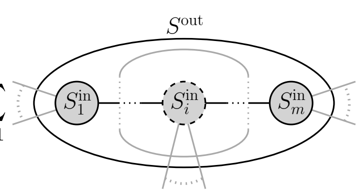

$$-$$

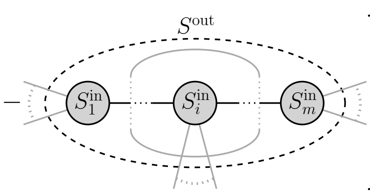

$$\left.\vphantom{\sum_{i=1}^m}\right] \tag{3.168}$$

where the dashed tubings above correspond to deleting that tubing, $Y^{\text{out}} = \sum_{e\in\mathcal{E}^{\text{out}}} Y_e$ and $\mathcal{E}^{\text{out}}$ is the set of edges that are *wholly within* S^{out} (i.e., not are crossed by S^{out}). It is easy to see that $\sum_{i=1}^m S_i^{\text{in}} - S^{\text{out}}$ is only a function of the Y_i since each vertex is encircled the same number of times in the collection of the S_i^{in} and S^{out}. Then all edges that cross S^{out} are also crossed by the S_i^{in} and therefore cancel in the difference. Hence, we are left with twice[24] the sum of all Y_i's wholly within S^{out}.

The simplest example is the 2-site chain, which has one complete non-crossing tubing

$$\hat{\Omega}_2^{(0)} = \frac{2Y}{S_1S_2S_3} =$$

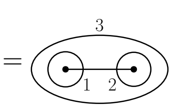

$$. \tag{3.169}$$

[24] The factor of two comes from the fact that the collection of S_i^{in} must cross each edge wholly within S^{out} twice.

Choosing $S^{\text{out}} = S_3$ and $S_i^{\text{in}} = S_i$, we can multiply the canonical function by unity

$$\hat{\Omega}_2^{(0)} = \overbrace{\frac{S_1 + S_2 - S_3}{2Y}}^{=1}\hat{\Omega}_2^{(0)} =$$

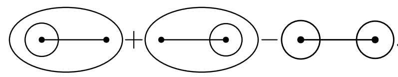

Now that we have understood how to partial fraction the maximal non-crossing tubings it is fairly straightforward to show that the terms in the canonical function that correspond to maximal codimenson degenerate boundaries come with the same relative sign.

While more complicated, it is also straightforward to verify that the dlog-forms corresponding to non-maximal codimension degenerate boundaries always come in linear combinations without relative signs. For example, suppose we want to know the linear combination of the degenerate propagators

$$\frac{1}{S_5 S_9 S_3} =$$

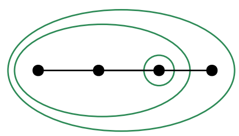

$$, \quad \frac{1}{S_5 S_8 S_3} =$$

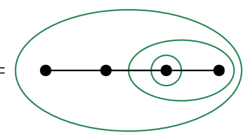

$$, \tag{3.170}$$

that appear in the canonical form. From the set of compatible complete tubings (3.149), it is easy to see that the only dlog 4-forms containing both (3.170) contain an S_1 or S_2. However, it turns out the the coefficients of $1/(S_5S_9S_3S_2)$ and $1/(S_5S_8S_3S_2)$ vanish. Therefore, we seek the coefficients of

$$\frac{1}{S_5 S_9 S_3 S_2} =$$

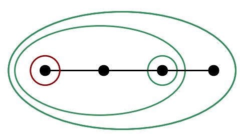

$$, \quad \frac{1}{S_5 S_8 S_3 S_2} =$$

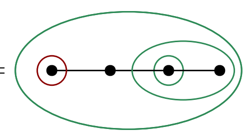

$$, \tag{3.171}$$

Using crosses to denote the choice of S^{out} and S_i^{in} we partial fraction each term in the canonical function throwing away all terms the do not contain (3.171)

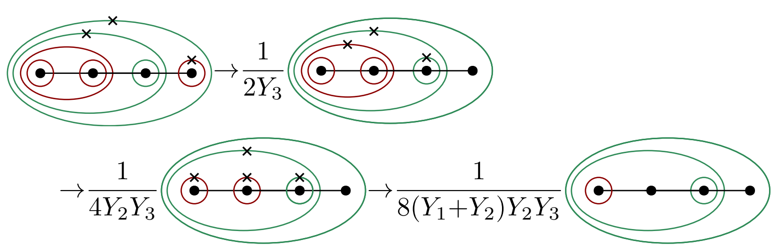

(3.172)

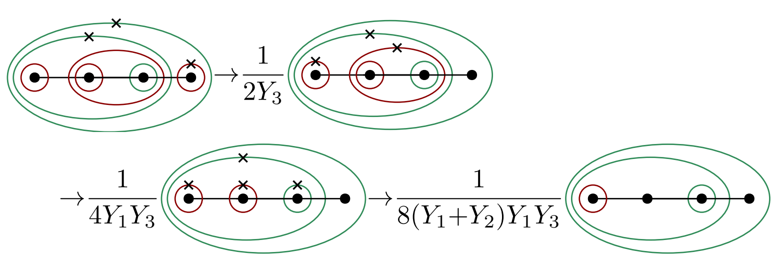

(3.173)

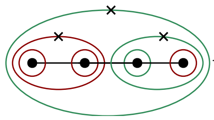 $\rightarrow \dfrac{1}{2Y_2}$ 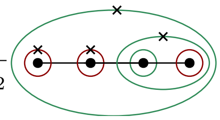

$\rightarrow \dfrac{1}{4(Y_1+Y_2)Y_2}$ 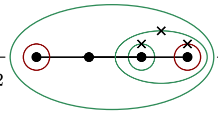 $\rightarrow \dfrac{1}{8(Y_1+Y_2)Y_2Y_3}$ 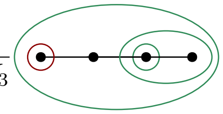 , (3.174)

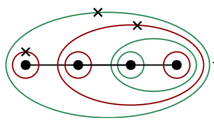 $\rightarrow \dfrac{-1}{2Y_1}$ 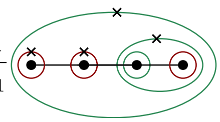

$\rightarrow \dfrac{-1}{4Y_1(Y_1+Y_2)}$ 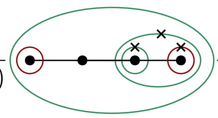 $\rightarrow \dfrac{-1}{8Y_1(Y_1+Y_2)Y_3}$ 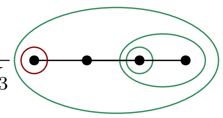 . (3.175)

Adding equations (3.172)-(3.175) together, one finds

$\dfrac{1}{8Y_1Y_2Y_3}\Bigg[$ 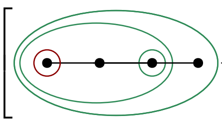 $+$ 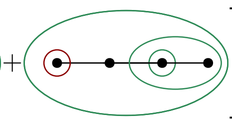 $\Bigg] = \dfrac{1}{8Y_1Y_2Y_3S_1}\left(\dfrac{1}{S_5S_9S_3}+\dfrac{1}{S_5S_9S_3}\right).$ (3.176)

To turn this into the dlog-form of interest, we shift $\mathbf{x} \to \mathbf{X}$ and multiply by the volume form $\mathrm{d}^4\mathbf{x}$

$$
\begin{aligned}
\frac{\mathrm{d}^4\mathbf{x}}{B_1}\left(\frac{1}{B_5B_9B_3}+\frac{1}{B_5B_8B_3}\right) &= \frac{\mathrm{d}^4\mathbf{x}}{\mathrm{d}B_5\wedge\mathrm{d}B_9\wedge\mathrm{d}B_3\wedge\mathrm{d}B_1}\mathrm{dlog}[5,9,3,1] \\
&\quad + \frac{\mathrm{d}^4\mathbf{x}}{\mathrm{d}B_5\wedge\mathrm{d}B_8\wedge\mathrm{d}B_3\wedge\mathrm{d}B_1}\mathrm{dlog}[5,8,3,1]\,, \\
&= \mathrm{dlog}[5,\tfrac{8}{9},3,1]\,.
\end{aligned}
\tag{3.177}
$$

The additive positivity of the partial fractioned canonical function is reflected in the fact that the pair of crossing hyperplanes in the degenerate boundary (B_8 and B_9) appear as a ratio in the above dlog-form.

Chapter 4

Hidden Zeros of the Cosmological Wavefunction

This chapter is based on the work [156].

Scattering amplitudes in certain quantum field theories have recently been shown to possess a remarkable property called hidden zeros which are special kinematic configurations of the scattering data for which the amplitudes vanish [157]. Furthermore, amplitudes in $\mathrm{Tr}(\phi^3)$ theory, the non-linear sigma model, and Yang-Mills theory exhibit a novel factorization property, termed splitting, near the kinematical locus of their hidden zeros [158, 157]. While the factorization of an amplitude on its poles is dictated by unitarity, the physical origin of splitting on its hidden zeros remains less understood. Recent progress in this regard has shown that the existence of hidden zeros in these theories is intimately tied to the color-kinematics duality [159, 160, 161] and enhanced ultraviolet scaling under BCFW shifts [162]; see also [163, 164, 165, 166, 167] for other recent work on hidden zeros and splittings. Earlier examples of amplitude zeros include the Adler zeros of pion amplitudes [168], the radiation zero in vector boson pair production [169], and zeros in dual resonant amplitudes studied in the early days of string theory [170].

The past few years have also seen considerable progress in our understanding of the analytic structure of observables in cosmological spacetimes from underlying combinatorial and geometric structures. In particular, the Bunch-Davies wavefunction for individual graphs in a theory of conformally coupled scalars can be described combinatorially by graph tubings and geometrically as the canonical form of the cosmological polytope [171] (see [172] for a review). More recently, it was shown in [173] that the graph associahedron encodes the combinatorics of graph tubings for single graphs, forming the building blocks for the cosmohedron – the geometric object capturing sums over graphs contributing to the $\mathrm{Tr}(\phi^3)$ wavefunction.

Given the crucial role of geometry (specifically, the ABHY associahedron [9]) in revealing hidden zeros of $\mathrm{Tr}(\phi^3)$ scattering amplitudes through its "flattening" limits, it is natural to explore whether similar features arise in cosmology. In this paper, we investigate hidden zeros of the cosmological Bunch-Davies wavefunction, focusing on flat-space wavefunction coefficients in a theory of massless scalars with a ϕ^3 interaction, which has been extensively studied in the literature [73, 70, 49, 76, 75, 139, 131, 135, 133, 125, 174]. Unlike the case of flat-space amplitudes, where hidden zeros emerge from full on-shell amplitudes obtained by summing over all Feynman diagrams, we study the structure of hidden zeros in individual diagrams contributing to wavefunction coefficients. By leveraging the geometry of the graph associahedron, we reveal how these zeros manifest in cosmological observables, offering a new perspective on their analytic properties.

The paper is organized as follows. We begin in section 4.1 by establishing notation for the (stripped) wavefunction coefficients corresponding to the various graph topologies (tree-level and one-loop) studied in this work. In section 4.2 we establish notation for the three different types of cosmological zeros that we will call wavefunction, factorization, and parametric zeros, and work out a couple of examples in detail. We show in section 4.3 that just as the amplitude zeros in $\mathrm{Tr}(\phi^3)$ theory can be represented geometrically through various "flattening" limits of the associated geometry (the ABHY associahedron) parametric zeros emerge from flattening the geometry that encodes the wavefunction. This geometry, which we call the *cosmological* graph associahedron, is a non-simple polytope that arises from the cosmological limit of the graph associahedron introduced in [173]. We also discuss the geometric and physical origins of the wavefunction and factorization zeros. In section 4.4 we present a surprising connection between the stripped wavefunction coefficients of chain graphs and scattering amplitudes in $\mathrm{Tr}(\phi^3)$ theory. This connection remarkably allows us to use the zeros for the wavefunction associated to a single graph to find the zeros of amplitudes in $\mathrm{Tr}(\phi^3)$ theory, which involve a sum over many Feynman graphs. We conclude in 5.4 with a discussion on the scope of our findings and present ideas for future investigations.

4.1 (Stripped) wavefunctions

Arkani-Hamed, Benincasa and Postnikov showed that the wavefunction coefficients[1] for a theory of conformally coupled scalars (with polynomial interactions) in an FRW spacetime possess a remarkable combinatorial and geometric description [171] that is independent of Feynman diagrams. Our focus in this paper will be on the flat-space wavefunctions as their FRW counterparts can be obtained via a simple integral transform. The combinatorial definition of the contribution $\psi_{\mathcal{G}}$ to the n-site ℓ-loop[2] wavefunction $\psi_n^{(\ell)}$ from a single graph $\mathcal{G}$ proceeds by encircling various subgraphs of $\mathcal{G}$ with tubes to create a graph tubing. A *tube* τ of $\mathcal{G}$ contains two pieces of information: the set of sites v encircled and the set of edges e crossed. At tree-level, a tube τ is unambiguously defined by specifying the sites it encloses, but at loop level one must also specify the edges that are crossed.

If the tube τ encircles a subgraph with m sites, we refer to it as an m-tube. To compute the wavefunction, we first generate the set of all compatible (non-intersecting) complete tubings T of $\mathcal{G}$. A *tubing* is a collection of tubes and a *complete tubing* T is a maximal set of non-overlapping tubes.

[1] Henceforth, we will simply call these *wavefunctions* to avoid clutter.

[2] For loop graphs, $\psi_n^{(\ell)}$ is the *loop integrand*.

We then assign to each complete tubing the inverse of the product of all of the energy factors S_τ associated to the constituent tubings, and sum over all possible compatible complete tubings of $\mathcal{G}$. This leads to a remarkably simple formula for the wavefunction:

$$\psi_{\mathcal{G}} = \sum_{\mathsf{T}} \prod_{\tau \in \mathsf{T}} \frac{1}{S_\tau}\,, \qquad \text{where} \qquad S_\tau = \sum_{\text{sites } v \in \tau} X_v + \sum_{\text{edges } e \text{ that cross } \tau} Y_e\,, \tag{4.1}$$

where X_v is the sum of the external energies at site v and Y_e is the energy exchanged through the internal edge e of $\mathcal{G}$.

For a given graph $\mathcal{G}$, a certain subset of tubes is common to all complete tubings T and hence give factors common to every term in the corresponding expression for the wavefunction. Therefore, we define the *stripped* wavefunction $\tilde{\psi}_{\mathcal{G}}$, which is associated to a maximal collection of compatible tubes, $\tilde{\mathsf{T}}$, that do not include the total energy n-tube S_{total} (the unique tube encircling all sites and no edges) or the 1-tubes $S_1, \ldots, S_n$ that encircle a single site:

$$\psi_{\mathcal{G}} = \frac{1}{S_1 \ldots S_n S_{\text{total}}} \times \left(\sum_{\tilde{\mathsf{T}}} \prod_{\tau \in \tilde{\mathsf{T}}} \frac{1}{S_\tau} \right) = \frac{1}{S_1 \ldots S_n S_{\text{total}}} \times \tilde{\psi}_{\mathcal{G}}\,. \tag{4.2}$$

Just like the wavefunction ψ, its stripped counterpart $\tilde{\psi}$ also has an independent geometric and combinatorial interpretation: it was recently shown that $\tilde{\psi}_{\mathcal{G}}$ is the canonical function of the graph associahedron $\mathcal{AG}$ whose face structure reflects the combinatorics of the tubings $\tilde{\mathsf{T}}$ [173]. While often non-simple, the cosmological limit of this graph associahedron, $\tilde{\mathcal{A}}_{\mathcal{G}}$, better reflects the physical properties of the wavefunction (see section 4.3). In the remainder of this work, we will focus on the properties of the stripped wavefunction $\tilde{\psi}$ and deduce which of these carry over to the full wavefunction ψ.

In the next three subsections we introduce three distinct graph topologies relevant for wavefunctions in a theory with a cubic interaction: the n-chain graph and a specific class of n-star graphs at tree level, as well as the one-loop n-gon graph. We establish notation for the constituent energy factors S_τ that appear in the various graph topologies with explicit examples.

4.1.1 The n-chain

For n-chains, we use the following convention to label the site and edge energies X_v and Y_e:

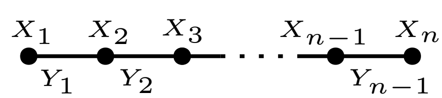

.

Then, given a tube $\tau = \{i, i+1, \ldots, i+k\}$ of the n-chain, the corresponding energy factor S_τ is given via (4.1) by

$S_{i\,i+1\ldots i+k} =$ 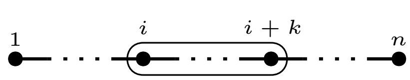

$= X_i + \cdots + X_{i+k} + Y_{i-1} + Y_{i+k}\,, \quad (4.3)$

where $Y_0 = Y_n = 0$ and the total energy n-tube is $S_{\text{total}} = S_{12\ldots n} = \sum_{i=1}^{n} X_i$. To compute the stripped wavefunction of the n-chain, we list its complete compatible tubings $\tilde{\mathsf{T}}$ and use (4.2). For example, the stripped wavefunction for the 3-chain is simply

$\tilde{\psi}_{3\text{-chain}} =$ 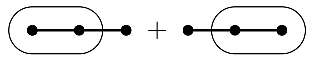 $= \dfrac{1}{S_{12}} + \dfrac{1}{S_{23}}\,, \qquad (4.4)$

while the expression for the 4-chain is

$\tilde{\psi}_{4\text{-chain}} =$ 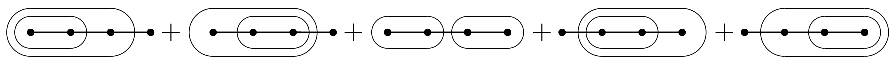

$$
\begin{aligned}
&= \frac{1}{S_{123}}\left(\frac{1}{S_{12}} + \frac{1}{S_{23}}\right) + \frac{1}{S_{12}S_{34}} + \frac{1}{S_{234}}\left(\frac{1}{S_{23}} + \frac{1}{S_{34}}\right) \\
&= \frac{1}{S_{123}}\tilde{\psi}_{3\text{-chain}}(1,2,3) + \frac{1}{S_{12}S_{34}} + \frac{1}{S_{234}}\tilde{\psi}_{3\text{-chain}}(2,3,4)\,,
\end{aligned} \tag{4.5}
$$

where the numbers in brackets denote the labels of the ordered sites of the chain subgraphs. As we have advertised on the last line of (4.5), it is clear that for general n, the stripped wavefunction exhibits a recursive structure allowing it to be expressed in terms of chain subgraphs as

$$
\tilde{\psi}_{n\text{-chain}} = \sum_{i=1}^{n-1} \frac{1}{S_{1\cdots i}S_{i+1\cdots n}} \tilde{\psi}_{i\text{-chain}}(1,\cdots,i) \times \tilde{\psi}_{n-i\text{-chain}}(i{+}1,\cdots,n)\,, \tag{4.6}
$$

except that the factor $1/S_1$ should be omitted in the $i = 1$ term and the factor $1/S_n$ should be omitted in the $i = n-1$ term. In applying this formula we note that $\tilde{\psi}_{1\text{-chain}} = \tilde{\psi}_{2\text{-chain}} = 1$.

4.1.2 The n-star

Next, we consider the n-star defined and labeled as follows:

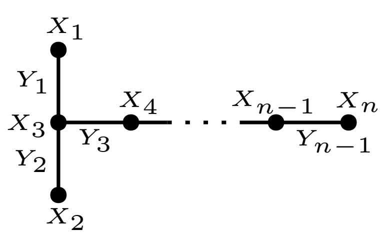

.

This graph can be arranged by connecting an $(n{-}2)$-chain and two 2-chains to a single central site with valence three. As with chain graphs, we specify a tube τ by the list of sites encircled: $\tau = \{i_1, \ldots, i_k\} \subset \{1, \ldots, n\}$ ordered such that $i_j < i_{j+1}$. The energy factors S_τ depend on which subset of the sites $\{1, 2, 3\}$ are included in the tube:

$$
\begin{gathered}
S^*_{134\ldots k} = X_1 + X_3 + \cdots + X_k + Y_2 + Y_k\,, \qquad S^*_{234\ldots k} = X_2 + X_3 + \cdots + X_k + Y_1 + Y_k\,, \\
S^*_{34\ldots k} = X_3 + \cdots + X_k + Y_1 + Y_2 + Y_k\,, \qquad S^*_{1234\ldots k} = X_1 + \cdots + X_k + Y_k\,, \\
S_{i\,i+1\ldots k} = X_i + \cdots + X_k + Y_{i-1} + Y_k\,, \quad \forall\ i \geq 4\,,
\end{gathered} \tag{4.7}
$$

where we have introduced the notation S^* for energy factors associated with tubings exclusive to the n-star, with no analog for n-chains. Note that the $S_{i\,i+1\ldots k}$ for $i \geq 4$ are simply the tubes of an $(n{-}3)$-chain (4.3) and the total energy tube is that of the n-chain, i.e. $S_{\text{total}} = S_{12\ldots n} = \sum_{i=1}^{n} X_i$.

For example, the stripped wavefunction for the 4-star can be expressed in the above notation as

$$\tilde{\psi}_{4\text{-star}} =$$

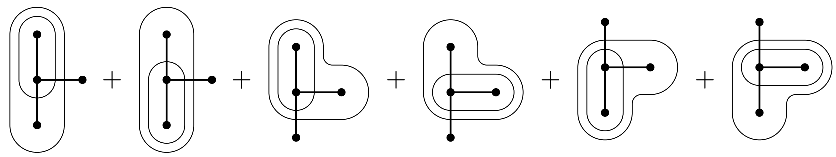

$$
\begin{aligned}
&= \frac{1}{S^*_{123}}\left(\frac{1}{S^*_{13}}+\frac{1}{S^*_{23}}\right) + \frac{1}{S^*_{134}}\left(\frac{1}{S^*_{13}}+\frac{1}{S^*_{34}}\right) + \frac{1}{S^*_{234}}\left(\frac{1}{S^*_{23}}+\frac{1}{S^*_{34}}\right) , \\
&= \frac{1}{S^*_{123}}\tilde{\psi}_{3\text{-chain}}(1,3,2) + \frac{1}{S^*_{134}}\tilde{\psi}_{3\text{-chain}}(1,3,4) + \frac{1}{S^*_{234}}\tilde{\psi}_{3\text{-chain}}(2,3,4) \, . \qquad (4.8)
\end{aligned}
$$

Like with chain topologies, the stripped wavefunction of the general n-star can be constructed recursively; this time, in terms of both chain and star subgraphs

$$
\begin{aligned}
\tilde{\psi}_{n\text{-star}} = {} & \frac{1}{S^*_{123}S_{45\ldots n}}\tilde{\psi}_{3\text{-chain}}(1,3,2) \times \tilde{\psi}_{n-3\text{-chain}}(4,\ldots,n) + \sum_{i=1}^{2}\frac{1}{S^*_{i3\cdots n}}\tilde{\psi}_{n-1\text{-chain}}(i,3,\ldots,n) \\
& + \sum_{i=1}^{n-4}\frac{1}{S^*_{123\ldots n-i}S_{n-i+1\ldots n}}\tilde{\psi}_{n-i\text{-star}}(1,\ldots,n-i) \times \tilde{\psi}_{i\text{-chain}}(n-i+1,\ldots,n) \ , \qquad (4.9)
\end{aligned}
$$

except that all $1/S_n$ factors should be omitted in the above expression. The seed of this recursive formula is the expression (4.8) for the 4-star, which gives a recursive relation for the n-star purely in terms of chain subgraphs.

4.1.3 The n-gon

For graphs corresponding to loop integrands, we only need to consider the 1-loop n-gon since any other graph can be obtained by gluing trees to the n-gon. We arrange the n sites of the n-gon on a circle in a clockwise manner:

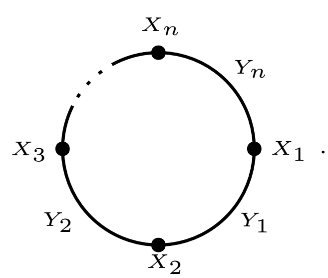

The indices labeling the sites of the n-gon are to be interpreted cyclically. The energy tubes S_τ contributing to $\tilde{\psi}_{n\text{-gon}}$ are specified by a list of cyclically consecutive sites $\tau = \{i, i+1, \ldots, j\}$

$$S_{i\,i+1\ldots j} =$$

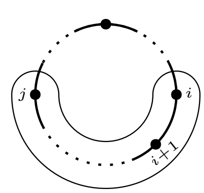

$$= X_i + \cdots + X_j + Y_{i-1} + Y_j \, , \qquad (4.10)$$

for all tubes other than the total energy tube S_{total}. One should think of the tubes in (4.10) as starting at i and ending at j; in particular, tubes that start at i and end at $j = i-1$, i.e.

$\tau = \{i, i+1, \ldots, i-1\}$ also contribute to the stripped wavefunction. We label the total energy tube by $\tau = \{1, 2, \ldots, n, 1\} = \{i, i+1, \ldots, n, 1, \ldots, i\}$ and draw it as:

$$S_{\text{total}} = S_{12\cdots n1} =$$

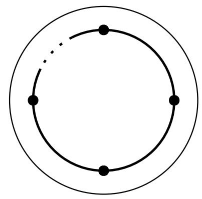

$$= \sum_{i=1}^{n} X_i \,. \tag{4.11}$$

Notice that both tubes $\tau = \{1, 2, \ldots, n\}$ and $\tau = \{1, 2, \ldots, n, 1\}$ include all sites. However, the two are distinct – the former crosses the edge labeled by Y_n while the latter does not cross any edge. This is because at loop-level specifying only the set of sites enclosed is is not enough to uniquely fix a tube. To keep the notation light for n-gons, we fix this ambiguity by including the site labeled 1 twice in the total energy tube. One should think of this tube as starting and ending at the same site.

Using the notation we have introduced, the 3-gon can for example be expressed as

$$\tilde{\psi}_{3\text{-gon}} =$$

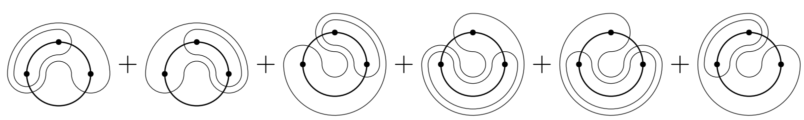

$$\begin{aligned}
&= \frac{1}{S_{123}}\left(\frac{1}{S_{12}} + \frac{1}{S_{23}}\right) + \frac{1}{S_{231}}\left(\frac{1}{S_{23}} + \frac{1}{S_{31}}\right) + \frac{1}{S_{312}}\left(\frac{1}{S_{31}} + \frac{1}{S_{12}}\right), \\
&= \frac{1}{S_{123}}\tilde{\psi}_{3\text{-chain}}(1,2,3) + \frac{1}{S_{231}}\tilde{\psi}_{3\text{-chain}}(2,3,1) + \frac{1}{S_{312}}\tilde{\psi}_{3\text{-chain}}(3,1,2)\,.
\end{aligned} \tag{4.12}$$

The recursive pattern demonstrated in the last line above persists for general n-gons and the corresponding stripped wavefunction can also be written for any n solely in terms of the n-chain via

$$\tilde{\psi}_{n\text{-gon}} = \sum_{\sigma} \frac{1}{S_\sigma} \tilde{\psi}_{n\text{-chain}}(\sigma[1, \cdots, n])\,, \tag{4.13}$$

where σ is a cyclic permutation of the site labels $\{1, \cdots, n\}$.

Arbitrary graphs. For an arbitrary tree- or loop-level graph one can systematically derive formulas analogous to (4.6), (4.9), and (4.13), so that ultimately any stripped wavefunction can be constructed recursively by "gluing" chains together.

4.2 Cosmological zeros

In this section we introduce three categories of linear conditions on the energy factors for which (stripped) wavefunctions vanish that we call wavefunction zeros (section 4.2.1), factorization zeros (section 4.2.2) and parametric zeros (section 4.2.3). In sections 4.2.4 and 4.2.5 we exhibit these types of zeros in two detailed examples.

4.2.1 Wavefunction zeros

We begin with a class of zeros that is possessed by the chain graphs only. One can easily verify that for $n > 2$, the wavefunction of the n-chain obtained from (4.1) vanishes when the following $n-2$ conditions are satisfied:

$$S_{12\cdots n-1} - S_{1\cdots i} + S_{i+1\cdots n} = 0 \text{ for all } 2 \leq i \leq n-2 \quad \text{and} \quad S_{12\cdots n-1} + S_{23\cdots n} = 0\,. \tag{4.14}$$

We call these *wavefunction zeros* because these are zeros of both the full wavefunction $\psi_{n\text{-chain}}$ and its stripped counterpart $\tilde{\psi}_{n\text{-chain}}$.

In fact the n-chain wavefunction satisfies a universal splitting property near its wavefunction zero. Consider a kinematic configuration $\mathcal{S}_i$ in which all of the conditions (4.14) are satisfied except that for a single $i \in \{2, \ldots, n-2\}$ we have

$$S_{12\cdots n-1} - S_{1\cdots i} + S_{i+1\cdots n} \neq 0\,. \tag{4.15}$$

Then one can easily check that the n-chain wavefunction $\psi_{n\text{-chain}}$ splits into a product of factors involving chains obtained by "splitting" the n-chain between sites i and $i+1$:

$$\psi_{n\text{-chain}}|_{\mathcal{S}_i} = \frac{S_{12\cdots n-1} - S_{1\cdots i} + S_{i+1\cdots n}}{S_{12\cdots n}S_{12\cdots n-1}} \times \psi_{i\text{-chain}}(1, \cdots, i) \times \psi_{n-i\text{-chain}}(i+1, \cdots, n)\,. \tag{4.16}$$

This splitting property makes manifest the existence of a zero at the locus (4.14). When interpreting the equation (4.16) and several similar ones that follow, it is crucial to keep in mind that the energy factors involving the "split" i-th and $(i+1)$-th sites in the subgraphs on the right-hand side are identified with those that appear in the parent n-site graph on the left; in other words, despite being exterior sites of the subgraph, i and $i+1$ still carry the same interior energy factors as before. Let us illustrate this point explicitly by way of an example for $n = 4$ and $i = 2$ where we look at the locus

$$\mathcal{S}_2 = \{S_{123} + S_{234} = 0\}\,. \tag{4.17}$$

A short calculation reveals that

$\psi_{4\text{-chain}}|_{\mathcal{S}_2} =$ 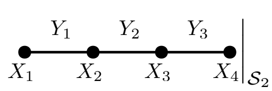

$= \dfrac{S_{123} - S_{12} + S_{34}}{S_{1234}S_{123}} \times$ 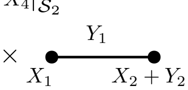

$\times$ 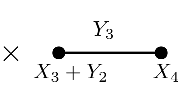

$$= \frac{S_{123} - S_{12} + S_{34}}{S_{1234}S_{123}} \times \psi_{2\text{-chain}}(1,2) \times \psi_{2\text{-chain}}(3,4)\,, \tag{4.18}$$

where, as indicated by the pictures on the second line, we have

$$\psi_{2\text{-chain}}(1,2) = \frac{1}{S_1 S_2 S_{12}} = \frac{1}{(X_1 + Y_1)(X_2 + Y_1 + Y_2)(X_1 + X_2 + Y_2)}\,, \tag{4.19}$$

$$\psi_{2\text{-chain}}(3,4) = \frac{1}{S_3 S_4 S_{34}} = \frac{1}{(X_3 + Y_2 + Y_3)(X_4 + Y_3)(X_3 + X_4 + Y_2)}\,. \tag{4.20}$$

A similar splitting property exists on the locus $\mathcal{S}$ on which all of the conditions in (4.14) except that $S_{12\cdots n-1} + S_{23\cdots n} \neq 0$. In this case,

$$\psi_{n\text{-chain}}|_{\mathcal{S}} = \frac{S_{12\cdots n-1} + S_{23\cdots n}}{S_{12\cdots n} S_{12\cdots n-1}} \times \psi_{1\text{-chain}}(1) \times \psi_{n-1\text{-chain}}(2, 3, \cdots, n) \tag{4.21}$$

$$= \frac{S_{12\cdots n-1} + S_{23\cdots n}}{S_{12\cdots n} S_{23\cdots n-1}} \times \psi_{n-1\text{-chain}}(1, 2, \cdots, n{-}1) \times \psi_{1\text{-chain}}(n)\,, \tag{4.22}$$

where the symmetry of the chain under reversal of the labeling is reflected in the existence of two equivalent formulas; each manifests the wavefunction zero on the locus (4.14). Again, we note that the wavefunctions on the right-hand side of (4.22) must be properly interpreted in terms of shifted energy variables. For example, at $n = 4$ we have

$$\psi_{4\text{-chain}}|_{\mathcal{S}} = \frac{S_{123} + S_{234}}{S_{1234} S_{123}} \times$$ 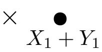 $$\times$$ 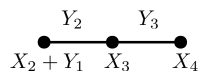

$$= \frac{S_{123} + S_{234}}{S_{1234} S_{123}} \times \psi_{1\text{-chain}}(1) \times \psi_{3\text{-chain}}(2, 3, 4)\ \ , \tag{4.23}$$

where in this case

$$\psi_{1\text{-chain}}(1) = \frac{1}{S_1} = \frac{1}{X_1 + Y_1}\,, \tag{4.24}$$

$$\psi_{3\text{-chain}}(2, 3, 4) = \frac{\frac{1}{S_{23}} + \frac{1}{S_{34}}}{S_2 S_3 S_4 S_{234}} = \frac{\frac{1}{X_2+X_3+Y_1+Y_3} + \frac{1}{X_3+X_4+Y_2}}{(X_2 + Y_1 + Y_2)(X_3 + Y_2 + Y_3)(X_4 + Y_3)(X_2 + X_3 + X_4 + Y_1)}\,. \tag{4.25}$$

4.2.2 Factorization zeros

It is well-known that wavefunctions obey factorization on the residues of their physical poles at $S_{\tau \in \mathsf{T}} = 0$ [73, 79, 123], with the residue on the total energy pole at $S_{\text{total}} = 0$ famously being the corresponding flat-space S-matrix element. Note that a subset of the energy factors, namely the ones $\{S_1, \ldots, S_n, S_{\text{total}}\}$ that belong to tubes in T but not in $\tilde{\mathsf{T}}$ and arise from the prefactor in (4.2), are not poles of stripped n-site wavefunctions. We will refer to these energy factors as the *parameters* of a stripped n-site wavefunction. In this section, we demonstrate that stripped wavefunctions also exhibit factorization when any one of the parameters S_j corresponding to an interior site[3] is set to zero. These factorizations imply that the stripped wavefunction associated to any graph must exhibit zeros associated to its various subgraphs; we call these *factorization zeros*.

n-chain. For any $j \in \{2, \ldots, n-1\}$ it follows from (4.6) and the definition (4.3) after a little bit of work that

$$\tilde{\psi}_{n\text{-chain}}|_{S_j=0} = \frac{S_{12\cdots n}}{S_{1\cdots j} S_{j\cdots n}} \times \tilde{\psi}_{j\text{-chain}}(1, \cdots, j) \times \tilde{\psi}_{n-j+1\text{-chain}}(j, \cdots, n)\,. \tag{4.26}$$

[3] An interior site is one that is adjacent to at least two other sites. Specifically, in an n-chain the sites labeled $i \in \{2, \ldots, n-1\}$ are interior, in an n-star the sites labeled $i \in \{3, \ldots, n-1\}$ are interior, while in an n-gon all sites are interior. The remaining sites are called exterior.

As always, following the discussion below (4.16), we emphasize that the energy factors at site j on the right-hand side are the same as in the parent graph on the left-hand side. We note that (4.26) explains why the 3-chain has no factorization zeros: on the support of the only possible factorization condition $S_2 = 0$, the 3-chain factorizes into a product of two 2-chains, which do not have any zeros of their own since $\tilde{\psi}_{\text{2-chain}} = 1$.

n-star. For the n-star there are two distinct types of factorization limits depending on whether we factor at the trivalent site or (for $n > 4$) at one of the other $n-4$ interior sites. In the former case, it follows from (4.9) that

$$\tilde{\psi}_{n\text{-star}}|_{S_3^*=0} = \frac{S_{12\cdots n}}{S_{13}^* S_{23}^* S_{3\cdots n}^*} \times \tilde{\psi}_{\text{2-chain}}(1,3) \times \tilde{\psi}_{\text{2-chain}}(2,3) \times \tilde{\psi}_{n-2\text{-chain}}(3,4,\cdots,n)\,, \tag{4.27}$$

while in the latter case we have for $j \in \{4,\ldots,n{-}1\}$ that

$$\tilde{\psi}_{n\text{-star}}|_{S_j=0} = \frac{S_{1234\cdots n}}{S_{j\cdots n} S_{1234\cdots j}^*} \times \tilde{\psi}_{j\text{-star}}(1,\cdots,j) \times \tilde{\psi}_{n-j+1\text{-chain}}(j,\cdots,n)\,. \tag{4.28}$$

We note that the 4-star has no factorization zeros since the only factorization (4.27) leads to a product of three 2-chains which are each just $\tilde{\psi}_{\text{2-chain}} = 1$.

n-gons. Using the recursion (4.13) one can see for any $i \in \{1,\ldots,n\}$ the n-gon "factors" as

$$\tilde{\psi}_{n\text{-gon}}|_{S_i=0} = \tilde{\psi}_{n+1\text{-chain}}(i,i{+}1,\cdots,n,1,2,\cdots,i)\,. \tag{4.29}$$

Arbitrary graphs. Any zero of a stripped wavefunction appearing on the right-hand side of a factorization can be considered a "factorization zero" of the parent stripped wavefunction. However, in order to enumerate all of the distinct zeros arising from an arbitrary tree- or loop-level graph, it is sufficient to look at its chain subgraphs, after using the fact that any graph can be broken into chains by taking some sequence of $S_i \to 0$ limits at various interior sites i. Moreover, for any tree graph, tabulating the wavefunction zeros of all chain subgraphs is sufficient to give the full set of distinct factorization zeros due to a cancellation of total energy factors in intermediate steps. These phenomena are exhibited by the examples worked out in detail in sections 4.2.4 and 4.2.5 below.

4.2.3 Parametric zeros

It is evident that the right-hand side of the factorization (4.26) of the n-chain vanishes when the total energy factor $S_{12\ldots n}$ is zero. The same is true for the n-star as seen from (4.27) and (4.28). Finally, by taking the $S_j \to 0$ limit on both sides of the factorization (4.29), it is clear that the n-gon inherits the zeros of the chain appearing on the right-hand side of (4.29). We refer to zeros of this type as *parametric zeros* since they involve simply setting certain parameters of the stripped wavefunction to zero. In summary, parametric zeros for the three relevant graph topologies are given by:

$$n\text{-chain:} \quad S_i = 0 \text{ and } S_{\text{total}} = 0 \text{ for any } i \in \{2, \dots, n{-}1\}\,, \tag{4.30}$$

$$n\text{-star:} \quad S_3^* = 0 \text{ and } S_{\text{total}} = 0\,, \quad \text{or} \quad S_i = 0 \text{ and } S_{\text{total}} = 0 \text{ for any } i \in \{4, \dots, n{-}1\}\,, \tag{4.31}$$

$$n\text{-gon:} \quad S_i = 0 \text{ and } S_j = 0 \text{ and } S_{\text{total}} = 0 \text{ for any } i, j \in \{1, \dots, n\} \text{ and } i \neq j\,. \tag{4.32}$$

4.2.4 Example: the 5-star

The stripped wavefunction $\tilde{\psi}_{\text{5-star}}$ of the 5-star has no wavefunction zeros (since only chains have wavefunction zeros) and, according to (4.31), two parametric zeros: at $S_3^* = S_{12345} = 0$ and at $S_4 = S_{12345} = 0$. Let us now classify its factorization zeros, which arise from two possible factorizations: at $S_3^* = 0$ or at $S_4 = 0$.

On the support of $S_3^* = 0$ (which we denote graphically by drawing a dashed circle around site 3), (4.27) tells us that the stripped wavefunction factors into a certain prefactor times the product of its constituent chain subgraphs, two of which are trivial due to $\tilde{\psi}_{\text{2-chain}} = 1$:

$$\tilde{\psi}_{\text{5-star}}|_{S_3^*=0} =$$
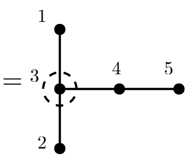

$$= \frac{S_{12345}}{S_{13}^* S_{23}^* S_{345}^*} \times 1 \times 1 \times \tilde{\psi}_{\text{3-chain}}(3,4,5)\,. \tag{4.33}$$

This vanishes if we further impose the wavefunction zero condition (4.14) for the 3-chain subgraph $\tilde{\psi}_{\text{3-chain}}(3,4,5)$ given by the relation

$$S_{34}^* + S_{45} = 0\,. \tag{4.34}$$

Therefore, $S_3^* = S_{34}^* + S_{45} = 0$ constitutes a factorization zero of $\tilde{\psi}_{\text{5-star}}$.

On the other hand, on the support of $S_4 = 0$, (4.28) tells us that

$$\tilde{\psi}_{\text{5-star}}|_{S_4=0} =$$
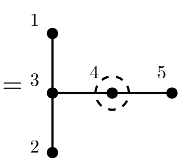

$$= \frac{S_{12345}}{S_{1234}^* S_{45}} \times \tilde{\psi}_{\text{4-star}}(1,2,3,4) \times 1\,. \tag{4.35}$$

Now $\tilde{\psi}_{\text{4-star}}$ does not possess any wavefunction zeros (since only chains have those), and it does not possess any factorization zeros (see the comment under (4.28)); the only possible path to zero is via the parametric zero of the 4-star $\tilde{\psi}_{\text{4-star}}(1,2,3,4)$ at $S_3^* = S_{1234}^* = 0$. However, on the support of $S_3^* = 0$, the stripped wavefunction of the 4-star subgraph further factors into

$$\tilde{\psi}_{\text{5-star}}|_{S_3^*=S_4=0} = \frac{S_{12345}}{S_{1234}^* S_{45}} \times$$
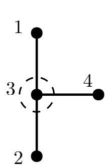

$$\times$$
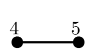

$$= \frac{S_{12345}}{S_{13}^* S_{23}^* S_{34}^* S_{45}} \times$$
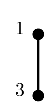

$$\times$$
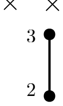

$$\times$$

$$. \tag{4.36}$$

Note in the second equality the factor S_{1234}^* has canceled out and therefore the second condition of the parametric zero is rendered useless. With only 2-chains remaining in the product, we find no factorization zeros of $\tilde{\psi}_{5\text{-star}}$ on the locus $S_4 = 0$. Note that had we started with an $(n{>}5)$-star graph, we would have reached an $(n{-}3)$-chain, and its wavefunction zeros would have led to factorization zeros of $\tilde{\psi}_{(n>5)\text{-star}}$ in this step.

4.2.5 Example: the 3-gon

The stripped wavefunction $\tilde{\psi}_{3\text{-gon}}$ of the 3-gon has no wavefunction zeros (since only chains have wavefunction zeros) and three parametric zeros, at the loci given by (4.32). Let us now classify its factorization zeros. According to (4.29) it "factors" at $S_1 = 0$ into the 4-chain

$$\tilde{\psi}_{3\text{-gon}}|_{S_1=0} =$$ 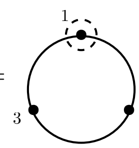

$$=$$ 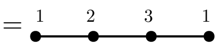

$$= \tilde{\psi}_{4\text{-chain}}(1,2,3,1)\,. \tag{4.37}$$

The 4-chain appearing here has parametric zeros, but these are the same as the parametric zeros of the 3-gon itself that we already listed. In addition, the 4-chain vanishes at the wavefunction zero given by (4.14). Since we could have factored at sites 2 or 3, altogether we obtain three distinct factorization zeros of the 3-gon, at the loci

$$S_1 = S_{123} + S_{231} = S_{12} - S_{31} + S_{231} = 0\,, \tag{4.38}$$
$$S_2 = S_{231} + S_{312} = S_{23} - S_{12} + S_{312} = 0\,, \tag{4.39}$$
$$S_3 = S_{312} + S_{123} = S_{31} - S_{23} + S_{123} = 0\,. \tag{4.40}$$

These arguments straightforwardly generalize to the n-gon, which inherits the wavefunction zeros of the $(n{+}1)$-chain on the locus $S_i = 0$ for any i.

4.3 The geometric origins of cosmological zeros

In section 4.3.1, we construct in kinematic space the graph associahedron associated to a stripped wavefunction and discuss a particular cosmological limit that degenerates the graph associahedron into a (generically non-simple) polytope relevant to our analysis of cosmological zeros. Through explicit examples in sections 4.3.2 and 4.3.3, we show that a graph associahedron can be expressed in terms of its constituent Minkowski summands; moreover, we demonstrate that tuning the parameters in a particular manner causes the cosmological graph associahedron to flatten (i.e., the polytope drops in dimension), thereby providing a geometric origin for the parametric zeros of section 4.2.3. In section 4.3.4, we discuss the geometric origin of the wavefunction and factorization zeros of sections 4.2.1 and 4.2.2 through the lens of the vanishing locus of the adjoint polynomial.

4.3.1 Graph associahedra and the cosmological limit

It has been recently shown [173] that the stripped wavefunction $\tilde{\psi}$ associated to a single Feynman graph $\mathcal{G}$ is the canonical form of a polytope called a graph associahedron $\mathcal{A}_{\mathcal{G}}$ (slightly different than

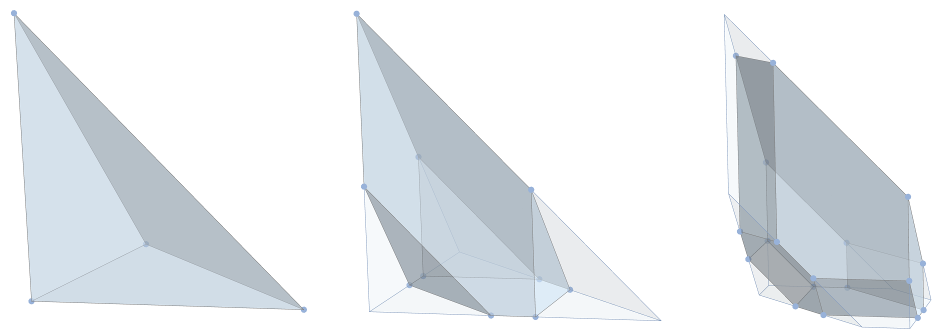

Figure 4.1: Truncating a 3-simplex to carve out the graph associahedron $\mathcal{A}_{\text{5-star}}$. Left: we begin with the simplex cut out by the 2-tube hyperplanes $\{S^*_{13}, S^*_{23}, S^*_{34}, S_{45}\} = 0$. Middle: the vertices of the simplex are truncated by the 4-tube hyperplanes $\{S^*_{1234}, S^*_{1345}, S^*_{2345}\} = 0$. Right: the edges of the simplex are truncated by the 3-tube hyperplanes $\{S^*_{123}, S^*_{134}, S^*_{234}, S^*_{345}\} = 0$.

the one used in the mathematical literature), whose facet structure reflects the combinatorics of the tubings $\tilde{\mathsf{T}}$ of $\mathcal{G}$. These graph associahedra are facets of larger polytopes called cosmohedra [173], which encode the full flat-space wavefunctions (summed over all contributing Feynman diagrams) of a colored version of the uncolored theory studied in this paper at the level of individual diagrams. In this section we provide an algorithm for constructing graph associahedra based on simplex truncation introduced by Carr and Devadoss in [175, 176]; a complementary construction was recently given in [177, 178].

To construct the graph associahedron associated to a single graph $\mathcal{G}$ relevant for the cosmological context, we modify the Carr-Devadoss algorithm so that 2-tubes replace 1-tubes as the fundamental building blocks. This is natural because the energy factors of 1-tubes only appear as overall factors in the wavefunction associated to $\mathcal{G}$. Also, our construction will heavily rely on the fact that the energy factors satisfy the linear relations

$$S_{\tau_1} + S_{\tau_2} = S_{\tau_1 \cup \tau_2} + S_{\tau_1 \cap \tau_2} \,, \tag{4.41}$$

when $\tau_1 \cap \tau_2$ is non-empty. Note that beyond tree-level one must be careful in interpreting this formula since the order of the indices that define a tube matters. For example, already at one-loop τ_1 can intersect τ_2 twice – at both ends of τ_1 – and the operation $\cap$ can only be thought of as acting on the tube not the indices labeling a tube.

Let $\mathcal{T}_k$ denote the set of all k-tubes of some graph $\mathcal{G}$ and let $m = |\mathcal{T}_2| = n{+}\ell{-}1$ be the total number of 2-tubes. The graph associahedron $\mathcal{A}_\mathcal{G}$ can be realized as a simple $(m{-}1)$-dimensional polytope in an m-dimensional ambient space $\mathbb{R}^m$ with coordinates $S_{\tau\in\mathcal{T}_2}$ labeled by the 2-tubings. To construct $\mathcal{A}_\mathcal{G}$ we start with the $(m{-}1)$-simplex (see for example figure 4.1 left) defined by intersecting $\{S_\tau \geq 0 : \tau \in \mathcal{T}_2\} \subset \mathbb{R}^m$ with the hyperplane

$$\sum_{\tau\in\mathcal{T}_2} S_\tau = S_{\text{total}} + \sum_{\text{interior sites}\, v} \Big(c_v(\tau_{\text{total}}) - 1\Big)\, S_v \,, \tag{4.42}$$

where τ_{total} is the total energy tube[4], the second sum includes only the interior sites of $\mathcal{G}$, and $c_v(\tau)$

[4] Recall that $\tau_{\text{total}} = \{1, \cdots, n\}$ for chains and stars while $\tau_{\text{total}} = \{1, \cdots, n, 1\}$ for n-gons.

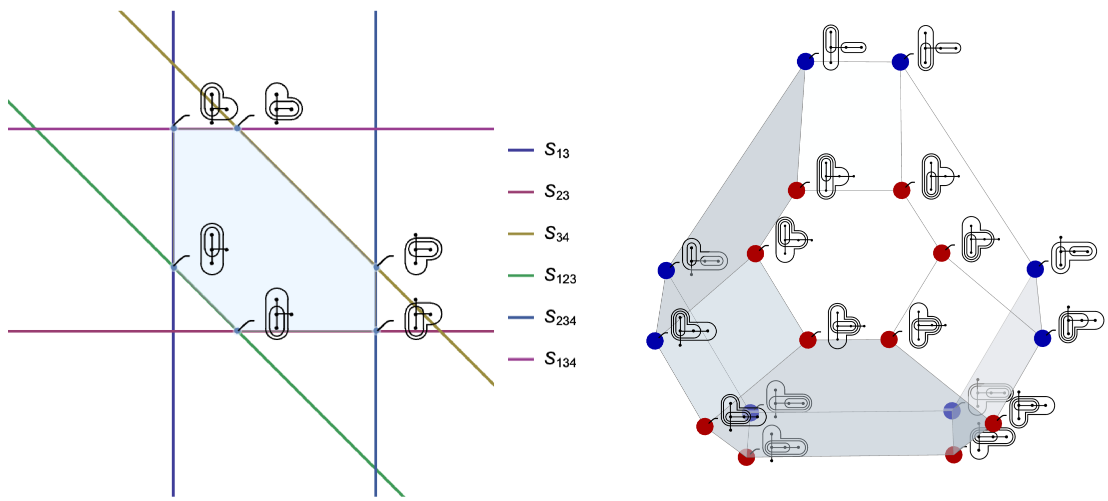

Figure 4.2: The graph associahedra $\mathcal{A}_{4\text{-star}}$ (left) and $\mathcal{A}_{5\text{-star}}$ (right), with vertices labeled by complete tubings.

is the number of 2-tubes in τ that include the interior site v. Then, for each $k \in \{3, \ldots, n+\ell-1\}$, each $(m-k)$-dimensional facet of the simplex is truncated by the hyperplanes $S_{\tau\in\mathcal{T}_k} = 0$ where S_τ is defined by

$$\sum_{\tau'\in\mathcal{T}_2\,:\,\tau'\subset\tau} S_{\tau'} = S_\tau + \sum_{\text{interior sites}\, v} \Big(c_v(\tau) - 1\Big) S_v - \delta_\tau\,, \tag{4.43}$$

where the δ_τ are positive parameters whose role will be explained shortly. See figure 4.1 for a visualization of this process. Also note that while the 2-tubes are naturally distinguished by the Carr-Devadoss construction, one could choose any cardinality-m subset of the energy variables S_τ (for $\tau \in \tilde{\mathsf{T}}$) as coordinates for the ambient space.

Now, in order to avoid cutting the simplex too deeply and to ensure that the resulting polytope remains simple, we require that the δ_τ's introduced in (4.43) satisfy the bounds

$$\delta_\tau > 0 \text{ for all } \tau \quad \text{and} \quad \delta_{\tau_1} + \delta_{\tau_2} > \delta_{\tau_1\cup\tau_2} + \delta_{\tau_1\cap\tau_2} \text{ when } \tau_1 \cap \tau_2 \neq \emptyset\,, \tag{4.44}$$

as well as

$$0 < \delta_{\tau\in\mathcal{T}_3} < S_v < S_{\text{total}} \text{ for all internal sites } v\,. \tag{4.45}$$

The boundary of the region defined by $\{S_{\tau\in\mathcal{T}_k} \geq 0 : 2 \leq k \leq n-1\}$ then provides a realization of the graph associahedron $\mathcal{A}_\mathcal{G}$ as the boundary of an $(m-1 = n+\ell-2)$-dimensional polytope. Each complete compatible tubing $\tilde{\mathsf{T}}$ of the stripped wavefunction $\tilde{\psi}_\mathcal{G}$ corresponds to a vertex of $\mathcal{A}_\mathcal{G}$ where $\cap_{\tau\in\tilde{\mathsf{T}}}\{S_\tau = 0\}$. Figure 4.2 depicts the graph associahedra for the 4- and 5-star graphs.

By construction, the non-zero δ_τ ensure that the graph associahedron $\mathcal{A}_\mathcal{G}$ is always a simple polytope. While $\mathcal{A}_\mathcal{G}$ does describe the combinatorics of compatible tubings of $\mathcal{G}$, the energy factors

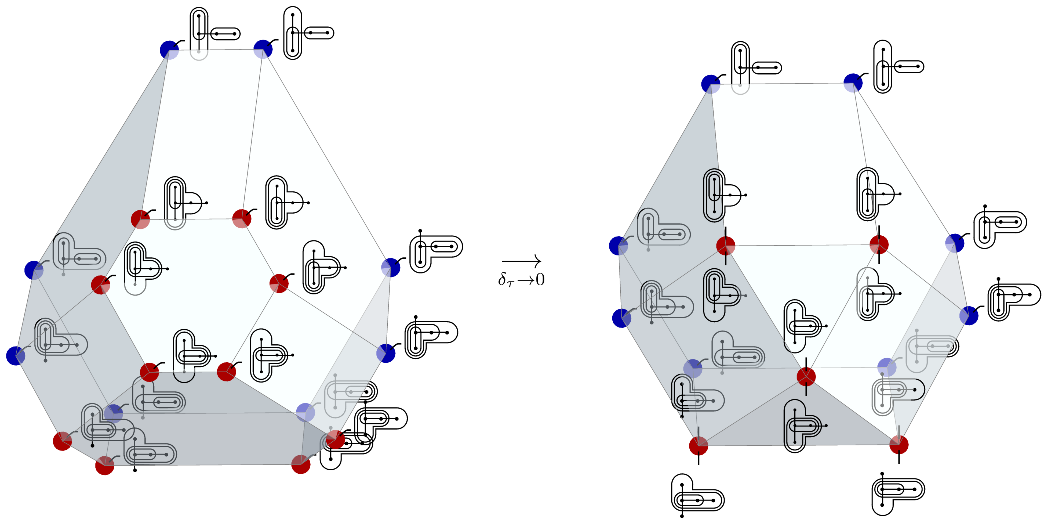

Figure 4.3: Left: the graph associahedron $\mathcal{A}_{5\text{-star}}$ ($\delta_\tau \neq 0$); the f-vector of this simple polytope is (18,27,11). Right: the cosmological graph associahedron $\tilde{\mathcal{A}}_{5\text{-star}}$ ($\delta_\tau = 0$); the f-vector of this non-simple polytope is (13,22,11). Note that as expected, the number of facets remains the same, while the number of edges and vertices decreases. The vertices that remain simple in the $\delta_\tau \to 0$ limit are colored blue, while all others are colored red.

defined by (4.43) do not in general satisfy the relations (4.41) required for the cosmological application. This requires taking the limit $\delta_\tau \to 0$, which results in a non-simple polytope when $n + \ell > 4$. We will call the resulting polytope $\tilde{\mathcal{A}}_{\mathcal{G}} := \lim_{\delta_\tau \to 0} \mathcal{A}_{\mathcal{G}}$ the *cosmological graph associahedron* associated to $\mathcal{G}$. Figure 4.3 shows the degeneration from the simple δ-deformed graph associahedron to the non-simple cosmological graph associahedron for the 5-star graph.

Even though we are primarily interested in the cosmological limit $\delta_\tau \to 0$, the polytope $\mathcal{A}_{\mathcal{G}}$ is an important intermediate step that encodes useful combinatorial information. Moreover, the canonical function of the cosmological graph associahedron $\tilde{\mathcal{A}}_{\mathcal{G}}$, defined by taking the $\delta_\tau \to 0$ limit of the canonical function of the simple polytope $\mathcal{A}_{\mathcal{G}}$, is precisely the stripped wavefunction $\tilde{\psi}_{\mathcal{G}}$. Note that this limit is automatically realized when the energy factors S_τ are parameterized directly in terms of the energy variables X_v and Y_e of section 4.1.

4.3.2 Parametric zeros: examples of simple polytopes

In this section, we illustrate how the parametric zeros of section 4.2.3 can be seen as flattening limits of the cosmological graph associahedron for three examples – the 4-chain, the 4-star and the 3-gon. For these examples $n + \ell = 4$ and, consequently, both $\mathcal{A}_{\mathcal{G}}$ and $\tilde{\mathcal{A}}_{\mathcal{G}}$ are simple polytopes that are topologically equivalent. Nevertheless they are geometrically distinct, having different Minkowski summands and flattening behaviors. Aside from selected comments, we set the δ_τ to zero from the beginning and explore the properties of $\tilde{\mathcal{A}}_{\mathcal{G}}$ in the following.

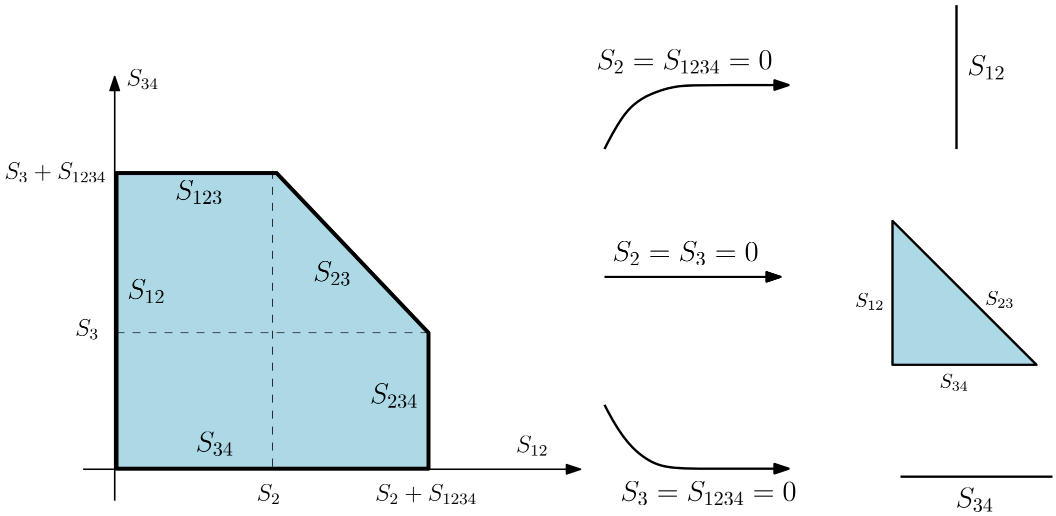

Figure 4.4: The cosmological graph associahedron $\tilde{\mathcal{A}}_{\text{4-chain}}$ and its Minkowski summands, showing that the polytope collapses in the upper and lower limits, corresponding to parametric zeros of $\tilde{\psi}_{\text{4-chain}}$, but not in the center limit.

The 4-chain. Following section 4.3.1, we carve out the cosmological graph associahedron $\tilde{\mathcal{A}}_{\text{4-chain}}$ in kinematic space with coordinates (S_{12}, S_{34}) and parameters (S_2, S_3, S_{1234}) via the inequalities

$$\begin{gathered} S_{12} \geq 0\,, \qquad S_{34} \geq 0\,, \qquad S_{23} = S_2 + S_3 + S_{1234} - S_{12} - S_{34} \geq 0\,, \\ S_{123} = S_3 + S_{1234} - S_{34} \geq 0\,, \qquad S_{234} = S_2 + S_{1234} - S_{12} \geq 0\,, \end{gathered} \tag{4.46}$$

which describes a pentagon. This polytope and its Minkowski summands are presented in figure 4.4. From (4.30), we expect the associated stripped wavefunction $\tilde{\psi}_{\text{4-chain}}$ to have two parametric zeros, at

$$S_2 = S_{1234} = 0 \qquad \text{and at} \qquad S_3 = S_{1234} = 0\,. \tag{4.47}$$

As shown in the top and bottom right of figure 4.4, these limits evidently collapse the pentagon to a vertical or horizontal line segment, respectively. In both cases the stripped wavefunction $\tilde{\psi}_{\text{4-chain}}$ vanishes and the polytope $\tilde{\mathcal{A}}_{\text{4-chain}}$ collapses in dimension to one of its 1-dimensional Minkowski summands. On the other hand, the limit $S_2 = S_3 = 0$ collapses the pentagon to its 2-dimensional Minkowski summand – the triangle (center right of figure 4.4). Since the polytope does not drop in dimension, this limit does not correspond to a zero of the stripped wavefunction.

The 4-star. Again following the prescription of section 4.3.1 and choosing coordinates (S^*_{13}, S^*_{23}) with (S^*_3, S_{1234}) as parameters, the cosmological graph associahedron $\tilde{\mathcal{A}}_{\text{4-star}}$ is the hexagon in figure 4.5 carved out by the inequalities

$$\begin{gathered} S^*_{13} \geq 0\,, \qquad S^*_{23} \geq 0\,, \qquad S^*_{34} = S_{1234} + 2S^*_3 - S^*_{13} - S^*_{23} \geq 0\,, \\ S^*_{134} = S^*_{13} + S^*_{34} - S^*_3 \geq 0\,, \qquad S^*_{123} = S^*_{13} + S^*_{23} - S^*_3 \geq 0\,, \qquad S^*_{234} = S^*_{23} + S^*_{34} - S^*_3 \geq 0\,. \end{gathered} \tag{4.48}$$

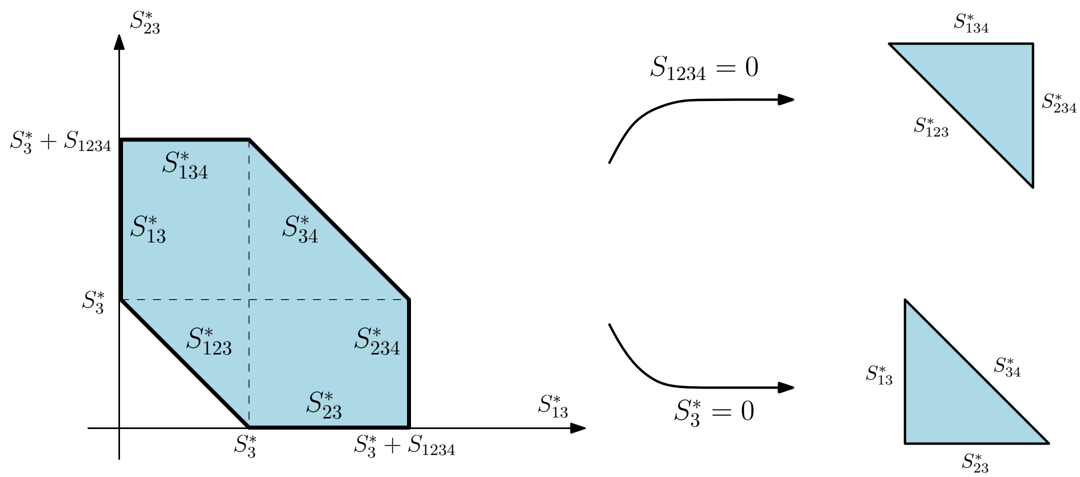

Figure 4.5: The cosmological graph associahedron $\tilde{\mathcal{A}}_{\text{4-star}}$ and its Minkowski summands, showing that the polytope does not collapse in either of the limits shown.

We expect the sole zero of $\tilde{\psi}_{\text{4-star}}$ to be the parametric zero at (see (4.31))

$$S^*_3 = S_{1234} = 0\,. \tag{4.49}$$

Note that the 4-star has only two parameters in contrast to three for the 4-chain. Setting either of them to zero collapses the hexagon to one of its two Minkowski summands – the triangles shown on the right of figure 4.5. Since the polytope does not drop in dimension, these limits do not correspond to zeros of $\tilde{\psi}_{\text{4-star}}$. The parametric zero (4.49) corresponds to collapsing the hexagon down to a point – a 2-dimensional drop.

The above observations are simple consequences of the linear relations (4.41) and the cosmological limit. The δ-deformed graph associahedron $\mathcal{A}_{\text{4-star}}$ behaves more like $\tilde{\mathcal{A}}_{\text{4-chain}}$ since the nonzero δ_τ behave as extra parameters. Indeed, one can find flattening limits of $\mathcal{A}_{\text{4-star}}$ that only drop the dimension of the polytope by one instead of two.

The 3-gon. Our final example of a simple cosmological graph associahedron is $\tilde{\mathcal{A}}_{\text{3-gon}}$. Choosing coordinates (S_{12}, S_{23}) with parameters $(S_1, S_2, S_3, S_{1231})$, the 3-gon inequalities are

$$\begin{gathered} S_{12} \geq 0\,, \qquad S_{23} \geq 0\,, \qquad S_{31} = S_{1231} + S_1 + S_2 + S_3 - S_{12} - S_{23} \geq 0\,, \\ S_{123} = S_{12} + S_{23} - S_2 \geq 0\,, \quad S_{231} = S_{23} + S_{31} - S_3 \geq 0\,, \quad S_{312} = S_{31} + S_{12} - S_1 \geq 0\,. \end{gathered} \tag{4.50}$$

The inequalities again carve out a hexagon, as shown in figure 4.6. From (4.32) we expect that $\tilde{\psi}_{\text{3-gon}}$ as three parametric zeros, at

$$S_1 = S_2 = S_{1231} = 0\,, \qquad S_2 = S_3 = S_{1231} = 0\,, \qquad \text{and } S_3 = S_1 = S_{1231} = 0\,, \tag{4.51}$$

corresponding to flattening limits of the hexagon to 1-dimensional Minkowski summands as shown in figure 4.6 (right). Interestingly, note that although both $\tilde{\mathcal{A}}_{\text{4-star}}$ and $\tilde{\mathcal{A}}_{\text{3-gon}}$ are hexagons, the existence of two extra parameters in the latter implies that its associated Minkowski summands are 1-dimensional line segments.

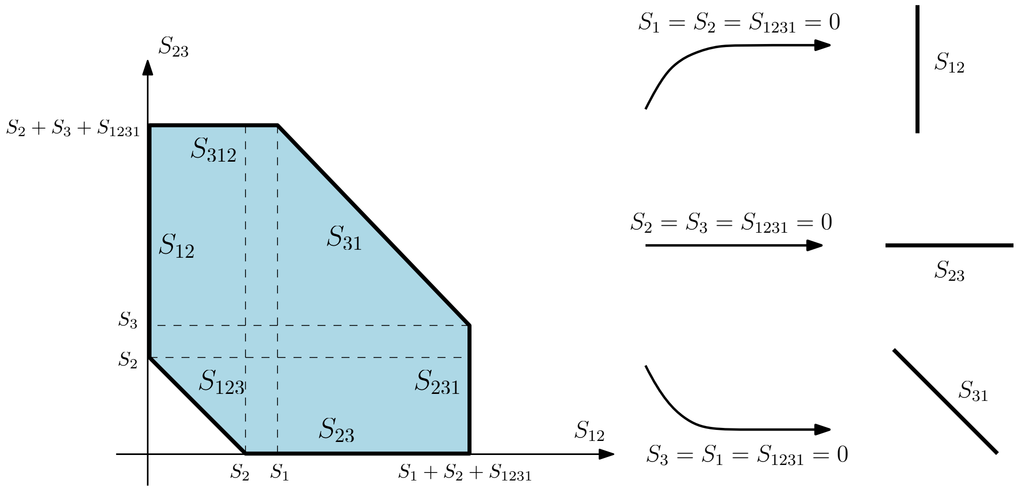

Figure 4.6: The graph associahedron $\tilde{\mathcal{A}}_{\text{3-gon}}$ and its Minkowski summands. Note that here we only show the lower-dimensional Minkowski summands, not the full Minkowski decomposition of the hexagon. In particular we do not show the summand that corresponds to the limit $S_1 = S_2 = S_3 = 0$, since that leaves a 2-dimensional simplex.

4.3.3 Parametric zeros: examples of non-simple polytopes

Starting in 3-dimensions the distinction between the graph associahedron $\mathcal{A}_{\mathcal{G}}$ and its cosmological limit $\tilde{\mathcal{A}}_{\mathcal{G}}$ becomes more apparent: the former is simple while the latter is not.

The 5-chain. Choosing (S_{12}, S_{23}, S_{45}) as coordinates with parameters $(S_2, S_3, S_4, S_{12345})$, the simple polytope $\mathcal{A}_{\text{5-chain}}$ is defined by the inequalities

$$\begin{gathered}S_{12}\geq 0\,,\qquad S_{23}\geq 0\,,\qquad S_{45}\geq 0\,,\quad S_{34}{=}S_{12345}{+}S_2{+}S_3{+}S_4{-}S_{12}{-}S_{23}{-}S_{45}\geq 0\,,\\ S_{123}=\delta_{123}{+}S_{12}{+}S_{23}{-}S_2\geq 0\,,\quad S_{234}=\delta_{234}{+}S_{23}{+}S_{34}{-}S_3\geq 0\,,\quad S_{345}=\delta_{345}{+}S_{34}{+}S_{45}{-}S_4\geq 0\,,\\ S_{1234}=\delta_{1234}{+}S_{12}{+}S_{23}{+}S_{34}{-}S_2{-}S_3\geq 0\,,\quad S_{2345}=\delta_{2345}{+}S_{12}{+}S_{23}{+}S_{34}{+}S_{45}{-}S_2{-}S_3{-}S_4\geq 0\,.\end{gathered}\tag{4.52}$$

The graph associahedron $\mathcal{A}_{\text{5-chain}}$ and its cosmological limit $\tilde{\mathcal{A}}_{\text{5-chain}}$ are depicted in figure 4.7.

As expected from (4.30), the sequential limit $\lim_{S_{12345}\to 0}\lim_{S_i\to 0}\tilde{\mathcal{A}}_{\text{5-chain}}$ flattens the polytope for $i = 2, 3, 4$. An example of this is shown in the left of figure 4.8. On the other hand, the polytope cannot be flattened by keeping the total energy factor non-zero. For example, the sequential limit $\lim_{S_3\to 0}\lim_{S_2\to 0}\tilde{\mathcal{A}}_{\text{5-chain}}$ is still a 3-dimensional polytope (see the right of figure 4.8) and consequently does not correspond to a zero of $\tilde{\psi}_{\text{5-chain}}$.

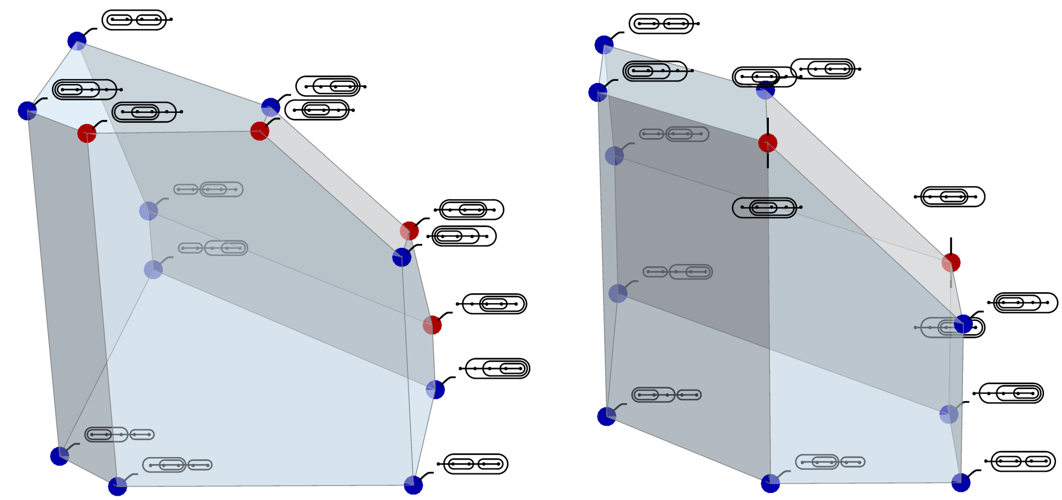

Figure 4.7: The polytopes $\mathcal{A}_{\text{5-chain}}$ (simple with f-vector (14,21,9)) and $\tilde{\mathcal{A}}_{\text{5-chain}}$ (non-simple with f-vector (12,19,9)) for the 5-chain graph. The blue vertices remain simple in the cosmological limit $\delta_\tau \to 0$ while the red vertices become non-simple.

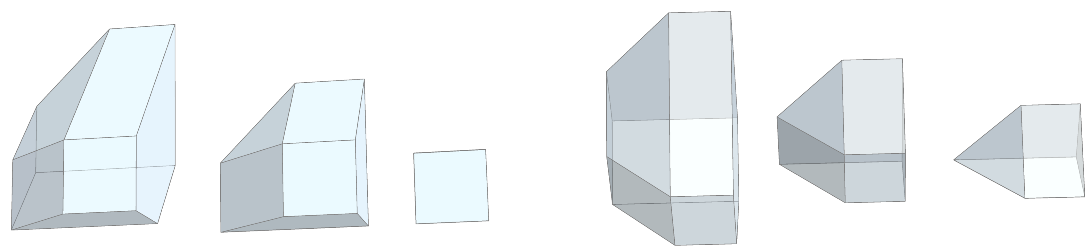

Figure 4.8: Left: the sequential limit $\lim_{S_{12345}\to 0}\lim_{S_2\to 0}\tilde{\mathcal{A}}_{\text{5-chain}}$. The polytope drops in dimension, signaling the parametric zero of $\tilde{\psi}_{\text{5-chain}}$. Right: the sequential limit $\lim_{S_3\to 0}\lim_{S_2\to 0}\tilde{\mathcal{A}}_{\text{5-chain}}$. The polytope does not drop in dimension indicating that this limit does not lead to a parametric zero.

The 5-star. In the coordinates $(S^*_{13}, S^*_{23}, S^*_{34})$ with parameters (S^*_3, S_4, S_{12345}), the inequalities that define the graph associahedron $\mathcal{A}_{\text{5-star}}$ are

$$\begin{aligned}
&S^*_{13} \geq 0\,, \qquad\qquad S^*_{23} \geq 0\,, \qquad\qquad S^*_{34} \geq 0\,,\\
&S_{45} = S_{12345}+2S^*_3+S_4-S^*_{13}-S^*_{23}-S^*_{34} \geq 0\,, &&S^*_{123} = \delta_{123}+S^*_{13}+S^*_{23}-S^*_3 \geq 0\,,\\
&S^*_{345} = \delta_{345}-S^*_{13}-S^*_{23}+S_{12345}+2S^*_3 \geq 0\,, &&S^*_{134} = \delta_{134}+S^*_{13}+S^*_{34}-S^*_3 \geq 0\,,\\
&S^*_{234} = \delta_{234}+S^*_{23}+S^*_{34}-S^*_3 \geq 0\,, &&S^*_{1234} = \delta_{1234}+S^*_{13}+S^*_{23}+S^*_{34}-2S^*_3 \geq 0\,,\\
&S^*_{1345} = \delta_{1345}-S^*_{23}+S_{12345}+S^*_3 \geq 0\,, &&S^*_{2345} = \delta_{2345}-S^*_{13}+S_{12345}+S^*_3 \geq 0\,.
\end{aligned} \tag{4.53}$$

The graph associahedron $\mathcal{A}_{\text{5-star}}$ and its cosmological limit $\tilde{\mathcal{A}}_{\text{5-star}}$ are shown in figure 4.3.

The 5-star exhibits two distinct flavors of parametric zeros; both are depicted in figure 4.9. The parametric zero defined by the sequential limit $\lim_{S_{12345}\to 0}\lim_{S^*_3\to 0}\tilde{\mathcal{A}}_{\text{5-star}}$ behaves like that of the 4-star where the dimension of the polytope drops by two: from a 3-dimensional polytope to a 1-dimensional line. The only other parametric zero, corresponding to the sequential limit

$\lim_{S_{12345}\to 0}\lim_{S_4\to 0}\tilde{\mathcal{A}}_{5\text{-star}}$, behaves like that of the 5-chain since the polytope dimension only drops by one.

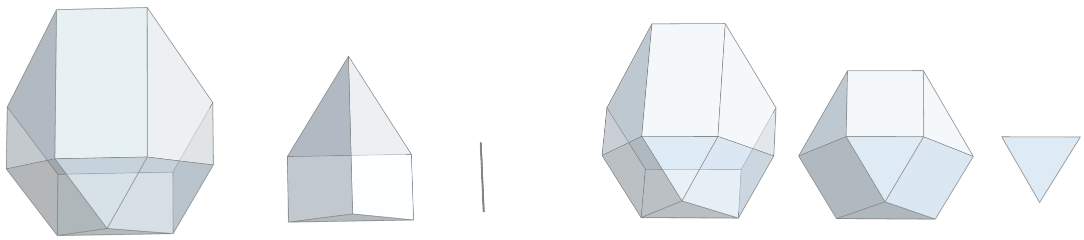

Figure 4.9: The sequential limits $\lim_{S_{12345}\to 0}\lim_{S_3^*\to 0}\tilde{\mathcal{A}}_{5\text{-star}}$ (left, showing a 2-dimensional drop) and $\lim_{S_{12345}\to 0}\lim_{S_4\to 0}\tilde{\mathcal{A}}_{5\text{-star}}$ (right, showing a 1-dimensional drop).

The 4-gon. In the coordinates (S_{12}, S_{23}, S_{34}) with parameters $(S_1, S_2, S_3, S_4, S_{12341})$, the inequalities that define $\mathcal{A}_{4\text{-gon}}$ are

$$\begin{aligned}
&S_{12} \geq 0\,, && S_{23} \geq 0\,,\\
&S_{34} \geq 0\,, && S_{41} = S_{12341}{+}S_1{+}S_2{+}S_3{+}S_4{-}S_{12}{-}S_{23}{-}S_{34} \geq 0\,,\\
&S_{123} = \delta_{123}{+}S_{12}{-}S_2{+}S_{23} \geq 0\,, && S_{341} = \delta_{341}{+}S_{12341}{+}S_2{+}S_1{+}S_3{-}S_{12}{-}S_{23}\,,\\
&S_{234} = \delta_{234}{+}S_{23}{-}S_3{+}S_{34} \geq 0 \geq 0\,, && S_{412} = \delta_{412}{+}S_{12341}{+}S_2{+}S_3{+}S_4{-}S_{23}{-}S_{34} \geq 0\,,\\
&S_{1234} = \delta_{1234}{-}S_2{-}S_3{+}S_{12}{+}S_{23}{+}S_{34} \geq 0\,, && S_{2341} = \delta_{2341}{+}S_{12341}{+}S_1{+}S_2{-}S_{12} \geq 0\,,\\
&S_{3412} = \delta_{3412}{+}S_{12341}{+}S_2{+}S_3{-}S_{23} \geq 0\,, && S_{4123} = \delta_{4123}{+}S_{12341}{+}S_3{+}S_4{-}S_{34} \geq 0\,.
\end{aligned} \tag{4.54}$$

Both the graph associahedron $\mathcal{A}_{4\text{-gon}}$ and its cosmological limit $\tilde{\mathcal{A}}_{4\text{-gon}}$ are depicted in figure 4.10. The parametric zeros of $\tilde{\psi}_{4\text{-gon}}$ correspond to flattening limits where the dimension of the polytope drops by one. To illustrate this we demonstrate the flattening corresponding to the parametric zero $S_1 = S_2 = S_{12341} = 0$ in figure 4.11.

4.3.4 Wavefunction and factorization zeros from the adjoint polynomial

Unlike the parametric zeros discussed above, the wavefunction zeros of n-chains discussed in section 4.2.1 (and consequently, the factorization zeros of arbitrary graphs) are not realized as flattening limits of the associated cosmological graph associahedra. Instead, we will now illustrate that they can be understood from a geometric perspective by studying the adjoint polynomial of the associated polytope; in particular, we will see that while all of the parametric zeros are accessible from within the positive region (by dialing various positive parameters to zero), the factorization and wavefunction zeros lie outside of it. We utilize the 4-chain as an illustrative example throughout this section.

The numerator of a canonical function is called the *adjoint polynomial* of the associated polytope. For example, bringing the expression (4.5) for the 4-chain stripped wavefunction $\tilde{\psi}_{4\text{-chain}}$ onto a

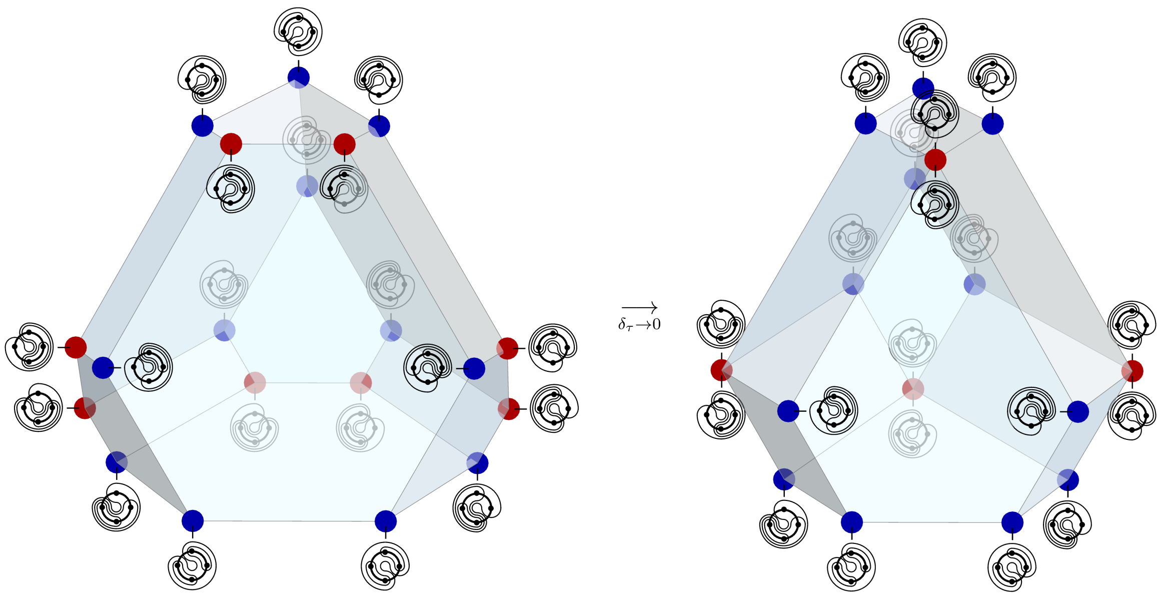

Figure 4.10: The polytopes $\mathcal{A}_{\text{4-gon}}$ (simple with f-vector $(20, 30, 12)$) and $\tilde{\mathcal{A}}_{\text{4-gon}}$ (non-simple with f-vector $(16, 26, 12)$) for the 4-gon graph. The blue vertices remain simple in the cosmological limit $\delta_\tau \to 0$ while the red vertices become non-simple.

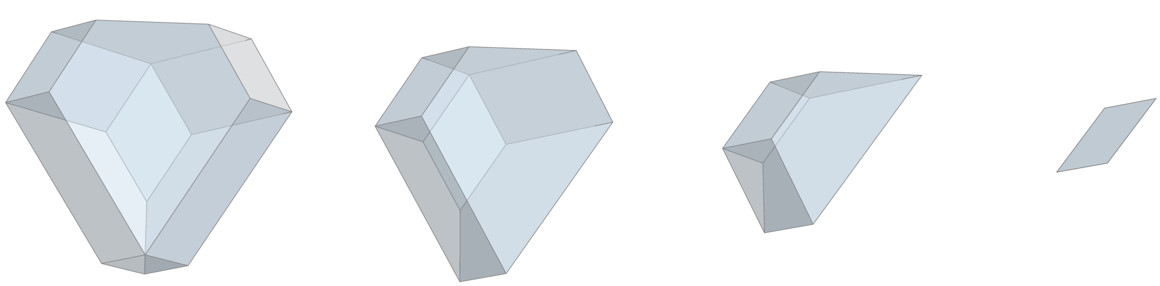

Figure 4.11: The sequential limit $\lim_{S_{12341}\to 0} \lim_{S_2 \to 0} \lim_{S_1 \to 0} \tilde{\mathcal{A}}_{\text{4-gon}}$, showing a 1-dimensional drop.

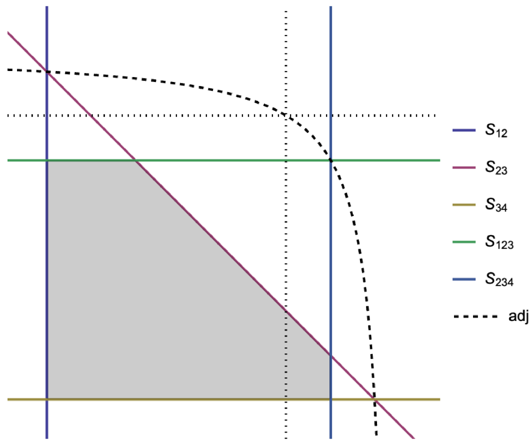

Figure 4.12: The hyperplane arrangement corresponding to the 4-chain graph. The horizontal and vertical axes are the coordinate axes of the variables S_{12} and S_{34}, respectively. The solid colored lines are the vanishing loci of the indicated energy factors S_τ while the dashed curve is the vanishing locus of the adjoint polynomial in (4.55). The horizontal and vertical dotted lines are the vanishing loci of (4.59) and (4.60), respectively. Left: arrangement for generic values of the parameters (S_2, S_3, S_{1234}). Right: degeneration of the arrangement obtained by shrinking an external bounded region (specifically, the triangle on the right) by setting $S_{23} + S_{34} - S_{234} = S_3 = 0$. Note how the adjoint polynomial factors such that one factor lies on top of the horizontal dotted line. Similarly at $S_{12} + S_{23} - S_{123} = S_2 = 0$ the adjoint polynomial factors such that one factor lies on top of the vertical dotted line.

common denominator gives

$$\begin{aligned}\tilde{\psi}_{\text{4-chain}} &= \frac{\text{adj}}{S_{12}S_{23}S_{34}S_{123}S_{234}}\,, \\ \text{adj} &= S_{12}\left(S_{123}\left(S_{23}+S_{34}\right)+S_{234}S_{34}\right)+S_{23}S_{234}\left(S_{123}+S_{34}\right).\end{aligned} \tag{4.55}$$

The corresponding cosmological graph associahedron $\tilde{\mathcal{A}}_{\text{4-chain}}$ is the interior of the region bounded by the hyperplanes $S_{12} = S_{23} = S_{34} = S_{123} = S_{234} = 0$ corresponding to the denominator factors in (4.55). For generic positive values of the parameters (S_2, S_3, S_{1234}), this region is the pentagon in (S_{12}, S_{34})-space depicted in figure 4.12. The vanishing locus of the adjoint polynomial, shown as a dashed line, passes through all points where the hyperplanes intersect outside of the pentagon; this property ensures that the canonical form has zero residue at these points.

According to the analysis of section 4.2, we know that $\tilde{\psi}_{\text{4-chain}}$ has (by splitting the graph at site 2 or at site 3) factorization zeros at

$$S_2 = S_{1234} + S_3 - S_{12} = 0 \qquad \text{and} \qquad S_3 = S_{1234} + S_2 - S_{34} = 0\,, \tag{4.56}$$

and a wavefunction zero at

$$S_{123} - S_{12} + S_{34} = S_{123} + S_{234} = 0\,. \tag{4.57}$$

Here we want to think of these as conditions on the variables (S_{12}, S_{34}) for fixed values of the parameters (S_2, S_3, S_{1234}); therefore we use (4.41) to reexpress (4.57) as

$$\begin{aligned} S_{123} + S_{234} = (S_{1234} + S_2 - S_{34}) + (S_{1234} + S_3 - S_{12}) = 0\,, \\ S_{123} - S_{12} + S_{34} = S_{1234} + S_3 - S_{12} = 0\,. \end{aligned} \tag{4.58}$$

In general the adjoint polynomial is a high degree polynomial whose roots may be difficult to analyze, while the wavefunction and factorization zeros are always linear conditions on the variables. In order to see how it encodes the wavefunction and factorization zeros in our example, let us take a limit in the parameters that shrinks one of the external bounded regions in the hyperplane arrangement. When this happens the vertices forming the region collide and become part of the polytope; such a degeneration of the hyperplane arrangement leads to a factorization of the adjoint polynomial.

For example, setting $S_3 = S_{23}+S_{34}-S_{234} = 0$ leads to the configuration in the right of figure 4.12, where the triangle to the right of the pentagon has shrunk. In this limit, the adjoint polynomial factors as

$$\mathrm{adj}|_{S_3=0} = S_{234}S_{1234}\left(S_{1234} + S_2 - S_{34}\right)\,, \tag{4.59}$$

where we have used (4.41). The first factor above cancels the S_{234} pole in the denominator of $\tilde{\psi}_{\text{4-chain}}$ while the vanishing locus of the last factor corresponds to the horizontal dotted line in figure 4.12. This provides a geometric interpretation for the second factorization zero listed in (4.56).

Similarly setting $S_2 = S_{12}+S_{23}-S_{123} = 0$ shrinks the triangle above the pentagon in figure 4.12 and the adjoint polynomial factors as

$$\mathrm{adj}|_{S_2=0} = S_{123}S_{1234}\left(S_{1234} + S_3 - S_{12}\right)\,, \tag{4.60}$$

where we have again used (4.41). The first factor above cancels the S_{123} pole in the denominator of $\tilde{\psi}_{\text{4-chain}}$ while the vanishing locus of the last factor corresponds to the vertical dashed line in the figure. This provides a geometric interpretation for the first factorization zero listed in (4.56).

There is a third external bounded region – the triangle to the upper right of the pentagon – that can be shrunk by setting the total energy parameter S_{1234} to zero. In this limit the adjoint polynomial again factors, but one of the factors cancels one of the poles in the stripped wavefunction:

$$\tilde{\psi}_{\text{4-chain}}|_{S_{1234}=0} = \frac{S_2S_3(S_2+S_3-S_{12}-S_{34})}{S_{12}(S_2+S_3-S_{12}-S_{34})S_{34}(S_3-S_{34})(S_2-S_{12})} = \frac{S_2S_3}{S_{12}S_{34}(S_3-S_{34})(S_2-S_{12})}\,, \tag{4.61}$$

so there is no novel zero associated with this limit; we do however see the two parametric zeros (4.47) of $\tilde{\psi}_{\text{4-chain}}$ from this formula.

Finally we turn to the wavefunction zero (4.58), and we see now that it has a trivial explanation: it lies at the intersection of the two factorization zeros listed in (4.56)! For chain graphs it is always the case that the wavefunction zero lies at an intersection of different factorization zeros, but this does not happen for other graph topologies. This may be one way to see why chain graphs "accidentally" have wavefunction zeros that general graphs do not.

4.4 Cosmological ABHY associahedra

In this section, we present a surprising connection between the (tree-level) scattering *amplitudes* of a colored (i.e., matrix-valued) scalar field with a $\mathrm{Tr}(\phi^3)$ interaction (which have full Poincaré symmetry) and the stripped cosmological wavefunctions (which lack time-translation invariance) associated to *individual* chain graphs. We begin in section 4.4.1 with a lightning review of the color-ordered amplitudes in $\mathrm{Tr}(\phi^3)$ theory, the geometries that encodes them (the ABHY associahedra), and their hidden zeros discovered in [157]. In section 4.4.2, we present an explicit map between the kinematic variables appearing in the n-chain stripped wavefunction and those of the $(n{+}1)$-point color-ordered amplitude in $\mathrm{Tr}(\phi^3)$ theory before explaining how the cosmological zeros studied in this paper map to their amplitude counterparts.

4.4.1 A review of the hidden zeros of $\mathrm{Tr}(\phi^3)$ theory

Kinematic mesh. Each n-point color-ordered amplitude in $\mathrm{Tr}(\phi^3)$ theory, denoted by $A_n^{\mathrm{Tr}(\phi^3)}$, is a function of the $n(n{-}1)/2$ Lorentz-invariant dot products of momenta $p_i \cdot p_j$. Thanks to momentum conservation only $n(n{-}3)/2$ of these are independent (in arbitrary spacetime dimension), which coincides with the number of *planar kinematic variables* $X_{i,j}$[5] defined by

$$X_{i,j} = (p_i + \cdots + p_{j-1})^2 \,, \tag{4.62}$$

where we take the momenta to be on-shell so that $X_{i,i+1} = p_i^2 = 0$ and subscripts are always understood mod n. These planar variables comprise the complete set of propagators that appear in $A_n^{\mathrm{Tr}(\phi^3)}$. We then define the *non-planar variables* $c_{ij} \equiv -2p_i \cdot p_j$ for $|i{-}j| \geq 2$, which can be expressed in terms of the $X_{i,j}$ via

$$c_{i,j} = X_{i,j} + X_{i+1,j+1} - X_{i,j+1} - X_{i+1,j} \,. \tag{4.63}$$

This identity motivates organizing both sets of variables in a *kinematic mesh* [9, 179], where the planar variables label vertices and the non-planar variables are associated to specific diamonds, as seen in figure 4.13 for the 5-point case.

ABHY associahedron. A *kinematic basis* is a choice of $n{-}3$ planar variables and $(n{-}2)(n{-}3)/2$ non-planar variables that are independent, which means that all of the $X_{i,j}$ can be expressed uniquely in terms of the variables in a basis. The former are treated as coordinates on an $(n{-}3)$-dimensional subspace of the $n(n{-}3)/2$-dimensional kinematic space, while the latter are thought of as parameters that specify the hypersurface. The ABHY construction [9] realizes the associahedron in this hyperplane as an $(n{-}3)$-dimensional polytope whose canonical function equals the amplitude $A_n^{\mathrm{Tr}(\phi^3)}$. For example at $n = 5$ the associahedron is a pentagon (identical to the 4-chain graph associahedron from figure 4.4) and the associated canonical function is

$$A_5^{\mathrm{Tr}(\phi^3)} = \frac{1}{X_{1,3}X_{1,4}} + \frac{1}{X_{2,4}X_{2,5}} + \frac{1}{X_{1,3}X_{3,5}} + \frac{1}{X_{1,4}X_{2,4}} + \frac{1}{X_{2,5}X_{3,5}} \,. \tag{4.64}$$

[5] These should not be confused with the site energies X_v of cosmological wavefunctions in (4.1).

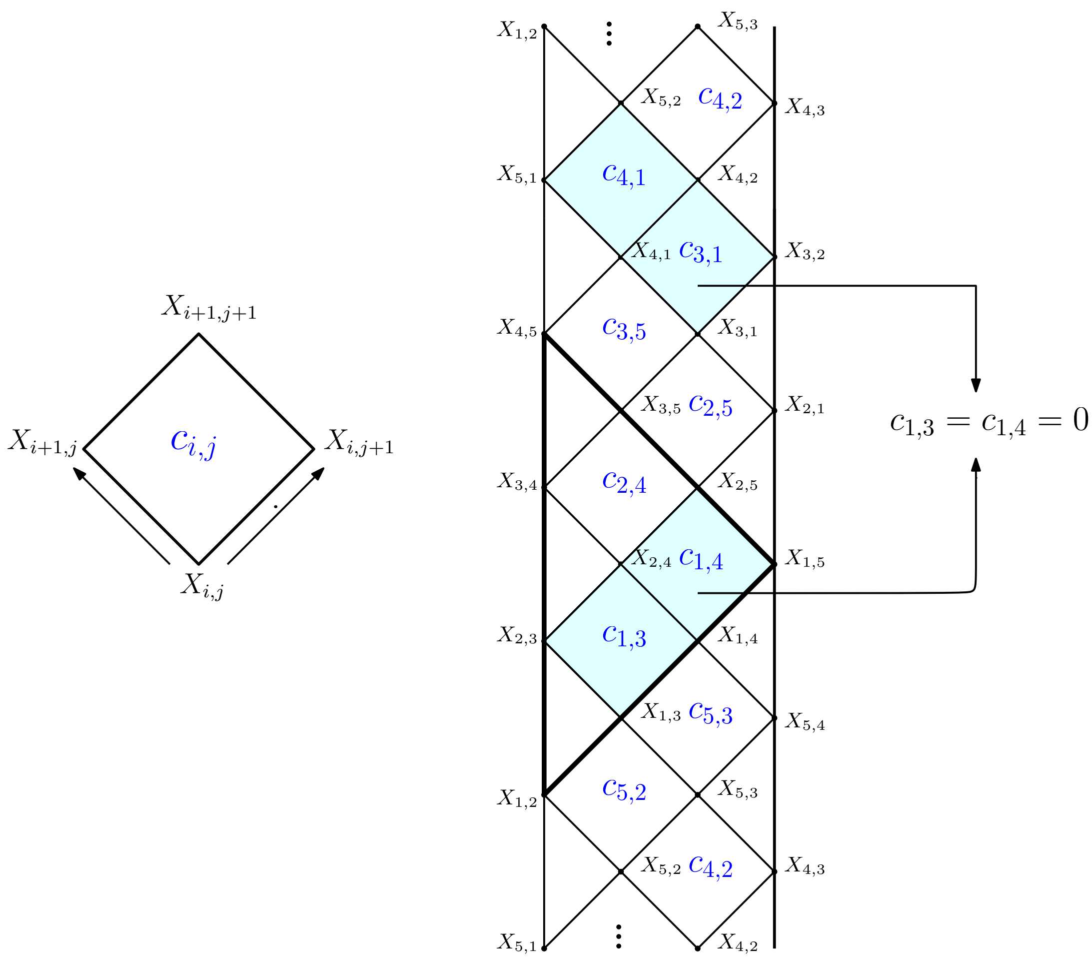

Figure 4.13: The 5-point kinematic mesh (right) with legend (left). The kinematic basis associated to the triangular region highlighted in bold is $\{X_{1,3}, X_{1,4}, c_{1,3}, c_{1,4}, c_{2,4}\}$. As an example of a zero of the amplitude $A_5^{\mathrm{Tr}(\phi^3)}$, we highlight the case of $c_{1,3} = c_{1,4} = 0$ associated to the maximal rectangle in blue.

Zeros. The zeros of $\mathrm{Tr}(\phi^3)$ amplitudes are reached by picking a maximal rectangular region in the kinematic mesh and setting to zero all of the $c_{i,j}$ inside it [157]. In the 5-point example, one such zero is reached by setting $c_{1,3} = c_{1,4} = 0$, which is associated to the maximal rectangle with top and bottom vertices $X_T = X_{2,5}$ and $X_B = X_{1,3}$ respectively, as shown in figure 4.13.

In addition, there is a splitting property associated to a near-zero configuration which states that on the locus where all of the non-planar variables except one in a maximal triangle are zero, the amplitude factors into

$$A_n^{\mathrm{Tr}(\phi^3)} \to \left(\frac{1}{X_B} + \frac{1}{X_T}\right) \times A_{\mathrm{down}}^{\mathrm{Tr}(\phi^3)} \times A_{\mathrm{up}}^{\mathrm{Tr}(\phi^3)} \,, \tag{4.65}$$

with appropriate kinematics for the up- and down- sub-amplitudes. In the example shown in the figure, i.e. the zero of $A_5^{\mathrm{Tr}(\phi^3)}$ at $c_{1,3} = c_{1,4} = 0$, relaxing the first condition leads to

$$A_5^{\mathrm{Tr}(\phi^3)}|_{c_{1,4}=0} = \frac{c_{1,3}}{X_{1,3}X_{2,5}} \times \left(\frac{1}{X_{1,4}} + \frac{1}{X_{3,5}}\right), \tag{4.66}$$

while relaxing the second condition leads to

$$A_5^{\mathrm{Tr}(\phi^3)}|_{c_{1,3}=0} \frac{c_{1,4}}{X_{1,3}X_{2,5}} \times \left(\frac{1}{X_{2,4}} + \frac{1}{X_{3,5}}\right). \tag{4.67}$$

We refer the reader to [157] for a detailed analysis of these zeros and how they can be realized as flattening limits of the ABHY associahedron.

4.4.2 From cosmological to amplitudes zeros

It is already clear that the $\mathrm{Tr}(\phi^3)$ story closely resembles that of the cosmological zeros we studied in section 4.3. We now present a concrete connection between the stripped wavefunctions for n-chains and the color-ordered scattering amplitudes in $\mathrm{Tr}(\phi^3)$ theory (similar connections have been discussed recently in [177, 178]). To start with we identify the planar variable $X_{i,j}$ of $A_{n+1}^{\mathrm{Tr}(\phi^3)}$ with the energy factor S_τ associated to the tube $\tau = \{i, i+1, \ldots, j-1\}$:

$$S_{i\ldots j-1} \equiv X_{i,j} \qquad |i-j| \geq 2\,, \tag{4.68}$$

with $X_{i,i+1} = 0$ as discussed above. Note that this identification does not determine the energy parameters S_i associated to 1-tubes, and in particular does not require that we must take them to vanish. It is easy to see that the stripped wavefunction $\tilde{\psi}_{n\text{-chain}}$ of the n-chain is identical to the $(n+1)$-point $\mathrm{Tr}(\phi^3)$ scattering amplitude $A_{n+1}^{\mathrm{Tr}(\phi^3)}$ under (4.68). For example, the five terms in (4.5) for $\tilde{\psi}_{4\text{-chain}}$ become identical to the five terms in the 5-point amplitude $A_5^{\mathrm{Tr}(\phi^3)}$ shown in (4.64).

Next let us understand how the non-planar variables $c_{i,j}$ defined in (4.63) map to the parameters $\{S_2, S_3, \ldots, S_{n-1}, S_{12\ldots n}\}$ of the n-chain. Using the map (4.68) along with the linear relations of the n-chain obtained from (4.41), we observe that:

1. The $n-2$ parameters associated to energy 1-tubes of interior sites map according to

$$S_i = c_{i-1,i+1} \qquad \text{for } 2 \leq i \leq n-1\,. \tag{4.69}$$

2. A total of $(n-1)(n-4)/2$ non-planar variables vanish identically on the support of (4.41):

$$\begin{aligned} &c_{1,4} = c_{1,5} = \cdots = c_{1,n-1} = 0\,, \\ &c_{i,i+3} = c_{i,i+4} = \cdots = c_{i,n} = 0 \qquad\qquad \text{for } 2 \leq i \leq n-3\,. \end{aligned} \tag{4.70}$$

3. The total energy factor $S_{1\ldots n}$ maps to

$$S_{12\ldots n} = c_{1,n}\,. \tag{4.71}$$

4. The remaining $n-3$ non-planar variables map to linear combinations of the parameters and energy factors $S_{\tau \in \tilde{\mathsf{T}}}$ of the n-chain graph; these can be worked out on a case-by-case basis.

We call the image of the n-chain cosmological graph associahedron $\tilde{\mathcal{A}}_{n\text{-chain}}$ under this map the *cosmological ABHY associahedron*.

Note that the map explicitly breaks the $\mathbb{Z}_{n+1}$ cyclic symmetry of the amplitude $A_{n+1}^{\mathrm{Tr}(\phi^3)}$. Thus unlike for the ABHY associahedron, different cyclic permutations of the cosmological ABHY associahedron are not related to each other by different choices of kinematic basis. The form of the map given above is tuned to the choice of coordinates provided by the ray-like triangulation of $A_{n+1}^{\mathrm{Tr}(\phi^3)}$. We refer the reader to [157] for additional details; for our purpose it is enough to state that elements of the kinematic basis associated to this triangulation are those that live inside a maximal triangular region in the kinematic mesh (see figure 4.13).

Another key difference between the ABHY associahedron and its cosmological counterpart arises from the vanishing non-planar variables (4.70). The vanishing of these parameters of the ABHY associahedron causes vertices to collide, resulting in a non-simple polytope as discussed in section 4.3.1.

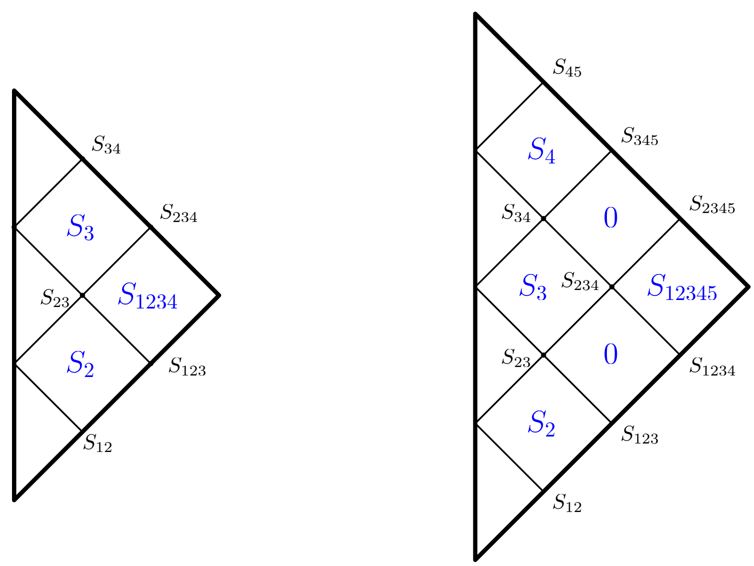

Figure 4.14: The ray-like subregion of the cosmological kinematic mesh for the 4- and 5-chain graphs.

It is instructive to utilize our map between the kinematic variables $\{X_{i,j}, c_{i,j}\}$ of $\mathrm{Tr}(\phi^3)$ theory and the energy factors S_τ of cosmological wavefunctions to translate the kinematic mesh associated to the former into a *cosmological kinematical mesh* for the stripped n-chain wavefunction $\tilde{\psi}_{n\text{-chain}}$. Figure 4.14 shows, for $n = 4, 5$, the portion of the cosmological kinematic mesh corresponding to the ray-like triangulation subregion of the full mesh.

Given this surprising connection between stripped wavefunctions for n-chains and $(n+1)$-point amplitudes in $\mathrm{Tr}(\phi^3)$ theory, it is natural to ask whether the cosmological zeros of the former, that we have studied in section 4.2, map naturally to the zeros of the latter that were characterized in [157]. We now illustrate how this works using the 4-chain as an example.

First we consider the parametric zeros (4.30), which map to

$$S_2 = S_{1234} = 0 \;\to\; c_{1,3} = c_{1,4} = 0\,, \tag{4.72}$$

$$S_3 = S_{1234} = 0 \;\to\; c_{1,4} = c_{2,4} = 0\,, \tag{4.73}$$

reproducing two of the zeros of the amplitude $A_5^{\mathrm{Tr}(\phi^3)}$. Note that like for the 5-point amplitude, the parametric zeros of the 4-chain are also reached by setting all of the parameters inside a maximal rectangle of the cosmological kinematic mesh to zero, shown in this example in the left of figure 4.14. This is a generic feature – setting the parameters inside a maximal rectangle in the ray-like subregion of the cosmological kinematic mesh for the n-chain enumerates all parametric zeros (4.30) for the stripped wavefunction $\tilde{\psi}_{n\text{-chain}}$, and these zeros correspond to a subset of the zeros of the $(n{+}1)$-point amplitude $A_{n+1}^{\mathrm{Tr}(\phi^3)}$. Figure 4.14 (right) demonstrates this feature for $n = 5$.

To access the other zeros of $A_{n+1}^{\mathrm{Tr}(\phi^3)}$, one needs to go beyond the ray-like subregion of the cosmological kinematic mesh. As discussed earlier, this does not correspond to a simple change of kinematic basis for the cosmological ABHY associahedron. The two factorization zeros for the 4-chain map to two more zeros of the 5-point amplitude according to

$$S_3 = S_{12} + S_{23} = 0 \;\to\; c_{2,4} = c_{2,5} = 0\,, \tag{4.74}$$

$$S_2 = S_{23} + S_{34} = 0 \;\to\; c_{1,3} = c_{3,5} = 0\,, \tag{4.75}$$

while the sole wavefunction zero (4.14) gives the final zero of $A_5^{\mathrm{Tr}(\phi^3)}$:

$$S_{123} - S_{12} + S_{34} = S_{123} + S_{234} = 0 \;\to\; c_{2,5} = c_{3,5} = 0\,. \tag{4.76}$$

Thus, we see that the zeros of the stripped wavefunction $\tilde{\psi}_{4\text{-chain}}$ associated to the single 4-chain graph non-trivially map to all five zeros of the 5-point amplitude $A_5^{\mathrm{Tr}(\phi^3)}$, which is given by a sum of contributions from 5 distinct graphs.

Again, this is a generic feature that extends to all n. In addition to the zeros, the near-zero splitting associated to $\mathrm{Tr}(\phi^3)$ amplitudes is also reproduced by the stripped wavefunction: one can readily check that the splitting associated to the near-zero loci of the stripped wavefunction, described in section 4.2, reproduces the splitting property of the $\mathrm{Tr}(\phi^3)$ amplitudes given in (4.65). The only subtlety in checking this is that for generic n-chains, the near-zero splitting proceeds straightforwardly except for the fact that one needs to account for the $c_{i,j}$ variables that vanish at the outset (4.70). These coincide with the non-simple vertices of the cosmological ABHY associahedron. Given a maximal rectangle, one cannot turn these vanishing $c_{i,j}$ back on; however, the other non-trivial $c_{i,j}$ variables can be turned on in the usual manner to observe the near-zero splitting described above.

4.5 Discussion and outlook

In this paper, we have classified the linear zero conditions for the flat-space (stripped) wavefunction coefficients (associated to a single Feynman graph $\mathcal{G}$) into parametric, wavefunction and factorization zeros. The wavefunction zeros (section 4.2.1) are exclusive to graphs of chain topology and cause both the wavefunction and its stripped counterpart to exhibit a universal splitting behavior on its near-zero locus. The factorization zeros (section 4.2.2) rely on first factorizing an arbitrary graph $\mathcal{G}$ solely into its constituent chain subgraphs and then localizing on to the wavefunction zeros of all such chain subgraphs. Finally, the parametric zeros (section 4.2.3) of a graph $\mathcal{G}$ are seen to arise as flattening limits of the associated cosmological graph associahedron $\tilde{\mathcal{A}}_{\mathcal{G}}$ – a non-simple polytope obtained from a certain cosmological limit of the graph associahedron $\mathcal{A}_{\mathcal{G}}$. While the wavefunction and factorization zeros are not discoverable as flattening limits of $\tilde{\mathcal{A}}_{\mathcal{G}}$, they still admit geometric interpretations: new zero conditions on the coordinates are discovered by degenerating the hyperplane arrangement so that the adjoint polynomial (numerator of the wavefunction) factors into linear pieces. Finally, we see a surprising connection between the stripped wavefunction coefficients of chain graphs to scattering amplitudes in $\mathrm{Tr}(\phi^3)$ theory. This connection remarkably allows us to use the zeros for the wavefunction associated to a single graph to find the zeros of amplitudes in $\mathrm{Tr}(\phi^3)$ theory, which involve a sum over many Feynman graphs.

We note that while we have focused on an uncolored scalar theory with a ϕ^3 interaction, the analysis of this paper generalizes to arbitrary polynomial ϕ^p interactions in a straightforward manner. Indeed the zero loci of specific graphs remain unchanged upon changing the valence of the scalar self-interaction. On the other hand, the definitions of the energy factors in terms of which these zero loci are expressed will have to be changed accordingly.

While the central objects of interest in this paper have been the flat-space wavefunction coefficients, it is important to note that they serve as universal integrands for their counterparts in a generic power-law FRW spacetime with scale factor $a(\eta) = \eta^{-1-\varepsilon}$ and cubic interactions[6]

$$\psi_{n,\mathrm{FRW}}^{(\ell)} = \int_0^\infty \left(\prod_v \mathrm{d}x_v \; x_v^\varepsilon\right) \psi_n^{(\ell)}(x_v + X_v, Y_e) \; . \tag{4.77}$$

Here, the site energies of the flat wavefunction (defined in (4.1)) are shifted by x_v and then integrated over the kernel $x_1^\varepsilon \cdots x_n^\varepsilon$. Consequently, the zeros of the universal integrand $\psi_n^{(\ell)}$ studied here naturally carry over to wavefunction coefficients in power-law FRW cosmologies $\psi_{n,\mathrm{FRW}}^{(\ell)}$.

Also, while our analysis is centered around the flat-space wavefunction corresponding to a single Feynman graph $\mathcal{G}$, it would be natural to perform the same analysis of the zeros for the $\mathrm{Tr}(\phi^3)$ cosmological wavefunction that involves a sum over Feynman diagrams [173]. Just as the parametric zeros of $\mathcal{G}$ were discovered from flattening limits of the (non-simple) cosmological graph associahedron as discussed in section 4.3, it would be interesting to study if the zeros for the $\mathrm{Tr}(\phi^3)$ wavefunction arise from flattening the associated geometry – the cosmohedron [173].

In section 4.4, we discussed that the graph associahedra for n-chains are simply the classical associahedra, which is of cluster type A_{n-2}, while the n-gons at 1-loop are of type B_{n-1}. Cluster string integrals [180] exist for such associahedra, paving the way for stringy formulations of wavefunction coefficients associated with single graphs in cosmology – an active area of ongoing research.

[6] The integration kernel depends on the valency of the interaction.

From a more physical perspective, it is important to understand the physical origin of the zeros for the cosmological wavefunction studied in this paper. Recasting the conditions of the n-chain wavefunction zero (4.14) explicitly in terms of its energy variables

$$X_i = 0 \quad \text{for} \quad 3 \leq i \leq n-2\,, \qquad Y_1 = -X_1 - 2X_2\,, \qquad Y_{n-1} = -2X_{n-1} - X_n\,, \tag{4.78}$$

we observe that the associated kinematics exhibit multi-soft limits, i.e the energy of the external leg at the i-th site vanishes: $X_i = |\vec{k}_i| = 0$ for $3 \leq i \leq n-2$. It would be interesting to see if the kinematics of such zeros could be exploited to better understand the soft behavior of the wavefunction coefficients. Also at the level of flat-space amplitudes, the existence of hidden zeros are linked to the color-kinematics duality and can be derived from the Bern-Carrasco-Johansson (BCJ) relations [160]. To that end, understanding the symmetry arguments behind the cosmological zeros is an important direction we leave for future study.

Finally, it would also be interesting to see if the flat-space (stripped) wavefunction can be uniquely fixed from its zeros, as was recently shown to be true for amplitudes in $\mathrm{Tr}(\phi^3)$ theory [162].

Chapter 5

On the Unitarity of Coon Amplitude

This chapter is based on the work [181].

A four-point amplitude that: i) is crossing symmetric in $s \leftrightarrow t$, ii) has polynomial residues, and iii) is meromorphic (with simple poles only), was first introduced by Veneziano in 1968 [15][1]:

$$\mathcal{A}^V(s,t) = -(s+t)^{\alpha_0-1}\frac{\Gamma(-\alpha_0-s)\Gamma(-\alpha_0-t)}{\Gamma(-2\alpha_0-s-t)} \ . \tag{5.1}$$

Its worldsheet realization as a dual resonance model in an operator formalism was established later [16, 17, 18]. Owing to an infinite product representation of the gamma function, the simple pole structure of the Veneziano amplitude is made manifest by the expression:

$$\mathcal{A}^V(s,t) = \frac{1}{st}\prod_{n=1}^{\infty}\frac{1-\frac{s+t}{n}}{\left(1-\frac{s}{n}\right)\left(1-\frac{t}{n}\right)} \ , \tag{5.2}$$

which holds when $\alpha_0 = 0$.

A year later, an investigation into the uniqueness of the Veneziano amplitude led Coon to suggest a more generic infinite product representation albeit with logarithmic Regge trajectories [19][2]:

$$\mathcal{A}^C(s,t) = (q-1)\exp\left(\frac{\log\sigma\log\tau}{\log q}\right)\prod_{n=0}^{\infty}\frac{\left(1-\frac{q^n}{\sigma\tau}\right)\left(1-q^{n+1}\right)}{\left(1-\frac{q^n}{\sigma}\right)\left(1-\frac{q^n}{\tau}\right)} \ , \tag{5.3}$$

where

$$\sigma = 1-(1-q)(\alpha_0+s) \ , \qquad \tau = 1-(1-q)(\alpha_0+t) \ , \tag{5.4}$$

[1] Here the parameter $\alpha_0 = 0$ for type-I superstrings and $\alpha_0 = 1$ for bosonic strings. In some papers on this subject, α_0 is used interchangeably with m^2.

[2] It is worth noting that this representation of the amplitude was not first adopted in [19], but originally appeared in later papers by the same author [182]. More recently, beginning with the work of [2], it has become conventional to adopt this infinite product representation.

and $q \in [0,1]$ is an arbitrary parameter[3].

In this chapter we focus on the Coon amplitude, which smoothly interpolates between the Veneziano amplitude as $q \to 1$ and scalar field theory as $q \to 0$:

$$\mathcal{A}^C(s,t) \xrightarrow{q\to 0} \frac{1}{s+\alpha_0} + \frac{1}{t+\alpha_0} + 1 \ . \tag{5.5}$$

Following its inception, many aspects of the Coon amplitude have been studied in some detail, including its n-point generalization [183], prescriptions for factorization [184, 185], a loop-order extension [186], and its operator formulations [187, 188, 189, 190][4]. However, the physical origin of the Coon amplitude is not yet clear, and a worldsheet realization of the amplitude remains elusive (see [193] for attempts in this direction by q-deforming the worldsheet conformal group). One of its key physical features is the appearance of an infinite tower of massive states in the form an accumulation point spectrum (similar to that in the hydrogen atom); such features have also been observed in several recent studies in different physical scenarios [194, 195]. More recently, the authors of [196] have attempted to reproduce such accumulation-like aspects of the Coon amplitude by virtue of open string scattering on D-branes in an AdS background. Also, multi-parameter spaces of four-point amplitudes satisfying the above constraints i)-iii) have been introduced in [21, 22] with further modified spin-dependent Regge trajectories.

A necessary condition for the Coon amplitude to have physical relevance is that it must be unitary. An early attempt to analyze unitarity was carried out in [20] where it was claimed that the Coon amplitude is *ghost-free*. A more careful and detailed analysis on this issue was carried out more recently in [2]. It was demonstrated by numerical methods that there exists a curve in (q, D) space separating regions where the Coon amplitude does or does not satisfy unitarity in D (spacetime) dimensions. They also analytically show the existence of a certain critical value $q = q_\infty(-\alpha_0)$ where the amplitude switches from being unitary in all dimensions to having a critical dimension. However, an analytic analysis of the unitarity of the Coon amplitude for all (q, D) is still an outstanding problem. In this chapter, we study the positivity of the Coon amplitude's partial wave expansion coefficients, in a spirit similar to the recent techniques developed for the Veneziano amplitude in [1]. In doing so, we make small strides towards an analytic analysis of Coon unitarity. We achieve this by utilizing several elements of q-calculus which have been well studied in the literature [197, 198].

This chapter is organized as follows. In section 5.1, we derive a novel contour integral representation for the partial wave expansion coefficients $B_{n,j}^{(D)}(q)$. In section 5.2 we analyze Regge trajectories (leading and beyond), finding that the leading and sub-leading Regge trajectories are manifestly unitary, while unitarity fails for a certain region in (q, D) space for the sub-sub-leading coefficient $B_{3,0}^{(D)}(q)$. Finally, in section 5.3, we strive towards obtaining a double-contour integral representation for the coefficients in the near Veneziano case $(1-q \ll 1)$ and apply our formula to study their

[3] In principle, the deformation parameter q could be any real number, but it is easy to see that there is no chance for the amplitude to be unitarity if q is outside $[0,1]$.

[4] We refer the interested reader to [191, 192] for an early review on the subject.

asymptotic behavior. We conclude with a discussion of our results and possible future directions in section 5.4.

5.1 A contour integral representation for partial wave coefficients

In this section, we establish a contour integral representation for the partial wave expansion of Coon amplitude. The analysis here closely follows a q-generalization of the derivation presented in section 3.1 of [1].

5.1.1 A contour representation

Our starting point is the representation of $\mathcal{A}^{\mathrm{C}}(s,t)$ in terms of the q-gamma function[5]:

$$\mathcal{A}^{\mathrm{C}}(s,t) = q^{\alpha_q(s)\alpha_q(t)-\alpha_q(s)-\alpha_q(t)} \frac{\Gamma_q(-\alpha_q(s))\Gamma_q(-\alpha_q(t))}{\Gamma_q(1-\alpha_q(s)-\alpha_q(t))} \ . \tag{5.6}$$

This expression can also be recast as a q-beta function. Utilizing its integral representation (5.110) (for more details, refer to Appendix 5.5.3) one can rewrite the amplitude as a "Koba-Nielsen" like integral [191]:

$$\mathcal{A}^{\mathrm{C}}(s,t) = \frac{q^{\alpha_q(s)\alpha_q(t)-\alpha_q(s)-\alpha_q(t)}}{[-\alpha_q(s)]_q} \int_0^1 d_q z \ z^{-\alpha_q(s)}(1-qz)_q^{-\alpha_q(t)-1} \ . \tag{5.7}$$

We note that the arguments that appear in the q-gamma functions of (5.6) are the non-linear q-deformed Regge trajectories defined by

$$\alpha_q(s) \equiv \frac{\ln \sigma}{\ln q} = \frac{\ln\left(1-s(1-q)\right)}{\ln q} \ , \tag{5.8}$$

in contrast to the linear Regge trajectories $s = \lim_{q\to 1}\alpha_q(s)$ that appear in the Veneziano amplitude (5.1).

From the integral representation (5.7), we can extract the residue polynomials on the massive poles at $s = [n]_q$

$$\mathcal{A}^{\mathrm{C}}(s,t) \to \frac{1}{s-[n]_q} \times R^C_{[n]_q}(t) \ , \tag{5.9}$$

where the q-integers $[n]_q$ are defined in (5.79). Then unitarity is equivalent to the condition that each residue polynomial admits a partial wave expansion in terms of D-dimensional Gegenbauer polynomials

$$R^C_{[n]_q}(t) = \sum_j B^{(D)}_{n,j}(q)\, G^{(D)}_j(t) \ , \tag{5.10}$$

with all of the coefficient functions $B^{(D)}_{n,j}(q)$ non-negative.

[5] Our normalization matches the one stated in recent literature [199].

To determine $R^C_{[n]_q}(t)$, we note that the singularities in s all come from the region of integration near $z \to 0$. To that end, we Taylor expand the integrand around $z = 0$ using $(1-qz)_q^{-\alpha_q(t)-1} = \sum_{k=0}^{\infty} a_k(q,t) z^k$, which implies that the Coon amplitude can be written as

$$\mathcal{A}^{\mathrm{C}}(s,t) = \frac{q^{\alpha_q(s)\alpha_q(t)-\alpha_q(s)-\alpha_q(t)}}{[-\alpha_q(s)]_q} \sum_{k=0}^{\infty} a_k(q,t) \frac{1}{[k+1-\alpha_q(s)]_q} \ , \tag{5.11}$$

where we have utilized the identity

$$\int_0^1 d_q z \ z^{-\alpha_q(s)+k} = \frac{1}{[k+1-\alpha_q(s)]_q} \ . \tag{5.12}$$

Evaluating the residue polynomial $R^C_{[n]_q}(t)$, we obtain

$$R^C_{[n]_q}(t) = \lim_{s \to [n]_q} (s-[n]_q)\mathcal{A}^{\mathrm{C}}(s,t) = \frac{1}{[-n]_q} q^{\alpha_q(t)(n-1)-n} \lim_{s \to [n]_q} \sum_{k=0}^{\infty} a_k \frac{s-[n]_q}{[k+1-\alpha_q(s)]_q} \ , \tag{5.13}$$

where we have used the fact that $\alpha_q(s) = n$ in the limit $s \to [n]_q$. The only term that survives is the one corresponding to $k = n-1$, for which the residue polynomial reduces to

$$R^C_{[n]_q}(t) = \frac{q^{\alpha_q(t)(n-1)-n}}{[-n]_q} \lim_{s \to [n]_q} a_{n-1} \frac{s-[n]_q}{[n-\alpha_q(s)]_q} \ . \tag{5.14}$$

Manipulating the limit in the above expression and using the fact that

$$q^{\alpha_q(t)(n-1)-n} = \exp \alpha_q(t)(n-1) \, \log q - n \log q = (1+(q-1)t)^{n-1} q^{-n} \ , \tag{5.15}$$

we obtain

$$R^C_{[n]_q}(t) = a_{n-1}(q,t) \frac{q^n}{[n]_q} (1+(q-1)t)^{n-1} \ , \tag{5.16}$$

where we have used the property $[-n]_q = q^{-n}[n]_q$ of q-integers. We can now obtain the Taylor series coefficients a_n as a contour integral around $z = 0$ by Cauchy's theorem

$$a_n(q,t) = \oint_{z=0} \frac{dz}{2\pi i} \frac{(1-qz)_q^{-\alpha_q(t)-1}}{z^{n+1}} \ , \tag{5.17}$$

which finally gives us the expression for the residue polynomial $R^C_{[n]_q}(t)$ as a contour integral around $z = 0$:

$$R^C_{[n]_q}(t) = (1+(q-1)t)^{n-1} \frac{q^n}{[n]_q} \oint_{z=0} \frac{dz}{2\pi i} \frac{(1-qz)_q^{-\alpha_q(t)-1}}{z^n} \ . \tag{5.18}$$

Next, we would like to compute the partial wave coefficients by expanding $R^C_{[n]_q}(t)$ in terms of the D-dimensional Gegenbauer polynomials[6] $G_j^{(D)}(x)$, where $x = \cos\theta$ and is related to t as

[6] It might seem mathematically more natural to expand in the q-deformed Gegenbauer polynomials (also known as Rogers polynomials) [200], but the physical interpretation of such an expansion would be unclear. Unitarity demands that the coefficient of each Gegenbauer polynomial must be non-negative; it is not clear what this fact implies for the coefficients of an expansion in q-deformed Gegenbauer polynomials. If a function admitting a non-negative expansion in terms of Gegenbauer polynomials is said to satisfy unitarity, then perhaps a function admitting a non-negative expansion in terms of q-deformed Gegenbauer polynomials should be said to satisfy q-nitarity.

$t = \frac{s(x-1)}{2} = \frac{[n]_q(x-1)}{2}$ on the resonance $s = [n]_q$. We shall make use of the Rodrigues formula for $G_j^{(D)}(x)$:

$$G_j^{(D)}(x) = (-1)^j \alpha_{j,D}(1-x^2)^{-\delta}\partial_x^j(1-x^2)^{\delta+j} \ , \tag{5.19}$$

where $\alpha_{j,D} = (2\delta+1)_j/(2^j j!(\delta+1)_j)$ with $\delta = \frac{D-4}{2}$. Now, orthogonality allows us to expand any smooth function $F(x)$ in terms of these Gegenbauer polynomials as $F(x) = \sum_{j=0}^{\infty} F_j G_j^{(D)}(x)$, where

$$F_j = n_{j,D}\int_{-1}^{1} dx(1-x^2)^{\delta} G_j^{(D)}(x)F(x) \ , \quad n_{j,D} = j!\frac{2^{2\delta}\left(j+\delta+\frac{1}{2}\right)\left[\Gamma\left(\delta+\frac{1}{2}\right)\right]^2}{\pi\Gamma(j+2\delta+1)} \ . \tag{5.20}$$

Using the Rodrigues formula (5.19), one can integrate by parts j times to obtain for the coefficients $F_j = \int_{-1}^{1} dx(1-x^2)^{\delta+j}\partial_x^j F(x)$, where we have suppressed the overall positive factor $n_{j,D}$. We can apply this form to extract the coefficients in the Gegenbauer expansion of the residue polynomial which can be written as (5.10). Integrating by parts leaves us with the Gegenbauer coefficients $B_{n,j}^{(D)}(q)$ expressed as

$$B_{n,j}^{D}(q) = c_{n,j}^{D}(q)\oint_{z=0}\frac{dz}{z^n}H_q(z) \ , \tag{5.21}$$

where

$$c_{n,j}^{D}(q) = q^n\frac{2^{D-3}}{[n]_q^{D+j-2}}\frac{(j+\frac{D-3}{2})\Gamma\left(\frac{D-3}{2}\right)}{\sqrt{\pi}\Gamma(j+\frac{D-2}{2})} > 0 \ , \tag{5.22}$$

is an overall, manifestly positive constant, and

$$H_q(z) = \int_{-[n]_q}^{0} dt(-t(t+[n]_q))^{\frac{D-4}{2}+j}\partial_t^j[(1-(1-q)t)^{n-1}(1-qz)_q^{-\alpha_q(t)-1}] \ . \tag{5.23}$$

We note that in the limit $q \to 1$, the result (5.23) is in perfect agreement with the t-integral given by (C.9) corresponding to the type-I superstring amplitude ($a = 0$) in [1]. Unfortunately, compared to the analysis in that paper, for general q it appears difficult to further find representations that diagonalize the action of the differential operator ∂_t^j on the q-function in (5.23). This is a roadblock to further manipulating the t-integral to attain a double-contour representation along the lines of [1]. Instead, we now highlight the utility of (5.23) for recovering several existing results before moving on to discuss novel applications in section 5.2.

5.1.2 The critical value $q = 2/3$

In this section we demonstrate that the coefficients $B_{n,j}^{D}(q)$ given in (5.21) are non-negative in arbitrary dimension D for $q \leq 2/3$, recovering a result of [2] in the $\alpha_0 \to 0$ limit.

Starting from (5.21) and (5.23) and applying the residue theorem we have

$$B_{n,j}^{D}(q) = c_{n,j}^{D}(q)\frac{1}{[n-1]_q!}D_q^{(n-1)}H_q(0) \ , \tag{5.24}$$

where

$$\frac{1}{[n-1]_q!}D_q^{(n-1)}H_q(0) = \frac{(-1)^{n-1}q^{\frac{n(n-1)}{2}}}{[n-1]_q!}\int_{-[n]_q}^{0} dt(-t(t+[n]_q))^{\frac{D-4}{2}}\partial_t^j\prod_{k=1}^{n-1}\left(\frac{1-q^{-k}}{1-q}-t\right) \ ,$$

where $D_q^{(n-1)}$ denotes the Jackson q-derivative operated $(n-1)$-times with respect to z and we have made use of the identity (5.96). Now making the substitution $t \to -[n]_q t$ and manipulating the finite product in the integrand yields the following result

$$\begin{aligned}\frac{1}{[n-1]_q!}&D_q^{(n-1)}H_q(0)\\ &= \frac{(-1)^{n-1+j}q^{\frac{n(n-1)}{2}}}{[n]_q!}[n]_q^{n+D+j-3}\int_0^1 dt(t(1-t))^{\frac{D-4}{2}+j}\partial_t^j\prod_{k=1}^{n-1}\left(-\frac{q^{-k}-1}{1-q^n}+t\right)\ ,\end{aligned}$$

and therefore for the coefficients, one arrives at

$$B_{n,j}^D(q) = \frac{2^{D-3}(-1)^j}{\sqrt{\pi}}\frac{\left(\frac{D-3}{2}+j\right)\Gamma\left(\frac{D-3}{2}\right)}{\Gamma\left(\frac{D-2}{2}+j\right)}\frac{q^{\frac{n(n+1)}{2}}[n]_q^{n-1}}{[n]_q!}\int_0^1 dt(t(1-t))^{\frac{D}{2}-2+j}\partial_t^j\prod_{k=1}^{n-1}\left(\frac{q^{-k}-1}{1-q^n}-t\right)\ . \tag{5.25}$$

Finally we consider the substitution $t = \frac{1-x}{2}$, and the integral looks as follows[7]

$$B_{n,j}^D(q) \propto \int_{-1}^1 dx(1-x^2)^{\frac{D}{2}-2+j}\partial_x^j\prod_{k=1}^{n-1}\left(\frac{2q^{-k}-3+q^n}{1-q^n}+x\right)\ . \tag{5.26}$$

The above integral is manifestly positive if all roots of the polynomial in the product are negative. This is the case if $2q^{-k}-3+q^n \geq 0$ so if the minimum value of the LHS satisfies this then it will be positive for all k. So we take $k=1$ which implies $2q^{-1}-3+q^n \geq 0$, but since this is a decreasing function of n it is minimised as $n \to \infty$ and we get

$$2q^{-1}-3 \geq 0 \implies q_{\text{crit}} = \frac{2}{3}\ . \tag{5.27}$$

Therefore, we conclude that the Coon amplitude is manifestly unitary for $q \leq 2/3$ for any spacetime dimensions D, in agreement with the results of [2].

5.1.3 Some coefficients at small n and j

Using the finite product formula (5.26), we list in table 5.1 some of the low-lying partial wave coefficients for the Coon amplitude; for comparison, we list the corresponding coefficients for the Veneziano amplitude in table 5.2.

In table 5.1 we have defined:

$$b_{3,0}^D(q) = \frac{q^3\left[4(D-1)+2q(D-1)-6q^2(D-1)-q^3(5D-6)-2q^4(D-2)+3Dq^5+2Dq^6+Dq^7\right]}{4(D-1)(1+q)(1+q+q^2)}\ , \tag{5.28}$$

[7] Up to a positive constant of proportionality that depends on q, n and D.

	$j=0$	$j=1$	$j=2$	$j=3$
$n=1$	q			
$n=2$	$\frac{q^2(1-q)(2+q)}{2(1+q)}$	$\frac{q^3}{2(D-3)}$		
$n=3$	$b^D_{3,0}(q)$	$\frac{q^4(1-q)(1+3q+2q^2+q^3)}{2(D-3)(1+q)}$	$\frac{q^6(1+q+q^2)}{2(D-1)(D-3)(1+q)}$	
$n=4$	$(1-q)b^D_{4,0}(q)$	$b^D_{4,1}(q)$	$(1-q)b^D_{4,2}(q)$	$\frac{3q^{10}(1+q)(1+q^2)^2}{4(D-3)(D^2-1)(1+q+q^2)}$

Table 5.1: Values of $B^D_{n,j}(q)$ for Coon amplitude for low lying (n,j). All the leading and sub-leading Regge coefficients are manifestly positive for $D \geq 4$. Expressions for the coefficients $b^D_{3,0}, b^D_{4,0}, b^D_{4,1}$ and $b^D_{4,2}$ are too long to fit inside the table and are given in equations (5.28-5.31).

	$j=0$	$j=1$	$j=2$	$j=3$
$n=1$	1			
$n=2$	0	$\frac{1}{2(D-3)}$		
$n=3$	$\frac{10-D}{24(D-1)}$	0	$\frac{3}{4(D-1)(D-3)}$	
$n=4$	0	$\frac{11-D}{12(D+1)(D-3)}$	0	$\frac{2}{(D^2-1)(D-3)}$

Table 5.2: Values of $B^D_{n,j}$ for the Veneziano amplitude for low lying (n,j). These results were listed for example in [1].

$$
\begin{aligned}
b^D_{4,0}(q) = {}& \frac{q^4}{8(D-1)(1+q^2)(1+q+q^2)}\Big[8(D-1)+4(D-1)q+4(D-1)q^2 \\
& + 2(8-7D)q^3 + 2(10-7D)q^4 + 16(2-D)q^5 - 3(3D-10)q^6 + 4(7+D)q^7 \\
& + (22+5D)q^8 + 8(2+D)q^9 + 5(2+D)q^{10} + 2(2+D)q^{11} + (2+D)q^{12}\Big] , \qquad (5.29)\\
b^D_{4,1}(q) = {}& \frac{q^5}{8(D-3)(1+D)(1+q+q^2)(1+q+q^2+q^3)}\Big[4(1+D)+12(1+D)q+12(1+D)q^2 \\
& - 24(1+D)q^4 - 3(6+7D)q^5 - 2(4+7D)q^6 - 3(D-2)q^7 + 12(2+D)q^8 + 9(2+D)q^9 \\
& + 6(2+D)q^{10} + 3(2+D)q^{11}\Big] , \qquad (5.30)\\
b^D_{4,2}(q) = {}& \frac{q^7(1+q^2)(2+6q+12q^2+9q^3+6q^4+3q^5)}{4(D-3)(D-1)(1+q+q^2)} . \qquad (5.31)
\end{aligned}
$$

The coefficients derived in the tables above are found to be in agreement with certain recent results in the literature:

- The values of $B^D_{n,j}(q)$ listed in table 5.1 are in agreement with the results of [199], where the authors computed the closed-form expressions for the Coon amplitude partial-wave coefficients up to $n=3$.
- An explicit formula for the coefficient $B^D_{n,j}(q)$, in fact for a four-parameter generalization of the Coon amplitude, was written as a nested four-fold sum in (67) of [21].
- Moreover, it is easy to check that in the $q \to 1$ limit, table 5.1 reduces to the coefficients $B^D_{n,j}$ for the Veneziano amplitude listed in table 5.2. These were first derived in [1] for arbitrary spacetime dimensions D and in [201] for the limiting case of $D=4$.

Further, we notice manifest positivity of the leading and sub-leading Regge coefficients i.e., $B^D_{n,n-1}$ and $B^D_{n,n-2}$ for $n \in \{1, 2, 3, 4\}$ in arbitrary D. We demonstrate the latter fact for any general n in section 5.2.1 and then later around $q = 1$ for any j in the large n limit in section 5.3.2.

5.2 Regge Trajectories

In this section, we analyze the positivity of partial wave coefficients on Regge trajectories, where $j = n - k$ for some fixed k. The leading Regge trajectory has $j = n - 1$, which is the highest spin for a given level n. We find that the leading and first sub-leading Regge coefficients are manifestly positive in all dimensions, but that unitarity breaks down in certain regions of (q, D) parameter space starting with the sub-sub-leading Regge coefficients $B^D_{n,n-3}(q)$.

5.2.1 Leading and sub-leading Regge coefficients

We first determine the partial wave coefficients $B^D_{n,n-1}(q)$ of the Coon amplitude on the leading Regge trajectory. As before, our starting point is the contour expression for the partial wave coefficients (5.21) with $(n, j) = (n, n - 1)$:

$$B^D_{n,n-1}(q) = c^D_{n,n-1}(q) \frac{D^{(n-1)}_q H_q(0)}{[n-1]_q!} \ . \tag{5.32}$$

Now, performing the Jackson q-derivative $(n - 1)$-times on (5.23) (with $j = n - 1$) in the usual manner, we obtain for this derivative

$$\begin{aligned} \frac{D^{(n-1)}_q H_q(0)}{[n-1]_q!} &= \frac{q^{\frac{n(n-1)}{2}}(n-1)!}{[n-1]_q!} \int_{-[n]_q}^{0} dt(-t(t+[n]_q))^{\frac{D-6}{2}+n} \\ &= \frac{q^{\frac{n(n-1)}{2}}(n-1)!}{[n]_q!} [n]_q^{D-4+2n} \frac{\Gamma\left(\frac{D}{2}-2+n\right)^2}{\Gamma(D-4+2n)} \ , \end{aligned} \tag{5.33}$$

where in reaching the final equality we have made a change of variable $t' = -\frac{t}{[n]_q}$, and then evaluated the t-integral. Plugging in the value for the prefactor $c^D_{n,n-1}(q)$ leads us to the final expression for the leading Regge trajectory coefficient $B^D_{n,n-1}(q)$ which reads as

$$B^D_{n,n-1}(q) = 2^{2-2n} q^{\frac{n(n+1)}{2}} \frac{(n-1)![n]_q^{n-1}}{[n]_q!} \frac{\Gamma\left(\frac{D-3}{2}\right)}{\Gamma\left(\frac{D-5}{2}+n\right)} > 0 \ . \tag{5.34}$$

We see that the above expression is clearly manifestly positive in arbitrary spacetime dimensions D. The above result is in agreement with the following special cases that have been recently derived in the literature:

- The leading Regge coefficient for the Coon amplitude (5.34) coincides with that of the Veneziano case as derived in [1]. To see this, we take the $q \to 1$ limit of (5.34) and see that this agrees with eq. (4.38) in that reference with $\Delta = 1$.

- The formula above also coincides with the recently derived partial wave coefficients in [202] for the Coon amplitude in $D = 4$. To make contact with their result, we set $n \to n+1$ for the relevant terms (as $j_{\text{max}} = n$ for the open, bosonic string which is the case considered in [202]) and take the $D \to 4$ limit of (5.34). To that end, we obtain

$$\lim_{D\to 4} B^D_{n,n}(q) = \frac{\sqrt{\pi}}{2^{2n}} q^{\frac{n(n+1)}{2}} \frac{n!}{\Gamma\left(n+\frac{1}{2}\right)} \frac{[n]_q^{n-1}}{[n-1]_q!} \ . \tag{5.35}$$

  Expressing the q-factorials as an infinite product and rearranging the terms in (5.35), we see that it exactly coincides with the expression in [202] with $\alpha_0 = 0$.

- In the further special case of the Veneziano amplitude in $D = 4$, the result (5.34) in the $D = 4, q \to 1$ limit coincides with the expression derived in [201].

We now move on to the sub-leading Regge trajectory where we can follow a similar prescription to determine the coefficient $B^D_{n,n-2}(q)$. Setting $j = n-2$ in (5.21) and acting with the q-derivatives gives

$$B^D_{n,n-2} = -c^D_{n,n-2} \frac{q^{\frac{n(n-1)}{2}}(n-2)!}{[n]_q!} \int_{-[n]_q}^0 dt(-t(t+[n]_q))^{\frac{D}{2}+n-4} \sum_{k=1}^{n-1} \left(\frac{1-q^{-k}}{1-q} - t \right) \ . \tag{5.36}$$

Considering a similar change of variables as before where $t' = -\frac{t}{[n]_q}$ and computing the sum using $\sum_{k=1}^{n-1}\left(\frac{q^{-k}-1}{1-q^n} - t\right) = \frac{q^{-n+1}}{1-q^n} - \frac{n}{1-q^n} - (n-1)t$ leaves us with the t-integral to evaluate. Evaluating this t-integral and inserting the expressions for the prefactor $c^D_{n,n-2}(q)$ from (5.22), one finally obtains for the sub-leading Regge trajectory coefficient $B^D_{n,n-1}(q)$ to be:

$$B^D_{n,n-2}(q) = 2^{3-2n} q^{\frac{n(n-1)}{2}} (1-q) \frac{[n]_q^{n-2}(n-2)!}{[n]_q!} \frac{\Gamma\left(\frac{D-3}{2}\right)}{\Gamma\left(\frac{D-7}{2}+n\right)} \times f(n,q) \ , \tag{5.37}$$

where the polynomial $f(n,q)$ is defined as

$$f(n,q) = \frac{2q + (n-1)(1-q)q^{2n} + q^n(1-3n(1-q)-3q)}{(1-q)^3} \ . \tag{5.38}$$

Although this form is clearly not manifestly positive, it can be written as

$$f(n,q) = \sum_{k=1}^{n-2}(k+1)kq^k + \sum_{k=1}^{n} k(n-1)q^{2n-k-1} > 0 \ , \tag{5.39}$$

which is manifestly positive, thereby proving that the sub-leading Regge coefficients $B^D_{n,n-2}$ are positive for *all* n, q and D. We can easily see that the above expression (5.37) for the sub-leading Regge coefficient of the Coon amplitude approaches zero in the $q \to 1$ limit:

$$\lim_{q\to 1} B^D_{n,n-2} = 0 \ , \tag{5.40}$$

which is the expected result for the Veneziano amplitude for the case when $n + j \in 2\mathbb{Z}$ as shown in [1, 201].

5.2.2 Sub-sub-leading Regge trajectory

We now move on to analyze the sub-sub-leading Regge coefficient $B^D_{n,n-3}(q)$. Starting again from (5.21, 5.23) and following a similar prescription as in the previous sub-section, we have:

$$B^D_{n,n-3}(q) = q^{\frac{n(n+1)}{2}} 2^{D-3} \frac{(n+\frac{D-9}{2})\Gamma\left(\frac{D-3}{2}\right)}{\sqrt{\pi}\Gamma(n+\frac{D-8}{2})} \frac{(n-3)!}{[n]_q!}[n]_q^{n-1} \times \int_0^1 dt (t(1-t))^{\frac{D-10}{2}+n} \sum_{j=1}^{n-1}\sum_{k=j+1}^{n-1}\left(\frac{q^{-j}-1}{1-q^n}-t\right)\left(\frac{q^{-k}-1}{1-q^n}-t\right) . \tag{5.41}$$

Performing the double sum gives us the following rather complicated expression

$$\begin{aligned} B^D_{n,n-3}(q) = 2^{4-2n} q^{\frac{1}{2}n(n-3)}[n]_q^{n-1} \frac{(n-3)!}{[n]_q!} \frac{\Gamma\left(\frac{D-3}{2}\right)}{\Gamma\left(n+\frac{D-9}{2}\right)} \Bigg[& \frac{q^{2n}(n-2)(n-1)(D+2n-6)}{2(2n+D-7)} \\ + \frac{4q^3}{(1-q)^2(1+q)} + \frac{2n(n-1)q^{2n}}{(1-q^n)^2} + & \frac{q^{2n}(4q-2n(2-n(1-q))(1+q))}{(1-q^2)(1-q^n)} \\ - \frac{2q^{1+n}(3n(1+q)-2(2+q))}{1-q^2} \Bigg] . & \end{aligned} \tag{5.42}$$

One can easily verify that in taking the $q \to 1$ limit, one arrives at the following result

$$B^D_{n,n-3}(q) \xrightarrow{q\to 1} \frac{2^{5-2n} n^{n-3}(7-D+n)(D-9+2n)\Gamma\left(\frac{D-3}{2}\right)}{48\,\Gamma\left(\frac{D-5}{2}+n\right)} , \tag{5.43}$$

and then using the Legendre duplication formula:

$$\Gamma\left(\frac{z}{2}\right)\Gamma\left(\frac{z+1}{2}\right) = 2^{1-z}\sqrt{\pi}\Gamma(z) , \qquad \forall z \in \mathbb{C}/\mathbb{Z}_{\leq 0} \tag{5.44}$$

one obtains the result derived in [1] for the type-I superstring amplitude for $\Delta = 3$.

Like the sub-leading Regge coefficients, the sub-sub-leading case (5.42) is not manifestly positive for general q. Moreover, on plotting the first few low-level coefficients (see figure 5.1) we see that for certain values of q and D, the coefficient for the $n = 3$ level starts becoming negative (indicated in the figure by the red patch). We note from figure 5.1 that the coefficient $B^D_{3,0}(q)$ vanishes as $q \to 1, D \to 10$ which is the behavior one would expect for the Veneziano amplitude coefficient $B^D_{3,0} = \frac{10-D}{24(D-1)}$ (from table 5.2). Similarly for the $n = 4$ coefficient, we continue to see a small red patch around $q = 1$ and $D = 10$ (albeit smaller), but the patch completely disappears for the $n = 5$ coefficient (see figure 5.2). We will show in section 5.3 that all Regge coefficients of the Coon amplitude for large values of n are manifestly positive in a neighborhood of $q = 1$.

5.2.3 Leading versus sub-leading Regge behaviour as $n \to \infty$

We now compare the leading, sub-leading, and sub-sub-leading Regge coefficients that we calculated in the last two sections for various values of level n. In figure 5.3 we compare these coefficients for the first 25 levels for various values of q in $D = 10$. We can see that unless q is very close to 1, the sub-leading coefficients always dominate over the leading ones. This is clearly the case with the

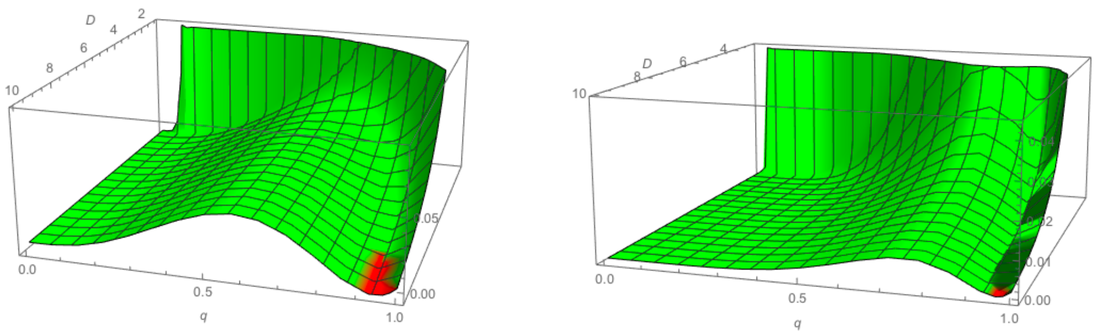

(a) The coefficient $B^D_{3,0}(q)$ (b) The coefficient $B^D_{4,1}(q)$

Figure 5.1: The green region indicates positivity while the red region shows where the indicated partial wave coefficients become negative. We also note from the plot that the coefficient $B^D_{3,0} \to 0$ as $q \to 1, D \to 10$ which is consistent with the expression $B^D_{3,0}$ obtained in [1]. On the right, we continue to see the negative patch (although smaller) in the plot (b) very close to the critical dimension $D = 10$ of the Veneziano amplitude ($q \to 1$).

first three sub-plots in figure 5.3. Therefore, away from the Veneziano case, our numerical results support the hypothesis that $B^D_{n,n-\Delta_1} > B^D_{n,n-\Delta_2}$ for $\Delta_1 > \Delta_2$ as $n \to \infty$. Thus the positivity of the leading Regge trajectory is sufficient to conclude that all Regge trajectories are positive-definite in the asymptotic limit. In fact, one can easily verify numerically that this true $\forall\ D \geq 4$. However, as one reaches closer to the Veneziano case (the last subplot in the figure) this pattern breaks down and one needs to go to larger and larger values of n to recover this trend. In such a case, the pattern depends greatly on the order of limits and there may be some doubt about whether positivity indeed holds on all Regge trajectories as $n \to \infty$. In order to close this gap, we turn our attention in the next section to an analysis of the $q \approx 1$ region of parameter space, showing that the Regge coefficients are indeed positive for any D as $n \to \infty$.

5.3 Coon amplitude around $q = 1$

So far, our single-contour expression (5.21) for the partial wave coefficients $B^D_{n,j}(q)$ of the Coon amplitude has found applications in evaluating certain low-lying coefficients and obtaining analytic, manifestly positive expressions for the leading and sub-leading Regge trajectories. It has also helped us obtain a closed-form expression for the sub-sub-leading Regge trajectory which showed us the first signs of the breakdown of positivity. To gain further understanding of the Gegenbauer coefficients, we must strive towards obtaining a double-contour integral representation for them, in a spirit close to the analysis in [1] for the Veneziano amplitude. In moving towards a double-contour integral representation for the Coon amplitude coefficients, we encounter difficulties mainly arising from technical obscurities in dealing with q-deformed quantities in the integrand. While a double-contour integral representation eludes us, we attempt to consider small deviations around the Veneziano amplitude by Taylor expanding our single-contour expression (5.21) around $q = 1$, up to the first

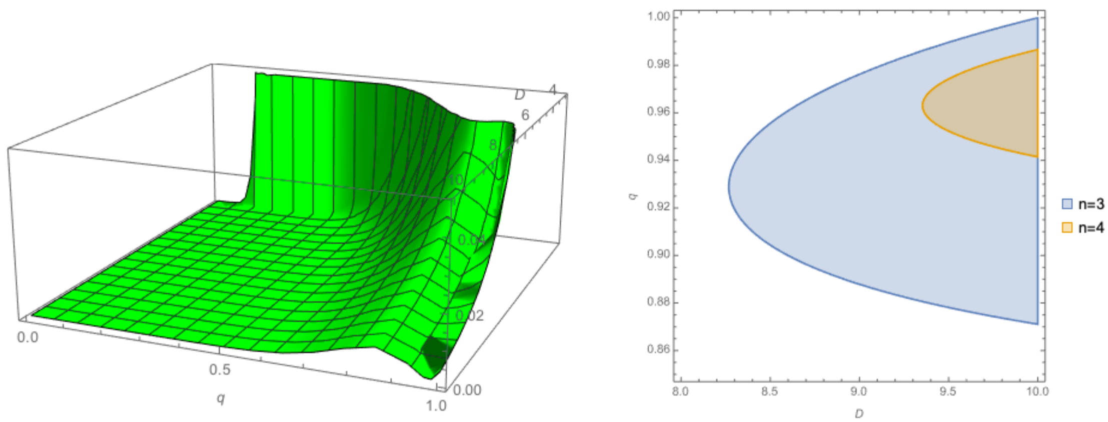

(a) The coefficient $B^D_{5,2}(q)$ (b) Non-unitary regions for $B^D_{n,n-3}(q)$

Figure 5.2: On moving to the next sub-sub-leading Regge coefficient $B^D_{5,2}(q)$ in the plot (a), we see that the negative patch disappears and the surface becomes positive for all values of $q \in [0, 1]$ and $D \in [4, 10]$. The region plot (b) shows more clearly the negative patches for $B^D_{n,n-3}(q)$ in (q, D) parameter space. The tip of the non-unitary region lies at $q = 0.9289\ldots$, $D = 8.2672\ldots$; the exact numbers are roots of sixth order polynomial equations following from (5.42) with $n = 3$.

order. As we shall see in this section, this would help us obtain a $\mathcal{O}(1-q)$ correction to the double-contour integral representation of the Veneziano coefficients [1]. The upshot is that we get a crude understanding of the structures one would naively expect in a generic double-contour integral representation for the Coon amplitude (in a higher-order expansion). Our $\mathcal{O}(1-q)$ double-contour expression will also help us understand applications related to the asymptotics of these coefficients which we show to be manifestly positive, thus validating our discussion at the end of section 5.2.3 on analytic grounds.

5.3.1 Towards a double-contour representation

To help us obtain a $\mathcal{O}(1-q)$ double-contour correction to the Veneziano amplitude ($q = 1$), we start by considering small deviations around $q = 1$. To that end, we perform a Taylor expansion of our single-contour expression (5.21) around $q = 1$ up to the first order. We refer the reader to Appendix 5.6 for the Taylor expansion of the various q-deformed quantities that appear in the integrand of (5.21). We achieve this by dividing the integrand into two parts: i) the first order expansion of the portion inside the derivative of (5.23) is shown explicitly in (5.117), ii) while the expansion of the remaining part of the integrand along with measure has been dealt with in (5.113). We can try to condense these integrals by introducing the H-integral along the lines of [1] as follows[8]:

$$H^{(r,s)}_{n,j}(t') = \int^{t'} dt \frac{(-t)^{\frac{D-4}{2}+j+r}(t+n)^{\frac{D-4}{2}+j+s}}{(1-z)^{t+1}} \ , \quad r, s \in \mathbb{Z} \ . \tag{5.45}$$

[8]We note that our definition of the H-integral slightly differs from [1] by an extra factor of $(1-z)$ in the denominator and the inclusion of the integer parameters r, s.

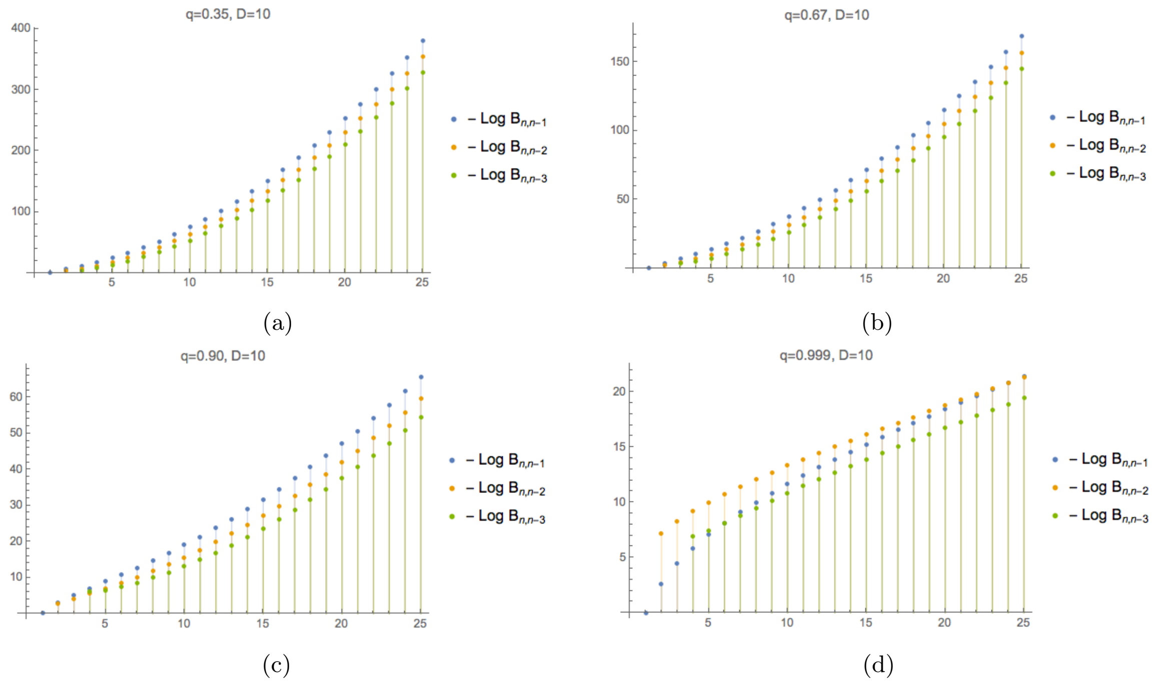

Figure 5.3: Coefficients of leading, sub-leading and sub-sub-leading Regge trajectories for various values of q for $\alpha_0 = 0$. From plot (a), (b) and (c) it is clear that $B^{10}_{n,n-3} > B^{10}_{n,n-2} > B^{10}_{n,n-1}\ \forall n$. However, for plot (d) this is only true for larger values of n.

We leave the exact details of manipulating these H-integrals (where one can express its integrand as a total derivative) to Appendix 5.6. However, to perform an expansion of the Gegenbauer coefficients (5.21), we must find an appropriate contour expression around $z = 0$. To that end, we define a generalized basis of integrals which we term as the $\mathcal{H}$-integrals:

$$\mathcal{H}^{(a,b,c,r,s)}_{n,j}(t') := \oint \frac{dz}{2\pi i}\frac{1}{z^{n+a}}\frac{1}{(1-z)^b}(-\log(1-z))^{j+c}H^{(r,s)}_{n,j}(t')\ , \tag{5.46}$$

where $a \in \mathbb{Z}_{\leq 0}$ and $b, c, r, s \in \mathbb{Z}$ parameterize the above set of integrals. We observe that these integrals satisfy the following property

$$\begin{aligned}\mathcal{H}^{(a,b,c,r,s)}_{n,j}(-n) &= (-1)^{n+j+a+c}\oint \frac{dz}{z^{n+a}}(1-z)^{a+b}(-\log(1-z))^{j+c}H^{(s,r)}_{n,j}(0)\\ &= (-1)^{n+j+a+c}\mathcal{H}^{(a,-a-b,c,s,r)}_{n,j}(0)\ ,\end{aligned} \tag{5.47}$$

with the details of the derivation presented in Appendix 5.6. Making use of the above identity and performing certain algebraic manipulations (for the explicit details we refer the reader again to Appendix 5.6), we finally obtain a double-contour integral representation for the $\mathcal{H}$-integral expressed as[9]

$$\mathcal{H}_{n,j}^{(a,b,c,r,s)}(0) = (-1)^{r+s}\Gamma\left(j+r+\frac{D-2}{2}\right)\Gamma\left(j+s+\frac{D-2}{2}\right) \times \oint_{u=0}\frac{du}{2\pi i}\oint_{v=0}\frac{dv}{2\pi i}\frac{(v-u)^{j+c}e^{-bu}e^{(a+b)v}}{(uv)^{\frac{D-2}{2}+j}u^r v^s (e^v-e^u)^{n+a}}\,. \tag{5.48}$$

We now wish to express our first-order expansions of the two terms in the integrand, namely (5.113) and (5.117), in terms of the above-introduced basis integrals $\mathcal{H}_{n,j}^{(a,b,c,r,s)}(0)$. The contour integral of (5.113) is rewritten in the above basis as

$$\begin{aligned}\oint_{z=0}\frac{dz}{2\pi i}\frac{1}{z^n}(5.113) &= (1-(-1)^{n+j})\mathcal{H}_{n,j}^{(0,0,0,0,0)} \\ &- (1-q)\Bigg\{\frac{n-1}{2}\left(\frac{D-2}{2}+j\right)(1-(-1)^{n+j})\mathcal{H}_{n,j}^{(0,0,0,0,0)} \\ &+ \frac{n-1}{2}\left[\mathcal{H}_{n,j}^{(0,0,1,1,0)} + (-1)^{n+j}\mathcal{H}_{n,j}^{(0,0,1,0,1)}\right] \\ &+ \left(\frac{D-4}{2}+j\right)\frac{n(n-1)}{2}\left[\mathcal{H}_{n,j}^{(0,0,0,0,-1)} - (-1)^{n+j}\mathcal{H}_{n,j}^{(0,0,0,-1,0)}\right] \\ &+ \frac{n-1}{2}\left(\frac{D-4}{2}+j\right)\left[\mathcal{H}_{n,j}^{(0,0,0,1,-1)} - (-1)^{n+j}\mathcal{H}_{n,j}^{(0,0,0,1,-1)}\right]\Bigg\}\,,\end{aligned} \tag{5.49}$$

where we have made use of the identity (5.47) to rewrite $\mathcal{H}_{n,j}^{(0,0,0,0,0)}(-n)$ in terms of the basis integrals. Similarly, we have for the contour integral of (5.117) around $z=0$:

$$\begin{aligned}\oint_{z=0}\frac{dz}{2\pi i}\frac{1}{z^n}(5.117) &= (1-(-1)^{n+j})\mathcal{H}_{n,j}^{(0,0,0,0,0)} - (1-q)\Bigg\{\left(nj-\frac{j(j+1)}{2}\right)\mathcal{H}_{n,j}^{(0,0,-1,0,0)}(1+(-1)^{n+j}) \\ &- \frac{1}{2}\left[\mathcal{H}_{n,j}^{(-1,1,0,2,0)} + (-1)^{n+j}\mathcal{H}_{n,j}^{(-1,0,0,0,2)} + \mathcal{H}_{n,j}^{(0,0,1,2,0)} + (-1)^{n+j}\mathcal{H}_{n,j}^{(0,0,1,0,2)}\right] \\ &+ j\left[\mathcal{H}_{n,j}^{(-1,1,-1,1,0)} - (-1)^{n+j}\mathcal{H}_{n,j}^{(-1,0,-1,0,1)} + \mathcal{H}_{n,j}^{(0,0,0,1,0)} - (-1)^{n+j}\mathcal{H}_{n,j}^{(0,0,0,0,1)}\right] \\ &- \frac{j(j-1)}{2}\left[\mathcal{H}_{n,j}^{(-1,1,-2,0,0)} + (-1)^{n+j}\mathcal{H}_{n,j}^{(-1,0,-2,0,0)}\right]\Bigg\}\,,\end{aligned} \tag{5.50}$$

where we note that all the master $\mathcal{H}$-integrals in the above two equations are evaluated at $z=0$, i.e., $\mathcal{H}_{n,j}^{(a,b,c,r,s)}(0)$. We see that the first terms in both (5.49) and (5.50) coincide with that obtained for the Veneziano amplitude in [1]. The remaining terms arise from considering $\mathcal{O}(1-q)$ corrections.

Now, an expression that shows up quite often in relations (5.49) and (5.50) is of the form $\mathcal{H}_{n,j}^{(a,b,c,r,s)} - (-1)^{n+j+a+c}\mathcal{H}_{n,j}^{(a,-a-b,c,s,r)}$, which we can further simplify by combining the two terms into one expression. First, we consider an interchange in $u\leftrightarrow v$, $r\leftrightarrow s$ and $b\to -a-b$ in (5.48), by virtue of which we arrive at the following

$$\mathcal{H}_{n,j}^{(a,-a-b,c,s,r)}(0) = (-1)^{r+s+n+j+a+c}\Gamma\left(j+r+\frac{D-2}{2}\right)\Gamma\left(j+s+\frac{D-2}{2}\right) \times \oint_{v=0}\frac{dv}{2\pi i}\oint_{u=0}\frac{du}{2\pi i}\frac{(v-u)^{j+c}e^{-bu}e^{(a+b)v}}{(uv)^{\frac{D-2}{2}+j}u^r v^s (e^v-e^u)^{n+a}}\,. \tag{5.51}$$

[9] In [1], the coefficient $B_{n,j}^{\text{open}}$ is proportional to the integral $\mathcal{H}_{n,j}^{(0,0,0,0,0)}(0)$ which exactly matches with their result (C.17).

But, we then notice that

$$
\begin{aligned}
\mathcal{H}_{n,j}^{(a,b,c,r,s)} - & (-1)^{n+j+a+c}\mathcal{H}_{n,j}^{(a,-a-b,c,s,r)} \\
&= (-1)^{r+s}\Gamma\left(j+r+\frac{D-2}{2}\right)\Gamma\left(j+s+\frac{D-2}{2}\right) \\
&\quad \times \left(\oint_{u=0}\frac{du}{2\pi i}\oint_{v=0}\frac{dv}{2\pi i} - \oint_{v=0}\frac{dv}{2\pi i}\oint_{u=0}\frac{du}{2\pi i}\right)\frac{(v-u)^{j+c}e^{-bu}e^{(a+b)v}}{(uv)^{\frac{D-2}{2}+j}u^r v^s (e^v-e^u)^{n+a}} \\
&= (-1)^{r+s+1}\Gamma\left(j+r+\frac{D-2}{2}\right)\Gamma\left(j+s+\frac{D-2}{2}\right) \\
&\quad \times \oint_{u=0}\frac{du}{2\pi i}\oint_{v=u}\frac{dv}{2\pi i}\frac{(v-u)^{j+c}e^{-bu}e^{(a+b)v}}{(uv)^{\frac{D-2}{2}+j}u^r v^s (e^v-e^u)^{n+a}} \ ,
\end{aligned}
\tag{5.52}
$$

where we made use of the identity familiar to us from two-dimensional CFT for contour integrals (for example, refer to section 6.1.2 of [203])

$$
\oint_{v=0}\frac{dv}{2\pi i}\oint_{u=0}\frac{du}{2\pi i} - \oint_{u=0}\frac{du}{2\pi i}\oint_{v=0}\frac{dv}{2\pi i} = \oint_{u=0}\frac{du}{2\pi i}\oint_{v=u}\frac{dv}{2\pi i} \ . \tag{5.53}
$$

Observing the above identities, we immediately see that the number of terms in (5.49, 5.50) can be exactly reduced to half if we make the following choice for our basis integrals:

$$
\begin{aligned}
\mathcal{I}_{n,j}^{(a,b,c,r,s)}(0) = (-1)^{r+s+1}&\Gamma\left(j+r+\frac{D-2}{2}\right)\Gamma\left(j+s+\frac{D-2}{2}\right) \\
&\times \oint_{u=0}\frac{du}{2\pi i}\oint_{v=u}\frac{dv}{2\pi i}\frac{(v-u)^{j+c}e^{-bu}e^{(a+b)v}}{(uv)^{\frac{D-2}{2}+j}u^r v^s (e^v-e^u)^{n+a}} \ .
\end{aligned}
\tag{5.54}
$$

we therefore classify the $\mathcal{I}$-integrals (5.54) as our new basis integrals. Finally rewriting (5.49) and (5.50) in terms of our new basis of $\mathcal{I}$-integrals (5.54) and combining it with the Taylor expansion of the coefficients, we arrive at the following more compact expression

$$
\begin{aligned}
B_{n,j}^D(q) = c_{n,j}^D\Bigg\{&\mathcal{I}_{n,j}^{(0,0,0,0,0)} + (1-q)\Bigg[\left(\frac{D-2}{4}(n-1)-n\right)\mathcal{I}_{n,j}^{(0,0,0,0,0)} \\
&- \frac{n-1}{2}\mathcal{I}_{n,j}^{(0,0,1,1,0)} - \left(\frac{D-4}{2}+j\right)\frac{n(n-1)}{2}\mathcal{I}_{n,j}^{(0,0,0,0,-1)} \\
&- \frac{n-1}{2}\left(\frac{D-4}{2}+j\right)\mathcal{I}_{n,j}^{(0,0,0,1,-1)} - \left(nj-\frac{j(j+1)}{2}\right)\mathcal{I}_{n,j}^{(0,0,-1,0,0)} \\
&+ \frac{1}{2}\left(\mathcal{I}_{n,j}^{(-1,1,0,2,0)} + \mathcal{I}_{n,j}^{(0,0,1,2,0)}\right) - j\left(\mathcal{I}_{n,j}^{(-1,1,-1,1,0)} + \mathcal{I}_{n,j}^{(0,0,0,1,0)}\right) \\
&+ \frac{j(j-1)}{2}\mathcal{I}_{n,j}^{(-1,1,-2,0,0)}\Bigg]\Bigg\} \ .
\end{aligned}
\tag{5.55}
$$

Rewriting the above explicitly in terms of the double contour integral representation (5.54), we get

$$
B_{n,j}^D(q) = -c_{n,j}^D(0)\Gamma\left(j+\frac{D-2}{2}\right)^2\oint_{u=0}\frac{du}{2\pi i}\oint_{v=u}\frac{dv}{2\pi i}\frac{(v-u)^{j-2}}{(uv)^{\frac{D-2}{2}+j}(e^v-e^u)^n}\mathscr{F}_{n,j}^D(u,v;q) \ , \tag{5.56}
$$

where the function $\mathscr{F}^D_{n,j}(u,v;q)$ is given by the relation

$$\begin{aligned}\mathscr{F}^D_{n,j}(u,v;q) = (v-u)^2 + (1-q)\Bigg[&\left(\left(\frac{D-2}{4}\right)(n-1) - n\right)(v-u)^2 \\ &+ \frac{n-1}{2}\left(j+\frac{D-2}{2}\right)\frac{(v-u)^3}{u} + \left(j+\frac{D-4}{2}\right)\frac{n(n-1)}{2}v \\ &- \frac{n-1}{2}\frac{(v-u)^2 v}{u} - \left(nj - \frac{j(j+1)}{2}\right)(v-u) \\ &+ \frac{1}{2u^2}\left(j+\frac{D}{2}\right)\left(j+\frac{D-2}{2}\right)\left[(v-u)^3 + (v-u)^2(e^{v-u}-1)\right] \\ &+ \frac{1}{u}j\left(j+\frac{D-2}{2}\right)\left[(e^{v-u}-1)(v-u)+1\right] + \frac{j(j-1)}{2}(e^{v-u}-1)\Bigg] + \mathcal{O}(1-q)^2 \ ,\end{aligned} \tag{5.57}$$

where as before, the first term in (5.57) coincides with that obtained for the Veneziano amplitude in [1] while the remaining terms arise from considering $\mathcal{O}(1-q)$ corrections.

5.3.2 Applications

Equipped with the first order $(1-q)$ correction to the double-contour integral representation for the Veneziano amplitude [1], we see glimpses of the structures one can expect as one flows away from $q = 1$ from the relations (5.56, 5.57). While this double-contour correction has little use in studying manifest unitarity around $q = 1$[10], we put this relation to use by studying the asymptotics of the Gegenbauer coefficients in two regimes: i) for fixed spin j, and ii) for fixed $\Delta = n - j$ (Regge trajectories).

Fixed j asymptotics

We use our first order q-extension to the double contour integral representation for studying asymptotics (i.e., the large n limit) at fixed spin j. We start by writing the $\mathcal{H}$-integrals

$$\mathcal{H}^{(a,b,c,r,s)}_{n,j}(0) \propto \oint_{u=0}\frac{du}{2\pi i}\oint_{v=0}\frac{dv}{2\pi i}\frac{(v-u)^{j+c}e^{-bu}e^{(a+b)v}}{(uv)^{\frac{D-2}{2}+j}u^r v^s(e^v-e^u)^{n+a}} \ , \tag{5.58}$$

and simply change variables to

$$u = \log(1-x) \ , \qquad v = \log(1-y) \ , \tag{5.59}$$

to obtain the integral

$$\begin{aligned}\mathcal{H}^{(a,b,c,r,s)}_{n,j}(0) \propto \oint_{x=0}\frac{dx}{2\pi i}\oint_{y=0}\frac{dy}{2\pi i}&\frac{1}{(1-x)^{1+b}(1-y)^{1-a-b}\log(1-x)^{\frac{D-2}{2}-c+r}\log(1-y)^{\frac{D-2}{2}-c+s}} \\ &\times\frac{1}{(x-y)^{n-j-c+a}}\left(\frac{\frac{1}{\log(1-x)}-\frac{1}{\log(1-y)}}{x-y}\right)^{j+c} \ .\end{aligned} \tag{5.60}$$

[10]In fact we observe that studying positivity on a term-by-term basis leads us to conclude that the first order correction is not manifestly positive in any dimension D. This only concludes that not all terms in the Taylor expansion of $\mathscr{F}^D_{n,j}$ are manifestly positive, but that does not rule out the possibility for the function itself to be positive for all $q \in [0,1]$ once the entire series is summed over.

Each of the three factors in the above integrand is a function with strictly positive Taylor coefficients when expanded first around $y = 0$ followed by $x = 0$. Such a function is termed as a *positive* function. As a result, the coefficients picked out by the residue integral will be positive as well. We manipulate each of the factors in the above integrand one-by-one. The positivity of the first factor is positive based on the arguments presented in Appendix A of [1]. Specifically, in the factor

$$\log(1-y)^{1-\frac{D}{2}+c-s} = (-y)^{1-\frac{D}{2}+c-s} \times \sum_{m=0}^{\infty} c_m y^m \approx (-y)^{1-\frac{D}{2}+c-s} , \tag{5.61}$$

we note that only the leading term contributes in the $n \to \infty$ limit. For the binomial expansion[11]

$$\begin{aligned}(x-y)^{-n+j+c-a} &= \sum_{m=0}^{\infty} \binom{n+a-j-c+m-1}{m} x^{-n-a+j+c-m} y^m \\ &\approx \binom{2n+2a-2j-2c-2}{n+a-j-c-1} x^{-2n-2a+2j+2c+1} y^{n+a-j-c-1} ,\end{aligned} \tag{5.62}$$

where we have used the fact that the maximum binomial coefficient $\binom{n}{m}$ is obtained for $m = \lfloor \frac{n}{2} \rfloor$ and contributes solely to the sum in the large n limit. The third factor in the integrand admits an expansion whose coefficients are all positive:

$$\left(\frac{\frac{1}{\log(1-x)} - \frac{1}{\log(1-y)}}{x-y} \right)^{j+c} = \frac{1}{(xy)^{j+c}} + \sum_{m=0}^{\infty} c_m \sum_{k=0}^{m-1} x^{m-1-k} y^k \approx \frac{1}{(xy)^{j+c}} , \tag{5.63}$$

where only the first term survives in the asymptotic regime. Using the above results and performing the y-integral where we pick up the residue at $y = 0$[12], we get

$$\mathcal{H}_{n,j}^{(a,b,c,r,s)} \sim \frac{n^{j+s+\frac{D-4}{2}}}{(j+s+\frac{D-4}{2})!} \oint_{x=0} \frac{dx}{2\pi i} \frac{x^{-n-a-j-s-\frac{D-4}{2}}}{(1-x)^{1+b}(-\log(1-x))^{\frac{D-2}{2}+r-c}} . \tag{5.64}$$

where we have used Stirling's approximation on the factorials $n! \sim \sqrt{2\pi n}\left(\frac{n}{e}\right)^n$. We first deform the above contour that runs around 0 to the Hankel contour $\mathcal{C}$ that runs from below around the branch cut (see Figure VI.2 in [204] for exact details) and then perform a change of variables $x = 1 + \frac{t}{n}$ to obtain

$$\begin{aligned}\mathcal{H}_{n,j}^{(a,b,c,r,s)} &\sim \frac{n^{j+s+\frac{D-4}{2}}}{(j+s+\frac{D-4}{2})!} \oint_{t=0} \frac{dt}{2\pi i} \frac{1}{n} \frac{\left(1+\frac{t}{n}\right)^{-n-a-j-s-\frac{D-4}{2}}}{\left(-\frac{t}{n}\right)^{1+b}\left(-\log\left(-\frac{t}{n}\right)\right)^{\frac{D-2}{2}+r-c}} \\ &= \frac{(-1)^{1+b} n^{j+s+\frac{D-4}{2}+b}}{(j+s+\frac{D-4}{2})!(\log n)^{\frac{D-2}{2}+r-c}} \oint_{t=0} \frac{dt}{2\pi i} \frac{\left(1+\frac{t}{n}\right)^{-n-a-j-s-\frac{D-4}{2}}}{t^{1+b}\left(1-\frac{\log(-t)}{\log(n)}\right)^{\frac{D-2}{2}+r-c}} .\end{aligned} \tag{5.65}$$

[11] We note that the binomial coefficient in (5.62) is always positive for the $\mathcal{H}$-integrals contributing at $\mathcal{O}(1-q)$. At subsequent higher orders, this term would have to be dealt with differently.

[12] When computing the residue in y, the greatest contribution comes from the highest possible power from (5.62) as the binomial coefficients grow rapidly with n. For the other two factors (5.61, 5.63), we simply pick up their leading coefficients in the $n \to \infty$ limit.

The above integrand converges uniformly for any bounded domain on the t-plane and hence we replace it with its value at large n which leads us to

$$\mathcal{H}_{n,j}^{(a,b,c,r,s)} \sim \frac{(-1)^{1+b} n^{j+s+\frac{D-4}{2}+b}}{\left(j+s+\frac{D-4}{2}\right)!(\log n)^{\frac{D-2}{2}+r-c}} \oint_{t=0} \frac{dt}{2\pi i} \frac{e^{-t}}{t^{1+b}} \; . \tag{5.66}$$

Performing the final contour integral and restoring the proportionality factors we omitted in writing (5.58), we finally find the asymptotics for the $\mathcal{H}$-integrals in the $n \to \infty$ regime to be

$$\mathcal{H}_{n,j}^{(a,b,c,r,s)} \overset{n\to\infty}{\sim} \frac{n^{j+s+b+\frac{D-4}{2}} \left(j+r+\frac{D-4}{2}\right)!}{(\log n)^{\frac{D-2}{2}+r-c}} \; . \tag{5.67}$$

On plugging the above result into (5.49, 5.50) and keeping only those terms that have the fastest n-growth (i.e., those terms with the largest power of n), we have for the actual residue (including the factors contributing from the coefficient $c_{n,j}^D$):

$$\begin{aligned} B_{n,j}^D(q) \overset{n\to\infty}{\sim} & \frac{2^{D-3}}{\sqrt{\pi}} \left(j + \frac{D-3}{2}\right) \Gamma\left(\frac{D-3}{2}\right) \frac{1}{n^{D/2} (\log(n))^{\frac{D-2}{2}}} \\ & \times \left[(1-(-1)^{n+j}) + (1-q)(-1)^{n+j} \frac{n^2 \log(n)}{2} + \mathcal{O}\big[(1-q)^2; n^2\big]\right] \; . \end{aligned} \tag{5.68}$$

We make a couple of interesting observations for the fixed j asymptotics described by the above relation:

- We note that (5.68) is consistent with the formula (4.17) derived in [1]. For $n+j \in 2\mathbb{Z}$, the leading order contribution vanishes as expected and we have the first-order contribution to the asymptotics whose values are *positive*:

$$B_{n,j}^D(q) \overset{n\to\infty}{\sim} (1-q) \frac{2^{D-4}}{\sqrt{\pi}} \left(j + \frac{D-3}{2}\right) \Gamma\left(\frac{D-3}{2}\right) \frac{1}{(n \log(n))^{\frac{D-4}{2}}} > 0 \; . \tag{5.69}$$

  For $n+j \in 2\mathbb{Z}+1$, both terms in (5.68) contribute with the first-order term giving a negative contribution.

- We note from (5.68) that the first-order contribution grows *faster* in comparison to the leading order term at a rate $\sim n^2 \log(n)$.

Regge asymptotics

For studying the second type of asymptotics, namely the Regge behavior, we keep $\Delta = n - j$ fixed and take $n \to \infty$. We begin by first writing our basis integrals (5.54) in a form similar to the one in [1]

$$\oint_{u=0} \frac{du}{2\pi i} \oint_{v=u} \frac{dv}{2\pi i} \frac{1}{(uv)^{\frac{D-2}{2}} u^r v^s} \left(\frac{u^{-1}-v^{-1}}{e^v - e^u}\right)^n \left(u^{-1}-v^{-1}\right)^{-\Delta} (v-u)^c \frac{e^{-bu} e^{(a+b)v}}{(e^v-e^u)^a} \; . \tag{5.70}$$

As already mentioned in [1], in the large n limit it is enough to truncate the Taylor expansion of the second term to third order in $(v-u)$ in order to achieve the largest powers of n. Hence one has

$$\frac{u^{-1}-v^{-1}}{e^v-e^u}=\frac{e^{-u}}{u^2}\left(1-\frac{(u+2)(v-u)}{2u}+\frac{(u^2+6u+12)(v-u)^2}{12u^2}\right)+\mathcal{O}(v-u)^3\ . \tag{5.71}$$

Then circling around the saddle point at $u=-2$, we can set $u=-2$ wherever doing so gives a non-zero contribution and $u=v$ wherever the poles are absent[13]. We get[14]

$$\mathcal{I}^{(a,b,c,r,s)}_{n,n-\Delta}\propto \oint_{u=0}\frac{du}{2\pi i}\oint_{v=u}\frac{dv}{2\pi i}\frac{1}{u^{D-2+r+s-2\Delta}}\left(1+\frac{(u+2)(u-v)}{4}+\frac{(v-u)^2}{12}\right)^n\frac{1}{(v-u)^{\Delta-c}}\frac{1}{(1-e^{u-v})^a}, \tag{5.72}$$

to perform the above integral in the $n\to\infty$ we follow similar procedure as in [1]. First consider substituting $t=(v-u)\sqrt{n}$ and use the fact that $(1+\frac{a}{n})^n\sim e^a$ when $n\to\infty$. Now, since $a\in\mathbb{Z}_{\le 0}$ and the fact that the integral is non-zero if and only if $\Delta>c$, we can simply interchange the integral and take residue w.r.t u to get:

$$\mathcal{I}^{(a,b,c,r,s)}_{n,n-\Delta}\propto\frac{n^{-\frac{3\Delta-c-5}{2}+2n+D+r+s}(-1)^{r+s+1}}{(2n-2\Delta+D+r+s-3)!}\oint_{t=0}\frac{dt}{2\pi i}\frac{1}{t^{\Delta-c}}\left(1-\frac{t}{4\sqrt{n}}\right)^{2n}\exp(\frac{1}{2}\sqrt{n}t+\frac{t^2}{12})\ .$$

Using the fact that in the limit $n\to\infty$

$$\left(1-\frac{t}{4\sqrt{n}}\right)^{2n}\exp(\frac{1}{2}\sqrt{n}t+\frac{t^2}{12})=\exp(\frac{t^2}{48})+\mathcal{O}(n^{-\frac{1}{2}})\ , \tag{5.73}$$

the remaining t-integral is then evaluated as

$$\oint_{t=0}\frac{1}{2\pi i}\frac{1}{t^{\Delta-c}}\exp(\frac{t^2}{48})=\frac{1}{(\frac{\Delta-c-1}{2})!}\left(\frac{1}{48}\right)^{\frac{\Delta-c-1}{2}}\ , \tag{5.74}$$

which holds for any $\Delta>c$. Then finally using Stirling's approximation as before, we get that the basis integrals in the $n\to\infty$ limit is

$$\mathcal{I}^{(a,b,c,r,s)}_{n,n-\Delta}\propto\frac{(-1)^{r+s+1}}{\sqrt{\pi n}}\frac{2^{2c+4-D-r-s-2n}}{(\frac{\Delta-c-1}{2})!}\left(\frac{n}{3}\right)^{\frac{\Delta-c-1}{2}}e^{2n}\ . \tag{5.75}$$

Putting in the constants of proportionality, we finally arrive at

$$\mathcal{I}^{(a,b,c,r,s)}_{n,n-\Delta}\sim\frac{2^{2c+5-D-r-s-2n}\sqrt{\pi}}{3^{\frac{\Delta-c-1}{2}}\,(\frac{\Delta-c-1}{2})!}n^{2n+r+s+D-4-\frac{3\Delta+c}{2}}\ . \tag{5.76}$$

Plugging this into (5.55) and again retaining only those terms that have the fastest n-growth, we find for $n+j\in 2\mathbb{Z}+1$

$$B^D_{n,n-\Delta}\overset{n\to\infty}{\sim}\frac{2^{\frac{3}{2}-2n}}{3^{\frac{\Delta-1}{2}}}\frac{e^n}{\sqrt{\pi}}\frac{\Gamma\left(\frac{D-3}{2}\right)}{\Gamma\left(\frac{\Delta+1}{2}\right)}n^{\frac{\Delta-D+1}{2}}\left(1+(1-q)\frac{n^3}{24(\Delta+1)}\right)>0\ ,\qquad\forall\Delta\in\{1,\dots,n\}\ , \tag{5.77}$$

[13] For more details look at section 4.3.2 in [1].

[14] The constant of proportionality comes from the gamma functions and the $(-1)^{r+s+1}$ factor in (5.117).

where as for $n+j \in 2\mathbb{Z}$, we get

$$B^D_{n,n-\Delta} \overset{n\to\infty}{\sim} (1-q)\frac{2^{-\frac{3}{2}-2n}}{3^{\frac{\Delta+1}{2}}}\frac{e^n}{\sqrt{\pi}}\frac{\Gamma\left(\frac{D-3}{2}\right)}{\Gamma\left(\frac{\Delta+1}{2}\right)}\frac{n^{\frac{\Delta-D+7}{2}}}{\Delta+1} > 0\ , \qquad \forall \Delta \in \{1,\dots,n\}\ . \tag{5.78}$$

We now make a couple of crucial observations for the Regge asymptotics described by the above relations (5.77, 5.78):

- Note the manifest *positivity* at first order for both $n+j \in 2\mathbb{Z}$ and $n+j \in 2\mathbb{Z}+1$, unlike the fixed spin case where we saw this only for $n+j \in 2\mathbb{Z}$. This combined with our numerical analysis away from $q=1$ in section 5.2.3 allows us to conclude positivity for all Regge trajectories for any $q \in [0,1]$ and any spacetime dimension $D \geq 4$ in the large n limit. This is consistent with the main result in [202] for $D=4$ and $m^2=0$.
- Once again, we see that the first-order corrections grow *faster* than the leading Veneziano term at a rate $\sim n^3$.

5.4 Outlook and discussions

Here we reflect on some of the key results of this chapter and discuss the potential scope for future work and some open questions. The main results are summarized as under:

- Our contour integral representation of the Coon amplitude partial wave coefficients $B^D_{n,j}(q)$ given by (5.21) establishes manifest *positivity* for the leading and sub-leading Regge sectors in arbitrary spacetime dimensions D.
- Our closed-form, analytic expression of the sub-sub-leading Regge trajectory (5.42) reveals the first signatures of breakdown of positivity for certain critical values of q, D as seen from figures 5.1 and 5.2.
- We consider a perturbative expansion near the Veneziano amplitude ($q=1$) to get first glimpses of the mathematical structures that one ought to encounter in a double-contour representation for the Coon amplitude coefficients $B^D_{n,j}(q)$, in a spirit similar to the Veneziano case [1]. In particular, we arrive at a generalized basis of integrals that we expect to show up at all orders in the $(1-q)$ expansion. Studying the properties of these basis integrals, we derive a double-contour representation for the first $\mathcal{O}(1-q)$ contribution to the coefficients $B^D_{n,j}(q)$. This expression finds applications in studying the $n\to\infty$ asymptotic limit of Regge trajectories.
- For q not very close to 1, our numerical analysis from section 5.2.3 suggests the positivity of *all* Regge trajectories based on the manifest positivity of the leading Regge coefficient. For $q \sim 1$ the numerical analysis is unreliable; however, our analytic expressions (5.77, 5.78) assert the positivity of such Regge trajectories in the asymptotic regime for arbitrary D. A similar discussion also holds that argues for the positivity of fixed j asymptotics based on the numerical analysis presented in appendix 5.7 and the analytic expression (5.68).

We know from the work of [2] that the Coon amplitude is unitary in all dimensions for $q \leq \frac{2}{3}$ and that there exists a unitary envelope for $q \in (\frac{2}{3}, 1)$ (which our analysis confirms). On the other hand, figure 5.2(b) establishes a minimal region in (q, D) parameter space in which the Coon amplitude is definitely not unitary. It remains an open problem to analytically prove or disprove unitarity elsewhere within $q \in [0, 1)$, $D \in (4, 10]$. Our results (based on numerical experimentation for q not close to 1, and on analytic analysis for q near 1) suggest that the region in (q, D) space is excluded by demanding that $B^{(D)}_{n+m,m}(q) \geq 0$ always sits *inside* the region excluded by demanding that $B^{(D)}_{n,0}(q) \geq 0$. If true, then the boundary of the excluded region in (q, D) space can be determined entirely from the latter. We plot the regions excluded by demanding that $B^{(D)}_{n,0}(q) \geq 0$ for several values of n in Fig. 5.4. Tantalizingly, these plots suggest (but again, do not prove) that the regions excluded by considering larger values of n lie at smaller values of q than those at smaller values of n. If this is true, it means that the analytic shape of the boundary curve for any finite value of q is, in principle, analytically determinable from explicit knowledge of $B^{(D)}_{n,0}(q)$.

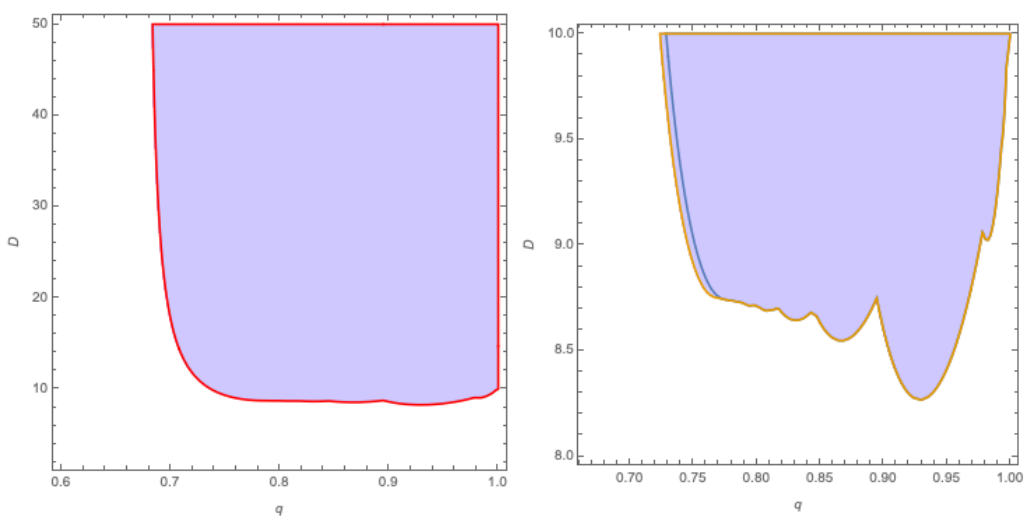

(a) (b)

Figure 5.4: Plots indicating the unitarity envelope for the Coon amplitude, computed analytically from $B^{D}_{n,0}(q)$ with a cutoff $n_{\max}$. The Coon amplitude violates unitarity in the shaded region of (q, D) parameter space. Plot (a), with $n_{\max} = 8$, already agrees well with the numerically computed unitarity envelope depicted by the red-dotted curve ($m^2 = 0$ case) in Fig. 3 of [2]. Plot (b) is a closeup of the region $q \in [2/3, 1]$, $D \in [8, 10]$, showing the small change as we increase the cutoff from $n_{\max} = 10$ (dark blue) to $n_{\max} = 13$ (gold). We speculate that the $q \gtrsim 0.77$ part of the boundary curve is already stable (which in particular would mean we know its shape analytically), while the excluded region grows slowly to the left as the cutoff is increased.

A general proof of unitarity in certain regions may be attainable either from an amplitudes perspective or a q-string analog of the *no-ghost* theorem. The former approach has been recently pioneered in [1] for the Veneziano amplitude, which served as our main source of inspiration to address this question for Coon. It would be very interesting to extend our analysis to the new classes of four-point amplitudes recently constructed in [21, 22]. Of course, it would also be very interesting to explore higher-point amplitudes, which we expect will lead to much more stringent constraints on unitarity than four-point amplitudes do.

5.5 Appendix: A primer on q-analysis

In this appendix, we present some important q-theory machinery that is central to our manipulations in passing from Veneziano to the Coon amplitude. We refer the interested reader to standard texts on the subject [197, 198] for extensive details. We first define the q-integers $[n]_q$ (also known as the q-bracket of ordinary non-negative integers n) by[15]:

$$[n]_q = \frac{1-q^n}{1-q} \ , \tag{5.79}$$

where q is a fixed real number $0 < q < 1$. As with all q-deformed objects, one recovers the original identity or expression in the limit $q \to 1$. For the q-integers defined above, one can easily check that $\lim_{q\to 1}[n]_q = n$. With that, the definition of the q-factorial arises naturally:

$$[n]_q! = [1]_q \cdot [2]_q \cdots [n]_q = \frac{(q;q)_n}{(1-q)^n} \ , \tag{5.80}$$

where in the final equality we have introduced the q-Pochhammer symbol defined by

$$(a;q)_n = \prod_{j=0}^{n-1}(1-aq^j) \ . \tag{5.81}$$

This is a q-analog of the ordinary Pochhammer symbol $(x)_n$ in the sense that $\lim_{q\to 1}\frac{(q^x;q)_n}{(1-q)^n} = (x)_n$ $\forall x \in \mathbb{R}$. We note that the q-Pochhammer symbol has an infinite product representation (unlike its ordinary counterpart):

$$(a,q)_\infty = \prod_{j=0}^{\infty}(1-aq^j) \ . \tag{5.82}$$

However, for most of the analysis in this chapter, we shall use the q-Pochhammer notation established in [205]:

$$(a+b)_q^n = \prod_{j=0}^{n-1}(a+q^j b) \ , \tag{5.83}$$

$$(1+a)_q^\infty = \prod_{j=0}^{\infty}(1+q^j a) \ , \tag{5.84}$$

$$(1+a)_q^t = \frac{(1+a)_q^\infty}{(1+q^t a)_q^\infty} \ , \qquad \forall t \in \mathbb{C} \ . \tag{5.85}$$

We note that the infinite product (5.83) is convergent since $0 < q < 1$.

[15]It is useful to note that this particular choice of defining the q-integers (among many other possible options) provides a natural starting point to define q-analogs of other associated quantities like the q-factorial, q-Pochhammer and so on.

5.5.1 Elements of q-calculus

We introduce some basic notions of q-calculus that prove handy in computing derivatives and integrals of q-deformed quantities. We first introduce the q-derivative given by

$$D_q f(x) = \frac{f(qx) - f(x)}{(q-1)x} \ . \tag{5.86}$$

Consequently, we define the notion of the q-antiderivative given by

$$\int f(x) d_q x = (1-q)x \sum_{j=0}^{\infty} q^j f(q^j x) \ , \tag{5.87}$$

with the series being called the *Jackson integral* of $f(x)$. The two definitions (5.86) and (5.87) combine to give the fundamental theorem of q-calculus.

Theorem A.1.1 (*Fundamental theorem of q-calculus*) If $F(x)$ is an antiderivative of $f(x)$ and $F(x)$ is continuous at $x = 0$, we have

$$\int_a^b f(x) d_q x = F(b) - F(a) \ , \tag{5.88}$$

where $0 \leq a < b \leq \infty$.

Corollary A.1.1 If $f'(x)$ exists in a neighbourhood of $x = 0$ and is continuous at $x = 0$, where $f'(x)$ denotes the ordinary derivative of $f(x)$, we have

$$\int_a^b D_q f(x) d_q x = f(b) - f(a) \ . \tag{5.89}$$

We list some of the important properties of these q-derivatives and Jackson integrals as follows:

$$\int_a^b f(x) d_q x := \int_0^b f(x) d_q x - \int_0^a f(x) d_q x \ . \tag{5.90}$$

We also have a natural formula of q-integration by parts:

$$\int_0^a g(x) D_q f(x) d_q x = f(x) g(x) \Big|_0^a - \int_0^a f(qx) D_q g(x) d_q x \ , \tag{5.91}$$

which follows from the q-Leibniz rule[16]

$$D_q(f(x)g(x)) = f(qx) D_q g(x) + g(x) D_q f(x) \ . \tag{5.92}$$

However, one should note that there does not exist a general chain rule for q-derivatives. An exception is the derivative of a function of the form $f(u(x))$, where $u(x) = \alpha x^\beta$ with α, β being constants, for which we have

$$D_q f(u(x)) = (D_{q^\beta} f)(u(x)) \cdot D_q u(x) \tag{5.93}$$

$$\int_{u(a)}^{u(b)} f(u) d_q u = \int_a^b f(u(x)) D_{q^{1/\beta}} u(x) d_{q^{1/\beta}} x. \tag{5.94}$$

[16] We note that by symmetry, we can interchange f and g, and obtain another equivalent version of the q-Leibniz rule $D_q(f(x)g(x)) = f(x) D_q g(x) + g(qx) D_q f(x)$.

We list below a few known examples of basic q-derivatives that follow immediately from the q-Leibniz rule and the definitions (5.83)-(5.85):

$$D_q x^t = [t]_q x^{t-1} \ , \tag{5.95}$$

$$D_q(Ax+b)_q^n = [n]_q A(Ax+b)_q^{n-1} \ , \tag{5.96}$$

$$D_q(a+Bx)_q^n = [n]_q B(a+Bqx)_q^{n-1} \ . \tag{5.97}$$

For an extensive list of results, we refer the reader to [205].

5.5.2 Lambert series

We briefly review the Lambert series which comes in handy when dealing with the Taylor expansion of the contour integral (5.21) around $q=1$, as shown later in Appendix 5.6. For any $s \in \mathbb{C}$ and $z>0$, the Lambert series is defined as the following convergent sum [206, 207]:

$$\mathcal{L}_q(s,z) = \sum_{k=1}^{\infty} \frac{k^s q^{kz}}{1-q^k} \ , \tag{5.98}$$

where $q \in [0,1)$. The Lambert series is closely related to the q-Pochhammer symbol via the identity:

$$\log{(1-q^z)_q^\infty} = -\mathcal{L}_q(-1,z) \ . \tag{5.99}$$

To derive this rather important identity, we first consider

$$\begin{aligned}\log(1-q^z)_q^\infty &= \log\prod_{n=0}^{\infty}(1-q^{n+z}) = \sum_{n=0}^{\infty}\log(1-q^{n+z}) \\ &= -\sum_{n=0}^{\infty}\sum_{k=1}^{\infty}\frac{q^{k(n+z)}}{k} \ ,\end{aligned} \tag{5.100}$$

where the second equality follows from Taylor expanding the logarithm around $z=0$. Now since we assume that $z>0$ and $q \in [0,1)$, the two sums converge and we can therefore interchange them to sum over the n series first

$$\log(1-q^z)_q^\infty = -\sum_{k=1}^{\infty}\frac{q^{kz}}{k}\sum_{n=0}^{\infty}q^{kn} \tag{5.101}$$

$$= -\sum_{k=1}^{\infty}\frac{1}{k}\frac{q^{kz}}{1-q^k} = -\mathcal{L}_q(-1,z) \tag{5.102}$$

to get the desired result. In going from the first to the second line, we have summed over the geometric series for $q^k \in [0,1)$, and in the final expression we employed the definition of the Lambert series (5.98).

5.5.3 q-gamma and q-beta functions

We introduce the q-analogs of the standard gamma and Euler-beta functions whose various representations are central to our analysis. We start with reviewing the q-deformation of the simplest transcendental function in analysis, the exponential, for which there exists two q-analogs, namely:

$$E_q^x = \sum_{n=0}^{\infty} q^{n(n-1)/2} \frac{x^n}{[n]_q!} = (1+(1-q)x)_q^{\infty} \ , \tag{5.103}$$

$$e_q^x = \sum_{n=0}^{\infty} \frac{x^n}{[n]_q!} = \frac{1}{(1-(1-q)x)_q^{\infty}} \ . \tag{5.104}$$

The two definitions are unfortunately not equivalent but instead inverses of each other:

$$e_q^x E_q^{-x} = E_q^x e_q^{-x} = 1 \ , \tag{5.105}$$

with their q-derivatives being

$$D_q e_q^x = e_q^x \ , \qquad D_q E_q^x = E_q^{qx} \ . \tag{5.106}$$

Similarly, there are two equivalent definitions of the trigonometric functions which we will not review here (one can refer to [205, 197] for more details).

We now define the q-gamma function which admits the following infinite product representation:

$$\Gamma_q(t) := \frac{(1-q)_q^{t-1}}{(1-q)^{t-1}} = \frac{\prod_{n=0}^{\infty} 1 - q^{t-1+n}}{(1-q)^{t-1}} \ , \qquad t > 0 \ . \tag{5.107}$$

It also has several integral representations one of which is

$$\Gamma_q(t) = \int_0^{1/(1-q)} x^{t-1} E_q^{-qx} d_q x \ . \tag{5.108}$$

As in the standard case, one can also define the q-beta function in terms of these q-gamma functions as follows

$$B_q(s,t) := \frac{\Gamma_q(t)\Gamma_q(s)}{\Gamma_q(t+s)} \ , \tag{5.109}$$

which also has a useful integral representation of the form

$$B_q(s,t) = \int_0^1 x^{t-1}(1-qx)_q^{s-1} d_q x \ . \tag{5.110}$$

5.6 Appendix: Details of the derivation for the $\mathcal{O}(1-q)$ double-contour representation

5.6.1 Relevant Taylor expansions

In this appendix we fill in the details regarding crucial Taylor expansions in section 5.3. To consider small deformations around the Veneziano amplitude, we Taylor expand our integral result (5.21) around $q = 1$ up to first order. To that end, we manipulate the q-deformed quantities one by one. At first, we deal with the coefficients $c_{n,j}^D(q)$ for which we get

$$c_{n,j}^D(q) = c_{n,j}^D + c_{n,j}^D \left(\frac{D+j-2}{2}(n-1) - n \right) (1-q) + \mathcal{O}(1-q)^2 \ . \tag{5.111}$$

Moreover, we note that $(1-(1-q)t)^{n-1} = 1-(n-1)(1-q)t+\mathcal{O}(1-q)^2$. Now, the slightly trickier part is Taylor expanding the integration range, the measure and the integrand $(t+[n]_q)^{\frac{D-4}{2}+j}$, we get:

$$\begin{aligned}
&\int_{-[n]_q}^{0} dt(-t(t+[n]_q))^{\frac{D-4}{2}+j}(1-z)^{-t-1} \\
&= \int_{-n\left(1-\frac{n-1}{2}(1-q)\right)}^{0} dt\,(-t(t+n))^{\frac{D-4}{2}+j}\left(1-\left(\frac{D-4}{2}+j\right)\frac{n(n-1)}{2(t+n)}(1-q)\right)(1-z)^{-t-1} \\
&\qquad + \mathcal{O}(1-q)^2 \;.
\end{aligned} \tag{5.112}$$

Considering the substitution $t \to t(1-\frac{n-1}{2}(1-q))$ we finally get

$$\begin{aligned}
&\int_{-[n]_q}^{0} dt(-t(t+[n]_q))^{\frac{D-4}{2}+j}(1-z)^{-1-t}(-\log(1-z))^j \\
&\quad = \int_{-n}^{0} dt\,(-t(t+n))^{\frac{D-4}{2}+j}\,(1-z)^{-1-t}(-\log(1-z))^j \\
&\quad - (1-q)\Bigg[\frac{n-1}{2}\left(\frac{D-2}{2}+j\right)\int_{-n}^{0} dt\,(-t(t+n))^{\frac{D-4}{2}+j}\,(1-z)^{-1-t} \\
&\quad - \frac{n-1}{2}\log(1-z)\int_{-n}^{0} dt(-t)^{\frac{D-2}{2}+j}(t+n)^{\frac{D-4}{2}+j}(1-z)^{-1-t} \\
&\quad + \left(\frac{D-4}{2}+j\right)\frac{n(n-1)}{2}\int_{-n}^{0} dt(-t)^{\frac{D-4}{2}+j}(t+n)^{\frac{D-6}{2}+j}(1-z)^{-1-t} \\
&\quad + \frac{n-1}{2}\left(\frac{D-4}{2}+j\right)\int_{-n}^{0} dt(-t)^{\frac{D-2}{2}+j}(t+n)^{\frac{D-6}{2}+j}(1-z)^{-1-t}\Bigg](-\log(1-z))^j \;.
\end{aligned} \tag{5.113}$$

Finally we Taylor expand the $(1-qz)_q^{-\alpha_q(t)-1}$ term inside the derivative in equation (5.21), but first note

$$(1-qz)_q^x \equiv \frac{(1-qz)_q^\infty}{(1-q^{1+x}z)_q^\infty} = \exp\left\{\mathcal{L}_q\left(-1,\frac{\log zq^{1+x}}{\log q}\right)-\mathcal{L}_q\left(-1,\frac{\log zq}{\log q}\right)\right\} \;, \tag{5.114}$$

where we made use of the crucial identity derived in the previous section given by equation (5.99). For $x=-\alpha_q(t)-1$, we have:

$$(1-qz)_q^{-\alpha_q(t)-1} = \exp\left\{\sum_{k=1}^{\infty}\frac{z^k(1-(1-q)t)^{-k}}{k(1-q^k)} - \sum_{k=1}^{\infty}\frac{z^kq^k}{k(1-q^k)}\right\} \;.$$

Taylor expanding to first order around $q=1$ we get

$$\begin{aligned}
(1-qz)_q^{-\alpha_q(t)-1} &= \exp\left\{(1+t)\sum_{k=1}^{\infty}\frac{z^k}{k}+\frac{t^2}{2}(1-q)\sum_{k=1}^{\infty}\frac{k+1}{k}z^k\right\} \\
&= (1-z)^{-1-t}\left[1+\left(\frac{1-q}{2}\right)\left(\frac{z}{1-z}-\log(1-z)\right)t^2\right]+\mathcal{O}(1-q)^2.
\end{aligned} \tag{5.115}$$

Putting this back into the integral we get

$$\int_{-n}^{0} dt(-t(t+n))^{\frac{D-4}{2}+j}\partial_t^j\left\{(1-z)^{-1-t}\left[1-(n-1)(1-q)t+(1-q)\left(\frac{z}{1-z}-\log(1-z)\right)\frac{t^2}{2}\right]\right\}\ , \tag{5.116}$$

and, differentiating w.r.t t, we get

$$\begin{aligned}
&\int_{-n}^{0} dt\ (-t(t+n))^{\frac{D-4}{2}+j}\partial_t^j\left\{(1-z)^{-1-t}\left[1-(n-1)(1-q)t+(1-q)\left(\frac{z}{1-z}-\log(1-z)\right)\frac{t^2}{2}\right]\right\}\\
&=(-\log(1-z))^j\int_{-n}^{0} dt\ (-t(t+n))^{\frac{D-4}{2}+j}(1-z)^{-1-t}\\
&-(1-q)\Bigg\{(n-1)\Bigg[j(-\log(1-z))^{j-1}\int_{-n}^{0} dt\ (-t(t+n))^{\frac{D-4}{2}+j}(1-z)^{-1-t}\\
&\qquad\qquad-(-\log(1-z))^j\int_{-n}^{0} dt\ (-t)^{\frac{D-2}{2}+j}(t+n)^{\frac{D-4}{2}+j}(1-z)^{-1-t}\Bigg]\\
&\qquad-\frac{1}{2}\left(\frac{z}{1-z}-\log(1-z)\right)\Bigg[j(j-1)(-\log(1-z))^{j-2}\int_{-n}^{0} dt\ (-t(t+n))^{\frac{D-4}{2}+j}(1-z)^{-1-t}\\
&\qquad\qquad-2j(-\log(1-z))^{j-1}\int_{-n}^{0} dt\ (-t)^{\frac{D-2}{2}+j}(t+n)^{\frac{D-4}{2}+j}(1-z)^{-1-t}\\
&\qquad\qquad+(-\log(1-z))^j\int_{-n}^{0} dt\ (-t)^{\frac{D}{2}+j}(t+n)^{\frac{D-4}{2}+j}(1-z)^{-1-t}\Bigg]\Bigg\}\ .
\end{aligned} \tag{5.117}$$

Combining (5.111), (5.113) and (5.117), we have the $\mathcal{O}(1-q)$ Taylor expansion of the $H_q(z)$ integral.

5.6.2 Deriving double contour integral representation of $\mathcal{H}$-integrals

We now derive the double contour integral representation for the $\mathcal{H}$-basis integrals we introduced in section 5.3. The derivation is more or less a generalization of the one presented in [1]. First consider the H-integral already defined in section 5.3

$$H_{n,j}^{(r,s)}(t')=\int^{t'} dt\frac{(-t)^{\frac{D-4}{2}+j+r}(t+n)^{\frac{D-4}{2}+j+s}}{(1-z)^{t+1}}\ , \tag{5.118}$$

where $r,s\in\mathbb{Z}$. Substituting $u=\log(1-z)$, we have

$$\begin{aligned}
H_{n,j}^{(r,s)}(t')&=e^{nu}\int^{t'} du\, e^{-(t+1+n)u}(-t)^{\frac{D-4}{2}+j+r}(t+n)^{\frac{D-4}{2}+j+s}\\
&=(-1)^{s+r}e^{(n-1)u}\partial_u^{\frac{D-4}{2}+j+s}\int^{t'} du\, e^{-(t+n)u}t^{\frac{D-4}{2}+j+r}\ ,
\end{aligned} \tag{5.119}$$

we try to realize the integrand as a total derivative by observing the following fact:

$$\begin{aligned}
\partial_t\left(\frac{e^{-(t+n)u}}{u^{j+r+\frac{D-2}{2}}}\sum_{k=0}^{j+r+\frac{D-4}{2}}\frac{(tu)^k}{k!}\right)&=\frac{e^{-(t+n)u}}{u^{j+r+\frac{D-4}{2}}}\left(-\sum_{k=0}^{j+r+\frac{D-4}{2}}\frac{(tu)^k}{k!}+\sum_{k=0}^{j+r+\frac{D-6}{2}}\frac{(tu)^k}{k!}\right)\\
&=-\frac{e^{-(t+n)u}t^{\frac{D-4}{2}+j+r}}{(j+r+\frac{D-4}{2})!}\ .
\end{aligned} \tag{5.120}$$

This implies that the integrand can be rewritten as a total derivative

$$e^{-(t+n)u}t^{\frac{D-4}{2}+j+r} = \left(j+r+\frac{D-4}{2}\right)!\,\partial_t\left(\frac{e^{-(t+n)u}}{u^{\frac{D-2}{2}+j+r}}\sum_{k=0}^{j+r+\frac{D-4}{2}}\frac{(tu)^k}{k!}\right)\,, \tag{5.121}$$

which means that the H-integral can be written as

$$H_{n,j}^{(r,s)}(t') = (-1)^{s+r+1}e^{(n-1)u}\left(j+r+\frac{D-4}{2}\right)!\partial_u^{j+s+\frac{D-4}{2}}\left(\frac{e^{-(t'+n)u}}{u^{j+r+\frac{D-2}{2}}}\sum_{k=0}^{j+r+\frac{D-4}{2}}\frac{(t'u)^k}{k!}\right)\,. \tag{5.122}$$

We now define the generalised basis for our double contour integral representation already introduced section 5.3:

$$\mathcal{H}_{n,j}^{(a,b,c,r,s)}(t') := \oint \frac{dz}{2\pi i}\frac{1}{z^{n+a}}\frac{1}{(1-z)^b}(-\log(1-z))^{j+c}H_{n,j}^{(r,s)}(t')\,. \tag{5.123}$$

We note that from the Taylor expansions (5.112), (5.115) and (5.117), it is clear that these are the only integrals that show up at any order in the perturbation series and thus serve as a complete basis for a Taylor expansion around $q=1$ of the partial wave coefficients.

Moving on, let us first demonstrate how one can relate $\mathcal{H}_{n,j}^{(a,b,c,r,s)}(-n)$ with $\mathcal{H}_{n,j}^{(a,b,c,r,s)}(0)$ of which we find a double contour integral representation later on. Consider the substitution $z \to z/(z-1)$ and $t \to -t-n$ then (5.118) at $t'=-n$ becomes

$$\begin{aligned} H_{n,j}^{(r,s)}(-n) &= \int^{-n}\frac{dt}{(1-z)^{1+t}}(-t)^{\frac{D-4}{2}+j+r}(t+n)^{\frac{D-4}{2}+j+s}\,,\\ &= -\int^{0}dt(1-z)^{1-t-n}(-t)^{\frac{D-4}{2}+j+s}(t+n)^{\frac{D-4}{2}+j+r}\,,\\ &= -(1-z)^{2-n}H_{n,j}^{(s,r)}(0)\,. \end{aligned} \tag{5.124}$$

Then (5.123) at $t'=-n$ becomes

$$\begin{aligned} \mathcal{H}_{n,j}^{(a,b,c,r,s)}(-n) &= (-1)^{n+j+a+c}\oint\frac{dz}{z^{n+a}}(1-z)^{a+b}(-\log(1-z))^{j+c}H_{n,j}^{(s,r)}(0)\\ &= (-1)^{n+j+a+c}\mathcal{H}_{n,j}^{(a,-a-b,c,s,r)}(0)\,. \end{aligned} \tag{5.125}$$

Now combining the above results with our observation in (5.122) and considering the substitution $u = \log(1-z)$ we arrive at

$$\begin{aligned} \mathcal{H}_{n,j}^{(a,b,c,r,s)}(0) &= (-1)^{j+c+r+s}\left(j+\frac{D-4}{2}+r\right)!\\ &\times\oint\frac{du}{2\pi i}\frac{1}{(1-e^u)^{n+a}}e^{(n-b)u}u^{j+c}\partial_u^{j+\frac{D-4}{2}+s}\left(\frac{e^{-nu}}{u^{\frac{D-2}{2}}+j+r}\right)\,. \end{aligned} \tag{5.126}$$

Performing an integration by parts $j+s+\frac{D-4}{2}$ times in u, the above integral is recast as

$$\mathcal{H}_{n,j}^{(a,b,c,r,s)}(0) = (-1)^{c+r+\frac{D-4}{2}}\left(j+r+\frac{D-2}{2}\right)!\oint_{u=0}\frac{du}{2\pi i}\frac{e^{-nu}}{u^{\frac{D-2}{2}+j+r}}\partial_u^{\frac{D-2}{2}+j+s}\left(\frac{e^{(n-b)u}u^{j+c}}{(1-e^u)^{n+a}}\right)\,. \tag{5.127}$$

This is followed by rewriting the derivative as a residue integral using the identity

$$\partial_u^J f(u) = (-1)^J \oint_{v=0} \frac{dv}{2\pi i} \frac{J!}{v^{J+1}} f(u-v) \ , \tag{5.128}$$

with $J = j + s + \frac{D-4}{2}$. This gives us

$$\begin{aligned}\mathcal{H}_{n,j}^{(a,b,c,r,s)}(0) = (-1)^{j+c+r+s}\Gamma\left(j+r+\frac{D-2}{2}\right)\Gamma\left(j+s+\frac{D-2}{2}\right)\\ \times \oint_{u=0} \frac{du}{2\pi i} \frac{e^{-nu}}{u^{\frac{D-2}{2}+j+r}} \oint_{v=0} \frac{dv}{2\pi i} \frac{1}{v^{\frac{D-2}{2}+j+s}} \frac{e^{(n-b)(u-v)}(u-v)^{j+c}}{(1-e^{u-v})^{n+a}} \ .\end{aligned} \tag{5.129}$$

Rearranging the terms, we finally obtain a double-contour integral representation for the $\mathcal{H}$-integral as follows

$$\begin{aligned}\mathcal{H}_{n,j}^{(a,b,c,r,s)}(0) = (-1)^{r+s}\Gamma\left(j+r+\frac{D-2}{2}\right)\Gamma\left(j+s+\frac{D-2}{2}\right)\\ \times \oint_{u=0} \frac{du}{2\pi i} \oint_{v=0} \frac{dv}{2\pi i} \frac{(v-u)^{j+c}e^{-bu}e^{(a+b)v}}{(uv)^{\frac{D-2}{2}+j}u^r v^s (e^v - e^u)^{n+a}} \ .\end{aligned} \tag{5.130}$$

5.7 Appendix: Numerics for fixed j asymptotics

In this appendix we present certain graphical plots of the coefficients $B_{n,j}^D(q)$ for certain *fixed* values of j, that are central to the discussion concerning their positivity in the asymptotic regime ($n \to \infty$) in section 5.4.

We observe that these coefficients die off rapidly for $n \gg 1$, $q \ll 1$. It is also clear that the coefficients follow a monotonically decreasing sequence with respect to spin j. In the special case of $D = 4$, the noted pattern is consistent with the graphical analysis presented in [202]. However, we also see from figure 5.5 that closer to $q = 1$, the coefficients die off less and less rapidly as j increases. Moreover, the pattern of the coefficients around $q = 1$ is highly unpredictable as it is non-trivial to analyze their convergent behaviour for larger values of n. One can check graphically that this behaviour stabilizes for sufficiently small values of $(1-q)$ and significantly large values of n, such that one recovers a decaying pattern similar to the plots in figure 5.5 which is in qualitative agreement with the expression (5.68).

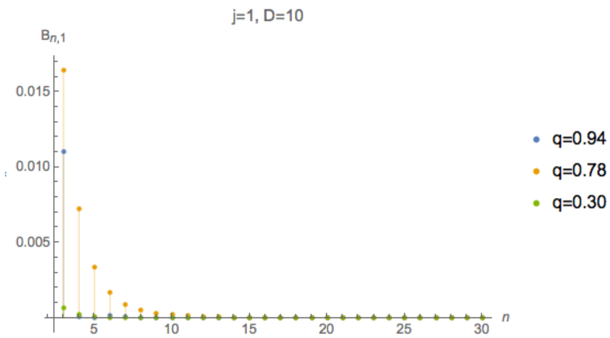

(a)

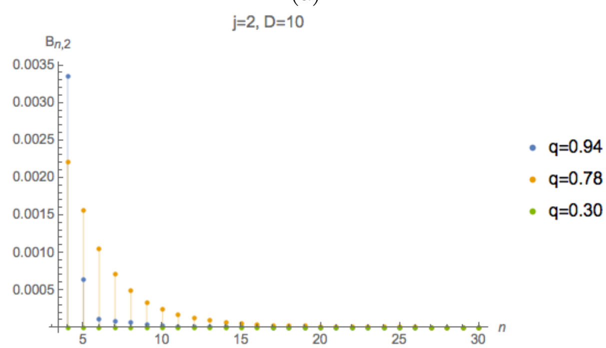

(b)

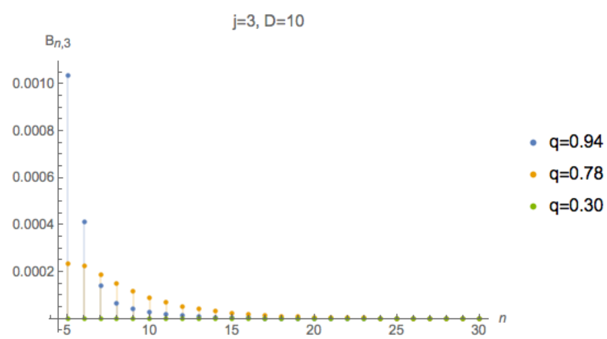

(c)

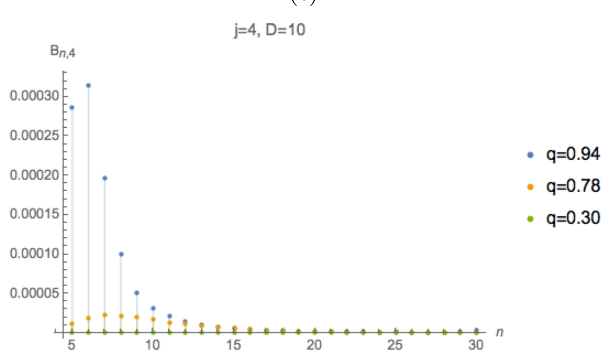

(d)

Figure 5.5: This plots the coefficients $B^D_{n,j}(q)$ for fixed values of $j \in \{1, 2, 3, 4\}$ and $D = 10$.

Chapter 6

Scalar-Graviton Amplitudes and Celestial Holography

This chapter is based on the work [208].

Understanding how bulk translational symmetry emerges is one of the central problems in the celestial holography program. In addition to being constrained by conformal invariance, correlation functions in celestial conformal field theory (CCFT) [25, 23, 24] must also obey translation invariance. This acts as an "external symmetry" and forces low point correlators to be distributional [26]. These effects are not as stark at higher points where the correlators are non-distributional. However, the positions of the operators are still constrained and cannot be chosen to lie arbitrarily on the celestial sphere [27]. Such correlation functions are exotic from the perspective of a 2D conformal field theory and are one of the main roadblocks to finding a top-down description of CCFT. Indeed many of the existing top-down constructions [209, 210, 211] correspond to theories in the bulk which differ from Yang-Mills or GR in significant ways.

One way to circumvent this difficulty has been to introduce nontrivial backgrounds in the bulk [28, 29, 30, 31, 32, 33, 34, 35, 36, 37, 38, 39]. The backgrounds must not only be Lorentz invariant — thus preserving the 2D conformal symmetry of the CCFT — but should also maintain the asymptotic flatness of the 4D bulk spacetime. The celestial counterparts of scattering amplitudes on these backgrounds typically have a number of desirable features. Firstly, they are unconstrained by translation invariance: the background acts as a source/sink of momentum. Consequently, they resemble traditional CFT correlators. Secondly, they have better convergence properties and we avoid having to deal with divergent integrals. Finally, for well-chosen backgrounds, the OPEs and symmetry algebras of the resulting theory resemble those of the CCFT without a background [28, 33, 40]. These properties suggest that the CFT from which these correlators arise might be closely related to the background-free CCFT. Moreover, the semblance of these correlators to those of a traditional CFT makes it easier to identify an independent definition. We refer the reader to [31, 41] for some progress in this direction in the case of Yang-Mills theory.

In this work, we are concerned with gravity amplitudes in 4D Minkowski and Klein spacetimes [42]. In particular, our interests lie in generalizing the results of [40], where the authors considered gluon amplitudes on a massive scalar background, to gravity amplitudes. The scalar was not colored and interacted with gluons only via a non-minimal coupling which gave rise to particularly simple amplitudes. A straightforward extension of this to gravity is impossible since a non-dynamical scalar background breaks diffeomorphism invariance. Moreover, it is impossible to avoid a minimal coupling of the scalar to gravitons. Thus, amplitudes involving n gravitons and one scalar will necessarily involve a scalar exchange. Nevertheless, we will show that the celestial counterparts of these amplitudes exhibit all of the desirable properties mentioned in the previous paragraph.

This paper is structured as follows. In Section 6.1, we describe the precise quantity of interest and its relation to scattering amplitudes. In Section 6.2, we compute scattering amplitudes involving two, three, and four gravitons and a single massive scalar. To our knowledge, these amplitudes have not appeared in the literature before. We then use these to compute the associated celestial correlators in Section 6.3. The OPE of two positive helicity gravitons extracted from these correlators is consistent with the usual OPE as shown in Section 6.4. However, the celestial avatar of the leading soft theorem appears to be slightly different, which we expand on in Section 6.5. Finally, we end with some outlook and discussions in Section 6.6.

6.1 Preliminaries

In this paper, we will be concerned with scattering amplitudes involving n massless gravitons and a single massive scalar. We will always label the graviton momenta by $p_1, \dots, p_n$ and the scalar momentum will be denoted by p_{n+1}. In order to compute the corresponding celestial amplitudes, it is convenient to use the following parametrization for the massless momenta:

$$p_i = \epsilon_i \omega_i \left(1 + z_i \bar{z}_i, z_i + \bar{z}_i, z_i - \bar{z}_i, 1 - z_i \bar{z}_i\right), \qquad i = 1, \dots, n \ . \tag{6.1}$$

This parametrization is written for a spacetime with $(2,2)$ signature (specifically $(+,-,+,-)$). ω_i is a positive real number while $z_i, \bar{z}_i$ are real and independent. $\epsilon_i = \pm 1$ is the direction of the momentum. The parametrization for $(3,1)$ signature is obtained by Wick rotating the third component. The scattering amplitude will be written in terms of spinor helicity variables, which for the momentum parametrization above, take the form

$$\lambda_i = \sqrt{2\omega_i}\epsilon_i \begin{pmatrix} 1 \\ z_i \end{pmatrix}, \qquad \tilde{\lambda}_i = \sqrt{2\omega_i} \begin{pmatrix} 1 \\ \bar{z}_i \end{pmatrix}, \qquad i = 1, \dots, n \ . \tag{6.2}$$

The analogous parametrization for the massive scalar momentum (also in $(2,2)$ signature) is

$$p_{n+1} = \frac{m\epsilon_{n+1}}{2y} \left(1 + y^2 + z_{n+1}\bar{z}_{n+1}, z_{n+1} + \bar{z}_{n+1}, z_{n+1} - \bar{z}_{n+1}, 1 - y^2 - z_{n+1}\bar{z}_{n+1}\right) \ . \tag{6.3}$$

Here $\epsilon_{n+1} = \pm 1$ is the direction of the momentum, $y, z_{n+1}, \bar{z}_{n+1}$ are real and independent with $y > 0$. The celestial amplitude can be obtained from the momentum space scattering amplitude by changing the basis from plane waves to conformal primary wavefunctions. For the case of n massless and one massive particle, this is implemented by [25, 24]

$$\begin{aligned}
&\tilde{\mathcal{A}}^{\epsilon}_{n+1}\left(\{\Delta_1, z_1, \bar{z}_1\}^{J_1}, \ldots, \{\Delta_n, z_n, \bar{z}_n\}^{J_n}; \{\Delta_{n+1}, w, \bar{w}\}\right) = \\
&\qquad \frac{m^2}{4}\int_0^\infty \prod_{i=1}^{n} \frac{d\omega_i}{\omega_i}\omega_i^{\Delta_i} \int_0^\infty \frac{dy}{y^3}\int_{-\infty}^{\infty} dz_{n+1}\, d\bar{z}_{n+1} \\
&\qquad\qquad G_{\Delta_{n+1}}\left(y, z_{n+1}, \bar{z}_{n+1}; w, \bar{w}\right)\mathcal{A}_{n+1}\left(p_1^{J_1}, \ldots, p_n^{J_n}, p_{n+1}\right) \ .
\end{aligned} \tag{6.4}$$

Here $J_1, \ldots, J_n$ are the helicities of the massless particles and

$$G_{\Delta}\left(y, z_{n+1}, \bar{z}_{n+1}; w, \bar{w}\right) = \left(\frac{y}{y^2 + |z_{n+1} - w|^2}\right)^{\Delta} \tag{6.5}$$

is the bulk-to-boundary propagator. The superscript ϵ in (6.4) is meant to indicate the dependence of the celestial amplitude on the directions of the momenta. The quantity of interest in this paper is[1]

$$\begin{aligned}
\tilde{\mathrm{A}}_n &= \langle\langle \mathcal{O}_{\Delta_1, J_1}\left(z_1, \bar{z}_1\right) \ldots \mathcal{O}_{\Delta_n, J_n}\left(z_n, \bar{z}_n\right)\rangle\rangle \\
&\equiv \sum_{\epsilon_i} \tilde{\mathcal{A}}^{\epsilon}_{n+1}\left(\left\{\Delta_1, z_1, \bar{z}_1\right\}^{J_1}, \ldots, \left\{\Delta_n, z_n, \bar{z}_n\right\}^{J_n}; \{0, w, \bar{w}\}\right)
\end{aligned} \tag{6.6}$$

whose features we now explain. But first, we pause to make a comment on notation. We will use $\langle\langle \ldots \rangle\rangle$ and $\tilde{\mathrm{A}}_n$ interchangeably — the former being used more often for brevity and the latter when we wish to emphasize its nature as a CCFT correlator. Implicit in both is the fact that we have set the conformal dimension of the scalar, Δ_{n+1} to 0. The subscript on $\tilde{\mathrm{A}}_n$ matches the number of operators in the double brackets $\langle\langle \ldots \rangle\rangle$ and is one less than the subscript on the corresponding momentum space scattering amplitude. Returning to the features of $\tilde{\mathrm{A}}_n$, firstly note that setting $\Delta_{n+1} = 0$ eliminates all dependence on the scalar coordinates $w, \bar{w}$. The RHS of (6.6) behaves like an n-point correlator[2] — a claim that shall be supported by the computations in this paper. When ϕ is a non-dynamical field, this has the interpretation of being the Mellin transform of amplitude on a scalar background and has been studied for gluons in [28]. These amplitudes take on a particularly simple form [212] due to the absence of scalar exchange contributions to the amplitude. Upon including gravity, we must promote ϕ to a dynamical field and include the resulting scalar exchange terms in the amplitude

Secondly, despite the absence of manifest Lorentz invariance due to the presence of a three-dimensional integral, (6.6) is indeed Lorentz invariant. The three-dimensional measure corresponds to integration over the Lorentz invariant phase space of one massive particle:

$$\int \frac{d^4Q}{(2\pi)^4}\,\delta^{+}\left(Q^2 - m^2\right) = \int \frac{d^3\vec{Q}}{(2\pi)^3\, 2Q^0} = \frac{m^2}{4}\int_0^\infty \frac{dy}{y^3}\int_{-\infty}^{\infty} dz\, d\bar{z}\ . \tag{6.7}$$

[1] The double brackets in the LHS of (6.6) is meant to serve as a reminder of the presence of the massive scalar profile and we use $\tilde{\mathrm{A}}$ for the celestial amplitude with the conformal dimension of the scalar set to 0.

[2] In the celestial amplitude wherein the conformal dimension of the scalar has been set to zero, the subscript n of $\tilde{\mathcal{A}}_n$ counts only the number of gravitons.

Here Q is an off-shell momentum which is put on-shell (with positive energy) by the δ function. Once this is on-shell, we can use a parametrization similar to (6.3) and perform a change of variables as shown in the second equality above.

Finally, we sum over the directions ϵ_i purely for practical purposes since this simplifies computations, particularly in Klein space. This simplification has already been exploited before [213, 47, 214].[3]

6.2 Massive scalar-graviton scattering amplitudes

We must first construct the scattering amplitudes in a theory of scalars and gravitons. We will make a choice for the three-point amplitudes motivated by the results of [28]. In this work, the authors considered gluons coupled to a single massive, uncolored scalar which resulted in the following three-point amplitudes

$$\mathcal{A}_3\left(1^+,2^+,3^-\right)=\kappa_{1,1,-1}\frac{[12]^3}{[23][31]},\qquad \mathcal{A}_3(1^+,2^+,3^\phi)=\kappa_{1,1,0}[12]^2\ . \tag{6.8}$$

Here and in the rest of this paper, we will leave the momentum-conserving delta function implicit while writing scattering amplitudes in momentum space. The authors of [28] worked in $(2,2)$ signature and this corresponded to introducing terms proportional to $\phi\,\mathrm{Tr}\,(F_+)^2$ in the Lagrangian where

$$F_+^{a\,\mu\nu}=\frac{1}{2}\left(F^{a\,\mu\nu}+\frac{1}{2}\epsilon^{\mu\nu\rho\sigma}F^a_{\rho\sigma}\right) \tag{6.9}$$

is the self-dual gauge field strength.[4] $\kappa_{1,1,-1}$ is the Yang-Mills coupling and $\kappa_{1,1,0}$ is related by some numerical factor to the Wilson coefficient of the non-minimal $\phi\,\mathrm{Tr}\,(F_+)^2$ interaction. The scalar is uncolored and does not couple minimally to the gluon.

The analogous three-point amplitudes in gravity can be easily written down and take the following form

$$\mathcal{A}_3\left(1^{++},2^{++},3^{--}\right)=\kappa_{2,2,-2}\frac{[12]^6}{[23]^2[13]^2}\ ,\qquad \mathcal{A}_3\left(1^{++},2^{++},3^\phi\right)=\kappa_{2,2,0}\,[12]^4\ . \tag{6.10}$$

However, it is also necessary to introduce the scalar-graviton minimal coupling [216]

$$\mathcal{A}_3\left(1^{++},2^\phi,3^\phi\right)=\kappa_{2,0,0}\frac{\langle\xi_1|p_2|1]}{\langle\xi_1 1\rangle}\frac{\langle\xi_2|p_2|1]}{\langle\xi_2 1\rangle}\ , \tag{6.11}$$

where ξ_1,ξ_2 indicate arbitrary reference spinors. From the Lagrangian perspective, minimal coupling is unavoidable in order to maintain diffeomorphism invariance. From a pure amplitudes perspective, as we will show later, any four-point amplitude constructed without the minimal coupling (6.11) is inconsistent with the soft graviton theorem. Finally, we note that the amplitudes in (6.10, 6.11) arise from terms that are schematically of the form $R^2\phi, R\phi^2$ in the Lagrangian.

[3] This procedure computes the celestial amplitude for certain "boost + $\mathbb{Z}_2$" eigenstates [215].

[4] This is real in (2,2) signature.

These three-point amplitudes serve as seeds for the construction of four- and higher-point ones. We utilize recursion relations, in particular, those generated by a three-line shift [217] for their construction, which begins with defining

$$\hat{\lambda}_i = \lambda_i - z w_i X \ , \qquad i = 1,2,3 \tag{6.12}$$

such that $w_i \tilde{\lambda}_i = 0$ and X is an arbitrary reference spinor that must drop out at the end. A particularly convenient choice is

$$w_1 = [23] \ , \quad w_2 = [31] \ , \quad w_3 = [12] \ . \tag{6.13}$$

The three shifted momenta are now complex and functions of z. Locality dictates that poles can occur at

$$z_\star \quad \text{such that} \quad \hat{P}^2 = 0 \quad \text{or} \quad \hat{P}^2 = m^2 \ , \tag{6.14}$$

where $\hat{P}$ is a sum of external momenta necessarily involving at most two of $\hat{p}_1, \hat{p}_2, \hat{p}_3$. The residues on these poles are governed by unitarity implying that they factorize into a product of lower point amplitudes. The amplitude can thus be written as (assuming that there is no contribution from the pole at infinity)

$$\mathcal{A}_n \equiv \mathcal{A}_n(0) = \sum_{z_\star} \left[\mathcal{A}_m^{(L)}(z_\star) \frac{1}{P^2} \mathcal{A}_{n-m}^{(R)}(z_\star) + \mathcal{A}_m^{(L)}(z_\star) \frac{1}{P^2 - m^2} \mathcal{A}_{n-m}^{(R)}(z_\star) \right] \ . \tag{6.15}$$

We will now employ this to construct the four- and five-point graviton-scalar amplitudes.

6.2.1 Four-point amplitudes

We first consider the amplitude $\mathcal{A}\left(1^{++}, 2^{++}, 3^{++}, 4^{\phi}\right)$ which receives contributions from both scalar and graviton exchange channels

$$\mathcal{A}_4\left(1^{++}, 2^{++}, 3^{++}, 4^{\phi}\right) \equiv \mathcal{A}_4^{gr,s} + \mathcal{A}_4^{gr,t} + \mathcal{A}_4^{gr,u} + \mathcal{A}_4^{sc,s} + \mathcal{A}_4^{sc,t} + \mathcal{A}_4^{sc,u}. \tag{6.16}$$

The first of these terms corresponds to an s-channel graviton exchange

$$\mathcal{A}_4^{gr,s} = \tag{6.17}$$

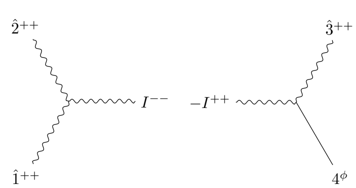

$$= \mathcal{A}_3\left(\hat{1}, \hat{2}, P\right) \frac{1}{P^2} \mathcal{A}_3\left(\hat{3}, 4, -P\right) \ ,$$

with the value of $z_\star$ given by

$$\left(\hat{p}_1 + \hat{p}_2\right)^2 = 0 \implies z_\star = \frac{\langle 12 \rangle}{w_1 \langle X2 \rangle - w_2 \langle X1 \rangle} \ . \tag{6.18}$$

Using the three-point amplitudes in (6.10, 6.11), this evaluates to

$$\begin{aligned}\mathcal{A}_4^{gr,s} &= \kappa_{2,2,-2}\left(\frac{[12]^3}{[2I][I1]}\right)^2\frac{1}{\langle 12\rangle[21]}\kappa_{2,2,0}[3I]^4 \\ &= -\kappa_{2,2,-2}\kappa_{2,2,0}\frac{[12]}{\langle 12\rangle}\frac{[3|p_4|X\rangle^4}{\langle 1X\rangle^2\langle 2X\rangle^2}\ .\end{aligned} \tag{6.19}$$

Similarly, the s-channel scalar exchange term is

$$\mathcal{A}_4^{sc,s} = \tag{6.20}$$

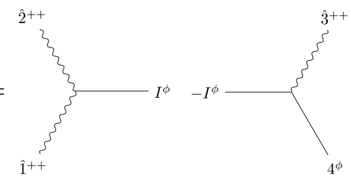

$$\begin{aligned}&= \mathcal{A}_3\left(\hat{1},\hat{2},P\right)\frac{1}{P^2-m^2}\mathcal{A}_3\left(\hat{3},4,-P\right) \\ &= \kappa_{2,2,0}[12]^4\frac{1}{s-m^2}\kappa_{2,0,0}\frac{[3|p_4|\xi_1\rangle}{\langle\hat{3}\xi_1\rangle}\frac{[3|p_4|\xi_2\rangle}{\langle\hat{3}\xi_2\rangle}\ .\end{aligned}$$

Here $s = (p_1+p_2)^2$ is the usual Mandelstam invariant. The remaining terms can be obtained by the replacements $1 \leftrightarrow 3$ and $2 \leftrightarrow 3$. Adding all of these terms and setting the arbitrary reference spinors $\xi_1 = \xi_2 = X$, we finally get

$$\begin{aligned}\mathcal{A}_4\left(1^{++},2^{++},3^{++},4^\phi\right) = -\kappa_{2,2,-2}\kappa_{2,2,0}\frac{[12]}{\langle 12\rangle}\frac{[3|p_4|X\rangle^4}{\langle 1X\rangle^2\langle 2X\rangle^2} &+ \kappa_{2,0,0}\kappa_{2,2,0}\frac{[12]^4}{s-m^2}\frac{[3|p_4|X\rangle^2}{\langle 3X\rangle^2} \\ + \qquad (2\leftrightarrow 3) \qquad &+ \qquad (1\leftrightarrow 3)\ .\end{aligned}$$

The spinor X is arbitrary and the amplitude must be independent of it. It can be checked that the dependence on the arbitrary spinor X drops out *only* if $\kappa_{2,0,0} = \kappa_{2,2,-2}$ and in that case the expression simplifies to

$$\begin{aligned}\mathcal{A}_4\left(1^{++},2^{++},3^{++},4^\phi\right) &= \kappa_{2,2,-2}\kappa_{2,2,0}m^4\frac{[12]}{\langle 12\rangle}\frac{[23]}{\langle 23\rangle}\frac{[31]}{\langle 31\rangle} \\ &\times\left(-2+\frac{s}{s-m^2}+\frac{t}{t-m^2}+\frac{u}{u-m^2}\right),\end{aligned} \tag{6.21}$$

with $t = (p_1+p_4)^2$ and $u = (p_1+p_3)^2$. We pause here to point out that this expression involves a nontrivial cancellation of the X dependence between the graviton exchange terms (which arise from the non-minimal coupling $\kappa_{2,2,0}$) and the scalar exchange terms (arising from the minimal coupling $\kappa_{2,0,0}$). This affirms the statement made at the beginning of this section that the presence of this minimal coupling is crucial to have a consistent and non-zero four-point amplitude. Furthermore, it is also necessary to have $\kappa_{2,0,0} = \kappa_{2,2,-2}$ — a relation that is to be expected on grounds of the equivalence principle. It is interesting to compare this to the four-point amplitude involving one scalar and three positive helicity gluons originally computed in [212] to be

$$\mathcal{A}_4(1^+,2^+,3^+,4^\phi) = \kappa_{1,1,-1}\kappa_{1,1,0}\,\frac{m^4}{\langle 12\rangle\langle 23\rangle\langle 13\rangle}\ . \tag{6.22}$$

This amplitude is particularly simple since the absence of the gluon-scalar minimal coupling eliminates massive exchange contributions.

Moving on to the other four-point amplitudes in this theory, $\mathcal{A}\left(1^{++},2^{++},3^{\phi},4^{\phi}\right)$ has been computed in [218] via BCFW recursion relations to be

$$\mathcal{A}_4\left(1^{++},2^{++},3^{\phi},4^{\phi}\right)=\kappa_{2,2,-2}^2 m^4\frac{[12]^4}{s\left(t-m^2\right)\left(u-m^2\right)}\ . \tag{6.23}$$

Finally, the amplitude $\mathcal{A}\left(1^{++},2^{++},3^{--},4^{\phi}\right)$ cannot be computed by a three-line shift (or using BCFW recursion). We provide an independent derivation of this amplitude in Appendix 6.7 and show that it is given by

$$\mathcal{A}_4\left(1^{++},2^{++},3^{--},4^{\phi}\right)=\kappa_{2,2,0}\kappa_{2,-2,-2}\frac{[12]^6\langle 23\rangle^2\langle 13\rangle^2}{\left(s-m^2\right)tu}\ . \tag{6.24}$$

6.2.2 Five-point amplitudes

The five-point computation proceeds in a similar, albeit more complicated manner to that at four points. The three-line shift in (6.12) and the associated recursion relation imply that the amplitude $\mathcal{A}\left(1^{++},2^{++},3^{++},4^{++},5^{\phi}\right)$ receives contributions from 18 compatible factorization channels.

$$\mathcal{A}_5\left(1^{++},2^{++},3^{++},4^{++},5^{\phi}\right)=\sum_{i=1}^{3}\sum_{j=i+1}^{4}\left(\mathcal{A}_5^{gr,i,j}+\mathcal{A}_5^{sc,i,j}\right)+\sum_{i=1}^{3}\mathcal{A}_5^{sc,i,5}. \tag{6.25}$$

They can be divided into five classes with $\mathcal{A}_5^{gr,1,2},\mathcal{A}_5^{gr,3,4},\mathcal{A}_5^{sc,1,2},\mathcal{A}_5^{sc,3,4},\mathcal{A}_5^{gr,1,5}$ being their representatives. The rest can be obtained by making appropriate replacements on the external legs. As we will now demonstrate, it will be useful to set $X=\lambda_4$.

Evaluation of $\mathcal{A}_5^{gr,3,4}$ and $\mathcal{A}_5^{sc,3,4}$

These classes of terms arise from graviton and scalar exchanges and correspond to the momentum $\left(\hat{p}_1+p_4\right)^2$ going on-shell.

$$\mathcal{A}_5^{gr,3,4} = \tag{6.26}$$

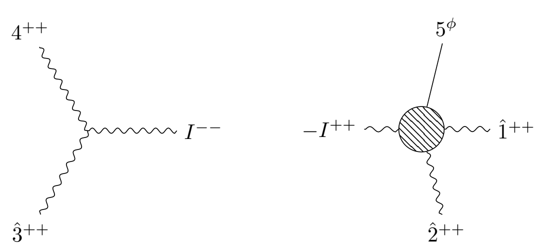

$$\begin{aligned}
&=\mathcal{A}_3\left(\hat{3}^{++},4^{++},I^{--}\right)\frac{1}{P^2}\mathcal{A}_4\left(-I^{++},\hat{2}^{++},\hat{1}^{++},5^{\phi}\right)\\
&=\left(\frac{[34]^3}{[4I][I3]}\right)^2\frac{1}{\langle 34\rangle[43]}\frac{[12]}{\langle\hat{1}\hat{2}\rangle}\frac{[2I]}{\langle\hat{2}I\rangle}\frac{[I1]}{\langle I\hat{1}\rangle}\\
&\qquad\times\left(-2+\frac{s_{\hat{1}\hat{2}}}{s_{\hat{1}\hat{2}}-m^2}+\frac{s_{\hat{2}\hat{3}4}}{s_{\hat{2}\hat{3}4}-m^2}+\frac{s_{\hat{1}\hat{3}4}}{s_{\hat{1}\hat{3}4}-m^2}\right)\ ,
\end{aligned}$$

where we've used the notation $s_{ij} = (p_i + p_j)^2$, $s_{ijk} = (p_i + p_j + p_k)^2$. After some manipulation, this term takes the form

$$\mathcal{A}_5^{gr,3,4} = -\frac{[34]}{\langle 34\rangle}\frac{[12]}{\langle \hat{1}\hat{2}\rangle}\frac{\left[2|\hat{3}+4|X\right\rangle \left[1|\hat{3}+4|X\right\rangle}{\langle 3X\rangle\langle 4X\rangle\langle \hat{1}\hat{3}\rangle\langle \hat{2}4\rangle}\left[-2 + \frac{s_{\hat{1}\hat{2}}}{s_{\hat{1}\hat{2}} - m^2} + \frac{s_{\hat{2}\hat{3}4}}{s_{\hat{2}\hat{3}4} - m^2} + \frac{s_{\hat{1}\hat{3}4}}{s_{\hat{1}\hat{3}4} - m^2}\right] . \quad (6.27)$$

The shifted spinors are determined by first solving $\langle \hat{3}4\rangle = 0$ for z. This gives

$$z = \frac{\langle 34\rangle}{\langle X4\rangle} , \quad \hat{\lambda}_1 = \lambda_1 - \frac{[23]\langle 34\rangle}{[12]\langle X4\rangle}X , \quad \hat{\lambda}_2 = \lambda_2 - \frac{[31]\langle 34\rangle}{[12]\langle X4\rangle}X , \quad \hat{\lambda}_3 = \frac{\langle X3\rangle}{\langle X4\rangle}\lambda_4 . \quad (6.28)$$

Plugging all of this into (6.27), we find that

$$\mathcal{A}_5^{gr,3,4} \propto \langle X4\rangle , \quad (6.29)$$

which vanishes when $X = \lambda_4$. A similar analysis for the scalar exchange diagrams shows that it also vanishes. Thus all diagrams in this class do not contribute to the amplitude and we have

$$\mathcal{A}_5^{gr,1,4} = \mathcal{A}_5^{gr,2,4} = \mathcal{A}_5^{gr,3,4} = \mathcal{A}_5^{sc,1,4} = \mathcal{A}_5^{sc,2,4} = \mathcal{A}_5^{sc,3,4} = 0 . \quad (6.30)$$

Evaluation of $\mathcal{A}_5^{gr,1,2}$

This class of terms arises from the momentum $(\hat{p}_1 + \hat{p}_2)^2$ going on-shell and corresponds to the exchange of a graviton. This channel cannot be obtained from (6.26) because the shift does not treat p_4 on the same footing as p_1, p_2, p_3.

$\mathcal{A}_5^{gr,1,2} =$

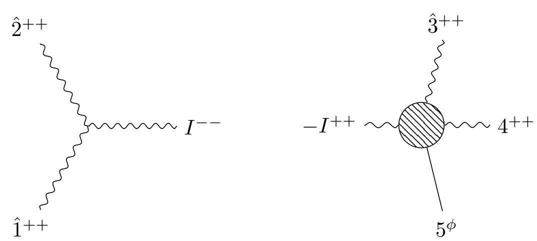

(6.31)

$$= \mathcal{A}_3\left(\hat{1}^{++}, \hat{2}^{++}, I^{--}\right)\frac{1}{P^2}\mathcal{A}_4\left(-I^{++}, \hat{3}^{++}, 4^{++}, 5^{\phi}\right)$$
$$= \left(\frac{[12]^3}{[2I][I1]}\right)^2 \frac{1}{\langle 12\rangle[21]}\frac{[34][4I][I3]}{\langle \hat{3}\hat{4}\rangle\langle 4I\rangle\langle I\hat{3}\rangle}$$
$$\times\left(-2 + \frac{s_{\hat{3}4}}{s_{\hat{3}4} - m^2} + \frac{s_{\hat{1}\hat{2}4}}{s_{\hat{1}\hat{2}4} - m^2} + \frac{s_{\hat{1}\hat{2}\hat{3}}}{s_{\hat{1}\hat{2}\hat{3}} - m^2}\right) .$$

The kinematic invariants involving shifted spinors can be evaluated by first determining the value of z for this channel by setting $\langle \hat{1}\hat{2}\rangle = 0$ and plugging in this value of z into (6.12). By doing this, we get

$$\langle \hat{3}4\rangle = \langle 34\rangle, \qquad \langle 4I\rangle = -1, \qquad \langle I\hat{3}\rangle = -\frac{s_{123}}{[3|p_1 + p_2|4\rangle} \quad (6.32)$$
$$s_{\hat{1}\hat{2}4} = s_{124} - s_{12}, \qquad s_{\hat{1}\hat{2}\hat{3}} = s_{123} .$$

This brings this term to the form

$$\mathcal{A}_5^{gr,1,2} = -\frac{[12]}{\langle 12\rangle}\frac{[34]}{\langle 34\rangle}\frac{[14]}{\langle 14\rangle}\frac{[24]}{\langle 24\rangle}\left(\frac{1}{s_{24}}+\frac{1}{s_{14}}\right)\frac{[3|p_5|4\rangle^2}{s_{123}} \times \left(-2+\frac{s_{34}}{s_{34}-m^2}+\frac{s_{14}+s_{24}}{s_{14}+s_{24}-m^2}+\frac{s_{123}}{s_{123}-m^2}\right) \ . \quad (6.33)$$

Evaluation of $\mathcal{A}_5^{sc,1,5}$

This class of terms arises from the momentum $(\hat{p}_1+p_5)^2$ going on-shell and corresponds to a scalar exchange.

$$\mathcal{A}_5^{sc,1,5} = \quad (6.34)$$

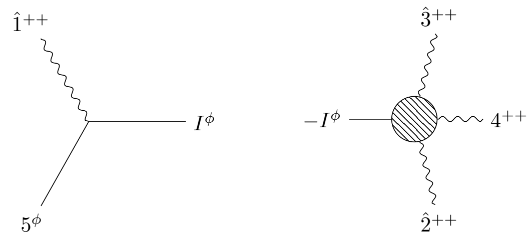

$$= \mathcal{A}_3\left(\hat{1}^{++},5^{\phi},I^{\phi}\right)\frac{1}{P^2-m^2}\mathcal{A}_4\left(-I^{\phi},\hat{3}^{++},4^{++},\hat{2}^{++}\right)$$

$$= \frac{[1|p_5|\xi_1\rangle\,[1|p_5|\xi_2\rangle}{\langle\hat{1}\xi_1\rangle\langle\hat{2}\xi_2\rangle}\frac{1}{s_{15}-m^2}\frac{[23][34][42]}{\langle\hat{2}\hat{3}\rangle\langle\hat{3}4\rangle\langle 4\hat{2}\rangle} \times\left(-2+\frac{s_{\hat{3}4}}{s_{\hat{3}4}-m^2}+\frac{s_{\hat{3}\hat{2}}}{s_{\hat{3}\hat{2}}-m^2}+\frac{s_{\hat{2}4}}{s_{\hat{2}4}-m^2}\right) \ .$$

In this case, the kinematic invariants involving shifted momenta evaluate to

$$\langle\hat{2}\hat{3}\rangle = \frac{s_{15}-s_{23}-m^2}{[23]} \ , \qquad s_{\hat{2}\hat{3}} = s_{23}-s_{15}+m^2 \ , \qquad s_{\hat{3}4} = s_{34} \ , \qquad s_{\hat{2}4} = s_{24} \ . \quad (6.35)$$

Setting $\xi_1=\xi_2=\lambda_4$ for simplicity, we get

$$\mathcal{A}_5^{sc,1,2} = \frac{[23]}{\langle 23\rangle}\frac{[34]}{\langle 34\rangle}\frac{[24]}{\langle 24\rangle}\frac{[14]}{\langle 14\rangle}\frac{s_{23}}{s_{14}}\frac{[1|p_5|4\rangle^2}{(s_{15}-m^2)\,(s_{15}-s_{23}-m^2)} \times\left(-2+\frac{s_{34}}{s_{34}-m^2}+\frac{s_{123}+s_{14}}{s_{123}+s_{14}-m^2}+\frac{s_{24}}{s_{24}-m^2}\right).$$

Evaluation of $\mathcal{A}_5^{sc,1,2}$

This final class of terms also corresponds to a scalar exchange but arises from the momentum

$(\hat{p}_1+\hat{p}_2)^2$ going on-shell.

$$\mathcal{A}_5^{sc,1,2} = \tag{6.36}$$

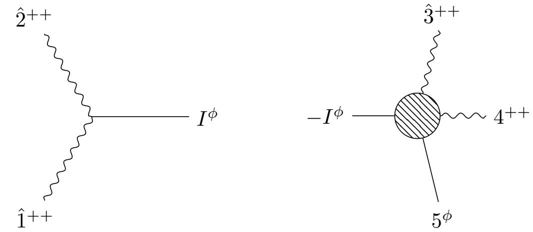

$$= \mathcal{A}_3\left(\hat{1}^{++},\hat{2}^{++},I^{\phi}\right)\frac{1}{P^2-m^2}\mathcal{A}_4\left(-I^{\phi},\hat{3}^{++},4^{++},5^{\phi}\right)$$

$$= [12]^4\,\frac{1}{s_{12}-m^2}\,\frac{[34]^4}{s_{\hat{3}4}\left(s_{\hat{1}\hat{2}4}-m^2\right)\left(s_{\hat{1}\hat{2}\hat{3}}-m^2\right)}\ .$$

Here the shifted momenta are determined by $\langle\hat{1}\hat{2}\rangle[12]=m^2$ and this term evaluates to

$$\mathcal{A}_5^{sc,1,2} = \frac{[12]^4[34]^4}{\left(s_{12}-m^2\right)s_{34}\left(s_{123}-m^2\right)\left(s_{14}+s_{24}\right)}\ . \tag{6.37}$$

This completes the computation of $\mathcal{A}_5\left(1^{++},2^{++},3^{++},4^{++},5^{\phi}\right)$. In computing this amplitude using the recursion relations, we have implicitly assumed that there is no contribution from a pole at infinity in the complex z plane. In order to verify the validity of this assumption, we have checked that the amplitude we computed has all the correct soft and collinear limits.

6.3 Celestial amplitudes

We are interested in evaluating the celestial amplitudes corresponding to the bulk scattering amplitudes of the previous section. As explained in Section 6.1, we are interested in the correlators obtained by setting $\Delta=0$, where Δ is the conformal dimension of the massive scalar. Since all the dependence on the scalar coordinates drops out of the correlation functions, we will refer to the celestial counterparts of $n+1$-point bulk scattering amplitudes as n-point correlators. This is further supported, as we will now show, by the structure of these correlators.

6.3.1 Two-point function

The momentum space three-point amplitude (6.10), written using the parameterization (6.1, 6.3) is given by

$$\mathcal{A}_3\left(1^{++},2^{++},3^{\phi}\right) = \kappa_{2,2,0}\,m^4\,\frac{\bar{z}_{12}^2}{z_{12}^2}\delta^{(4)}\left(p_1+p_2+Q\right)\ . \tag{6.38}$$

We have made use of momentum conservation ($\langle 12\rangle[12]=m^2$) in arriving at the above form. The corresponding celestial amplitude integrated over the scalar phase space is given by the expression

$$\begin{aligned}&\tilde{\mathrm{A}}_2\left(\{\Delta_1,z_1,\bar{z}_1\}^{++},\{\Delta_2,z_2,\bar{z}_2\}^{++}\right)\\ &=\kappa_{2,2,0}\sum_{\epsilon_1,\epsilon_3}\int_0^{\infty}dy\,dz_3\,d\bar{z}_3\,\frac{m^2}{4y^3}\times\int_0^{\infty}d\omega_1\,d\omega_2\,\omega_1^{\Delta_1-1}\,\omega_2^{\Delta_2-1}\,\frac{\bar{z}_{12}^2}{z_{12}^2}\,\delta^{(4)}\left(p_1+p_2+Q\right)\ .\end{aligned} \tag{6.39}$$

We can use the δ-function to solve for $y, z, \bar{z}, \omega_1$ to get

$$\delta^{(4)}\left(p_1+p_2+Q\right)=\frac{1}{|J|}\delta\left(y-y^{\star}\right)\delta\left(\bar{z}_3-\bar{z}_3^{\star}\right)\delta\left(z_3-z_3^{\star}\right)\delta\left(\omega_1-\omega_1^{\star}\right)\ , \tag{6.40}$$

where[5]

$$\omega_1^{\star}=\frac{m^2}{4\epsilon_1\epsilon_2 z_{12}\bar{z}_{12}\omega_2},\qquad y^{\star}=\frac{-2m\epsilon_2\epsilon_3 z_{12}\bar{z}_{12}\omega_2}{m^2+4z_{12}\bar{z}_{12}\omega_2^2},\qquad J=\frac{m^2 z_{12}\bar{z}_{12}\epsilon_1\epsilon_2\omega_2}{(y^{\star})^3}\ . \tag{6.41}$$

After integrating over $y, z_3, \bar{z}_3, \omega_1$, we get

$$\tilde{\mathrm{A}}_2=\kappa_{2,2,0}m^2\left(\frac{\bar{z}_{12}}{z_{12}}\right)^2\sum_{\epsilon_1,\epsilon_3}\int_0^{\infty}d\omega_2\left(\frac{m^2}{4\epsilon_1\epsilon_2 z_{12}\bar{z}_{12}\omega_2}\right)^{\Delta_1}\omega_2^{\Delta_2-1}\,\Theta\left(\omega_1^{\star}\right)\,\Theta\left(y^{\star}\right)\ . \tag{6.42}$$

The integral over the δ-function gives rise to the two Θ functions since the y, ω_1 integrals are over $\mathbb{R}^+$. The sum over ϵ_3 eliminates $\Theta\left(y^{\star}\right)$ while the sum over ϵ_1 eliminates $\Theta\left(\omega_1^{\star}\right)$ yielding

$$\tilde{\mathrm{A}}_2=\kappa_{2,2,0}m^2\left|\frac{\bar{z}_{12}}{z_{12}}\right|^2\left|\frac{m^2}{4z_{12}\bar{z}_{12}}\right|^{\Delta_1}\int_0^{\infty}d\omega_2\,\omega_2^{\Delta_2-\Delta_1-1}\ . \tag{6.43}$$

Performing the ω_2 integral, we obtain the final result for the two-point celestial correlator

$$\langle\langle\mathcal{O}_{\Delta_1}^{++}\left(z_1,\bar{z}_1\right)\mathcal{O}_{\Delta_2}^{++}\left(z_2,\bar{z}_2\right)\rangle\rangle\equiv\tilde{\mathrm{A}}_2=\kappa_{2,2,0}m^2\left|\frac{\bar{z}_{12}}{z_{12}}\right|^2\left|\frac{m^2}{4z_{12}\bar{z}_{12}}\right|^{\Delta_1}\times 2\pi\delta\left(\Delta_1-\Delta_2\right)\ . \tag{6.44}$$

We see that the resulting object indeed resembles a two-point correlation function as in an ordinary CFT.

It is also natural to consider correlation functions like $\langle\mathcal{O}_{\Delta_1}^{++}\left(z_1,\bar{z}_1\right)\mathcal{O}_{\Delta_2}^{0}\left(z_2,\bar{z}_2\right)\mathcal{O}_{0}^{0}\left(z_3,\bar{z}_3\right)\rangle$. Interpreting it as a two-point function of a graviton and scalar, we expect it to vanish from the 2D CFT perspective. However, it is nonzero and is suggestive of the fact that additional insertions of the scalar cannot be treated on the same footing as gravitons. We leave the exploration of such correlators and their meaning to future work, noting for now that the singular part of the graviton OPE does not involve the scalar, so the set of correlators $\langle\langle\ldots\rangle\rangle$ with only graviton insertions forms a self-consistent sector in some sense, similar in spirit to studying a current algebra independently from any actual CFT.[6]

6.3.2 Three-point functions

$\langle\langle\mathcal{O}_{\Delta_1}^{++}\,\mathcal{O}_{\Delta_2}^{++}\,\mathcal{O}_{\Delta_3}^{++}\rangle\rangle$

The three-point functions are computed from momentum space four-point scattering amplitudes. We start with (6.21) which we write as

$$\mathcal{A}_4\left(1^{++},2^{++},3^{++},4^{\phi}\right)=\mathcal{A}_4^{gr}+\mathcal{A}_4^{sc,s}+\mathcal{A}_4^{sc,t}+\mathcal{A}_4^{sc,u}, \tag{6.45}$$

[5] We have not displayed the solutions for $z_3, \bar{z}_3$ since they are not required for this computation.

[6] We thank Sruthi Narayanan for bringing this to our attention.

with $\mathcal{A}_4^{gr}$ representing the contribution of graviton exchange in all channels. As in the previous section, the δ-function is used to eliminate the scalar momentum variables $z_4, \bar{z}_4, y$ as well as ω_3

$$\delta^{(4)}\left(p_1+p_2+p_3+Q\right)=\frac{1}{|J|}\delta\left(y-y^\star\right)\delta\left(\bar{z}-\bar{z}_\star\right)\delta\left(z-z_\star\right)\delta\left(\omega_3-\omega_3^\star\right)\ , \tag{6.46}$$

with

$$\omega_3^\star=\frac{\epsilon_3}{4}\frac{m^2-4\omega_1\omega_2 z_{12}\bar{z}_{12}\epsilon_1\epsilon_2}{z_{13}\bar{z}_{13}\epsilon_1\omega_1+z_{23}\bar{z}_{23}\epsilon_2\omega_2}\quad,\quad y^\star=-\frac{2m\epsilon_4\left(z_{13}\bar{z}_{13}\epsilon_1\omega_1+z_{23}\bar{z}_{23}\epsilon_2\omega_2\right)}{m^2+4\left(\epsilon_1\omega_1 z_{13}+\epsilon_2\omega_2 z_{23}\right)\left(\epsilon_1\omega_1\bar{z}_{13}+\epsilon_2\omega_2\bar{z}_{23}\right)}\ ,$$
$$J=\frac{m^2}{y^3}\left(z_{13}\bar{z}_{13}\epsilon_1\omega_1+z_{23}\bar{z}_{23}\epsilon_2\omega_2\right)\ . \tag{6.47}$$

The resulting three-point celestial correlator for both the graviton and scalar exchanges is given by

$$\tilde{\mathrm{A}}_3=\frac{1}{4}\sum_{\epsilon_i}\int_0^\infty d\omega_1\, d\omega_2\, \omega_1^{\Delta_1-1}\,\omega_2^{\Delta_2-1}\frac{\left(\omega_3^\star\right)^{\Delta_3-1}}{\left|z_{13}\bar{z}_{13}\epsilon_1\omega_1+z_{23}\bar{z}_{23}\epsilon_2\omega_2\right|}\Theta\left(y^\star\right)\Theta\left(\omega_3^\star\right)\mathcal{A}_4. \tag{6.48}$$

We will now compute the above integral for each term in $\mathcal{A}_4$ (6.45), whose explicit form in the momentum space is given by the relation (6.21).

Mellin transform of $\mathcal{A}_4^{gr}$

In the parametrization of (6.1), the graviton exchange term of the amplitude is

$$\mathcal{A}_4^{gr}=-2\kappa_{2,2,-2}\kappa_{2,2,0}m^4\frac{\bar{z}_{12}\bar{z}_{23}\bar{z}_{31}}{z_{12}z_{23}z_{31}}. \tag{6.49}$$

Plugging this into (6.48) and performing the sum over ϵ_3, ϵ_4 gives

$$\tilde{\mathrm{A}}_3^{gr}=-2^{1-2\Delta_3}\kappa_{2,2,-2}\kappa_{2,2,0}m^4\frac{\bar{z}_{12}\bar{z}_{23}\bar{z}_{31}}{z_{12}z_{23}z_{31}}\sum_{\epsilon_1,\epsilon_2}\int_0^\infty d\omega_1\, d\omega_2\, \omega_1^{\Delta_1-1}\,\omega_2^{\Delta_2-1}$$
$$\times\left|m^2-4\omega_1\omega_2 z_{12}\bar{z}_{12}\epsilon_1\epsilon_2\right|^{\Delta_3-1}\left|z_{13}\bar{z}_{13}\epsilon_1\omega_1+z_{23}\bar{z}_{23}\epsilon_2\omega_2\right|^{-\Delta_3}. \tag{6.50}$$

Changing variables to

$$\omega_1=\frac{m}{2}\left(\frac{|z_{23}\bar{z}_{23}|}{|z_{12}\bar{z}_{12}|\,|z_{13}\bar{z}_{13}|}\right)^{\frac{1}{2}}\sqrt{\frac{Y}{X}}\quad,\quad \omega_2=\frac{m}{2}\left(\frac{|z_{13}\bar{z}_{13}|}{|z_{12}\bar{z}_{12}|\,|z_{23}\bar{z}_{23}|}\right)^{\frac{1}{2}}\sqrt{XY}\quad,\quad \epsilon_1\epsilon_2=\epsilon\ , \tag{6.51}$$

brings the integral to the form

$$\tilde{\mathrm{A}}_3^{gr}=-\kappa_{2,2,-2}\kappa_{2,2,0}\,\mathcal{Z}\left(z_{ij},\bar{z}_{ij}\right)\sum_{\epsilon}f_1\left(\Delta_i,\alpha_1\right)\,f_2\left(\Delta_i,\alpha_2\right)\ , \tag{6.52}$$

with

$$\mathcal{Z}=2^{-\beta-3}m^{\beta+5}\frac{\bar{z}_{12}\bar{z}_{23}\bar{z}_{13}}{z_{12}z_{23}z_{13}}\left|z_{12}\bar{z}_{12}\right|^{\frac{\Delta_3-\Delta_1-\Delta_2}{2}}\left|z_{23}\bar{z}_{23}\right|^{\frac{\Delta_1-\Delta_2-\Delta_3}{2}}\left|z_{13}\bar{z}_{13}\right|^{\frac{\Delta_2-\Delta_1-\Delta_3}{2}}\ , \tag{6.53}$$

being a standard conformal factor and $\beta=-3+\sum_{i=1}^3\Delta_i$. f_1 and f_2 are integrals over the variables X and Y respectively and depend on the $z_{ij},\bar{z}_{ij}$ only through

$$\alpha_1=\epsilon\,\mathrm{sgn}\left(z_{13}\bar{z}_{13}z_{23}\bar{z}_{23}\right),\quad \alpha_2=\epsilon\,\mathrm{sgn}\left(z_{12}\bar{z}_{12}\right). \tag{6.54}$$

The f_1, f_2 integrals are now readily performed giving us

$$f_1\left(\Delta_i, \alpha_1\right) \equiv \int_0^\infty dX\, X^{\frac{\Delta_2-\Delta_1+\Delta_3}{2}-1} \left|X+\alpha_1\right|^{-\Delta_3}$$
$$= \frac{\Gamma\left(\frac{\Delta_2+\Delta_3-\Delta_1}{2}\right)\Gamma\left(\frac{\Delta_1-\Delta_2+\Delta_3}{2}\right)}{\Gamma\left(\Delta_3\right)} \begin{cases} 1 & \alpha_1 = 1 \\ \frac{\cos\left(\frac{\pi}{2}(\Delta_1-\Delta_2)\right)}{\cos\frac{\pi}{2}\Delta_3} & \alpha_1 = -1 \ , \end{cases} \tag{6.55}$$

and

$$f_2\left(\Delta_i, \alpha_2\right) \equiv \int_0^\infty dY\, Y^{\frac{\Delta_1-\Delta_3+\Delta_2}{2}-1} \left|1-\alpha_2 Y\right|^{\Delta_3-1}$$
$$= \frac{1}{\pi}\Gamma\left(\frac{\Delta_1+\Delta_2-\Delta_3}{2}\right)\Gamma\left(\frac{2-\Delta_1-\Delta_2-\Delta_3}{2}\right)\Gamma\left(\Delta_3\right)$$
$$\times \begin{cases} 2\sin\frac{\pi}{2}\left(\Delta_1+\Delta_2\right)\cos\frac{\pi}{2}\Delta_3 & \alpha_2 = 1 \\ \sin\pi\Delta_3 & \alpha_2 = -1 \ . \end{cases} \tag{6.56}$$

Putting all of this together, we finally get two regions for the graviton exchange term

$$\tilde{\mathrm{A}}_3^{gr} = -\kappa_{2,2,-2}\kappa_{2,2,0}\, \mathcal{Z}\left(z_{ij}, \bar{z}_{ij}\right) \mathcal{G}^{gr}\left(\Delta_i\right) \ \times \ \begin{cases} \mathcal{S}_+ & \left(z_{12}\bar{z}_{12}z_{13}\bar{z}_{13}z_{23}\bar{z}_{23}\right) > 0 \\ \mathcal{S}_- & \left(z_{12}\bar{z}_{12}z_{13}\bar{z}_{13}z_{23}\bar{z}_{23}\right) < 0 \ , \end{cases} \tag{6.57}$$

where

$$\mathcal{G}^{gr}\left(\Delta_i\right) = \frac{1}{\pi}\,\Gamma\left(\frac{2-\Delta_1-\Delta_2-\Delta_3}{2}\right)\Gamma\left(\frac{\Delta_1+\Delta_2-\Delta_3}{2}\right)$$
$$\times\,\Gamma\left(\frac{\Delta_2+\Delta_3-\Delta_1}{2}\right)\Gamma\left(\frac{\Delta_1-\Delta_2+\Delta_3}{2}\right) \ , \tag{6.58}$$

and

$$\mathcal{S}_+ = \sin\frac{\pi}{2}\left(\Delta_1+\Delta_2+\Delta_3\right) + \sin\frac{\pi}{2}\left(\Delta_1+\Delta_2-\Delta_3\right)$$
$$+ \sin\frac{\pi}{2}\left(\Delta_1-\Delta_2+\Delta_3\right) + \sin\frac{\pi}{2}\left(\Delta_2-\Delta_1+\Delta_3\right) \ ,$$
$$\mathcal{S}_- = \sin\pi\Delta_1 + \sin\pi\Delta_2 + \sin\pi\Delta_3 \ . \tag{6.59}$$

Mellin transform of $\mathcal{A}_4^{sc,s}, \mathcal{A}_4^{sc,t}$ and $\mathcal{A}_4^{sc,u}$

We only need to evaluate the s-channel exchange since the other channels can be simply obtained from this by interchanging $1 \leftrightarrow 3$ and $2 \leftrightarrow 3$. Moreover, since we have the following relation between the graviton and scalar exchange terms

$$\mathcal{A}_4^{sc,s} = -\frac{1}{2}\mathcal{A}_4^{gr} \times \frac{4\epsilon_1\epsilon_2\omega_1\omega_2 z_{12}\bar{z}_{12}}{4\epsilon_1\epsilon_2\omega_1\omega_2 z_{12}\bar{z}_{12} - m^2} \ , \tag{6.60}$$

their Mellin transforms are quite similar. Following the steps that led from (6.49) to (6.52), we get

$$\tilde{\mathrm{A}}_3^{sc,s} = \frac{1}{2}\kappa_{2,2,-2}\kappa_{2,2,0}\, \mathcal{Z}\left(z_{ij}, \bar{z}_{ij}\right) \sum_\epsilon \epsilon\, f_1\left(\Delta_i, \alpha_1\right) f_3\left(\Delta_i, \alpha_2\right) \ , \tag{6.61}$$

where

$$f_3\left(\Delta_i,\alpha_2\right)\equiv\int_0^\infty dY\,Y^{\frac{\Delta_1-\Delta_3+\Delta_2}{2}}\left|1-\alpha_2 Y\right|^{\Delta_3-2}\operatorname{sgn}\left(1-\alpha_2 Y\right)$$
$$=\frac{1}{\pi}\Gamma\left(\frac{2+\Delta_1+\Delta_2-\Delta_3}{2}\right)\Gamma\left(\frac{2-\Delta_1-\Delta_2-\Delta_3}{2}\right)\Gamma\left(\Delta_3-1\right)$$
$$\times\begin{cases}-2\sin\frac{\pi}{2}\left(\Delta_1+\Delta_2\right)\cos\frac{\pi}{2}\Delta_3 & \alpha_2=1\\ \sin\pi\Delta_3 & \alpha_2=-1\ .\end{cases} \tag{6.62}$$

We can now put together the celestial amplitude corresponding to the s-channel exchange by summing over ϵ resulting in

$$\tilde{\mathrm{A}}_3^{sc,s}=-\frac{1}{2}\kappa_{2,2,-2}\kappa_{2,2,0}\,\mathcal{Z}\left(z_{ij},\bar{z}_{ij}\right)\mathcal{G}^{sc,s}\left(\Delta_i\right)\ \times\begin{cases}\mathcal{S}_+ & \left(z_{12}\bar{z}_{12}z_{13}\bar{z}_{13}z_{23}\bar{z}_{23}\right)\ >\ 0\\ \mathcal{S}_- & \left(z_{12}\bar{z}_{12}z_{13}\bar{z}_{13}z_{23}\bar{z}_{23}\right)\ <\ 0\end{cases} \tag{6.63}$$

where

$$\mathcal{G}^{sc,s}\left(\Delta_i\right)=\frac{1}{\pi}\Gamma\left(\frac{2-\Delta_1-\Delta_2-\Delta_3}{2}\right)\Gamma\left(\frac{\Delta_1+\Delta_2-\Delta_3+2}{2}\right)$$
$$\times\Gamma\left(\frac{\Delta_1-\Delta_2+\Delta_3}{2}\right)\Gamma\left(\frac{\Delta_2+\Delta_3-\Delta_1}{2}\right)\frac{\Gamma\left(\Delta_3-1\right)}{\Gamma\left(\Delta_3\right)}\ , \tag{6.64}$$

and $\mathcal{S}_\pm$ were defined in (6.59). The invariance of $\mathcal{S}_\pm$ under cyclic permutations of the conformal dimensions Δ_i allows us to write the all-plus three-point expression in a compact manner by combining (6.57) and (6.63) as follows:

$$\langle\langle\mathcal{O}^{++}_{\Delta_1}\,\mathcal{O}^{++}_{\Delta_2}\,\mathcal{O}^{++}_{\Delta_3}\rangle\rangle=\tilde{\mathrm{A}}_3^{gr}+\tilde{\mathrm{A}}_3^{sc,s}+\tilde{\mathrm{A}}_3^{sc,t}+\tilde{\mathrm{A}}_3^{sc,u} \tag{6.65}$$
$$=-\kappa_{2,2,-2}\kappa_{2,2,0}\,\mathcal{Z}\left(z_{ij},\bar{z}_{ij}\right)\left[\mathcal{G}^{gr}+\frac{1}{2}\left(\mathcal{G}^{sc,s}+\mathcal{G}^{sc,t}+\mathcal{G}^{sc,u}\right)\right]$$
$$\times\begin{cases}\mathcal{S}_+ & \left(z_{12}\bar{z}_{12}z_{13}\bar{z}_{13}z_{23}\bar{z}_{23}\right)\ >\ 0\\ \mathcal{S}_- & \left(z_{12}\bar{z}_{12}z_{13}\bar{z}_{13}z_{23}\bar{z}_{23}\right)\ <\ 0\ ,\end{cases}$$

where $\mathcal{G}^{sc,t}(\Delta_i)$ and $\mathcal{G}^{sc,u}(\Delta_i)$ are obtained from $\mathcal{G}^{sc,s}(\Delta_i)$ given in (6.64) by interchanging $\Delta_1\leftrightarrow\Delta_3$ and $\Delta_2\leftrightarrow\Delta_3$ respectively.

$\langle\langle\mathcal{O}^{++}_{\Delta_1}\,\mathcal{O}^{++}_{\Delta_2}\,\mathcal{O}^{--}_{\Delta_3}\rangle\rangle$

We now present the three-point function involving two positive and one negative helicity graviton derived from the momentum-space four-point amplitude given by (6.24), which in the parameterization of (6.1) takes the form

$$\mathcal{A}(1^{++},2^{++},3^{--},4^{\phi})=4^3\kappa_{2,2,0}\kappa_{2,-2,-2}\frac{\bar{z}_{12}^6z_{23}z_{13}}{\bar{z}_{23}\bar{z}_{13}}\frac{\epsilon_1\epsilon_2\omega_1^3\omega_2^3}{4\epsilon_1\epsilon_2\omega_1\omega_2z_{12}\bar{z}_{12}-m^2}\ . \tag{6.66}$$

The computation of this Mellin transform is very similar to the previous cases and we omit all details. The final result takes the form

$$\begin{aligned}\tilde{\mathrm{A}}_3\left(\{\Delta_1, z_1, \bar{z}_1\}^{++}, \{\Delta_2, z_2, \bar{z}_2\}^{++}, \{\Delta_3, z_3, \bar{z}_3\}^{--}\right) \\ = \kappa_{2,2,0}\,\kappa_{2,-2,-2}\,\tilde{\mathcal{Z}}\left(z_{ij}, \bar{z}_{ij}\right)\sum_{\epsilon}\epsilon\, f_1\left(\Delta_i, \alpha_1\right)\, f_4\left(\Delta_i, \alpha_2\right)\ ,\end{aligned} \tag{6.67}$$

where

$$\tilde{\mathcal{Z}} = 2^{-\beta-4} m^{\beta+5}\,\frac{\bar{z}_{12}^6 z_{23} z_{13}}{\bar{z}_{23}\bar{z}_{13}}\left|z_{12}\bar{z}_{12}\right|^{\frac{\Delta_3-\Delta_1-\Delta_2-6}{2}}\left|z_{23}\bar{z}_{23}\right|^{\frac{\Delta_1-\Delta_2-\Delta_3}{2}}\left|z_{13}\bar{z}_{13}\right|^{\frac{\Delta_2-\Delta_1-\Delta_3}{2}}\ , \tag{6.68}$$

is now the appropriate conformal factor, $f_1\left(\Delta_i, \alpha_1\right)$ is the same integral as in (6.55) and

$$\begin{aligned} f_4\left(\Delta_i, \alpha_2\right) &\equiv \int_0^\infty dY\, Y^{\frac{\Delta_1-\Delta_3+\Delta_2}{2}+4}\left|1-\alpha_2 Y\right|^{\Delta_3-2}\operatorname{sgn}\left(1-\alpha_2 Y\right) \\ &= \frac{1}{\pi}\Gamma\left(\frac{6+\Delta_1+\Delta_2-\Delta_3}{2}\right)\Gamma\left(\frac{-2-\Delta_1-\Delta_2-\Delta_3}{2}\right)\Gamma\left(\Delta_3-1\right) \\ &\qquad\times\begin{cases}-2\sin\frac{\pi}{2}\left(\Delta_1+\Delta_2\right)\cos\frac{\pi}{2}\Delta_3 & \alpha_2=1 \\ \sin\pi\Delta_3 & \alpha_2=-1\,.\end{cases}\end{aligned} \tag{6.69}$$

Putting all of this together, the result is

$$\langle\langle\mathcal{O}^{++}_{\Delta_1}\mathcal{O}^{++}_{\Delta_2}\mathcal{O}^{--}_{\Delta_3}\rangle\rangle = -\kappa_{2,-2,-2}\kappa_{2,2,0}\,\tilde{\mathcal{Z}}\left(z_{ij}, \bar{z}_{ij}\right)\tilde{\mathcal{G}}\left(\Delta_i\right)\ \times\begin{cases}\mathcal{S}_+ & \left(z_{12}\bar{z}_{12}z_{13}\bar{z}_{13}z_{23}\bar{z}_{23}\right)\ >\ 0 \\ \mathcal{S}_- & \left(z_{12}\bar{z}_{12}z_{13}\bar{z}_{13}z_{23}\bar{z}_{23}\right)\ <\ 0\ ,\end{cases} \tag{6.70}$$

where

$$\begin{aligned}\tilde{\mathcal{G}}\left(\Delta_i\right) = \frac{1}{\pi}\Gamma\left(\frac{-2-\Delta_1-\Delta_2-\Delta_3}{2}\right)\Gamma\left(\frac{\Delta_1+\Delta_2-\Delta_3+6}{2}\right) \\ \times\Gamma\left(\frac{\Delta_1-\Delta_2+\Delta_3}{2}\right)\Gamma\left(\frac{\Delta_2+\Delta_3-\Delta_1}{2}\right)\frac{\Gamma\left(\Delta_3-1\right)}{\Gamma\left(\Delta_3\right)}\ ,\end{aligned} \tag{6.71}$$

and $\mathcal{S}_\pm$ were defined in (6.59).

6.3.3 Four-point function

The four-point function can be obtained from the five-point amplitude computed in Section 6.2 starting from the definition

$$\tilde{\mathrm{A}}_4 \equiv \frac{m^2}{4}\int_0^\infty\frac{dy}{y^3}\int_{-\infty}^\infty dz_5\,d\bar{z}_5\int_0^\infty\prod_{i=1}^4\frac{d\omega_i}{\omega_i}\,\omega_i^{\Delta_i}\delta^{(4)}\left(\sum_{i=1}^5 p_i\right)\mathcal{A}_5\ . \tag{6.72}$$

Due to the complexity of this amplitude, we will evaluate the corresponding celestial correlator only in Minkowski space. In this case, the regions on which the constraints imposed by the Θ functions are satisfied can be enumerated. As we will see below, a simplification occurs since $\bar{z}_i$ are the complex conjugates of z_i and we have $\bar{z}_i z_i = |z_i|^2 > 0$.[7] As before, we can first eliminate the coordinates of the scalar and one energy using

$$\delta^{(4)}\left(\sum_{i=1}^{5} p_i\right) = \frac{1}{|J|}\delta\left(\omega_4 - \omega_4^\star\right)\delta\left(z_5 - z_5^\star\right)\delta\left(\bar{z}_5 - \bar{z}_5^\star\right)\delta\left(y - y^\star\right) \ , \tag{6.73}$$

$$\omega_4^\star = \frac{m^2 - 4z_{12}\bar{z}_{12}\epsilon_1\epsilon_2\omega_1\omega_2 - 4z_{13}\bar{z}_{13}\epsilon_1\epsilon_3\omega_1\omega_3 - 4z_{23}\bar{z}_{23}\epsilon_2\epsilon_3\omega_2\omega_3}{4\epsilon_4\left(z_{14}\bar{z}_{14}\epsilon_1\omega_1 + z_{24}\bar{z}_{24}\epsilon_2\omega_2 + z_{34}\bar{z}_{34}\epsilon_3\omega_3\right)} \ ,$$

$$J = -\frac{m^2\epsilon_5\left(z_{14}\bar{z}_{14}\epsilon_1\omega_1 + z_{24}\bar{z}_{24}\epsilon_2\omega_2 + z_{34}\bar{z}_{34}\epsilon_3\omega_3\right)}{y^3} \ ,$$

$$y^\star = \frac{-2m\epsilon_5\left(z_{14}\bar{z}_{14}\epsilon_1\omega_1 + z_{24}\bar{z}_{24}\epsilon_2\omega_2 + z_{34}\bar{z}_{34}\epsilon_3\omega_3\right)}{m^2 + 4\left(z_{14}\epsilon_1\omega_1 + z_{24}\epsilon_2\omega_2 + z_{34}\epsilon_3\omega_3\right)\left(\bar{z}_{14}\epsilon_1\omega_1 + \bar{z}_{24}\epsilon_2\omega_2 + \bar{z}_{34}\epsilon_3\omega_3\right)} \ .$$

In arriving at the above result, we have made use of the parametrization

$$p_i = \epsilon_i\,\omega_i\left(1 + z_i\bar{z}_i, z_i + \bar{z}_i, i\left(z_i - \bar{z}_i\right), 1 - z_i\bar{z}_i\right) \ , \tag{6.74}$$

which is appropriate for Minkowski space. Performing the $y, z_5, \bar{z}_5, \omega_4$ integrals, we get

$$\tilde{\mathrm{A}}_4 \equiv \int\prod_{i=1}^{3} d\omega_i\,\omega_i^{\Delta_i - 1}\frac{1}{|J|}\delta\left(\omega_4 - \omega_4^\star\right)\delta\left(z_5 - z_5^\star\right)\delta\left(\bar{z}_5 - \bar{z}_5^\star\right)\delta\left(y - y^\star\right) \times \left(\omega_4^\star\right)^{\Delta - 4 - 1}\Theta\left(y^\star\right)\Theta\left(\omega_1^\star\right)\mathcal{A}_5 \ . \tag{6.75}$$

We do not sum over the directions as in the previous sections. We find it easier to solve the Θ function constraints and evaluate the amplitude for each case. Once we have these correlators, the summation can be trivially carried out. It is easy to see that the two Θ functions in (6.75) reduce to

$$\begin{aligned}\Theta\left(y^\star\right)\Theta\left(\omega_4^\star\right) =& \Theta\left(-\epsilon_5\left(z_{14}\bar{z}_{14}\epsilon_1\omega_1 + z_{24}\bar{z}_{24}\epsilon_2\omega_2 + z_{34}\bar{z}_{34}\epsilon_3\omega_3\right)\right) \\ & \Theta\left(\epsilon_4\epsilon_5\left(-m^2 + 4z_{12}\bar{z}_{12}\epsilon_1\epsilon_2\omega_1\omega_2 + 4z_{13}\bar{z}_{13}\epsilon_1\epsilon_3\omega_1\omega_3 + 4z_{23}\bar{z}_{23}\epsilon_2\epsilon_3\omega_2\omega_3\right)\right) .\end{aligned} \tag{6.76}$$

The constraints imposed by these Θ functions on $\omega_1, \omega_2, \omega_3$ contours are most easily worked out by first changing variables to

$$\omega_1 = \frac{m}{2}\left|\frac{z_{34}}{z_{13}z_{14}}\right|\tilde{\omega}_1,\ \omega_2 = \frac{m}{2}\left|\frac{z_{14}z_{34}}{z_{13}}\right|\frac{1}{|z_{24}|^2}\tilde{\omega}_2,\ \omega_3 = \frac{m}{2}\left|\frac{z_{14}}{z_{13}z_{34}}\right|\tilde{\omega}_3 \ . \tag{6.77}$$

The constraints can now be written purely in terms of the $\tilde{\omega}_i, \epsilon_i$, the conformal cross ratio $z = \frac{z_{12}z_{34}}{z_{13}z_{24}}$ and its conjugate:

$$\begin{aligned}\Theta\left(y^\star\right)\Theta\left(\omega_4^\star\right) =& \Theta\left(-\epsilon_5\left(\epsilon_1\tilde{\omega}_1 + \epsilon_2\tilde{\omega}_2 + \epsilon_3\tilde{\omega}_3\right)\right) \\ & \Theta\left(\epsilon_4\epsilon_5\left(-1 + \epsilon_1\epsilon_2\left|z\right|\tilde{\omega}_1\tilde{\omega}_2 + \epsilon_1\epsilon_3\tilde{\omega}_1\tilde{\omega}_3 + \epsilon_2\epsilon_3\left|1 - z\right|\tilde{\omega}_2\tilde{\omega}_3\right)\right) \ .\end{aligned} \tag{6.78}$$

Before enumerating all the regions, it helps to note that the Θ functions are invariant under three operations

[7]Note that in this section the symbols $z_i, \bar{z}_i, z, \bar{z}$ are all complex, and $||$ denotes the modulus of the complex number. In the previous sections, they were real and we used $||$ to denote the absolute value of these real numbers.

1. $\epsilon_1\tilde{\omega}_1 \leftrightarrow \epsilon_2\tilde{\omega}_2$

2. $\epsilon_1\tilde{\omega}_1 \leftrightarrow \epsilon_3\tilde{\omega}_3$ and $|z| \leftrightarrow |1-z|$

3. $\epsilon_2\tilde{\omega}_2 \leftrightarrow \epsilon_3\tilde{\omega}_3$ and $|z| \leftrightarrow |1-z|$.

Moreover, we regard combinations of ϵ_i differing by an overall sign to be equivalent and set $\epsilon_5 = -1$ in everything that follows. These imply that we can obtain all possible regions from the ones shown in Table 2.1. The combinations $\epsilon_1 = \epsilon_2 = \epsilon_3 = -\epsilon_4 = 1$ and $\epsilon_1 = \epsilon_2 = \epsilon_4 = -\epsilon_3 = -1$ are not listed in this table as they lead to empty regions.

Region	ϵ_1	ϵ_2	ϵ_3	ϵ_4	Constraints
$\mathcal{R}_1$	1	1	1	1	$\tilde{\omega}_1 > 0, \quad \tilde{\omega}_2 < \frac{1}{\lvert z\rvert^2\tilde{\omega}_1}, \quad 0 < \tilde{\omega}_3 < \frac{1-\tilde{\omega}_1\tilde{\omega}_2\lvert z\rvert^2}{\tilde{\omega}_1+\tilde{\omega}_2\lvert 1-z\rvert^2}$
$\mathcal{R}_2$	1	1	-1	1	$\tilde{\omega}_1 > 0, \quad \tilde{\omega}_2 < \frac{1}{\lvert z\rvert^2\tilde{\omega}_1}, \quad 0 < \tilde{\omega}_3 < \tilde{\omega}_1 + \tilde{\omega}_2$
$\mathcal{R}_3$	1	1	-1	1	$\tilde{\omega}_1 > 0, \quad \tilde{\omega}_2 > \frac{1}{\lvert z\rvert^2\tilde{\omega}_1}, \quad \frac{\tilde{\omega}_1\tilde{\omega}_2\lvert z\rvert^2-1}{\tilde{\omega}_1+\tilde{\omega}_2\lvert 1-z\rvert^2} < \tilde{\omega}_3 < \tilde{\omega}_1 + \tilde{\omega}_2$
$\mathcal{R}_4$	1	-1	-1	1	$\tilde{\omega}_1 > 0, \quad 0 < \tilde{\omega}_2 < \tilde{\omega}_1, \quad 0 < \tilde{\omega}_3 < \tilde{\omega}_1 - \tilde{\omega}_2$
$\mathcal{R}_5$	1	1	1	-1	$\tilde{\omega}_1 > 0, \quad 0 < \tilde{\omega}_2 < \frac{1}{\lvert z\rvert^2\tilde{\omega}_1}, \quad \tilde{\omega}_3 > \frac{1-\lvert z\rvert^2\tilde{\omega}_1\tilde{\omega}_2}{\tilde{\omega}_1+\tilde{\omega}_2\lvert 1-z\rvert^2}$
$\mathcal{R}_6$	1	1	1	-1	$\tilde{\omega}_1 > 0, \quad \tilde{\omega}_2 > \frac{1}{\lvert z\rvert^2\tilde{\omega}_1}, \quad \tilde{\omega}_3 > 0$
$\mathcal{R}_7$	1	1	-1	-1	$\tilde{\omega}_1 > 0, \quad \tilde{\omega}_2 > \frac{1}{\lvert z\rvert^2\tilde{\omega}_1}, \quad \tilde{\omega}_3 < \frac{\lvert z\rvert^2\tilde{\omega}_1\tilde{\omega}_2-1}{\tilde{\omega}_1+\lvert 1-z\rvert^2\tilde{\omega}_2}$

Table 6.1: A list of regions carved out by the Θ function constraints for different values of ϵ_i. The regions for any combinations of ϵ_i not listed here are either empty or are related to the listed ones via symmetries. In all of these cases we have set $\epsilon_5 = -1$.

The variable change (6.77) also vastly simplifies (6.73) to

$$\begin{aligned} \omega_4^\star &= -\frac{m\epsilon_4}{2}\left|\frac{z_{13}}{z_{14}z_{34}}\right| \frac{\left(1-|z|^2\epsilon_1\epsilon_2\tilde{\omega}_1\tilde{\omega}_2 - \epsilon_1\epsilon_3\tilde{\omega}_1\tilde{\omega}_3 - |1-z|^2\,\epsilon_2\epsilon_3\tilde{\omega}_2\tilde{\omega}_3\right)}{(\epsilon_1\tilde{\omega}_1+\epsilon_2\tilde{\omega}_2+\epsilon_3\tilde{\omega}_3)}\ , \\ J &= -\frac{m^3\epsilon_5}{2y^3}\left|\frac{z_{14}z_{34}}{z_{13}}\right|(\epsilon_1\tilde{\omega}_1+\epsilon_2\tilde{\omega}_2+\epsilon_3\tilde{\omega}_3)\ . \end{aligned} \tag{6.79}$$

and the integral for the celestial correlator

$$\begin{aligned} \tilde{\mathrm{A}}_4 = \mathcal{Z}\int_{\mathcal{R}_i} d\omega_1\, d\omega_2\, d\omega_3\, \omega_1^{\Delta_1-1}\omega_2^{\Delta_2-1}\omega_3^{\Delta_3-1}\left(\epsilon_1\tilde{\omega}_1+\epsilon_2\tilde{\omega}_2+\epsilon_3\tilde{\omega}_3\right)^{-\Delta_4} \\ \left(1-|z|^2\epsilon_1\epsilon_2\tilde{\omega}_1\tilde{\omega}_2-\epsilon_1\epsilon_3\tilde{\omega}_1\tilde{\omega}_3-|1-z|^2\,\epsilon_2\epsilon_3\tilde{\omega}_2\tilde{\omega}_3\right)^{\Delta_4-1}\mathcal{A}_5^\star\ . \end{aligned} \tag{6.80}$$

$\mathcal{A}_5^\star$ is meant to represent the five-point amplitude after imposing momentum conservation and the variable change in (6.77) and

$$\begin{aligned} \mathcal{Z} = |z_{34}|^{\frac{1}{2}(\Delta_1+\Delta_2-\Delta_3-\Delta_4-1)}\,|z_{13}|^{\frac{1}{2}(-\Delta_1-\Delta_2-\Delta_3+\Delta_4+1)} \\ |z_{14}|^{\frac{1}{2}(-\Delta_1+\Delta_2+\Delta_3-\Delta_4+1)}\,|z_{24}|^{1-\Delta_2}\left(\frac{m}{2}\right)^{-5+\sum_{i=1}^4\Delta_i}\ , \end{aligned} \tag{6.81}$$

is the standard conformal factor.

It is prudent to first identify a few classes of integrals that arise in the computation of the correlator above. To this end, it is necessary to rewrite the five-point amplitude (6.25) using the variables (6.77) as in Appendix 6.8. We can check that all the terms $\mathcal{A}_5^{gr,1,2,(i)}$ (defined in Appendix 6.8) lead to the following class of integrals

$$I^{(1)}_{\mathcal{R}_i}\left(\alpha,\beta,\gamma,\delta,\rho,a,b,c\right)=\int_{\mathcal{R}_i} d\tilde{\omega}_1\, d\tilde{\omega}_2\, d\tilde{\omega}_3 \tilde{\omega}_1^{\alpha}\, \tilde{\omega}_2^{\beta}\, \tilde{\omega}_3^{\gamma}\left(1-\hat{s}\right)^{\delta}\hat{s}^{a}\left(\epsilon_1\tilde{\omega}_1+\epsilon_2\tilde{\omega}_2+\epsilon_3\tilde{\omega}_3\right)^{\rho}$$
$$\left(\hat{s}\epsilon_3\tilde{\omega}_3+\epsilon_1\tilde{\omega}_1+\epsilon_2\tilde{\omega}_2\right)^{b}\left(\hat{s}\left(\epsilon_1\tilde{\omega}_1+\epsilon_2\tilde{\omega}_2\right)+\epsilon_3\tilde{\omega}_3\right)^{c}\ ,\quad (6.82)$$

$$\begin{aligned}
&I^{(2)}_{\mathcal{R}_i}\left(\alpha,\beta,\gamma,\delta,\rho,a,b,c,d,e\right)\\
&\quad=\int_{\mathcal{R}_i} d\tilde{\omega}_1\, d\tilde{\omega}_2\, d\tilde{\omega}_3 \tilde{\omega}_1^{\alpha}\, \tilde{\omega}_2^{\beta}\, \tilde{\omega}_3^{\gamma}\left(1-\hat{s}\right)^{\delta}\left(\epsilon_1\tilde{\omega}_1+\epsilon_2\tilde{\omega}_2+\epsilon_3\tilde{\omega}_3\right)^{\rho}\left(\epsilon_2\tilde{\omega}_2+\epsilon_3\tilde{\omega}_3\right)^{d}\\
&\qquad\times\left(\hat{s}\left(\epsilon_2\tilde{\omega}_2+\epsilon_3\tilde{\omega}_3\right)+\epsilon_1\tilde{\omega}_1\right)^{a}\left(\hat{s}\epsilon_3\tilde{\omega}_3+\epsilon_1\tilde{\omega}_1+\epsilon_2\tilde{\omega}_2\right)^{b}\\
&\qquad\times\left(1+|z|^2\tilde{\omega}_2^2+\left(z+\bar{z}\right)\epsilon_2\epsilon_3\tilde{\omega}_2\tilde{\omega}_3+\tilde{\omega}_3^2\right)^{c}\left(\epsilon_2\tilde{\omega}_2\hat{s}+\epsilon_1\tilde{\omega}_1+\epsilon_3\tilde{\omega}_3\right)^{e}\ ,
\end{aligned}\quad (6.83)$$

where $\hat{s}=|z|\epsilon_1\epsilon_2\tilde{\omega}_1\tilde{\omega}_2+\epsilon_1\epsilon_3\tilde{\omega}_1\tilde{\omega}_3+|1-z|\,\epsilon_2\epsilon_3\tilde{\omega}_2\tilde{\omega}_3$. The exponents represented by Greek letters can take complex values while the Latin ones only take on integer values. All of the terms in $\tilde{\mathrm{A}}_4$ can be expressed in terms of these integrals. This decomposition can be performed easily using Mathematica.

The integrals in (6.82, 6.83) must first be regulated with appropriate $i\epsilon$ prescriptions. Here, we must distinguish between the factors with Greek and Latin exponents. The former are positive in all the regions $\mathcal{R}_i$ as they are just the arguments of the Θ functions. Consequently, they do not require $i\epsilon$ prescriptions. However, the factors with integer exponents introduce new singularities which sometimes intersect the regions $\mathcal{R}_i$. The necessary $i\epsilon$ prescription follows from the corresponding Feynman $i\epsilon$ for the propagators in the tree amplitude. We will now tacitly assume such a prescription and outline how we can derive a Mellin-Barnes representation for these integrals. Applying the Mellin-Barnes decomposition formula[8]

$$\frac{1}{(A_1+\cdots+A_n)^{\lambda}}=\frac{1}{(2\pi i)^{n-1}\Gamma(\lambda)}\int\prod_{i=1}^{n-1}dx_i\,A_i^{x_i}A_n^{-\lambda-x_1-\cdots-x_{n-1}}$$
$$\times\prod_{i=1}^{n-1}\Gamma(-x_i)\Gamma(\lambda+x_1+\cdots+x_{n-1})\ ,\quad (6.84)$$

to each factor with an integer exponent yields an integral of the form

$$\mathcal{I}^{(j)}_{\mathcal{R}_i}=\int\prod_{k=1}^{r}dx_k\,G\left(x_1,\ldots,x_r,a,b,c,d,e,z,\bar{z}\right)\mathcal{J}_{\mathcal{R}_i}\ .\quad (6.85)$$

This generic form is motivated by the observation that each of the factors A_i in the Mellin-Barnes decomposition is a product of powers of $\tilde{\omega}_1,\tilde{\omega}_2,\tilde{\omega}_3,z$ and $\bar{z}$. This modifies the exponents of $\tilde{\omega}_1,\tilde{\omega}_2,\tilde{\omega}_3$

[8]Here and henceforth, we will suppress the contour of integration. It is understood that these contours run upward along the imaginary axis such that the poles separate into left and right ones. For more details, please refer to [219].

from α, β, γ in (6.82, 6.83) to A, B and C. The function $G(x_1, \ldots, x_r, a, b, c, d, e)$ is a universal (independent of the regions $\mathcal{R}_i$) factor containing all the Γ functions and powers of $z, \bar{z}$ arising from (6.84). r is an integer that represents the total number of Mellin variables that must be introduced to achieve this form. We have also defined

$$\mathcal{J}_{\mathcal{R}_i} = \int_{\mathcal{R}_i} d\tilde{\omega}_1\, d\tilde{\omega}_2\, d\tilde{\omega}_3\, \tilde{\omega}_1^A\, \tilde{\omega}_2^B\, \tilde{\omega}_3^C\, (1-\hat{s})^\delta \left(\epsilon_1\tilde{\omega}_1 + \epsilon_2\tilde{\omega}_2 + \epsilon_3\tilde{\omega}_3\right)^\rho \ . \tag{6.86}$$

We can now complete the reduction to Mellin-Barnes form more efficiently by performing some of the integrals and identifying them with well-known hypergeometric functions. The details of this somewhat lengthy procedure are relegated to Appendix 6.9. Here, we merely present the final result:

$$\mathcal{J}_{\mathcal{R}_4} = \int \prod_{i=1}^{4} dx_{r+i}\, \mathcal{G}\left(x_{r+1}, \ldots, x_{r+4}\right) (z-1)^{x_{r+2}} \left(\bar{z}-1\right)^{x_{r+3}} \left(1 - |z|^2\right)^{x_{r+4}} , \tag{6.87}$$

where $\mathcal{G}$ is defined in (6.133).

6.4 Graviton OPEs

We can obtain the graviton OPEs (for positive helicity gravitons) from the three-point correlator (6.57, 6.63). Since the OPE is local and is insensitive to insertions far away from the position of the relevant operators, we expect it to agree with the OPE derived for correlators without a massive scalar. Consider the limit as $z_{23} \to 0$ in which we have for the conformal factor

$$\mathcal{Z} \xrightarrow{2\|3} 2^{2-2\Delta_1} m^{2\Delta_1+2} \frac{\bar{z}_{13}^2}{z_{13}^2} \frac{\bar{z}_{23}}{z_{23}} \left|z_{13}\bar{z}_{13}\right|^{-\Delta_1} (-i\pi)\, \delta\left(\Delta_2 + \Delta_3 - \Delta_1\right) \ . \tag{6.88}$$

In arriving at this result, we have made use of the identity [220]

$$\lim_{\nu\to 0} \nu^{z-\Delta}\, \Gamma\left(\Delta - z\right) = -2\pi i \delta\left(\Delta - z\right) \ . \tag{6.89}$$

The terms in the three-point correlator now become

$$\begin{aligned} \tilde{\mathrm{A}}_3^{gr} \xrightarrow{2\|3} & -2i\kappa_{2,2,-2} \frac{\bar{z}_{23}}{z_{23}} \frac{1}{\pi} \Gamma\left(1-\Delta_2-\Delta_3\right) \Gamma\left(\Delta_2\right) \Gamma\left(\Delta_3\right) \\ & \times \left(\sin\pi\Delta_2 + \sin\pi\Delta_3 + \sin\pi\left(\Delta_2+\Delta_3\right)\right) \tilde{\mathrm{A}}_2 \\ = & -2\kappa_{2,2,-2} \frac{\bar{z}_{23}}{z_{23}} \Big(B(\Delta_2, \Delta_3) + B(1-\Delta_2-\Delta_3, \Delta_3) + B(1-\Delta_2-\Delta_3, \Delta_2) \Big) \tilde{\mathrm{A}}_2 \ , \end{aligned} \tag{6.90}$$

$$\begin{aligned} \tilde{\mathrm{A}}_3^{sc,s} \xrightarrow{2\|3} & -i\kappa_{2,2,-2} \frac{\bar{z}_{23}}{z_{23}} \frac{1}{\pi} \Gamma\left(1-\Delta_2-\Delta_3\right) \Gamma\left(\Delta_2+1\right) \Gamma\left(\Delta_3-1\right) \\ & \times \left(-\sin\pi\Delta_2 - \sin\pi\Delta_3 - \sin\pi\left(\Delta_2+\Delta_3\right)\right) \tilde{\mathrm{A}}_2 \\ = & -\kappa_{2,2,-2} \frac{\bar{z}_{23}}{z_{23}} \Big(B(\Delta_2+1, \Delta_3-1) - B(1-\Delta_2-\Delta_3, \Delta_3-1) + B(1-\Delta_2-\Delta_3, \Delta_2+1) \Big) \tilde{\mathrm{A}}_2 \ , \end{aligned} \tag{6.91}$$

$$
\begin{aligned}
\tilde{\mathrm{A}}_3^{sc,u} &\xrightarrow{2\|3} -i\kappa_{2,2,-2}\frac{\bar{z}_{23}}{z_{23}}\frac{1}{\pi}\Gamma\left(1-\Delta_2-\Delta_3\right)\Gamma\left(\Delta_3+1\right)\Gamma\left(\Delta_2-1\right) \\
&\qquad\qquad \times\left(-\sin\pi\Delta_2-\sin\pi\Delta_3-\sin\pi\left(\Delta_2+\Delta_3\right)\right)\tilde{\mathrm{A}}_2 \\
&= -\kappa_{2,2,-2}\frac{\bar{z}_{23}}{z_{23}}\Big(B(\Delta_2-1,\Delta_3+1)-B(1-\Delta_2-\Delta_3,\Delta_2-1)+B(1-\Delta_2-\Delta_3,\Delta_3+1)\Big)\tilde{\mathrm{A}}_2\ ,
\end{aligned}
\tag{6.92}
$$

while $\tilde{\mathrm{A}}_3^{sc,t}$ is subleading in this limit and hence we drop it. Here $B(x,y)$ is the Euler beta function. Now, if we write the OPE as

$$
\mathcal{O}^{++}_{\Delta_2}\left(z_2,\bar{z}_2\right)\mathcal{O}^{++}_{\Delta_3}\left(z_3,\bar{z}_3\right)\sim\frac{\bar{z}_{23}}{z_{23}}C^{\Delta_2+\Delta_3}_{\Delta_2,\Delta_3}\,\mathcal{O}^{++}_{\Delta_2+\Delta_3}\left(z_3,\bar{z}_3\right)+\dots\ ,
\tag{6.93}
$$

we can read off the OPE coefficient to be

$$
\begin{aligned}
C^{\Delta}_{\Delta_2,\Delta_3} &= -\kappa_{2,2,-2}\Big(2B(\Delta_2,\Delta_3)+2B(1-\Delta_2-\Delta_3,\Delta_3)+2B(1-\Delta_2-\Delta_3,\Delta_2) \\
&\qquad +B(\Delta_2+1,\Delta_3-1)-B(1-\Delta_2-\Delta_3,\Delta_3-1)-B(1-\Delta_2-\Delta_3,\Delta_2+1) \\
&\qquad +B(\Delta_2-1,\Delta_3+1)-B(1-\Delta_2-\Delta_3,\Delta_2-1)-B(1-\Delta_2-\Delta_3,\Delta_3+1)\Big) \\
&= -\kappa_{2,2,-2}\Big(B(\Delta_2-1,\Delta_3-1)-B(\Delta_2-1,3-\Delta_2-\Delta_3)-B(\Delta_3-1,3-\Delta_2-\Delta_3)\Big)\ ,
\end{aligned}
\tag{6.94}
$$

where we have used the following identities:

- $B(\Delta_2-1,\Delta_3+1)+B(\Delta_2+1,\Delta_3-1)+2B(\Delta_2,\Delta_3)-B(\Delta_2-1,\Delta_3-1)=0$
- $B(1-\Delta_2-\Delta_3,\Delta_2-1)+B(1-\Delta_2-\Delta_3,\Delta_2+1)-2B(1-\Delta_2-\Delta_3,\Delta_2)$
  $-B(\Delta_2-1,3-\Delta_2-\Delta_3)=0$
- $B(1-\Delta_2-\Delta_3,\Delta_3-1)+B(1-\Delta_2-\Delta_3,\Delta_3+1)-2B(1-\Delta_2-\Delta_3,\Delta_3)$
  $-B(\Delta_3-1,3-\Delta_2-\Delta_3)=0$,

to simplify the OPE coefficients in the final equality above. This OPE coefficient cannot be directly compared with those obtained in [221, 222] as it does not correspond to OPEs of incoming or outgoing operators, but to specific linear combinations of them. We can use the OPEs of [221, 222] to derive the appropriate quantity for comparison. To do this, we start by considering[9,10]

$$
\sum_{\epsilon_3=\pm1}\mathcal{O}^{++,+1}_{\Delta_2}\,\mathcal{O}^{++,\epsilon_3}_{\Delta_3}=\mathcal{O}^{++,+1}_{\Delta_2}\,\mathcal{O}^{++,+1}_{\Delta_3}+\mathcal{O}^{++,+1}_{\Delta_2}\mathcal{O}^{++,-1}_{\Delta_3}.
\tag{6.95}
$$

Applying the usual OPE we get,

$$
\begin{aligned}
\sum_{\epsilon_3=\pm1}\mathcal{O}^{++,+1}_{\Delta_2}\,\mathcal{O}^{++,\epsilon_3}_{\Delta_3}\sim -\kappa_{2,2,-2}\frac{\bar{z}_{23}}{z_{23}}\Big(&B(\Delta_2-1,\Delta_3-1)\,\mathcal{O}^{++,+1}_{\Delta_2+\Delta_3} \\
&-B(\Delta_2-1,3-\Delta_2-\Delta_3)\,\mathcal{O}^{++,+1}_{\Delta_2+\Delta_3} \\
&-B(\Delta_3-1,3-\Delta_2-\Delta_3)\mathcal{O}^{++,-1}_{\Delta_2+\Delta_3}\Big)\ .
\end{aligned}
\tag{6.96}
$$

[9] We set $\epsilon_2=1$ since there are only two inequivalent choices for ϵ_1,ϵ_2 up to an overall sign.

[10] We suppress all the coordinate dependence of the operators.

If we now insert this into a three-point function and sum over the directions of the new insertion, we get

$$\sum_{\epsilon_1,\epsilon_3}\langle\langle\mathcal{O}^{++,\epsilon_1}_{\Delta_1}\,\mathcal{O}^{++,+1}_{\Delta_2}\,\mathcal{O}^{++,\epsilon_3}_{\Delta_3}\rangle\rangle \sim -\kappa_{2,2,-2}\frac{\bar{z}_{23}}{z_{23}}\Big(B(\Delta_2-1,\Delta_3-1)-B(\Delta_2-1,3-\Delta_2-\Delta_3)$$
$$-B(\Delta_3-1,3-\Delta_2-\Delta_3)\Big)\sum_{\epsilon_1}\langle\langle\mathcal{O}^{++,\epsilon_1}_{\Delta_1}\mathcal{O}^{++}_{\Delta_2+\Delta_3}\rangle\rangle\ , \tag{6.97}$$

matching the expression for the OPE coefficient obtained in (6.94). This shows that the OPEs in the presence of a massive scalar are consistent with those in its absence.

6.5 The conformally soft graviton theorem

The computations of the previous sections have shown that celestial amplitudes involving n gravitons and a massive scalar behave like n-point graviton correlators when the conformal dimension of the scalar is taken to vanish. We will now examine whether this similarly persists for the conformal soft theorems [223]. In this paper, we will only examine the leading soft theorem leaving the others for future work. In momentum space, the leading soft theorem [224] for an amplitude with n positive helicity gravitons and a massive scalar is

$$\mathcal{A}_{n+1}\left(\varepsilon p_1^{++},p_2^{++},\ldots,p_n^{++},p_{n+1}\right)\xrightarrow{\varepsilon\to 0}\frac{1}{\varepsilon}S\left[p_1^{++}\right]\mathcal{A}_n\left(p_2^{++},\ldots,p_n^{++},p_{n+1}\right)+\mathcal{O}\left(\varepsilon^0\right)\ , \tag{6.98}$$

where $S\left[p_1^{++}\right]$ is the relevant soft factor given by

$$S\left[p_1^{++}\right]=\sum_{i=2}^{n+1}\frac{\epsilon_{\mu\nu}\left(p_1\right)p_i^{\mu}p_i^{\nu}}{p_i\cdot p_1}\ , \tag{6.99}$$

and $\epsilon_{\mu\nu}\left(p_1\right)$ is the polarization tensor of the soft graviton, which takes the form

$$\epsilon^{\mu\nu}\left(p_1\right)=\frac{\langle x|\gamma^{\mu}|1]}{\langle x1\rangle}\frac{\langle y|\gamma^{\nu}|1]}{\langle y1\rangle}\ , \tag{6.100}$$

for a positive helicity graviton. Here x,y are two arbitrary reference spinors. The soft factor is independent of the specific choice of x,y on the support of momentum conservation (which always holds upon including the momentum of the massive scalar). A compact expression can be obtained by setting $x=\lambda_2, y=\lambda_3$. Note that there is a sum over all the other particles involved in the amplitude. For the four-point amplitude $\mathcal{A}_4\left(1^{++},2^{++},3^{++},4^{\phi}\right)$ in (6.21), this becomes

$$S\left[p_1^{++}\right]=\frac{[12]}{\langle 12\rangle}\frac{[13]}{\langle 13\rangle}\frac{\langle 23\rangle^2}{t-m^2}=\frac{\bar{z}_{12}\bar{z}_{13}z_{23}^2}{z_{12}z_{13}}\frac{\omega_2\omega_3}{2m\omega_1}\frac{y}{y^2+z_{14}\bar{z}_{14}}. \tag{6.101}$$

It can be checked that the momentum-space amplitude (6.21) satisfies the soft theorems. It is worth noting that the leading soft behavior arises entirely from the term in the amplitude that corresponds to the exchange of the massive scalar. Indeed, without this, the amplitude would fail to satisfy the soft graviton theorem as already stated in Section 6.2. In order to examine the celestial avatar of this statement, we must compute

$$\lim_{\Delta_1\to 1}(\Delta_1-1)\,\tilde{\mathcal{A}}^{\epsilon}_{n+1}=\frac{m^2}{4}\oint_{\omega_1=0}d\omega_1\int_0^\infty\prod_{i=2}^{n}\frac{d\omega_i}{\omega_i}\omega_i^{\Delta_i}\int_0^\infty\frac{dy}{y^3} \times\int_{-\infty}^{\infty}dz_{n+1}\,d\bar{z}_{n+1}\,G_{\Delta_{n+1}}\left(z_{n+1},\bar{z}_{n+1},w,\bar{w}\right)\mathcal{A}_{n+1} \tag{6.102}$$

where we have used the definition (6.4) and the identity

$$\lim_{\varepsilon\to 0}\varepsilon\,|x|^{\varepsilon-1}=\delta\left(x\right), \tag{6.103}$$

which holds for functions falling off at infinity at least as fast as x^{-b} for some $b>0$. For the four-point amplitude under consideration, this turns into

$$\lim_{\Delta_1\to 1}(\Delta_1-1)\,\tilde{\mathcal{A}}_4=\frac{m}{8}\frac{\bar{z}_{12}\bar{z}_{13}z_{23}^2}{z_{12}z_{13}}\int\frac{dy}{y^3}\,dz_4\,d\bar{z}_4 d\omega_2\,d\omega_3\,\omega_2^{\Delta_2}\,\omega_3^{\Delta_3} \times\left(\frac{y}{y^2+(z_4-w)(\bar{z}_4-\bar{w})}\right)^{\Delta_4}\left(\frac{y}{y^2+z_{14}\bar{z}_{14}}\right)\mathcal{A}_3\,. \tag{6.104}$$

We must now set $\Delta_4=0$ in order to obtain the conformal soft theorem for the correlators considered in this paper. The presence of the soft factor prevents us from interpreting this quantity as a lower point celestial amplitude with $\Delta_4=0$. In fact, this can be interpreted as a new correlator with $\Delta_4=1$ and the scalar coordinates being $\{z_1,\bar{z}_1\}$. Thus, we can write

$$\lim_{\Delta_1\to 1}(\Delta_1-1)\,\tilde{\mathcal{A}}_4\left(\{\Delta_1,z_1,\bar{z}_1\},\{\Delta_2,z_2,\bar{z}_2\},\{\Delta_3,z_3,\bar{z}_3\},\{\Delta_4,w,\bar{w}\}\right) =\frac{1}{2m}\frac{\bar{z}_{12}\bar{z}_{13}z_{23}^2}{z_{12}z_{13}}\tilde{\mathcal{A}}_3\left(\{\Delta_2+1,z_2,\bar{z}_2\},\{\Delta_3+1,z_3,\bar{z}_3\},\{1,z_1,\bar{z}_1\}\right)\,. \tag{6.105}$$

This compact version of the conformally soft theorem involves shifting all the conformal dimensions and is ostensibly very different from the massless version in [223]. However, this is merely an artefact of the choice of reference spinors. Indeed, keeping x,y arbitrary will lead to a version of the conformally soft graviton theorem which involves multiple terms, each involving only one shifted conformal dimension. This is also supported by the following direct computation

$$\lim_{\Delta_1\to 1}(\Delta_1-1)\tilde{\mathrm{A}}_3=\frac{m^2}{2}\frac{\bar{z}_{12}^3z_{23}^2}{z_{12}^3z_{13}^2}\left|\frac{m^2}{4z_{23}\bar{z}_{23}}\right|^{\Delta_3}\left|\frac{m^2z_{13}\bar{z}_{13}}{4z_{12}\bar{z}_{12}z_{23}\bar{z}_{23}}\right|^{\frac{\Delta_2-\Delta_3+1}{2}} \times\begin{cases}\frac{\pi}{\cos\left(\frac{\pi}{2}(\Delta_2-\Delta_3)\right)} & ;\ \mathrm{sgn}(z_{12}\bar{z}_{12}z_{23}\bar{z}_{23})>0\\ -\pi\tan\left(\frac{\pi}{2}(\Delta_2-\Delta_3)\right) & ;\ \mathrm{sgn}(z_{12}\bar{z}_{12}z_{23}\bar{z}_{23})<0\ .\end{cases} \tag{6.106}$$

This suggests that the leading soft theorem relates the set of correlators with vanishing scalar conformal dimension to those with unit conformal dimension. It would be intriguing to investigate if this has an interpretation along the lines of [225, 226]. The connection between soft theorems and Ward identities of asymptotic symmetries in the presence of massive particles has been studied in [227, 228] in general. It would also be interesting to see if any lessons could be extracted from this analysis.

6.6 Outlook and discussion

The correlators computed in this paper are well-defined and non-distributional, resembling ordinary CFT correlators. This computation opens up several lines of investigation. The first of these is understanding whether the remaining soft theorems are modified, along with their associated symmetries. Next is understanding the singularity structure of these correlators either using the Mellin Barnes representations (6.87) and generalizing the analysis in [229] or using the Euler integral representation (6.82, 6.83) and methods in [94, 68]. A particularly interesting question is understanding how the massive exchange is manifest in the singularity structure. Another question that would benefit from further investigation is if an on-shell version of the correlators in [230] agrees with those in this paper. This would provide a connection between the two different definitions. The final and perhaps most interesting and challenging question is whether we can identify a 2D CFT that reproduces the correlation functions in this paper.

6.7 Appendix: Derivation of the $\mathcal{A}(1^{++}, 2^{++}, 3^{--}, 4^{\phi})$ amplitude

This amplitude is not constructible via BCFW or three-line shift recursions. The simplest way to derive this amplitude is by appealing to consistent factorization and locality along the lines of [216]. The basic procedure is to compute the residues on all factorization channels by multiplying the appropriate three-point amplitudes and then guessing an expression that correctly reproduces all of them. For the case at hand, we begin by computing the residue in the u-channel corresponding to a graviton exchange. This is

$$\underset{[13]\to 0}{\text{Res}}\, \mathcal{A}_4\left(1^{++}, 2^{++}, 3^{--}, 4^{\phi}\right) = \frac{1}{\langle 13\rangle} \tag{6.107}$$

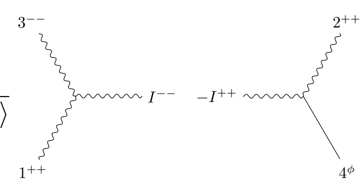

$$\begin{aligned}
&= \frac{1}{\langle 13\rangle}\kappa_{2,2,-2}\left(\frac{\langle 3I\rangle^3}{\langle I1\rangle\langle 13\rangle}\right)^2 \kappa_{2,2,0}\,[2I]^4 \\
&= \kappa_{2,2,0}\kappa_{2,2,-2}\frac{[12]^6\langle 23\rangle^2\langle 13\rangle^2}{\langle 13\rangle t^2}\,.
\end{aligned} \tag{6.108}$$

The expression above has a double pole in t which would be unphysical in an amplitude. However, on the support of $u=0$, we have $s-m^2=-t$. An ansatz for the amplitude is thus

$$\mathcal{A}_4\left(1^{++}, 2^{++}, 3^{--}, 4^{\phi}\right) = \kappa_{2,2,0}\kappa_{2,2,-2}\frac{[12]^6\langle 23\rangle^2\langle 13\rangle^2}{t\,u\,(s-m^2)}\,. \tag{6.109}$$

It can be checked that this correctly reproduces the t- and u-channel residues and has the correct soft limits.

6.8 Appendix: Expressions for various terms in the five-point amplitude

This appendix contains expressions for all the terms in (6.25) written in terms of the variables introduced in (6.77).

$$\begin{aligned}
\mathcal{A}_5^{gr,1,2,(1)} &\equiv \frac{[12]}{\langle 12\rangle}\frac{[34]}{\langle 34\rangle}\frac{[14]}{\langle 14\rangle}\frac{[24]}{\langle 24\rangle}\frac{\langle 3|p_5|4\rangle^2}{s_{24}}\frac{2}{s_{123}} = \frac{\bar z}{z}\frac{\bar z_{13}^2\bar z_{24}^2}{z_{13}^2 z_{24}^2}\epsilon_2\epsilon_3\frac{\tilde\omega_3}{\tilde\omega_2}\frac{2\left(\epsilon_1\tilde\omega_1+\epsilon_2\tilde\omega_2\left(1-\bar z\right)\right)^2}{\hat s} \\
\mathcal{A}_5^{gr,1,2,(2)} &\equiv \frac{[12]}{\langle 12\rangle}\frac{[34]}{\langle 34\rangle}\frac{[14]}{\langle 14\rangle}\frac{[24]}{\langle 24\rangle}\frac{\langle 3|p_5|4\rangle^2}{s_{14}}\frac{2}{s_{123}} = \frac{\bar z}{z}\frac{\bar z_{13}^2\bar z_{24}^2}{z_{13}^2 z_{24}^2}\epsilon_1\epsilon_3\frac{\tilde\omega_3}{\tilde\omega_1}\frac{2\left(\epsilon_1\tilde\omega_1+\epsilon_2\tilde\omega_2\left(1-\bar z\right)\right)^2}{\hat s}
\end{aligned}\tag{6.110}$$

$$\begin{aligned}
\mathcal{A}_5^{gr,1,2,(3)} &\equiv -\frac{[12]}{\langle 12\rangle}\frac{[34]}{\langle 34\rangle}\frac{[14]}{\langle 14\rangle}\frac{[24]}{\langle 24\rangle}\frac{\langle 3|p_5|4\rangle^2}{s_{24}}\frac{s_{34}}{s_{34}-m^2}\frac{1}{s_{123}} = \frac{\bar z}{z}\frac{\bar z_{13}^2\bar z_{24}^2}{z_{13}^2 z_{24}^2}\epsilon_2\frac{\tilde\omega_3^2}{\tilde\omega_2}\frac{\left(\epsilon_1\tilde\omega_1+\epsilon_2\tilde\omega_2\left(1-\bar z\right)\right)^2}{\hat s\epsilon_3\tilde\omega_3+\epsilon_1\tilde\omega_1+\epsilon_2\tilde\omega_2}\frac{\hat s-1}{\hat s} \\
\mathcal{A}_5^{gr,1,2,(4)} &\equiv -\frac{[12]}{\langle 12\rangle}\frac{[34]}{\langle 34\rangle}\frac{[14]}{\langle 14\rangle}\frac{[24]}{\langle 24\rangle}\frac{\langle 3|p_5|4\rangle^2}{s_{14}}\frac{s_{34}}{s_{34}-m^2}\frac{1}{s_{123}} = \frac{\bar z}{z}\frac{\bar z_{13}^2\bar z_{24}^2}{z_{13}^2 z_{24}^2}\epsilon_2\frac{\tilde\omega_3^2}{\tilde\omega_1}\frac{\left(\epsilon_1\tilde\omega_1+\epsilon_2\tilde\omega_2\left(1-\bar z\right)\right)^2}{\hat s\epsilon_3\tilde\omega_3+\epsilon_1\tilde\omega_1+\epsilon_2\tilde\omega_2}\frac{\hat s-1}{\hat s}
\end{aligned}\tag{6.111}$$

$$\begin{aligned}
\mathcal{A}_5^{gr,1,2,(5)} &\equiv -\frac{[12]}{\langle 12\rangle}\frac{[34]}{\langle 34\rangle}\frac{[14]}{\langle 14\rangle}\frac{[24]}{\langle 24\rangle}\frac{\langle 3|p_5|4\rangle^2}{s_{24}}\frac{s_{14}+s_{24}}{s_{14}+s_{24}-m^2}\frac{1}{s_{123}} \\
&= \frac{\bar z}{z}\frac{\bar z_{13}^2\bar z_{24}^2}{z_{13}^2 z_{24}^2}\epsilon_2\epsilon_3\frac{\tilde\omega_3}{\tilde\omega_2}\frac{\left(\epsilon_1\tilde\omega_1+\epsilon_2\tilde\omega_2\left(1-\bar z\right)\right)^2\left(\epsilon_1\tilde\omega_1+\epsilon_2\tilde\omega_2\right)}{\hat s\left(\epsilon_1\tilde\omega_1+\epsilon_2\tilde\omega_2\right)+\epsilon_3\tilde\omega_3}\frac{1-\hat s}{\hat s} \\
\mathcal{A}_5^{gr,1,2,(6)} &\equiv -\frac{[12]}{\langle 12\rangle}\frac{[34]}{\langle 34\rangle}\frac{[14]}{\langle 14\rangle}\frac{[24]}{\langle 24\rangle}\frac{\langle 3|p_5|4\rangle^2}{s_{14}}\frac{s_{14}+s_{24}}{s_{14}+s_{24}-m^2}\frac{1}{s_{123}} \\
&= \frac{\bar z}{z}\frac{\bar z_{13}^2\bar z_{24}^2}{z_{13}^2 z_{24}^2}\epsilon_2\epsilon_3\frac{\tilde\omega_3}{\tilde\omega_1}\frac{\left(\epsilon_1\tilde\omega_1+\epsilon_2\tilde\omega_2\left(1-\bar z\right)\right)^2\left(\epsilon_1\tilde\omega_1+\epsilon_2\tilde\omega_2\right)}{\hat s\left(\epsilon_1\tilde\omega_1+\epsilon_2\tilde\omega_2\right)+\epsilon_3\tilde\omega_3}\frac{1-\hat s}{\hat s}
\end{aligned}\tag{6.112}$$

$$\begin{aligned}
\mathcal{A}_5^{gr,1,2,(7)} &\equiv -\frac{[12]}{\langle 12\rangle}\frac{[34]}{\langle 34\rangle}\frac{[14]}{\langle 14\rangle}\frac{[24]}{\langle 24\rangle}\frac{\langle 3|p_5|4\rangle^2}{s_{24}}\frac{1}{\hat s-1} = \frac{\bar z}{z}\frac{\bar z_{13}^2\bar z_{24}^2}{z_{13}^2 z_{24}^2}\epsilon_2\epsilon_3\frac{\tilde\omega_3}{\tilde\omega_2}\frac{\left(\epsilon_1\tilde\omega_1+\epsilon_2\tilde\omega_2\left(1-\bar z\right)\right)^2}{1-\hat s} \\
\mathcal{A}_5^{gr,1,2,(8)} &\equiv -\frac{[12]}{\langle 12\rangle}\frac{[34]}{\langle 34\rangle}\frac{[14]}{\langle 14\rangle}\frac{[24]}{\langle 24\rangle}\frac{\langle 3|p_5|4\rangle^2}{s_{14}}\frac{1}{\hat s-1} = \frac{\bar z}{z}\frac{\bar z_{13}^2\bar z_{24}^2}{z_{13}^2 z_{24}^2}\epsilon_2\epsilon_3\frac{\tilde\omega_3}{\tilde\omega_2}\frac{\left(\epsilon_1\tilde\omega_1+\epsilon_2\tilde\omega_2\left(1-\bar z\right)\right)^2}{1-\hat s}
\end{aligned}\tag{6.113}$$

$$\begin{aligned}
\mathcal{A}_5^{sc,1,2(1)} &\equiv -\frac{[23][34][24][14]\,\langle 1|p_5|4\rangle^2}{\langle 23\rangle\langle 34\rangle\langle 24\rangle\langle 14\rangle s_{14}}\frac{2}{s_{15}-s_{23}-m^2} \\
&= 2\frac{\bar z_{13}^2\bar z_{24}^2}{z_{13}^2 z_{24}^2}\frac{1-\bar z}{1-z}\left(\bar z\epsilon_2\tilde\omega_2+\epsilon_3\tilde\omega_3\right)^2\frac{\epsilon_1\tilde\omega_1+\epsilon_2\tilde\omega_2+\epsilon_3\tilde\omega_3}{\epsilon_1\tilde\omega_1+\hat s\left(\epsilon_2\tilde\omega_2+\epsilon_3\tilde\omega_3\right)} \\
\mathcal{A}_5^{sc,1,2(2)} &\equiv \frac{[23][34][24][14]\,\langle 1|p_5|4\rangle^2}{\langle 23\rangle\langle 34\rangle\langle 24\rangle\langle 14\rangle s_{14}}\frac{2}{s_{15}-m^2} \\
&= -2\frac{\bar z_{13}^2\bar z_{24}^2}{z_{13}^2 z_{24}^2}\frac{1-\bar z}{1-z}\left(\bar z\epsilon_2\tilde\omega_2+\epsilon_3\tilde\omega_3\right)^2\epsilon_1\tilde\omega_1\frac{\epsilon_1\tilde\omega_1+\epsilon_2\tilde\omega_2+\epsilon_3\tilde\omega_3}{1+|z|\,\tilde\omega_2^2+\left(z+\bar z\right)\epsilon_2\epsilon_3\tilde\omega_2\tilde\omega_3+\tilde\omega_3^2}
\end{aligned}\tag{6.114}$$

$$\begin{aligned}
\mathcal{A}_5^{sc,1,2(3)} &\equiv \frac{[23][34][24][14]\,[1|p_5|4\rangle^2}{\langle 23\rangle\langle 34\rangle\langle 24\rangle\langle 14\rangle s_{14}} \frac{1}{s_{15}-s_{23}-m^2} \frac{s_{34}}{s_{34}-m^2} \\
&= \frac{\bar{z}_{13}^2\bar{z}_{24}^2}{z_{13}^2 z_{24}^2} \frac{1-\bar{z}}{1-z} \frac{\epsilon_3\tilde{\omega}_3 \left(\bar{z}\epsilon_2\tilde{\omega}_2+\epsilon_3\tilde{\omega}_3\right)^2 \left(\epsilon_1\tilde{\omega}_1+\epsilon_2\tilde{\omega}_2+\epsilon_3\tilde{\omega}_3\right)(1-\hat{s})}{\left(\epsilon_1\tilde{\omega}_1+\hat{s}\left(\epsilon_2\tilde{\omega}_2+\epsilon_3\tilde{\omega}_3\right)\right)\left(\hat{s}\epsilon_3\tilde{\omega}_3+\epsilon_1\tilde{\omega}_1+\epsilon_2\tilde{\omega}_2\right)} \\
\mathcal{A}_5^{sc,1,2(4)} &\equiv -\frac{[23][34][24][14]\,[1|p_5|4\rangle^2}{\langle 23\rangle\langle 34\rangle\langle 24\rangle\langle 14\rangle s_{14}} \frac{1}{s_{15}-m^2} \frac{s_{34}}{s_{34}-m^2} \\
&= -\frac{\bar{z}_{13}^2\bar{z}_{24}^2}{z_{13}^2 z_{24}^2} \frac{1-\bar{z}}{1-z} \frac{\left(\bar{z}\epsilon_2\tilde{\omega}_2+\epsilon_3\tilde{\omega}_3\right)^2 \epsilon_1\epsilon_3\tilde{\omega}_1\tilde{\omega}_3 \left(\epsilon_1\tilde{\omega}_1+\epsilon_2\tilde{\omega}_2+\epsilon_3\tilde{\omega}_3\right)(1-\hat{s})}{\left(1+|z|^2\tilde{\omega}_2^2+(z+\bar{z})\,\epsilon_2\epsilon_3\tilde{\omega}_2\tilde{\omega}_3+\tilde{\omega}_3^2\right)\left(\hat{s}\epsilon_3\tilde{\omega}_3+\epsilon_1\tilde{\omega}_1+\epsilon_2\tilde{\omega}_2\right)}
\end{aligned} \tag{6.115}$$

$$\begin{aligned}
\mathcal{A}_5^{sc,1,2(5)} &\equiv \frac{[23][34][24][14]\,[1|p_5|4\rangle^2}{\langle 23\rangle\langle 34\rangle\langle 24\rangle\langle 14\rangle s_{14}} \frac{1}{s_{15}-s_{23}-m^2} \frac{s_{123}+s_{14}}{s_{123}+s_{14}-m^2} \\
&= -\frac{\bar{z}_{13}^2\bar{z}_{24}^2}{z_{13}^2 z_{24}^2} \frac{1-\bar{z}}{1-z} \left(\bar{z}\epsilon_2\tilde{\omega}_2+\epsilon_3\tilde{\omega}_3\right)^2 \frac{\epsilon_1\tilde{\omega}_1+\epsilon_2\tilde{\omega}_2+\epsilon_3\tilde{\omega}_3}{\left(\epsilon_2\tilde{\omega}_2+\epsilon_3\tilde{\omega}_3\right)(\hat{s}-1)} \\
\mathcal{A}_5^{sc,1,2(6)} &\equiv -\frac{[23][34][24][14]\,[1|p_5|4\rangle^2}{\langle 23\rangle\langle 34\rangle\langle 24\rangle\langle 14\rangle s_{14}} \frac{1}{s_{15}-m^2} \frac{s_{123}+s_{14}}{s_{123}+s_{14}-m^2} \\
&= \frac{\bar{z}_{13}^2\bar{z}_{24}^2}{z_{13}^2 z_{24}^2} \frac{1-\bar{z}}{1-z} \frac{\left(\bar{z}\epsilon_2\tilde{\omega}_2+\epsilon_3\tilde{\omega}_3\right)^2 \epsilon_1\tilde{\omega}_1 \left(\epsilon_1\tilde{\omega}_1+\epsilon_2\tilde{\omega}_2+\epsilon_3\tilde{\omega}_3\right)\left(\epsilon_1\tilde{\omega}_1+\hat{s}\left(\epsilon_2\tilde{\omega}_2+\epsilon_3\tilde{\omega}_3\right)\right)}{\left(1+|z|^2\tilde{\omega}_2^2+(z+\bar{z})\,\epsilon_2\epsilon_3\tilde{\omega}_2\tilde{\omega}_3+\tilde{\omega}_3^2\right)\left(\epsilon_2\tilde{\omega}_2+\epsilon_3\tilde{\omega}_3\right)(\hat{s}-1)}
\end{aligned} \tag{6.116}$$

$$\begin{aligned}
\mathcal{A}_5^{sc,1,2(7)} &\equiv \frac{[23][34][24][14]\,[1|p_5|4\rangle^2}{\langle 23\rangle\langle 34\rangle\langle 24\rangle\langle 14\rangle s_{14}} \frac{1}{s_{15}-s_{23}-m^2} \frac{s_{24}}{s_{24}-m^2} \\
&= \frac{\bar{z}_{13}^2\bar{z}_{24}^2}{z_{13}^2 z_{24}^2} \frac{1-\bar{z}}{1-z} \frac{\left(\epsilon_1\tilde{\omega}_1+\epsilon_2\tilde{\omega}_2+\epsilon_3\tilde{\omega}_3\right)\left(\bar{z}\epsilon_2\tilde{\omega}_2+\epsilon_3\tilde{\omega}_3\right)^2 \epsilon_2\tilde{\omega}_2 (1-\hat{s})}{\epsilon_1\tilde{\omega}_1+\hat{s}\left(\epsilon_2\tilde{\omega}_2+\epsilon_3\tilde{\omega}_3\right)\left(\epsilon_2\tilde{\omega}_2\hat{s}+\epsilon_1\tilde{\omega}_1+\epsilon_3\tilde{\omega}_3\right)} \\
\mathcal{A}_5^{sc,1,2(8)} &\equiv -\frac{[23][34][24][14]\,[1|p_5|4\rangle^2}{\langle 23\rangle\langle 34\rangle\langle 24\rangle\langle 14\rangle s_{14}} \frac{1}{s_{15}-m^2} \frac{s_{24}}{s_{24}-m^2} \\
&= -\frac{\bar{z}_{13}^2\bar{z}_{24}^2}{z_{13}^2 z_{24}^2} \frac{1-\bar{z}}{1-z} \frac{\left(\bar{z}\epsilon_2\tilde{\omega}_2+\epsilon_3\tilde{\omega}_3\right)^2 \epsilon_1\epsilon_2\tilde{\omega}_1\tilde{\omega}_2 \left(\epsilon_1\tilde{\omega}_1+\epsilon_2\tilde{\omega}_2+\epsilon_3\tilde{\omega}_3\right)(1-\hat{s})}{1+|z|^2\tilde{\omega}_2^2+(z+\bar{z})\,\epsilon_2\epsilon_3\tilde{\omega}_2\tilde{\omega}_3+\tilde{\omega}_3^2\left(\epsilon_2\tilde{\omega}_2\hat{s}+\epsilon_1\tilde{\omega}_1+\epsilon_3\tilde{\omega}_3\right)}\ .
\end{aligned} \tag{6.117}$$

6.9 Appendix: Reduction of $\mathcal{J}_{\mathcal{R}_4}$ to a Mellin-Barnes integral

Start by changing variables to $\tilde{\omega}_1 = \tilde{\omega}_3 X, \tilde{\omega}_2 = \tilde{\omega}_3 Y$. This transforms (6.86) to

$$\begin{aligned}
\mathcal{J}_{\mathcal{R}_4} = \int_0^\infty dY \int_{1+Y}^\infty dX\, X^A\, Y^B\, (X-Y-1)^\rho \\
\int_0^\infty d\tilde{\omega}_3\, \tilde{\omega}_3^{A+B+C+2+\rho} \left[1+\tilde{\omega}_3^2\left(|z|^2 XY + X - Y\,|1-z|^2\right)\right]^\delta\ .
\end{aligned} \tag{6.118}$$

We pause here to draw attention to the fact that the integral is well-defined as the integrand is strictly positive in the integration domain. The $\tilde{\omega}_3$ integral evaluates to

$$\int_0^\infty d\tilde{\omega}_3\, \tilde{\omega}_3^{A+B+C+2+\rho} \left[1 + \tilde{\omega}_3^2 \left(|z|^2 XY + X - Y\,|1-z|^2\right)\right]^\delta$$
$$= \mathcal{G}_1 \left(|z|^2 XY + X - Y\,|1-z|^2\right)^{-\frac{1}{2}(3+A+B+C+\rho)} \, , \quad (6.119)$$

with

$$\mathcal{G}_1 = \frac{1}{2\Gamma(-\delta)} \Gamma\left(-\frac{1}{2}(3+A+B+C+\rho+2\delta)\right)\Gamma\left(\frac{1}{2}(3+A+B+C+\rho)\right) \, . \quad (6.120)$$

After this, (6.86) reads,

$$\mathcal{J}_{\mathcal{R}_4} = \mathcal{G}_1 \int_0^\infty dY \int_{1+Y}^\infty dX\, X^A Y^B\, (X-Y-1)^\rho \left(|z|^2 XY + X - Y\,|1-z|^2\right)^{-\frac{1}{2}(3+A+B+C+\rho)} \, . \quad (6.121)$$

The evaluation of the integral over X is expedited by the further change of variables, $t = \frac{-1+X-Y}{X-Y}$ as seen below:

$$\mathcal{J}_{\mathcal{R}_4} = \mathcal{G}_1 \int_0^\infty dY\, Y^B\, (1+Y)^A\, w_2^{-\frac{3+A+B+C+\rho}{2}}$$
$$\times \int_0^1 dt\, t^\rho\, (1-t)^{-\frac{1+A+\rho-B-C}{2}} \left(1 - \frac{Y}{Y+1} t\right)^A \left(1 + \frac{w_1}{w_2} t\right)^{-\frac{3+A+B+C+\rho}{2}} \, . \quad (6.122)$$

Here, $w_1 = Y(1-Y)\,|z|^2 - 2Y\, Re(z)$, $w_2 = 1 + Y^2\,|z|^2 + 2Y\, Re(z)$. We can recognize the integral over t as a representation of the Appell F_1 function and write

$$\int_0^1 dt\, t^\rho\, (1-t)^{-\frac{1+A+\rho-B-C}{2}} \left(1 - \frac{Y}{Y+1} t\right)^A \left(1 + \frac{w_1}{w_2} t\right)^{-\frac{3+A+B+C+\rho}{2}}$$
$$= \mathcal{G}_2\, F_1\left(\rho+1; -A, \frac{3+A+B+C+\rho}{2}; \frac{3-A+B+C+\rho}{2}; \frac{Y}{Y+1}, -\frac{w_1}{w_2}\right)$$
$$= \mathcal{G}_2 \left(\frac{w_1+w_2}{w_2}\right)^{-1-\rho} {}_2F_1\left(-A, 1+\rho, \frac{1}{2}(3-A+B+C+\rho), \frac{w_1 + Y(w_1+w_2)}{(w_1+w_2)(1+Y)}\right), \quad (6.123)$$

with $\mathcal{G}_2 = \frac{\Gamma(\rho+1)\Gamma\left(\frac{1-A+B+C-\rho}{2}\right)}{\Gamma\left(\frac{3-A+B+C+\rho}{2}\right)}$ and we have used an identity of the Appell F_1 in arriving at the final equality. Plugging in the values of w_1, w_2, we see that the argument of the hypergeometric ${}_2F_1$

$$0 < \frac{w_1 + Y(w_1+w_2)}{(w_1+w_2)(1+Y)} = \frac{Y\,|1-z|^2}{(1+y)(1+y\,|z|^2)} < 1 \, . \quad (6.124)$$

This allows us to use the relevant Mellin-Barnes representation of the Gauss hypergeometric function,

$${}_2F_1(a,b,c,z) = \frac{\Gamma(c)}{2\pi i \Gamma(a)\Gamma(b)\Gamma(c-a)\Gamma(c-b)}$$
$$\times \int ds\, \Gamma(-s)\Gamma(c-a-b-s)\Gamma(a+s)\Gamma(b+s)\,(1-z)^s \, . \quad (6.125)$$

In applying this formula, we introduce a new Mellin variable x_{r+1} in addition to the $x_1, \ldots, x_r$ introduced in (6.85). Thus,

$$\mathcal{J}_{\mathcal{R}_4} = \int dx_{r+1}\, \mathcal{G}_3\left(x_{r+1}\right) \int_0^\infty dY\, Y^B \left(1+Y\right)^{A-x_{r+1}} \left(1+y\,|z|^2\right)^{-1-\rho-x_{r+1}} \times \left(1+y\,z\right)^{-\frac{1}{2}(1+A+B+C-\rho-x_{r+1})} \left(1+y\,\bar{z}\right)^{-\frac{1}{2}(1+A+B+C-\rho-x_{r+1})} \;, \quad (6.126)$$

where

$$\mathcal{G}_3\left(x_{r+1}\right) = \Gamma(-x_{r+1})\,\Gamma\left(-x_{r+1} + \frac{1}{2}(A+B+C-\rho)\right)\Gamma(-A+x_{r+1}) \times \Gamma(\rho+1+x_{r+1})\frac{\Gamma\left(\frac{1}{2}(3+A+B+C+\rho+2\delta)\right)}{2\Gamma(-A)\Gamma(-\delta)} \;. \quad (6.127)$$

A final change of variables $Y = \frac{\eta}{1-\eta}$ turns the integral into

$$\mathcal{J}_{\mathcal{R}_4} = \int dx_{r+1}\, \mathcal{G}_3\left(x_{r+1}\right) \int_0^1 d\eta\, \eta^B \left(1-\eta\right)^{x_{r+1}+C} \left(1-\left(1-|z|^2\right)\eta\right)^{-1-\rho-x_{r+1}} \times \left(1-\eta\left(1-z\right)\right)^{-\frac{1}{2}(1+A+B+C-\rho-x_{r+1})} \left(1-\eta\left(1-\bar{z}\right)\right)^{-\frac{1}{2}(1+A+B+C-\rho-x_{r+1})} \;, \quad (6.128)$$

which can immediately be recognized as the integral representation of a type D Lauricella function,

$$\mathcal{J}_{\mathcal{R}_4} = \int dx_{r+1}\, \mathcal{G}_4\left(x_{r+1}\right) F_D^{(3)}\left(a_1; b_1, b_2, b_3, c_1; 1-z, 1-\bar{z}, 1-|z|^2\right) \;, \quad (6.129)$$

where

$$\begin{aligned} \mathcal{G}_4\left(x_{r+1}\right) &= \mathcal{G}_3\left(x_{r+1}\right) \frac{\Gamma\left(B+1\right)\Gamma\left(-x_{r+1}+C+1\right)}{\Gamma\left(-x_{r+1}+B+C+2\right)} \;, \\ a_1 &= B+1, \quad b_1 = b_2 = \frac{1}{2}\left(1+A+B+C-\rho-x_{r+1}\right) \;, \\ b_3 &= 1+\rho-x_{r+1}, \quad c_1 = -x_{r+1}+B+C+2 \;. \end{aligned} \quad (6.130)$$

To complete the reduction, we now use the Mellin-Barnes representation of the Lauricella function [231]

$$F_D^{(m)}\left(a_1; b_m, \ldots, b_m; c_1, x_1, \ldots, x_m\right) = \left(\frac{1}{2\pi i}\right)^m \int \prod_{i=1}^m dt_i\, \Gamma\left(-t_i\right)\left(-x_i\right)^{t_i} \frac{\Gamma\left(c_1\right)\Gamma\left(a_1+\sum_{i=1}^m t_i\right)\prod_{i=1}^m \Gamma\left(b_i+t_i\right)}{\Gamma\left(a\right)\Gamma\left(c_1+\sum_{i=1}^m t_i\right)\prod_{i=1}^m \Gamma\left(b_i\right)} \;, \quad (6.131)$$

to get the final Mellin-Barnes form

$$\mathcal{J}_{\mathcal{R}_4} = \int \prod_{i=1}^4 dx_{r+i}\, \mathcal{G}\left(x_{r+1}, \ldots, x_{r+4}\right)\left(z-1\right)^{x_{r+2}}\left(\bar{z}-1\right)^{x_{r+3}}\left(1-|z|^2\right)^{x_{r+4}} \;, \quad (6.132)$$

with

$$\mathcal{G}\left(x_{r+1}, \ldots, x_{r+4}\right) = \left[\prod_{i=1}^4 \Gamma\left(-x_{r+i}\right)\right] \frac{\Gamma\left(a_1+\sum_{i=2}^4 x_{r+i}\right)}{\Gamma\left(c_1+\sum_{i=2}^4 x_{r+i}\right)} \left[\prod_{i=2}^4 \frac{\Gamma\left(b_1+x_{r+i}\right)}{\Gamma\left(b_i\right)}\right] \Gamma\left(c_1-a_1\right)\mathcal{G}_3 \;. \quad (6.133)$$

Chapter 7

Correlators of Four Light-ray Operators in CCFT

This chapter is based on the work [214].

Light-ray operators appear in Lorentzian CFTs [232, 233, 234] in general, and in celestial CFT (CCFT) in particular [43, 44]. Their role in CCFT is tied fundamentally to the problem of finding a suitable basis of operators. It was shown in [45] that certain three-point correlators involving light-ray operators take the form of standard three-point CFT correlators. This is in contrast to the distributional nature of CCFT three-point functions [24]. These operators were further studied and their contribution to the OPE of CCFT primaries was identified in [235]. It was also noted in [45] that the light transform is related to Witten's half Fourier transform and particularly the conformal primary twistor eigenstate can be written as a linear combination of light transformed boost eigenstates. Moreover, the light transform unravels symmetries of CCFT. In a single helicity sector, the symmetry algebra for gravity is enhanced beyond the asymptotic analysis to include a $w_{1+\infty}$ symmetry. In [46], Strominger recognized that the $w_{1+\infty}$ mode is essentially the light transform of the soft current mode. Furthermore, light-ray operators seem to be generically exchanged in CCFT as shown by the conformal block decomposition in [44]. To gain a better understanding of the role played by light-ray operators in CCFT, the computation of correlators involving light-ray operators is essential and is the theme of the current paper.

Four-point correlators involving one and two gluon light-ray operators were computed in [47, 48]. They are non-distributional and correctly reproduce the contribution of light-ray operators to the OPE. This contribution is invisible from the collinear limits of the four-point celestial amplitude. In this paper, we build on our results from [47] and compute correlators of four gluon light-ray operators. We find that they can be expressed in terms of Fox H-functions [236, 237, 238, 239, 240] and generalized I-functions [241, 242]. We also analyze scalar amplitudes involving the exchange of a massive scalar.

The paper is organized as follows. In Section 7.1, we compute the four light-ray gluon correlator.

We flesh out the computation of light-ray correlators involving the exchange of a massive scalar in Section 7.2. The paper ends with a number of appendices which contain technical details of some computations as well as a variety of other results. Appendices 7.3.1 and 7.3.2 are devoted to providing explicit expressions for various integrals used throughout the paper. Appendix 7.4 defines the relevant special functions. Appendix 7.5 describes the technical details involved in the evaluation of the four gluon light transform. Appendix 7.6 contains the derivation of various OPEs from the collinear limits of the scalar light-ray correlator. Finally, Appendix 7.7 describes the conformal block decomposition of the scalar light-ray correlator.

7.1 Four light-ray correlator for gluons

Light-ray operators are naturally defined in a Lorentzian CFT which is achieved by working in a (2,2) signature bulk spacetime [42]. We start with the four-point gluon celestial amplitude in this spacetime, which was first computed in [47] (the analogous result in a (3,1) signature bulk spacetime was first computed in [24]) [1]

$$\begin{aligned}&\langle\mathcal{O}_{\Delta_1,-}(z_1,\bar{z}_1)\mathcal{O}_{\Delta_2,-}(z_2,\bar{z}_2)\,\mathcal{O}_{\Delta_3,+}(z_3,\bar{z}_3)\mathcal{O}_{\Delta_4,+}(z_4,\bar{z}_4)\rangle\\&\quad=\ \pi\,\mathrm{d}(\beta)\delta(z-\bar{z})\mathrm{sgn}\left(\frac{z}{z-1}\right)|z|^3\,|1-z|^{1-\Delta_2-\Delta_3}\,X\left(z_{ij},\bar{z}_{ij}\right)\ ,\end{aligned}\tag{7.1}$$

where [2]

$$\begin{aligned}X(z_{ij},\bar{z}_{ij})\ &=\ \frac{1}{|z_{12}|^{h_1+h_2}|z_{34}|^{h_3+h_4}}\left|\frac{z_{24}}{z_{14}}\right|^{h_{12}}\left|\frac{z_{14}}{z_{13}}\right|^{h_{34}}\frac{1}{|\bar{z}_{12}|^{\bar{h}_1+\bar{h}_2}|\bar{z}_{34}|^{\bar{h}_3+\bar{h}_4}}\left|\frac{\bar{z}_{24}}{\bar{z}_{14}}\right|^{\bar{h}_{12}}\left|\frac{\bar{z}_{14}}{\bar{z}_{13}}\right|^{\bar{h}_{34}}\ ,\\h_i\ &=\ \frac{\Delta_i+J_i}{2}\quad,\quad\bar{h}_i\ =\ \frac{\Delta_i-J_i}{2}\quad,\quad h_{ij}\ =\ h_i-h_j\quad,\quad\bar{h}_{ij}\ =\ \bar{h}_i-\bar{h}_j\quad,\end{aligned}\tag{7.2}$$

and

$$\begin{aligned}z_{ij}\ &=\ z_i-z_j\quad,\quad\bar{z}_{ij}\ =\ \bar{z}_i-\bar{z}_j\quad,\quad z\ =\ \frac{z_{12}z_{34}}{z_{13}z_{24}}\quad,\\J_1\ &=\ J_2=-J_3=-J_4=-1\quad,\quad\beta\ =\ \sum_{i=1}^{4}\Delta_i-4\quad.\end{aligned}\tag{7.3}$$

[1] For readers not familiar with the celestial holography program and celestial amplitudes, we briefly recap the setup in this footnote. Generally, the boundary operator $\mathcal{O}^{\epsilon}_{\Delta,J}(z,\bar{z})$ is defined by taking the inner product of the bulk spin-s operator $\hat{\mathcal{O}}^s$ and the conformal primary wavefunction defined on a Cauchy slice [243], that is $\mathcal{O}^{\pm}_{\Delta,J}(z,\bar{z})=i(\hat{\mathcal{O}}^s(X^\mu),\Phi_{\Delta,J}(X^\mu_{\mp};z,\bar{z}))_\Sigma$, and we take the Cauchy slice to null infinity. The ϵ labels the incoming and outgoing modes. These operators can be interpreted as conformal primaries in celestial CFT with conformal dimension Δ and spin J. For massless particles, the correlation functions in celestial CFT, also called celestial amplitudes, can be computed by Mellin transforms of momentum space amplitudes [24]. The 2D spin J is identical to the 4D helicity. In this paper, we further adopt the definition $\mathcal{O}\sim\mathcal{O}^{\mathrm{in}}+\mathcal{O}^{\mathrm{out}}$ for the same reason as in [47].

[2] Note that we are using a slightly different pre-factor in this paper. We can compare the two using the equation $\prod_{i<j}|z_{ij}|^{\frac{h}{3}-h_i-h_j}\,|\bar{z}_{ij}|^{\frac{\bar{h}}{3}-\bar{h}_i-\bar{h}_j}=X\left(z_{ij},\bar{z}_{ij}\right)|z|^{\frac{h}{3}}\,|\bar{z}|^{\frac{\bar{h}}{3}}\,|1-z|^{\frac{h}{3}-h_2-h_3}\,|1-\bar{z}|^{\frac{\bar{h}}{3}-\bar{h}_2-\bar{h}_3}$.

Light-ray operators are defined by

$$\begin{aligned}\mathbf{L}[\mathcal{O}_{\Delta,J}](z,\bar{z}) &:= \int_{-\infty}^{\infty} \frac{dz'}{|z'-z|^{2-\Delta-J}}\, \mathcal{O}_{\Delta,J}(z',\bar{z})\ , \\ \bar{\mathbf{L}}[\mathcal{O}_{\Delta,J}](z,\bar{z}) &:= \int_{-\infty}^{\infty} \frac{d\bar{z}'}{|\bar{z}'-\bar{z}|^{2-\Delta+J}}\, \mathcal{O}_{\Delta,J}(z,\bar{z}')\ .\end{aligned} \tag{7.4}$$

We will refer to these as the "holomorphic" and "anti-holomorphic" light-ray operators respectively. Note that the conformal weights of $\mathbf{L}[\mathcal{O}_{\Delta,J}]$ are $\left(1-\frac{\Delta+J}{2}, \frac{\Delta-J}{2}\right)$ and those of $\bar{\mathbf{L}}[\mathcal{O}_{\Delta,J}]$ are $\left(\frac{\Delta+J}{2}, 1-\frac{\Delta-J}{2}\right)$.

In this section, we will compute the correlator involving two holomorphic and two anti-holomorphic light-ray operators

$$\begin{aligned}&\langle \bar{\mathbf{L}}[\mathcal{O}_{\Delta_1,-}](z_1,\bar{z}_1)\, \bar{\mathbf{L}}[\mathcal{O}_{\Delta_2,-}](z_2,\bar{z}_2)\, \mathbf{L}[\mathcal{O}_{\Delta_3,+}](z_3,\bar{z}_3)\, \mathbf{L}[\mathcal{O}_{\Delta_4,+}](z_4,\bar{z}_4)\rangle \\ &= \int_{-\infty}^{\infty} \frac{d\bar{z}_1'}{|\bar{z}_1'-\bar{z}_1|^{1-\Delta_1}} \frac{d\bar{z}_2'}{|\bar{z}_2'-\bar{z}_2|^{1-\Delta_2}} \frac{dz_3'}{|z_3'-z_3|^{1-\Delta_3}} \frac{dz_4'}{|z_4'-z_4|^{1-\Delta_4}} \\ &\qquad \times \langle \mathcal{O}_{\Delta_1,-}(z_1,\bar{z}_1')\mathcal{O}_{\Delta_2,-}(z_2,\bar{z}_2')\, \mathcal{O}_{\Delta_3,+}(z_3',\bar{z}_3)\mathcal{O}_{\Delta_4,+}(z_4',\bar{z}_4)\rangle\ .\end{aligned} \tag{7.5}$$

After performing the $\bar{z}_1'$ integral using the delta function in (7.1) and changing variables to

$$t \;=\; \frac{\bar{z}_{12'}\,\bar{z}_{34}}{\bar{z}_{13}\,\bar{z}_{2'4}}\ , \quad x \;=\; \frac{z_{12}\,z_{3'4'}}{z_{13'}\,z_{24'}}\ , \quad y \;=\; \frac{z_{12}\,z_{34'}}{z_{13}\,z_{24'}}\ , \tag{7.6}$$

we end up with

$$\begin{aligned}&\langle \bar{\mathbf{L}}[\mathcal{O}_{\Delta_1,-}](z_1,\bar{z}_1)\, \bar{\mathbf{L}}[\mathcal{O}_{\Delta_2,-}](z_2,\bar{z}_2)\, \mathbf{L}[\mathcal{O}_{\Delta_3,+}](z_3,\bar{z}_3)\, \mathbf{L}[\mathcal{O}_{\Delta_4,+}](z_4,\bar{z}_4)\rangle \\ &= \pi\,\delta(\beta)\,X(z_{ij},\bar{z}_{ij})\,\left|\frac{z}{\bar{z}}\right|^{\frac{\Delta_1+\Delta_2-2}{2}} |1-z|^{2-\Delta_2-\Delta_4}\,\mathcal{G}(z,\bar{z})\ .\end{aligned} \tag{7.7}$$

The pre-factor X now involves the conformal weights of the light-ray operators which are

$$\begin{aligned}(h_1,\bar{h}_1) &= \left(\frac{\Delta_1-1}{2}, \frac{1-\Delta_1}{2}\right)\ , \quad (h_2,\bar{h}_2) = \left(\frac{\Delta_2-1}{2}, \frac{1-\Delta_2}{2}\right)\ , \\ (h_3,\bar{h}_3) &= \left(\frac{1-\Delta_3}{2}, \frac{\Delta_3-1}{2}\right)\ , \quad (h_4,\bar{h}_4) = \left(\frac{1-\Delta_4}{2}, \frac{\Delta_4-1}{2}\right)\ ,\end{aligned} \tag{7.8}$$

and

$$\begin{aligned}\mathcal{G}(z,\bar{z}) \;:=\; \int_{-\infty}^{\infty} dt\,dx\,dy\,\frac{1}{x\,(x-1)}&|\bar{z}-t|^{\Delta_2-1}\,|y-z|^{\Delta_4-1}\,|1-t|^{\Delta_4-2}\,|x-t|^{\Delta_1-1} \\ &\times |x-y|^{\Delta_3-1}\,|y-1|^{\Delta_2-2}\ .\end{aligned} \tag{7.9}$$

Our strategy to compute this integral is to first reduce it to an integral over the product of the following four-marked point integrals:

$$\mathcal{F}_1(z,x) = \int_{-\infty}^{\infty} dy\,|y-z|^{\Delta_4-1}|x-y|^{\Delta_3-1}|y-1|^{\Delta_2-2}\ , \tag{7.10}$$

$$\mathcal{F}_2(x,\bar{z}) = \int_{-\infty}^{\infty} dt\,|x-t|^{\Delta_1-1}|1-t|^{\Delta_4-2}|\bar{z}-t|^{\Delta_2-1}\ . \tag{7.11}$$

These integrals were first encountered in the evaluation of correlators with two light-ray operators in [47] and can be expressed in terms of Gauss hypergeometric functions. For a complete description of these results, we refer the reader to Appendix 7.3.1. The desired form for $\mathcal{G}(z,\bar{z})$ is

$$\mathcal{G}(z,\bar{z}) = \int_{-\infty}^{\infty} \frac{dx}{x(x-1)}\,\mathcal{F}_1(z,x)\,\mathcal{F}_2(x,\bar{z})\ . \tag{7.12}$$

For simplicity, we will focus on the case $z, \bar{z} \in [0,1]$ for which the x integral splits into two regions: [3]

$$\begin{aligned}
\mathcal{G}(z,\bar{z}) \;&=\; \mathcal{G}(z,\bar{z})\Big|_{\mathrm{I}} + \mathcal{G}(z,\bar{z})\Big|_{\mathrm{II}} \\
&=\; \int_{-\infty}^{1} dx\,\frac{1}{x(x-1)}\,\mathcal{F}_1(z,x)|_{x,z<1}\,\mathcal{F}_2(x,\bar{z})|_{x,\bar{z}<1} \\
&\quad+\int_{1}^{\infty} dx\,\frac{1}{x(x-1)}\,\mathcal{F}_1(z,x)|_{z<1<x}\,\mathcal{F}_2(x,\bar{z})|_{\bar{z}<1<x}\ .
\end{aligned} \tag{7.13}$$

The integrals can be explicitly evaluated in terms of Fox H-functions [236, 237, 238, 239, 240] and I-functions [241, 242] which are special functions belonging to a general class of Mellin-Barnes integrals. Here, we flesh out the evaluation of $\mathcal{G}(z,\bar{z})\big|_{\mathrm{II}}$ and refer the reader to Appendix 7.4 for more details of these special functions and to Appendix 7.5 for the evaluation of $\mathcal{G}(z,\bar{z})\big|_{\mathrm{I}}$ (the details heavily rely on the ordering we choose for x, z, and $\bar{z}$).

7.1.1 Evaluation of $\mathcal{G}(z,\bar{z})\big|_{\mathrm{II}}$

Evaluating $\mathcal{G}(z,\bar{z})\big|_{\mathrm{II}}$using the definitions of $\mathcal{F}_1(z,x)$ and $\mathcal{F}_2(x,\bar{z})$ in (7.34) and (7.36) results in a sum of four integrals, one of which is

$$\begin{aligned}
\mathcal{G}(z,\bar{z})\big|_{\mathrm{II}} \supset \int_{1}^{\infty} \frac{dx}{x\,(x-1)}\,(1-\bar{z})^{1-\Delta_3}\,(1-z)^{1-\Delta_1}\,C\left(\Delta_4,\Delta_1-1\right)\,C\left(\Delta_2,\Delta_3-1\right)& \\
\times\,{}_2F_1\left(1-\Delta_3,\Delta_1-1,\Delta_4+\Delta_1-1,\frac{1-x}{1-z}\right)& \\
\times\,{}_2F_1\left(1-\Delta_1,\Delta_3-1,\Delta_2+\Delta_3-1,\frac{1-x}{1-\bar{z}}\right)&,
\end{aligned} \tag{7.14}$$

where we've eliminated the absolute value signs keeping in mind that we're working in the region $0 < z, \bar{z} < 1 < x$. We then use the Mellin-Barnes representation of the Gauss hypergeometric function

$${}_2F_1[a,b,c;-|z|] = \frac{1}{2\pi i}\frac{\Gamma(c)}{\Gamma(a)\Gamma(b)}\int_{-i\infty}^{i\infty} ds\,\frac{\Gamma(-s)\Gamma(a+s)\Gamma(b+s)}{\Gamma(c+s)}\,|z|^s\ , \tag{7.15}$$

[3]The x-integral in $\mathcal{G}$ function (7.12) seems to contain singularities at $x = 0$ and $x = 1$ and require prescriptions. However, this is not needed since after splitting the integration range the x-integrals reduce to standard Euler Beta/Gauss ${}_2F_1$ hypergeometric/Appell F_1 functions.

to obtain

$$\begin{aligned}\mathcal{G}(z,\bar{z})\big|_{\mathrm{II}} \supset \frac{1}{(2\pi i)^2}\,(1-\bar{z})^{1-\Delta_3}\,(1-z)^{1-\Delta_1}\,C\left(\Delta_4,\Delta_1-1\right)C\left(\Delta_2,\Delta_3-1\right)\\ \times\int_{-i\infty}^{i\infty} ds_1 \frac{\Gamma\left(\Delta_4+\Delta_1-1\right)}{\Gamma\left(1-\Delta_3\right)\Gamma\left(\Delta_1-1\right)}\frac{\Gamma\left(-s_1\right)\Gamma\left(1-\Delta_3+s_1\right)\Gamma\left(\Delta_1-1+s_1\right)}{\Gamma\left(\Delta_4+\Delta_1-1+s_1\right)}(1-z)^{-s_1}\\ \times\int_{-i\infty}^{i\infty} ds_2 \frac{\Gamma\left(\Delta_2+\Delta_3-1\right)}{\Gamma\left(1-\Delta_1\right)\Gamma\left(\Delta_3-1\right)}\frac{\Gamma\left(-s_2\right)\Gamma\left(1-\Delta_1+s_2\right)\Gamma\left(\Delta_3-1+s_2\right)}{\Gamma\left(\Delta_2+\Delta_3-1+s_2\right)}(1-\bar{z})^{-s_2}\\ \times\int_1^{\infty} dx\,x^{-1}\,(x-1)^{-1+s_1+s_2}\ .\end{aligned} \tag{7.16}$$

The x-integral evaluates to $B\left(s_1+s_2,1-s_1-s_2\right)$ and comparing with equations (7.42), (7.43), we can identify the residual double Mellin-Barnes to be

$$\begin{aligned}&\frac{1}{(2\pi i)^2}\int_{-i\infty}^{i\infty} ds_1\,ds_2\,\left[\Gamma\left(1-s_1-s_2\right)\Gamma\left(s_1+s_2\right)\right]\times\left[\frac{\Gamma\left(-s_1\right)\Gamma\left(1-\Delta_3+s_1\right)\Gamma\left(\Delta_1-1+s_1\right)}{\Gamma\left(\Delta_4+\Delta_1-1+s_1\right)}\right]\\ &\qquad\times\left[\frac{\Gamma\left(-s_2\right)\Gamma\left(1-\Delta_1+s_2\right)\Gamma\left(\Delta_3-1+s_2\right)}{\Gamma\left(\Delta_2+\Delta_3-1+s_2\right)}\right]\times(1-\bar{z})^{-s_2}\,(1-z)^{-s_1}\\ &=\mathrm{H}^{1,1:\,2,1;\,2,1}_{1,1:\,2,2;\,2,2}\left(\begin{array}{c|c} 1-z & (0,1):\,(1,\Delta_1+\Delta_4-1,1,1);\,(1,\Delta_2+\Delta_3-1,1,1)\\ 1-\bar{z} & (0,1):\,(1-\Delta_3,\Delta_1-1,1,1);\,(1-\Delta_1,\Delta_3-1,1,1)\end{array}\right)\ .\end{aligned} \tag{7.17}$$

The remaining three integrals can be performed in a similar manner. The final result is thus a sum of four Fox H-functions as seen below:

$$\begin{aligned}\mathcal{G}(z,\bar{z})\big|_{\mathrm{II}} &= \int_1^{\infty}\frac{dx}{x(x-1)}\,\mathcal{F}_1(z,x)\Big|_{z<1<x}\,\mathcal{F}_2(x,\bar{z})\Big|_{\bar{z}<1<x}\\ &=|1-z|^{1-\Delta_1}|1-\bar{z}|^{1-\Delta_3}C(\Delta_4,\Delta_1-1)C(\Delta_2,\Delta_3-1)\frac{\Gamma(\Delta_2+\Delta_3-1)\Gamma(\Delta_1+\Delta_4-1)}{\Gamma(1-\Delta_1)\Gamma(\Delta_3-1)\Gamma(1-\Delta_3)\Gamma(\Delta_1-1)}\\ &\quad\times\mathrm{H}^{1,1:\,2,1;\,2,1}_{1,1:\,2,2;\,2,2}\left(\begin{array}{c|c} 1-z & (0,1):\,(1,\Delta_1+\Delta_4-1,1,1);\,(1,\Delta_2+\Delta_3-1,1,1)\\ 1-\bar{z} & (0,1):\,(1-\Delta_3,\Delta_1-1,1,1);\,(1-\Delta_1,\Delta_3-1,1,1)\end{array}\right)\\ &+\Bigg\{|1-z|^{1-\Delta_1}|1-\bar{z}|^{\Delta_2-1}C(\Delta_4,\Delta_1-1)C(\Delta_1,\Delta_4-1)\frac{(\Gamma(\Delta_1+\Delta_4-1))^2}{\Gamma(1-\Delta_3)\Gamma(\Delta_1-1)\Gamma(1-\Delta_2)\Gamma(\Delta_4-1)}\\ &\quad\times\mathrm{H}^{1,1:\,2,1;\,2,1}_{1,1:\,2,2;\,2,2}\left(\begin{array}{c|c} 1-z & (\Delta_1+\Delta_4-2,1):\,(1,\Delta_1+\Delta_4-1,1,1);\,(1,\Delta_1+\Delta_4-1,1,1)\\ 1-\bar{z} & (\Delta_1+\Delta_4-2,1):\,(1-\Delta_3,\Delta_1-1,1,1);\,(1-\Delta_2,\Delta_4-1,1,1)\end{array}\right)\\ &\quad+\left(z\leftrightarrow\bar{z},\Delta_1\leftrightarrow\Delta_3,\Delta_2\leftrightarrow\Delta_4\right)\Bigg\}\\ &+|1-z|^{\Delta_4-1}|1-\bar{z}|^{\Delta_2-1}\,C(\Delta_3,\Delta_2-1)\,C(\Delta_1,\Delta_4-1)\frac{\Gamma(\Delta_2+\Delta_3-1)\Gamma(\Delta_1+\Delta_4-1)}{\Gamma(1-\Delta_4)\Gamma(\Delta_2-1)\Gamma(1-\Delta_2)\Gamma(\Delta_4-1)}\\ &\quad\times\mathrm{H}^{1,1:\,2,1;\,2,1}_{1,1:\,2,2;\,2,2}\left(\begin{array}{c|c} 1-z & (0,1):\,(1,\Delta_2+\Delta_3-1,1,1);\,(1,\Delta_1+\Delta_4-1,1,1)\\ 1-\bar{z} & (0,1):\,(1-\Delta_4,\Delta_2-1,1,1);\,(1-\Delta_2,\Delta_4-1,1,1)\end{array}\right)\ .\end{aligned} \tag{7.18}$$

The evaluation of $\mathcal{G}(z,\bar{z})\big|_{\mathrm{I}}$is more involved due to the presence of additional singular points at $x=z,\bar{z}$ in the x-integral. The x-integrals generically evaluate to an Appell function F_1 and contributes an additional Mellin-Barnes integral. The resulting special function is a generalization of the Fox H-function, called the I-function. We relegate the details of this computation to Appendix 7.5.

7.1.2 Conformal block decomposition

Note that as shown in (7.12), the cross ratios z and $\bar{z}$ only occur in the hypergeometric functions. For each $\mathcal{F}_1$ and $\mathcal{F}_2$, we know how to do the conformal block decompositions for the simplest gluon exchange term, namely the first terms in both (7.33) and (7.35) based on the results in [47]. This lets us read off the the conformal block decomposition for this subset of terms in the first integral in (7.13). Since the analysis is identical to the one in [47], we do not present the details here but merely note that the spectrum of exchanged states is

$$(h, \bar{h}) \;=\; \left(\frac{\Delta_1+\Delta_2}{2} - 1 + m, \frac{\Delta_3+\Delta_4}{2} - 1 + n\right) \quad m, n \in \mathbb{Z}_{\geq 0}\ . \tag{7.19}$$

7.2 Light-ray correlators for scalars

In this section, we consider the scattering of four massless scalars mediated by a massive one. Throughout this section, we will drop the spin label on the CCFT operators. The amplitude is [4]

$$\mathbf{M}\,(s,t) = g^2\left(\frac{1}{m^2-s} \;+\; \frac{1}{m^2-t} \;+\; \frac{1}{m^2+s+t}\right)\ . \tag{7.20}$$

where

$$s = -4\,\varepsilon_3\varepsilon_4\,\omega_3\omega_4\,z_{34}\bar{z}_{34} \quad , \quad t = -4\,\varepsilon_2\varepsilon_4\,\omega_2\omega_4\,z_{24}\bar{z}_{24}\ , \tag{7.21}$$

The analog of (7.1) for this theory is

$$\begin{aligned}
&\langle\, \mathcal{O}_{\Delta_1}(z_1,\bar{z}_1)\mathcal{O}_{\Delta_2}(z_2,\bar{z}_2)\mathcal{O}_{\Delta_3}(z_3,\bar{z}_3)\mathcal{O}_{\Delta_4}(z_4,\bar{z}_4)\,\rangle \\
&= N(\beta)\,|z(1-z)|^{\frac{\beta}{2}+2}\,|1-z|^{-\Delta_2-\Delta_3}\,\mathrm{d}(z-\bar{z})\,X(z_{ij},\bar{z}_{ij})\Bigg\{[\mathrm{sgn}((z-1)z_{34}z_{23}z_{24})\mathrm{sgn}(\bar{z}_{23}\bar{z}_{24}\bar{z}_{34})]^{-\frac{\beta}{2}}|z|^{-\frac{\beta}{2}} \\
&\quad +\ [\mathrm{sgn}((1-z)zz_{12}z_{13}z_{23})\mathrm{sgn}(\bar{z}_{12}\bar{z}_{13}\bar{z}_{23})]^{-\frac{\beta}{2}}\ +\ [\mathrm{sgn}(-zz_{12}z_{14}z_{24})\mathrm{sgn}(\bar{z}_{12}\bar{z}_{14}\bar{z}_{24})]^{-\frac{\beta}{2}}|1-z|^{-\frac{\beta}{2}}\Bigg\}\,,
\end{aligned} \tag{7.22}$$

where

$$N(\beta) \;=2^{-\beta-2}\,g^2\,\pi\,|m|^{\beta-2}\,\csc\frac{\beta\pi}{2}\quad . \tag{7.23}$$

The presence of the mass term leads to residual sgn functions even after the summation over ϵ_i. This impacts the computation of light-ray correlators. In the limit $m\to\infty$ with g/m held fixed, the exchange interaction effectively reduces to a contact interaction and $N(\beta)\to \mathrm{d}(\beta)$ as pointed out in [44]. In particular, the sgn functions vanish in this limit and the correlator resembles that of gluons.

7.2.1 Two light-ray correlator

Owing to the differences cited above, the correlator involving two light-ray operators differs from that of gluons. This correlator is also essential in computing the four light-ray correlator. The final

[4]This amplitude was also considered in [44, 244] where the authors restricted themselves to different channels in order to analyze the conformal block decomposition. Restrictions of this sort are not feasible for the purpose of computing light transforms in the formalism of our paper.

result can still be expressed in terms of Gauss hypergeometric functions albeit with more complicated coefficients. Starting with (7.22), we have

$$
\begin{aligned}
&\langle\, \bar{\mathbf{L}}[\mathcal{O}_{\Delta_1}](z_1,\bar{z}_1)\bar{\mathbf{L}}[\mathcal{O}_{\Delta_2}](z_2,\bar{z}_2)\mathcal{O}_{\Delta_3}(z_3,\bar{z}_3)\mathcal{O}_{\Delta_4}(z_4,\bar{z}_4)\,\rangle \\
&= \int_{-\infty}^{\infty} \frac{d\bar{z}_1'}{|\bar{z}_1'-\bar{z}_1|^{2-\Delta_1}} \frac{d\bar{z}_2'}{|\bar{z}_2'-\bar{z}_2|^{2-\Delta_2}} \langle\, \mathcal{O}_{\Delta_1}(z_1,\bar{z}_1')\mathcal{O}_{\Delta_2}(z_2,\bar{z}_2')\mathcal{O}_{\Delta_3}(z_3,\bar{z}_3)\mathcal{O}_{\Delta_4}(z_4,\bar{z}_4)\,\rangle \\
&= N(\beta)\, X(z_{ij},\bar{z}_{ij})\, |\bar{z}|^{\frac{\Delta_3+\Delta_4}{2}-\frac{\beta}{2}}\, |z|^{\frac{\Delta_3+\Delta_4}{2}}\, \mathcal{F}_\phi(z,\bar{z}) \ ,
\end{aligned}
\tag{7.24}
$$

where $\mathcal{F}_\phi(z,\bar{z})$ is again an integral over four marked points:

$$
\begin{aligned}
\mathcal{F}_\phi(z,\bar{z}) \ &= \ \int_{-\infty}^{\infty} dt\, |z-t|^{\Delta_1-2}\, |\bar{z}-t|^{\Delta_2-2}\, |1-t|^{\Delta_4-1-\frac{\beta}{2}} \\
&\times \Big\{ [\mathrm{sgn}((z-1)z_{34}z_{23}z_{24})\mathrm{sgn}(\bar{z}_{13}\bar{z}_{14}\bar{z}_{34}(1-t))]^{-\frac{\beta}{2}}|z|^{-\frac{\beta}{2}} \\
&\quad + \ [\mathrm{sgn}((1-z)z_{12}z_{13}z_{23})\mathrm{sgn}(\bar{z}_{13}\bar{z}_{14}\bar{z}_{34}(1-t))]^{-\frac{\beta}{2}} \\
&\quad + \ [\mathrm{sgn}((z-1)z_{12}z_{14}z_{24})\mathrm{sgn}(\bar{z}_{13}\bar{z}_{14}\bar{z}_{34}(1-t))]^{-\frac{\beta}{2}}|1-z|^{-\frac{\beta}{2}} \Big\} \\
&= \ \mathcal{F}_{\phi,1}(z,\bar{z}) + \mathcal{F}_{\phi,2}(z,\bar{z}) + \mathcal{F}_{\phi,3}(z,\bar{z}) \ .
\end{aligned}
\tag{7.25}
$$

$X(z_{ij},\bar{z}_{ij})$ is the suitable pre-factor for the correlator which has conformal weights

$$
\begin{aligned}
(h_1,\bar{h}_1) &= \left(\frac{\Delta_1}{2}, 1-\frac{\Delta_1}{2}\right) \quad , \quad (h_2,\bar{h}_2) = \left(\frac{\Delta_2}{2}, 1-\frac{\Delta_2}{2}\right) \quad , \\
(h_3,\bar{h}_3) &= \left(\frac{\Delta_3}{2}, \frac{\Delta_3}{2}\right) \qquad , \qquad (h_4,\bar{h}_4) = \left(\frac{\Delta_4}{2}, \frac{\Delta_4}{2}\right) \ .
\end{aligned}
\tag{7.26}
$$

The s-, t-, and u-channels (in the bulk) contribute different sign functions to the integral (7.25). These eventually lead to different phases in the coefficient of the Gauss hypergeometric functions. The integral can be evaluated by using techniques similar to those of [47] and for $0<z<\bar{z}<1$, we find

$$
\begin{aligned}
\mathcal{F}_{\phi,i}(z,\bar{z})|_{z,\bar{z}<1\,\cup\, z,\bar{z}>1} \ &= \mathcal{S}_i(z_{ab})\,|1-z|^{\frac{\beta}{2}-\Delta_3}\, C^{(1)}\left(\Delta_4-\frac{\beta}{2}, \Delta_3-\frac{\beta}{2}\right) \\
&\qquad \times\ {}_2F_1\left(2-\Delta_2, \Delta_3-\frac{\beta}{2}, \Delta_3+\Delta_4-\beta, \frac{\bar{z}-z}{1-z}\right) \\
&+ \mathcal{S}_i(z_{ab})\,|\bar{z}-z|^{\Delta_1+\Delta_2-3}\,|1-z|^{\Delta_4-1-\frac{\beta}{2}}\, C\left(\Delta_1-1, \Delta_2-1\right) \\
&\qquad \times\ {}_2F_1\left(\Delta_1-1, 1+\frac{\beta}{2}-\Delta_4, \Delta_1+\Delta_2-2, \frac{\bar{z}-z}{1-z}\right) \ ,
\end{aligned}
\tag{7.27}
$$

where

$$
C^{(1)}(a,b) \ := \ e^{-\frac{\beta}{2}i\pi}B(a,b) + B(a,1-a-b) + B(b,1-a-b) \tag{7.28}
$$

and

$$
\mathcal{S}_i(z_{ab}) \ = \ \begin{cases} [-\mathrm{sgn}(z_{34}z_{23}z_{24})\mathrm{sgn}(\bar{z}_{13}\bar{z}_{14}\bar{z}_{34})]^{-\frac{\beta}{2}}|z|^{-\frac{\beta}{2}} & i=1 \\ [\mathrm{sgn}(z_{12}z_{13}z_{23})\mathrm{sgn}(\bar{z}_{13}\bar{z}_{14}\bar{z}_{34})]^{-\frac{\beta}{2}} & i=2 \\ [-\mathrm{sgn}(z_{12}z_{14}z_{24})\mathrm{sgn}(\bar{z}_{13}\bar{z}_{14}\bar{z}_{34})]^{-\frac{\beta}{2}}|1-z|^{-\frac{\beta}{2}} & i=3 \end{cases} \tag{7.29}
$$

The phase factor $(-1)^{-\frac{\beta}{2}} = e^{-\frac{\beta}{2}i\pi}$ comes from the sign functions. The result for the other regions can be found in Appendix 7.3.2.

7.2.2 Four light-ray correlator

The computation of the correlator involving four scalar light-ray operators begins in a manner analogous to Section [7.1].

$$\begin{aligned}
&\langle\,\bar{\mathbf{L}}[\mathcal{O}_{\Delta_1}](z_1,\bar z_1)\bar{\mathbf{L}}[\mathcal{O}_{\Delta_2}](z_2,\bar z_2)\mathbf{L}[\mathcal{O}_{\Delta_3}](z_3,\bar z_3)\mathbf{L}[\mathcal{O}_{\Delta_4}](z_4,\bar z_4)\,\rangle \\
&= \; N(\beta)\,|\bar z|^{\frac{\Delta_3+\Delta_4}{2}-\frac{\beta}{2}}\,|z|^{2-\frac{\Delta_3+\Delta_4}{2}}|1-z|^{\frac{\Delta_1+\Delta_3-\Delta_2-\Delta_4}{2}}\,X(z_{ij},\bar z_{ij}) \\
&\quad\times \int_{-\infty}^{\infty} dx \int_{-\infty}^{\infty} dy\,|1-y|^{\Delta_2-1-\frac{\beta}{2}}\,|z-y|^{\Delta_4-2}|x-y|^{\Delta_3-2} \\
&\quad\times \int_{-\infty}^{\infty} dt\,|x-t|^{\Delta_1-2}\,|\bar z-t|^{\Delta_2-2}\,|1-t|^{\Delta_4-1-\frac{\beta}{2}}\,S_\phi(x,y,t)
\end{aligned} \tag{7.30}$$

where

$$\begin{aligned}
S_\phi(x,y,t) \;=\; \Big\{ & [\mathrm{sgn}(x(y-1)(1-t))\mathrm{sgn}(z_{12}z_{13}z_{23})\mathrm{sgn}(\bar z_{13}\bar z_{14}\bar z_{34})]^{-\frac{\beta}{2}}|x|^{-\frac{\beta}{2}} \\
& + \;[\mathrm{sgn}((1-y)(1-t))\mathrm{sgn}(z_{12}z_{13}z_{23})\mathrm{sgn}(\bar z_{13}\bar z_{14}\bar z_{34})]^{-\frac{\beta}{2}} \\
& + \;[\mathrm{sgn}((x-1)(1-y)(1-t))\mathrm{sgn}(z_{12}z_{13}z_{23})\mathrm{sgn}(\bar z_{13}\bar z_{14}\bar z_{34})]^{-\frac{\beta}{2}}|1-x|^{-\frac{\beta}{2}} \Big\}\,,
\end{aligned} \tag{7.31}$$

and the conformal weights in the $X(z_{ij},\bar z_{ij})$ function are

$$\begin{aligned}
(h_1,\bar h_1) &= \left(\frac{\Delta_1}{2}, 1-\frac{\Delta_1}{2}\right) \quad , \quad (h_2,\bar h_2) = \left(\frac{\Delta_2}{2}, 1-\frac{\Delta_2}{2}\right) \quad , \\
(h_3,\bar h_3) &= \left(1-\frac{\Delta_3}{2}, \frac{\Delta_3}{2}\right) \quad , \quad (h_4,\bar h_4) = \left(1-\frac{\Delta_4}{2}, \frac{\Delta_4}{2}\right) \quad .
\end{aligned} \tag{7.32}$$

The sgn functions hinder the factorization of this integral and we cannot express this in a form similar to (7.12). However, we can proceed by breaking up the integral into regions where they have fixed signs and then perform the integral using tricks similar to Section [7.1]. The final result is then expressible in terms of Fox H-functions and I-functions, as in the gluon case.

7.3 Appendix: The library of four-marked-point integrals

This appendix is devoted to tabulating all four-marked-point integrals encountered in the gluon and scalar light transform calculations.

7.3.1 Gluon integrals

$$\begin{aligned}
&\mathcal{F}_1(z,x)|_{z,x<1\,\cup\,z,x>1} \\
&\quad= |x-1|^{1-\Delta_1}\,{}_2F_1\left(1-\Delta_4,\Delta_1-1,\Delta_1+\Delta_2-2,\frac{x-z}{x-1}\right)C(\Delta_2-1,\Delta_1-1) \\
&\quad+ |x-1|^{\Delta_2-2}|z-x|^{\Delta_3+\Delta_4-1}\,{}_2F_1\left(2-\Delta_2,\Delta_3,\Delta_3+\Delta_4,\frac{x-z}{x-1}\right)C(\Delta_3,\Delta_4)
\end{aligned} \tag{7.33}$$

$$\begin{aligned}
&\mathcal{F}_1(z,x)|_{z<1<x\,\cup\,z>1>x} \\
&\quad = |1-z|^{1-\Delta_1}\,{}_2F_1\left(1-\Delta_3,\Delta_1-1,\Delta_4+\Delta_1-1,-\frac{|x-1|}{|1-z|}\right)C(\Delta_4,\Delta_1-1) \\
&\quad + |x-1|^{\Delta_3+\Delta_2-2}|1-z|^{\Delta_4-1}\,{}_2F_1\left(1-\Delta_4,\Delta_2-1,\Delta_3+\Delta_2-1,-\frac{|x-1|}{|1-z|}\right)C(\Delta_3,\Delta_2-1)
\end{aligned} \tag{7.34}$$

$$\begin{aligned}
&\mathcal{F}_2(x,\bar{z})|_{\bar{z},x<1\,\cup\,\bar{z},x>1} \\
&\quad = |x-1|^{1-\Delta_3}\,{}_2F_1\left(1-\Delta_2,\Delta_3-1,\Delta_3+\Delta_4-2,\frac{\bar{z}-x}{1-x}\right)C(\Delta_4-1,\Delta_3-1) \\
&\quad + |x-1|^{\Delta_4-2}|\bar{z}-x|^{\Delta_1+\Delta_2-1}\,{}_2F_1\left(2-\Delta_4,\Delta_1,\Delta_1+\Delta_2,\frac{\bar{z}-x}{1-x}\right)C(\Delta_1,\Delta_2)
\end{aligned} \tag{7.35}$$

$$\begin{aligned}
&\mathcal{F}_2(x,\bar{z})|_{\bar{z}<1<x\,\cup\,\bar{z}>1>x} \\
&\quad = |1-\bar{z}|^{1-\Delta_3}\,{}_2F_1\left(1-\Delta_1,\Delta_3-1,\Delta_2+\Delta_3-1,-\frac{|x-1|}{|1-\bar{z}|}\right)C(\Delta_2,\Delta_3-1) \\
&\quad + |x-1|^{\Delta_1+\Delta_4-2}|1-\bar{z}|^{\Delta_2-1}\,{}_2F_1\left(1-\Delta_2,\Delta_4-1,\Delta_1+\Delta_4-1,-\frac{|x-1|}{|1-\bar{z}|}\right)C(\Delta_1,\Delta_4-1)
\end{aligned} \tag{7.36}$$

where

$$C(a,b) = B(a,b) + B(a,1-a-b) + B(b,1-a-b) \quad , \quad B(a,b) = \frac{\Gamma(a)\Gamma(b)}{\Gamma(a+b)}\,. \tag{7.37}$$

7.3.2 Scalar integrals

$$\begin{aligned}
\mathcal{F}_{\phi,i}(z,\bar{z})|_{z,\bar{z}<1\,\cup\,z,\bar{z}>1} \;&= \mathcal{S}_i(z_{ab})\,\Bigg[|1-z|^{\frac{\beta}{2}-\Delta_3}\,C^{(1)}\left(\Delta_4-\frac{\beta}{2},\Delta_3-\frac{\beta}{2}\right) \\
&\qquad \times\,{}_2F_1\left(2-\Delta_2,\Delta_3-\frac{\beta}{2},\Delta_3+\Delta_4-\beta,\frac{\bar{z}-z}{1-z}\right) \\
&+\;\; |\bar{z}-z|^{\Delta_1+\Delta_2-3}\,|1-z|^{\Delta_4-1-\frac{\beta}{2}}\,C\left(\Delta_1-1,\Delta_2-1\right) \\
&\qquad \times\,{}_2F_1\left(\Delta_1-1,1+\frac{\beta}{2}-\Delta_4,\Delta_1+\Delta_2-2,\frac{\bar{z}-z}{1-z}\right)\Bigg]
\end{aligned} \tag{7.38}$$

$$\begin{aligned}
\mathcal{F}_{\phi,i}(z,\bar{z})|_{z<1<\bar{z}\,\cup\,z>1>\bar{z}} \;&= \mathcal{S}_i(z_{ab})\,\Bigg[|\bar{z}-1|^{\frac{\beta}{2}-\Delta_3}\,C^{(1,2)}\left(\Delta_2-1,\Delta_3-\frac{\beta}{2}\right) \\
&\qquad \times\,{}_2F_1\left(\Delta_3-\frac{\beta}{2},2-\Delta_1,\Delta_2+\Delta_3-1-\frac{\beta}{2},-\frac{|1-z|}{|\bar{z}-1|}\right) \\
&+\;\; |1-z|^{\Delta_1+\Delta_4-2-\frac{\beta}{2}}|\bar{z}-1|^{\Delta_2-2}\,C^{(3)}\left(\Delta_1-1,\Delta_4-\frac{\beta}{2}\right) \\
&\qquad \times\,{}_2F_1\left(\Delta_4-\frac{\beta}{2},2-\Delta_2,\Delta_1+\Delta_4-1-\frac{\beta}{2},-\frac{|1-z|}{|\bar{z}-1|}\right)\Bigg]
\end{aligned} \tag{7.39}$$

where

$$\begin{aligned}
C^{(1)}(a,b) \;&:= e^{-\frac{\beta}{2}i\pi}B(a,b) + B(a,1-a-b) + B(b,1-a-b) \\
C^{(1,2)}(a,b) \;&:= e^{-\frac{\beta}{2}i\pi}\,B(a,b) + e^{-\frac{\beta}{2}i\pi}\,B(a,1-a-b) + B(b,1-a-b) \\
C^{(3)}(a,b) \;&:= B(a,b) + B(a,1-a-b) + e^{-\frac{\beta}{2}i\pi}\,B(b,1-a-b)
\end{aligned} \tag{7.40}$$

and

$$\mathcal{S}_i(z_{ab}) \;=\; \begin{cases} [-\mathrm{sgn}(z_{34}z_{23}z_{24})\mathrm{sgn}(\bar{z}_{13}\bar{z}_{14}\bar{z}_{34})]^{-\frac{\beta}{2}}|z|^{-\frac{\beta}{2}} & i=1 \\ [\mathrm{sgn}(z_{12}z_{13}z_{23})\mathrm{sgn}(\bar{z}_{13}\bar{z}_{14}\bar{z}_{34})]^{-\frac{\beta}{2}} & i=2 \\ [-\mathrm{sgn}(z_{12}z_{14}z_{24})\mathrm{sgn}(\bar{z}_{13}\bar{z}_{14}\bar{z}_{34})]^{-\frac{\beta}{2}}|1-z|^{-\frac{\beta}{2}} & i=3 \end{cases} \tag{7.41}$$

7.4 Appendix: Definitions of Fox H-function and Generalized I-function

Central to our discussion of the four-light transforms are special functions that belong to a general class of Mellin-Barnes type integrals, namely the Fox H-function [236, 237, 238, 239, 240] and the recently introduced generalized I-function [241, 242]. In this appendix, we briefly introduce the definitions of the bivariate Fox H-function $\mathrm{H}(x,y)$ and the generalized I-function of r-variables $\mathrm{I}(z_1,\ldots,z_r)$.

Fox H-function of two variables The Fox H-function of two variables $\mathrm{H}(x,y)$ (with the third characteristic) is defined as

$$\begin{aligned} \mathrm{H}(x,y) &= \mathrm{H}^{m_1,n_1:\,m_2,n_2;\,m_3,n_3}_{p_1,q_1:\,p_2,q_2;\,p_3,q_3}\left(\begin{array}{c|c} x & (\alpha^{(1)}_{p_1},a^{(1)}_{p_1})\,:\,(\alpha^{(2)}_{p_2},a^{(2)}_{p_2});\,(\alpha^{(3)}_{p_3},a^{(3)}_{p_3}) \\ y & (\beta^{(1)}_{q_1},b^{(1)}_{q_1})\,:\,(\beta^{(2)}_{q_2},b^{(2)}_{q_2});\,(\beta^{(3)}_{q_3},b^{(3)}_{q_3}) \end{array}\right) \\ &= \frac{1}{(2\pi i)^2}\int_{-i\infty}^{+i\infty} ds \int_{-i\infty}^{+i\infty} dt\,\phi_1(s+t)\,\phi_2(s)\,\phi_3(t)\,x^{-s}\,y^{-t}\ , \end{aligned} \tag{7.42}$$

where

$$\begin{aligned} \phi_1(s+t) &= \frac{\prod_{j=1}^{m_1}\Gamma\Big(\beta^{(1)}_j+b^{(1)}_j(s+t)\Big)\prod_{j=1}^{n_1}\Gamma\Big(1-\alpha^{(1)}_j-a^{(1)}_j(s+t)\Big)}{\prod_{j=n_1+1}^{p_1}\Gamma\Big(\alpha^{(1)}_j+a^{(1)}_j(s+t)\Big)\prod_{j=m_1+1}^{q_1}\Gamma\Big(1-\beta^{(1)}_j-b^{(1)}_j(s+t)\Big)}\ , \\ \phi_2(s) &= \frac{\prod_{j=1}^{m_2}\Gamma\Big(\beta^{(2)}_j+b^{(2)}_j s\Big)\prod_{j=1}^{n_2}\Gamma\Big(1-\alpha^{(2)}_j-a^{(2)}_j s\Big)}{\prod_{j=n_2+1}^{p_2}\Gamma\Big(\alpha^{(2)}_j+a^{(2)}_j s\Big)\prod_{j=m_2+1}^{q_2}\Gamma\Big(1-\beta^{(2)}_j-b^{(2)}_j s\Big)}\ , \\ \phi_3(t) &= \frac{\prod_{j=1}^{m_3}\Gamma\Big(\beta^{(3)}_j+b^{(3)}_j t\Big)\prod_{j=1}^{n_3}\Gamma\Big(1-\alpha^{(3)}_j-a^{(3)}_j t\Big)}{\prod_{j=n_3+1}^{p_3}\Gamma\Big(\alpha^{(3)}_j+a^{(3)}_j t\Big)\prod_{j=m_3+1}^{q_3}\Gamma\Big(1-\beta^{(3)}_j-b^{(3)}_j t\Big)}\ . \end{aligned} \tag{7.43}$$

The variables x and y are not equal to zero and an empty product is interpreted as unity. The parameters m_j, n_j, p_j, q_j $(j=1,2,3)$ are non-negative integers such that $0 \le m_j \le p_j$ and $0 \le n_j \le q_j$. The Latin letters $a^{(k)}_j, b^{(k)}_j$ are all positive quantities, while the Greek letters $\alpha^{(k)}_j, \beta^{(k)}_j$ are all complex numbers. For a detailed discussion on the convergence of H-functions, we refer the reader to [237].

Generalized I-function The I-function can be regarded as the generalization of the Fox-H functions. They were introduced recently in [241, 242] where their properties have been studied. The I-function of r-variables $\mathrm{I}(z_1, \ldots, z_r)$ is defined as

$$\mathrm{I}^{0,n:\, m_1,n_1;\,\ldots;\, m_r,n_r}_{p,q:\, p_1,q_1;\,\ldots;\, p_r,q_r}\left(\begin{array}{c|c} z_1 & \\ \vdots & \begin{array}{l}(\alpha_j; a_j^{(i)}; A_j)_{1,p} :\ (\gamma_j^{(1)}, c_j^{(1)}; C_j^{(1)})_{1,p_1}; \ldots; (\gamma_j^{(r)}, c_j^{(r)}; C_j^{(r)})_{1,p_r} \\ (\beta_j; b_j^{(i)}; B_j)_{1,q} :\ (\delta_j^{(1)}, d_j^{(1)}; D_j^{(1)})_{1,q_1}; \ldots; (\delta_j^{(r)}, d_j^{(r)}; D_j^{(r)})_{1,q_r}\end{array} \\ z_r & \end{array}\right)$$
$$= \frac{1}{(2\pi i)^r}\int_{-i\infty}^{+i\infty} \cdots \int_{-i\infty}^{+i\infty} ds_1 \ldots ds_r\, \phi(s_1, \ldots, s_r)\, \theta_1(s_1) \ldots \theta_r(s_r)\, z_1^{s_1} \ldots z_r^{s_r} \;, \tag{7.44}$$

where $\phi(s_1, \ldots, s_r)$, $\theta_i(s_i)$ for $i = 1, \ldots, r$ are given by

$$\phi(s_1, \ldots, s_r) = \frac{\prod_{j=1}^{n} \Gamma^{A_j}\left(1 - \alpha_j + \sum_{i=1}^{r} a_j^{(i)} s_i\right)}{\prod_{j=n+1}^{p} \Gamma^{A_j}\left(\alpha_j - \sum_{i=1}^{r} a_j^{(i)} s_i\right) \prod_{j=1}^{q} \Gamma^{B_j}\left(1 - \beta_j + \sum_{i=1}^{r} b_j^{(i)} s_i\right)} \;,$$
$$\theta_i(s_i) = \frac{\prod_{j=1}^{n_i} \Gamma^{C_j^{(i)}}\left(1 - \gamma_j^{(i)} + c_j^{(i)} s_i\right) \prod_{j=1}^{m_i} \Gamma^{D_j^{(i)}}\left(\delta_j^{(i)} - d_j^{(i)} s_i\right)}{\prod_{j=n_i+1}^{p_i} \Gamma^{C_j^{(i)}}\left(\gamma_j^{(i)} - c_j^{(i)} s_i\right) \prod_{j=m_i+1}^{q_i} \Gamma^{D_j^{(i)}}\left(1 - \delta_j^{(i)} + d_j^{(i)} s_i\right)} \;, \tag{7.45}$$

where z_i for $i = 1, \ldots, r$ are not equal to zero and an empty product is interpreted as unity as before. The parameters $n, p, q, m_j, n_j, p_j, q_j$ $(j = 1, \ldots, r)$ are non-negative integers such that $0 \leq n \leq p, q \geq 0, 0 \leq n_j \leq p_j$, and $0 \leq m_j \leq q_j$ $(j = 1, \ldots, r)$ (not all can be zero simultaneously). Crucially for our discussion related to light transforms, the definition of the I-function of r-variables presented above holds good even if some of the Latin letters $a_j^{(i)}, b_j^{(i)}, c_j^{(i)}, d_j^{(i)}$ are *zero* or *negative numbers*. In such cases, there exists certain transformation formulae relating them to other I-functions [242]. The Greek letters $\alpha_j, \beta_j, \gamma_j^{(i)}, \delta_j^{(i)}$ are all complex numbers and the exponents $A, B, C^{(i)}, D^{(i)}$ of the various Gamma functions appearing in (7.45) may assume non-integer values. In all the cases considered in this paper, the exponents will always be *unity*.

7.5 Appendix: Evaluation of $\mathcal{G}(z,\bar{z})\big|_{\mathrm{I}}$

In this appendix, we will demonstrate the procedure to evaluate $\mathcal{G}(z,\bar{z})\big|_{\mathrm{I}}$in eq(7.13). We again choose to work in the configuration where $0 < z < \bar{z} < 1$, for which the integral in the first region $\mathcal{G}(z,\bar{z})\big|_{\mathrm{I}}$ further breaks down into three regions:

$$\begin{aligned}\mathcal{G}(z,\bar{z})\Big|_{\mathrm{I}} &= \int_{-\infty}^{1} dx\, \frac{1}{x(x-1)}\, \mathcal{F}_1(z,x)|_{x,z<1}\, \mathcal{F}_2(x,\bar{z})|_{x,\bar{z}<1} \\ &= \int_{-\infty}^{z} \frac{dx}{x(x-1)}\, \mathcal{F}_1(z,x)\Big|_{x<z<1} \mathcal{F}_2(x,\bar{z})\Big|_{x<\bar{z}<1} + \int_{z}^{\bar{z}} \frac{dx}{x(x-1)}\, \mathcal{F}_1(z,x)\Big|_{z<x<1} \mathcal{F}_2(x,\bar{z})\Big|_{x<\bar{z}<1} \\ &\quad + \int_{\bar{z}}^{1} \frac{dx}{x(x-1)}\, \mathcal{F}_1(z,x)\Big|_{z<x<1} \mathcal{F}_2(x,\bar{z})\Big|_{\bar{z}<x<1} \;.\end{aligned} \tag{7.46}$$

Focusing on the second term of (7.46) and using the results in Appendix 7.3, we have

$$
\begin{aligned}
\mathcal{G}(z,\bar z)\Big|_{\mathrm{I}} &\supset C(\Delta_3,\Delta_4)\,C(\Delta_2,\Delta_4-1)\,|\bar z-1|^{\Delta_2+\Delta_4-2} \\
&\quad \int_z^{\bar z}\frac{dx}{x(1-x)}\,|x-1|^{\Delta_2-2}|z-x|^{\Delta_3+\Delta_4-1}|x-\bar z|^{\Delta_1-1} \\
&\quad \times\ {}_2F_1\left(2-\Delta_2,\Delta_3,\Delta_3+\Delta_4;-\frac{|x-z|}{|1-x|}\right){}_2F_1\left(1-\Delta_1,\Delta_2,\Delta_2+\Delta_4-1;-\frac{|\bar z-1|}{|x-\bar z|}\right)\,.
\end{aligned}
\tag{7.47}
$$

Proceeding as we did in Section 7.1.1, we first recast the Gauss hypergeometric functions as contour integrals over exponents s_1, s_2 as in (7.15). We can then perform the x-integral as below.

$$
\begin{aligned}
&\int_z^{\bar z}\frac{dx}{x(1-x)}\,(1-x)^{\Delta_2-2-s_1}(x-z)^{\Delta_3+\Delta_4-1+s_1}\,(\bar z-x)^{\Delta_1-1-s_2} \\
&= (\bar z-z)^{3-\Delta_2+s_1-s_2}\,\bar z^{\Delta_1-s_2-1}z^{s_2-\Delta_1}\,(1-\bar z)^{\Delta_2-s_1-3}\,B(\Delta_1-s_2,\Delta_3+\Delta_4+s_1) \\
&\qquad\qquad \times F_1\left(\Delta_1-s_2,-s_2,3+s_1-\Delta_2,4-\Delta_2+s_1-s_2;-\left|\frac{\bar z-z}{\bar z}\right|,-\left|\frac{\bar z-z}{z(1-\bar z)}\right|\right)
\end{aligned}
\tag{7.48}
$$

To proceed further, we make use of the following contour integral representation of the Appell F_1 hypergeometric function

$$
\begin{aligned}
&F_1(a,b_1,b_2,c;-|z_1|,-|z_2|) \\
&= \frac{1}{(2\pi i)^2}\frac{\Gamma(c)}{\Gamma(a)\Gamma(b_1)\Gamma(b_2)} \\
&\quad \times\int_{-i\infty}^{i\infty} ds_3\,ds_4\,\frac{\Gamma(-s_3)\Gamma(-s_4)\Gamma(b_1+s_3)\Gamma(b_2+s_4)\Gamma(a+s_3+s_4)}{\Gamma(c+s_3+s_4)}\,|z_1|^{s_3}|z_2|^{s_4}\,.
\end{aligned}
\tag{7.49}
$$

The final result is now a four-fold Mellin Barnes integral and can be identified with the 4-variable I-function

$$
\begin{aligned}
\mathcal{G}(z,\bar z)\Big|_{\mathrm{I}} &\supset\ |\bar z|^{\Delta_1-1}|z|^{-\Delta_1}|\bar z-z|^{3-\Delta_2}|1-\bar z|^{\Delta_2-\Delta_1-\Delta_3-1} \\
&\quad \times\ \frac{\Gamma(\Delta_3+\Delta_4)\Gamma(\Delta_2+\Delta_4-1)}{\Gamma(2-\Delta_2)\Gamma(\Delta_3)\Gamma(1-\Delta_1)\Gamma(\Delta_2)}C(\Delta_3,\Delta_4)\,C(\Delta_2,\Delta_4-1) \\
&\quad \times\ \mathrm{I}^{0,3:1,2;0,2;1,0;1,0}_{3,1:2,2;2,1;0,1;0,1}\left(\begin{array}{c|c} z_1 & (\alpha_j;a_j^{(i)};A_j)_{1,3}:\,(\gamma_j^{(1)},c_j^{(1)};C_j^{(1)})_{1,2};\ldots;(\gamma_j^{(4)},c_j^{(4)};C_j^{(4)})_{1,0} \\ \vdots & \\ z_4 & (\beta_j;b_j^{(i)};B_j)_{1,1}:\,(\delta_j^{(1)},d_j^{(1)};D_j^{(1)})_{1,2};\ldots;(\delta_j^{(4)},d_j^{(4)};D_j^{(4)})_{1,1}\end{array}\right)
\end{aligned}
\tag{7.50}
$$

where the entries of the above I-function are:

- variables z_i: $z_1=\left|\frac{\bar z-z}{1-\bar z}\right|$, $z_2=\left|\frac{(1-\bar z)z}{(\bar z-z)\bar z}\right|$, $z_3=\left|\frac{\bar z-z}{z}\right|$, and $z_4=\left|\frac{\bar z-z}{z(1-\bar z)}\right|$;
- exponents of the Gamma functions: $A_j = B_j = C_j^{(i)} = D_j^{(i)} = 1$;
- coefficients $c_j^{(i)} = d_j^{(i)} = 1$;
- $\alpha_1 = 1$, $a_1 = (0,-1,1,0)$; $\alpha_2 = \Delta_2 - 2$, $a_2 = (1,0,0,1)$;
  $\alpha_3 = 1-\Delta_1$, $a_3 = (0,-1,1,1)$;
- $\beta_1 = \Delta_2 - 3$, $b_1 = (1,-1,1,1)$;

- $\gamma_j^{(1)} = \left(\Delta_2 - 1, 1 - \Delta_3\right)$; $\gamma_j^{(2)} = \left(\Delta_1, 1 - \Delta_2\right)$;
- $\delta_j^{(1)} = \left(0, \Delta_2 - 2\right)$; $\delta_1^{(2)} = 2 - \Delta_2 - \Delta_4$; $\delta_j^{(3)} = \delta_j^{(4)} = 0$.

The remaining integrals in (7.46) can be computed in a similar manner and can be shown to be some I-function of *four* variables.

7.6 Appendix: OPEs from the collinear limits of the four-point scalar amplitude

In this Appendix, we study the various collinear limits of (7.24).

Scalar - scalar collinear limit We consider taking the limit $z_{34} \to 0$ starting from a region with $0 < z, \bar{z} < 1$. We can then make use of (7.24) and (7.27) and the correlator reduces to

$$\begin{aligned}
&\left\langle \bar{\mathbf{L}}[\mathcal{O}_{\Delta_1}](z_1,\bar{z}_1)\bar{\mathbf{L}}[\mathcal{O}_{\Delta_2}](z_2,\bar{z}_2)\mathcal{O}_{\Delta_3}(z_3,\bar{z}_3)\mathcal{O}_{\Delta_4}(z_4,\bar{z}_4)\right\rangle \\
&\overset{3||4}{\to} N(\beta)\,|z_{12}|^{2+\frac{\beta}{2}-\Delta_1-\Delta_2}|z_{14}|^{-2+\Delta_2-\frac{\beta}{2}}|z_{24}|^{-2+\Delta_1-\frac{\beta}{2}} \\
&\left[1+e^{-\frac{\beta}{2}i\pi}\right]\left\{\frac{C^{(1)}\left(\Delta_4-\frac{\beta}{2},\Delta_3-\frac{\beta}{2}\right)}{|\bar{z}_{34}|^{\frac{\beta}{2}}}\,|\bar{z}_{14}|^{\Delta_1-2}|\bar{z}_{24}|^{\Delta_2-2}\right. \\
&\qquad\left.+\;C(\Delta_1-1,\Delta_2-1)\,|\bar{z}_{34}|^{\frac{\beta}{2}-\Delta_3-\Delta_4+1}\,\frac{|\bar{z}_{12}|^{\Delta_1+\Delta_2-3}}{|\bar{z}_{14}|^{\Delta_2-1}|\bar{z}_{24}|^{\Delta_1-1}}\right\} \\
&+\;N(\beta)\,|z_{12}|^{2-\Delta_1-\Delta_2}|z_{14}|^{-2+\Delta_2}|z_{24}|^{-2+\Delta_1}|z_{34}|^{-\frac{\beta}{2}} \\
&\left[-\mathrm{sgn}(z_{34}\bar{z}_{34})\right]^{-\frac{\beta}{2}}\left\{\frac{C^{(1)}\left(\Delta_4-\frac{\beta}{2},\Delta_3-\frac{\beta}{2}\right)}{|\bar{z}_{34}|^{\frac{\beta}{2}}}\,|\bar{z}_{14}|^{\Delta_1-2}|\bar{z}_{24}|^{\Delta_2-2}\right. \\
&\qquad\left.+\;C(\Delta_1-1,\Delta_2-1)\,|\bar{z}_{34}|^{\frac{\beta}{2}-\Delta_3-\Delta_4+1}\,\frac{|\bar{z}_{12}|^{\Delta_1+\Delta_2-3}}{|\bar{z}_{14}|^{\Delta_2-1}|\bar{z}_{24}|^{\Delta_1-1}}\right\}\;.
\end{aligned} \tag{7.51}$$

Note that the leading term is of $\mathcal{O}\left(z_{34}^0\right)$. This is to be expected as three-point amplitudes involving a massive particle do not produce collinear divergences. In order to read off the OPE, we must first express the parts dependent on coordinates $z_1, z_2, z_3, \bar{z}_1, \bar{z}_2, \bar{z}_3$ as a three-point function. We can do this simply using dimensional analysis. As an example, the fact that

$$\begin{aligned}
&\left\langle \bar{\mathbf{L}}[\mathcal{O}_{\Delta_1}](z_1,\bar{z}_1)\bar{\mathbf{L}}[\mathcal{O}_{\Delta_2}](z_2,\bar{z}_2)\,\mathcal{O}_{\Delta_3+\Delta_4-\frac{\beta}{2},\frac{\beta}{2}}(z_4,\bar{z}_4)\right\rangle \\
&\propto |z_{12}|^{2+\frac{\beta}{2}-\Delta_1-\Delta_2}|z_{14}|^{-2+\Delta_2-\frac{\beta}{2}}|z_{24}|^{-2+\Delta_1-\frac{\beta}{2}}|\bar{z}_{14}|^{\Delta_1-2}|\bar{z}_{24}|^{\Delta_2-2}
\end{aligned} \tag{7.52}$$

tells us that the first term in the OPE must contain an operator with conformal dimension $\Delta_3+\Delta_4-\frac{\beta}{2}$ and spin $\frac{\beta}{2}$. A similar analysis for the remaining terms lets us write the OPE as $z_{34}\to 0$ in the form

$$\begin{aligned}\mathcal{O}_{\Delta_3}(z_3,\bar{z}_3)\mathcal{O}_{\Delta_4}(z_4,\bar{z}_4) \;\sim\; & \rho_1\,\frac{C^{(1)}\left(\Delta_4-\frac{\beta}{2},\Delta_3-\frac{\beta}{2}\right)}{|\bar{z}_{34}|^{\frac{\beta}{2}}}\mathcal{O}_{\Delta_3+\Delta_4-\frac{\beta}{2},\frac{\beta}{2}}(z_4,\bar{z}_4)\\ &+\;\rho_2\,|\bar{z}_{34}|^{\frac{\beta}{2}-\Delta_3-\Delta_4+1}\,\bar{\mathbf{L}}[\mathcal{O}_{\Delta_3+\Delta_4-\frac{\beta}{2},\frac{\beta}{2}}](z_4,\bar{z}_4)\\ &+\;\rho_3\,[-\mathrm{sgn}(z_{34}\bar{z}_{34})]^{-\frac{\beta}{2}}\,\frac{C^{(1)}\left(\Delta_4-\frac{\beta}{2},\Delta_3-\frac{\beta}{2}\right)}{|z_{34}\bar{z}_{34}|^{\frac{\beta}{2}}}\,\mathcal{O}_{\Delta_3+\Delta_4-\beta}(z_4,\bar{z}_4)\\ &+\;\rho_4\,[-\mathrm{sgn}(z_{34}\bar{z}_{34})]^{-\frac{\beta}{2}}\,\frac{|\bar{z}_{34}|^{\frac{\beta}{2}-\Delta_3-\Delta_4+1}}{|z_{34}|^{\frac{\beta}{2}}}\,\bar{\mathbf{L}}[\mathcal{O}_{\Delta_3+\Delta_4-\beta}](z_4,\bar{z}_4)\quad .\end{aligned}\tag{7.53}$$

ρ_1, ρ_2, ρ_3, and ρ_4 can depend on the conformal dimensions but not on $z_3, z_4, \bar{z}_3, \bar{z}_4$.

Scalar light-ray - scalar light-ray collinear limit Next, we consider the limit $z_{12}\to 0$. Approaching from $0<z<\bar{z}<1$ as above, the correlator reduces to

$$\begin{aligned}&\langle\,\bar{\mathbf{L}}[\mathcal{O}_{\Delta_1}](z_1,\bar{z}_1)\bar{\mathbf{L}}[\mathcal{O}_{\Delta_2}](z_2,\bar{z}_2)\mathcal{O}_{\Delta_3}(z_3,\bar{z}_3)\mathcal{O}_{\Delta_4}(z_4,\bar{z}_4)\,\rangle\\ &\overset{1||2}{\to} N(\beta)\,|z_{12}|^{2+\frac{\beta}{2}-\Delta_1-\Delta_2}|z_{23}|^{-\Delta_3}|z_{24}|^{-\Delta_4}\\ &\quad\left[1+e^{-\frac{\beta}{2}i\pi}\right]\left\{\frac{C^{(1)}\left(\Delta_4-\frac{\beta}{2},\Delta_3-\frac{\beta}{2}\right)}{|\bar{z}_{34}|^{\frac{\beta}{2}}}\,|\bar{z}_{23}|^{\frac{\beta}{2}-\Delta_3}|\bar{z}_{24}|^{\frac{\beta}{2}-\Delta_4}\right.\\ &\qquad\left.+\;C(\Delta_1-1,\Delta_2-1)\,|\bar{z}_{12}|^{\Delta_1+\Delta_2-3}\,\frac{|\bar{z}_{34}|^{\Delta_1+\Delta_2-3-\frac{\beta}{2}}}{|\bar{z}_{23}|^{\frac{\beta}{2}+1-\Delta_4}|\bar{z}_{24}|^{\frac{\beta}{2}+1-\Delta_3}}\right\}\\ &\quad+\;N(\beta)\,|z_{12}|^{2-\Delta_1-\Delta_2}|z_{23}|^{\frac{\beta}{2}-\Delta_3}|z_{24}|^{\frac{\beta}{2}-\Delta_4}|z_{34}|^{-\frac{\beta}{2}}\\ &\quad[-\mathrm{sgn}(z_{34}z_{23}z_{24}\bar{z}_{23}\bar{z}_{24}\bar{z}_{34})]^{-\frac{\beta}{2}}\left\{\frac{C^{(1)}\left(\Delta_4-\frac{\beta}{2},\Delta_3-\frac{\beta}{2}\right)}{|\bar{z}_{34}|^{\frac{\beta}{2}}}\,|\bar{z}_{23}|^{\frac{\beta}{2}-\Delta_3}|\bar{z}_{24}|^{\frac{\beta}{2}-\Delta_4}\right.\\ &\qquad\left.+\;C(\Delta_1-1,\Delta_2-1)\,|\bar{z}_{12}|^{\Delta_1+\Delta_2-3}\,\frac{|\bar{z}_{34}|^{\Delta_1+\Delta_2-3-\frac{\beta}{2}}}{|\bar{z}_{23}|^{\frac{\beta}{2}+1-\Delta_4}|\bar{z}_{24}|^{\frac{\beta}{2}+1-\Delta_3}}\right\}\quad ,\end{aligned}\tag{7.54}$$

which implies the OPE

$$\begin{aligned}\bar{\mathbf{L}}[\mathcal{O}_{\Delta_1}](z_1,\bar{z}_1)\bar{\mathbf{L}}[\mathcal{O}_{\Delta_2}](z_2,\bar{z}_2)\;\sim\;& |z_{12}|^{2+\frac{\beta}{2}-\Delta_1-\Delta_2}\left\{\rho_1'\,\mathbf{S}[\mathcal{O}_{\Delta_1+\Delta_2-2-\frac{\beta}{2},-\frac{\beta}{2}}](z_2,\bar{z}_2)\right.\\ &\left.+\rho_2'\,C(\Delta_1-1,\Delta_2-1)\,|\bar{z}_{12}|^{\Delta_1+\Delta_2-3}\,\mathbf{L}[\mathcal{O}_{\Delta_1+\Delta_2-2-\frac{\beta}{2},-\frac{\beta}{2}}](z_2,\bar{z}_2)\right\}\\ &+|z_{12}|^{2-\Delta_1-\Delta_2}\left\{\rho_3'\,\mathbf{S}[\mathcal{O}_{\Delta_1+\Delta_2-2}](z_2,\bar{z}_2)\right.\\ &\left.+\rho_4'\,C(\Delta_1-1,\Delta_2-1)\,|\bar{z}_{12}|^{\Delta_1+\Delta_2-3}\,\mathbf{L}[\mathcal{O}_{\Delta_1+\Delta_2-2}](z_2,\bar{z}_2)\right\}\quad .\end{aligned}\tag{7.55}$$

Scalar light-ray - scalar collinear limit Finally, we consider the limit $z_{13} \to 0$. Since $z \to 1$ in this limit, it is helpful to use hypergeometric identities to rewrite the function $\mathcal{F}_{\phi,i}(z,\bar{z})$ in (7.27) as

$$\begin{aligned} \mathcal{F}_{\phi}(z,\bar{z})|_{z,\bar{z}<1\,\cup\, z,\bar{z}>1} &= \mathcal{S}_i(z)\,|z-\bar{z}|^{\frac{\beta}{2}-\Delta_3}\,C^{(3)}\left(\Delta_2-1,\Delta_3-\frac{\beta}{2}\right) \\ &\quad\times\,{}_2F_1\left(\Delta_3-\frac{\beta}{2},1-\Delta_4+\frac{\beta}{2},\Delta_2+\Delta_3-1-\frac{\beta}{2},-\frac{|z-1|}{|\bar{z}-z|}\right) \\ &+\mathcal{S}_i(z)\,|\bar{z}-z|^{\Delta_2-2}\,|1-z|^{\Delta_1+\Delta_4-2-\frac{\beta}{2}}\,C^{(3)}\left(\Delta_1-1,\Delta_4-\frac{\beta}{2}\right) \\ &\quad\times\,{}_2F_1\left(\Delta_1-1,2-\Delta_2,\Delta_1+\Delta_4-1-\frac{\beta}{2},-\frac{|z-1|}{|\bar{z}-z|}\right) \end{aligned} \tag{7.56}$$

which simplifies in the limit $z \to 1$, giving

$$\begin{aligned} &\langle\,\bar{\mathbf{L}}[\mathcal{O}_{\Delta_1}](z_1,\bar{z}_1)\bar{\mathbf{L}}[\mathcal{O}_{\Delta_2}](z_2,\bar{z}_2)\mathcal{O}_{\Delta_3}(z_3,\bar{z}_3)\mathcal{O}_{\Delta_4}(z_4,\bar{z}_4)\,\rangle \overset{2||3}{\to} N(\beta)\left[1+e^{-\frac{\beta}{2}i\pi}\right] \\ &\left\{\frac{C^{(3)}\left(\Delta_2-1,\Delta_3-\frac{\beta}{2}\right)}{|\bar{z}_{23}|^{\Delta_3-\frac{\beta}{2}}}\,|z_{12}|^{\Delta_4-2-\frac{\beta}{2}}|z_{24}|^{\Delta_1-2-\frac{\beta}{2}}|z_{14}|^{\frac{\Delta_2+\Delta_3-\Delta_1-\Delta_4}{2}}\,|\bar{z}_{14}|^{\Delta_1-2}|\bar{z}_{24}|^{2-\Delta_1-\Delta_4}\right. \\ &\left.+\;|z_{23}|^{\Delta_1+\Delta_4-2-\frac{\beta}{2}}|\bar{z}_{23}|^{\Delta_2-2}\,\frac{C^{(3)}\left(\Delta_1-1,\Delta_4-\frac{\beta}{2}\right)}{|z_{12}|^{\Delta_1}|z_{24}|^{\Delta_4}}\,\frac{|\bar{z}_{12}|^{2+\frac{\beta}{2}-\Delta_2-\Delta_3}}{|\bar{z}_{14}|^{\Delta_4-\frac{\beta}{2}}|\bar{z}_{24}|^{\frac{\beta}{2}}}\right\} \\ &+\;N(\beta)\left[-\mathrm{sgn}(z_{12}z_{14}z_{24}\bar{z}_{12}\bar{z}_{14}\bar{z}_{24})\right]^{-\frac{\beta}{2}} \\ &\left\{\frac{C^{(3)}\left(\Delta_2-1,\Delta_3-\frac{\beta}{2}\right)}{|\bar{z}_{23}|^{\Delta_3-\frac{\beta}{2}}|z_{23}|^{\frac{\beta}{2}}}\,|z_{12}|^{\Delta_4-2}|z_{24}|^{\Delta_1-2}|z_{14}|^{2-\Delta_1-\Delta_4}\,|\bar{z}_{14}|^{\Delta_1-2}|\bar{z}_{24}|^{2-\Delta_1-\Delta_4}\right. \\ &\left.+\;|z_{23}|^{2-\Delta_2-\Delta_3}|\bar{z}_{23}|^{\Delta_2-2}\,\frac{C^{(3)}\left(\Delta_1-1,\Delta_4-\frac{\beta}{2}\right)}{|z_{12}|^{\Delta_1-\frac{\beta}{2}}|z_{14}|^{\frac{\beta}{2}}|z_{24}|^{\Delta_4-\frac{\beta}{2}}}\,\frac{|\bar{z}_{12}|^{2+\frac{\beta}{2}-\Delta_2-\Delta_3}}{|\bar{z}_{14}|^{\Delta_4-\frac{\beta}{2}}|\bar{z}_{24}|^{\frac{\beta}{2}}}\right\}\;. \end{aligned} \tag{7.57}$$

This gives the corresponding OPE

$$\begin{aligned} \bar{\mathbf{L}}[\mathcal{O}_{\Delta_2}](z_2,\bar{z}_2)\mathcal{O}_{\Delta_3}(z_3,\bar{z}_3)\;\sim\;&\rho_1''\,\frac{C^{(3)}\left(\Delta_2-1,\Delta_3-\frac{\beta}{2}\right)}{|\bar{z}_{23}|^{\Delta_3-\frac{\beta}{2}}}\,\bar{\mathbf{L}}[\mathcal{O}_{\Delta_2+\Delta_3-\frac{\beta}{2},\frac{\beta}{2}}](z_3,\bar{z}_3) \\ &+\rho_2''\,|z_{23}|^{\Delta_1+\Delta_4-2-\frac{\beta}{2}}|\bar{z}_{23}|^{\Delta_2-2}\,\mathbf{L}[\mathcal{O}_{\Delta_2+\Delta_3-2-\frac{\beta}{2},-\frac{\beta}{2}}](z_3,\bar{z}_3) \\ &+\rho_3''\,\frac{C^{(3)}\left(\Delta_2-1,\Delta_3-\frac{\beta}{2}\right)}{|\bar{z}_{23}|^{\Delta_3-\frac{\beta}{2}}|z_{23}|^{\frac{\beta}{2}}}\,\bar{\mathbf{L}}[\mathcal{O}_{\Delta_2+\Delta_3-\beta}](z_3,\bar{z}_3) \\ &+\rho_4''\,|z_{23}|^{2-\Delta_2-\Delta_3}|\bar{z}_{23}|^{\Delta_2-2}\,\mathbf{L}[\mathcal{O}_{\Delta_2+\Delta_3-2}](z_3,\bar{z}_3)\quad. \end{aligned} \tag{7.58}$$

7.7 Appendix: Conformal block decomposition of the scalar light-ray correlator

In this appendix, we will compute the conformal block decompositions for the term corresponding to the primary operator exchange in the four-point scalar correlator containing two light-ray operators presented in (7.24). Again, we focus on the region $z, \bar{z} \in [0,1]$. Since (7.24) already takes the standard four-point function form, the function of cross ratios $G(z,\bar{z})$ can be read off as

$$G(z,\bar{z})|_{z,\bar{z}\in[0,1]} \;=\; \bar{z}^{-\frac{\beta}{2}}\,(z\bar{z})^{\frac{\Delta_3+\Delta_4}{2}}\,\mathcal{F}_\phi(z,\bar{z})|_{z,\bar{z}\in[0,1]} \;:=\; \mathcal{I}_1(z,\bar{z}) \;+\; \mathcal{I}_2(z,\bar{z}) \tag{7.59}$$

where

$$\begin{aligned}
\mathcal{I}_1(z,\bar{z}) \;&= S(z)\,\bar{z}^{-\frac{\beta}{2}}\,(z\bar{z})^{\frac{\Delta_3+\Delta_4}{2}}\,(1-z)^{\frac{\beta}{2}-\Delta_3}\,C^{(1)}\left(\Delta_4-\frac{\beta}{2},\Delta_3-\frac{\beta}{2}\right)\\
&\quad\times\;{}_2F_1\left(2-\Delta_2,\Delta_3-\frac{\beta}{2},\Delta_3+\Delta_4-\beta,\frac{\bar{z}-z}{1-z}\right)\\
\mathcal{I}_2(z,\bar{z}) \;&= S(z)\,\bar{z}^{-\frac{\beta}{2}}\,(z\bar{z})^{\frac{\Delta_3+\Delta_4}{2}}\,|\bar{z}-z|^{\Delta_1+\Delta_2-3}\,(1-z)^{\Delta_4-1-\frac{\beta}{2}}\,C\left(\Delta_1-1,\Delta_2-1\right)\\
&\quad\times\;{}_2F_1\left(\Delta_1-1,1+\frac{\beta}{2}-\Delta_4,\Delta_1+\Delta_2-2,\frac{\bar{z}-z}{1-z}\right)
\end{aligned} \tag{7.60}$$

and

$$S(z) \;=\; e^{-\frac{\beta}{2}i\pi}\,z^{-\frac{\beta}{2}} \;+\; 1 \;+\; e^{-\frac{\beta}{2}i\pi}\,(1-z)^{-\frac{\beta}{2}}\;. \tag{7.61}$$

We focus on the first term, which corresponds to the exchange of quasi-primary operators, and leave the decomposition of the second term, which corresponds to the exchange of light-ray operators, to future work. We proceed along the lines of [47, 213] in order to massage $\mathcal{I}_1(z,\bar{z})$ into a form from which the conformal block decomposition can be read off.

$$\begin{aligned}
\mathcal{I}_1(z,\bar{z}) \;&= e^{-\frac{\beta}{2}i\pi}\sum_{n=0}^{\infty}\tilde{a}_n\,k_{34}^{21}\left[\frac{\Delta_3+\Delta_4-\beta}{2}+n,\,\frac{\Delta_3+\Delta_4-\beta}{2}+n\right]\\
&\quad+\;\sum_{n,l=0}^{\infty}\tilde{b}_{n,l}\,k_{34}^{21}\left[\frac{\Delta_3+\Delta_4}{2}+n+l,\,\frac{\Delta_3+\Delta_4-\beta}{2}+n\right]\\
&\quad+\;e^{-\frac{\beta}{2}i\pi}\sum_{n,l=0}^{\infty}\tilde{c}_{n,l}\,k_{34}^{21}\left[\frac{\Delta_3+\Delta_4}{2}+n+l,\,\frac{\Delta_3+\Delta_4-\beta}{2}+n\right]
\end{aligned} \tag{7.62}$$

where recall that the conformal block is defined as [245]

$$k_{34}^{21}[h,\bar{h}] \;=\; z^h\,{}_2F_1(h-h_{12},h+h_{34},2h,z)\,\bar{z}^{\bar{h}}\,{}_2F_1(\bar{h}-\bar{h}_{12},\bar{h}+\bar{h}_{34},2\bar{h},\bar{z}) \tag{7.63}$$

and the coefficients are

$$\begin{aligned}
\tilde{a}_n \;&= C^{(1)}\left(\Delta_4-\frac{\beta}{2},\Delta_3-\frac{\beta}{2}\right)\frac{(2-\Delta_1)_n\,(2-\Delta_2)_n\,(\Delta_3-\frac{\beta}{2})_n\,(\Delta_4-\frac{\beta}{2})_n}{n!\,(\Delta_3+\Delta_4+n-1-\beta)_n\,(\Delta_3+\Delta_4-\beta)_{2n}}\\
\tilde{b}_{n,l} \;&= \tilde{a}_n\,\zeta_l\left(\frac{\Delta_3+\Delta_4-\beta}{2}+n,\frac{\beta}{2}\right)\\
\tilde{c}_{n,l} \;&= \tilde{a}_n\sum_{k=0}^{l}(-1)^k\binom{-\frac{\beta}{2}}{k}\,\zeta_{l-k}\left(\frac{\Delta_3+\Delta_4-\beta}{2}+n,k+\frac{\beta}{2}\right)\\
\zeta_l(h,r) \;&= \sum_{m=0}^{l}\frac{(-1)^m}{m!}\frac{(h-h_{12})_{l-m}(h+h_{34})_{l-m}(r+h+l-m-h_{12})_m(r+h+l-m+h_{34})_m}{(l-m)!(2h)_{l-m}(2r+2h+2l-1-m)_m}\;.
\end{aligned} \tag{7.64}$$

We can read off the spectrum of exchanged states in (7.62) to be

$$
\begin{aligned}
(h^{(1)}, \bar{h}^{(1)}) &= \left(\frac{\Delta_3 + \Delta_4 - \beta}{2} + n,\, \frac{\Delta_3 + \Delta_4 - \beta}{2} + n \right) \\
(h^{(2)}, \bar{h}^{(2)}) &= \left(\frac{\Delta_3 + \Delta_4}{2} + n + l,\, \frac{\Delta_3 + \Delta_4 - \beta}{2} + n \right)
\end{aligned}
\tag{7.65}
$$

where $n, l \in \mathbb{Z}_{\geq 0}$.

Bibliography

[1] N. Arkani-Hamed, L. Eberhardt, Y.-t. Huang, and S. Mizera, “On unitarity of tree-level string amplitudes,” *JHEP* **02** (2022) 197, 2201.11575.

[2] F. Figueroa and P. Tourkine, “Unitarity and Low Energy Expansion of the Coon Amplitude,” *Phys. Rev. Lett.* **129** (2022), no. 12 121602, 2201.12331.

[3] S. J. Parke and T. R. Taylor, “An Amplitude for n Gluon Scattering,” *Phys. Rev. Lett.* **56** (1986) 2459.

[4] R. Britto, F. Cachazo, B. Feng, and E. Witten, “Direct proof of tree-level recursion relation in Yang-Mills theory,” *Phys. Rev. Lett.* **94** (2005) 181602, hep-th/0501052.

[5] T. Cohen, H. Elvang, and M. Kiermaier, “On-shell constructibility of tree amplitudes in general field theories,” *JHEP* **04** (2011) 053, 1010.0257.

[6] N. Arkani-Hamed, J. L. Bourjaily, F. Cachazo, S. Caron-Huot, and J. Trnka, “The All-Loop Integrand For Scattering Amplitudes in Planar N=4 SYM,” *JHEP* **01** (2011) 041, 1008.2958.

[7] N. Arkani-Hamed and J. Trnka, “The Amplituhedron,” *JHEP* **10** (2014) 030, 1312.2007.

[8] S. De, D. Pavlov, M. Spradlin, and A. Volovich, “From Feynman diagrams to the amplituhedron: a gentle review,” 10, 2024. 2410.11757.

[9] N. Arkani-Hamed, Y. Bai, S. He, and G. Yan, “Scattering Forms and the Positive Geometry of Kinematics, Color and the Worldsheet,” *JHEP* **05** (2018) 096, 1711.09102.

[10] P. Banerjee, A. Laddha, and P. Raman, “Stokes polytopes: the positive geometry for ϕ^4 interactions,” *JHEP* **08** (2019) 067, 1811.05904.

[11] P. Raman, “The positive geometry for ϕ^p interactions,” *JHEP* **10** (2019) 271, 1906.02985.

[12] P. B. Aneesh, M. Jagadale, and N. Kalyanapuram, “Accordiohedra as positive geometries for generic scalar field theories,” *Phys. Rev. D* **100** (2019), no. 10 106013, 1906.12148.

[13] L. Ferro and T. Lukowski, “Amplituhedra, and beyond,” *J. Phys. A* **54** (2021), no. 3 033001, 2007.04342.

[14] E. Herrmann and J. Trnka, "The SAGEX review on scattering amplitudes Chapter 7: Positive geometry of scattering amplitudes," *J. Phys. A* **55** (2022), no. 44 443008, 2203.13018.

[15] G. Veneziano, "Construction of a crossing - symmetric, Regge behaved amplitude for linearly rising trajectories," *Nuovo Cim. A* **57** (1968) 190–197.

[16] L. Susskind, "Structure of hadrons implied by duality," *Phys. Rev. D* **1** (Feb, 1970) 1182–1186.

[17] T. Goto, "Relativistic quantum mechanics of one-dimensional mechanical continuum and subsidiary condition of dual resonance model," *Prog. Theor. Phys.* **46** (1971) 1560–1569.

[18] Y. Nambu, "Strings, Monopoles and Gauge Fields," *Phys. Rev. D* **10** (1974) 4262.

[19] D. D. Coon, "Uniqueness of the veneziano representation," *Phys. Lett. B* **29** (1969) 669–672.

[20] D. B. Fairlie and J. Nuyts, "A fresh look at generalized Veneziano amplitudes," *Nucl. Phys. B* **433** (1995) 26–40, hep-th/9406043.

[21] C. Cheung and G. N. Remmen, "Veneziano Variations: How Unique are String Amplitudes?," 2210.12163.

[22] N. Geiser and L. W. Lindwasser, "Generalized Veneziano and Virasoro amplitudes," 2210.14920.

[23] S. Pasterski and S.-H. Shao, "Conformal basis for flat space amplitudes," *Phys. Rev.* **D96** (2017), no. 6 065022, 1705.01027.

[24] S. Pasterski, S.-H. Shao, and A. Strominger, "Gluon Amplitudes as 2d Conformal Correlators," *Phys. Rev. D* **96** (2017), no. 8 085006, 1706.03917.

[25] S. Pasterski, S.-H. Shao, and A. Strominger, "Flat Space Amplitudes and Conformal Symmetry of the Celestial Sphere," *Phys. Rev. D* **96** (2017), no. 6 065026, 1701.00049.

[26] Y. T. A. Law and M. Zlotnikov, "Poincaré constraints on celestial amplitudes," *JHEP* **03** (2020) 085, 1910.04356. [Erratum: JHEP 04, 202 (2020)].

[27] S. Mizera and S. Pasterski, "Celestial geometry," *JHEP* **09** (2022) 045, 2204.02505.

[28] E. Casali, W. Melton, and A. Strominger, "Celestial amplitudes as AdS-Witten diagrams," *JHEP* **11** (2022) 140, 2204.10249.

[29] W. Fan, A. Fotopoulos, S. Stieberger, T. R. Taylor, and B. Zhu, "Celestial Yang-Mills amplitudes and D = 4 conformal blocks," *JHEP* **09** (2022) 182, 2206.08979.

[30] W. Fan, A. Fotopoulos, S. Stieberger, T. R. Taylor, and B. Zhu, "Elements of celestial conformal field theory," *JHEP* **08** (2022) 213, 2202.08288.

[31] S. Stieberger, T. R. Taylor, and B. Zhu, "Celestial Liouville theory for Yang-Mills amplitudes," *Phys. Lett. B* **836** (2023) 137588, 2209.02724.

[32] R. Gonzo, T. McLoughlin, and A. Puhm, "Celestial holography on Kerr-Schild backgrounds," *JHEP* **10** (2022) 073, 2207.13719.

[33] S. Banerjee, R. Mandal, A. Manu, and P. Paul, "MHV Gluon Scattering in the Massive Scalar Background and Celestial OPE," 2302.10245.

[34] T. Adamo, L. Mason, and A. Sharma, "MHV scattering of gluons and gravitons in chiral strong fields," *Phys. Rev. Lett.* **125** (2020), no. 4 041602, 2003.13501.

[35] T. Adamo, L. Mason, and A. Sharma, "Gluon Scattering on Self-Dual Radiative Gauge Fields," *Commun. Math. Phys.* **399** (2023) 1731–1771, 2010.14996.

[36] T. Adamo, L. Mason, and A. Sharma, "Graviton scattering in self-dual radiative space-times," *Class. Quant. Grav.* **40** (2023), no. 9 095002, 2203.02238.

[37] T. Adamo, G. Bogna, L. Mason, and A. Sharma, "Scattering on self-dual Taub-NUT," 2309.03834.

[38] T. Adamo, W. Bu, and B. Zhu, "Infrared structures of scattering on self-dual radiative backgrounds," 2309.01810.

[39] G. Bogna and L. Mason, "Yang-Mills form factors on self-dual backgrounds," *JHEP* **08** (2023) 165, 2305.07542.

[40] W. Melton, S. A. Narayanan, and A. Strominger, "Deforming soft algebras for gauge theory," *JHEP* **03** (2023) 233, 2212.08643.

[41] S. Stieberger, T. R. Taylor, and B. Zhu, "Yang-Mills as a Liouville Theory," 2308.09741.

[42] A. Atanasov, A. Ball, W. Melton, A.-M. Raclariu, and A. Strominger, "$(2,2)$ Scattering and the Celestial Torus," 2101.09591.

[43] E. Himwich, M. Pate, and K. Singh, "Celestial operator product expansions and $\mathrm{w}_{1+\infty}$ symmetry for all spins," *JHEP* **01** (2022) 080, 2108.07763.

[44] A. Atanasov, W. Melton, A.-M. Raclariu, and A. Strominger, "Conformal Block Expansion in Celestial CFT," 2104.13432.

[45] A. Sharma, "Ambidextrous light transforms for celestial amplitudes," *JHEP* **01** (2022) 031, 2107.06250.

[46] A. Strominger, "$w_{1+\infty}$ Algebra and the Celestial Sphere: Infinite Towers of Soft Graviton, Photon, and Gluon Symmetries," *Phys. Rev. Lett.* **127** (2021), no. 22 221601.

[47] Y. Hu, L. Lippstreu, M. Spradlin, A. Y. Srikant, and A. Volovich, "Four-point correlators of light-ray operators in CCFT," 2203.04255.

[48] S. Banerjee, R. Basu, and S. A. Bhatkar, "Light transformed gluon correlators in CCFT," 2203.06657.

[49] S. De and A. Pokraka, "Cosmology meets cohomology," *JHEP* **03** (2024) 156, 2308.03753.

[50] F. Cachazo, S. He, and E. Y. Yuan, "Scattering equations and Kawai-Lewellen-Tye orthogonality," *Phys. Rev. D* **90** (2014), no. 6 065001, 1306.6575.

[51] S. Mizera, "Scattering Amplitudes from Intersection Theory," *Phys. Rev. Lett.* **120** (2018), no. 14 141602, 1711.00469.

[52] H. Kawai, D. C. Lewellen, and S. H. H. Tye, "A Relation Between Tree Amplitudes of Closed and Open Strings," *Nucl. Phys. B* **269** (1986) 1–23.

[53] S. Mizera, "Combinatorics and Topology of Kawai-Lewellen-Tye Relations," *JHEP* **08** (2017) 097, 1706.08527.

[54] E. Casali, S. Mizera, and P. Tourkine, "Monodromy relations from twisted homology," *JHEP* **12** (2019) 087, 1910.08514.

[55] S. Stieberger, "A Relation between One-Loop Amplitudes of Closed and Open Strings (One-Loop KLT Relation)," 2212.06816.

[56] S. Mizera, "Kinematic Jacobi Identity is a Residue Theorem: Geometry of Color-Kinematics Duality for Gauge and Gravity Amplitudes," *Phys. Rev. Lett.* **124** (2020), no. 14 141601, 1912.03397.

[57] P. Mastrolia and S. Mizera, "Feynman Integrals and Intersection Theory," *JHEP* **02** (2019) 139, 1810.03818.

[58] H. Frellesvig, F. Gasparotto, S. Laporta, M. K. Mandal, P. Mastrolia, L. Mattiazzi, and S. Mizera, "Decomposition of Feynman Integrals on the Maximal Cut by Intersection Numbers," *JHEP* **05** (2019) 153, 1901.11510.

[59] S. Mizera, *Aspects of Scattering Amplitudes and Moduli Space Localization*. PhD thesis, Princeton, Inst. Advanced Study, 2020. 1906.02099.

[60] S. Mizera and A. Pokraka, "From Infinity to Four Dimensions: Higher Residue Pairings and Feynman Integrals," *JHEP* **02** (2020) 159, 1910.11852.

[61] H. Frellesvig, F. Gasparotto, S. Laporta, M. K. Mandal, P. Mastrolia, L. Mattiazzi, and S. Mizera, "Decomposition of Feynman Integrals by Multivariate Intersection Numbers," *JHEP* **03** (2021) 027, 2008.04823.

[62] S. Weinzierl, "On the computation of intersection numbers for twisted cocycles," *J. Math. Phys.* **62** (2021), no. 7 072301, 2002.01930.

[63] V. Chestnov, H. Frellesvig, F. Gasparotto, M. K. Mandal, and P. Mastrolia, "Intersection numbers from higher-order partial differential equations," *JHEP* **06** (2023) 131, 2209.01997.

[64] J. Chen, X. Jiang, C. Ma, X. Xu, and L. L. Yang, "Baikov representations, intersection theory, and canonical feynman integrals," 2202.08127.

[65] K. G. Chetyrkin and F. V. Tkachov, "Integration by Parts: The Algorithm to Calculate beta Functions in 4 Loops," *Nucl. Phys. B* **192** (1981) 159–204.

[66] T. Gehrmann and E. Remiddi, "Differential equations for two loop four point functions," *Nucl. Phys. B* **580** (2000) 485–518, hep-ph/9912329.

[67] S. Laporta, "High precision calculation of multiloop Feynman integrals by difference equations," *Int. J. Mod. Phys. A* **15** (2000) 5087–5159, hep-ph/0102033.

[68] S. Caron-Huot and A. Pokraka, "Duals of Feynman integrals. Part I. Differential equations," *JHEP* **12** (2021) 045, 2104.06898.

[69] S. Caron-Huot and A. Pokraka, "Duals of Feynman Integrals. Part II. Generalized unitarity," *JHEP* **04** (2022) 078, 2112.00055.

[70] A. Hillman, "Symbol Recursion for the dS Wave Function," 1912.09450.

[71] N. Arkani-Hamed, P. Benincasa, and A. Postnikov, "Cosmological polytopes and the wavefunction of the universe," 1709.02813.

[72] N. Arkani-Hamed and P. Benincasa, "On the Emergence of Lorentz Invariance and Unitarity from the Scattering Facet of Cosmological Polytopes," 1811.01125.

[73] P. Benincasa, "Cosmological Polytopes and the Wavefuncton of the Universe for Light States," 1909.02517.

[74] P. Benincasa and W. J. T. Bobadilla, "Physical representations for scattering amplitudes and the wavefunction of the universe," *SciPost Phys.* **12** (2022), no. 6 192, 2112.09028.

[75] N. Arkani-Hamed, D. Baumann, A. Hillman, A. Joyce, H. Lee, and G. L. Pimentel, "Differential Equations for Cosmological Correlators," 2312.05303.

[76] N. Arkani-Hamed, D. Baumann, A. Hillman, A. Joyce, H. Lee, and G. L. Pimentel, "Kinematic Flow and the Emergence of Time," 2312.05300.

[77] K. Matsumoto, "The monodromy representations of local systems associated with lauricella's,".

[78] P. Benincasa, "From the flat-space S-matrix to the Wavefunction of the Universe," 1811.02515.

[79] N. Arkani-Hamed, D. Baumann, H. Lee, and G. L. Pimentel, "The Cosmological Bootstrap: Inflationary Correlators from Symmetries and Singularities," *JHEP* **04** (2020) 105, 1811.00024.

[80] D. Baumann, D. Green, A. Joyce, E. Pajer, G. L. Pimentel, C. Sleight, and M. Taronna, "Snowmass White Paper: The Cosmological Bootstrap," in *Snowmass 2021*, 3, 2022. 2203.08121.

[81] E. Pajer, D. Stefanyszyn, and J. Supel, "The Boostless Bootstrap: Amplitudes without Lorentz boosts," *JHEP* **12** (2020) 198, 2007.00027. [Erratum: JHEP 04, 023 (2022)].

[82] N. Arkani-Hamed and J. Maldacena, "Cosmological collider physics," 1503.08043.

[83] D. Baumann, *Cosmology*. Cambridge University Press, 7, 2022.

[84] M. Juhnke-Kubitzke, L. Solus, and L. Venturello, "Triangulations of cosmological polytopes," 2303.05876.

[85] S.-J. Matsubara-Heo, S. Mizera, and S. Telen, "Four Lectures on Euler Integrals," 2306.13578.

[86] R. J. Eden, P. V. Landshoff, D. I. Olive, and J. C. Polkinghorne, *The analytic S-matrix*. Cambridge Univ. Press, Cambridge, 1966.

[87] Z. Bern, L. J. Dixon, D. C. Dunbar, and D. A. Kosower, "Fusing gauge theory tree amplitudes into loop amplitudes," *Nucl. Phys. B* **435** (1995) 59–101, hep-ph/9409265.

[88] R. Britto, F. Cachazo, and B. Feng, "Generalized unitarity and one-loop amplitudes in N=4 super-Yang-Mills," *Nucl. Phys. B* **725** (2005) 275–305, hep-th/0412103.

[89] V. A. Smirnov, *Feynman integral calculus*. Springer, Berlin, Heidelberg, 2006.

[90] M. Spradlin and A. Volovich, "Symbols of One-Loop Integrals From Mixed Tate Motives," *JHEP* **11** (2011) 084, 1105.2024.

[91] V. A. Smirnov, *Analytic tools for Feynman integrals*, vol. 250. 2012.

[92] C. Duhr, "Mathematical aspects of scattering amplitudes," in *Theoretical Advanced Study Institute in Elementary Particle Physics: Journeys Through the Precision Frontier: Amplitudes for Colliders*, pp. 419–476, 2015. 1411.7538.

[93] E. Gardi, S. Abreu, R. Britto, C. Duhr, and J. Matthew, "The diagrammatic coaction," *PoS* **LL2022** (2022) 015, 2207.07843.

[94] S. Mizera and S. Telen, "Landau discriminants," *JHEP* **08** (2022) 200, 2109.08036.

[95] S. Mizera, "Crossing symmetry in the planar limit," *Phys. Rev. D* **104** (2021), no. 4 045003, 2104.12776.

[96] M. Borinsky, H. J. Munch, and F. Tellander, "Tropical Feynman integration in the Minkowski regime," 2302.08955.

[97] J. M. Henn, "Multiloop integrals in dimensional regularization made simple," *Phys. Rev. Lett.* **110** (2013) 251601, 1304.1806.

[98] J. M. Henn, "Lectures on differential equations for Feynman integrals," *J. Phys. A* **48** (2015) 153001, 1412.2296.

[99] R. N. Lee and A. A. Pomeransky, "Critical points and number of master integrals," *JHEP* **11** (2013) 165, 1308.6676.

[100] T. Bitoun, C. Bogner, R. P. Klausen, and E. Panzer, "The number of master integrals as Euler characteristic," *PoS* **LL2018** (2018) 065, 1809.03399.

[101] K.-T. Chen, "Iterated path integrals," *Bulletin of the American Mathematical Society* **83** (1977), no. 5 831 – 879.

[102] C. Duhr and F. Dulat, "PolyLogTools — polylogs for the masses," *JHEP* **08** (2019) 135, 1904.07279.

[103] M. Yoshida, *Hypergeometric Functions, My Love: Modular Interpretations of Configuration Spaces*. Aspects of Mathematics. Vieweg+Teubner Verlag, 1997.

[104] K. Aomoto, M. Kita, T. Kohno, and K. Iohara, *Theory of Hypergeometric Functions*. Springer Monographs in Mathematics. Springer Japan, 2011.

[105] L. Kühne and L. Monin, "Faces of Cosmological Polytopes," 2209.08069.

[106] S. Albayrak, P. Benincasa, and C. D. Pueyo, "Perturbative Unitarity and the Wavefunction of the Universe," 2305.19686.

[107] K. Matsumoto, "Intersection numbers for logarithmic k-forms," *Osaka J. Math.* **35** (1998), no. 4 873–893.

[108] H. Frellesvig, F. Gasparotto, M. K. Mandal, P. Mastrolia, L. Mattiazzi, and S. Mizera, "Vector Space of Feynman Integrals and Multivariate Intersection Numbers," *Phys. Rev. Lett.* **123** (2019), no. 20 201602, 1907.02000.

[109] Z. Bern, V. Del Duca, L. J. Dixon, and D. A. Kosower, "All non-maximally-helicity-violating one-loop seven-gluon amplitudes in N=4 super-yang-Mills theory," *Phys. Rev. D* **71** (2005) 045006, hep-th/0410224.

[110] C. Anastasiou, R. Britto, B. Feng, Z. Kunszt, and P. Mastrolia, “D-dimensional unitarity cut method,” *Phys. Lett. B* **645** (2007) 213–216, hep-ph/0609191.

[111] R. Britto and B. Feng, “Unitarity cuts with massive propagators and algebraic expressions for coefficients,” *Phys. Rev. D* **75** (2007) 105006, hep-ph/0612089.

[112] G. Ossola, C. G. Papadopoulos, and R. Pittau, “Reducing full one-loop amplitudes to scalar integrals at the integrand level,” *Nucl. Phys. B* **763** (2007) 147–169, hep-ph/0609007.

[113] R. Britto and B. Feng, “Integral coefficients for one-loop amplitudes,” *JHEP* **02** (2008) 095, 0711.4284.

[114] J. L. Bourjaily, E. Herrmann, and J. Trnka, “Prescriptive Unitarity,” *JHEP* **06** (2017) 059, 1704.05460.

[115] B. Feng and H. Wang, “Reduction of one-loop integrals with higher poles by unitarity cut method,” *JHEP* **07** (2021) 204, 2104.00922.

[116] J. Chen, B. Feng, and L. L. Yang, “Intersection theory rules symbology,” 2305.01283.

[117] S. Abreu, R. Britto, and C. Duhr, “The SAGEX review on scattering amplitudes Chapter 3: Mathematical structures in Feynman integrals,” *J. Phys. A* **55** (2022), no. 44 443004, 2203.13014.

[118] P. Benincasa and F. Vazão, “The Asymptotic Structure of Cosmological Integrals,” 2402.06558.

[119] S. N. Karp and L. K. Williams, “The m=1 amplituhedron and cyclic hyperplane arrangements,” *Int. Math. Res. Not.* **5** (2019) 1401–1462, 1608.08288.

[120] H. Goodhew, S. Jazayeri, and E. Pajer, “The Cosmological Optical Theorem,” *JCAP* **04** (2021) 021, 2009.02898.

[121] H. Goodhew, S. Jazayeri, M. H. Gordon Lee, and E. Pajer, “Cutting cosmological correlators,” *JCAP* **08** (2021) 003, 2104.06587.

[122] S. Melville and E. Pajer, “Cosmological Cutting Rules,” *JHEP* **05** (2021) 249, 2103.09832.

[123] D. Baumann, W.-M. Chen, C. Duaso Pueyo, A. Joyce, H. Lee, and G. L. Pimentel, “Linking the singularities of cosmological correlators,” *JHEP* **09** (2022) 010, 2106.05294.

[124] D. Baumann, C. Duaso Pueyo, A. Joyce, H. Lee, and G. L. Pimentel, “The cosmological bootstrap: weight-shifting operators and scalar seeds,” *JHEP* **12** (2020) 204, 1910.14051.

[125] S. De and A. Pokraka, “A physical basis for cosmological correlators from cuts,” *JHEP* **03** (2025) 040, 2411.09695.

[126] D. Baumann, C. Duaso Pueyo, A. Joyce, H. Lee, and G. L. Pimentel, "The Cosmological Bootstrap: Spinning Correlators from Symmetries and Factorization," *SciPost Phys.* **11** (2021) 071, 2005.04234.

[127] E. Pajer, "Building a Boostless Bootstrap for the Bispectrum," *JCAP* **01** (2021) 023, 2010.12818.

[128] P. Benincasa and G. Dian, "The Geometry of Cosmological Correlators," 2401.05207.

[129] S. A. Salcedo, M. H. G. Lee, S. Melville, and E. Pajer, "The Analytic Wavefunction," *JHEP* **06** (2023) 020, 2212.08009.

[130] M. H. G. Lee, "From amplitudes to analytic wavefunctions," *JHEP* **03** (2024) 058, 2310.01525.

[131] S. He, X. Jiang, J. Liu, Q. Yang, and Y.-Q. Zhang, "Differential equations and recursive solutions for cosmological amplitudes," 2407.17715.

[132] F. Gasparotto, P. Mazloumi, and X. Xu, "Differential equations for tree–level cosmological correlators with massive states," 2411.05632.

[133] D. Baumann, H. Goodhew, and H. Lee, "Kinematic Flow for Cosmological Loop Integrands," 2410.17994.

[134] Y. Hang, "A Note on Kinematic Flow and Differential Equations for Two-Site One-Loop Graph in FRW Spacetime," 2410.17192.

[135] P. Benincasa, G. Brunello, M. K. Mandal, P. Mastrolia, and F. Vazão, "On one-loop corrections to the Bunch-Davies wavefunction of the universe," 2408.16386.

[136] J. Chen, B. Feng, and Y.-X. Tao, "Multivariate hypergeometric solutions of cosmological (dS) correlators by $\mathrm{d}\log$-form differential equations," 2411.03088.

[137] T. W. Grimm and A. Hoefnagels, "Reductions of GKZ Systems and Applications to Cosmological Correlators," 2409.13815.

[138] C. Fevola, G. L. Pimentel, A.-L. Sattelberger, and T. Westerdijk, "Algebraic Approaches to Cosmological Integrals," 2410.14757.

[139] B. Fan and Z.-Z. Xianyu, "Cosmological Amplitudes in Power-Law FRW Universe," 2403.07050.

[140] Z.-Z. Xianyu and J. Zang, "Inflation correlators with multiple massive exchanges," *JHEP* **03** (2024) 070, 2309.10849.

[141] Y. Ema and K. Mukaida, "Cutting rule for in-in correlators and cosmological collider," 2409.07521.

[142] D. Ghosh, E. Pajer, and F. Ullah, "Cosmological cutting rules for Bogoliubov initial states," 2407.06258.

[143] S. Agui Salcedo and S. Melville, "The cosmological tree theorem," *JHEP* **12** (2023) 076, 2308.00680.

[144] X. Tong, Y. Wang, and Y. Zhu, "Cutting rule for cosmological collider signals: a bulk evolution perspective," *JHEP* **03** (2022) 181, 2112.03448.

[145] D. Werth, "Spectral Representation of Cosmological Correlators," 2409.02072.

[146] M. Yoshida, *Hypergeometric functions, my love: modular interpretations of configuration spaces*, vol. 32. Springer Science & Business Media, 2013.

[147] M. H. G. Lee, C. McCulloch, and E. Pajer, "Leading loops in cosmological correlators," *JHEP* **11** (2023) 038, 2305.11228.

[148] N. Arkani-Hamed, Y. Bai, and T. Lam, "Positive Geometries and Canonical Forms," *JHEP* **11** (2017) 039, 1703.04541.

[149] A. McLeod, A. Pokraka, and L. Ren, "A diagrammatic coaction for cosmological correlators (work in progress)." Work in progress.

[150] S. Abreu, R. Britto, C. Duhr, E. Gardi, and J. Matthew, "From positive geometries to a coaction on hypergeometric functions," *JHEP* **02** (2020) 122, 1910.08358.

[151] R. C. Hwa and V. L. Teplitz, "Homology and feynman integrals," *(No Title)* (1966).

[152] P. Benincasa, A. J. McLeod, and C. Vergu, "Steinmann Relations and the Wavefunction of the Universe," *Phys. Rev. D* **102** (2020) 125004, 2009.03047.

[153] C. Dupont, "The orlik-solomon model for hypersurface arrangements," 2015.

[154] P. Orlik and L. Solomon, "Combinatorics and topology of complements of hyperplanes," *Inventiones mathematicae* **56** (1980), no. 2 167–189.

[155] F. Pham, *Singularities of integrals: Homology, hyperfunctions and microlocal analysis*. Universitext. Springer London, 2011.

[156] S. De, S. Paranjape, A. Pokraka, M. Spradlin, and A. Volovich, "Hidden Zeros of the Cosmological Wavefunction," 2503.23579.

[157] N. Arkani-Hamed, Q. Cao, J. Dong, C. Figueiredo, and S. He, "Hidden zeros for particle/string amplitudes and the unity of colored scalars, pions and gluons," *JHEP* **10** (2024) 231, 2312.16282.

[158] F. Cachazo, N. Early, and B. Giménez Umbert, "Smoothly splitting amplitudes and semi-locality," *JHEP* **08** (2022) 252, 2112.14191.

[159] Q. Cao, J. Dong, S. He, and C. Shi, "A universal splitting of tree-level string and particle scattering amplitudes," *Phys. Lett. B* **856** (2024) 138934, 2403.08855.

[160] C. Bartsch, T. V. Brown, K. Kampf, U. Oktem, S. Paranjape, and J. Trnka, "Hidden amplitude zeros from the double-copy map," *Phys. Rev. D* **111** (2025), no. 4 045019, 2403.10594.

[161] Y. Li, D. Roest, and T. ter Veldhuis, "Hidden Zeros in Scaffolded General Relativity and Exceptional Field Theories," 2403.12939.

[162] L. Rodina, "Hidden Zeros Are Equivalent to Enhanced Ultraviolet Scaling, and Lead to Unique Amplitudes in Tr(ϕ3) Theory," *Phys. Rev. Lett.* **134** (2025), no. 3 031601, 2406.04234.

[163] Y. Li, T. Wang, T. Brauner, and D. Roest, "Diagrammatic Derivation of Hidden Zeros and Exact Factorisation of Pion Scattering Amplitudes," 2412.14858.

[164] Y. Zhang, "On the new factorizations of Yang-Mills amplitudes," *JHEP* **02** (2025) 074, 2412.15198.

[165] B. Giménez Umbert and B. Sturmfels, "Splitting CEGM Amplitudes," 2501.10805.

[166] H. Huang, Y. Yang, and K. Zhou, "Note on hidden zeros and expansions of tree-level amplitudes," 2502.07173.

[167] J. V. Backus and L. Rodina, "Emergence of Unitarity and Locality from Hidden Zeros at One-Loop," 2503.03805.

[168] S. L. Adler, "Consistency conditions on the strong interactions implied by a partially conserved axial vector current," *Phys. Rev.* **137** (1965) B1022–B1033.

[169] L. J. Dixon, Z. Kunszt, and A. Signer, "Vector boson pair production in hadronic collisions at order α_s : Lepton correlations and anomalous couplings," *Phys. Rev. D* **60** (1999) 114037, hep-ph/9907305.

[170] A. D'Adda, S. Sciuto, R. D'Auria, and F. Gliozzi, "Zeros of dual resonant amplitudes," *Nuovo Cim. A* **5** (1971) 421–432.

[171] N. Arkani-Hamed, P. Benincasa, and A. Postnikov, "Cosmological Polytopes and the Wavefunction of the Universe," 1709.02813.

[172] P. Benincasa, "Amplitudes meet Cosmology: A (Scalar) Primer," 2203.15330.

[173] N. Arkani-Hamed, C. Figueiredo, and F. Vazão, "Cosmohedra," 2412.19881.

[174] Z.-Z. Du, "Hidden Adler zeros and soft theorems for inflationary perturbations," 2411.17591.

[175] M. Carr and S. L. Devadoss, "Coxeter complexes and graph-associahedra," math/0407229.

[176] S. L. Devadoss, "A realization of graph-associahedra," math/0612530.

[177] R. Glew and T. Lukowski, "Amplitubes: Graph Cosmohedra," 2502.17564.

[178] R. Glew, "Wavefunction coefficients from Amplitubes," 2503.13596.

[179] N. Arkani-Hamed, S. He, G. Salvatori, and H. Thomas, "Causal diamonds, cluster polytopes and scattering amplitudes," *JHEP* **11** (2022) 049, 1912.12948.

[180] N. Arkani-Hamed, S. He, and T. Lam, "Stringy canonical forms," *JHEP* **02** (2021) 069, 1912.08707.

[181] R. Bhardwaj, S. De, M. Spradlin, and A. Volovich, "On unitarity of the Coon amplitude," *JHEP* **08** (2023) 082, 2212.00764.

[182] D. D. Coon, U. P. Sukhatme, and J. Tran Thanh Van, "DUALITY AND PROTON PROTON SCATTERING AT ALL ANGLES," *Phys. Lett. B* **45** (1973) 287–291.

[183] M. Baker and D. D. Coon, "Dual resonance theory with nonlinear trajectories," *Phys. Rev. D* **2** (1970) 2349–2358.

[184] S. Yu, M. Baker, and D. Coon, "First and second factorization in a dual multiparticle theory with nonlinear trajectories," *Physical Review D* **5** (1972), no. 12 3108.

[185] M. Baker, S. Yu, and D. Coon, "Twist relation, third factorization, and the general vertex in a dual multiparticle theory with nonlinear trajectories," *Physical Review D* **6** (1972), no. 2 538.

[186] M. Baker and D. D. Coon, "Loop diagrams in dual-resonance theories with nonlinear trajectories," *Phys. Rev. D* **3** (1971) 2478–2485.

[187] M. Arik, D. D. Coon, and Y.-M. Lam, "OPERATOR ALGEBRA OF DUAL RESONANCE MODELS," *J. Math. Phys.* **16** (1975) 1776.

[188] D. D. Coon, S. Yu, and M. Baker, "Operator formulation of a dual multiparticle theory with nonlinear trajectories," *Phys. Rev. D* **5** (1972) 1429–1433.

[189] M. Chaichian, J. F. Gomes, and P. Kulish, "Operator formalism of q deformed dual string model," *Phys. Lett. B* **311** (1993) 93–97, hep-th/9211029.

[190] L. L. Jenkovszky, M. Kibler, and A. Mishchenko, "Two parametric quantum deformed dual amplitude," *Mod. Phys. Lett. A* **10** (1995) 51–60, hep-th/9407071.

[191] L. J. Romans, "A NEW FAMILY OF DUAL MODELS ('q strings'),".

[192] L. J. Romans, "Deforming the Veneziano model ('q strings')," *Conf. Proc. C* **8903131** (1989) 57–66.

[193] D. Bernard and A. LeClair, "q Deformation of SU(1,1) Conformal Ward Identities and q Strings," *Phys. Lett. B* **227** (1989) 417–423.

[194] Z. Bern, D. Kosmopoulos, and A. Zhiboedov, "Gravitational effective field theory islands, low-spin dominance, and the four-graviton amplitude," *J. Phys. A* **54** (2021), no. 34 344002, 2103.12728.

[195] S. Caron-Huot, Z. Komargodski, A. Sever, and A. Zhiboedov, "Strings from Massive Higher Spins: The Asymptotic Uniqueness of the Veneziano Amplitude," *JHEP* **10** (2017) 026, 1607.04253.

[196] J. Maldacena and G. N. Remmen, "Accumulation-point amplitudes in string theory," *JHEP* **08** (2022) 152, 2207.06426.

[197] V. G. Kac and P. Cheung, *Quantum calculus*, vol. 113. Springer, 2002.

[198] T. Ernst, *A comprehensive treatment of q-calculus*. Springer Science & Business Media, 2012.

[199] N. Geiser and L. W. Lindwasser, "Properties of infinite product amplitudes: Veneziano, Virasoro, and Coon," 2207.08855.

[200] G. Gasper and M. Rahman, *Basic Hypergeometric Series*. Encyclopedia of Mathematics and its Applications. Cambridge University Press, 2 ed., 2004.

[201] P. Maity, "Positivity of the Veneziano amplitude in D = 4," *JHEP* **04** (2022) 064, 2110.01578.

[202] J. Chakravarty, P. Maity, and A. Mishra, "On the positivity of Coon amplitude in D = 4," *JHEP* **10** (2022) 043, 2208.02735.

[203] P. Di Francesco, P. Mathieu, and D. Senechal, *Conformal Field Theory*. Graduate Texts in Contemporary Physics. Springer-Verlag, New York, 1997.

[204] P. Flajolet and R. Sedgewick, *Analytic Combinatorics*. Cambridge University Press, 2009.

[205] A. De Sole and V. Kac, "On integral representations of q-gamma and q-beta functions," *arXiv preprint math/0302032* (2003).

[206] S. Banerjee and B. Wilkerson, "Lambert series and q-functions near q= 1," *arXiv preprint arXiv:1602.01085* (2016).

[207] S. Banerjee and B. Wilkerson, "Asymptotic expansions of lambert series and related q-series," *International Journal of Number Theory* **13** (2017), no. 08 2097–2113.

[208] A. Ball, S. De, A. Yelleshpur Srikant, and A. Volovich, "Scalar-graviton amplitudes and celestial holography," *JHEP* **02** (2024) 097, 2310.00520.

[209] K. Costello, N. M. Paquette, and A. Sharma, "Top-Down Holography in an Asymptotically Flat Spacetime," *Phys. Rev. Lett.* **130** (2023), no. 6 061602, 2208.14233.

[210] K. Costello, N. M. Paquette, and A. Sharma, "Burns space and holography," 2306.00940.

[211] R. Bittleston, S. Heuveline, and D. Skinner, "The Celestial Chiral Algebra of Self-Dual Gravity on Eguchi-Hanson Space," 2305.09451.

[212] L. J. Dixon, E. W. N. Glover, and V. V. Khoze, "MHV rules for Higgs plus multi-gluon amplitudes," *JHEP* **12** (2004) 015, hep-th/0411092.

[213] W. Fan, A. Fotopoulos, S. Stieberger, T. R. Taylor, and B. Zhu, "Conformal Blocks from Celestial Gluon Amplitudes," 2103.04420.

[214] S. De, Y. Hu, A. Yelleshpur Srikant, and A. Volovich, "Correlators of four light-ray operators in CCFT," *JHEP* **10** (2022) 170, 2206.08875.

[215] C. Jorge-Diaz, S. Pasterski, and A. Sharma, "Celestial amplitudes in an ambidextrous basis," *JHEP* **02** (2023) 155, 2212.00962.

[216] N. Arkani-Hamed, T.-C. Huang, and Y.-t. Huang, "Scattering amplitudes for all masses and spins," *JHEP* **11** (2021) 070, 1709.04891.

[217] K. Risager, "A Direct proof of the CSW rules," *JHEP* **12** (2005) 003, hep-th/0508206.

[218] R. Britto, R. Gonzo, and G. R. Jehu, "Graviton particle statistics and coherent states from classical scattering amplitudes," *JHEP* **03** (2022) 214, 2112.07036.

[219] I. Dubovyk, J. Gluza, and G. Somogyi, "Mellin-Barnes Integrals: A Primer on Particle Physics Applications," *Lect. Notes Phys.* **1008** (2022) pp., 2211.13733.

[220] L. Donnay, S. Pasterski, and A. Puhm, "Asymptotic Symmetries and Celestial CFT," *JHEP* **09** (2020) 176, 2005.08990.

[221] S. Stieberger and T. R. Taylor, "Symmetries of Celestial Amplitudes," *Phys. Lett. B* **793** (2019) 141–143, 1812.01080.

[222] M. Pate, A.-M. Raclariu, A. Strominger, and E. Y. Yuan, "Celestial operator products of gluons and gravitons," *Rev. Math. Phys.* **33** (2021), no. 09 2140003, 1910.07424.

[223] A. Puhm, "Conformally Soft Theorem in Gravity," *JHEP* **09** (2020) 130, 1905.09799.

[224] S. Weinberg, "Infrared photons and gravitons," *Phys. Rev.* **140** (Oct, 1965) B516–B524.

[225] D. Kapec, Y. T. A. Law, and S. A. Narayanan, "Soft scalars and the geometry of the space of celestial conformal field theories," *Phys. Rev. D* **107** (2023), no. 4 046024, 2205.10935.

[226] D. Kapec, "Soft Particles and Infinite-Dimensional Geometry," 2210.00606.

[227] M. Campiglia and A. Laddha, "Asymptotic symmetries of gravity and soft theorems for massive particles," *JHEP* **12** (2015) 094, 1509.01406.

[228] M. Campiglia and A. Laddha, "Asymptotic symmetries of QED and Weinberg's soft photon theorem," *JHEP* **07** (2015) 115, 1505.05346.

[229] E. Y. Yuan, "Simplicity in AdS Perturbative Dynamics," 1801.07283.

[230] C. Sleight and M. Taronna, "Celestial Holography Revisited," 2301.01810.

[231] J. V. S. e. Tom H. Koornwinder (editor), *Encyclopedia of Special Functions: The Askey-Bateman Project - Volume 2. Multivariable Special Functions*. Encyclopedia of Special Functions: The Askey-Bateman Project 3 Hardback Books. Cambridge University Press, 1 ed., 2020.

[232] P. Kravchuk and D. Simmons-Duffin, "Light-ray operators in conformal field theory," *JHEP* **11** (2018) 102, 1805.00098.

[233] G. P. Korchemsky and A. Zhiboedov, "On the light-ray algebra in conformal field theories," *JHEP* **02** (2022) 140, 2109.13269.

[234] M. Kologlu, P. Kravchuk, D. Simmons-Duffin, and A. Zhiboedov, "The light-ray OPE and conformal colliders," *JHEP* **01** (2021) 128, 1905.01311.

[235] A. Guevara, "Celestial OPE blocks," 2108.12706.

[236] Y. N. Prasad and S. N. Singh, "Some expansion formulae for H-function of two variables involving Jacobi Polynomials," *Bulletin mathématique de la Société des Sciences Mathématiques de la République Socialiste de Roumanie* **21 (69)** (1977), no. 1/2 123–132.

[237] N. T. Hai and S. B. Yakubovich, *The Double Mellin-Barnes Type Integrals and Their Applications to Convolution Theory*. World Scientific, 1992.

[238] N. T. Hai, O. Marichev, and R. Buschman, "Theory of the general H-function of two variables," *The Rocky Mountain Journal of Mathematics* **22** (1992), no. 4 1317–1327.

[239] A. Kilbas, *H-Transforms: Theory and Applications*. Analytical Methods and Special Functions. CRC Press, 2004.

[240] J. Daiya, J. Ram, and D. Kumar, "The multivariable h-function and the general class of srivastava polynomials involving the generalized mellin-barnes contour integrals," *Filomat* **30** (2016), no. 6 1457–1464.

[241] A. Rathie, "A new generalization of generalized hypergeometric functions," *Le Matematiche* **52** (01, 1998) 1206.0350.

[242] P. Jayarama, V. Madam, and S. Kurumujji, "A Study of I-Function of Several Complex Variables," *International Journal of Engineering Mathematics* **2014** (01, 2014) 1–11.

[243] L. Donnay, S. Pasterski, and A. Puhm, "Goldilocks modes and the three scattering bases," *JHEP* **06** (2022) 124, 2202.11127.

[244] D. Nandan, A. Schreiber, A. Volovich, and M. Zlotnikov, "Celestial Amplitudes: Conformal Partial Waves and Soft Limits," *JHEP* **10** (2019) 018, 1904.10940.

[245] F. A. Dolan and H. Osborn, "Conformal Partial Waves: Further Mathematical Results," 1108.6194.